Open and Free http://www.zcyphygeodesy.com/en/

Precise Approximation of Earth Gravity Field and Geoid

PAGravf4.5 User Reference

- Multi-type data from terrestrial, maritime, aerial, or space-based observations
- Diverse Terrain Effects on Various gravity field Elements on or outside the Geoid
- Closed-Loop Analytical Operations between External Gravity Field Elements
- All-Element Analytical Modeling of Local Gravity Field in Full External Space
- Observation Error Assessment & Precise Computational Performance Control
- Gravity Exploration Modeling from Multi-Source Heterogeneous Observations

Chinese Academy of Surveying and Mapping

Chuanyin Zhang, March 2026, Beijing, China

Introduction to PAGravf4.5

PAGravf4.5 (**P**recise **A**pproximation of Earth **Grav**ity Field and Geoid, Version 4.5) is a comprehensive, Windows-based scientific computing suite specifically engineered for geophysical geodesy. The system architecture integrates five specialized subsystems:

(a) Analysis and Preprocessing of Earth gravity field data;

(b) Computation of Diverse Terrain Effects on various gravity field elements;

(c) High-Precision Gravity Field Approximation and full-element modeling;

(d) Optimization, Unification, and Application of regional height datums;

(e) Toolkit for Geodetic Data File Editing, Calculation, and Visualization.

Adhering strictly to the principles of physical geodesy, PAGravf4.5 establishes a unified analytical framework for computing diverse terrain effects across all external gravity field elements, significantly advancing capabilities in geophysical gravity exploration and gravity field data processing. The software employs a robust hybrid architecture that synergistically integrates spatial-domain boundary value problem (BVP) integrals with spectral-domain Spherical Radial Basis Function (SRBF) approximations. This enables full-space, all-element analytical modeling of the gravity field on and outside the geoid, utilizing multi-source, heterogeneous, varying-altitude, cross-distributed, and multi-type observations. Furthermore, PAGravf4.5 incorporates ingenious algorithms for gravity exploration modeling using multi-source heterogeneous geodetic data and for the optimization of height datums, thereby consolidating and expanding the practical utility of the Earth's gravity field theory.

PAGravf4.5 comprehensively encompasses the fundamental principles, core methodologies, and complete formalism of physical geodesy and the Earth's gravity field theory. It empowers users to explore and resolve complex geodetic challenges through analytical reasoning and advanced computational capabilities, serving as an invaluable resource for advanced education and professional training. The software effectively resolves a series of persistent technical challenges, including:

(1) The rigorous computation of diverse terrain effects on various gravity field elements;

(2) The realization of comprehensive, all-element analytical modeling using multi-source heterogeneous data;

(3) Gravity exploration modeling via the fusion of multi-source geodetic data;

(4) The optimization, unification, and refinement of regional height datums.

(5) The determination of external accuracy metrics, and precise control of computational performance.

These integrated capabilities markedly enhance the software's scientific robustness and application potential.

Target Audience

PAGravf4.5 is designed for undergraduates, graduate students, researchers, and engineering professionals in the following fields: Geodesy and Earth Sciences, Geology and Geophysics, Geomatics and GIS, Aerospace and Satellite Dynamics, and Seismology and Geodynamics.

Keywords: Terrain Effect; Gravity Field Approximation; Geoid; Spherical Radial Basis Function (SRBF); Height Datum; Geodetic Computation.

Website: https://www.zcyphygeodesy.com/en/
ZHANG Chuanyin (mailto: zpmzsyzcy1986@163.com)
Chinese Academy of Surveying & Mapping
March 2026, Beijing 100036, China

Contents

1. Architecture, Features, and Design Philosophy of PAGravf4.5

PAGravf4.5 (Precise Approximation for Earth Gravity Field and Geoid, Version 4.5) is a comprehensive, Windows-based scientific computing suite engineered specifically for geophysical geodesy.

Strictly adhering to the principles, theoretical foundations, and technical requirements of physical geodesy, PAGravf4.5 constructs a unified analytical algorithmic framework to compute diverse terrain effects on all gravity field elements on and outside the geoid. This architecture significantly enhances capabilities in gravity prospecting modeling and data processing, addressing the complex demands of modern geophysical geodesy.

PAGravf4.5 establishes a rigorous framework that synergizes spatial-domain boundary value problem integrals with spectral-domain Spherical Radial Basis Function (SRBF) approximations. This hybrid architecture effectively resolves persistent technical challenges, including: (a) the realization of all-element analytical modeling of the gravity field both on and outside the geoid; and (b) the determination of rigorous external accuracy metrics and the precise control of computational performance. Crucially, it enables comprehensive, all-element, full-space analytical modeling of the Earth's gravity field by deeply fusing multi-source, heterogeneous, varying-altitude, cross-distributed, and multi-type data encomp-

assing terrestrial, maritime, aerial, or space-based observations.

Furthermore, PAGravf4.5 incorporates a suite of ingenious algorithms grounded in physical geodesy principles, designed to create robust analytical gravity prospecting modeling methods using multi-source heterogeneous data, with the objective of optimizing and unifying regional height datums, thereby consolidating and expanding the practical utility of Earth's gravity field models and height datum products in scientific and engineering endeavors.

As a premier platform for education and research, PAGravf4.5 encompasses the fundamental principles, core methodologies, and exhaustive formulary of physical geodesy. It empowers users to explore and resolve complex geodetic challenges through analytical thinking and computational capabilities, serving as an indispensable asset for advancing higher education, facilitating knowledge dissemination, and catalyzing innovation within the geosciences. PAGravf4.5 is very helpful for empowering the exploration and resolution of complex geodetic challenges using physical geodetic ideas and thinking.

1.1 Computational Functional Architecture of PAGravf4.5

PAGravf4.5 is rigorously engineered around five tightly coupled, functionally specialized subsystems:

(a) Analysis and Preprocessing of Earth gravity field data;

(b) Computation of Diverse Terrain Effects on various gravity field elements;

(c) High-Precision Gravity Field Approximation and full-element modeling;

(d) Optimization, Unification, and Application of regional height datums; and

(e) Toolkit for Geodetic Data File Editing, Calculation, and Visualization.

(1) Development Environment and Hybrid Programming Paradigm

PAGravf4.5 was developed within the Microsoft Visual Studio 2017 x64 Integrated Development Environment (IDE), employing a strategic hybrid programming paradigm to leverage the distinct strengths of specialized languages:

(a) User Interface (UI) Layer: Implemented using QT C++ (compiled via the Visual C++ compiler), ensuring a responsive, intuitive, and cross-platform compatible graphical interface.

(b) Core Scientific Computation Layer: Computationally intensive numerical algorithms are implemented in Intel Fortran (Fortran 90 standard), capitalizing on Fortran's superior efficiency in array manipulation and scientific computing to guarantee high performance.

(c) Geodetic Data Visualization Layer: Scientific and geospatial graphics are rendered using the MathGL C++ library, enabling the generation of plots, maps, and visualizations of gravity field elements, terrain models, and processing results.

(2) PAGravf4.5 System Integration and Scale

This comprehensive, modular system comprises over 50 Win64 executable programs, collectively integrating nearly 600 functional modules. This extensive integration delivers a complete, professional-grade suite for physical geodetic scientific computation, fully addressing the diverse requirements of education, research, and application in geodesy and geophysics.

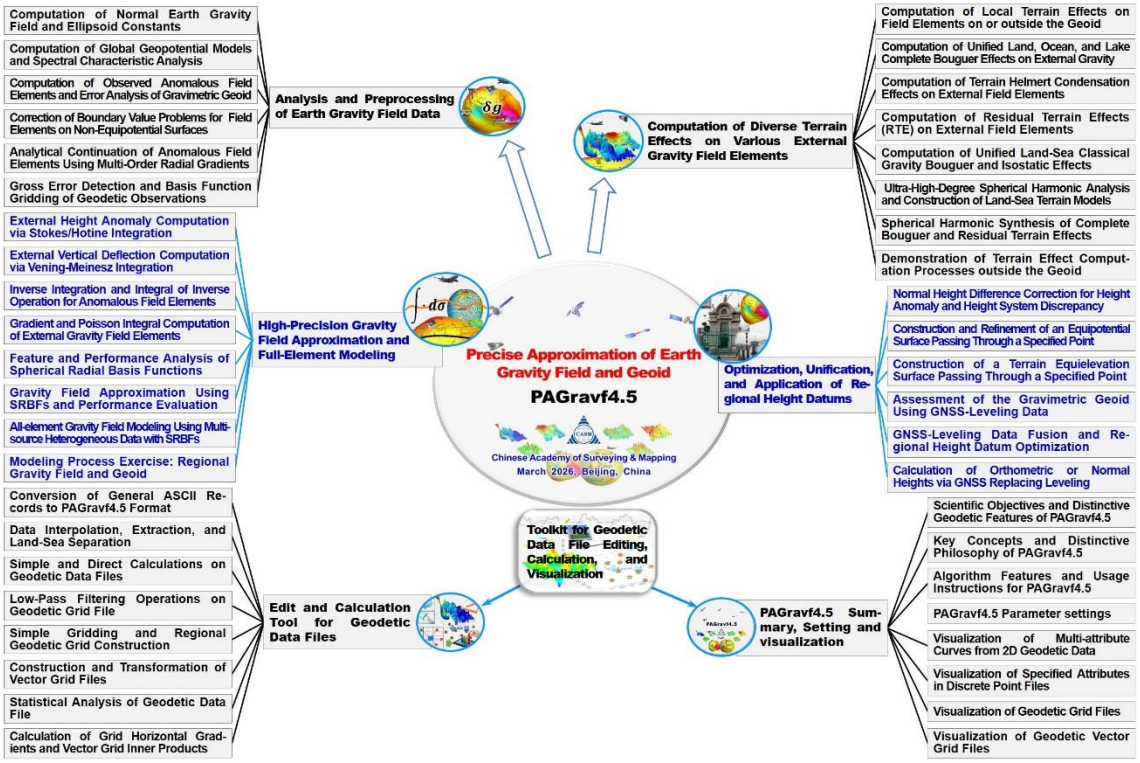

1.1.1 Analysis and Preprocessing of Earth Gravity Field Data

This subsystem executes foundational computational tasks for physical geodesy and gravimetric data processing. Core functionalities include:

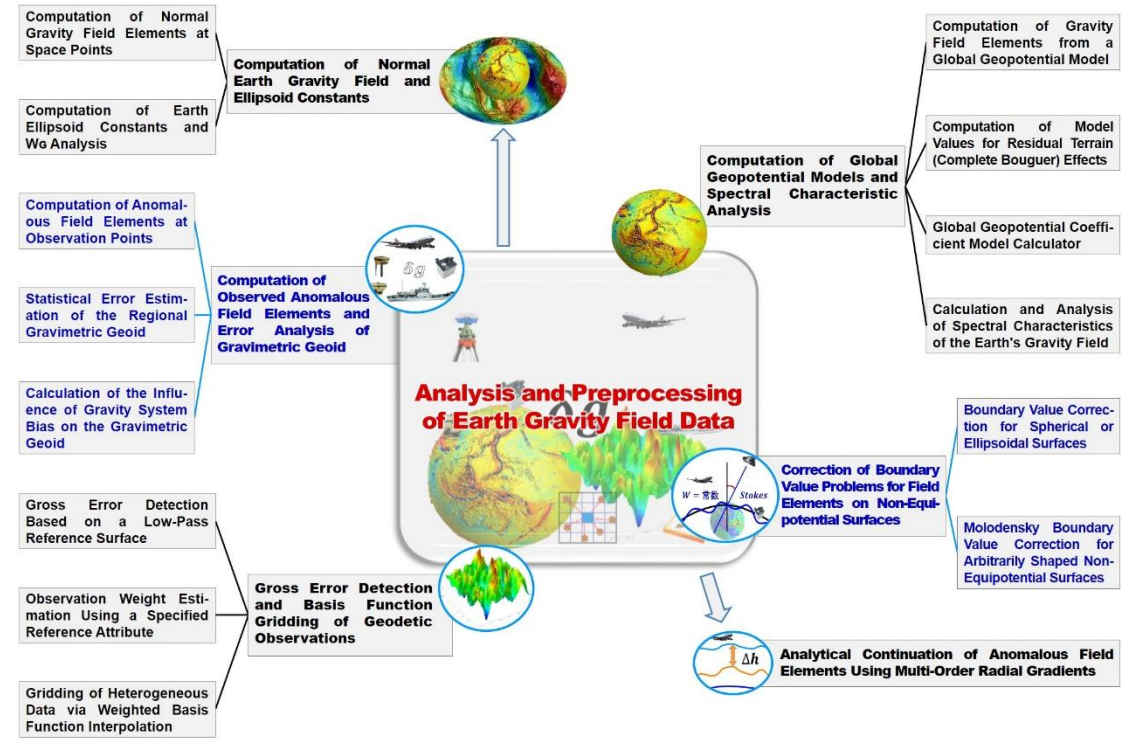

(a) Analysis and Computation of the Normal Gravity Field and Reference Ellipsoid Parameters.

(b) Computation and Spectral Analysis of Global Geopotential Models (GGMs).

(c) Reduction and Correction of Gravity Field Elements for solving the Geodetic Boundary Value Problem (GBVP).

(d) Processing of Gravity Field Observations, encompassing analytical continuation, gross error detection, and gridding operations.

1.1.2 Computation of Diverse Terrain Effects on Various External Gravity Field Elements

This subsystem establishes a unified analytical algorithmic framework dedicated to computing diverse terrain effects on various gravity field elements on or outside the geoid by formulating harmonic terrain fields in external space. Key capabilities include:

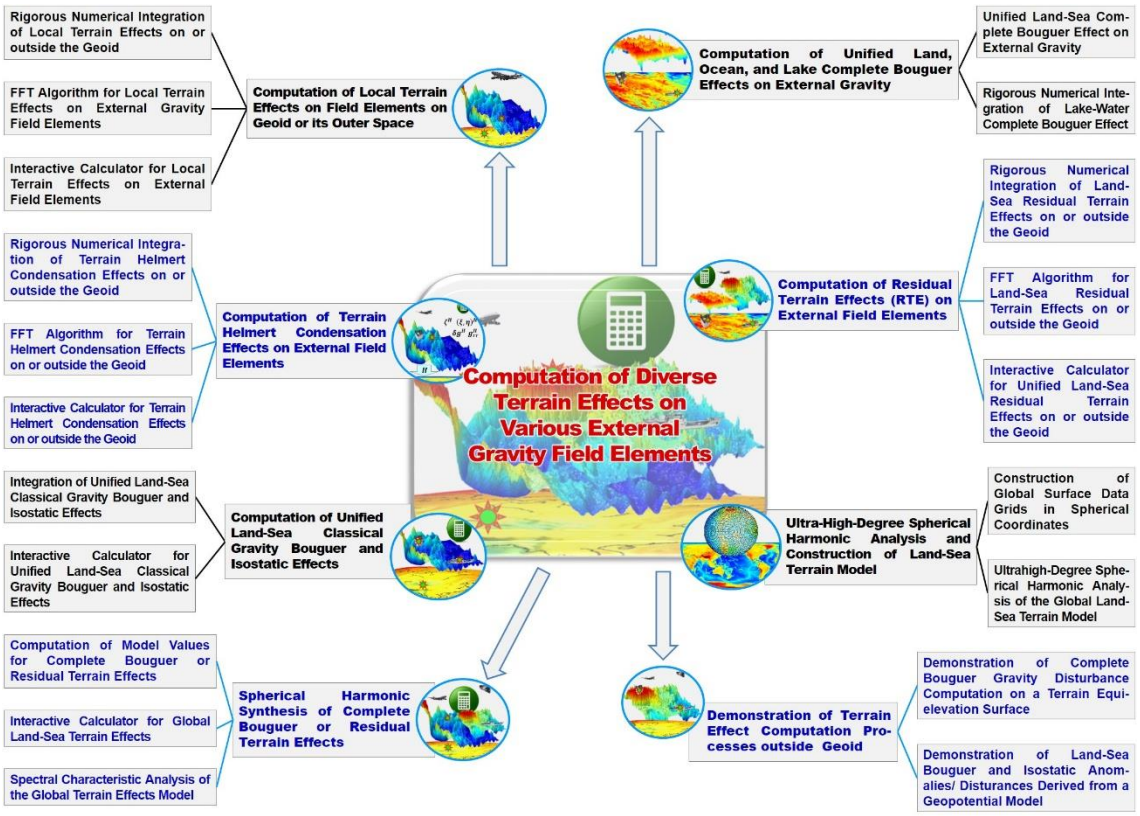

(a) Available Terrain Effect Strategies: Supports a wide array, including Local Terrain Effects, Terrain Bouguer Effects, Seawater Bouguer Effects, Crustal Isostatic Effects, Terrain Helmert Condensation Effects, and Residual Terrain Effects (RTE).

(b) Affected Gravity Field Elements: Encompasses the full spectrum: Geopotential, Disturbing Potential and Height Anomaly, Gravity, Gravity Disturbance and Gravity Anomaly, Vertical Deflection Vector, and Gravity Gradient Tensors.

(c) Spatial Domain Coverage: Supports high-precision computations for field elements located on or outside the geoid, ensuring seamless modeling continuity from the geoidal

surface to satellite altitudes.

1.1.3 High-Precision Gravity Field Approximation and Full-Element Modeling

This framework features a robust hybrid algorithmic architecture that synergizes spatial-domain and spectral-domain methods:

(a) Spatial-Domain Integration Algorithms (Geodetic Boundary Value Theory): Employs classical solutions including Stokes's, Hotine's, Vening Meinesz's, and various inverse operation integral formulas, effective for regional gravity field modeling.

(b) Spectral-Domain Spherical Radial Basis Function (SRBF): Utilizes SRBFs for gravity field representation, offering superior flexibility in spectral shaping and adeptness at handling irregularly distributed data, ideal for fusing multi-source heterogeneous observations.

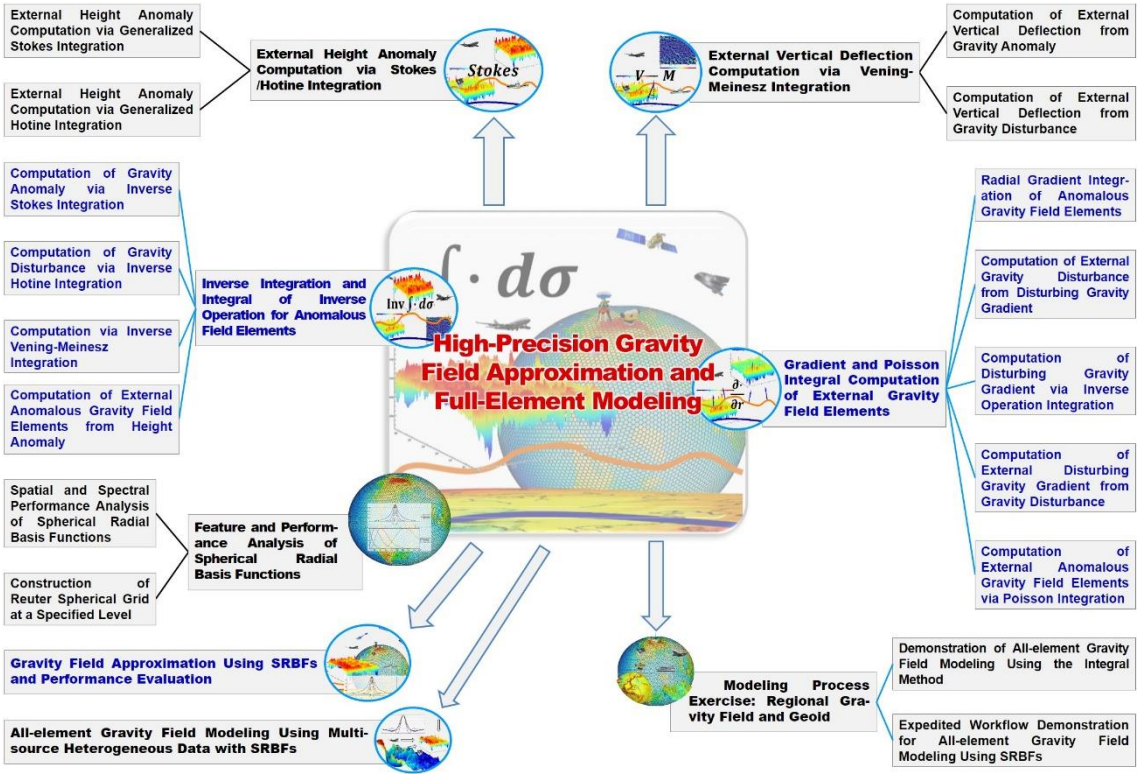

This integrated dual-domain framework enables full-space, all-element analytical modeling of the external gravity field directly using multi-source, heterogeneous, varying-altitude, cross-distributed, and multi-type data encompassing terrestrial, maritime, aerial, or space-based observations.

1.1.4 Optimization, Unification, and Application of Regional Height Datums

PAGravf4.5 develops a suite of ingenious algorithms grounded in physical geodesy principles, architected to address the practical challenges of optimizing and unifying regional height datums, playing a key role in consolidating the practical utility of the Earth's gravity field theory and data.

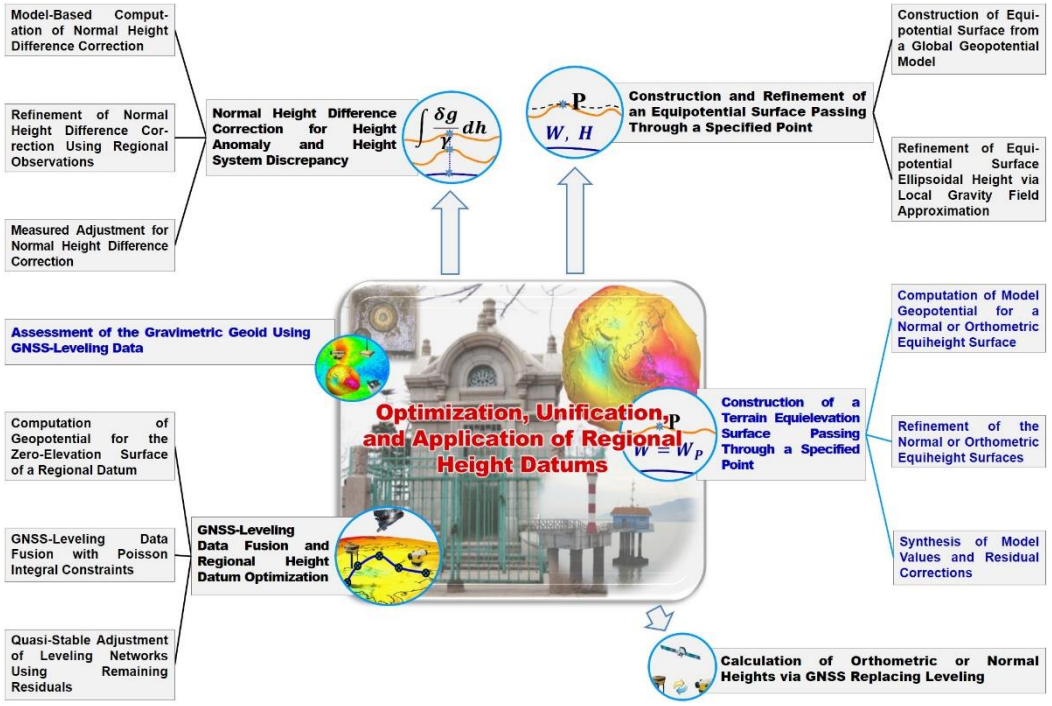

1.1.5 Toolkit for Geodetic Data File Editing, Calculation, and Visualization

This toolkit executes essential data manipulation and preprocessing tasks fundamental to geodetic workflows. Its core functionalities encompass format conversion, attribute editing, and preliminary statistical analysis, serving as the data preparation and conditioning hub within the PAGravf4.5 environment.

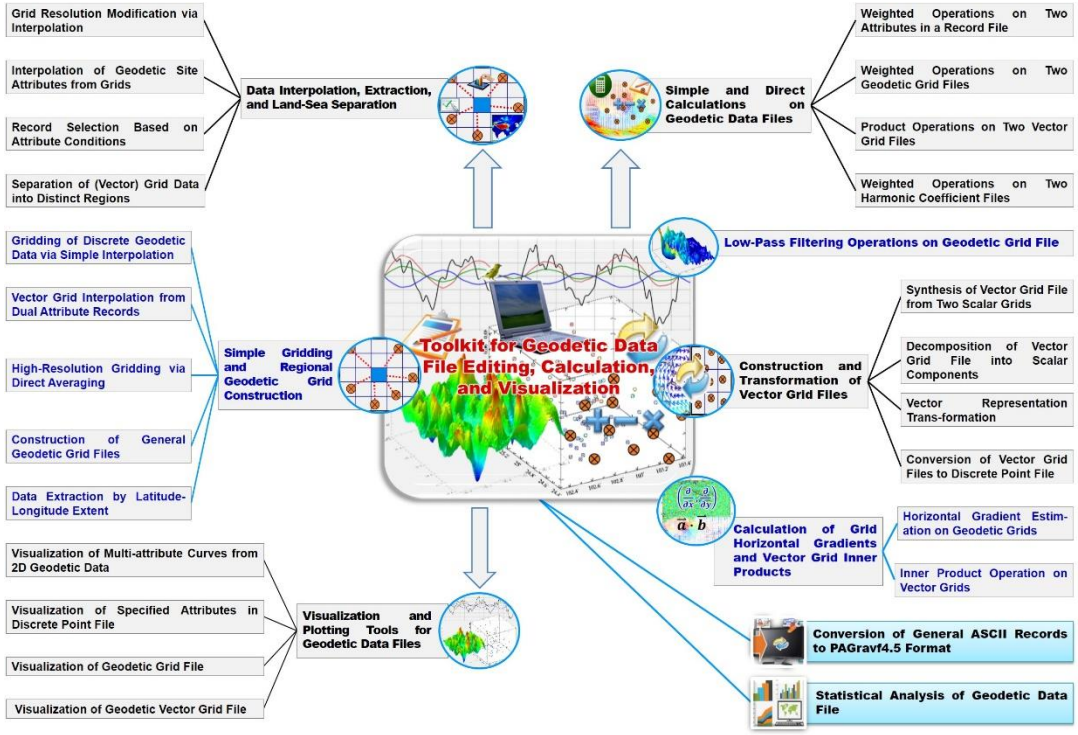

1.2 Scientific Objectives and Geodetic Features of PAGravf4.5

1.2.1 Scientific Objectives of PAGravf4.5

PAGravf4.5 is engineered to rigorously adhere to the theoretical foundations of physical geodesy. Its overarching scientific objectives are:

(a) To comprehensively resolve the complex diverse terrain effects on various gravity field elements both on and outside the geoid;

(b) To realize full-space, all-element analytical modeling of the gravity field and centimeter-level geoid;

(c) To achieve closed-loop analytical operations for various external anomalous gravity field elements;

(d) To significantly expand the computational capabilities and practical application scope of Earth's gravity field.

These objectives are realized through:

(a) Resolving Analytical Compatibility of Diverse Terrain Effects: Overcoming the challenge of achieving analytical compatibility and rigorously unified computation for diverse terrain effects on all gravity field elements.

(b) Constructing an Integrated Dual-Domain Algorithmic Framework: Establishing a robust framework that synergizes spatial-domain boundary-value integrals with spectral-domain SRBF approximations to enable comprehensive modeling using complex, multi-source data.

(c) Developing Ingenious Algorithms for Height Datum Optimization and Unification: Developing algorithms to facilitate analytical modeling of gravity exploration and the pivotal optimization and unification of regional height datums, strengthening the linkage between gravity field theory and height systems.

The scientific objectives of PAGravf4.5 are deeply interconnected, forming a logical progression from resolving fundamental computational issues (terrain effects) to constructing advanced integrated modeling systems, and finally to achieving height datum unification and gravity field application. This holistic design philosophy underscores its mission to "alleviate the critical scarcity of such computational resources in the global geoscience education landscape" and to "demonstrate the profound potential and elegance of geodesy." PAGravf4.5 is very helpful for empowering the exploration and resolution of complex geodetic challenges using physical geodetic ideas and thinking.

1.2.2 Distinctive Geodetic Features of PAGravf4.5

(a) Unified Analytical Computation Framework for Diverse Terrain Effects: A rigorously developed framework capable of precisely computing diverse terrain effects on a broad spectrum of gravity field elements on and outside the geoid, supporting advanced gravity exploration modeling.

(b) Integrated Dual-Domain Gravity Field Approximation Framework: A powerful hybrid computational framework combining spatial and spectral methods, achieving all-element analytical modeling and capable of processing and fusing multi-source, heterogeneous data.

(c) Quantitative Selection Criteria and Ingenious Algorithm Development: Introduces quantitative selection criteria for terrain effects and deploys a comprehensive suite of algorithms, with a paramount application directed toward the optimization and unification of regional height datums.

(d) Comprehensive Quality Control, Accuracy Assessment, and Performance Enhancement: Implements built-in functionalities for gross error detection, measurement of external accuracy indices, and control over computational quality, addressing long-standing technical bottlenecks.

1.3 Key Philosophy and Distinctive Ideas of PAGravf4.5

1.3.1 The Metrological Essence and Normative Constraints of Geodesy

Modern geodesy is fundamentally a metrological science dedicated to the precise global measurement of the Earth and the monitoring of global changes within the Earth system. The intrinsic attributes of its observables and measurement elements – objective uniqueness, precise measurability, and spatio-temporal unity – constitute the foundational and normative constraints that permeate all sub-disciplines of geodesy.

To articulate the core essence and metrological character of geodesy, we propose two pivotal conceptual pillars:

(1) General Geodetic Elements

All general geodetic elements, encompassing a broad spectrum of observables, parameters, and derived quantities, must rigorously adhere to the requirements of objective uniqueness and precise measurability. This ensures that every geodetic element within the geodetic framework is uniquely defined, reproducible, and quantifiable.

(2) Geodetic Datum Constants

Defined as time-invariant geodetic elements, geodetic datum constants must satisfy a stringent set of criteria: unique invariance, precise measurability, and conceptual independence from specific epochs and measurement errors. These criteria constitute the starting datum requirements of geodesy.

There exist exactly nine such Geodetic Datum Constants. They are mutually statistically independent and share no analytical functional relationships, yet collectively support the entire edifice of geodesy.

(3) The Nine Fundamental Geodetic Datum Constants

The Nine Constants form a minimal yet complete set required to define and express the Earth's position, orientation, rotation, and gravity field within an inertial or quasi-inertial reference system. This canonical set comprises:

(a) Origin of the Earth-Fixed Reference System: The mean center of mass (COM) of the Earth (contributing 3 constants: COM coordinates).

(b) Orientation of the Earth-Fixed Axes:

● The Reference Pole (the mean shape pole of the Earth, defining the z-axis orientation; 2 constants).

● The Zero Meridian (the reference meridian, defining the x -axis orientation, equivalent

to the Non-Rotating Origin [NRO] of the Geocentric Celestial Reference System [GCRS]; 1 constant).

(c) Fundamental Physical Constants:

● The global geopotential value (W_0), conventionally defining the geoid in gravity field space.

● The geocentric gravitational constant (GM).

● The mean angular velocity of Earth's rotation (ω).

Upon their definition via international convention and realization through precise measurement campaigns, these nine datum constants acquire a conventional nature. From the nine foundational constants, other geodetic constants (e.g., reference ellipsoid parameters) may be derived according to geodetic principles. These derived constants likewise inherit this conventional nature.

All these geodetic constants are characterized by:

● Unique invariance over long timescales (e.g., over decades);

● Conceptual freedom from notions of "error" and specific "epochs";

● Immunity to perturbations such as terrain effects, tidal effects, or loading deformation effects.

1.3.2 The Geoid, Height Datum, and Conceptual Updates

(1) The Geoid, Global Geopotential, and Normal Gravity Field

In accordance with the classical Gauss-Listing definition, the geoid is defined as the equipotential surface that best approximates the global mean sea level. This definition serves essentially as a specified convention in geodesy, establishing an invariant reference starting value for vertical positioning. The geopotential value associated with this Gaussian geoid is termed the Earth's geopotential constant, commonly known as the global geopotential and denoted as W_0.

The geoid is a specific equipotential surface defined in Earth-fixed reference system by a conventional constant geopotential value, W_0. Its geometric positioning within a terrestrial reference system is expressed in terms of geoid (ellipsoidal) height. Consequently, **the concept of the geoid can only be derived from the terrestrial reference system first.** Computing the geoid undulation (geoidal height) N necessitates the prior convention of a normal ellipsoid (or reference ellipsoid). A foundational geodetic requirement is that the normal geopotential (U_0) on the surface of this chosen ellipsoid must be equated to W_0 (i.e., $U_0 = W_0$), thereby rigorously linking the geometric starting surface to the physical gravity field.

The normal ellipsoid, which mathematically represents the normal gravity field, is defined by four fundamental geodetic constants. Among these, the geocentric gravitational constant (GM) and the mean Earth angular velocity (ω) are directly measurable physical quantities. The remaining two constants are: the Earth's semi-major axis (a); and one parameter selected from the set comprising the dynamic form factor (J_2), the normal geopotential on the ellipsoid surface (U_0), or the geometric flattening (f). For this latter pair, one must be specified to uniquely determine the other, ensuring a closed and consistent

normal gravity field.

Both the normal gravity field and the global geopotential W_0 inherently possess a conventional nature. For geodetic elements endowed with this conventional nature, once their constant values are established by international agreement, they must remain uniquely invariant over extended periods (e.g., decades). This temporal stability is paramount, as it guarantees the uniqueness of all associated gravity field elements (such as geoidal height and gravity anomalies) and ensures the analytical compatibility and consistency of the functional relationships interconnecting these geodetic elements across different measurement epochs and techniques.

Consequently, by virtue of their conventional definition, the normal gravity field and the geoidal geopotential (W_0) are immune to perturbations such as various terrain effects, tidal effects, or loading deformations. They are conceptually devoid of "measurement error" (**Error-Free**) and independent of any specific epoch (**Time-Invariant**), serving as stable, absolute references within the global geodetic framework against which all time-variable and relative measurements are compared.

(2) Implementation Principle for the Global Geopotential W_0 Consistent with the Gravimetric Geoid

The realization of W_0 may follow a rigorous, multi-step procedure using a precise global mean sea surface height grid and a latest global geopotential model:

(a) Estimation of Semi-major Axis (a): Utilizing an optimal global geopotential coefficient model (e.g., a high-degree EGM) in conjunction with a precise global mean sea surface height model (derived from satellite altimetry), the Earth's semi-major axis is estimated. This estimation strictly adheres to the Gauss-Listing convention, ensuring the defined geoid approximates the global mean sea level.

(b) Determination of Normal Ellipsoid Constants: Employing the measured second-degree zonal harmonic coefficient ($\bar{C}_{20}$, related to J_2 and consistent with the chosen a) from the global geopotential model, along with the known values of GM and ω, the four fundamental constants defining the Earth's normal ellipsoid is chosed.

(c) Calculation of U_0 and Conventional Assignment: The four constants enable the analytical calculation of the normal geopotential U_0 on the ellipsoid surface. The final, crucial step is the conventional assignment: defining U_0 as the global geopotential constant W_0 (i.e., $W_0 = U_0$). This process achieves the scientifically desired equivalence: $W_0 = U_0 = W_G$ (where W_G is the geopotential of the gravimetric geoid), thereby **unifying the geometric and physical geoid definitions**.

(3) Concept of the Analytical Geoid and Analytical Orthometric Height

The so-called "true" geoid (or terrain-corrected geoid), which attempts to account for topographic mass effects through reduction, suffers from decimeter-level uncertainties in continental mountainous regions. These uncertainties stem from necessary approximations in terrain density models and assumptions regarding methods of terrain mass reduction (e.g., Helmert condensation or complete Bouguer reduction). At the centimeter-level precision demanded, such a geoid fails to meet the fundamental constraints of uniqueness and precise

measurability required for valid geodetic element. Consequently, the geoidal height derived following such terrain adjustments is metrologically undefined; it is neither uniquely determinable nor does it possess an accepted concept of accuracy.

By rigorous constraints to the invariance of the external disturbing potential field, PAGravf4.5 employs analytical terrain mass adjustment strategies but does need not to know the specific adjustment process. Within this framework, the Analytical Geoid, defined by the geopotential W_0, is established as a uniquely defined and precisely measurable geodetic element. The corresponding Analytical Orthometric Height can be derived by determining mean gravity via analytical continuation from external gravity, and thus also becomes a uniquely defined and precisely measurable geodetic element. Numerically, the Analytical Orthometric Height exhibits closer agreement with Normal Height than with the classical Helmert orthometric height.

Unlike the Helmert orthometric height, both the Analytical Orthometric Height and the Normal Height strictly satisfy the datum conditions for GNSS Replacing Leveling. Furthermore, these two height systems share a rigorous analytical functional relationship within the framework of gravity field theory. This robust and consistent theoretical foundation is not Earth-specific; these two height systems can be directly extended and applied to other celestial bodies, such as the Moon and terrestrial planets.

(4) Definition of Geoid Geometric Deformation

The geodetic elevation (orthometric or normal height) of any terrain point is an objective quantity uniquely defined by its geopotential number. For a deforming Earth, the geopotential W changes objectively with time due to the redistribution of internal mass, inducing temporal variations in the geopotential number (and thus geometric elevation) of any point. Earth's deformation directly causes discrepancies of geopotential spatial distribution at two time epochs. This means that in the Earth-fixed reference system, the geometric positions of the geoid (where W_G remains unchanged) at two epochs differ, and this difference represents the geoid's geometric deformation.

(5) Applicability of the Geoid as the Zero-Height Surface

Geodetic elevation (orthometric or normal height) is rigorously defined in the Earth-fixed reference system grounded in gravity field theory. As geodetic elements, they are characterized by their uniqueness and measurability. However, the physical quantity they represent – the geopotential number – is inherently approximate, a limitation dictated by the geodetic definition of orthometric (or normal) height.

For any ground point where the normal height is zero, both its orthometric height and geopotential number are likewise zero. Its geopotential equals the geoid's geopotential constant, W_0 (or W_G). Consequently, this point must lie on the geoid. Therefore, the three surfaces – the zero orthometric height surface, the zero normal height surface, and the zero geopotential number surface – all coincide with the geoid. That is, regardless of whether one employs the orthometric height, normal height, or geopotential number system, the height starting datum surface is invariably the (global or regional) geoid (Zhang Chuanyin, 2017). Consequently, the reference starting surface for all three aforementioned height systems can

only be the geoid.

(6) The Inconsistency of Utilizing the Quasi-Geoid as the Reference Datum

In classical physical geodesy, the quasi-geoid is defined as the closed surface where the ellipsoidal height coincides with the height anomaly. It is often erroneously adopted as the reference starting surface for normal heights. However, this practice contradicts the rigorous geodetic definition of normal height.

Firstly, the geopotential of zero normal equiheight surface is equal to zero, which is the geoid, not the quasi-geoid. Secondly, for two points sharing identical latitude and longitudes but differing in altitude, their height anomalies are defferent. If the normal height system were referenced to the quasi-geoid, it would necessitate two non-coincident reference staring points at the vertical direction, thereby violating the uniqueness requirement of the normal height system.

Furthermore, actual observation points rarely coincide precisely with the Digital Elevation Model (DEM) surface used to construct the height anomaly model. For centimeter-level precision, a height-dependent correction, $\delta\zeta$, accounting for the height anomaly gradient (or gravity disturbance), must be applied.

Consequently, while the definition of the normal height system is theoretically rigorous, the use of the quasi-geoid as its reference surface is fundamentally flawed. PAGravf4.5 deliberately de-emphasizes the concept of the quasi-geoid and does not treat it as the reference starting surface for normal heights. Within the PAGravf4.5 framework, the height anomaly is strictly and uniquely correlated with its three-dimensional spatial position.

(7) Geometric Properties and Conceptual Updates of Height Systems

Both the orthometric and normal height systems are defined within an Earth-fixed reference system. Consider two surfaces of constant orthometric height, h_1 and h_2, such that their difference $\Delta\mathrm{h}_{12} = \mathrm{h}_2 - \mathrm{h}_1 = \mathrm{C} \neq 0$ is constant. The ellipsoidal height difference ΔH_{12} between the two surfaces is: $\Delta\mathrm{H}_{12} = \mathrm{H}_2 - \mathrm{H}_1 = (\mathrm{h}_2 + \mathrm{N}) - (\mathrm{h}_1 + \mathrm{N}) = \mathrm{h}_2 - \mathrm{h}_1 = \mathrm{C}$. This demonstrates that the ellipsoidal height difference between two constant orthometric height surfaces equals their orthometric height difference, independent of the geoidal height N. Therefore, all orthometric equi-height surfaces are parallel to the geoid, implying they share an identical geometric shape with the geoid.

It is particularly necessary to emphasize that the orthometric height is the straight-line distance from a ground point to the geoid, measured along the direction perpendicular to the geoidal surface. Due to the influence of vertical deflections and the curvature of normal gravity lines, the actual plumb line is an irregular curve. The length of this curved plumb line from the ground to the geoid is greater than the straight-line distance. The conventional view that orthometric height is the length of this irregular plumb line from the ground point to the geoid lacks a foundation in geodetic theory and is incorrect. Globally parallel closed surfaces do not exist in external Earth space. Since parallelism holds only in infinitesimally local spaces, orthometric height possesses typical local properties.

Normal height is also unique and measurable. However, since the height anomaly ζ varies with elevation, normal equi-height surfaces are not strictly parallel in the Earth-fixed

reference system. The signal of the height anomaly attenuates with increasing elevation. Consequently, the geometric shape of a normal equi-height surface becomes progressively smoother relative to the geoid as elevation increases.

In summary, Orthometric Height offers intuitive geometric measurement properties due to the parallelism of its equi-height surfaces with the geoid, while Normal Height aligns more closely with gravity field properties, as its equi-height surfaces smooth out with elevation increase, reflecting the attenuation of gravitational signals. Both height systems possess distinct advantages, limitations, and scientific applicability. Their coexistence is both necessary and scientifically justified.

1.3.3 Conceptual Analysis of Terrain Effects and Their Constraining Requirements

In physical geodesy, the treatment of topographic mass effects on various gravity field elements serves two fundamental objectives:

(a) Spectral Separation: To isolate ultra-short-wavelength components from discrete anomalous gravity field elements, thereby enhancing the performance of prediction, gridding, and numerical modeling.

(b) Approximation Enhancement: To improve the approximation of the ultra-short-wavelength gravity field by explicitly modeling the topographic mass contribution during gravity field recovery.

(1) Fundamental Principles for Optimizing the Selection of Terrain Effects

Analysis of terrain effects on any gravity field element necessitates the consideration of a triad of interdependent key factors: (a) The mass adjustment strategy employed; (b) The specific type of gravity field element subject to terrain influence (e.g., gravity disturbance, vertical deflection, height anomaly); (c) The spatial location of the field element.

By the chosen mass adjustment strategy, common types of terrain effects include, but are not limited to: Local Terrain Effect, Terrain Bouguer Effect, Seawater Bouguer Effect, Crustal Isostatic Effect, Terrain Helmert Condensation, and Residual Terrain Effect (RTE). Each type implies a distinct treatment of terrain or crustal masses.

To maximize the utility of terrain effects, PAGravf4.5 establishes a set of simplified yet quantitative criteria by the foundational tenets of physical geodesy.

(a) Criterion for Estimation/Gridding Enhancement

When the goal is to improve the accuracy of estimating or interpolating discrete anomalous field elements, terrain effect processing should yield a smoother residual field after the terrain effect removed. The optimization metric is straightforward: the standard deviation of the discrete residual field elements should decrease following terrain effect removal. A reduction in standard deviation directly indicates enhanced suitability for subsequent gridding or estimation.

(b) Criterion for Spectral Purity in Field Approximation

For applications focused on gravity field approximation, the ideal terrain effect should isolate ultra-short-wavelength components without biasing longer wavelengths. This dual-part criterion requires that: (i) The standard deviation of the anomalous field elements should decrease post-removal; and (ii) The spatial mean of the removed terrain effects, over scales

of tens of kilometers, should be negligible. This ensures the removed signal is strictly localized within ultra-short-wavelength components.

(c) Criterion Based on Signal Range-to-Noise Ratio (D/ε)

For a given anomalous field element and terrain effect type, the signal range-to-roise ratio D/ε – where D is the range (max-min difference) and ε is the standard deviation – serves as an indicator of the "spectral spikiness" or outlier character of the ultra-short-wavelength signal. Selecting a terrain effect with a high D/ε can improve the robustness and performance of data processing for that specific field element type.

(d) Criterion for Comparative Selection via Spectral Content

When multiple candidate terrain effect types exhibit similar D/ε magnitudes, a discriminatory criterion is applied: the ratio of the standard deviation of the terrain effects on gravity disturbances to those on height anomalies. A larger ratio suggests a richer proportion of short wavelength components, chosing the type of terrain effect beneficial for modeling the ultra-short-wavelength details of the geoid.

Hierarchy and Applicability of the Criteria: It is critical to recognize the hierarchical nature of these criteria. The first two are prescriptive technical regulations; they possess global applicability and represent mandatory requirements within the PAGravf4.5 processing chain. In contrast, the third and fourth are descriptive and advisory, serving as valuable technical references that require context-specific analysis.

Philosophical Underpinning: Ultimately, these four criteria are not rigid algorithmic prescriptions but rather operational translations of the core philosophical approach to terrain effects in physical geodesy. They provide a structured, intuitive framework. When confronted with complex real-world geodetic problems, practitioners should use the principles embedded within these criteria as a guide to develop tailored methodologies, refine algorithms, and formulate comprehensive technical implementation plans suited to the unique characteristics of the target region and dataset.

(2) Nature and Technical Characteristics of Terrain Effects on Gravity Field Elements

The nature of terrain effects exhibits significant variability, contingent upon the topographic relief of the computation region and the short-to-ultra-short-wavelength structure of the local gravity field. When addressing a specific region or specific target problem, it is imperative to pre-compute, compare, and analyze terrain effects of diverse natures on various gravity field elements. This analysis encompasses the statistical properties of diverse terrain effects on various elements such as height anomalies, gravity disturbances, vertical deflections, and gravity gradients, as well as their mutual discrepancies. The objective is to master the spectral-domain characteristics, algorithmic parameter attributes, and impact signatures of diverse terrain effects on different type field elements within the target region. Based on this comprehensive analysis, a highly adaptable terrain effect processing scheme can be devised.

It should be noted that, in scenarios characterized by low topographic relief, simple local gravity field structures, and dense observation distributions, the application of any terrain effect type may yield no improvement – or even degrade – the performance of estimating,

gridding, or approximating specific field elements.

To unify the conceptual framework of terrain effects, PAGravf4.5 rigorously distinguishes among three key dimensions: the nature of the terrain effect, the type of gravity field element affected, and the spatial location of that field element. For instance, applying three distinct effect types (Local Terrain Effect, Terrain Helmert Condensation, and Residual Terrain Effect) to the gravity disturbances at three different altitudes (on the ground, on the geoid, and outside the geoid) yields a total of 3 × 3 = 9 distinct terrain effect quantities.

(3) Terrain Effect Remove-Restore Scheme and Constraining Requirements

When terrain effects in the Earth's external space exhibit harmonic consistency, a Terrain Effect Remove-Restore Scheme – analogous to the reference global geopotential model remove-restore scheme – can be employed to enhance the performance and stability of gravity field approximation. The fundamental procedure is as follows:

(a) Remove: Compute and subtract the terrain effects from the source gravity field elements to obtain the residual field elements.

(b) Approximate: Utilize the residual field elements to solve for the residual target field elements via a gravity field approximation method.

(c) Restore: Compute and add the terrain effect back to the target field elements, thereby deriving the approximated solution for the target gravity field elements.

Any gravity field element in the Earth's external space represents the integrated effect of the entire Earth's masses; thus, it inherently includes the contribution of all terrain masses. However, any terrain effect is invariably subject to uncertainty. Accordingly, **terrain effects of any nature should not be employed as standalone geodetic observations for gravity field modeling, since they lack uniqueness and measurability and are not effective geodetic elements.**

Removing terrain effects from source field elements inevitably introduces uncertainty. To ensure that terrain effects play a constructive role and that the target field elements remain free from residual terrain effect uncertainty, this uncertainty must be effectively eliminated during the restore phase. Accordingly, terrain effect processing for gravity field approximation should adhere to two strict constraining requirements:

(a) Consistency of Model and Parameters: The terrain mass model (including the mass adjustment strategy) and the selected integration radius (or zone of influence) employed for computing terrain effects on both the source element and the target element must be identical.

(b) Analytic Harmonicity and Compatibility: In principle, terrain effects should be analytically harmonic. The algorithms for computing terrain effects on the source and target field elements must be fully analytically compatible. Specifically, the analytical functional relationship between the source and target terrain effects should be identical to the relationship between the source and target field elements.

Failure to satisfy either of the two constraining requirements will introduce uncontrollable uncertainty, thereby compromising both the performance fidelity and the quality control capability of the gravity field approximation process.

Historical Context and Scientific Rigor: In the era of classical terrestrial geodesy, gravity resources were scarce, characterized by extensive data gaps. It was hypothesized that a

correlation existed between the spatial variation of gravity anomalies and local topographic relief, leading to the use of terrain effects to interpolate gravity anomalies in these voids. However, in the contemporary context of rapid advancements in Earth gravity field measurement technologies and increasingly abundant observational resources, it is scientifically unsound to arbitrarily exaggerate the role and status of terrain effects in gravity field approximation without rigorous, detailed testing, analysis, and specific justification.

Summary: The philosophical foundation of terrain effect processing is "ends-driven pragmatism." It abandons the metaphysical pursuit of an "absolute true topographic gravity" and instead constructs a methodological system centered on statistical optimization and spectral analysis, bounded by data quality, and balancing regulatory rigidity with application flexibility. Within this framework, terrain effects are no longer a simple mirror of physical reality but serve as the useful mathematical bridge connecting discrete observational data with continuous gravity field models.

1.3.4 Classification and Solution Methodologies for Earth's Gravity Field Boundary Value Problems

Classifying the Earth's gravity field Boundary Value Problems (BVPs) exclusively within the framework of the classical first, second, and third BVPs of potential theory is insufficient for characterizing their integral solutions in a modern geodetic context. In classical potential theory, these categories prescribe the potential, its normal derivative (gravity disturbances), or the oblique derivative (gravity anomalies) on the boundary, respectively. However, this taxonomy fails when boundary values consist of quantities such as vertical deflections, gravity gradients, or other anomalous field elements for which no direct classical BVP category exists.

A comparative analysis of the derivation processes for the integral solutions of the Stokes problem (classically a third BVP) and the Hotine problem (classically a second BVP) reveals that their mathematical derivations are fundamentally identical. Conversely, comparing the Stokes problem with the Molodensky problem – both classically categorized as third BVPs – exposes significant discrepancies in both their derivation methodologies and the forms of their solutions. The Molodensky problem is demonstrably more complex than the Stokes problem.

Consequently, restricting the classification of external gravity field BVPs to the classical potential theory framework fails to meet the theoretical demands of modern gravity field approximation and obscures the intrinsic nature of these geodetic problems.

In practice, the fundamental nature of a gravity field BVP is dictated primarily by whether the boundary surface is an equipotential surface. Since most observational quantities (e.g., gravity, vertical deflections) are obtained in the local level (plumb line and horizontal plane) system at the observation point, PAGravf4.5 classifies all external BVPs – where the boundary value is any linear combination of partial derivatives of the disturbing potential in the local horizontal coordinate system – into two primary categories:

(a) Stokes-type Problem: Encompasses all BVPs where the boundary surface is an equipotential surface (e.g., the geoid or a level surface), and the boundary value is any linear

combination of partial derivatives of the disturbing potential in the local horizontal system.

(b) Molodensky-type Problem: Encompasses all BVPs where the boundary surface is not an equipotential surface (e.g., the Earth's topographical surface), and the boundary value is any linear combination of partial derivatives of the disturbing potential.

When the boundary surface is non-equipotential (a Molodensky-type problem), it can be addressed using one of the following four approaches:

(a) Analytical Continuation to an Equipotential Surface: Gravity field elements on the boundary (e.g., gravity anomalies, vertical deflections) are analytically continued onto a nearby equipotential surface. This transformation converts the boundary surface into an equipotential surface, thereby reducing the problem to a solvable Stokes-type formulation.

(b) Correction from Surface Normal to Plumb Line Direction: A correction is applied to the boundary values to account for the deviation between the surface's inner normal and the plumb line (vertical) direction. This adjustment effectively transforms the problem into a Stokes-type BVP.

(c) Direct Integral Solution on a Non-Equipotential Surface: The Molodensky BVP is solved directly on the actual, irregular boundary surface (e.g., the Earth's surface).

(d) Spectral-Domain Least Squares Approximation: The Molodensky BVP is solved using spectral-domain least squares collocation or spherical radial basis function approximation methods, which circumvent the complexities associated with the physical boundary surface.

Obtaining a rigorous closed-form integral solution for the Molodensky-type problem is mathematically intractable in many practical scenarios. Given that the integral solution of the Stokes-type problem also circumvents the complexities of terrain condensation when computing ground height anomalies, it is recommended that gravity field BVPs be addressed primarily using Stokes-type solution methods. Nevertheless, the theory of the Molodensky-type problem retains value for applications such as the reduction of gravity data to an equipotential surface and the quantitative analysis of approximation errors introduced by processing data on non-equipotential surfaces.

1.3.5 Fundamental Principles for Regional Gravity Field and Geoid Modeling

The precise determination of geoidal height at any point mandates global coverage of observational gravity field data. Regional datasets alone are insufficient to fully capture the medium- to long-wavelength components of the gravity field and the corresponding geoid undulations. In gravity field approximation, the accuracy of the recovered gravity field and geoid generally improves with increasing wavelength (i.e., larger spatial scales).

(1) The hierarchical control for Regional Gravity Field and Geoid Modeling

Based on this premise, a scientifically robust modeling principle of regional gravity field and geoid in PAGravf4.5: Employ an appropriate Global Geopotential Model (GGM) as both the reference field and the far-zone boundary condition. This step is critical for mitigating medium- to long-wavelength errors. Upon this foundation, all available regional and surrounding observational resources are integrated to enhance the accuracy of the medium- to short-wavelength components. The synergy of global reference control and local data integration enables high-precision modeling of the regional gravity field and geoid.

By analogous logic, for localized domains such as provinces or cities, a regional gravity field model should serve as the reference field to control the accumulation of medium- to short-wavelength errors. Local and surrounding data are then integrated, with the external regional model acting as the far-zone boundary constraint. This strategy aims to refine the short- to ultra-short-wavelength components of the geoid, achieving fine-scale modeling for the local area.

Consequently, in compliance with geodetic control principles, regional gravimetric geoid refinement schemes should adhere to a hierarchical control principle: "**The refinement of a gravimetric geoid for a sub-region shall utilize a gravity field model of a larger encompassing region as both the reference field and the far-zone boundary condition.**"

(2) GNSS/Leveling Data Fusion Requirements

The spirit leveling, which transfers height differences station-by-station, essentially measures the geopotential difference between leveling benchmarks. In principle, the relative error of this difference is independent of the total leveling route length.

For any specific region, there exists a critical spatial scale threshold. Below this threshold, the relative accuracy of gravimetric height anomaly differences between two points may be inferior to that of GNSS/leveling height anomaly differences. Therefore, algorithms fusing GNSS/leveling data with the gravimetric geoid should effectively integrate the high-precision medium- to long-wavelength components from gravity field modeling with the high-precision short- to ultra-short-wavelength components from the GNSS/leveling control network. Regarding error management, such algorithms must simultaneously suppress short-wavelength noise in gravimetric height anomalies while controlling long-distance error accumulation in GNSS/leveling height anomalies.

Furthermore, GNSS/leveling height anomalies, once properly referenced to an Earth-fixed system and reduced to the global height datum, qualify as general observational field elements. As such, they can be rigorously incorporated into the gravity field approximation and geoid modeling process alongside other heterogeneous data sources.

1.3.6 Error Analysis and Accuracy Assessment in Gravity Field Approximation

The Earth's gravity field is a continuous physical field permeating the entire Earth-fixed space. Consequently, gravity field elements can only be mathematically expressed as spatial averages over grids of finite resolution. This intrinsic characteristic fundamentally distinguishes gravity field elements from discrete geometric geodetic elements, such as point coordinates in a geodetic control network. As a result, error analysis and quality control for gravity field approximation cannot directly adopt the intuitive and point-to-point effective methods used in geometric geodesy.

However, all gravity field elements and their interrelationships exhibit high analytical correlation throughout the Earth's external space. The gravity field approximation problem is, in essence, a one-dimensional linear transformation between gravity field elements. By fully leveraging these intrinsic properties, it is possible to construct multiple analytical function constraints, significantly enriching the conceptual framework and strategic toolkit for error analysis and quality control in gravity field modeling.

1.3.6.1 Concepts of Observational Error and Target Element Accuracy

Gravity field elements are continuously differentiable in the Earth's external space or on boundary surfaces. Thus, although observation field elements are acquired at discrete points, the "observation field elements" functioning within gravity field approximation models are effectively the spatial averages of these observations at a specific resolution.

Spatial Domain: For instance, spatial-domain integration requires grid-averaged field elements on the boundary surface.

Spectral Domain: Truncating observational models at a maximum degree is mathematically equivalent to treating observation field elements as spatial averages at a corresponding resolution.

Similarly, target gravity field elements derived via approximation represent spatial averages corresponding to their effective resolution, not discrete point values.

Example: A 1′×1′ grid of approximated gravity disturbances represents the mean disturbance over each grid cell.

Principle: When computing a target element via spectral basis function expansion (e.g., spherical harmonics), series truncation implies the result is equivalent to the spatial average at the effective resolution.

Therefore, in the context of gravity field approximation, the definitions are as follows:

(a) Observational element Error:

Specifically refers to the error of its spatial average at a given resolution. This is termed the Spatial Representativeness Error, distinct from the point-wise observation error.

(b) Target Element Accuracy:

Refers to the accuracy of its spatial average at the effective resolution. This is termed the Spatial Representativeness Accuracy, rather than point-wise accuracy.

The spatial representativeness error of observational field elements depends on observation error, point distribution density, and local field structure. When observation accuracy is sufficiently high, this error is dominated by point density and local structure.

Example: If point observed gravity accuracy is 0.1 mGal but the representativeness error for a 1′×1′ gravity disturbance is 1 mGal, the latter is governed by point distribution density, field structure, and gridding algorithm performance. In such scenarios, further improving point observed gravity accuracy does not reduce the representativeness error. Historically, given the correlation between short-wavelength gravity field structures and undulating terrain, this was often termed Terrain Representativeness Error.

The spatial representativeness accuracy of a gravity field element grid depends on the approximation fidelity, spatial resolution, and the local gravity field structure (particularly short- and ultra-short-wavelength components) within each cell.

Important Reminder: The spatial resolution of gravity field elements is not a trivial geometric pixel average; its representativeness is intrinsically coupled to the local gravity field structure.

(a) Identical resolutions offer stronger representativeness in simple fields and weaker representativeness in complex ones.

(b) Field elements between grid cells contain rich spatial analytical functional relationships. Consequently, the information content within such a grid far exceeds what its geometric resolution alone suggests.

1.3.6.2 Theoretical Basis for Error Analysis and Accuracy Assessment

Earth's gravity field approximation is essentially a one-dimensional linear transformation within the gravity field's linear space. Field elements of the same type at different locations, different types, and various elements at different locations are all analytically correlated. These correlations can be analytically expressed via spatial-domain integral formulas or spectral-domain parameterized basis function expansions. Thus, Earth's gravity field signals possess high analyticity, pervasive throughout the external space. Leveraging this distinctive geophysical property allows for the extraction of weak signals from environments with strong observational noise – a feature distinguishing gravity field approximation from general geometric geodesy. For instance, based on this property, satellite gravity methods can effectively extract gravity field signals from environments with signal-to-noise ratios below 10^{-3}.

(1) When employing spatial-domain integral methods, two primary schemes exist for assessing the accuracy of local gravity field modeling:

Scheme I: Direct Derivation Based on the Integral Mathematical Model

This approach relies directly on the gravity field integral formula:

(a) Estimate Spatial Representativeness Error: Estimate the spatial representativeness error of the gridded observed field elements on the integration boundary (e.g., the gravity anomaly grid in Stokes' formula), accounting for errors introduced during discretization and gridding.

(b) Derive Error Propagation Formula: Derive an error propagation formula from the gravity field integral formula.

(c) Estimate Target Accuracy: Estimate the spatial representativeness accuracy of the target element, neglecting reference model errors.

Scheme II: Indirect Assessment Based on Analytical Functional Relationships

This approach is based on the analytical functional relationships between gravity field elements:

(a) Construct an Integral Algorithm: Formulate an algorithm where the target element is the integrand, its surface is the integration boundary, and discrete observed field elements serve as input reference truth values.

(b) Compute and Compare: Compute integral values at observation points. Statistically analyze the discrepancy between these integral values (possessing spatial representativeness accuracy) and the reference truth values (discrete observation accuracy). This yields the spatial representativeness error of the observed field elements via discrepancy statistics.

(c) Estimate Target Accuracy: Utilize the derived representativeness error from Step (b), following the procedure of Scheme I, to estimate the spatial representativeness accuracy of the target field elements.

(2) When approximating the gravity field using the spectral-domain least squares method with heterogeneous observations:

Such as in constructing Global Geopotential Models (GGMs) or Spherical Radial Basis Function (SRBF) models, error analysis and accuracy assessment can be rigorously implemented within the least squares framework. The specific procedural steps are:

(a) Residual Analysis and Extraction of Representativeness Error: Using the estimated spectral coefficients derived from the approximation, compute the estimated values for each type of observations at the observation points via spectral series expansion. Statistically analyze the residuals between these estimated values (which possess spatial representativeness accuracy) and the corresponding observations (treated as reference truth with their measurement accuracy). This yields the spatial representativeness error for each type of observations.

(b) Derivation of Error Propagation Formulas: Deduce the error propagation algorithm directly from the mathematical model of the spectral-domain least squares approximation.

(c) Computation of Accuracies: Utilizing the spatial representativeness errors of the various observations obtained in the previous step, apply the error propagation algorithm to compute the accuracy metrics of all spectral coefficients and the spatial representativeness accuracy of the target field elements.

Evidently, gravity field approximation methods can effectively determine the spatial representativeness error for any type of observed gravity field element, regardless of its origin (spaceborne, airborne, terrestrial, or marine). However, these methods cannot directly quantify the intrinsic accuracy of the measurement instrument. Gravity field approximation provides only an upper bound for the actual instrument error. Yet, it is the Spatial Representativeness Error that plays the decisive role in governing the fidelity and resolution of the final gravity field model.

1.4 Data Formats, Conventions, and Protocols in PAGravf4.5

1.4.1 Format Conventions for Geodetic Data Files

PAGravf4.5 utilizes five proprietary file formats. All algorithms operate on these native formats. The utility module [Conversion of General ASCII Records to PAGravf4.5 Format] serves as the primary interface for ingesting external text-based data. Users may generate numerical grids based on specified parameters via the [Simple Gridding and Regional Geodetic Grid Construction] module.

(1) Discrete Geodetic Record File

This format represents geodetic point data as a one-dimensional array of discrete observations.

File Header: Supports multiple header lines with unrestricted content and formatting, facilitating flexible metadata annotation.

Record Structure: Each row corresponds to a single observation site. Mandatory attributes, in sequential order, are: Site ID/Name, Longitude (decimal degrees), Latitude (decimal degrees), followed by optional attributes 4 through n.

Format Specification: All attributes must be numeric. The total number of attributes (n) shall not exceed 80. Attributes within a record are space-delimited.

(2) Geodetic Network Observation File

Designed for storing observational data from geodetic networks, including baseline vector components for Continuous Operating Reference Station (CORS) networks, height differences for leveling networks, or gravity differences for gravimetric networks.

File Header: A single header line defines critical structural parameters: character length of baseline/route names, character length of site names, and other relevant fields.

Record Structure: Each data row comprises: Baseline/Route Name, Start Site Coordinates (Longitude, Latitude, Height), End Site Coordinates (Longitude, Latitude, Height), followed by observed value. A sentinel value (e.g., 9999.999) denotes missing observations.

Network Topology Naming Convention: The topological relationship between baselines /routes and sites is encoded within their names. A baseline or route name is conventionally constructed by concatenating the names of its two endpoint site in the format B***A, where the placeholder (***) may contain additional identifiers.

○ Critical Constraint: All site names within a file must possess an identical character length. Consequently, the character length of any baseline/route name must be at least twice that of a station name.

(3) Geodetic Numerical Grid File

Geodetic numerical grid data is represented as a two-dimensional raster array.

File Header: A single header line precedes the data matrix, containing six essential georeferencing parameters (all in decimal degrees): Minimum Longitude, Maximum Longitude, Minimum Latitude, Maximum Latitude, Longitude Interval (cell width), and Latitude Interval (cell height).

Data Storage Order: Grid cell values are stored in row-major order: starting from the minimum latitude row, values are written for each column from minimum to maximum longitude, proceeding sequentially to subsequent latitude rows. Values within a row are space-delimited.

Semantic Interpretation: The value assigned to a grid cell represents the spatial average of the geodetic element over the grid cell's area. During numerical integration, the coordinates of the grid cell center are utilized to calculate the integral distance of the moving integral point (area element) to the computation point.

(4) Geodetic Vector Grid File

This format encapsulates a two-dimensional vector field by consecutively storing its primary (first) and secondary (second) component grids within a single file. The file header and the structure of the primary component grid strictly adhere to the specifications of the standard Geodetic Numerical Grid File [Section (3)]. The secondary component grid is appended immediately thereafter, following an identical row-major storage order and georeferencing convention.

In PAGravf4.5, geodetic vectors such as vertical deflections and tangential gravity

gradients are stored using this format.

(5) Spherical Harmonic Coefficient File

Tailored for storing models expressed as spherical harmonic expansions – a fundamental mathematical representation in physical geodesy for the Earth's gravity field.

Key models in PAGravf4.5 utilizing this format include:

- ○ Geopotential Coefficient Models (global gravity field models).
- ○ Terrain Mass Spherical Harmonic Coefficient Models (spectral decomposition of topographic masses).
- ○ Terrain Geopotential Coefficient Models (geopotential induced by terrain mass).

(a) File Header:

A single header line defines two essential scale parameters:

- ○ Geocentric Gravitational Constant (GM): units of $\times 10^{14}$ m^3/s^2.
- ○ Earth's Equatorial Radius (a): units of meters (m).

(b) Reference Surface Definition:

The surface spherical harmonic functions associated with the coefficients are defined on a reference sphere with a radius explicitly set to the Earth's equatorial radius (a) provided in the header.

(c) Coefficient Record Format:

Each spherical harmonic coefficient is stored as a distinct record: Degree n, Order m, C_nm, S_nm (, C_nm_error, S_nm_error). Where

- ○ n is the degree, and m is the order ($0 \leq m \leq n$).
- ○ C_nm and S_nm are the fully normalized spherical harmonic coefficients (cosine and sine terms, respectively).
- ○ C_nm_error and S_nm_error are optional fields for storing the respective coefficient standard errors or uncertainties.

(d) Ordering Flexibility:

PAGravf4.5 imposes no strict sequential requirement on the arrangement of coefficients by degree and order. The format accommodates incomplete sets of orders within a given degree, providing flexibility for truncated or irregularly sampled spectral models.

1.4.2 Units and Conventions for Primary Geodetic Quantities

(1) Unit Conventions for Anomalous Gravity Field Elements:

- ● Height Anomaly (ζ) or Geoidal Height (N): Meter (m).
- ● Gravity Anomaly (Δg) or Gravity Disturbance (δg): Milligal (mGal, 10^{-5} m/s^2).
- ● Vertical deflection (ξ, η): Arcsecond (″).
- ● Gravity Gradient (Γ): Eötvös (E, 10^{-9} s^{-2}).

(2) Unit of Terrain Effects:

The unit for the terrain effect on any gravity field element is identical to the unit of the field element itself.

(3) Ellipsoidal Geodetic Coordinates and Heights:

- ● Longitude (L): Decimal degrees.

- Latitude (B): Decimal degrees.
- Ellipsoidal Height (H): Meter (m).
- Normal Height (h) / Orthometric Height (h*) / Bathymetry: Meter (m).

(4) Vertical Deflection Vector (SW Convention):

The vertical deflection vector is resolved into two horizontal components within a South-West (SW) oriented local horizontal coordinate system. The first component (ξ) points toward South, and the second (η) toward West. Together with the gravity disturbance vector direction (approximately vertical), these three orthogonal directions form a right-handed, natural local coordinate system aligned with the local plumb line and horizon.

(5) Tangential Gravity Gradient Vector (NW Convention):

The tangential (horizontal) components of the gravity gradient tensor are represented as a vector in a North-West (NW) oriented local horizontal coordinate system. The first component points toward North, and the second toward West. This vector, combined with the radial component of the disturbing gravity gradient, forms a right-handed natural local coordinate system.

1.4.3 Instructional Demonstrations and Target Audience

(1) Tutorial Examples & Self-Study Guide:

Comprehensive example files for each module are provided in the directory C:\PAGravf4.5_win64en\examples: This folder includes a step-by-step operational process file (process.txt); example input and output data files; and Screenshots illustrating key interface operations.

Approximately 7 working days are required to complete all tutorial exercises. Upon completion, users will be equipped to operate PAGravf4.5 independently for professional applications.

(2) Target Audience and Disciplinary Scope:

PAGravf4.5 is designed for senior undergraduate students, graduate students, research scientists, and engineering professionals in the fields of Geodesy and Geophysics, Geology and Earth Sciences, Geomatics and Geographic Information Systems (GIS), as well as Seismology and Geodynamics.

1.5 Algorithm Features and Usage Instructions for PAGravf4.5

1.5.1 A Comprehensive Analytical Algorithm Framework for Terrain Effects

To facilitate the computation of diverse terrain effects on various gravity field elements on or outside the geoid, PAGravf4.5 has developed a comprehensive analytical algorithm framework characterized by:

(1) Theoretical Rigor and Numerical Precision:

The algorithmic formulations are theoretically analytic and rigorous. Numerical integration is implemented without computational error, while the accuracy of FFT-based fast algorithms is also controllable.

(2) Diversity and Flexibility:

The framework supports a wide spectrum of terrain effect types (e.g., Local Terrain

Effect, Terrain Bouguer Effect, Helmert Condensation Effect, and Residual Terrain Effect). The affected gravity field elements can be arbitrarily specified, including geopoential, height anomalies, gravity disturbances, vertical deflections, and gravity gradients.

(3) Analytical Consistency:

Terrain effects on different types of gravity field elements strictly adhere to the intrinsic analytical relationships of the field elements. This ensures refined and internally consistent algorithmic formulations, preserving the fundamental physical and mathematical properties of the gravity field throughout all computations.

(4) Code Efficiency via Analytical Compatibility:

The framework fully exploits the analytical compatibility among terrain effects of different natures, enabling compact and efficient code implementation. As demonstrated in Sections 7.5 – 7.8, many formulas share structural similarities. In PAGravf4.5, various terrain effect algorithms can be realized by invoking the same core codebase with parameter adjustments, significantly enhancing code reusability and maintainability.

1.5.2 Technical Characteristics of Local Gravity Field Integral Algorithms

(1) Fixed Integration Radius:

PAGravf4.5 implements gravity field integration with a fixed radius by controlling the domain of the integration kernel function. This applies to both numerical integration and Fast Fourier Transform (FFT)-based algorithms (which employ windowed kernels). This approach harmonizes and unifies various gravity field approximation methodologies. The 2D FFT utilizes a modified planar 2D kernel; within a latitude span of 10°, its computational accuracy shows no significant deviation from the 1D FFT method.

(2) Uniform Representation of Point Locations:

All point locations are uniformly expressed using ellipsoidal geodetic coordinates (latitude, longitude, and ellipsoidal height). This convention applies to boundary surfaces, observation points, computation points, and moving integration points (area or volume elements). The location of an integration grid cell is defined by the coordinates of its centroid. All integration distances are computed directly from these coordinates, ensuring a consistent geometric foundation.

(3) Equipotential Boundary Surface:

Most gravity field integral formulas (e.g., Hotine, Vening-Meinesz, and radial gradient integrals) derive from the solution to the Stokes Boundary Value Problem (BVP), which requires the boundary surface to be an equipotential surface (e.g., the geoid).

In PAGravf4.5, since anomalous gravity field elements and residual field elements (after reference geopotential model removal) exhibit low sensitivity to minor positional variations, the accuracy requirement for the ellipsoidal height representing the boundary surface may be relaxed. A height accuracy of no less than 10 meters is generally sufficient. This boundary surface can be constructed using a 360-degree geopotential coefficient model. For near-Earth applications, the ellipsoidal height grid of an orthometric (or normal) equi-height surface serves as an effective surrogate for the true equipotential surface.

1.5.3 Analytical Approximation of Gravity Field Using Multi-source Heterogeneous Data with SRBFs

PAGravf4.5 recommends three pivotal technical measures for the Spherical Radial Basis Function (SRBF) approximation algorithm. These measures render the algorithm robust against observational gross errors, prevent spectral leakage in target field elements, enhance the analytical rigor of approximation models, and enable all-element gravity field modeling from multi-source heterogeneous data.

(1) Edge Effect Suppression as an Alternative to Normal Equation Regularization

PAGravf4.5 proposes an algorithm that enhances parameter estimation performance by suppressing edge effects. When an SRBF center (node) lies at or outside the boundary of the ccomputation region, its corresponding SRBF coefficient is constrained to zero. This significantly improves the stability and reliability of SRBF coefficient estimation. The addition of boundary conditions can weaken the need for Tikhonov-type regularization, which might otherwise distort the analytical relationships between field elements.

(2) Normal Equation Normalization for Fusion of Heterogeneous observation Systems

PAGravf4.5 recommends a highly versatile method for the deep fusion of multi-source heterogeneous observation systems via the normalization of normal equations from different observation groups. This technique effectively manages the integration of diverse observation systems with vastly different covariance structures relative to the unknown coefficients, facilitating gravity field approximation through the fusion of heterogeneous gravity field observations. The method completely decouples the influence of the observation system model (covariance structure) from observation quality (errors or outliers). This separation ensures the fusion process remains immune to observational errors, type differences, or spatial distribution variations. This feature is particularly advantageous for fusing sparsely distributed data (e.g., limited astronomical vertical deflections or GNSS-leveling sites) and enables precise outlier detection.

(3) Cumulative SRBF Approximation for Optimal Gravity Field Recovery

A target field element is essentially the convolution of the observational field element with a SRBF filter. When target and observational elements differ in type, a single SRBF often fails to simultaneously match the spectral centers and bandwidths of both, inevitably causing spectral leakage. Moreover, factors beyond the Bjerhammar sphere burial depth (bandwidth parameter) – such as SRBF type, degree range, and SRBF node distribution – significantly impact gravity field approximation performance. Thus, optimizing approach based solely on burial depth is insufficient for optimal gravity field ecovery.

To address this, PAGravf4.5 proposes a Cumulative SRBF Approximation scheme. This scheme combines multiple SRBFs with distinct spectral centers and bandwidths to fully resolve the spectral signals of the target field element, thereby eliminating spectral leakage and achieving optimal field recovery. Each stage of residual approximation essentially treats the previous result as a reference gravity field, refining the residual target element according to the remove-restore principle.

1.5.4 Gravity Exploration Analytical Modeling using Multi-source Heterogeneous Data

PAGravf4.5 empowers users with high-precision analytical computation of diverse terrain effects on various gravity field elements on and outside the geoid. Concurrently, it features full-space, all-element gravity field analytical modeling capabilities that integrate multi-source, heterogeneous, varying-altitude, cross-distributed, and multi-type data encompassing terrestrial, maritime, aerial, and space-based observations. The synergy of these capabilities effectively resolves the analytical modeling challenges of geophysical gravity exploration under complex observational scenarios.

(1) Application Scenario

In any region globally, PAGravf4.5 can integrate multi-source heterogeneous data – including gravity, gravity gradients, (astronomical) vertical deflections, satellite altimetry, GNSS leveling, and satellite gravity – from spaceborne, airborne, terrestrial, and marine platforms. This facilitates the precise computation of land-sea unified Complete Bouguer gravity anomalies/disturbances, vertical deflections, and gradients, as well as unified Classical Bouguer and Isostatic anomalies/disturbances.

Gravity exploration analytical modeling using multi-source heterogeneous data can be achieved via the following four-step workflow:

(a) Define Scope and Model Type: Delineate the target region, computation surface, and exploration model type. Acquire all available gravity and other geodetic data within and surrounding the target region.

(b) Generate Target Field Grid Model: Utilize modules from the subsystem “High-Precision Gravity Field Approximation and Full-element Modeling” to compute a high-resolution grid model of the target field element on the specified computation surface.

(c) Compute Terrain Effect Grid Model: Employ modules from the subsystem “Computation of Diverse Terrain Effects on Various Gravity Field Elements” to derive a high-resolution grid model of the terrain effect consistent with the chosen exploration model.

(d) Synthesize Exploration Model: Directly subtract the terrain effect grid [Step (c)] from the gravity field element grid [Step (b)]. The result is a gravimetric exploration model that fully integrates all available gravity field data.

(2) Summary of Advantages

This scheme deeply fuses multi-source heterogeneous geodetic data within a unified mathematical framework, strictly adhering to model definitions to achieve high-precision analytical modeling. By circumventing traditional gravity reduction, continuation, and gridding operations, it effectively mitigates issues such as signal attenuation, non-analytical distortion, and error propagation inherent in conventional methods.

1.5.5 Algorithm and Computational Technical Route Optimization

The PAGravf4.5 algorithm system is designed with scientific rigor and comprehensiveness. In principle, it supports multiple schemes for computing diverse terrain effects on any gravity field element across all domains (space, air, land, and sea). Furthermore, it can derive various gravity field elements in external space from any single input type, ranging

from traditional quantities (gravity anomalies, vertical deflections) to diverse derivatives from Satellite-to-Satellite Tracking (SST) or satellite orbital perturbations. The applicable spatial domain encompasses the geoid and its external space.

Gravity field approximation theory in external space is founded on linear space. Accordingly, all terrain effect and gravity field approximation algorithms in PAGravf4.5 are linear. This linearity implies that injecting simulated spatial noise as the observed quantities yields an output that accurately characterizes the error distribution properties of the target field elements or terrain effects. Thus, PAGravf4.5 possesses robust capabilities for error simulation and analysis and can serve as a critical tool for optimizing gravity exploration modeling, field approximation algorithms, and technical routes.

Even for a single terrain effect type, multiple computational schemes are available in PAGravf4.5. For example, for the computation of land-sea unified Complete Bouguer effect, PAGravf4.5 can offer three distinct schemes and corresponding programs for user selection.

For specific objectives, users can select various algorithms, parameter sets, or diverse technical routes from PAGravf4.5. In practice, users should select, test, and evaluate the most suitable algorithms and relevant parameters based on the data conditions and local gravity field properties of the target region to optimize the technical route for their specific application.

1.5.6 Algorithm Performance and Parameter Testing Analysis

(1) Performance Testing and Analysis of Terrain Effect Algorithms

The Terrain Effect Optimization Criteria in PAGravf4.5 are grounded in the fundamental principles of physical geodesy. These criteria significantly reduce the complexity of terrain effect analysis and provide concrete, feasible technical pathways to leverage the critical role of terrain effects in gravity exploration modeling and gravity field approximation.

The nature of terrain effects varies significantly depending on topographic relief, local gravity field structure, and gravity field element typology within the target region. In the cases of the PAGravf4.5 terrain effect subsystem, a rugged mountainous region was selected for statistical analysis of the ratio between the range (max-min difference) and the standard deviation for diverse terrain effects on different types of field elements. Results indicate that, absent specific considerations of data distribution and field structure:

(a) Local Terrain Effects are beneficial for gravity data processing;

(b) Helmert Condensation is advantageous for gravity gradient data processing;

(c) Residual Terrain Effects are superior for geoid refinement.

Prior to actual computation, it is imperative to conduct comprehensive and meticulous testing of the terrain effect technical route for the target region. This process should be guided by quantitative criteria, accounting for topography characteristics, local gravity field structure, and available geodetic data resources. Only by ensuring a well-founded selection of algorithms and parameters can the technical applicability of the terrain effect processing scheme be effectively enhanced.

(2) Performance Testing of Gravity Field Approximation Algorithms

The performance of most gravity field approximation algorithms and parameter settings

can be validated using an ultra-high-degree geopotential coefficient model. In PAGravf4.5 local gravity field approximation examples, degrees 1–540 of the EGM2008 model serve as the reference field, while degrees 541–1800 constitute the residual anomalous field elements, providing a basis for statistical performance analysis.

Technical Workflow for Performance Testing:

(a) Input Selection: Select residual anomalous field elements as observational inputs.

(b) Computation: Invoke the local gravity field approximation algorithm under test to compute values for another set of residual field elements.

(c) Validation: Compare the computed values against the reference truth values (directly derived from degrees 541–1800 EGM2008 model). The discrepancies provide a quantitative evaluation of the algorithm's technical performance and parameter sensitivity.

PAGravf4.5 possesses the capability to compute full-space, all-element fields from a single observation type and supports cyclic calculations of the same element at identical points. By analyzing differences between cyclically computed results and original observations (reference truth), users can diagnose algorithmic characteristics, optimize configurations, and improve modeling schemes.

The module [All-element Gravity Field Modeling Using Multi-source Heterogeneous Data with SRBFs] inherently offers robust testing and validation capabilities.

For any specific objective, users may select from multiple algorithms, parameters, or technical routes. Practical implementation necessitates a thorough characterization of local data conditions and field properties to guide the rigorous selection, testing, and optimization of the most suitable approach.

(3) Built-in Case Studies in PAGravf4.5

PAGravf4.5 includes built-in case studies designed to demonstrate algorithmic capabilities under demanding conditions:

Terrain Effect Case: Selects a rugged region with an average elevation of 4,000 m and relief range exceeding 3,000 m to showcase detailed terrain effect characteristics.

Gravity Field Integral Case: Chooses a complex region rich in short-wavelength signals (residual gravity disturbances > 300 mGal after removing degrees ≤ 540) to illustrate local field approximation details.

Statistical results from these cases reflect the baseline performance of the corresponding algorithms. As their primary purpose is to illustrate computational workflows, they do not encompass exhaustive parameter optimization. Users are encouraged to explore further potential tailored to their specific application scenarios.

2. Analysis and Preprocessing of Earth Gravity Field Data

This subsystem is designed to perform comprehensive analytical and computational tasks for gravity field data processing. Its core functionalities include: (a) Analysis of the Normal Earth Gravity Field and Determination of Ellipsoid Constants. (b) Computation of Global Geopotential Models and Spectral Characterization. (c) Reduction and Correction of Gravity Field Elements for solving the Geodetic Boundary Value Problem (GBVP). (d) Processing of Gravity Observations, encompassing analytical continuation, gross error detection, and gridding operations.

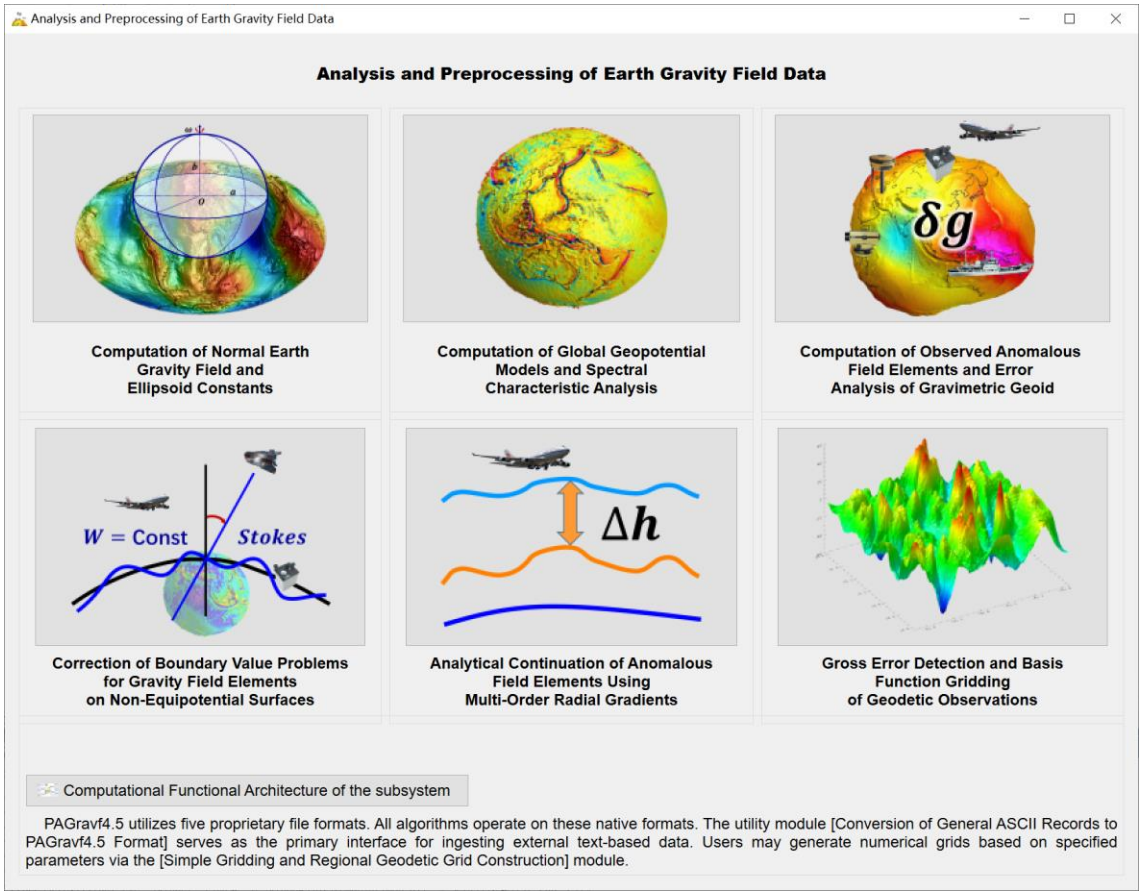

2.1 Computation of Normal Earth Gravity Field and Ellipsoid Constants

[Purpose] To compute normal gravity field elements at arbitrary points in Earth space, the geometric and physical constants of the normal Earth ellipsoid, and the geoidal geopotential (W_G) utilizing rigorous analytical algorithms based on spherical harmonic expansion.

Theoretical Basis: Within the framework of geodetic boundary value theory, the geoid is defined as the geometric realization of the constant geopotential surface $W_G = W_0$ in the Earth-fixed coordinate system, which is equivalent to determining the ellipsoidal height of the geoid. By definition, the geoidal geopotential W_G is strictly equal to the normal potential (U_0) of the reference normal ellipsoid.

2.1.1 Computation of Normal Gravity Field Elements at Space Points

[Function] Utilizing the spherical harmonic expansion formula, this module calculates: Normal Geopotential (unit: m²/s²); Normal Gravity (unit: mGal); Normal Gravity Gradient (unit: Eötvös, E); Direction of the Normal Gravity Vector (unit: arcminutes ['], expressed as the north declination relative to the Earth's center of mass); or, Direction of the Normal Gravity Gradient (unit: arcminutes ['], expressed as the north declination relative to the Earth's center of mass).

[Input File].

Record format: ID (Point Number/Name), Longitude (decimal degrees), Latitude (decimal degrees), Ellipsoidal Height (m), ...

[Parameter Settings]

Header Rows: Enter the number of header lines to skip in the input file.

Ellipsoidal Height Column Index: Enter the column ordinal number of the ellipsoidal height attribute in the record.

Element Selection: Select the specific normal gravity field elements to be computed.

[Output File]

File Content: A result file containing the computed normal gravity field elements.

Format: Appends one or more columns of computed values to each record of the source Space Computation Point File. Values are formatted to 4 significant figures.

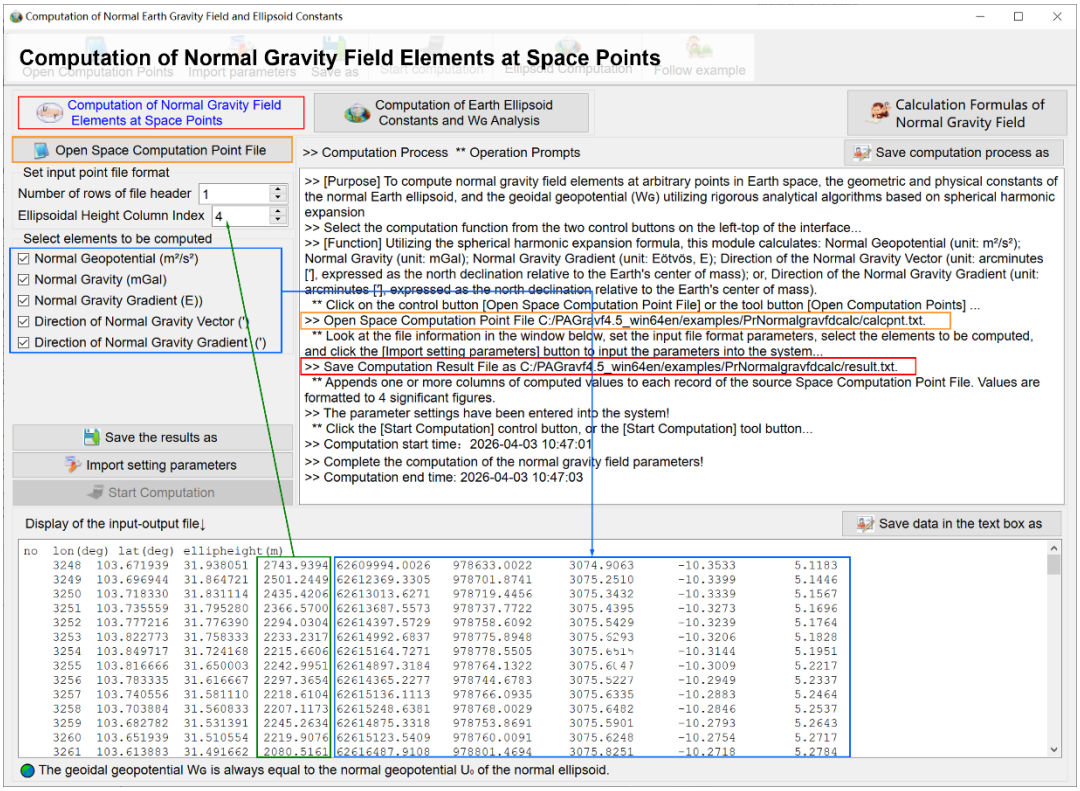

2.1.2 Computation of Earth Ellipsoid Constants and Wg Analysis

[Function] To derive the primary geometric and physical constants of the Earth ellipsoid from its four defining fundamental parameters.

[Parameter Settings]

Fundamental Parameters: Select the four basic parameters defining the Earth ellipsoid.

Fourth Parameter Options: The fourth parameter may be selected from the second-degree zonal harmonic coefficient ($\bar{C}_{20}$) from a global geopotential model; the dynamic form factor J_2; the reciprocal of flattening $1/f$; or, the normal geopotential of the ellipsoid (U_0).

Table 2.1 lists the scale parameters of several global geopotential models and the results of their geoidal geopotential calculations $W_G = U_0$.

Current Default: the coefficient $\bar{C}_{20}$ from the EGM2008 global geopotential model is currently selected as the fourth fundamental parameter.

[Output] Interactive Report: The program interface displays an interactive summary report of the computed Earth ellipsoid constants.

Tidal System Consistency: The tidal system of the generated normal ellipsoid is maintained consistent with the tidal system of the selected $\bar{C}_{20}$ or J_2 parameter.

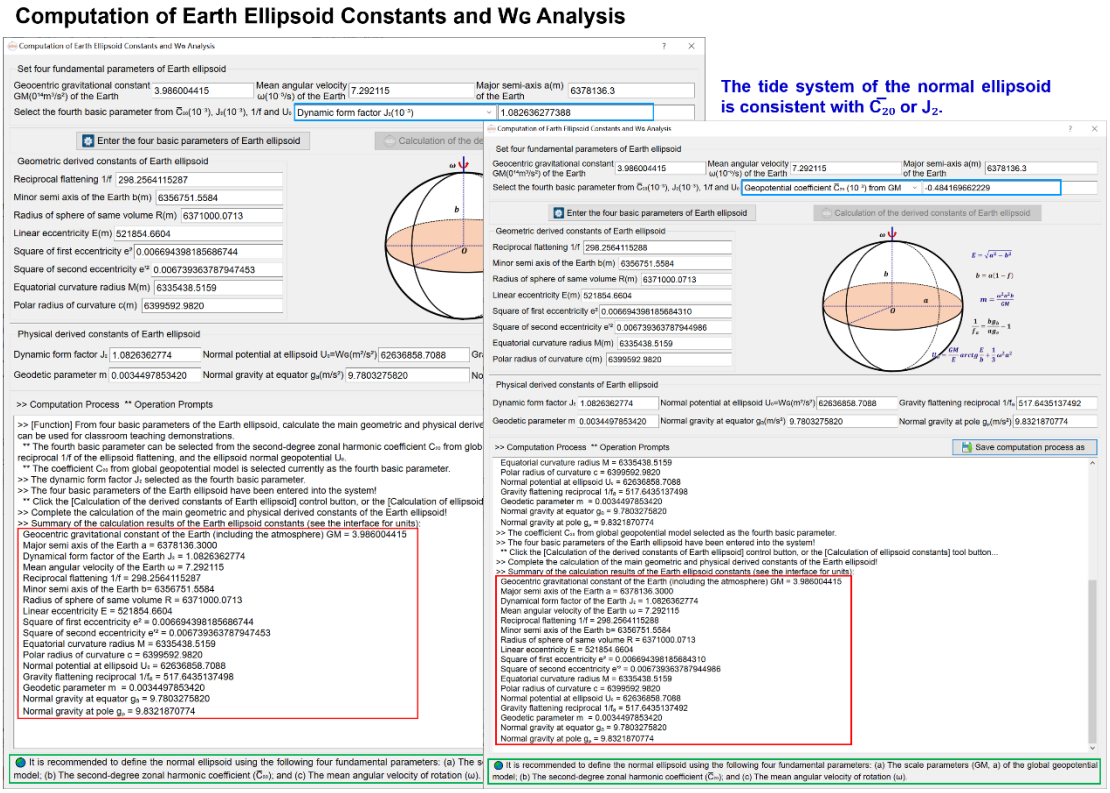

[Expert Recommendation (PAGravf4.5)]

It is recommended to define the normal ellipsoid using the following four fundamental parameters: (a) The scale parameters (GM, a) of the global geopotential model; (b) The second-degree zonal harmonic coefficient ($\bar{C}_{20}$); and (c) The mean angular velocity of rotation (ω).

Rationale: Adopting such a normal ellipsoid as the reference datum ensures that the second-degree zonal harmonic term of the anomalous gravity field vanishes (i.e., equals zero). This condition is critical for optimizing the convergence and accuracy of gravity field

approximation algorithms.

Table 2.1: The scale parameters of several global geopotential models and the results of their geoidal geopotential calculations $W_G = U_0$.

Geopotential Models	Scale Parameters		$\bar{C}_{20}\times10^{-4}$	$W_G = U_0(m^2/s^2)$	Tide System
	$GM\times10^{14}m^3/s^2$	a(m)			
EGM2008	3.986004415	6378136.3	-4.84165143791	62636858.392	tide free
EIGEN-6C4	3.986004415	6378136.46	-4.84165217061	62636856.834	zero tide
SGG-UGM2	3.986004415	6378136.3	-4.84168732275	62636858.644	zero tide
GOCO05c	3.986004415	6378136.3	-4.84169458843	62636858.694	zero tide
XGM2019	3.986004415	6378136.3	-4.84169494748	62636858.697	zero tide

2.2 Computation of Global Geopotential Models and Spectral Characteristic Analysis

[Purpose] To compute model values of anomalous gravity field elements at arbitrary points in Earth space using a global geopotential coefficient model. The module calculates the degree variance of geopotential coefficients, as well as the error degree variance and cumulative error of anomalous field elements, thereby providing an evaluation of the geopotential model's performance.

Single-Degree Analysis: When the specified minimum degree (n) equals the maximum degree, the program computes the contribution of degree-n geopotential coefficients to the anomalous gravity field elements. This functionality facilitates the analysis and evaluation of the model's spectral and spatial properties.

2.2.1 Computation of Gravity Field Elements from a Global Geopotential Model

[Function] Utilizing a global geopotential coefficient model, this module computes model values for (residual) height anomaly (m), gravity anomaly (mGal), gravity disturbance (mGal), vertical deflection vector (arcseconds [″], south, west components), disturbing gravity gradient (E, radial component), tangential gravity gradient vector (E, north, west components), or Laplace operator (E).

[Input Files]

(1) Global Geopotential Coefficient Model File.

Header Convention: The first row contains the model's scale parameters: the geocentric gravitational constant GM (10^{14} m^3/s^2) and the Earth's semi-major axis a (m).

Reference Sphere: Spherical harmonic functions are defined on a sphere of radius a.

(2) Space Computation Point File.

Format: Either a discrete computation point file or an ellipsoidal height grid file defining the computation surface.

Record Format (Discrete): ID (Point Number/Name), Longitude (decimal degrees), Latitude (decimal degrees), Ellipsoidal Height (m), ...

[Parameter Settings]

File Header Rows: Enter the number of header lines to skip in the point file.

Ellipsoidal Height Column Index: Enter the column ordinal number of the ellipsoidal height attribute in the record.

Degree Range: Input the minimum and maximum degrees for the geopotential model expansion.

- ○ If Min Degree = 1: Computes the full anomalous gravity field elements.
- ○ If Min Degree > 1: Computes the residual anomalous gravity field elements (high-frequency residuals).
- ○ Degree Truncation: The program automatically adopts the smaller of the model's maximum degree and the user-input maximum degree as the actual computation limit.

Element Selection: Select the type(s) of model gravity field elements to be computed.

Progress Monitoring: As the computation may be time-consuming, users can open the output file during processing to monitor progress in real-time.

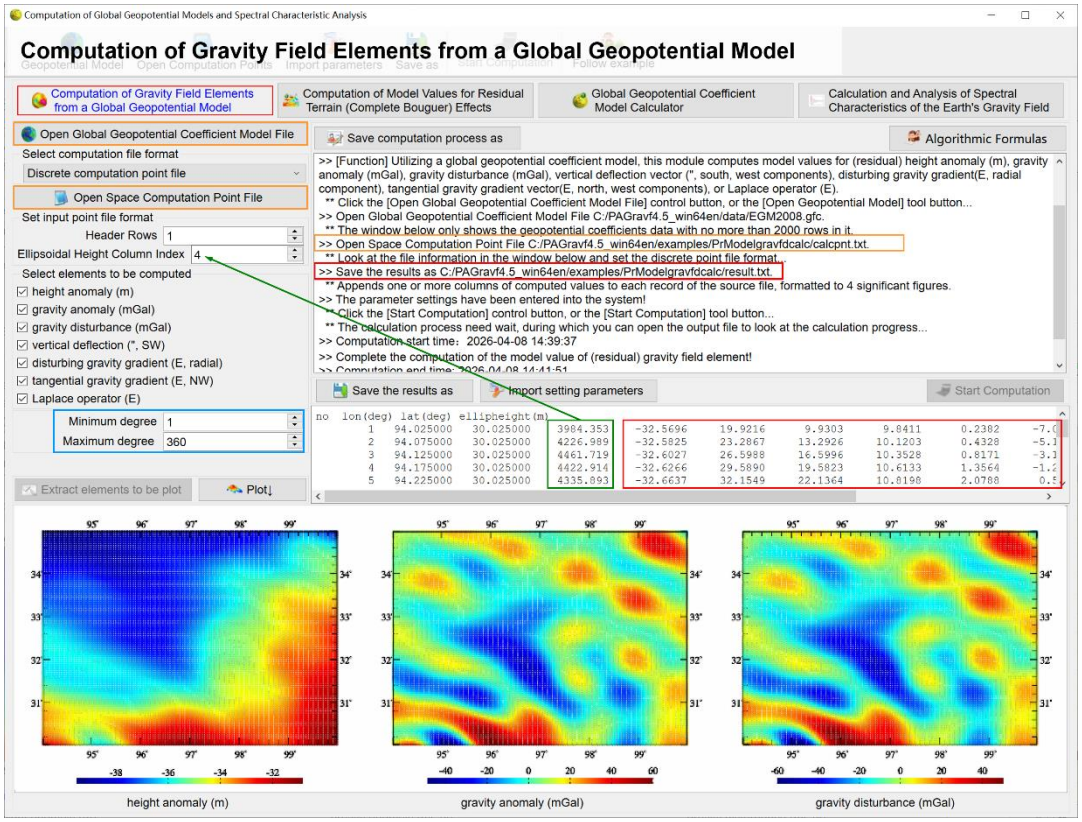

[Output File]

Primary Output File: Contains the model values of the (residual) anomalous gravity field elements.

- ○ Discrete Input Mode: Appends one or more columns of computed values to each record of the source file, formatted to 4 significant figures.
- ○ Grid Input Mode: Generates a new file containing Point ID, Longitude, Latitude, Ellipsoidal Height, and the computed model values.

Grid Output Files (Auto-generated) if grid Input: The program automatically generates

corresponding (residual) model value grid files in the current directory with the following extensions based on the selected element: height anomaly (*.ksi), gravity anomaly (*.gra), gravity disturbance (*.rga), vertical deflection vector (*.dft), disturbing gravity gradient (*.grr), tangential gravity gradient vector (*.hgd), or Laplace operator (*.lps) into the current directory. Where * is the user-defined output filename prefix

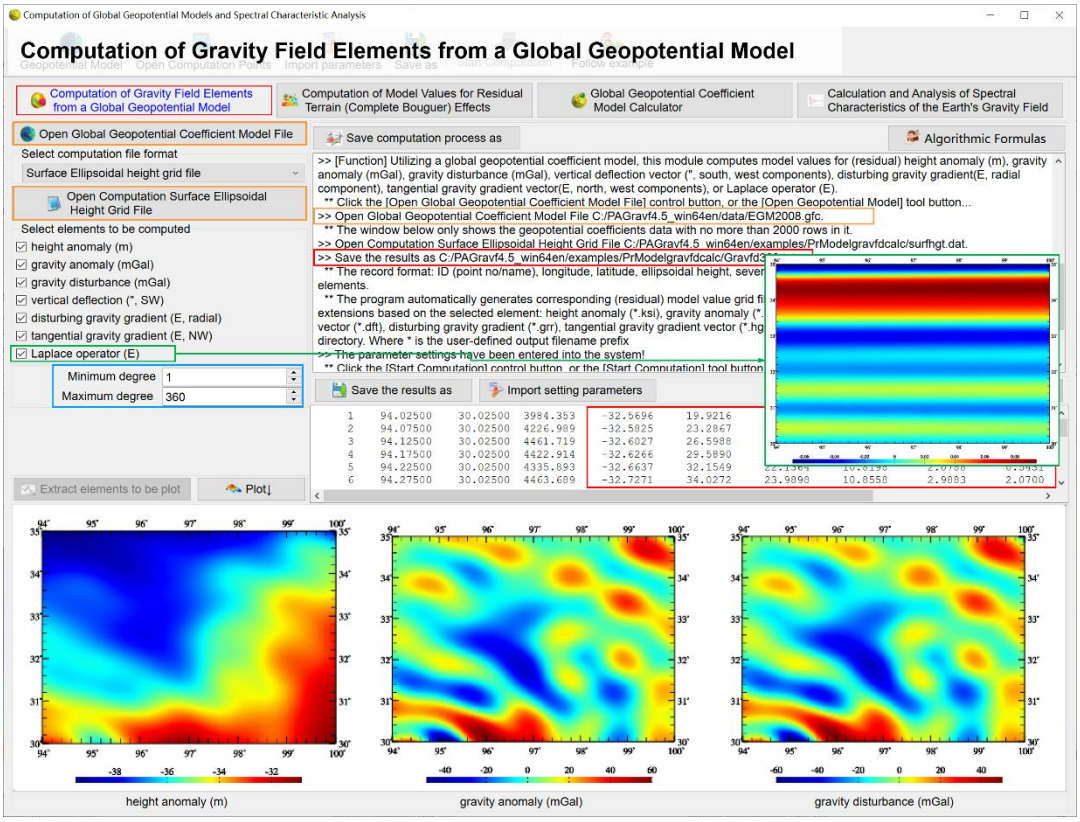

[Theoretical Validation: Laplace Operator]

Theoretically, the Laplace operator for any single degree n, cumulative degrees up to n, or degree band n_1 to n_2 should vanish (i.e., equal zero).

By computing the Laplace operator for specific degrees or ranges from a given global geopotential model, users can observe and evaluate the model's numerical stability and accuracy in both the spectral domain and the spatial domain.

2.2.2 Computation of Model Values for Residual Terrain (Complete Bouguer) Effects

[Function] Using a global land-sea terrain geopotential coefficient model (units: meters), this module computes model values for residual terrain effects (or complete Bouguer effects) on: height anomaly (m), gravity anomaly (mGal), gravity disturbance (mGal), vertical deflection vector (", south, west components), disturbing gravity gradient (radial, E), tangential gravity gradient vector (E, north, west components), or the Laplace operator.

Model Source: The required global land-sea terrain geopotential model can be generated using the module [Ultrahigh-Degree Land-Sea Terrain Spherical Harmonic Analysis and Model Construction].

[Input Files]

(1) Global Land-Sea Terrain Geopotential Model File

Header: Contains the scale parameters GM (10^{14} m^3/s^2) and a (m).

(2) Space Computation Point File

Supports discrete point files or ellipsoidal height grid files (format identical to Section 2.2.1).

[Parameter Settings]

Basic Settings: Input header rows and ellipsoidal height column index.

Degree Range: Specify the minimum and maximum degrees for the terrain geopotential model expansion.

- ○ If Min Degree = 1: Computes the land-sea complete Bouguer effects.
- ○ If Min Degree > 1: Computes the land-sea residual terrain effects (isolating the high-frequency topographic signal).
- ○ Degree Truncation: Automatically selects the minimum of the model's max degree and the input max degree.

Effect Type Selection: Choose the specific residual terrain (complete Bouguer) effects to compute.

Progress Monitoring: Real-time monitoring via the output file is supported during long computations.

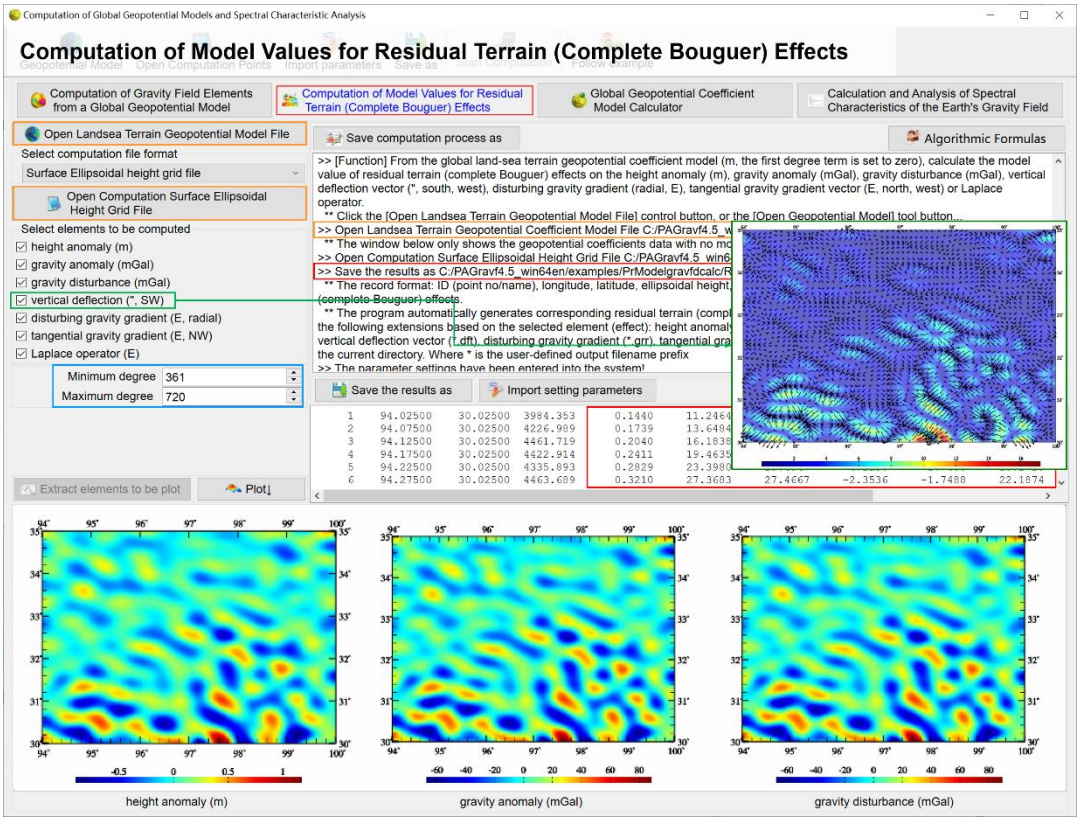

[Output File]

Primary Output File: Contains model values of the residual terrain (complete Bouguer)

effects.

○ Discrete Input Mode: Appends computed values to the source records (4 significant figures).

○ Grid Input Mode: Generates a comprehensive file with coordinates and computed effect values.

Grid Output Files (Auto-generated) if grid Input: The program automatically generates corresponding residual terrain (complete Bouguer) effects grid files in the current directory with the following extensions based on the selected element (effect): height anomaly (*.ksi), gravity anomaly (*.gra), gravity disturbance (*.rga), vertical deflection vector (*.dft), disturbing gravity gradient (*.grr), tangential gravity gradient vector (*.hgd), or Laplace operator (*.lps) into the current directory. Where * is the user-defined output filename prefix

[Performance Evaluation]

Similarly, by calculating the Laplace operator for specific degrees, cumulative sums, or degree bands from a given global terrain geopotential model, users can evaluate the spectral and spatial performance of both the terrain model itself and its derived residual terrain effect values.

2.2.3 Global Geopotential Coefficient Model Calculator

[Function] An interactive tool optimized for educational demonstrations and real-time computation. It computes model values for the following field elements based on a Global Geopotential Coefficient Model: Height Anomaly (m), Gravity Anomaly (mGal), Gravity Disturbance (mGal), Vertical Deflection Vector (arcseconds, South and West components), Disturbing Gravity Gradient (Radial component, E), Tangential Gravity Gradient Vector (E, North and West components), Laplace Operator (Eötvös), Gravity Gradient (E), and Geopotential (m^2/s^2).

Model Initialization: When loading an ultra-high-degree geopotential coefficient model, the system requires time to read and initialize the data. Please wait...

Real-time Computation: Once the model is loaded, users may iteratively input geodetic coordinates. The program will compute and display the model values for all field elements at the specified point in real-time.

Determination and Verification of the Geoidal Geopotential Constant (W_G): This calculator facilitates the verification that the geoidal geopotential W_G is identically equal to the normal potential U_0 of the reference ellipsoid. The procedure employs an iterative approach:

(a) Step 1 (Initialization): Given the latitude and longitude of an arbitrary point, initially set the ellipsoidal height to zero and compute the height anomaly.

(b) Step 2 (Iteration): Use the computed height anomaly from Step 1 as the new ellipsoidal height input for a subsequent computation.

(c) Convergence: When the newly computed height anomaly converges with the input ellipsoidal height, the point lies on the geoid. The geopotential value derived at this stage represents W_G, the potential of the gravimetric geoid.

Global Consistency Check: It is readily verified that the geopotential on the geoid is invariant and always equals W_G.

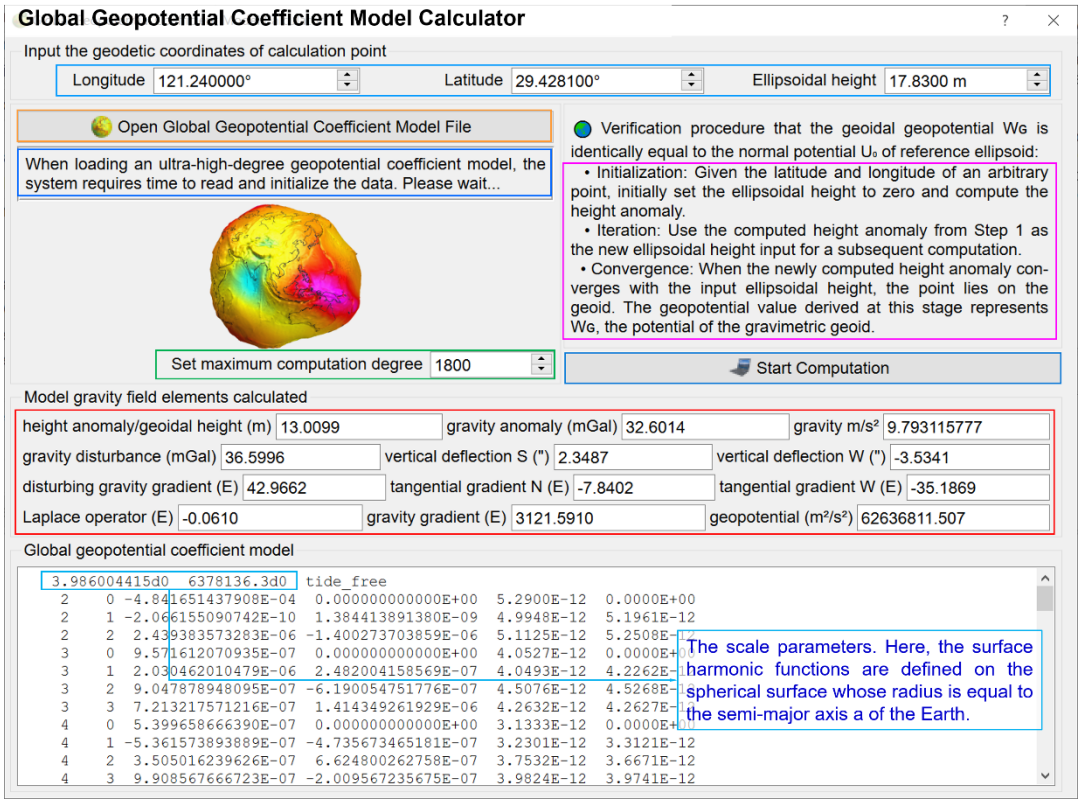

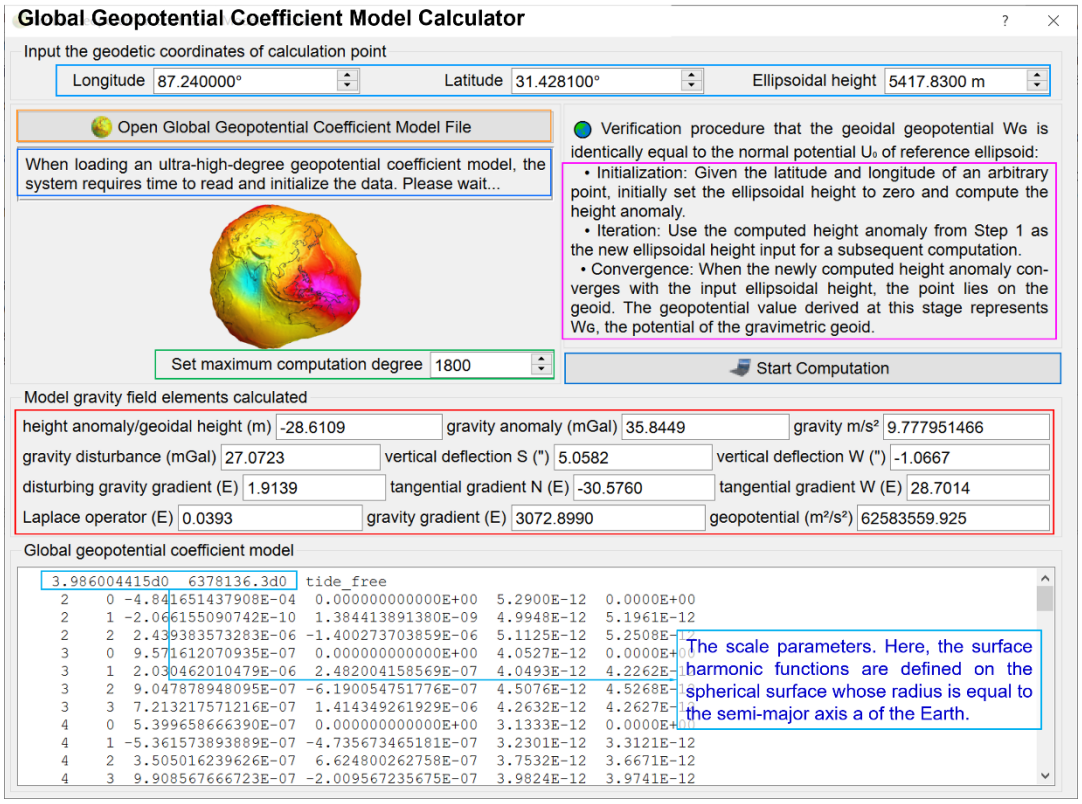

Validation via Laplace's Equation: According to Laplace's equation, the sum of the radial

component of the disturbing gravity gradient and the two tangential components should theoretically equal zero. This property serves as a metric to evaluate the numerical performance and consistency of the geopotential model.

2.2.4 Calculation and Analysis of Spectral Characteristics of the Earth's Gravity Field

[Function] To calculate and analyze the spectral properties of the Earth's gravity field using multiple global geopotential models. The module generates: Kaula rule curves, degree variance of geopotential coefficients, and error degree variance cumulative error curves for both the geoid and gravity anomaly.

This functionality enables a comparative analysis of the spectral behaviors and performance characteristics of different geopotential coefficient models.

[Workflow]

(a) Model Loading: Open at least two global geopotential coefficient model files. Additional models can be loaded as needed.

● The program supports the simultaneous plotting of spectral curves for up to ten (10) global geopotential models.

(b) Start Calculation: Click the [Start Calculation] button and wait for completion..

(c) Plotting: Enable visualization of spectral curves (Degree Variance, Error Variance, Cumulative Error for Geoid/Gravity).

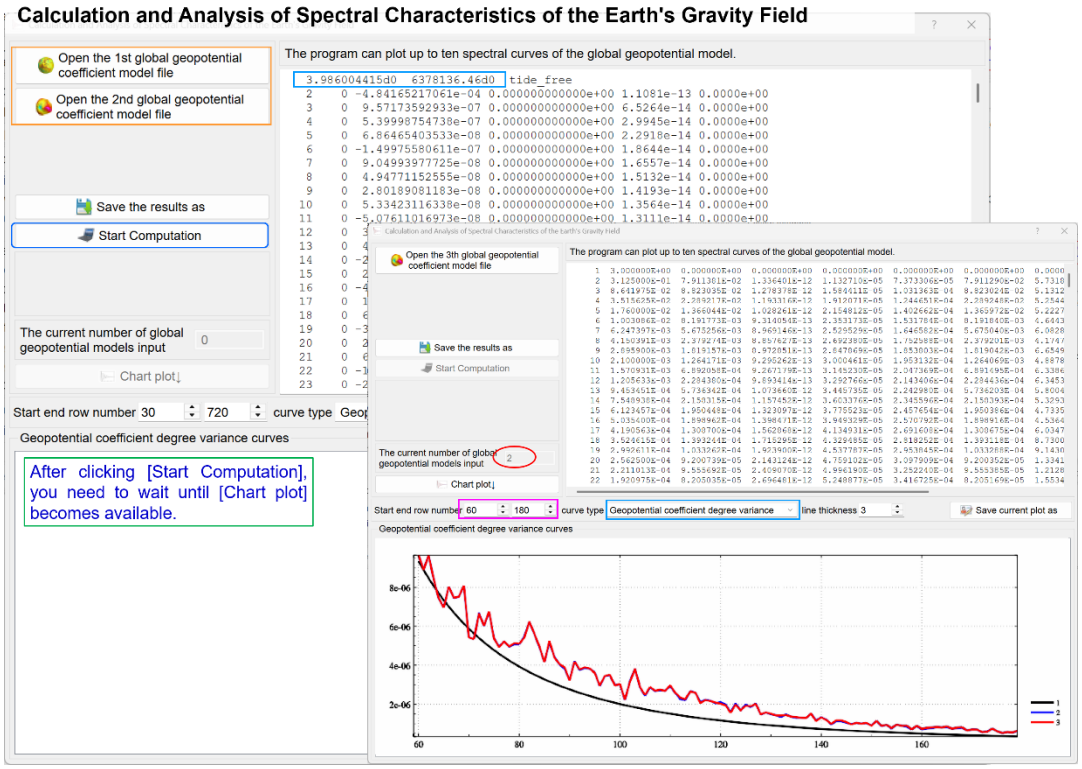

Note: Processing may take some time depending on the model degrees. Please wait until the [Plot Chart] button becomes enabled.

[Visualization Options]

Users can select to plot the following types of spectral curves: Geopotential Coefficient Degree Variance, Error Degree Variance, Cumulative Error for the Geoid, or Cumulative Error for Gravity Anomalies.

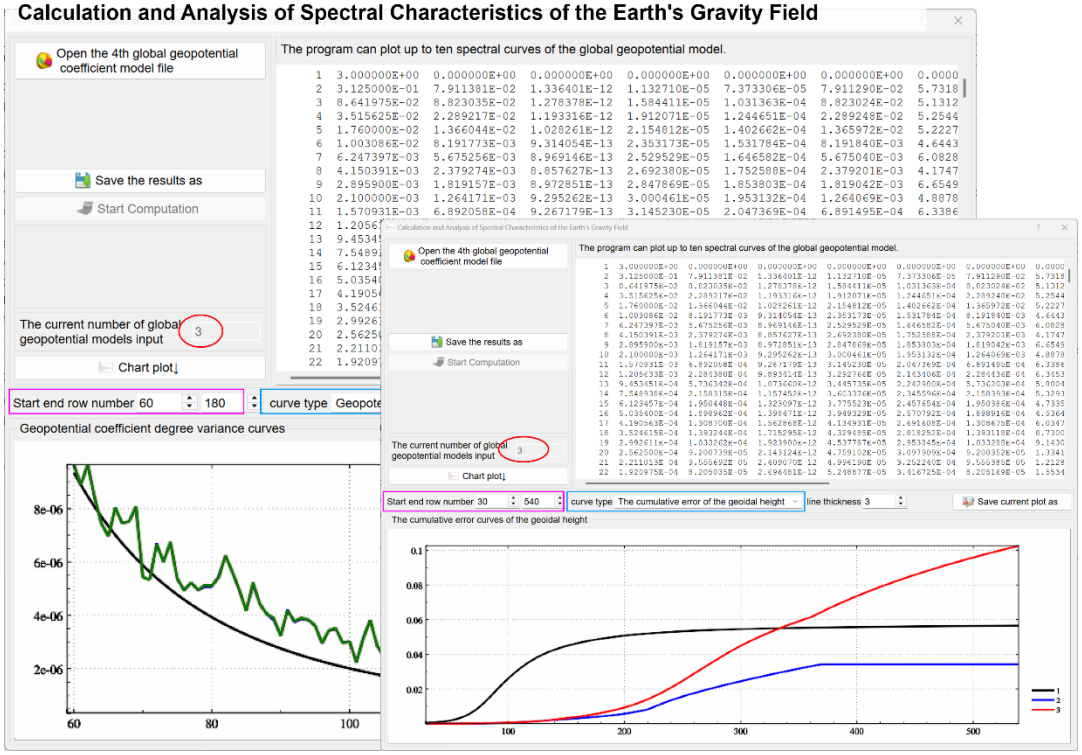

2.3 Computation of Observed Anomalous Field Elements and Error Analysis of Gravimetric Geoid

[Purpose] To compute gravity anomalies, gravity disturbances, or disturbing gravity gradients at observation points using observed gravity data. Furthermore, to estimate the impact of grid mean gravity errors and integration radius selection on the accuracy of the regional gravimetric geoid.

2.3.1 Computation of Anomalous Field Elements at Observation Points

[Function] Utilizing a rigorous spherical harmonic expansion formula to calculate normal gravity field elements, this module derives the anomalous observational field elements from observed gravity (mGal) or observed gravity gradients (E): Gravity Anomaly (mGal), Gravity Disturbance (mGal), or Disturbing Gravity Gradient (E, Radial component)

[Input File] Observed Gravity Data File.

Record Format: ID (Point Number/Name), Longitude (decimal degrees), Latitude (decimal degrees), Height (m), …, Observation Value, ...

[Parameter Settings]

Header Rows: Enter the number of header lines to skip.

Column Indices: Enter the column ordinal numbers for the height attribute and the observation attribute.

Computation Mode:

○ If the input height is Orthometric Height: The program computes the Gravity Anomaly.

○ If the input height is Ellipsoidal Height: The program computes the Gravity Disturbance or Disturbing Gravity Gradient.

[Output File]

The anomalous observational field element result file.

Format: Appends a single column of computed values (gravity anomaly, disturbance, or gradient) to each record of the input file. The values are formatted to 4 significant figures.

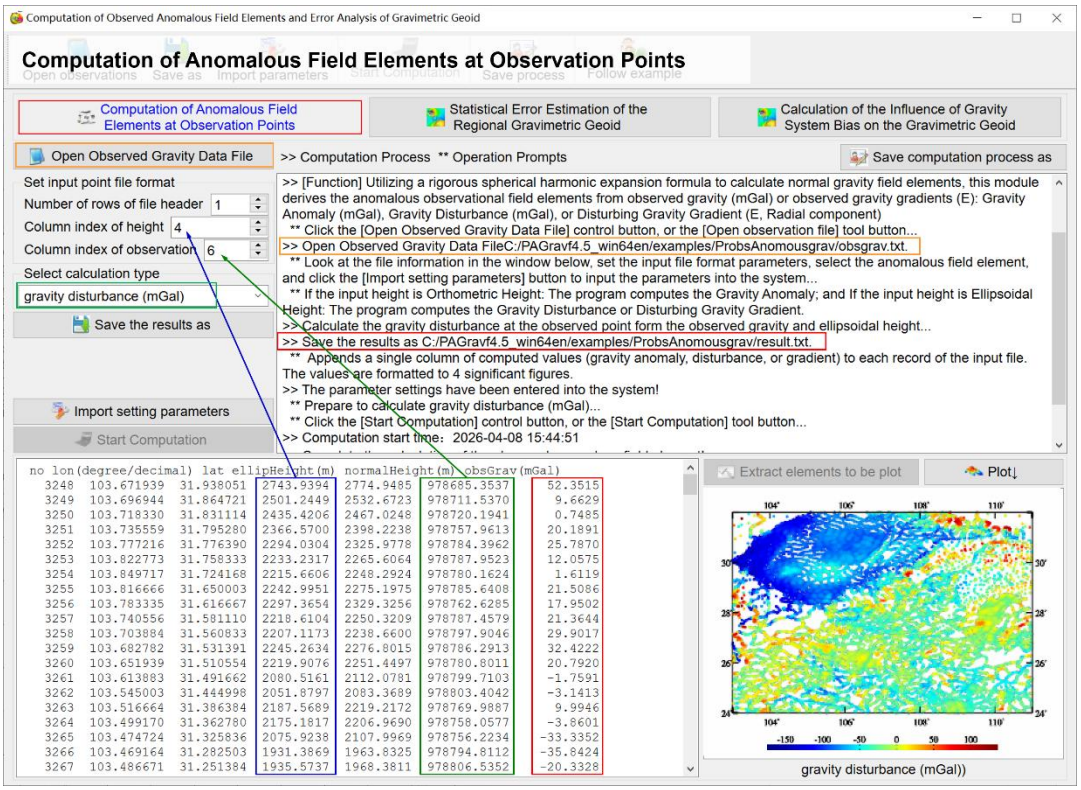

2.3.2 Statistical Error Estimation of the Regional Gravimetric Geoid

[Function] To estimate the error of the regional gravimetric geoid based on the spatial resolution and representative error of the grid mean gravity.

Theoretical Basis: The error analysis employs the Stokes/Hotine integral formula with a finite integration radius, assuming the far-zone effects of the residual anomalous gravity field are negligible.

Error Source Clarification: The term "grid mean gravity representative error" primarily refers to the terrain representation error. In general, the observation error introduced during the gridding process is significantly smaller than the error arising from terrain variability within the grid cell.

2.3.3 Calculation of the Influence of Gravity System Bias on the Gravimetric Geoid

[Function] To quantify the influence of systematic biases in gravity anomalies or gravity disturbances on the gravimetric geoid using the Stokes/Hotine integral formula.

Sources of Systematic Bias: Such biases may arise from: (a) Inconsistencies in the definition of the normal gravity field; (b) Non-uniformity in the vertical datum (height system); (c) Improper selection of the global geopotential constant (W_0); or (d) Errors in the gravity datum reference.

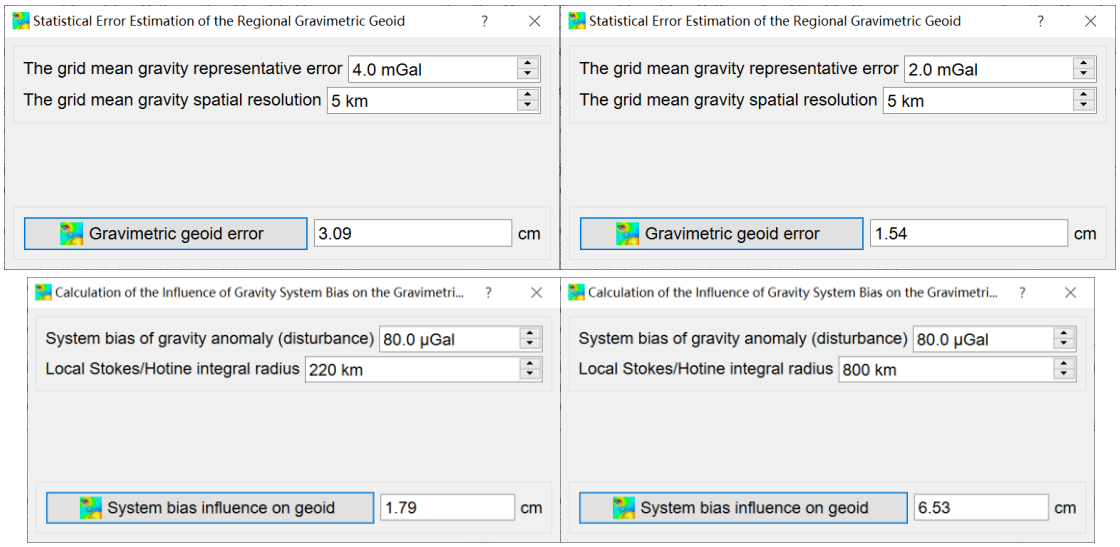

2.4 Correction of Boundary Value Problems for Gravity Field Elements on Non-Equipotential Surfaces

[Purpose] To apply reduction corrections to anomalous gravity field elements defined on spherical, ellipsoidal, or other non-equipotential surfaces. This process transforms the Molodensky-type problem (defined on a non-equipotential boundary surface) into the Stokes-type problem (defined on an equipotential boundary surface).

2.4.1 Boundary Value Correction for Spherical or Ellipsoidal Surfaces

[Function] Utilizing a global geopotential model, this module computes correction values (mGal) to reduce gravity disturbances/anomalies from a non-equipotential boundary (sphere/ellipsoid) to an equipotential surface. This mathematical transformation facilitates the conversion from a Molodensky-type problem to a Stokes-type problem.

Applications: (a) Ellipsoidal Reduction: Primarily employed for ellipsoidal harmonic analysis of the global gravity field using the Fast Fourier Transform (FFT) integral method. (b) Spherical Reduction: Commonly used for solving the Bjerhammar BVP (downward continuation to a reference Bjerhammar sphere).

[Input Files]

(1) Global Geopotential Coefficient Model File

Header: Contains scale parameters GM (10^{14} m^3/s^2) and a (m).

(2) Boundary Surface Computation Point File

Record Format: ID (Point Number/Name), Longitude (decimal degrees), Latitude (decimal degrees), Ellipsoidal Height (m), ...

[Parameter Settings]

Header Rows: Enter the number of header lines to skip in the point file.

Column Index: Enter the column ordinal numbers for the ellipsoidal height attribute.

Type Selection: Select the field element type and the boundary surface type (Spherical or Ellipsoidal).

Maximum Degree: Input the maximum degree for the geopotential coefficient model expansion.

○ Degree Truncation: The program automatically adopts the smaller of the model's maximum degree and the user-input maximum degree as the actual computation limit.

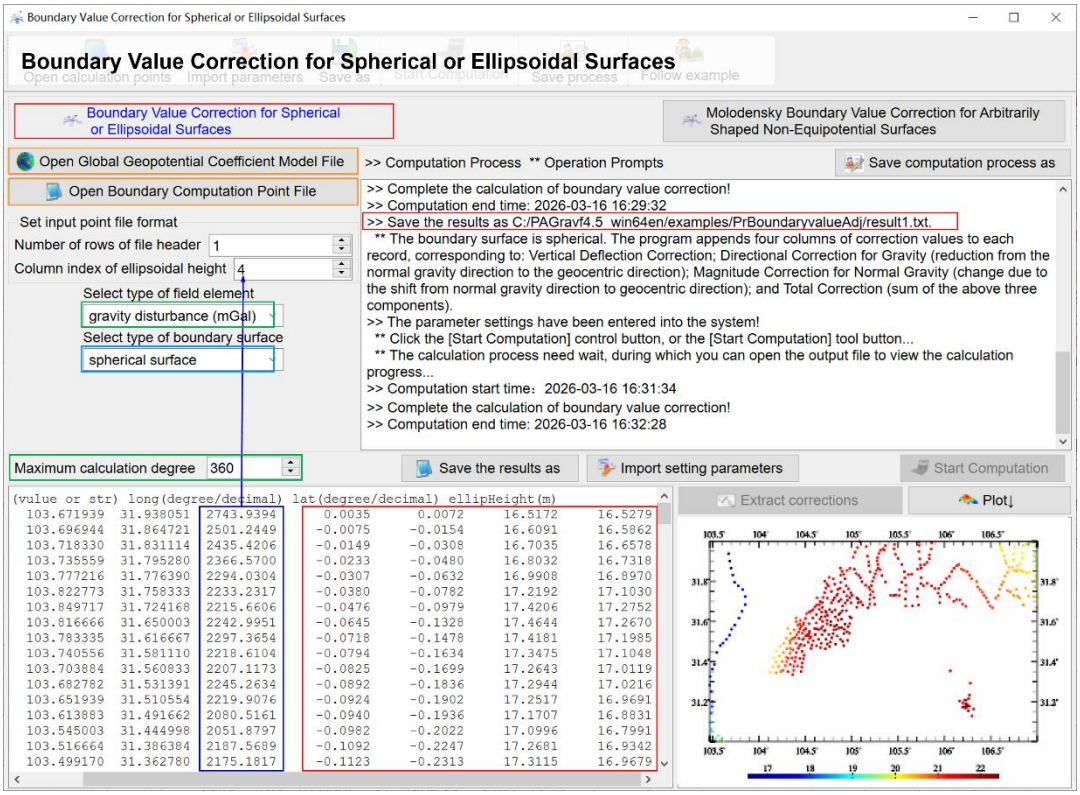

[Output File] The boundary value correction results file.

For Ellipsoidal Surfaces: Appends a single column containing the vertical deflection correction for gravity to each record of the input file.

For Spherical Surfaces: Appends four columns of correction values to each record, corresponding to: Vertical Deflection Correction; Directional Correction for Gravity (reduction from the normal gravity direction to the geocentric direction); Magnitude Correction for Normal Gravity (change due to the shift from normal gravity direction to geocentric direction); and Total Correction (sum of the above three components).

2.4.2 Molodensky Boundary Value Correction for Arbitrarily Shaped Non-Equipotential Surfaces

[Function] This module computes the Molodensky type-I corrections for gravity anomalies or gravity disturbances (mGal) defined on an arbitrary non-equipotential boundary surface (located on the ground or in the exterior space). The computation utilizes four datasets: a

grid of gravity anomalies/disturbances, a grid of height anomalies on the boundary, an ellipsoidal height grid defining the boundary surface, and an ellipsoidal height grid defining the reference equipotential surface (for the Stokes BVP).

Application of these corrections effectively reduces the complex Molodensky BVP to the classical Stokes BVP.

Applicability: The boundary surface may reside at any altitude above the geoid and may possess an irregular geometric configuration.

[Input Files]

(1) Boundary Surface Computation Point File: Coordinates of points on the non-equipotential surface.

(2) Boundary Surface Ellipsoidal Height Grid: Provides the geodetic coordinates of the non-equipotential boundary surface.

(3) Boundary Gravity Field Element Grid: Contains the observed gravity anomalies or disturbances.

(4) Boundary Height Anomaly Grid: Contains the height anomalies on the boundary surface.

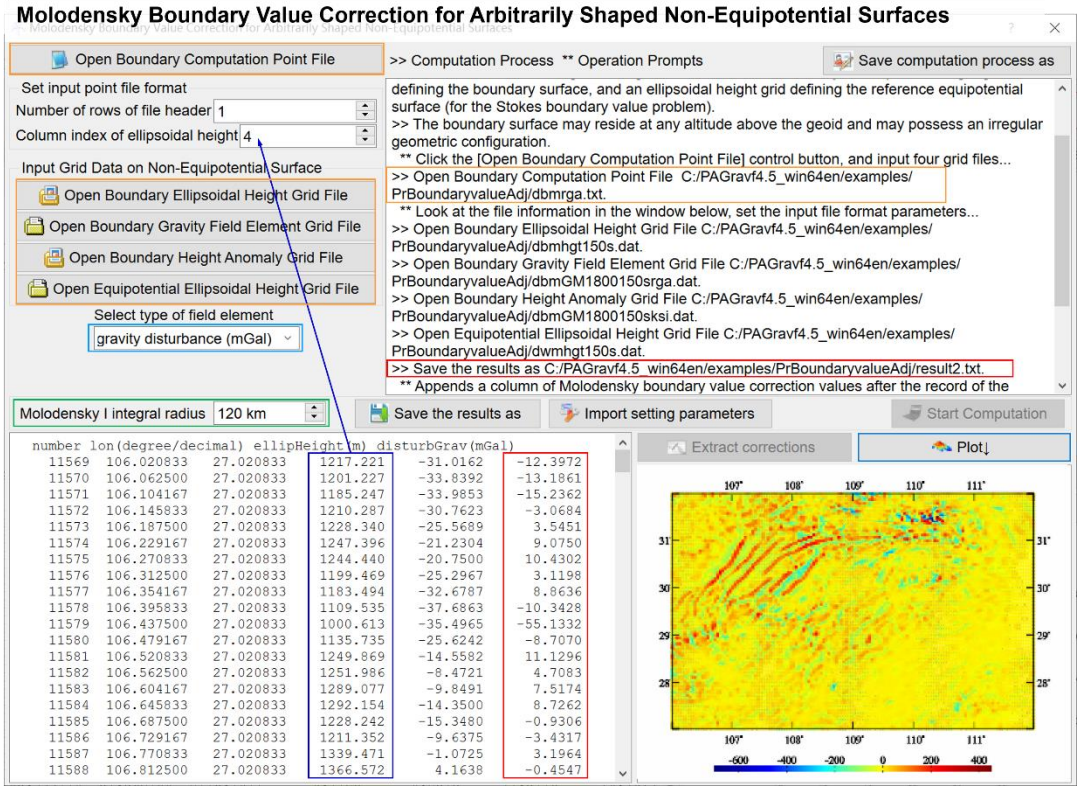

(5) Reference Equipotential Surface Ellipsoidal Height Grid: Provides the geodetic coordinates of the reference equipotential surface.

Consistency Requirement: All four input grid files must share identical grid specifications (resolution, and extent).

Type Matching: The type of gravity field element in the input grid must strictly correspond

to the selection made in the parameter panel.

[Parameter Settings]

Header Rows: Enter the number of header lines to skip in the computation point file.

Ellipsoidal Height Column Index: Enter the column ordinal number of the ellipsoidal height attribute in the file record.

Field Element Type: Select the specific type of gravity field element (Anomaly or Disturbance).

Integration Radius: Enter the numerical integration radius for Molodensky I item.

[Output File] The Molodensky boundary value correction file.

Appends a column of Molodensky boundary value correction values after the record of the source computation point file, keeping 4 significant figures.

Special Case: When the boundary surface is configured as the land terrain surface and the reference equipotential surface as the geoid, the algorithm computes the classical Molodensky I item (mGal).

2.5 Analytical Continuation of Anomalous Field Elements Using Multi-Order Radial Gradients

[Function] Based on the ellipsoidal height grid and the corresponding anomalous field element grid of the current altitude surface, this module computes 1st to 3rd order radial gradients using a rigorous radial gradient integral formula. Subsequently, it calculates the continuation corrections required to transform field elements from the current altitude to a target altitude.

[Input Files]

(1) Anomalous Field Element Grid File (Current Altitude Surface).

(2) Current Altitude Surface Ellipsoidal Height Grid File.

(3) Space Computation Point File for anomalous field elements.

Record Format: ID (Point Number/Name), Longitude (decimal degrees), Latitude (decimal degrees), Ellipsoidal height (m, current), ..., Ellipsoidal height (m, target), ...

[Parameter Settings]

Header Rows: Enter the number of header lines to skip in Space Point File.

Ellipsoidal Height Column Indics Enter the column ordinal number of the ellipsoidal height attribute for current and target field element.

Gradient Order: Specify the order of the radial gradient to be computed (1 – 3).

Integration Radius: Enter the radius for the radial gradient integration.

Constraints & Warnings: (a) Excessively large integration radii may induce significant edge effects. (b) The integration radius should be at least three times the vertical difference between the current and target altitudes (Δh).

[Output File] Analytical Continuation Result File.

Record Format: Appends 1 to 3 columns of gradient continuation correction values to each record of the source Computaion Point File. The values are formatted to 4 significant figures, and their units are identical to the input field element units.

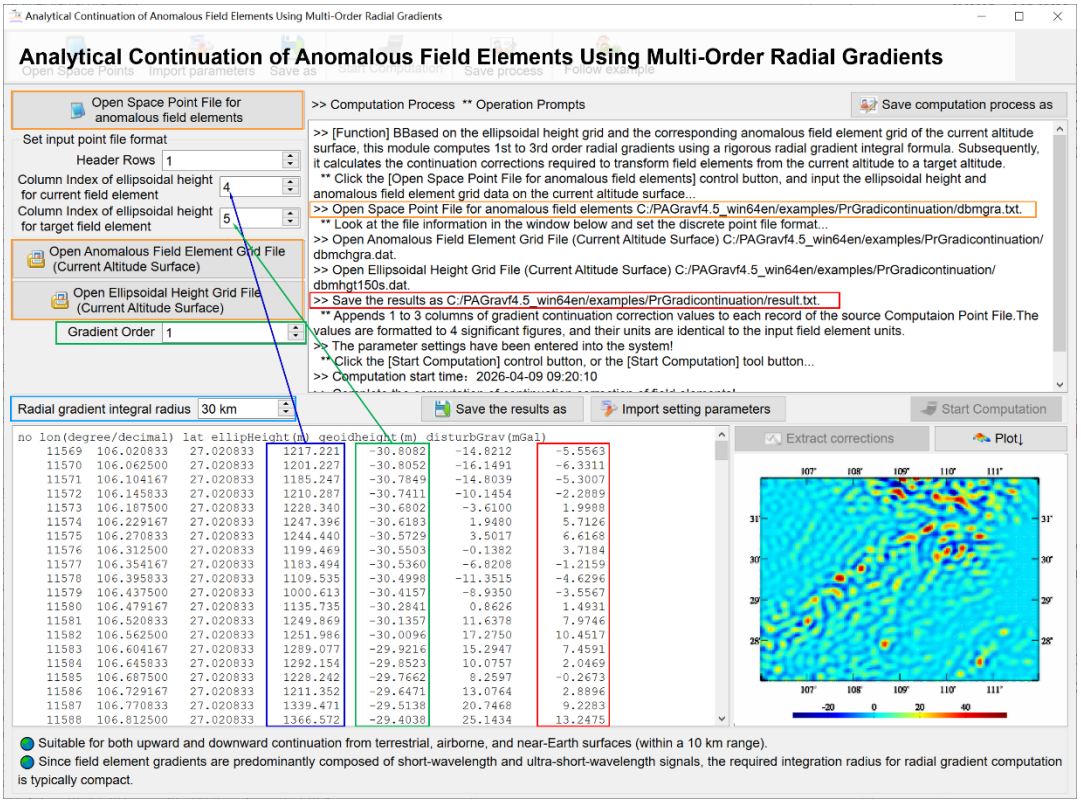

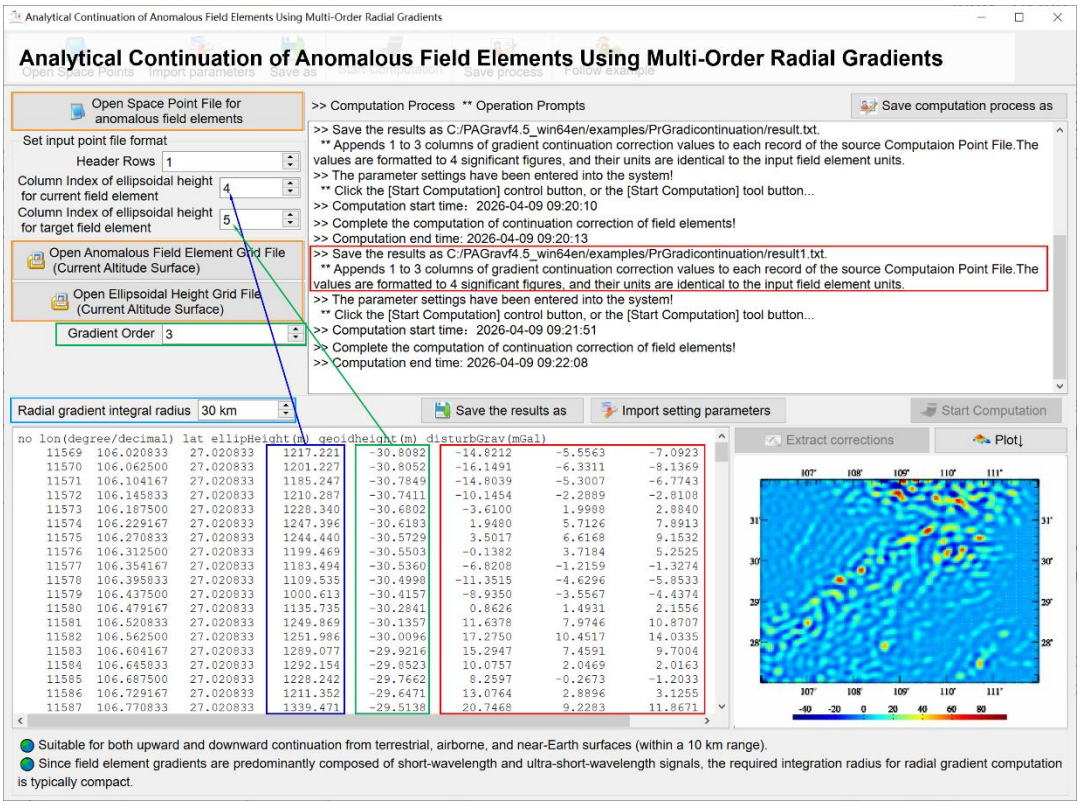

[Methodology & Advantages]

The Radial Gradient Continuation Method leverages the gradients of observed field elements to perform analytical continuation.

(a) Applicability: Suitable for both upward and downward continuation from terrestrial, airborne, and near-Earth surfaces (within a 10 km range).

(b) Spectral Characteristics: Since the field element gradients are predominantly composed of short-wavelength and ultra-short-wavelength signals, the required integration radius for radial gradient computation is typically compact.

[Recommended Workflow: PAGravf4.5 "Remove-Continuation-Restore" (RCR) Scheme]

PAGravf4.5 recommends an integrated approach combining an ultra-high-degree geopotential model with residual field element radial gradient continuation. The workflow proceeds as follows:

(a) Remove: Subtract the ultra-high-degree model values of the field elements at the current altitude to derive the residual field elements.

(b) Continue: Perform analytical continuation on the residual field elements using the radial gradient method.

(c) Restore: Add the ultra-high-degree model values of the field elements at the target altitude back to the continued residuals to obtain the final result.

2.6 Gross Error Detection and Basis Function Gridding of Geodetic Observations

2.6.1 Gross Error Detection Based on a Low-Pass Reference Surface

[Function] This module selects a low-pass grid as a reference surface to interpolate reference values for a specified attribute at discrete observation points. Subsequently, it detects and isolates records containing gross errors by analyzing the statistical properties of the residuals (differences between observed and reference values).

[Input Files]

(1) Discrete Geodetic Observation File (to be detect).

(2) Low-Pass Reference Surface Grid File.

Reference Surface Construction: The reference surface can be generated either by applying a low-pass filter to a simply gridded discrete dataset or by constructing a specific attribute grid via weighted basis function gridding.

Zero-Reference Mode: If a zero-value grid covering the observation area is used, the program performs simple statistical gross error detection.

[Parameter Settings]

Header Rows: Enter the number of header lines to skip.

Attribute Column Index: Enter the column ordinal number of the attribute to be detect.

Threshold Multiplier (n): Define the multiple of the standard deviation for outlier rejection.

Criterion: A record is flagged as a gross error if the absolute difference between its attribute value and the mean exceeds n times the standard deviation ($|\Delta| > n\,\sigma$).

[Output Files]

(1) Cleaned Discrete Point File: Contains only valid records, maintaining the original

input format.

(2) Gross Error Point File: Contains rejected records. The file header includes summary statistics of the residuals: Mean, Standard Deviation, Minimum, and Maximum.

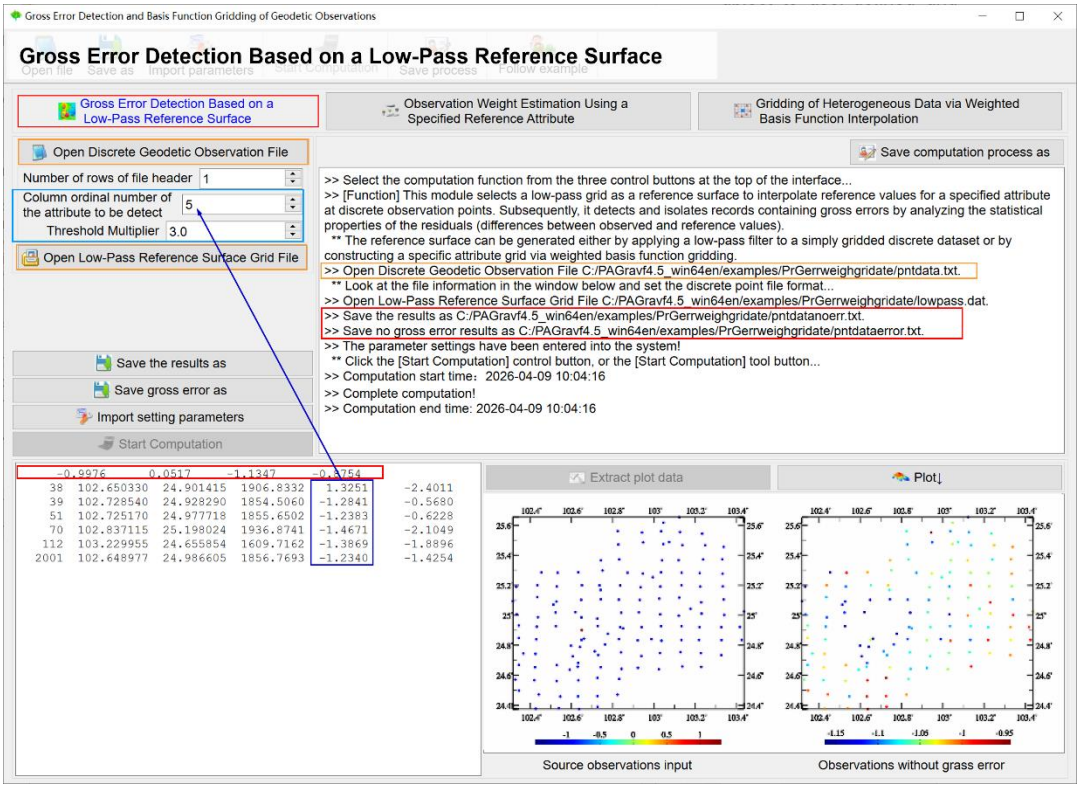

2.6.2 Observation Weight Estimation Using a Specified Reference Attribute

[Function] Estimates observation weights based on the statistical properties of a specified reference attribute within the input geodetic record file, utilizing the proprietary weight function defined by PAGravf4.5.

[Input File] Discrete Geodetic Observation File.

[Weight Function Model]

The weight function is defined as $w(x,a) = 10\sigma\sqrt{\sigma^2 + (ax)^2}$. Where: x is the reference attribute value, a is the user-defined smoothing factor, σ is the standard deviation of x (automatically computed by the program).

[Parameter Settings]

Header Rows: Enter the number of header lines to skip.

Reference Attribute Column Index: Enter the column ordinal number of the reference attribute.

Smoothing Factor a: A larger smoothing factor a results in a slower decay of the weight function w with increasing x, thereby assigning higher weights to observations with larger deviations and enhancing smoothing.

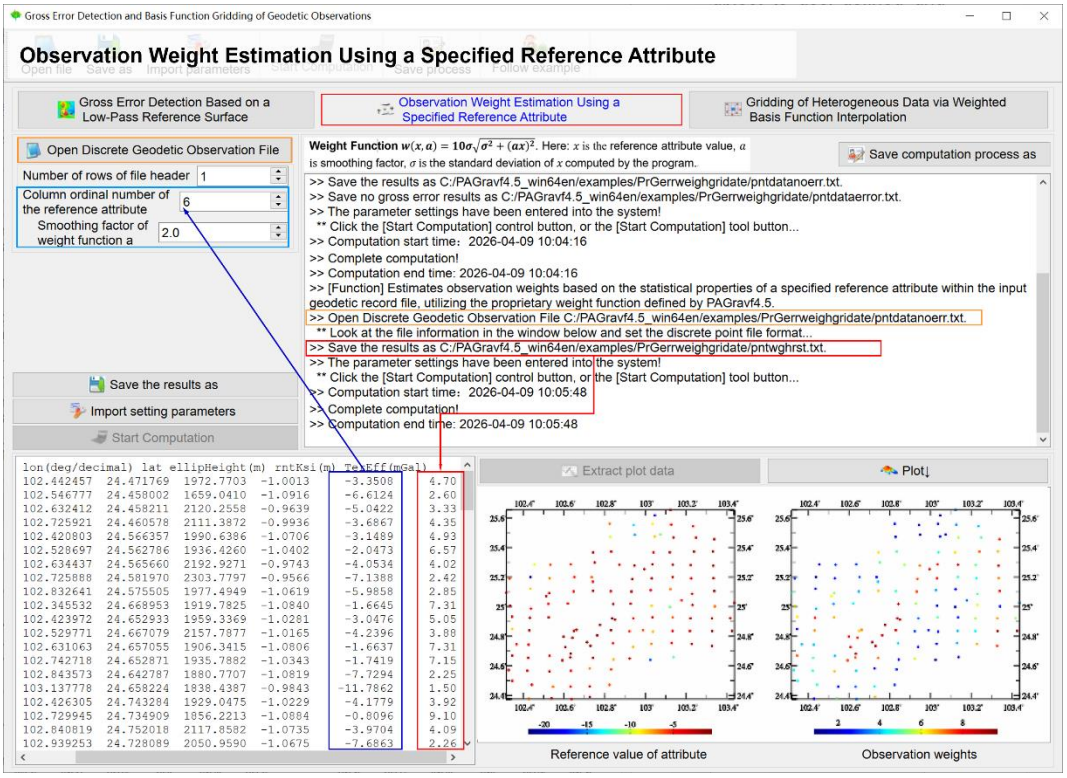

2.6.3 Gridding of Heterogeneous Data via Weighted Basis Function Interpolation

[Function] Generates a regular grid for a specified attribute from an input discrete geodetic point file using the Weighted Basis Function Interpolation, subject to user-defined grid specifications (extent and spatial resolution) and a selected basis function.

[Input File] Discrete Geodetic Observation File.

[Parameter Settings]

Header Rows: Enter the number of header lines to skip.

Column Indics: Enter the column ordinal number of the attribute to be gridded and its weight value.

Number of neighboring points: The number of nearest neighboring points used for interpolation.

Kurtosis of basis function: The smaller the kurtosis is (the slower the basis function value reduces with distance), the larger the number of neighboring points for the interpolation, the smoother the interpolation result, the weaker the edge effect and the stronger the interpolation ability for sparse data.

Grid Specifications: Define the output grid extent and resolution.

Basis Function Selection & Parameters:

- ○ Effect of Kurtosis: A lower kurtosis value induces a more gradual decay of the basis function with distance.
- ○ Interpolation Weight: Defined as the product of the attribute weight and the basis function value.

[Output File] Geodetic Grid File.

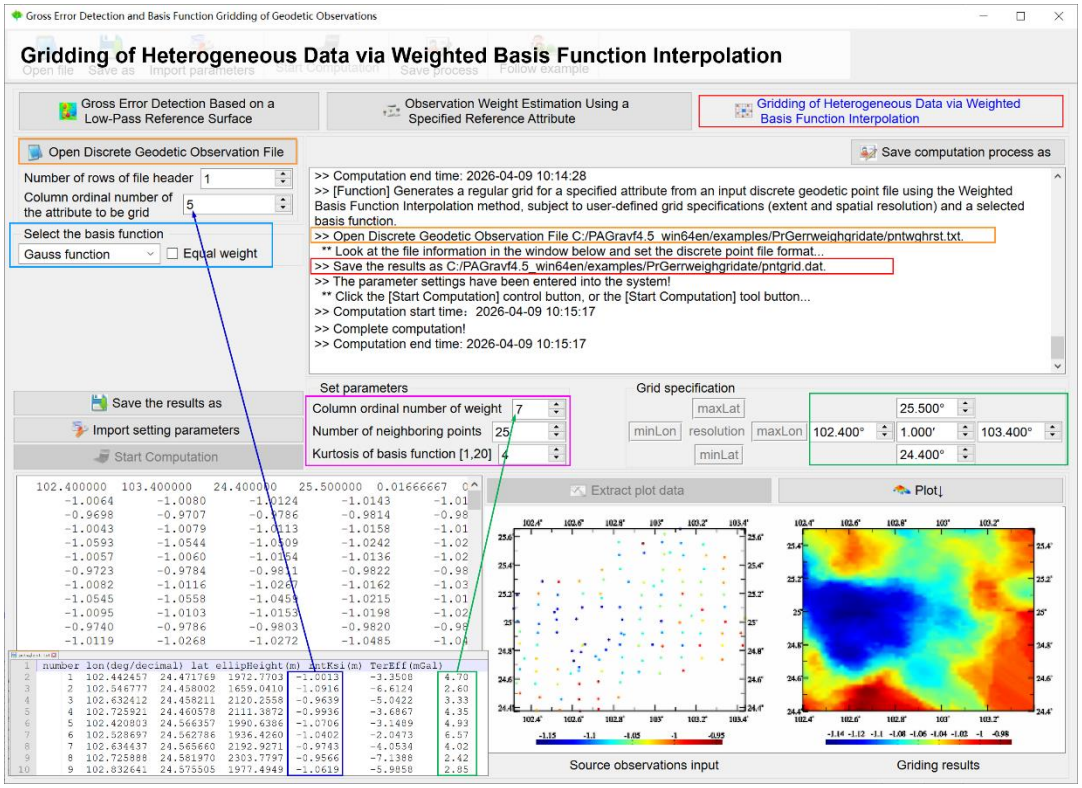

Note: This module is specifically engineered by PAGravf4.5, leveraging the intrinsic properties of general geophysical fields. It is optimized for the gridding of single-type, multi-source heterogeneous geophysical data.

3. Computation of Diverse Terrain Effects on Various External Gravity Field Elements

PAGravf4.5 establishes a unified analytical algorithm framework for computing diverse terrain effects on various gravity field elements on or outside the geoid. Designed to advance gravity prospecting modeling and enhance gravity field data processing. This subsystem can support a wide array, including local terrain effects, terrain Bouguer effects, seawater Bouguer effects, crustal isostatic effects, terrain Helmert condensation effects, and residual terrain effects (RTE).

The subsystem computes effects on the following gravity field elements: geopotential, disturbing potential and height anomaly, gravity, gravity disturbance and gravity anomaly, vertical deflection vector, and gravity gradient tensors. The framework can support high-precision computations for elements located on or outside the geoid, ensuring seamless modeling continuity from the geoidal surface to satellite altitudes.

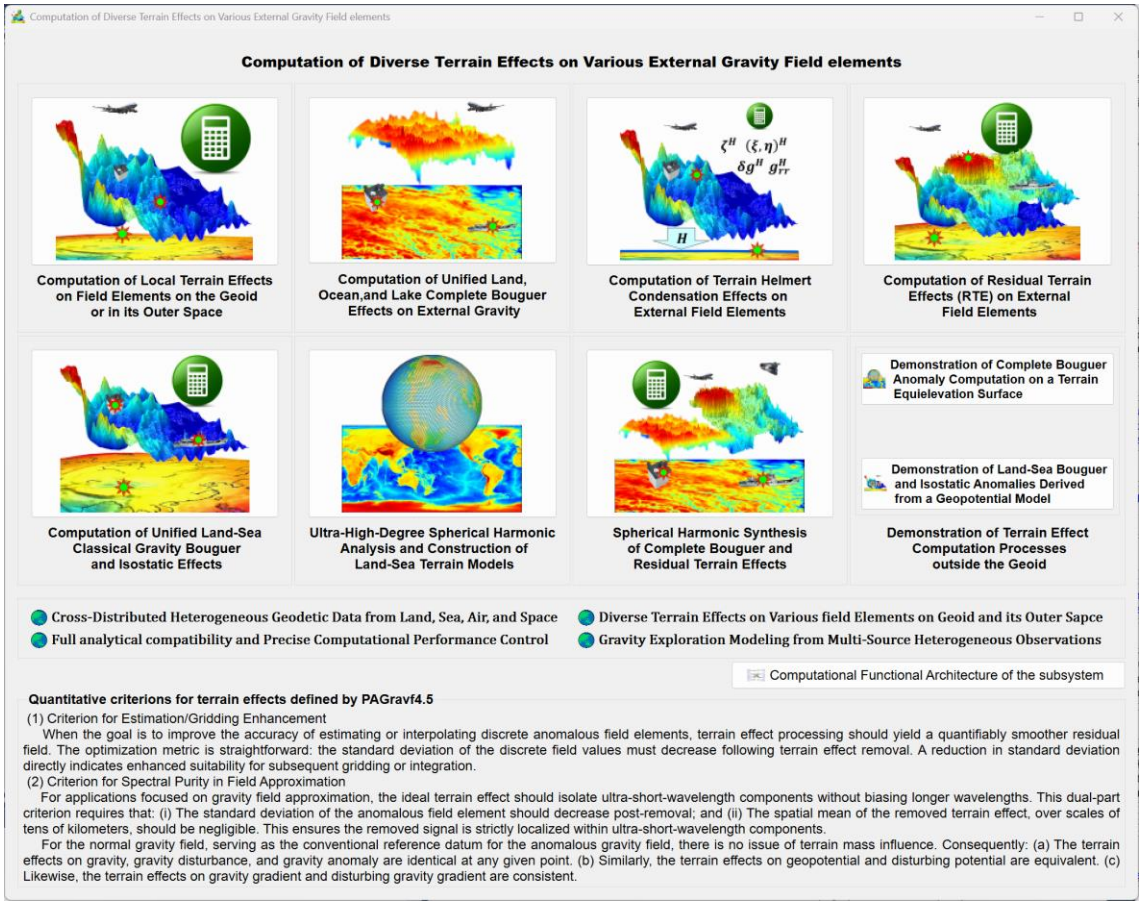

[Theoretical Basis]

For the normal gravity field, serving as the conventional reference datum for the anomalous gravity field, there is no issue of terrain mass influence. Consequently: (a) The terrain effects on gravity, gravity disturbance, and gravity anomaly are identical at any given point. (b) Similarly, the terrain effects on geopotential and disturbing potential are equivalent.

(c) Likewise, the terrain effects on gravity gradient and disturbing gravity gradient are consistent.

[Validation & Performance Analysis]

To validate and analyze the performance of these algorithms, the test of the software suite employs terrain data from representative rugged mountainous regions, characterized by a mean elevation of approximately 4,000 meters and topographic relief exceeding 3,000 meters. These tests facilitate a comprehensive understanding of various terrain effect characteristics.

3.1 Computation of Local Terrain Effects on Field Elements on or outside the Geoid

[Purpose] Utilizing either rigorous numerical integration or the Fast Fourier Transform (FFT) algorithm, this module computes local terrain effects on the following field elements on or outside the geoid (extending up to typical airborne altitudes): height anomaly (m), gravity (gravity anomaly/disturbance, mGal), vertical deflection (arcseconds [″], south and west components), or (disturbing) gravity gradient (E, radial component).

[Input Data Requirements]

(1) Ground Digital Elevation Model (DEM): Expressed in orthometric or normal heights.

(2) Ground Ellipsoidal Height Grid: Provides geodetic coordinates of the ground surface, essential for integration distance derivation.

[Physical Definitions & Relationships]

Terrain Effect vs. Terrain Correction: The terrain effect on a field element is defined as the negative of the classic terrain correction: $Local\ Terrain\ Effect = -Local\ Terrain\ Correction.$

Equivalence Principle: Given the invariance of the normal gravity field, the terrain effects on gravity disturbance and gravity anomaly are strictly equal to the terrain effect on gravity itself.

3.1.1 Rigorous Numerical Integration of Local Terrain Effects on External Field Elements

[Function] Utilizing a rigorous numerical integration algorithm, this module computes local terrain effects on various field elements at points located on or outside the geoid. Inputs include a Ground Digital Elevation Model (DEM) and a Ground Ellipsoidal Height Grid.

Target Elements: Height Anomaly (m), Gravity (Anomaly/Disturbance, mGal), Vertical Deflection (″; South/West components), or (Disturbing) Gravity Gradient (Eötvös; Radial component).

[Input Files]

(1) Ground DEM File: Expressed in orthometric or normal heights to characterize topographic relief.

(2) Ground Ellipsoidal Height Grid File: Provices the geodetic coordinates of ground surface, essential for deriving integration distances.

Requirement: Both files must share identical grid specifications.

(3) Space Computation Point File (discrete) or Computation Surface Ellipsoidal Height

Grid File.

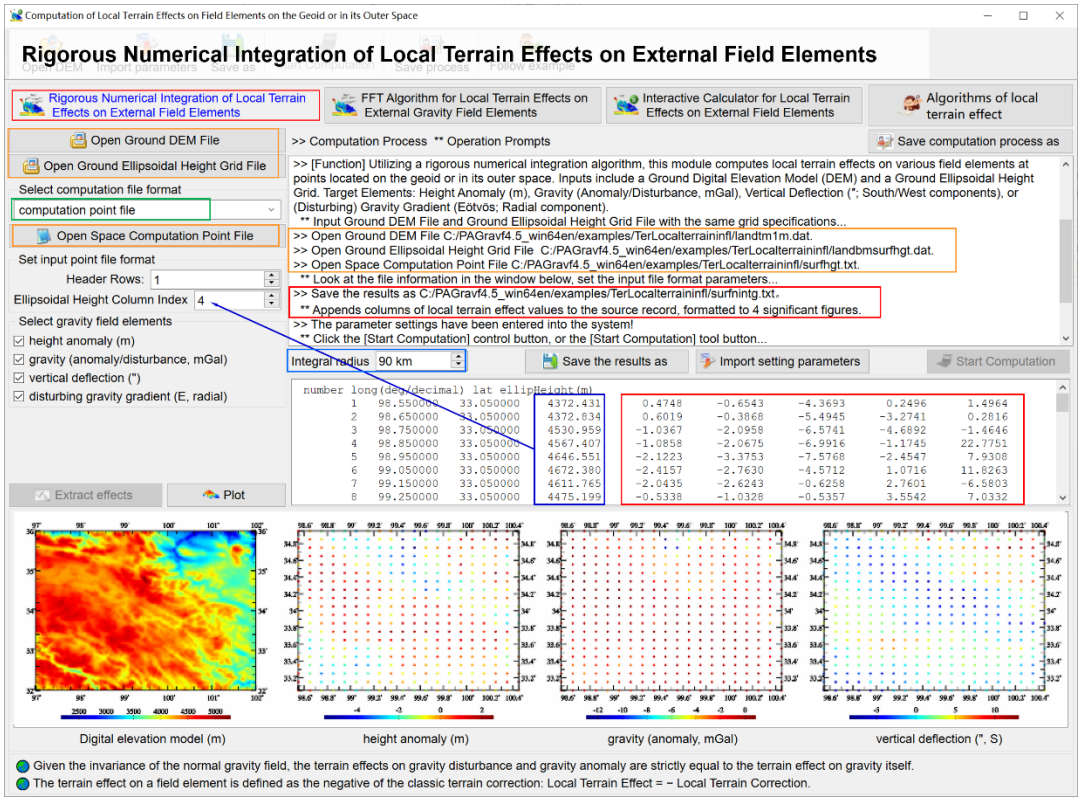
Computation of Local Terrain Effects on Field Elements on the Geoid or in its Outer Space
Rigorous Numerical Integration of Local Terrain Effects on External Field Elements
Rigorous Numerical Integration of Local Terrain Effects on External Field Elements
FFT Algorithm for Local Terrain Effects on External Gravity Field Elements
Interactive Calculator for Local Terrain Effects on External Field Elements
Algorithms of local terrain effect
Open Ground DEM File
Open Ground Ellipsoidal Height Grid File
Select computation file format
computation point file
Open Space Computation Point File
Set input point file format
Header Rows: 1
Ellipsoidal Height Column Index 4
Select gravity field elements
height anomaly (m)
gravity (anomaly/disturbance, mGal)
vertical deflection (")
disturbing gravity gradient (E, radial)
>> Computation Process ** Operation Prompts
Save computation process as
>> [Function] Utilizing a rigorous numerical integration algorithm, this module computes local terrain effects on various field elements at points located on the geoid or in its outer space. Inputs include a Ground Digital Elevation Model (DEM) and a Ground Ellipsoidal Height Grid. Target Elements: Height Anomaly (m), Gravity (Anomaly/Disturbance, mGal), Vertical Deflection (''; South/West components), or (Disturbing) Gravity Gradient (Eötvös; Radial component).
** Input Ground DEM File and Ground Ellipsoidal Height Grid File with the same grid specifications...
>> Open Ground DEM File C:/PAGravf4.5_win64en/examples/TerLocalterraininfl/landtm1m.dat.
>> Open Ground Ellipsoidal Height Grid File C:/PAGravf4.5_win64en/examples/TerLocalterraininfl/landbmsurfhgt.dat.
>> Open Space Computation Point File C:/PAGravf4.5_win64en/examples/TerLocalterraininfl/surfhgt.txt.
** Look at the file information in the window below, set the input file format parameters...
>> Save the results as C:/PAGravf4.5_win64en/examples/TerLocalterraininfl/surfnintg.txt.
** Appends columns of local terrain effect values to the source record, formatted to 4 significant figures.
>> The parameter settings have been entered into the system!
** Click the [Start Computation] control button, or the [Start Computation] tool button...
Integral radius 90 km
Save the results as
Import setting parameters
Start Computation
number long(dec/decimal) lat ellipHeight(m)
1 98.550000 33.050000 4372.431 0.4748 -0.6543 -4.3693 0.2496 1.4964
2 98.650000 33.050000 4372.834 0.6019 -0.3868 -5.4945 -3.2741 0.2816
3 98.750000 33.050000 4530.959 -1.0367 -2.0958 -6.5741 -4.6892 -1.4646
4 98.850000 33.050000 4567.407 -1.0858 -2.0675 -6.9916 -1.1745 22.7751
5 98.950000 33.050000 4646.551 -2.1223 -3.1753 -7.5768 -2.4547 7.9308
6 99.050000 33.050000 4672.380 -2.4157 -2.7630 -4.5712 1.0716 11.8263
7 99.150000 33.050000 4611.765 -2.0435 -2.6243 -0.6258 2.7601 -6.5803
8 99.250000 33.050000 4475.199 -0.5338 -1.0328 -0.5357 3.5542 7.0332
Extract effects
Plot
Digital elevation model (m)
height anomaly (m)
gravity (anomaly, mGal)
vertical deflection (", S)
Given the invariance of the normal gravity field, the terrain effects on gravity disturbance and gravity anomaly are strictly equal to the terrain effect on gravity itself.
The terrain effect on a field element is defined as the negative of the classic terrain correction: Local Terrain Effect = – Local Terrain Correction.

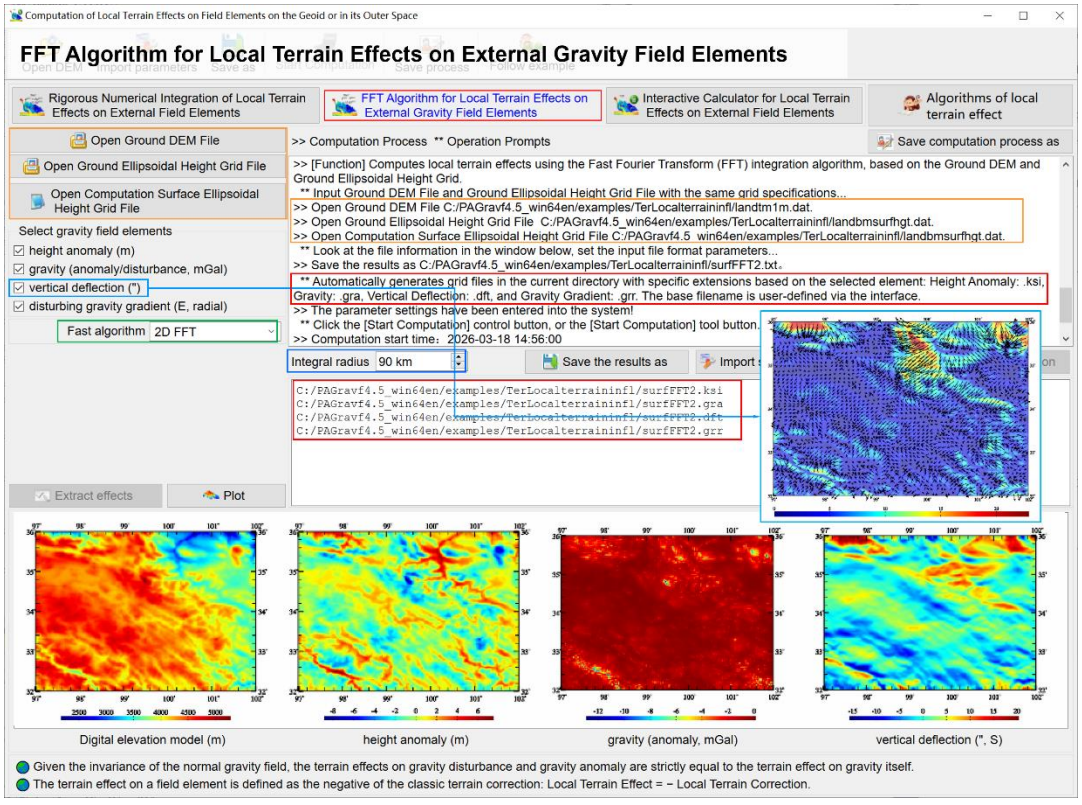
Computation of Local Terrain Effects on Field Elements on the Geoid or in its Outer Space
FFT Algorithm for Local Terrain Effects on External Gravity Field Elements
Rigorous Numerical Integration of Local Terrain Effects on External Field Elements
FFT Algorithm for Local Terrain Effects on External Gravity Field Elements
Interactive Calculator for Local Terrain Effects on External Field Elements
Algorithms of local terrain effect
Open Ground DEM File
Open Ground Ellipsoidal Height Grid File
Open Computation Surface Ellipsoidal Height Grid File
Select gravity field elements
height anomaly (m)
gravity (anomaly/disturbance, mGal)
vertical deflection (")
disturbing gravity gradient (E, radial)
Fast algorithm 2D FFT
>> Computation Process ** Operation Prompts
Save computation process as
>> [Function] Computes local terrain effects using the Fast Fourier Transform (FFT) integration algorithm, based on the Ground DEM and Ground Ellipsoidal Height Grid.
** Input Ground DEM File and Ground Ellipsoidal Height Grid File with the same grid specifications...
>> Open Ground DEM File C:/PAGravf4.5_win64en/examples/TerLocalterraininfl/landtm1m.dat.
>> Open Ground Ellipsoidal Height Grid File C:/PAGravf4.5_win64en/examples/TerLocalterraininfl/landbmsurfhgt.dat.
>> Open Computation Surface Ellipsoidal Height Grid File C:/PAGravf4.5_win64en/examples/TerLocalterraininfl/landbmsurfhgt.dat.
** Look at the file information in the window below, set the input file format parameters...
>> Save the results as C:/PAGravf4.5_win64en/examples/TerLocalterraininfl/surfFFT2.txt.
** Automatically generates grid files in the current directory with specific extensions based on the selected element: Height Anomaly: .ksi, Gravity: .gra, Vertical Deflection: .dft, and Gravity Gradient: .grr. The base filename is user-defined via the interface.
>> The parameter settings have been entered into the system!
** Click the [Start Computation] control button, or the [Start Computation] tool button.
>> Computation start time: 2026-03-18 14:56:00
Integral radius 90 km
Save the results as
C:/PAGravf4.5_win64en/examples/TerLocalterraininfl/surfFFT2.ksi
C:/PAGravf4.5_win64en/examples/TerLocalterraininfl/surfFFT2.gra
C:/PAGravf4.5_win64en/examples/TerLocalterraininfl/surfFFT2.dft
C:/PAGravf4.5_win64en/examples/TerLocalterraininfl/surfFFT2.grr
Extract effects
Plot
Digital elevation model (m)
height anomaly (m)
gravity (anomaly, mGal)
vertical deflection (", S)
Given the invariance of the normal gravity field, the terrain effects on gravity disturbance and gravity anomaly are strictly equal to the terrain effect on gravity itself.
The terrain effect on a field element is defined as the negative of the classic terrain correction: Local Terrain Effect = – Local Terrain Correction.

[Parameter Settings]

File Format: Configure input file parsing parameters.

Field Element Type: Select the specific gravity field element(s) for computation.

Integration Radius: Enter the radius for numerical integration.

[Output Files] The local terrain effect result file.

If discrete Input: Appends columns of local terrain effect values to the source record, formatted to 4 significant figures.

If grid Input: Outputs records as ID, Longitude, Latitude, Ellipsoidal Height, [Effect Values...], formatted to 4 significant figures.

Grid Output Files if grid Input: Automatically generates grid files in the current directory with specific extensions based on the selected element: Height Anomaly: .ksi, Gravity: .gra, Vertical Deflection: .dft, and Gravity Gradient: .grr. The base filename is user-defined via the interface.

[Case Study & Statistical Analysis]

Setup: A 1′×1′ resolution DEM was used with an integration radius of 90 km. The terrain surface was defined by the ground ellipsoidal height grid. A 1° marginal buffer zone was excluded to mitigate integration edge effects.

Statistics: As shown in Table 3.1, where D = Range [Max-Min], ε = Standard Deviation.

Table 3.1: Statistical Results of the Local Terrain Effects on Various Ground Gravity Field Elements

Field element type /Unit	Mean	Std. Dev. (ε)	Minimum	Maximum	D/ε
height anomaly (m)	-0.2233	1.4995	-8.9709	4.9249	9.3
gravity (anomaly, disturbance) (mGal)	-0.5364	0.7599	-14.3238	0.5061	19.5
vertical deflection (″, South)	1.0139	3.2809	-8.7789	13.2512	6.7
vertical deflection (″, West)	1.7161	3.2445	-6.8166	14.4212	6.5
gravity gradient (E)	1.3980	83.1923	-368.3504	493.4792	10.4

[Interpretation]

Significance of D/ε: A high ratio indicates that ultra-short-wavelength signals, while minor in total energy, exhibit prominent amplitudes (extreme local anomalies).

Applicability: A larger magnitude of terrain effect (higher D/ε) implies greater efficacy for correcting that specific field element.

Conclusion: In this scenario, gravity disturbance yields the highest ratio (19.5), demonstrating its high suitability for terrain correction. Conversely, vertical deflection shows the lowest ratios (~6.5), suggesting that local terrain effects are less dominant or effective for refining vertical deflection data in this context.

3.1.2 FFT Algorithm for Local Terrain Effects on External Gravity Field Elements

[Function] Computes local terrain effects using the Fast Fourier Transform (FFT)

integration algorithm, based on the Ground DEM and Ground Ellipsoidal Height Grid.

[Input Files]

(1) Ground DEM (Topographic relief) File.

(2) Ground Ellipsoidal Height Grid File.

(3) Computation Surface Ellipsoidal Height Grid File.

Requirement: All files must share identical grid specifications.

[Parameter Settings]

Field Element Type: Select target element.

Algorithm Variant: Choose between 1D-FFT or 2D-FFT.

Integration Radius: Enter the radius for integration FFT algorithm.

[Output Files]

Result File: Format: ID, Longitude, Latitude, Ellipsoidal Height, [Effect Values...] (4 significant figures).

Grid Files: Generates .ksi, .gra, .dft, .grr files as described in Section 3.1.1.

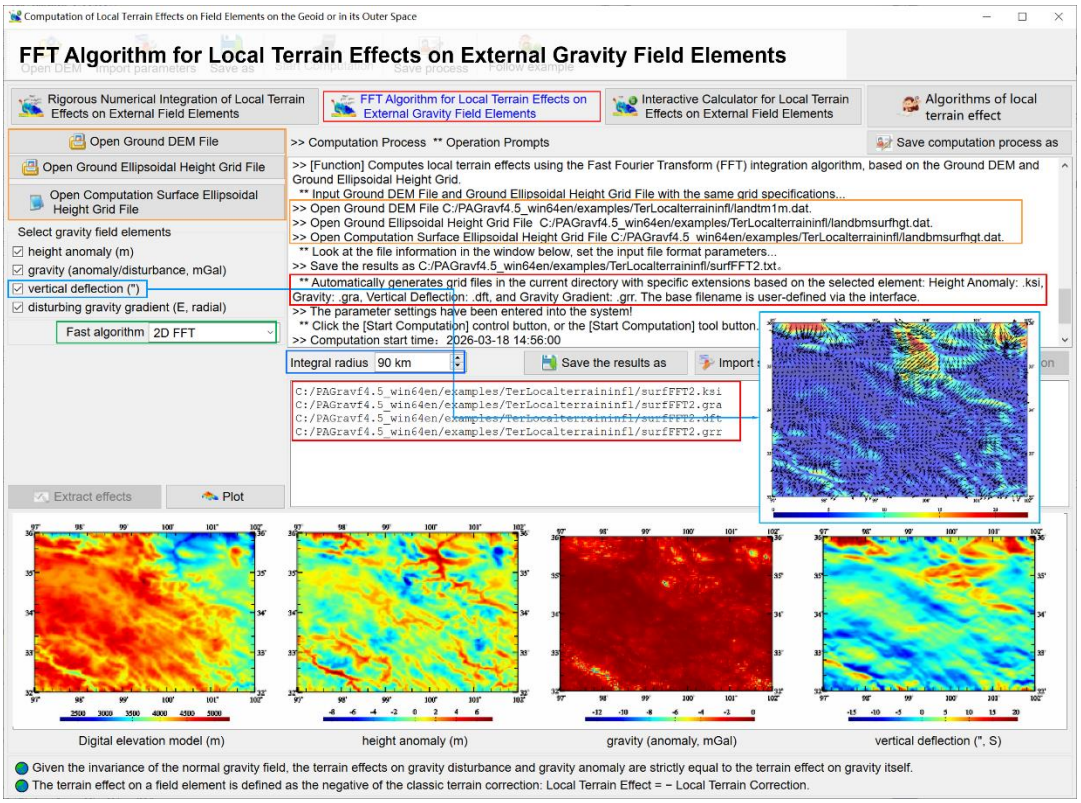

[Accuracy Assessment: FFT vs. Numerical Integration]

Using identical parameters, the differences between FFT results and rigorous numerical integration were analyzed, and the statistical results as shown in Table 3.2.

Table 3.2: Statistics for the differences between FFT results and rigorous numerical integration

Field Element / Unit	Algorithm	Mean Diff	Std. Dev. Diff	Min Diff	Max Diff
height anomaly (m)	FFT2	-0.0001	0.0138	-0.0686	0.0883

	FFT1	0.0012	0.0027	-0.0115	0.0110
gravity (anomaly, disturbance) (mGal)	FFT2	0.0352	0.2316	-0.7410	1.4406
	FFT1	0.0341	0.2298	-0.7602	1.3356
vertical deflection (″, South)	FFT2	-0.0082	0.0197	-0.1176	0.1275
	FFT1	-0.0026	0.0138	-0.1616	0.1538
vertical deflection (″, West)	FFT2	0.0018	0.0400	-0.3873	0.1555
	FFT1	0.0051	0.0198	-0.4444	0.2844
gravity gradient (E)	FFT2	0.0042	0.5176	-19.6242	10.5354
	FFT1	0.0036	0.5859	-21.2847	12.1181

The discrepancies between the rigorous numerical integration and the fast FFT algorithms are negligible. Furthermore, no significant difference exists between the 1D-FFT and 2D-FFT implementations.

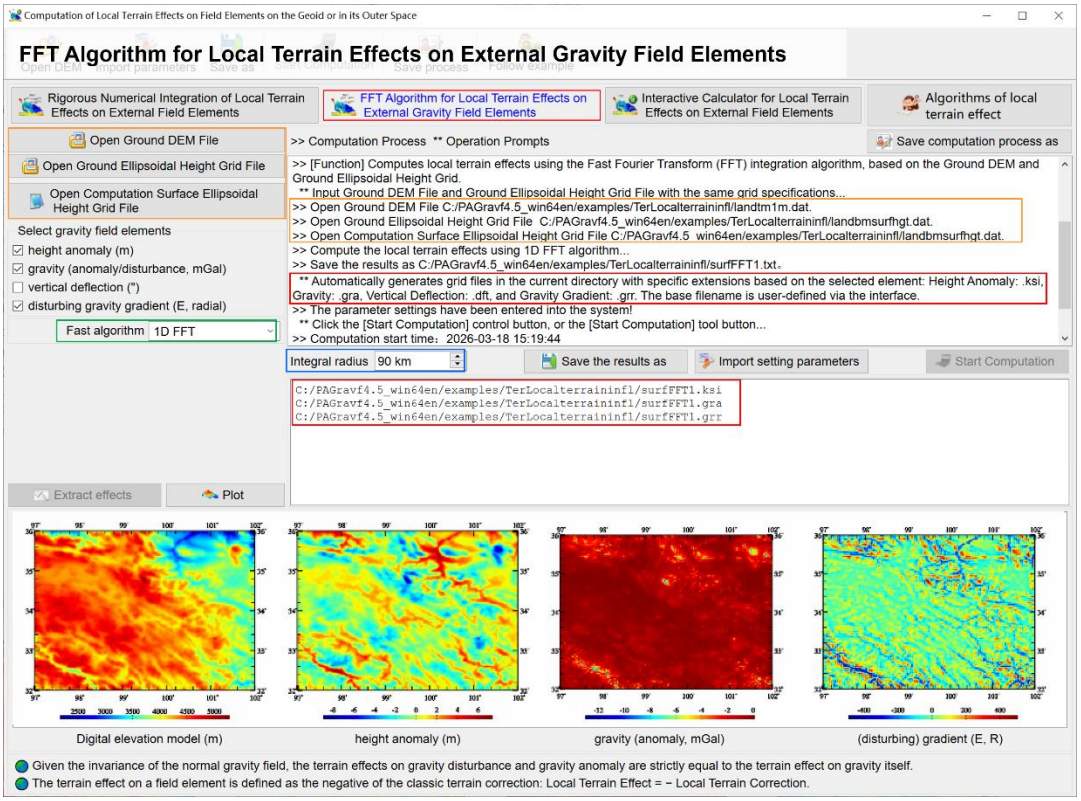

3.1.3 Interactive Calculator for Local Terrain Effects on External Field Elements

[Function] Provides a real-time interactive tool to compute the local terrain effects on gravity field elements at any user-defined geodetic point on or outside the geoid.

[Workflow]

Data Loading: Load the Ground DEM and Ground Ellipsoidal Height Grid (must share grid specs). The [Start Calculation] button activates upon successful loading.

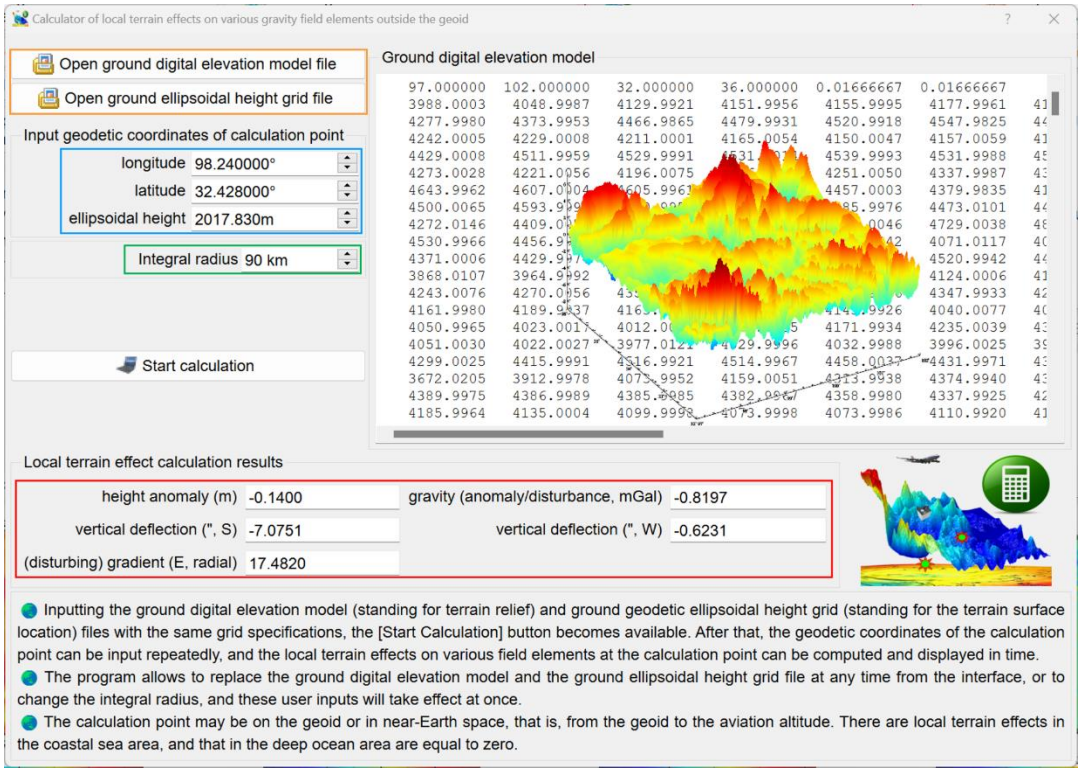

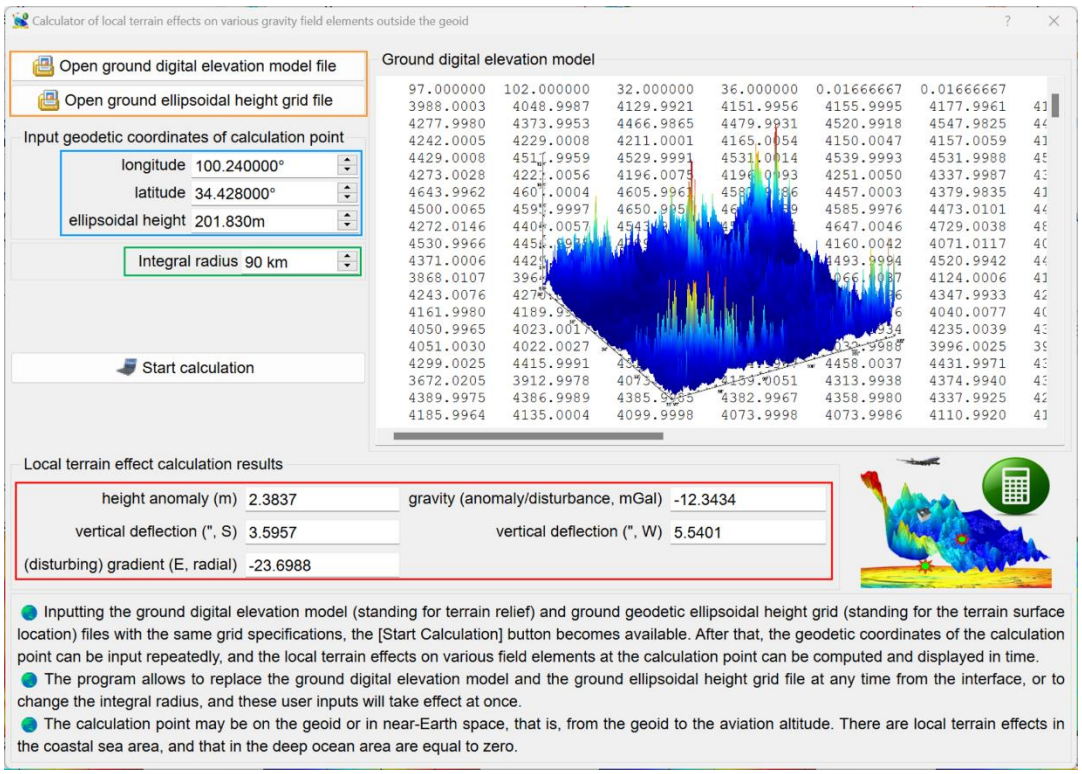

Real-Time Computation: Enter geodetic coordinates for computation points. The system

instantly calculates and displays the local terrain effects for all selected field elements.

Dynamic Updates: Users can dynamically swap input DEM/Height Grid files or adjust the Integration Radius via the interface. Changes take effect immediately for subsequent calculations.

[Applicability] Supports computation points spanning from the geoid up to typical airborne altitudes (near-Earth Space).

3.2 Computation of Unified Land, Ocean, and Lake Complete Bouguer Effects on External Gravity

[Purpose] Utilizing either rigorous numerical integration or the Fast Fourier Transform (FFT) algorithm, this module computes the unified land-sea Complete Bouguer effect on gravity anomaly or gravity disturbance (mGal) at points located on the geoid or in near-Earth space. Inputs include a land-sea terrain model and the land-sea surface ellipsoidal height grid.

[Physical Context & Application]

Magnitude: The Complete Bouguer effect on an anomalous field element typically far exceeds the magnitude of the element itself.

Disciplinary Usage:

- ○ Geophysics: Widely employed to probe the geometric structure of the gravity field.
- ○ Physical Geodesy: Due to the priority on quantitative accuracy, this effect is not applied directly. Instead, it serves as a fundamental component in deriving the Residual Terrain Effect (RTE).

Equivalence: Given the invariance of the normal gravity field, the Complete Bouguer effects on gravity disturbance and gravity anomaly are identical to that on gravity itself.

[Scope] Designed for the unified computation of Complete Bouguer effects across terrestrial regions, land-sea transition zones, and marine areas. Computation points may span from the geoid up to typical airborne altitudes.

[Automated Processing Logic]

The system dynamically adapts based on the input terrain model:

- ○ Terrestrial Mode: If sea bathymetrys in the model are set to zero, the program computes the land complete Bouguer effect.
- ○ Marine Mode: If terrain elevations are set to zero, the program computes the seawater complete Bouguer effect.

[Definition] The complete Bouguer effect is defined as the variation in the Earth's gravity field resulting from: The removal of topographic masses above the geoid; and the density compensation of seawater to the standard terrain density.

Consequently, oceanic seawater Bouguer effects persist in offshore terrestrial areas, while land local terrain effects exist in coastal marine regions.

3.2.1 Unified Land-Sea Complete Bouguer Effect on External Gravity

[Function] Computes the unified land-sea complete Bouguer effect on gravity (mGal) using rigorous numerical integration or FFT, based on a land-sea terrain model and the land-sea surface ellipsoidal height grid.

[Input Files]

(1) Land-Sea Terrain Model: Land elevation > 0; Sea bathymetry < 0 (negative values).

(2) Land-Sea Surface Ellipsoidal Height Grid: Provices the geodetic coordinates of Land-Sea Surface, essential for deriving integration distances.

Requirement: Both files must share identical grid specifications.

(3) Space Computation Point File OR Computation Surface Ellipsoidal Height Grid.

[Parameter Settings]

File Format: Configure input parsing parameters.

Algorithm: Select between rigorous numerical integration or FFT.

Integration Radii: Specify separate radii for Land and Sea components.

[Output File] Unified Complete Bouguer Effect File.

If discrete Input: Appends four columns to the source record (formatted to 4 significant figures): local terrain effect, spherical shell Bouguer effect, seawater complete Bouguer effect, and unified land-sea complete Bouguer effect.

If grid Input: Unified land-sea complete Bouguer effect grid File with identical grid specifications input.

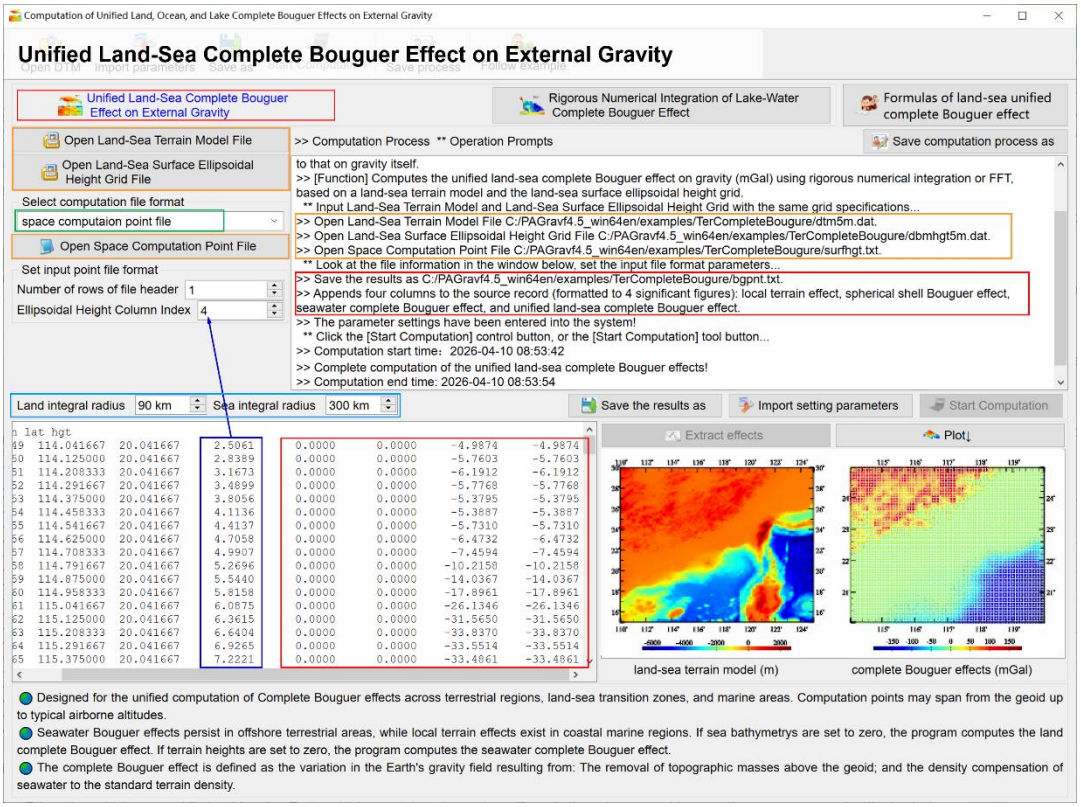

h	lat	hgt					
49	114.041667	20.041667	2.5061	0.0000	0.0000	-4.9874	-4.9874
50	114.125000	20.041667	2.8389	0.0000	0.0000	-5.7603	-5.7603
51	114.208333	20.041667	3.1673	0.0000	0.0000	-6.1912	-6.1912
52	114.291667	20.041667	3.4899	0.0000	0.0000	-5.7768	-5.7768
53	114.375000	20.041667	3.8056	0.0000	0.0000	-5.3795	-5.3795
54	114.458333	20.041667	4.1136	0.0000	0.0000	-5.3887	-5.3887
55	114.541667	20.041667	4.4137	0.0000	0.0000	-5.7310	-5.7310
56	114.625000	20.041667	4.7058	0.0000	0.0000	-6.4732	-6.4732
57	114.708333	20.041667	4.9907	0.0000	0.0000	-7.4594	-7.4594
58	114.791667	20.041667	5.2696	0.0000	0.0000	-10.2158	-10.2158
59	114.875000	20.041667	5.5440	0.0000	0.0000	-14.0367	-14.0367
60	114.958333	20.041667	5.8158	0.0000	0.0000	-17.8961	-17.8961
61	115.041667	20.041667	6.0875	0.0000	0.0000	-26.1346	-26.1346
62	115.125000	20.041667	6.3615	0.0000	0.0000	-31.5650	-31.5650
63	115.208333	20.041667	6.6404	0.0000	0.0000	-33.8370	-33.8370
64	115.291667	20.041667	6.9265	0.0000	0.0000	-33.5514	-33.5514
65	115.375000	20.041667	7.2221	0.0000	0.0000	-33.4861	-33.4861

[Case Study & Statistical Analysis]

Setup: A 5′×5′ land-sea terrain model was used. Integration radii were set to 90 km (land local terrain effect) and 300 km (seawater complete Bouguer effect). A 3° marginal buffer was excluded to mitigate edge effects.

Statistics: Results (Unit: mGal), and the statistical results as shown in Table 3.3.

Table 3.3: Statistics for the Unified land-sea complete Bouguer effect on ground gravity

Statistic (mGal)	Mean	Std. Dev.	Minimum	Maximum
Numerical integral	-17.2622	110.3575	-260.5460	562.1404
FFT2 – Numerical integral	1.7056	1.8637	0.0265	19.7512
FFT1 – Numerical integral	2.0864	2.2786	0.0268	19.3779
FFT2 – FFT1	-0.3808	0.7884	-3.3353	0.8730

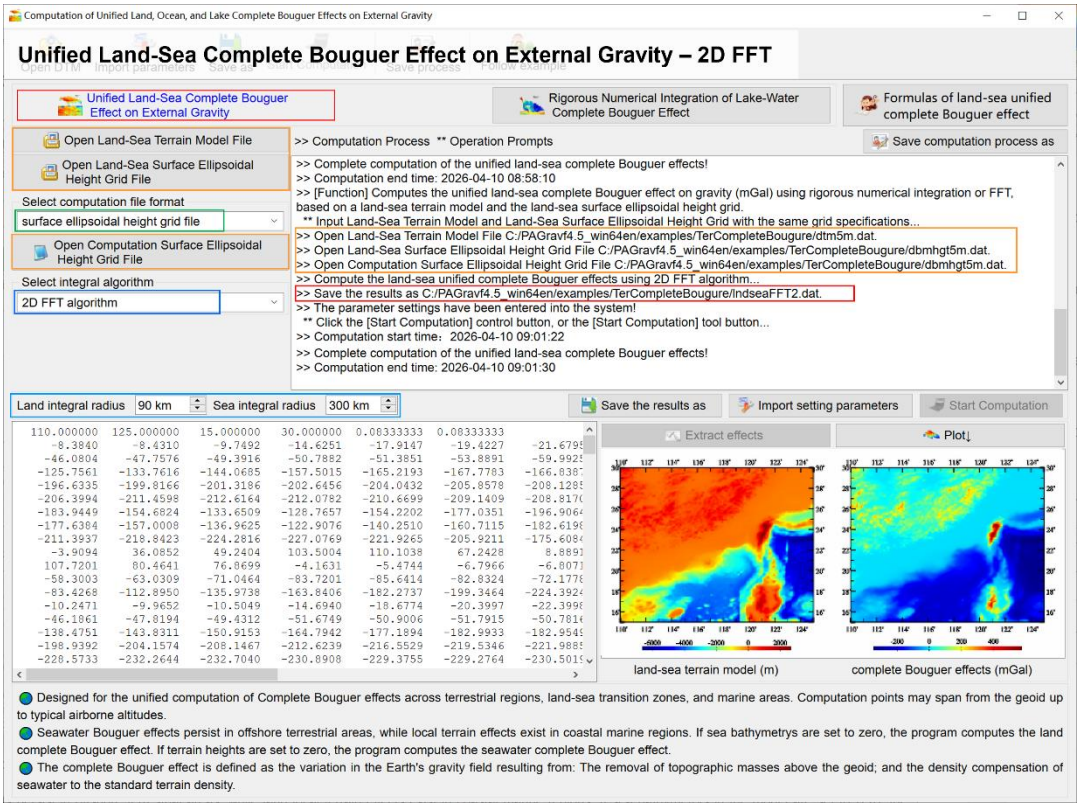

[Error Analysis & Recommendation]

Critical Issue: Given the substantial magnitude of the complete Bouguer effect, errors arising from the third-order approximation of topographic relief can, in certain scenarios, exceed the magnitude of the anomalous field element itself.

Recommended Strategy: PAGravf4.5 advises employing a "Remove-Restore" scheme for field elements beyond gravity:

- ○ Utilize a global land-sea terrain mass spherical harmonic coefficient model as the reference terrain field.
- ○ This approach effectively mitigates approximation errors inherent in limited-radius integrations.

Reference: For a detailed procedural walkthrough, see: [Demonstration of Complete Bouguer Anomaly Computation on a Terrain Equielevation Surface].

3.2.2 Rigorous Numerical Integration of Lake-Water Complete Bouguer Effect

[Function] Computes the lake-water complete Bouguer effect on gravity (mGal) using a rigorous numerical integration algorithm, based on a lake water-depth grid (zero over land) and the lake surface ellipsoidal height grid.

[Input Files]

(1) Lake Water-Depth Grid: Represents bathymetry; land areas are masked with zero.

(2) Lake Surface Ellipsoidal Height Grid: Provices the geodetic coordinates of Lake Surface, for integration distance derivation.

Requirement: Both files must share identical grid specifications.

(3) Space Computation Point File.

[Parameter Settings]

File Format: Configure input parsing parameters.

Integration Radius: Enter the radius for the lake effect integration.

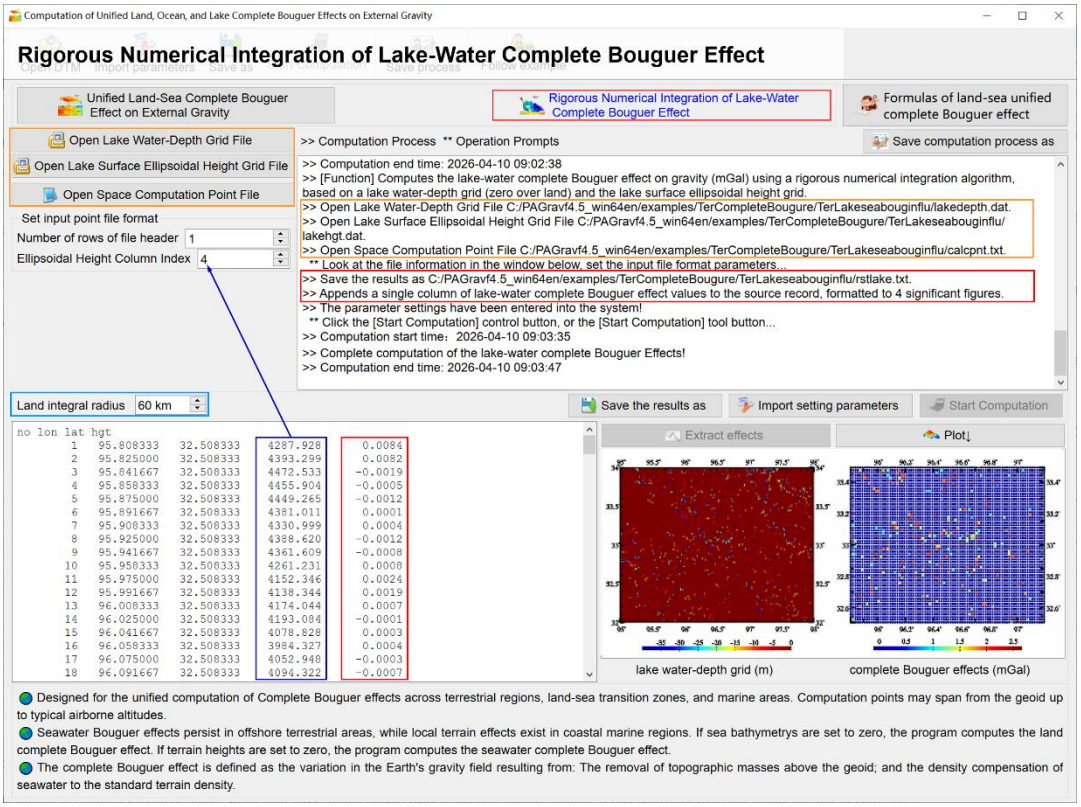

[Output File] Lake-Water Complete Bouguer Effect File.

Appends a single column of lake-water complete Bouguer effect values to the source record, formatted to 4 significant figures.

3.3 Computation of Terrain Helmert Condensation Effects on External Field Elements

[Purpose] Utilizing either rigorous numerical integration or the Fast Fourier Transform (FFT) algorithm, this module computes Terrain Helmert Condensation effects on various field

elements at points located on or outside the geoid.

Target Elements: Height Anomaly (m), Gravity (Anomaly/Disturbance, mGal), Vertical Deflection (″; South/West components), or (Disturbing) Gravity Gradient (E; Radial component).

[Scope & Physical Principle]

Spatial Domain: Computation points may span from the geoid up to typical airborne altitudes.

Mechanism: Since the normal gravity field is invariant, the Terrain Helmert Condensation effects on gravity, gravity disturbance and gravity anomaly are strictly identical.

Mass Conservation: Unlike local terrain or complete Bouguer effects, Helmert condensation preserves the total topographic mass. Consequently, the vertical component of the Helmert condensation effect is generally significantly smaller than both the complete Bouguer effect and the local terrain effect.

3.3.1 Rigorous Numerical Integration of Terrain Helmert Condensation Effects on or outside the Geoid

[Function] Computes Terrain Helmert Condensation effects using a rigorous numerical integration algorithm based on Ground DEM and Ground Surface Ellipsoidal Height Grid.

[Input Files]

(1) Ground DEM File: Expressed in orthometric or normal heights to characterize topographic relief.

(2) Ground Surface Ellipsoidal Height Grid File: Provices the geodetic coordinates of ground surface, for integration distance derivation.

Requirement: Both files must share identical grid specifications.

(3) Space Computation Point File or Computation Surface Ellipsoidal Height Grid File.

[Parameter Settings]

File Format: Configure input parsing parameters.

Field Element Type: Select target element(s).

Integration Radius: Enter the radius for numerical integration.

[Output Files]

Discrete Input: Appends columns of effect values to the source record (4 significant figures).

Grid Input: Outputs ID, Longitude, Latitude, Ellipsoidal Height, [Effect Values...] (4 significant figures).

Grid Output Files if Grid Input: Automatically generates files with extensions: .ksi (Height Anomaly), .gra (Gravity Anomaly), .rga (Gravity Disturbance), .dft (Vertical Deflection), and *.grr (Gravity Gradient).

[Case Study & Statistical Analysis]

Setup: 1′×1′ DEM, 90 km integration radius. A 1° marginal buffer was excluded.

Statistics: As shown in Table 3.4, where D = Range [Max-Min], ε = Standard Deviation.

Table 3.4: Statistical Results of Terrain Helmert Condensation Effects on Various Ground Gravity Field Elements

Field element type /Unit	Mean	Std. Dev. (ε)	Minimum	Maximum	D/ε
height anomaly (m)	-0.0005	0.0029	-0.0134	0.0180	1.6
gravity (anomaly, disturbance) (mGal)	0.2932	0.4168	-0.4313	3.1693	8.6
vertical deflection (″, South)	2.0301	6.5718	-17.5982	26.6152	6.8
vertical deflection (″, West)	3.4358	6.5000	-13.6625	28.9665	6.8
gravity gradient (E)	-0.3677	16.5856	-257.5543	112.1249	22.3

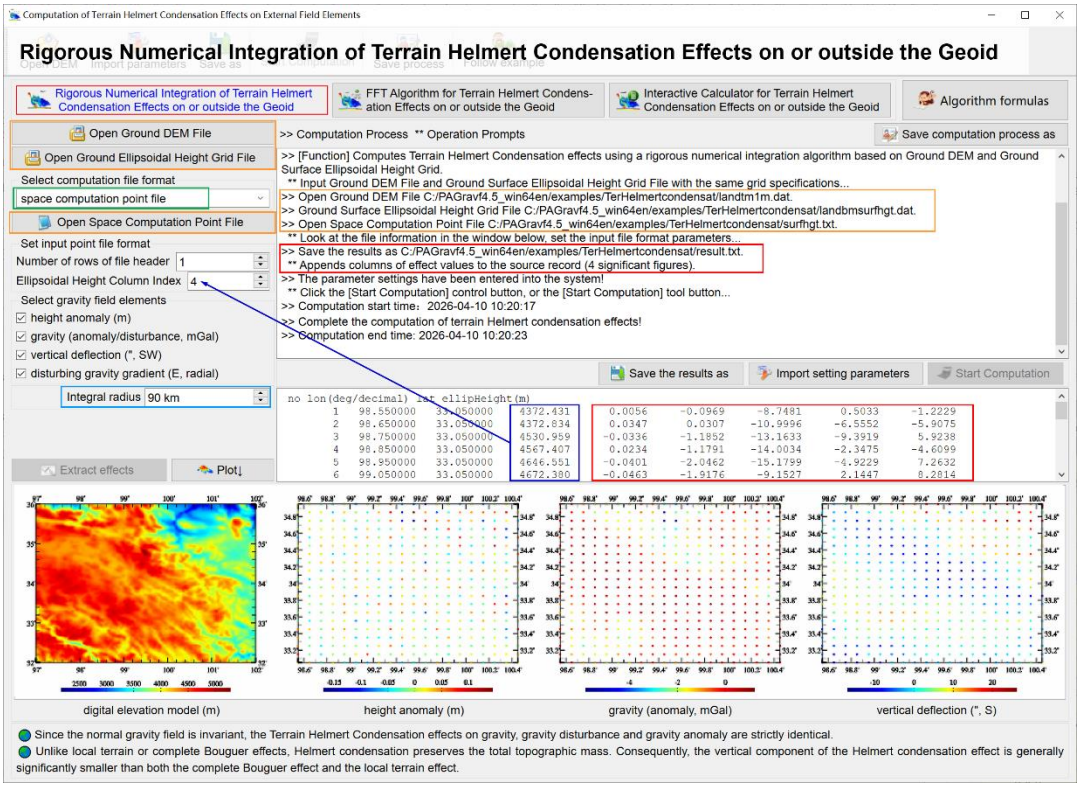

[Spectral Characteristics & Suitability Analysis]

Spectral Richness: Unlike the Local Terrain Effect, the Terrain Helmert Condensation effect is characterized by a significantly richer spectrum of ultra-short-wavelength components.

○ Near-shore: Non-zero effects persist due to land topography.

○ Deep Ocean: The effect vanishes (equals zero) in the absence of topographic masses.

Applicability Assessment (based on D/ε):

○ Optimal for Gravity Gradients: Due to its enhanced sensitivity to high-frequency signals, the Helmert condensation method demonstrates superior suitability for processing (disturbing) gravity gradient data (D/ε =22.3), outperforming the Local Terrain Effect.

○ Suboptimal for Long-Wavelength Fields: The method is less favorable for elements dominated by medium- and long-wavelength components. Specifically, it is not

recommended for geoid refinement (height anomaly determination), as the excessive high-frequency noise may obscure the broader geoidal undulations required for precise modeling (D/ε =1.6).

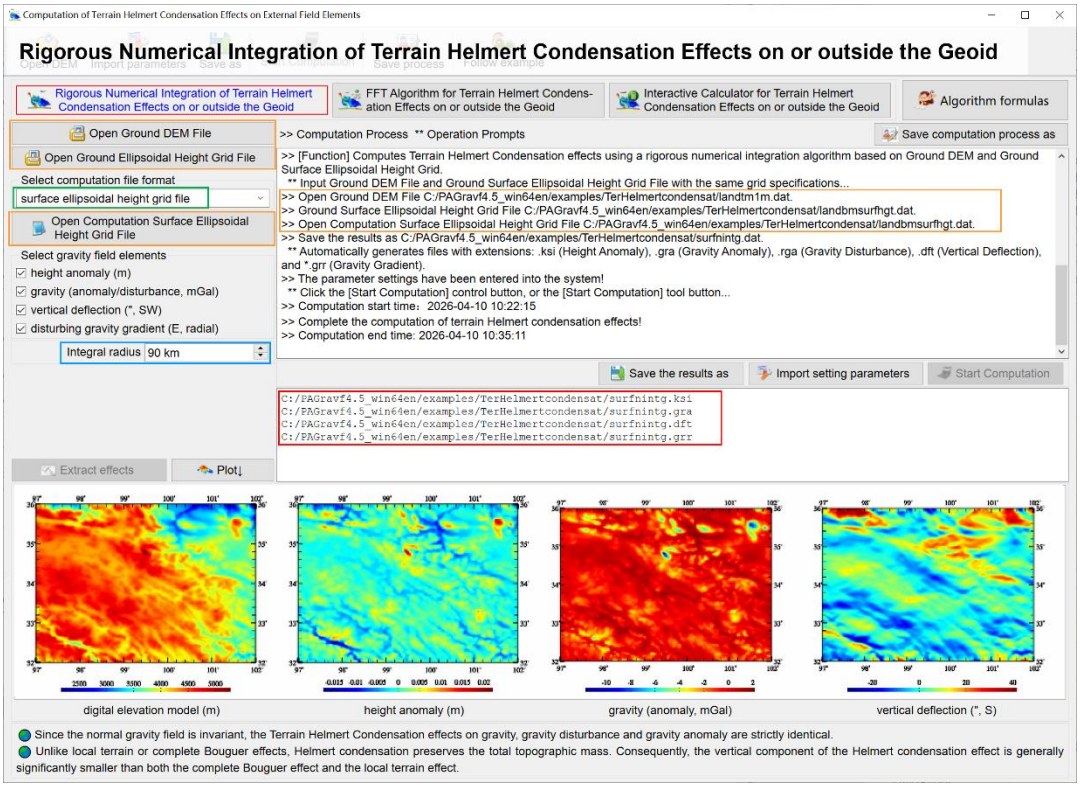

3.3.2 FFT Algorithm for Terrain Helmert Condensation Effects on or outside the Geoid

[Function] Computes Terrain Helmert Condensation effects using the Fast Fourier Transform (FFT) integration algorithm.

[Input Files] Ground DEM, Ground Ellipsoidal Height Grid, and Computation Surface Ellipsoidal Height Grid.

Requirement: All files must share identical grid specifications.

[Parameter Settings]

Field Element Type: Select target element.

Algorithm Variant: Choose between 1D-FFT or 2D-FFT.

Integration Radius: Enter the radius for integration FFT algorithm.

[Output Files]

Result File: Format: ID, Longitude, Latitude, Ellipsoidal Height, [Effect Values...] (4 significant figures).

Grid Files: Generates .ksi, .gra, .rga, .dft, *.grr files.

[Accuracy Assessment: FFT vs. Numerical Integration]

Using identical parameters, the differences between FFT results and rigorous numerical integration were analyzed, and the statistical results as shown in Table 3.5.

Table 3.5: Statistics for the differences between FFT results and rigorous numerical integration

Field Element / Unit	Algorithm	Mean Diff	Std. Dev. Diff	Min Diff	Max Diff
height anomaly (m)	FFT2	0.0008	0.0015	-0.0026	0.0064
	FFT1	0.0007	0.0015	-0.0027	0.0063
gravity (anomaly, disturbance) (mGal)	FFT2	0.0009	0.1262	-0.5535	0.6116
	FFT1	0.0025	0.1255	-0.5085	0.6768
vertical deflection (″, South)	FFT2	-0.0174	0.0404	-0.2220	0.1438
	FFT1	-0.0062	0.0240	-0.2359	0.2179
vertical deflection (″, West)	FFT2	0.0025	0.0804	-0.5046	0.2902
	FFT1	0.0093	0.0306	-0.6211	0.4129
gravity gradient (E)	FFT2	0.0062	0.4810	-17.1773	9.8987
	FFT1	0.0062	0.4799	-16.8811	9.8312

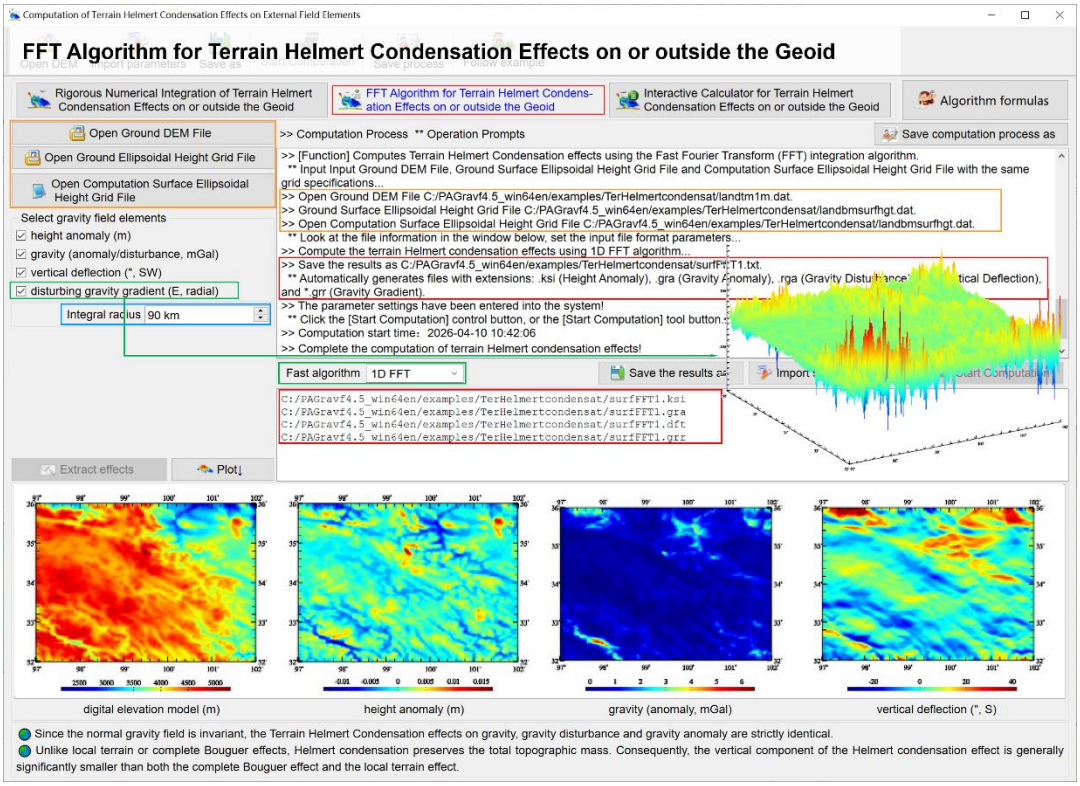

The discrepancies between rigorous numerical integration and fast FFT algorithms are negligible. No significant difference exists between 1D and 2D implementations.

3.3.3 Interactive Calculator for Terrain Helmert Condensation Effects on or outside the Geoid

[Function] Provides a real-time interactive tool to compute Terrain Helmert Condensation effects on gravity field elements at any user-defined geodetic point on or outside the geoid.

[Workflow]

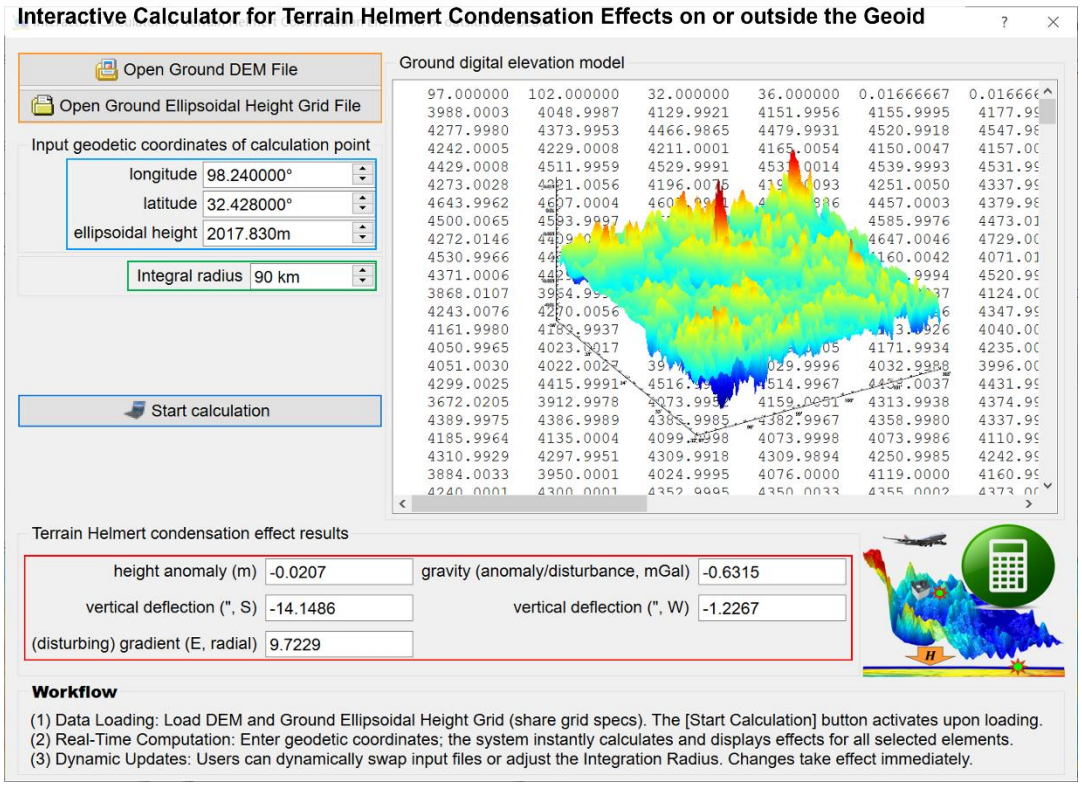

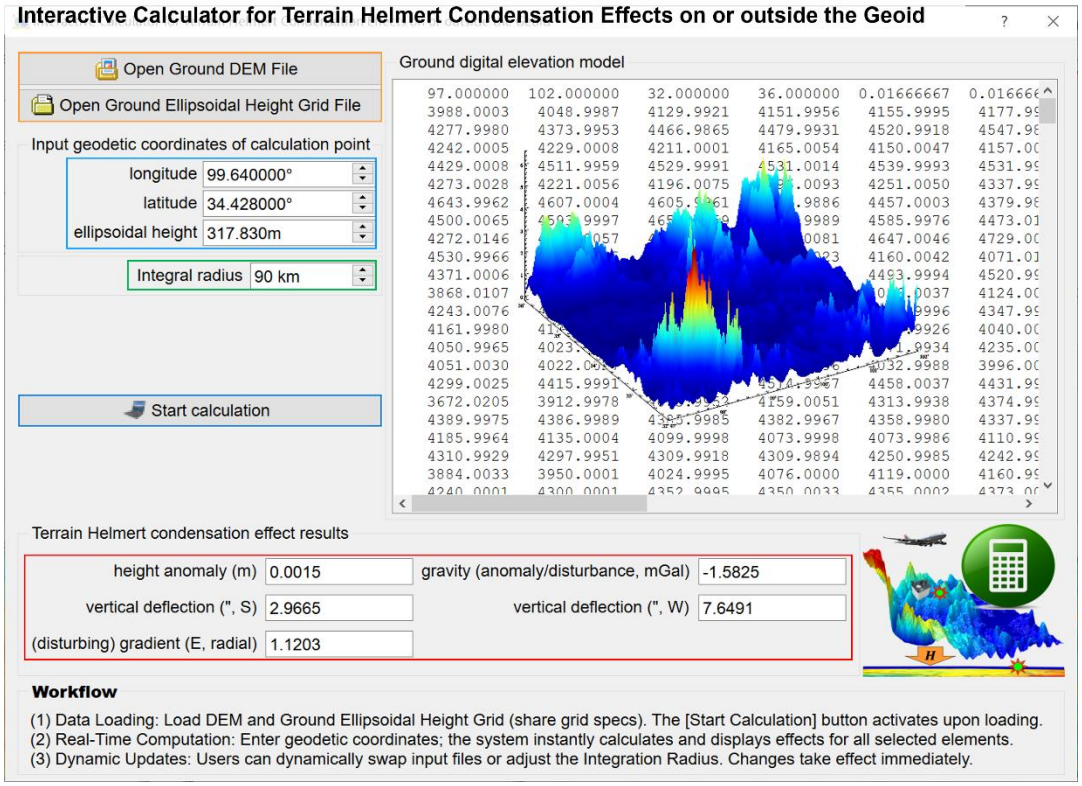

(1) Data Loading: Load DEM and Ground Surface Ellipsoidal Height Grid (must share grid specs). The [Start Calculation] button activates upon loading.

(2) Real-Time Computation: Enter geodetic coordinates; the system instantly calculates and displays effects for all field elements.

(3) Dynamic Updates: Users can dynamically swap input files or adjust the Integration Radius. Changes take effect immediately.

[Applicability] Supports computation points spanning from the geoid up to typical airborne altitudes.

In contrast to the local terrain and complete Bouguer effects, the Helmert condensation technique adheres to the principle of mass conservation, wherein the total topographic mass remains invariant. As a direct result, the vertical component of the terrain effect on gravity field elements generated by Helmert condensation is typically orders of magnitude smaller than that of the complete Bouguer effect and also diminishes relative to the local terrain effect.

3.4 Computation of Residual Terrain Effects (RTE) on External Field Elements

[Purpose] Computes Residual Terrain Effects (RTE) on height anomaly (m), gravity (anomaly/disturbance, mGal), vertical deflection (″; South/West components), and disturbing gravity gradient (E; radial component) on or outside the geoid, utilizing either rigorous numerical integration or the Fast Fourier Transform (FFT) algorithm, leveraging three core datasets: (a) High-resolution land-sea terrain model, (b) Low-pass land-sea terrain model and (c) Ellipsoidal height grid of the land-sea surface.

[Scope & Physical Definition]

(1) Spatial Domain: Computation points may span from the geoid to typical airborne altitudes.

(2) Definition: The Land-Sea Residual Terrain Effect is defined as the aggregate of the short-wavelength and ultra-short-wavelength spectral components of the land-sea complete Bouguer effect. Mathematically, it represents the difference between the effects of the high-resolution topography and its low-pass reference.

(3) Equivalence: Given the invariance of the normal gravity field, RTEs on gravity disturbance and gravity anomaly are strictly equivalent to the RTE on gravity itself.

(4) Reference Model Construction:

○ The low-pass model can be generated via spatial domain low-pass filtering or, preferably, via spherical harmonic synthesis from a global land-sea terrain mass coefficient model.

○ Recommendation: Spherical harmonic synthesis is strongly recommended to construct the low-pass reference, as it ensures a spectrally consistent separation of long-wavelength signals, thereby optimizing the approximation performance of the gravity field.

(5) Equivalence Principle: Given the invariance of the normal gravity field, the Residual Terrain Effects (RTEs) on gravity disturbance and gravity anomaly are strictly equal to the RTE on gravity itself.

3.4.1 Rigorous Numerical Integration of Land-Sea Residual Terrain Effects on or outside the Geoid

[Function] Computes RTEs using rigorous numerical integration based on the high-resolution and low-pass terrain models.

[Pre-processing Logic]

RTM Generation: The program computes the Residual Terrain Model (RTM) by subtracting the low-pass model from the high-resolution model (both must share identical grid specs).

Land-Sea Masking: The high-resolution model is employed to distinguish terrestrial and marine domains.

Zero-Degree Term Removal: Since finite-radius integration cannot account for the zero-degree term (DC component) of the terrain, the program automatically removes the mean value of the RTM prior to integration.

[Input Files]

(1) High-Resolution Land-Sea Terrain Model File [Terrain elevation > 0 (land); Bathymetric depth <0 (sea)].

(2) Low-Pass Land-Sea Terrain Model File.

(3) Land-Sea Surface Ellipsoidal Height Grid File: Provices the geodetic coordinates of Land-Sea Surface for integration distance derivation.

○ Requirement: All three files must share identical grid specifications.

(4) Space Computation Point File or Computation Surface Ellipsoidal Height Grid File.

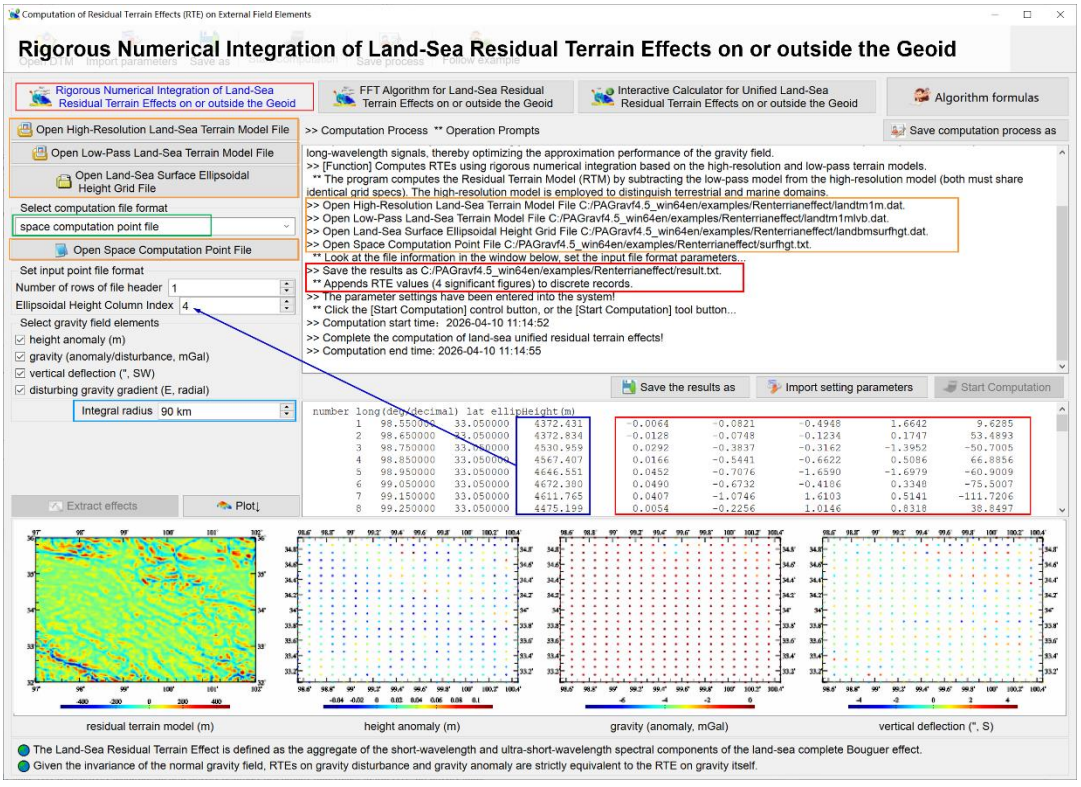

[Parameter Settings] File Format, Field Element Type, and Integration Radius.

[Output Files]

Result File: Appends RTE values (4 significant figures) to discrete records.

Grid Files: Generates .ksi, .gra, .dft, .grr files in the current directory.

[Case Study & Statistical Analysis]

Setup: 1′×1′ high-res model; Low-pass model synthesized from a degree-1440 global spherical harmonic model. Integration radius: 90 km. A 1° marginal buffer was excluded.

Statistics: As shown in Table 3.6, where D = Range [Max-Min], ε = Standard Deviation.

Table 3.6: Statistical Results of Land-sea Residual Terrain Effects on Various Ground Gravity Field Elements

Field element type /Unit	Mean	Std. Dev. (ε)	Minimum	Maximum	D/ε
height anomaly /m	0.0188	0.0566	-0.2151	0.3835	10.2
gravity(anomaly, disturbance) /mGal	0.5342	1.0570	-1.6605	13.2024	14.1
vertical deflection /S″	-0.0000	0.8730	-4.7838	4.6030	10.8
vertical deflection /W″	-0.0075	0.8157	-6.2512	5.1511	14.0
(disturbing) gravity gradient /E	-7.0310	300.1898	-928.6079	884.6364	6.0

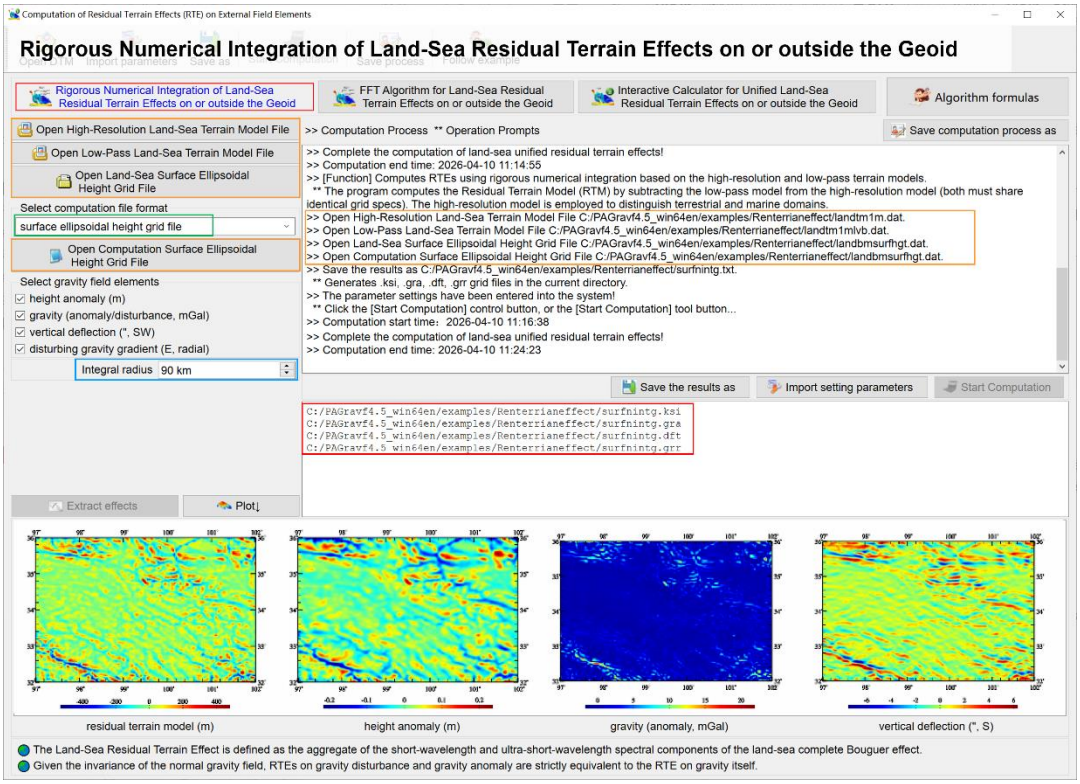

[Discussion & Applicability]

Special Case: If a zero-value grid serves as the low-pass model, the output approximates the Land-Sea Complete Bouguer effect (excluding far-zone contributions). In this scenario,

an integration radius ⩾ 300 km is required.

Spectral Control: The spectral characteristics of the RTM are directly regulated by the choice of the low-pass reference model.

Suitability Assessment: Based on the D/ε ratio (comparing against Local Terrain and Helmert Condensation effects):

○ Geoid Modeling: RTE is highly favorable for height anomaly determination (D/ε=10.2), as it preserves relevant medium-to-long wavelengths while removing smooth references.

○ Vertical Deflection: Suitable for processing vertical deflection data (e.g., satellite altimetry), showing balanced signal content ($D/\varepsilon \approx 10.8$ to 14.0).

○ Gravity Gradients: Less favorable. The removal of high-frequency components by the low-pass reference significantly attenuates the gradient signal (D/ε=6.0), making it less effective than other methods for this specific element.

Sign Distribution: RTE values exhibit bipolar behavior (positive and negative) across both terrestrial and marine regions, reflecting the residual nature of the topography.

3.4.2 FFT Algorithm for Land-Sea Residual Terrain Effects on or outside the Geoid

[Function] Computes RTEs using the Fast Fourier Transform (FFT) integration algorithm with the same input datasets as Section 3.4.1.

[Input Files]

(1) High-Resolution Land-Sea Terrain Model.

(2) Low-Pass Land-Sea Terrain Model.

(3) Land-Sea Surface Ellipsoidal Height Grid.

(4) Computation Surface Ellipsoidal Height Grid.

Requirement: All files must share identical grid specifications.

[Parameter Settings] Field Element Type, FFT Variant (1D/2D), and Integration Radius.

[Output Files]

Result File: Formatted records with 4 significant figures.

Grid Files: Automatic generation of .ksi, .gra, .dft, .grr files.

[Accuracy Assessment: FFT vs. Numerical Integration]

Using identical parameters, the differences between FFT results and rigorous numerical integration were analyzed, and the statistical results as shown in Table 3.7.

Table 3.7: Statistics for the differences between FFT results and rigorous numerical integration

Field Element / Unit	Algorithm	Mean Diff	Std. Dev. Diff	Min Diff	Max Diff
height anomaly (m)	FFT2	-0.0129	0.0335	-0.2051	0.1237
	FFT1	-0.0096	0.0242	-0.1514	0.0870
gravity (anomaly, disturbance) (mGal)	FFT2	0.1031	0.2585	-0.4320	3.0334
	FFT1	0.0328	0.2266	-0.7472	1.3431
vertical deflection (″, South)	FFT2	0.0001	0.3380	-1.7813	1.8500
	FFT1	0.0002	0.0021	-0.0248	0.0334

vertical deflection (″, West)	FFT2	0.0029	0.3145	-1.9819	2.3883
	FFT1	0.0001	0.0040	-0.1178	0.0822
gravity gradient (E)	FFT2	0.4968	15.1962	-67.4822	97.0052
	FFT1	-0.0239	0.3995	-10.3352	4.9832

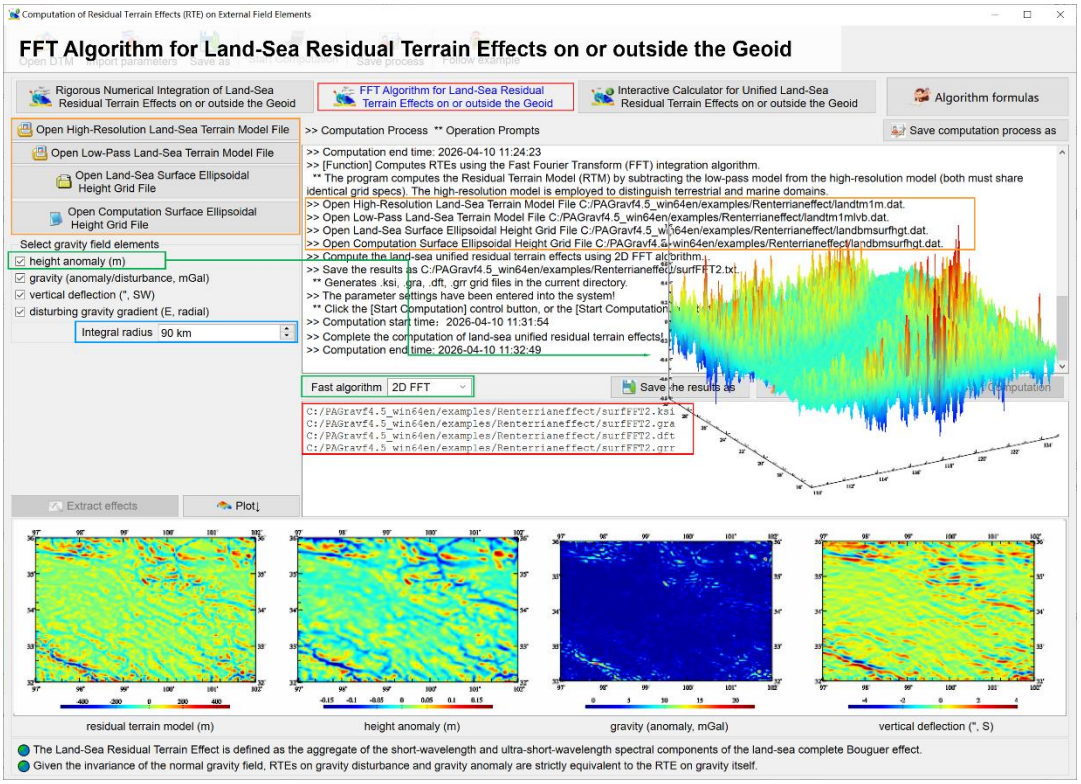

3.4.3 Interactive Calculator for Unified Land-Sea Residual Terrain Effects on or outside the Geoid

[Function] Computes unified land-sea residual terrain effects on height anomaly (m), gravity (anomaly/disturbance, mGal), vertical deflection (″; South/West components), and disturbing gravity gradient (E; radial component) at a user-defined point specified by its geodetic coordinates. The computation relies on three core datasets: (a) High-resolution land-sea terrain model, (b) Low-pass land-sea terrain model, and (c) land-sea surface ellipsoidal height grid.

Requirement: All input grids must share identical grid specifications.

[Workflow & Interaction]

Initialization: Upon loading the three required grid files (with matching specifications), the [Start Calculation] button is automatically activated.

Real-Time Computation: Users can iteratively input geodetic coordinates. The system instantly computes and displays the Residual Terrain Effects (or Complete Bouguer Effects, depending on the configuration) for all selected field elements at the specified location.

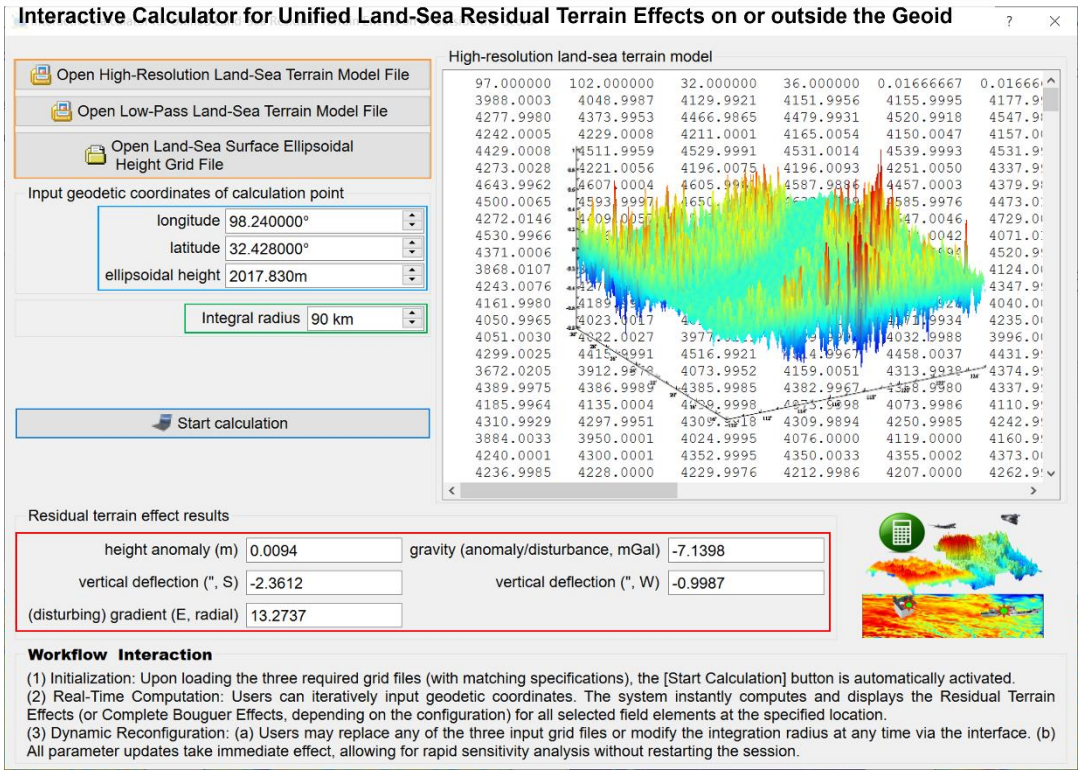

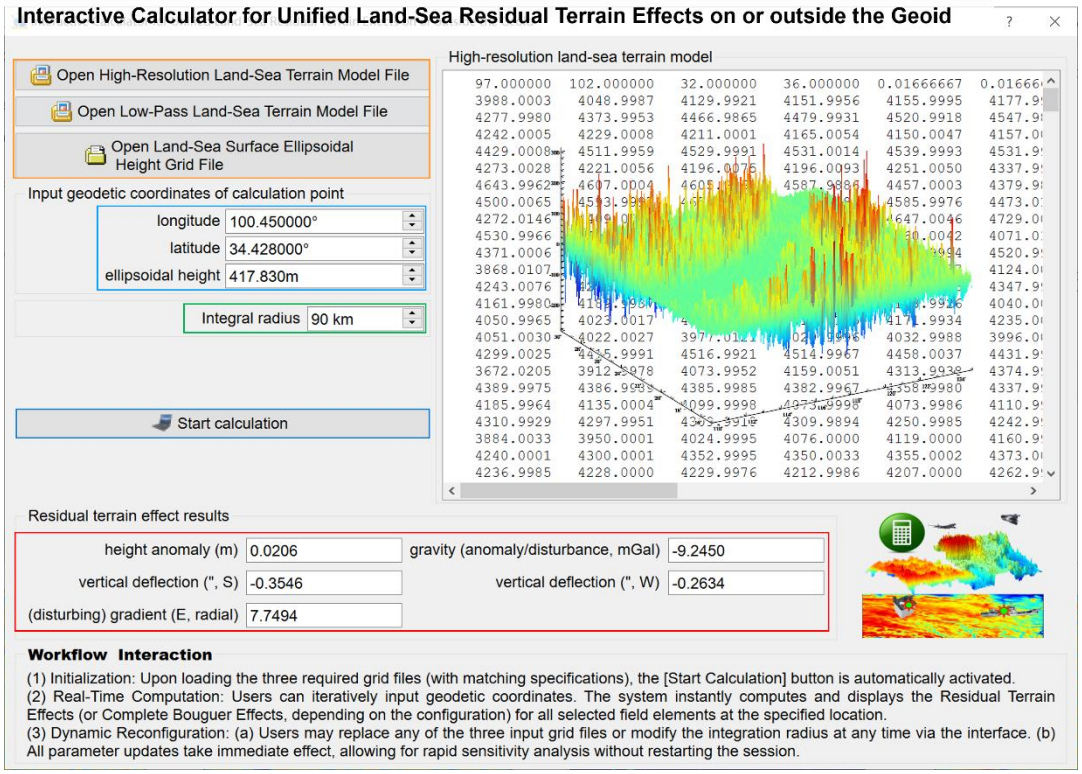

Dynamic Reconfiguration:

- Users may replace any of the three input grid files or modify the integration radius

at any time via the interface.

○ All parameter updates take immediate effect, allowing for rapid sensitivity analysis without restarting the session.

[Spatial Applicability]

Supports computation points spanning from the geoid up to typical airborne altitudes in near-Earth space.

3.5 Computation of Unified Land-Sea Classical Gravity Bouguer and Isostatic Effects

[Purpose] To compute the unified land-sea classical Bouguer effect and isostatic (equilibrium) effect on surface gravity, utilizing a land-sea terrain model.

Sign Convention: The terrain effect is defined as the negative of the classical terrain correction. Plane Layer Effect =− Plane Layer Correction; and Seawater Bouguer Effect =− Seawater Bouguer Correction.

The Classical Bouguer and Isostatic Gravity Anomales/Disturbances are strictly defined on the geoid. The computation points for Classical Bouguer and Isostatic Effects are defined only on land-sea surface.

3.5.1 Integration of Unified Land-Sea Classical Gravity Bouguer and Isostatic Effects

[Function] Computes the unified land-sea classical Bouguer and isostatic effects on surface gravity (mGal) based on the input land-sea terrain model and land-sea surface ellipsoidal height grid files.

[Input Files]

(1) Land-Sea Terrain Model File: Terrain elevation > 0 (land); Bathymetric depth <0 (sea).

(2) Land-Sea Surface Ellipsoidal Height Grid File: Provices the geodetic coordinates of the land-sea surface for integration distance derivation.

○ Requirement: Both files must share identical grid specifications.

(3) Land-sea Surface Computation Point File or Land-sea Computation Surface Ellipsoidal Height Grid File (for integration distance derivation).

[Parameter Settings]

File Format: Configure input parsing parameters.

Integration Algorithm: Select the numerical method.

Integration Radii: Specify distinct radii for land and sea domains.

Local Terrain Effect: Dominated by ultra-short-wavelength components; an integration radius of approximately 100 km is typically sufficient.

Seawater Bouguer & Isostatic Effects: Contain significant medium- and long-wavelength components; thus, their integration radii must be substantially larger than those used for local terrain effects to ensure full spectral capture.

[Output Files]

Discrete Input: Appends seven columns of effect values to the source record (4 significant figures): Local Terrain, Plane Layer, Seawater Bouguer, Land Isostatic, Ocean Isostatic, Total Bouguer, Total Isostatic.

Grid Input: Outputs formatted records: ID, Lon, Lat, h, [Seven Effect Values...].

Grid Output Files if Grid Input: Automatically generates: Unified Land-Sea Total Bouguer Effect: .bgr, and Unified Land-Sea Total Isostatic Effect: .ist.

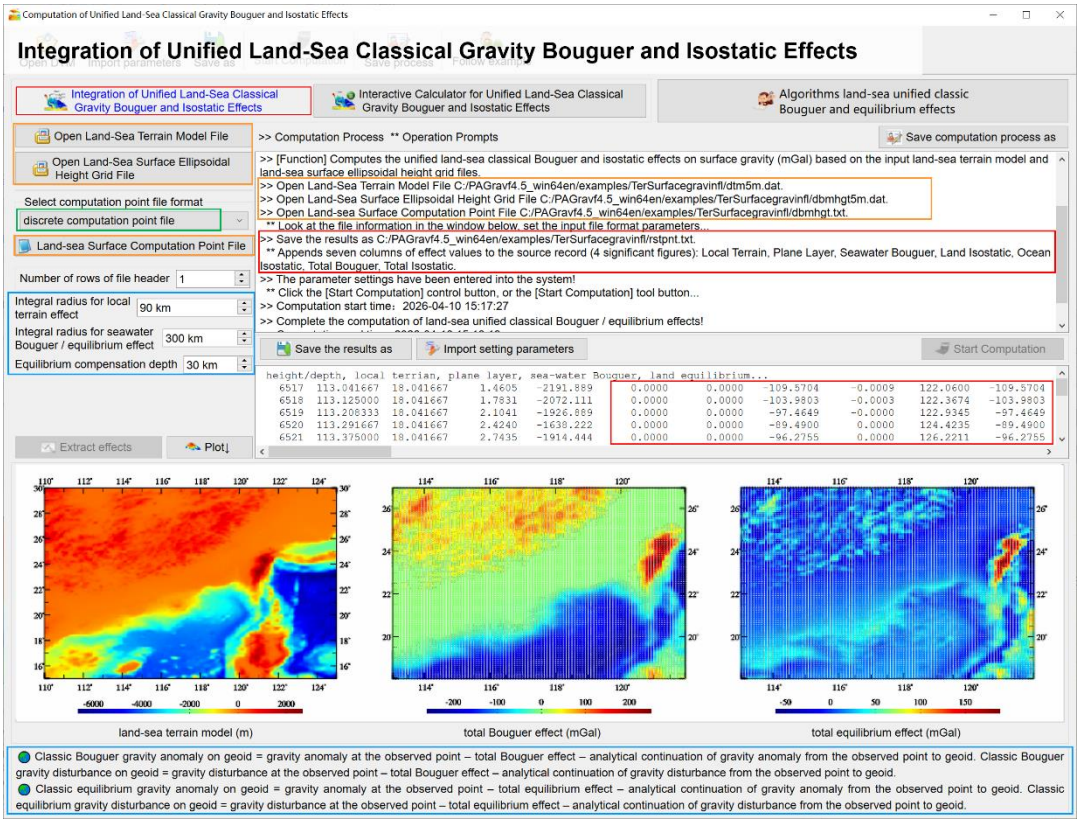

[Applicability & Post-Processing Workflow]

Scope: Designed for seamless computation across terrestrial, coastal transition, and marine domains.

Analytical Continuation: Users requiring analytical continuation (downward/upward continuation to the geoid) should utilize modules within the [Earth Gravity Field Data Analysis and Preprocessing] subsystem.

Two-Step Computation Protocol (The Classical Bouguer/Isostatic Gravity Anomaly (or Disturbance) on the Geoid is derived via the following rigorous two-step process):

● Acquire Observed Anomaly: Obtain the gravity anomaly or disturbance $\square g$ ($= \Delta g$ or δg) at the observation point from terrestrial, marine, or airborne observations (or a global geopotential model).

● Apply Corrections & Continuation:

○ Execute this program to obtain the Total Bouguer/Isostatic Effect (e^W).

○ Compute the Analytical Continuation term ($\square g^{ac}$) from the observation point to the geoid.

○ Final Formula: $\square g^W$ (Bouguer/Isostatic anomaly/disturbance on Geoid) $=$ $\square g$ (Observed anomaly/disturbance) $- e^W - \square g^{ac}$ (where $W = B$ or I, $\square = \Delta$ or δ).

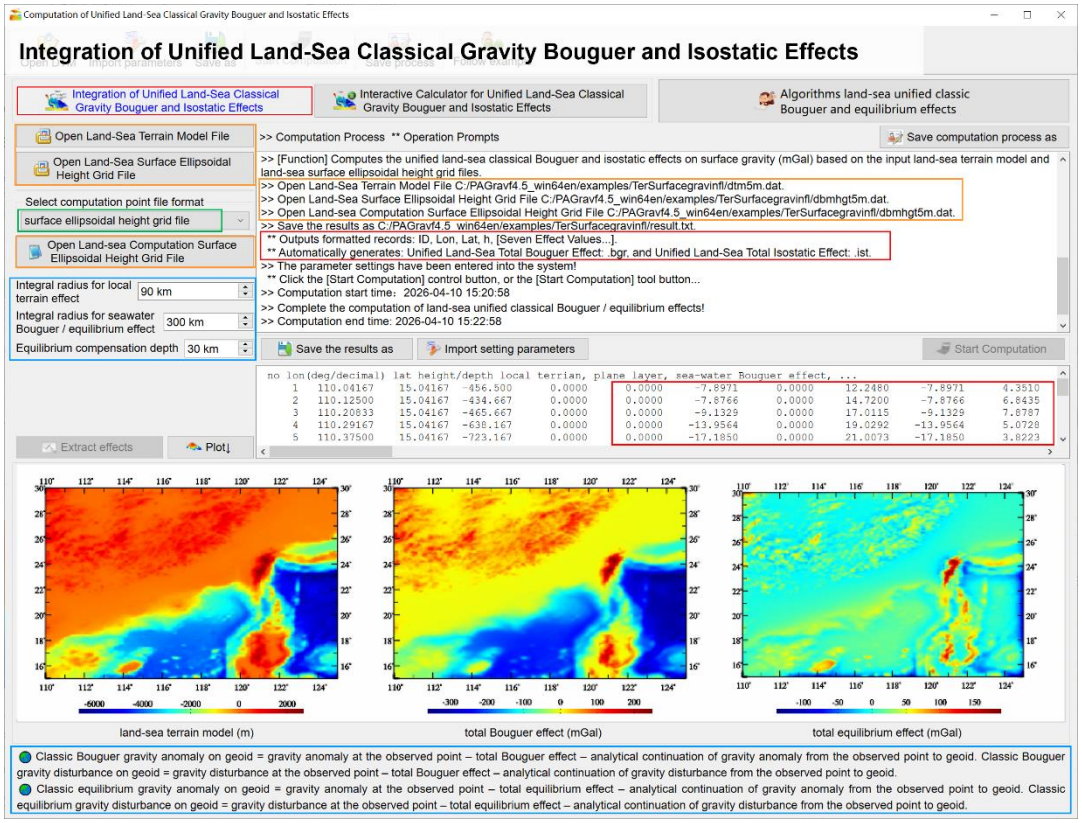

Classic Bouguer gravity anomaly on geoid = gravity anomaly at the observed point – total Bouguer effect – analytical continuation of gravity anomaly from the observed point to geoid. Classic Bouguer gravity disturbance on geoid = gravity disturbance at the observed point – total Bouguer effect – analytical continuation of gravity disturbance from the observed point to geoid.

Classic equilibrium gravity anomaly on geoid = gravity anomaly at the observed point – total equilibrium effect – analytical continuation of gravity anomaly from the observed point to geoid. Classic equilibrium gravity disturbance on geoid = gravity disturbance at the observed point – total equilibrium effect – analytical continuation of gravity disturbance from the observed point to geoid.

3.5.2 Interactive Calculator for Unified Land-Sea Classical Gravity Bouguer and Isostatic Effects

[Function] Provides a real-time interactive tool to compute unified land-sea classical Bouguer and isostatic effects (mGal) at any user-defined geodetic coordinate (Longitude/Latitude), based on the land-sea terrain model and land-sea surface ellipsoidal height grid files.

[Sign Conventions & Physical Characteristics] The computed effects generally adhere to the following sign conventions ('+' for positive, '-' for negative):

- Plane Layer Effect: Always (+)
- Seawater Bouguer Effect: Always (-)

- Land Isostatic Effect: Always (-)
- Ocean Isostatic Effect: Always (+)

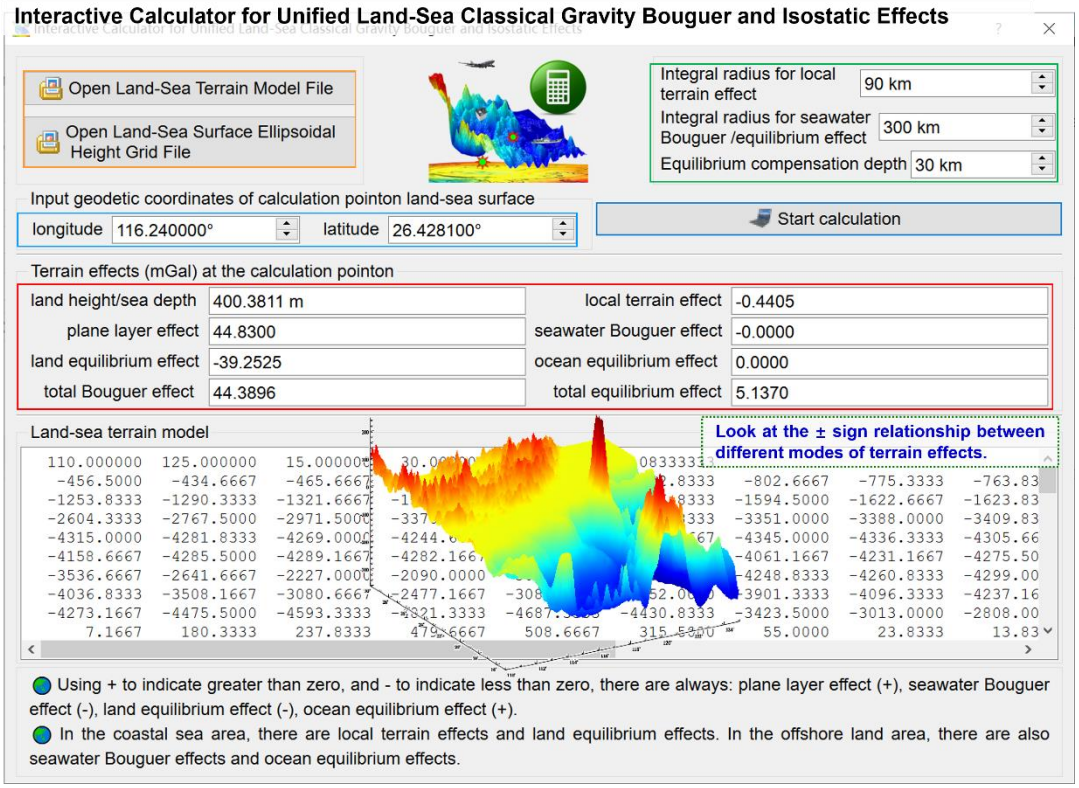

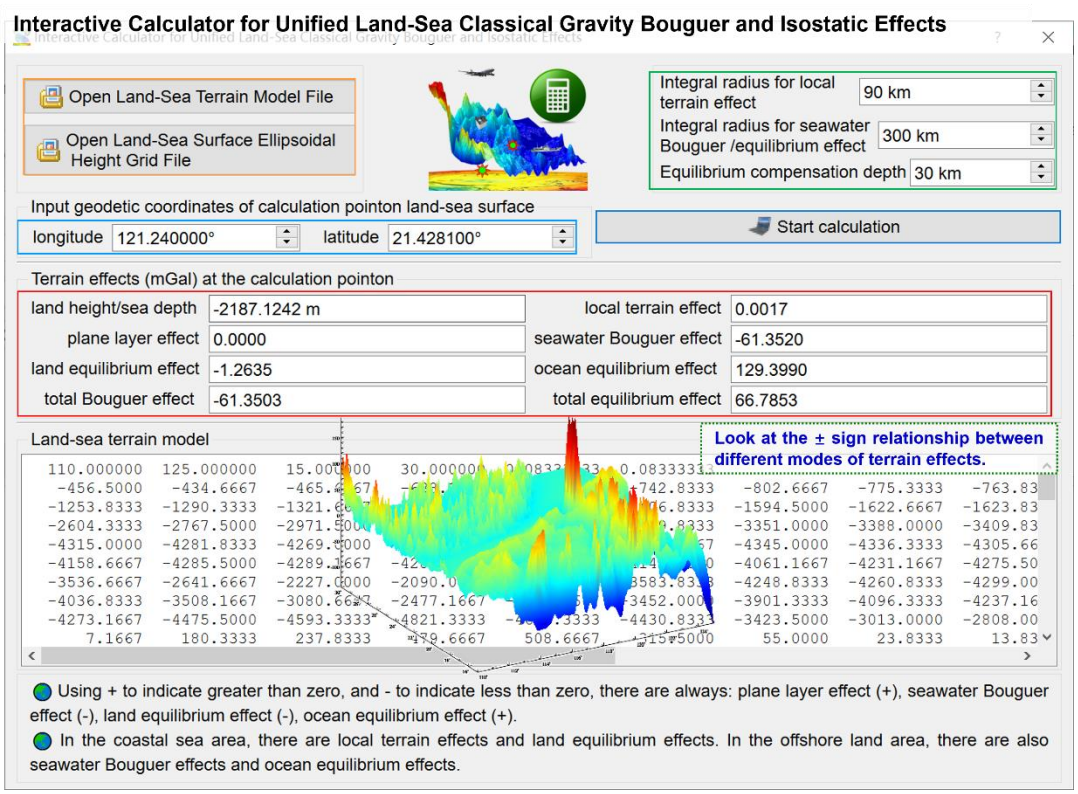

[Coastal Transition Behavior]

● Coastal Sea Areas: Results include contributions from Local Terrain Effects and Land Isostatic Effects due to proximity to land masses.

● Offshore Land Areas: Results include contributions from Seawater Bouguer Effects and Ocean Isostatic Effects due to proximity to marine basins.

[Mathematical Formulation] $\square g^{W} = \square g - e^{W} - \square g^{ac}$ (where $W = B$ or I, $\square = \Delta$ or δ).

● Δg^{B} /δg^{B}: Classical Bouguer gravity anomaly/disturbance on the geoid

● Δg^{I} /δg^{I}: Classical equilibrium gravity anomaly/disturbance on the geoid

● e^{B}/ e^{I}: Total Bouguer/ equilibrium effect

● Δg^{ac}/δg^{ac}: Analytical continuation of the gravity anomaly/disturbance from the observation point to the geoid

3.6 Ultra-High-Degree Spherical Harmonic Analysis and Construction of Land-Sea Terrain Model

[Purpose] To conduct spherical harmonic analysis on global land-sea terrain grids (encompassing topographic elevation and oceanic bathymetry) and construct a fully normalized global land-sea terrain mass spherical harmonic coefficient model. This model serves as the fundamental basis for computing unified land-sea complete Bouguer effects or residual terrain effects (RTE) on various gravity field elements, both on the geoid and throughout the exterior space of the Earth.

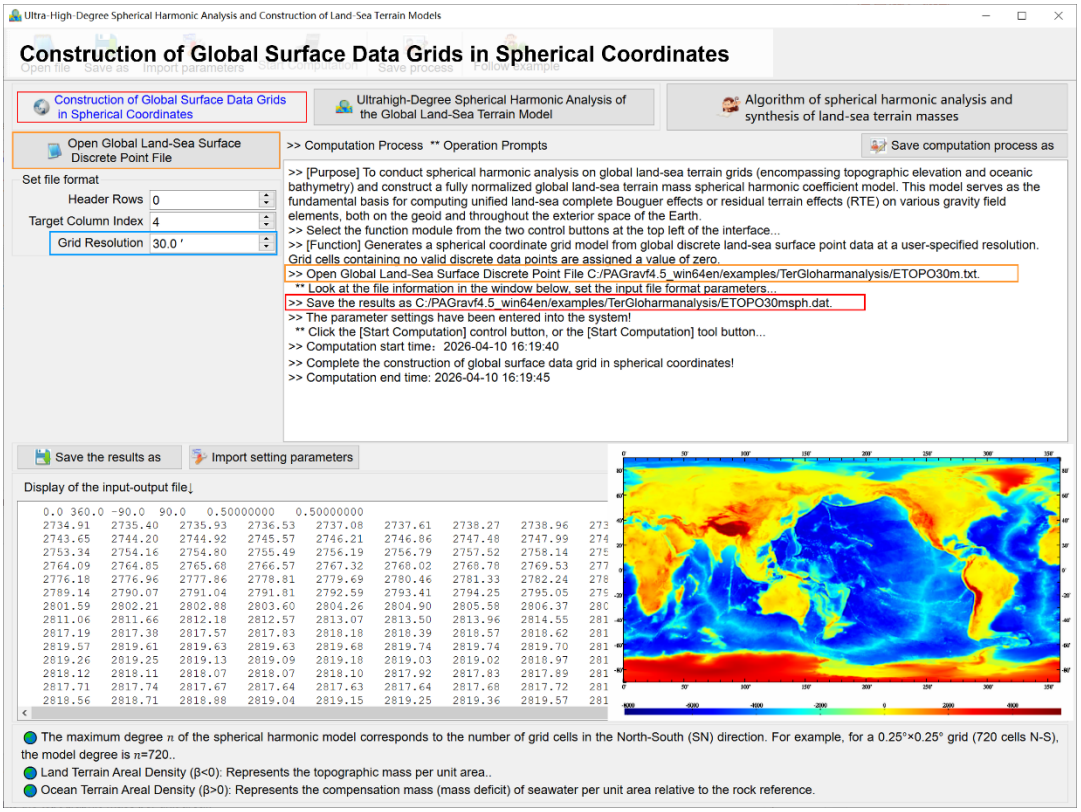

3.6.1 Construction of Global Surface Data Grids in Spherical Coordinates

[Function] Generates a spherical coordinate grid model from global discrete land-sea surface point data at a user-specified resolution. Grid cells containing no valid discrete data points are assigned a value of zero.

[Input File] Global Land-Sea Surface Discrete Point File.

Record Format: ID (Point Number/Name), Longitude, Latitude (decimal degrees), ..., Target Attribute, ...

[Parameter Settings]

File Header Rows: Enter the number of header lines to skip in the point file.

Target Column Index: Enter the column ordinal number of the attribute to be gridded.

Grid Resolution: Spatial resolution of the output grid (e.g., 0.25°×0.25°).

[Output File] Spherical Coordinate Grid File.

3.6.2 Ultrahigh-Degree Spherical Harmonic Analysis of the Global Land-Sea Terrain Model

[Function] Performs spherical harmonic analysis on the spherical grid model to derive the land-sea terrain mass expressed as areal density, generating a fully normalized global land-sea terrain mass spherical harmonic coefficient model (Unit: kg/m²).

[Physical Definitions & Sign Conventions]

Land Terrain Areal Density ($\beta<0$): Represents the topographic mass per unit area.

● $\beta = h\times\rho$, where h is the land surface elevation and ρ is the topographic mass density.

Ocean Terrain Areal Density ($\beta>0$): Represents the compensation mass (mass deficit) of seawater per unit area relative to the rock reference.

● $\beta = d\times(\rho_w-\rho)$, where d is the sea bathymetry and ρ_w is the seawater density.

[Degree Determination]

The maximum degree n of the spherical harmonic model corresponds to the number of grid cells in the North-South (NS) direction.

● Example: For a 0.25°×0.25° grid (720 cells NS), the model degree is n =720.

[Input File] Global Land-Sea Terrain Grid File (in spherical coordinates).

[Parameter Settings] Iteration Convergence Criteria: Define thresholds for terminating the iterative least-squares adjustment:

(1) Relative Residual Threshold (%): Terminate if the standard deviation (STD) of the residual areal density is $<a$ % of the STD of the source areal density.

(2) Convergence Rate Threshold (b ‰): Terminate if the difference between the residual STD of the current step and the previous step is $<b$ ‰ of the source STD.

(Termination occurs upon meeting either condition.)

[Output Files]

(1) Land-Sea Terrain Mass Spherical Harmonic Coefficient Model.

Coefficient File Header Information: The header includes critical scale and quality parameters: Geocentric Gravitational Constant (GM, 10^{14}m³/s²), Equatorial Radius (a, m), Zero-Degree Term ($a\,\Delta C$, kg/m²), and Relative Error (Θ%, Percentage ratio of the final

residual STD to the source grid STD).

Note: GM and a act as the scale parameters for the model.

Physical Interpretation of Low-Degree Terms

○ Zero-Degree Term (aC_{00}, kg/m²): Represents the variation in total Earth mass induced by terrain density changes. Under the principle of Earth Mass Conservation, this term is physically null and typically removed.

○ First-Degree Terms (ΔC_{10}, ΔC_{11}, ΔS_{11}): Represent the shift in the Earth's Center of Mass (Geocenter) caused by the redistribution of terrain mass.

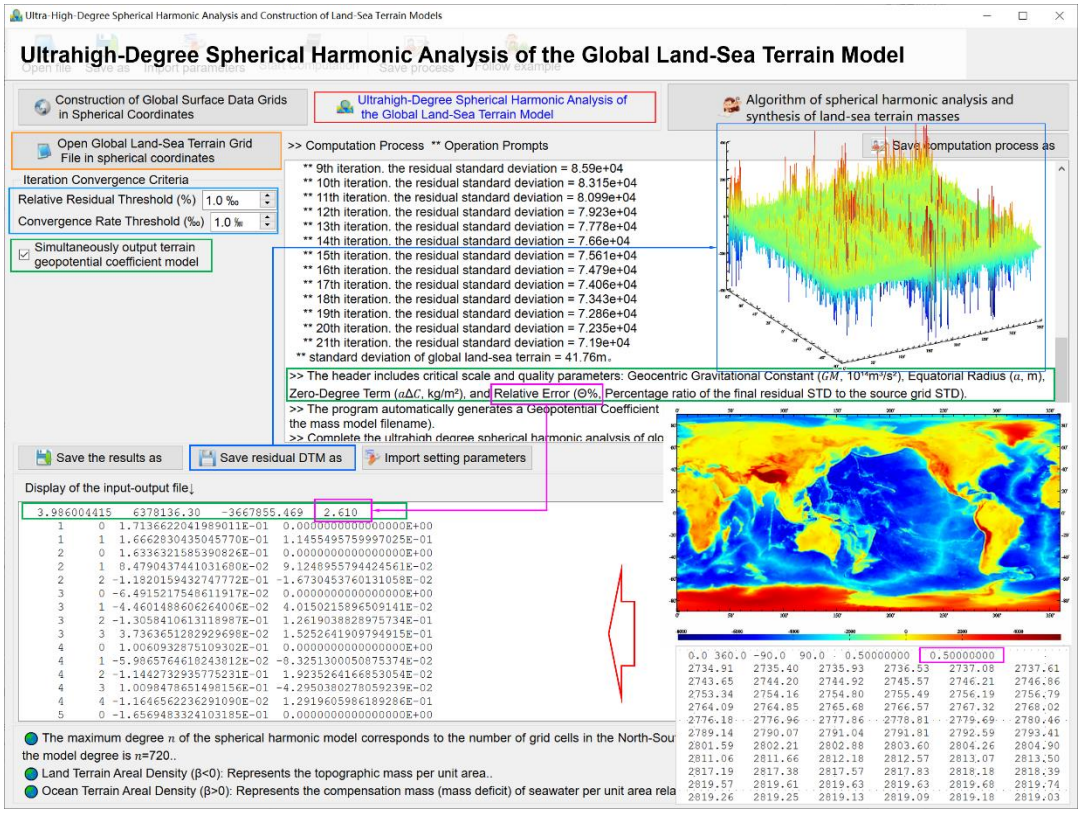

(2) Residual Land-Sea Terrain Grid File.

(3) Additional Output: The program automatically generates a Geopotential Coefficient Model file named *geop.dat in the current directory (where * matches the terrain mass coefficient model filename).

[Execution Monitoring]

● The computation employs an iterative algorithm and may require significant processing time.

● Users can monitor real-time progress by opening Harminf.txt in the current directory.

● Log Format: Iteration Count, Mean, Standard Deviation, Minimum, Maximum (statistics of the residual areal density).

3.7 Spherical Harmonic Synthesis of Complete Bouguer or Residual Terrain Effects

[Purpose] To perform spherical harmonic synthesis based on a global land-sea terrain mass spherical harmonic coefficient model (kg/m²) to derive:

(a) Model values of terrain elevation and sea bathymetry.

(b) Unified land-sea complete Bouguer effects or residual terrain effects (RTE) on various gravity field elements at points on the geoid or anywhere in the exterior Earth space.

(c) Comprehensive analysis of the spectral-domain and spatial-domain properties of global land-sea terrain effects.

[Physical Principles & Equivalence]

Since given the invariance of the normal gravity field, the terrain effect on gravity disturbance and gravity anomaly is strictly equivalent to the effect on gravity itself, and the terrain effect on the disturbing potential is strictly equivalent to the effect on the geopotential.

[Applicability] Designed for seamless computation across terrestrial, coastal transition, and marine domains. Computation points may reside on the geoid or at any altitude outside the geoid.

[Spectral Analysis Capabilities]

By setting identical minimum ($n_{\min}$) and maximum ($n_{\max}$) degrees, the program computes the contribution of specific degree-n coefficients to gravity field elements. Users can evaluate model performance by analyzing:

(a) Single-Degree Effects: Contribution from a specific degree n.

(b) Cumulative Effects: Summation from degree 1 up to n.

(c) Band-Pass Effects: Contribution within a specific degree band $n_{\min}$ to $n_{\max}$.

3.7.1 Computation of Model Values for Complete Bouguer or Residual Terrain Effects

[Function] Computes model values for terrain elevation/ sea bathymetry and unified land-sea effects (Complete Bouguer or RTE) on the following elements using spherical harmonic synthesis: Height Anomaly (m), Gravity (Anomaly/Disturbance, mGal), Vertical Deflection Vector (″; South/West components), Disturbing Gravity Gradient (E; Radial component), Tangential Gravity Gradient Vector (E; North/West components), and Disturbing Geopotential (m²/s²).

Note: The required coefficient model can be generated via Module 3.6.

[Input Files]

(1) Global Land-Sea Terrain Mass Spherical Harmonic Coefficient Model File (kg/m²).

Header Parameters: Geocentric Gravitational Constant (GM, 10^{14}m³/s²), Equatorial Radius (a, m), Zero-Degree Term ($a\Delta C$, kg/m²), and Relative Error (Θ%, Percentage ratio of the final residual STD to the source grid STD). (GM, a) serve as the scale parameters.

(2) Space Computation Point File OR Computation Surface Ellipsoidal Height Grid File.

Point File record Format: ID/Name, Longitude (deg), Latitude (deg), Ellipsoidal Height (m), ...

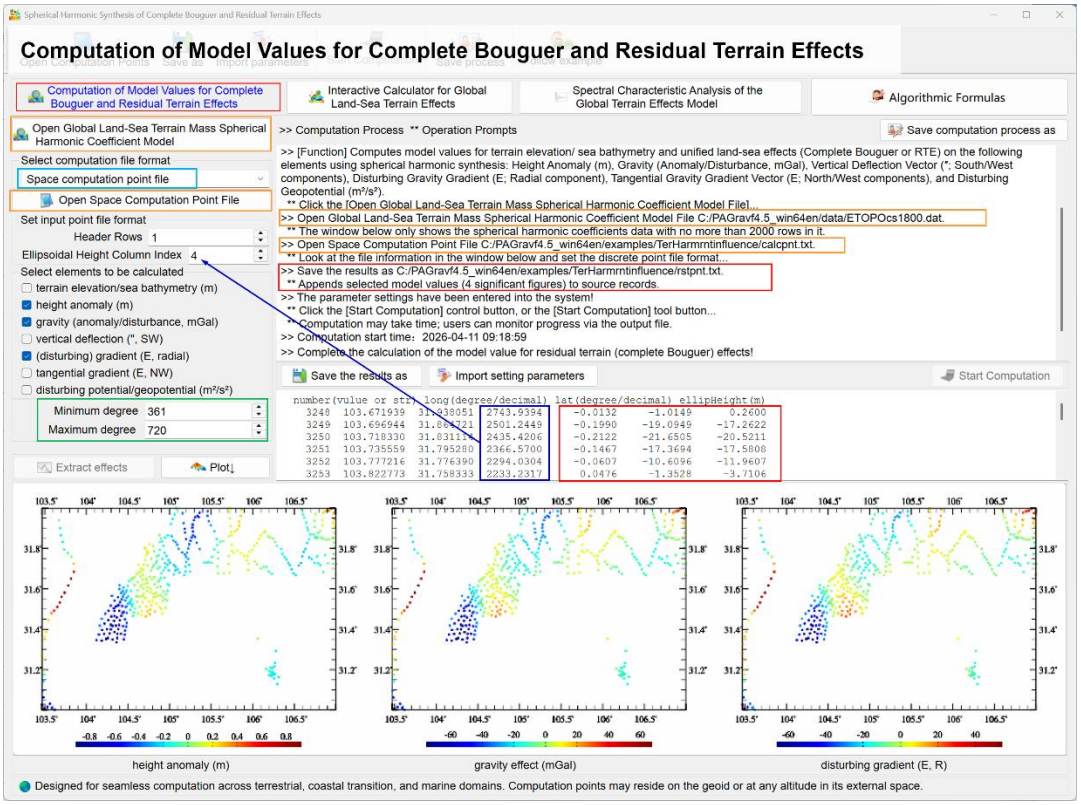

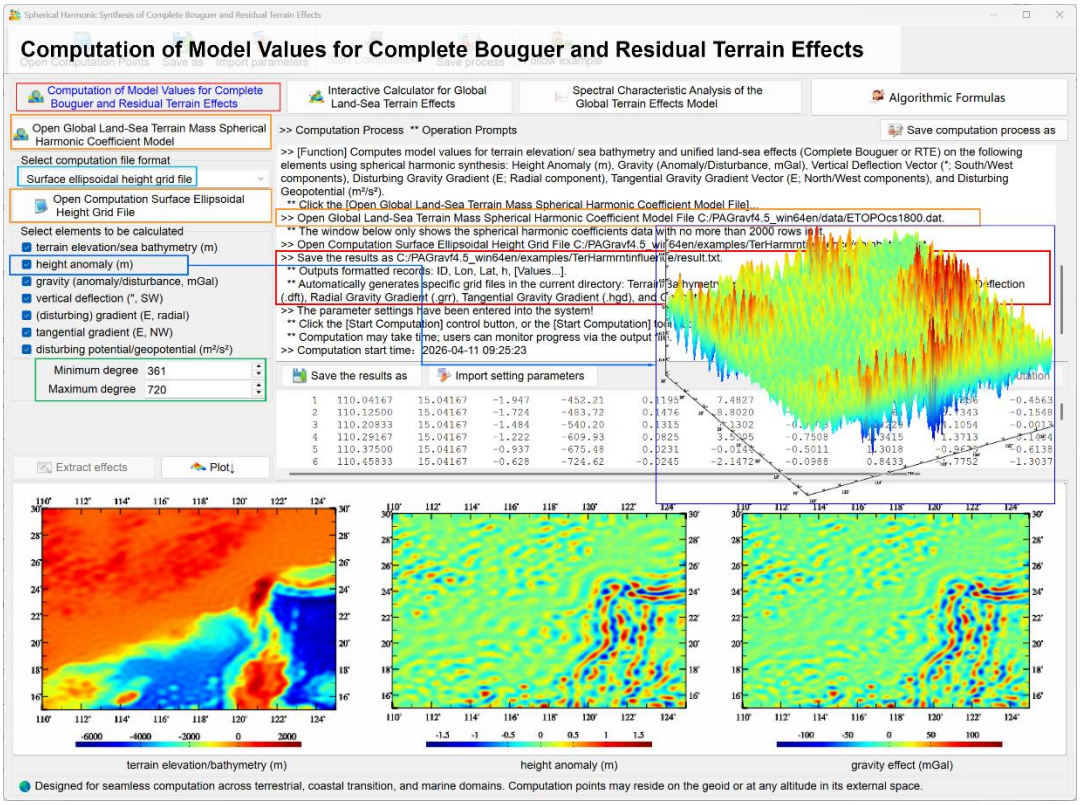

[Parameter Settings]

File Format: Define parsing rules for the input point file.

Degree Range: Specify $n_{\min}$ and $n_{\max}$.

○ Complete Bouguer Mode: Activated if $n_{\min}=1$.

○ Residual Terrain Mode: Activated if $n_{\min}>1$.

○ Truncation: Automatically adopts the smaller of the model's maximum degree and the user-input maximum degree as the actual computation limit.

Element Selection: Choose specific gravity field elements for computation.

[Execution Status]

Computation may take time; users can monitor progress via the output file.

[Output Files]

Discrete Input: Appends selected model values (4 significant figures) to source records.

Grid Input: Outputs formatted records: ID, Lon, Lat, h, [Values...].

Grid Output Files if Grid input: Automatically generates specific grid files in the current directory: Terrain/Bathymetry (m), Height Anomaly (.ksi), Gravity (.gra), Vertical Deflection (.dft), Radial Gravity Gradient (.grr), Tangential Gravity Gradient (.hgd), and Geopotential (.get).

Note: When computing elevation/bathymetry values, the ellipsoidal height of the computation point is ignored.

3.7.2 Interactive Calculator for Global Land-Sea Terrain Effects

[Function] Provides a real-time interactive tool to compute model values for terrain elevation/sea bathymetry and Complete Bouguer/RTE (including all vector and tensor components listed in 3.7.1) at any user-defined geodetic coordinate.

Use Case: Ideal for classroom demonstrations and rapid single-point queries.

Note: Loading ultra-high-degree models requires initialization; please wait during this process.

3.7.3 Spectral Characteristic Analysis of the Global Terrain Effects Model

[Function] Calculates the degree variances for the land-sea terrain geopotential models and a global geopotential model.

Property Analysis: Analyzes the spectral and spatial characteristics of Complete Bouguer and Residual Terrain effects based on the derived degree variance curves.

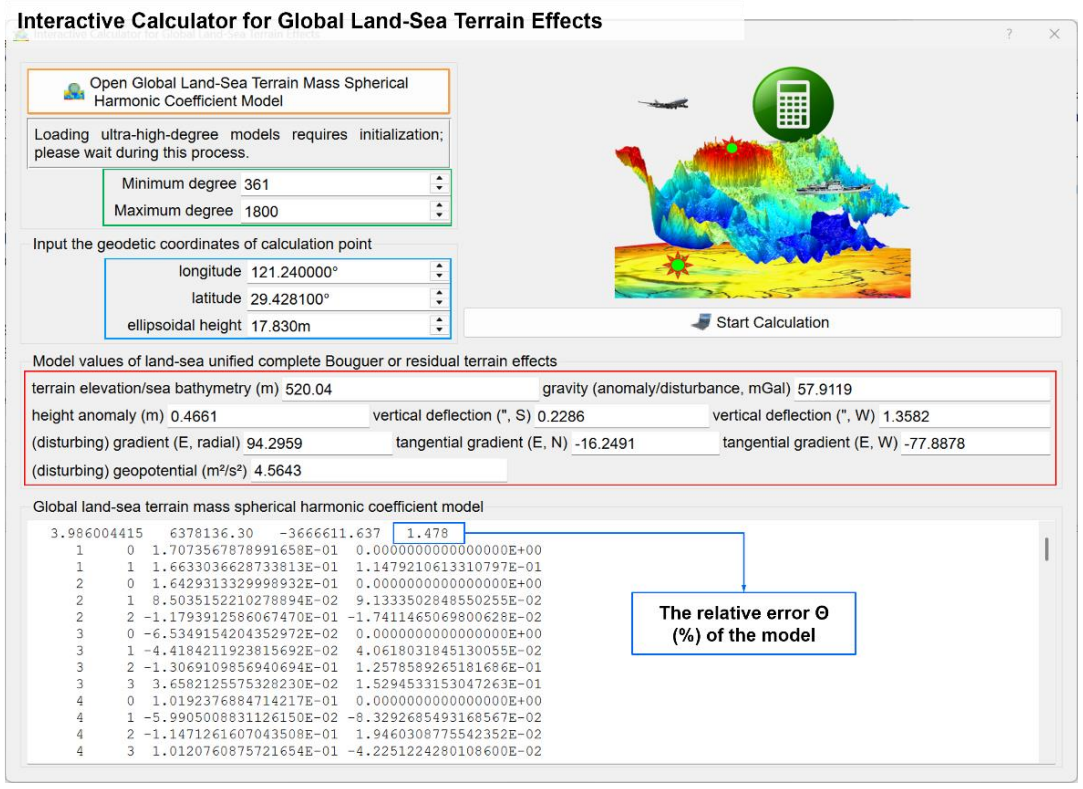
Interactive Calculator for Global Land-Sea Terrain Effects
Open Global Land-Sea Terrain Mass Spherical Harmonic Coefficient Model
Loading ultra-high-degree models requires initialization; please wait during this process.
Minimum degree 361
Maximum degree 1800
Input the geodetic coordinates of calculation point
longitude 121.240000°
latitude 29.428100°
ellipsoidal height 17.830m
Start Calculation
Model values of land-sea unified complete Bouguer or residual terrain effects
terrain elevation/sea bathymetry (m) 520.04
gravity (anomaly/disturbance, mGal) 57.9119
height anomaly (m) 0.4661
vertical deflection (", S) 0.2286
vertical deflection (", W) 1.3582
(disturbing) gradient (E, radial) 94.2959
tangential gradient (E, N) -16.2491
tangential gradient (E, W) -77.8878
(disturbing) geopotential (m²/s²) 4.5643
Global land-sea terrain mass spherical harmonic coefficient model
3.986004415 6378136.30 -3666611.637 1.478
1 0 1.7073567878991658E-01 0.0000000000000000E+00
1 1 1.6633036628733813E-01 1.1479210613310797E-01
2 0 1.6429313329998932E-01 0.0000000000000000E+00
2 1 8.5035152210278894E-02 9.1333502848550255E-02
2 2 -1.1793912586067470E-01 -1.7411465069800628E-02
3 0 -6.5349154204352972E-02 0.0000000000000000E+00
3 1 -4.4184211923815692E-02 4.0618031845130055E-02
3 2 -1.3069109856940694E-01 1.2578589265181686E-01
3 3 3.6582125575328230E-02 1.5294533153047263E-01
4 0 1.0192376884714217E-01 0.0000000000000000E+00
4 1 -5.9905008831126150E-02 -8.3292685493168567E-02
4 2 -1.1471261607043508E-01 1.9460308775542352E-02
4 3 1.0120760875721654E-01 -4.2251224280108600E-02
The relative error Θ (%) of the model

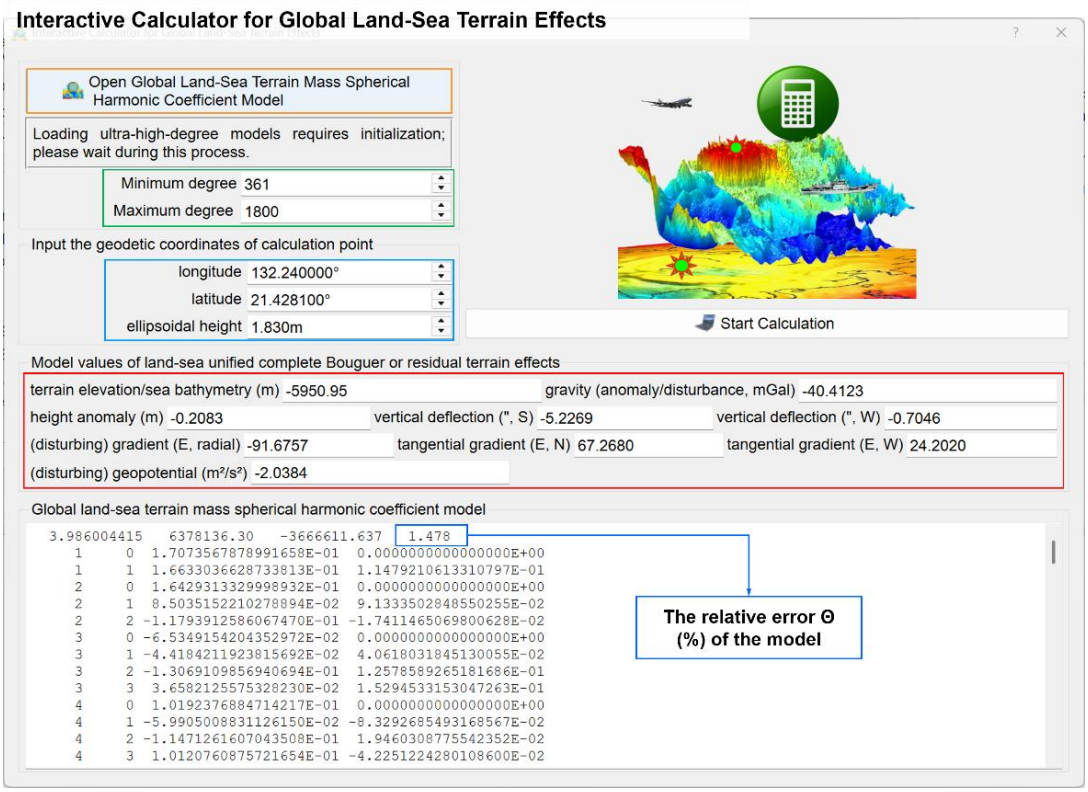
Interactive Calculator for Global Land-Sea Terrain Effects
Open Global Land-Sea Terrain Mass Spherical Harmonic Coefficient Model
Loading ultra-high-degree models requires initialization; please wait during this process.
Minimum degree 361
Maximum degree 1800
Input the geodetic coordinates of calculation point
longitude 132.240000°
latitude 21.428100°
ellipsoidal height 1.830m
Start Calculation
Model values of land-sea unified complete Bouguer or residual terrain effects
terrain elevation/sea bathymetry (m) -5950.95
gravity (anomaly/disturbance, mGal) -40.4123
height anomaly (m) -0.2083
vertical deflection (", S) -5.2269
vertical deflection (", W) -0.7046
(disturbing) gradient (E, radial) -91.6757
tangential gradient (E, N) 67.2680
tangential gradient (E, W) 24.2020
(disturbing) geopotential (m²/s²) -2.0384
Global land-sea terrain mass spherical harmonic coefficient model
3.986004415 6378136.30 -3666611.637 1.478
1 0 1.7073567878991658E-01 0.0000000000000000E+00
1 1 1.6633036628733813E-01 1.1479210613310797E-01
2 0 1.6429313329998932E-01 0.0000000000000000E+00
2 1 8.5035152210278894E-02 9.1333502848550255E-02
2 2 -1.1793912586067470E-01 -1.7411465069800628E-02
3 0 -6.5349154204352972E-02 0.0000000000000000E+00
3 1 -4.4184211923815692E-02 4.0618031845130055E-02
3 2 -1.3069109856940694E-01 1.2578589265181686E-01
3 3 3.6582125575328230E-02 1.5294533153047263E-01
4 0 1.0192376884714217E-01 0.0000000000000000E+00
4 1 -5.9905008831126150E-02 -8.3292685493168567E-02
4 2 -1.1471261607043508E-01 1.9460308775542352E-02
4 3 1.0120760875721654E-01 -4.2251224280108600E-02
The relative error Θ (%) of the model

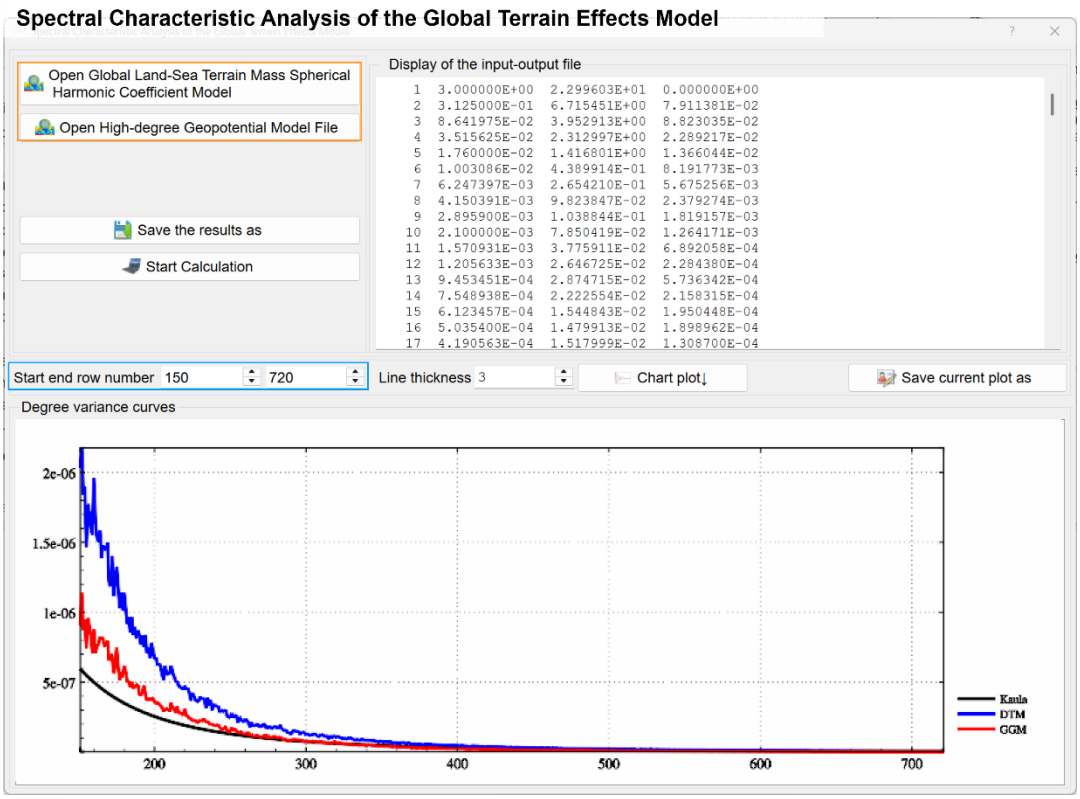

3.8 Demonstration of Terrain Effect Computation Processes on or outside the Geoid

3.8.1 Demonstration of Complete Bouguer Gravity Disturbance Computation on a Terrain Equielevation Surface

[Overview] This module demonstrates the fundamental workflow for computing unified land-sea complete Bouguer effects on gravities. Utilizing a Digital Elevation Model (DEM) and discrete gravity disturbances in near-Earth space derived from the EGM2008 geopotential model, the process employs a Remove-Restore scheme centered on Residual Terrain Effects (RTE). The target output is a grid of complete Bouguer gravity disturbances on a terrain equielevation surface, which simultaneously serves as the observation reduction surface.

[Physical Definition] The Complete Bouguer Effect is defined as the variation in the Earth's gravity field resulting from:

(1) The removal of topographic masses above the geoid.

(2) The compensation of seawater density to the land topographic density.

3.8.1.1 Input/Output Data and Related Terrain Models

Spatial Domains:

○ Terrain Data Domain (Extended Latitude and Longitude Extent): E94.5° – 99.5°, N30.5° – 34.5°.

○ Computation Domain (Result/Observation Extent): E95.0° – 99.0°, N31.0° – 34.0°.

○ Rationale: The extended extent encompasses the computation domain to suppress integration edge effects.

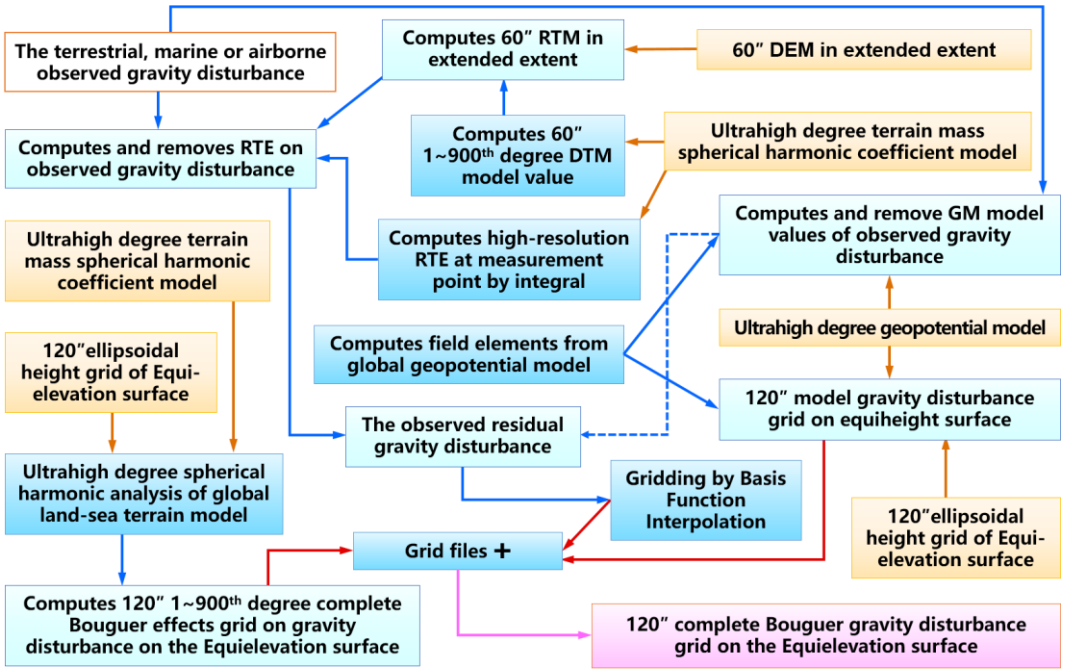

Computation Process of Complete Bouguer Gravity Disturbance on a Terrain Equielevation Surface

(1) Observed Gravity Disturbance File (Obsgrav.txt)

Source: Simulated gravity disturbances from degrees 2 to 1800 of the EGM2008 model.

Unified Processing: PAGravf4.5 applies identical algorithms to terrestrial, marine, and airborne data, eliminating the need to distinguish between ground, airborne altitude, or sea-surface observation points.

Record Format: ID, Longitude (°), Latitude (°), Ellipsoidal Height (m), Gravity Disturbance (mGal).

(2) Spherical Harmonic Coefficient Models

Terrain Mass Model: ETOPOcs1800.dat (1800-degree global land-sea terrain mass spherical harmonic coefficient model).

○ Generation: Derived via the [Ultrahigh-Degree Spherical Harmonic Analysis of the Global Land-Sea Terrain Model] function from the global 2′×2′ ETOPO2v2g model.

Geopotential Model: EGM2008.gfc (2190-degree EGM2008 model).

Path: C:\PAGravf4.5_win64en\data.

(3) Ground Digital Elevation Models (DEMs)

Coverage: Must exceed the computation extent to mitigate edge effects.

Dual-Resolution Requirement:

○ High-Resolution DEM (60″×60″, extdtm60s.dat): Used for data reduction (computing/removing RTE at observation points).

○ Target-Resolution DEM (120″×120″, extdtm120s.dat): Used for result restoration (restoring RTE to the output grid).

(4) Ground Ellipsoidal Height Grid (surfhgt60s.dat)

Resolution: 60″×60″.

Function: Provides the geodetic coordinates of residual terrain masses (integration moving cells), critical for high-precision RTE computation.

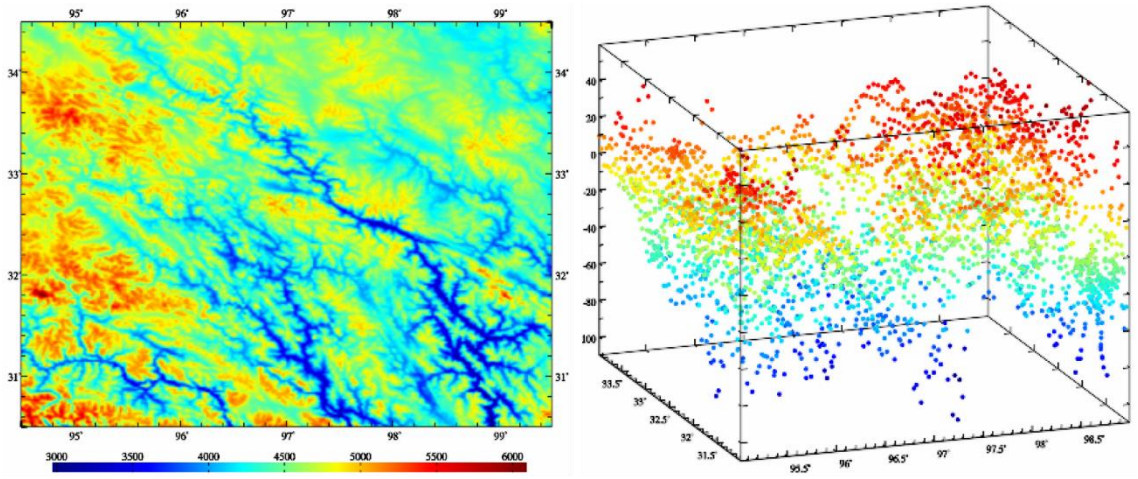

Ground digital elevation model (m) and gravity observation point distribution

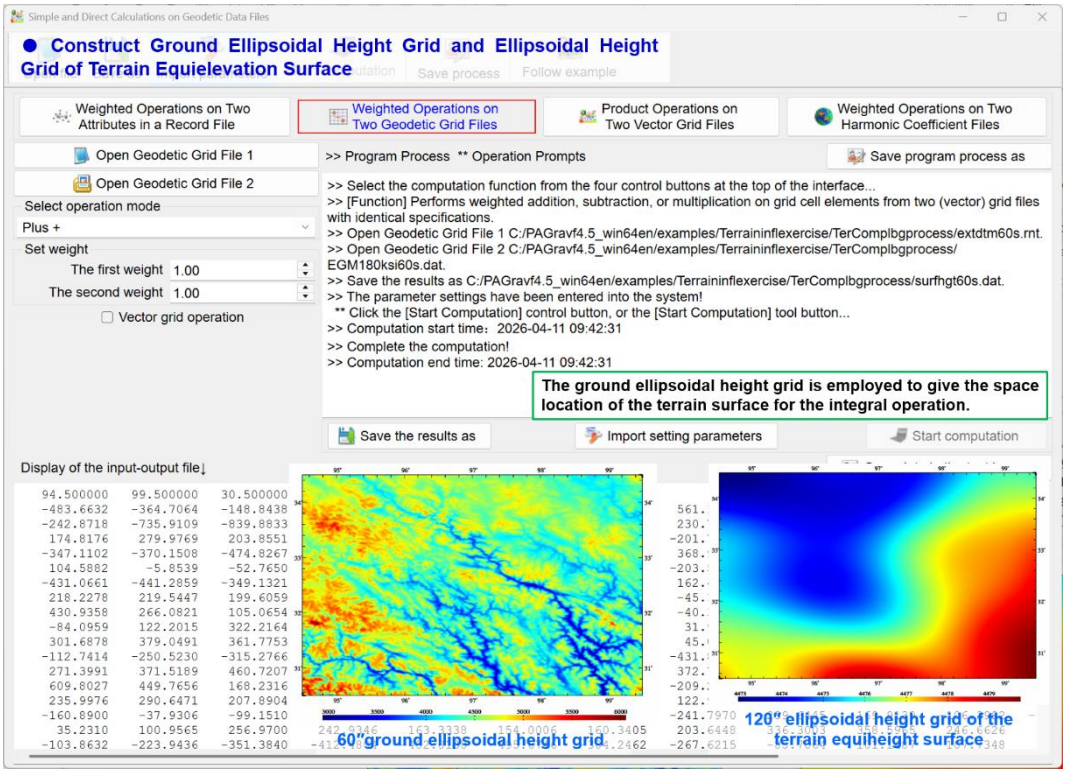

(5) Terrain Equielevation Surface Grid (equihgt120s.dat)

Resolution: 120″×120″.

Definition: Serves as both the reduction surface and the computation surface, treated physically as an equipotential surface.

Ellipsoidal Height h_e (Terrain Equielevation Surface) = N (EGM2008, 2 – 360) + h_e

(mean_DEM).

Theoretical Basis: Gridding is a non-analytical operation that can degrade the analytical nature of the gravity field. Performing such operations on an equipotential surface minimizes these adverse effects.

Special Case: If the normal/orthometric height of this surface is zero ($h_e = N$), it corresponds to the traditional geoid.

(6) Final Product:

A 120″×120″ grid of Complete Bouguer Gravity Disturbances on the terrain equielevation surface.

3.8.1.2 Workflow: Function Calls and Data Flow

(1) Compute and Remove the Model Elevations/Bathymetries, and then Construct 60″×60″ Residual Terrain Model (RTM)

Action: Compute and remove model terrain elevations/sea bathymetries.

Function: [Computation of Model Values for Complete Bouguer and Residual Terrain Effects].

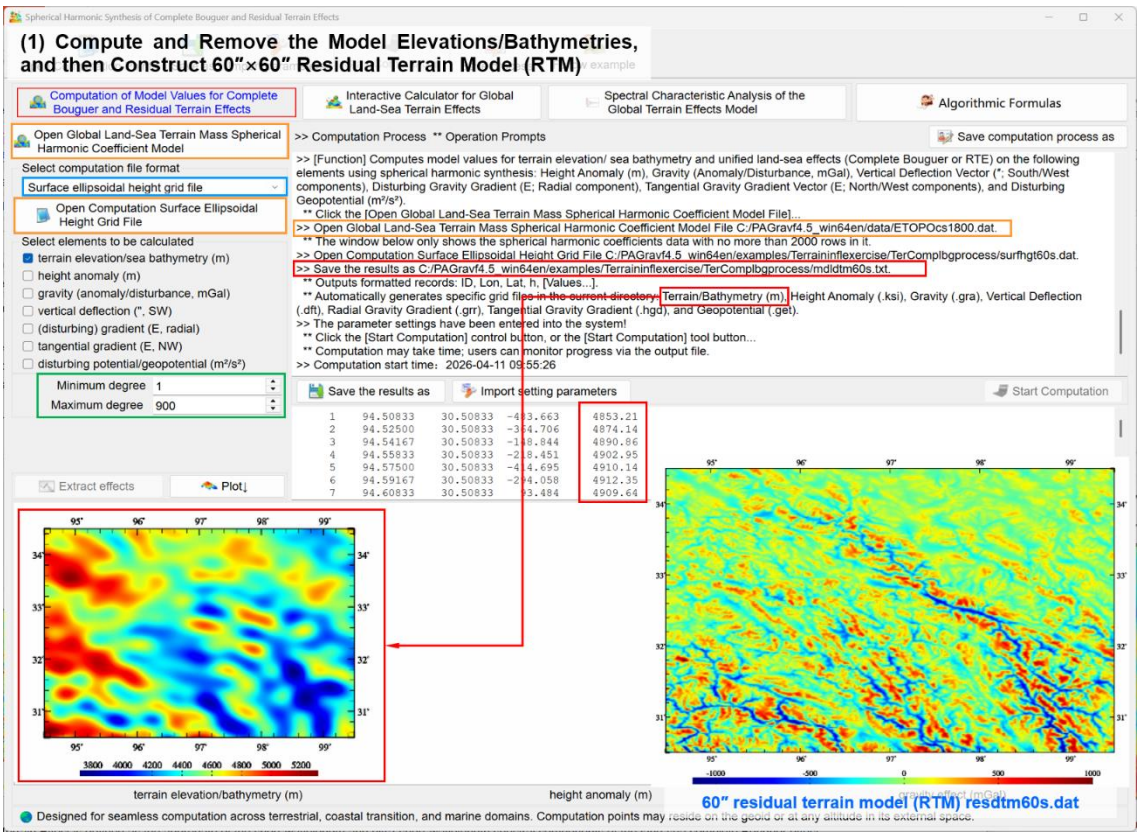

Parameters: Degrees 1 – 900; Type: Terrain Elevation/ Sea Bathymetry.

- ○ Inputs: ETOPOcs1800.dat, surfhgt60s.dat.
- ○ Output: Model terrain grid mdldtm60s.dtm.
- ○ Operation: $RTM = DTM\ (extdtm60s.dat) - DTM\ (mdldtm60s.dtm)$

Result: Extended extent 60″×60″ RTM grid resdtm60s.dat.

○ Inputs: ETOPOcs1800.dat, surfhgt120s.dat.

○ Output: Model terrain grid mdldtm120s.dtm.

○ Operation: $RTM = DTM\ (extdtm120s.dat) - DTM\ (mdldtm120s.dtm)$

Result: Extended extent 120″×120″ RTM grid resdtm120s.dat.

Statistics: See Table 3.8 (Mean, STD, Min, Max of RTM).

Table 3.8: Statistics for Residual Terrain Model

	Mean	STD	Minimum	Maximum
60″ RTM (m)	0.0053	175.5869	-959.5450	59.0160
120″ RTM (m)	0.0053	175.5869	-959.5450	886.2500

(2) Compute and Remove the Ultrahigh-degree Model Gravity Disturbances at the Observation Points

Action: Compute and subtract model gravity disturbances at observation points.

Function: [Computation of Gravity Field Elements from a Global Geopotential Model].

Parameters: Degrees 1 – 720; Type: Gravity Disturbance.

Inputs: EGM2008.gfc, Obsgrav.txt.

Output: Model disturbances Obsgravmdl.txt (Col 6).

○ Operation: δg (residual) = δg (obs, Col 5) – δg (model, Col 6).

○ Result: Residual gravity disturbance file Obsgravmdlresd.txt (Col 7).

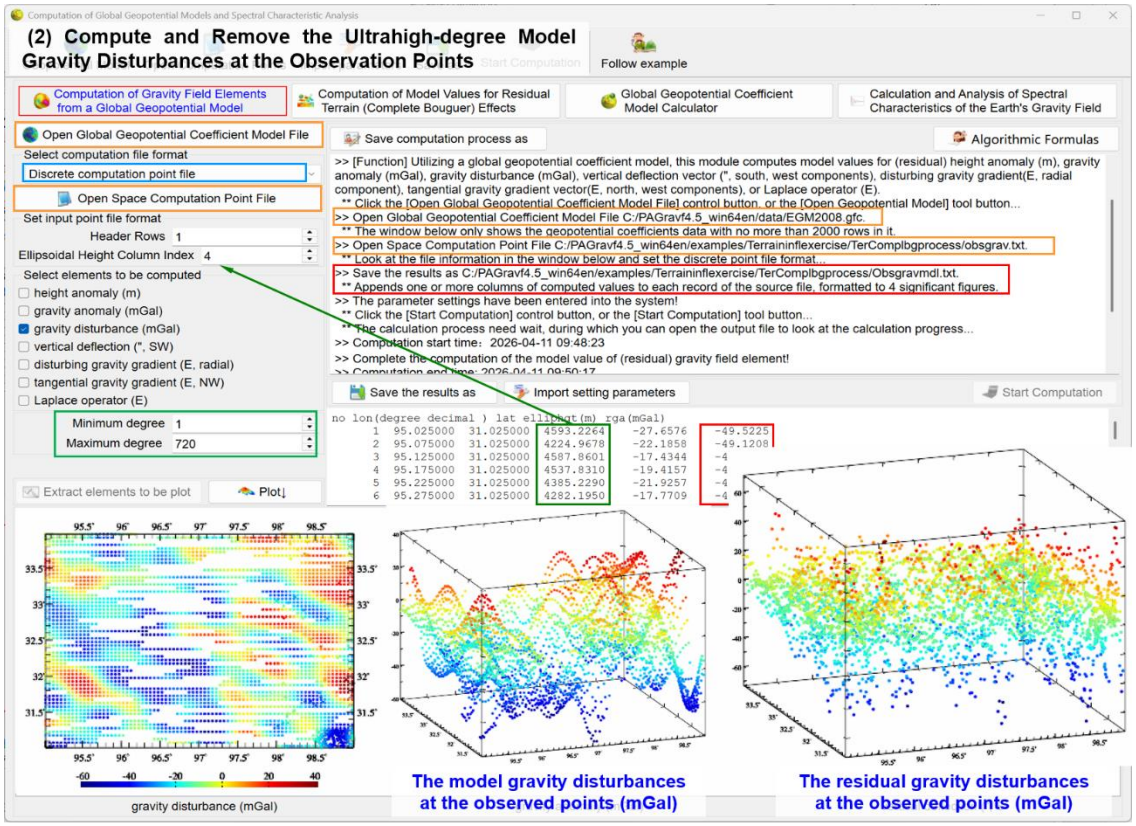

Statistics: See Table 3.9 (Significant reduction in STD after removing degrees 1 – 720).

Table 3.9: Statistics for gravity disturbances after removing the model values.

Observed points	Mean	STD	Minimum	Maximum
Observed gravity disturbance (mGal)	-15.6106	25.5080	-110.7251	59.0160
Residual of gravity disturbance (mGal)	-0.4881	17.4588	-74.6129	71.5003

(3) Compute and Remove the Residual Terrain Effects (RTE) on Gravity Disturbances at Observation Points

Action: Compute and subtract short-wavelength RTEs on gravity disturbances.

Function: [Rigorous Numerical Integration of Land-Sea Residual Terrain Effects].

Inputs: Obsgravmdlresd.txt, extdtm60s.dat (High-res), mdldtm60s.dtm (Low-pass), surfhgt60s.dat.

Parameter: Integration Radius = 90 km.

Output: RTE file Obsgravresdtm.txt (Col 8).

Operation: δg (final_res) = δg (residual, Col 7) – RTE (Col 8).

Result: Final residual gravity disturbance file Obsgravresidual.txt (Col 9).

Approximation: Continuation corrections for residual radial gradients are neglected (valid for elevation differences < 1000 m). Thus, δg (final_res) at the observation point ≈ its value on the equipotential surface.

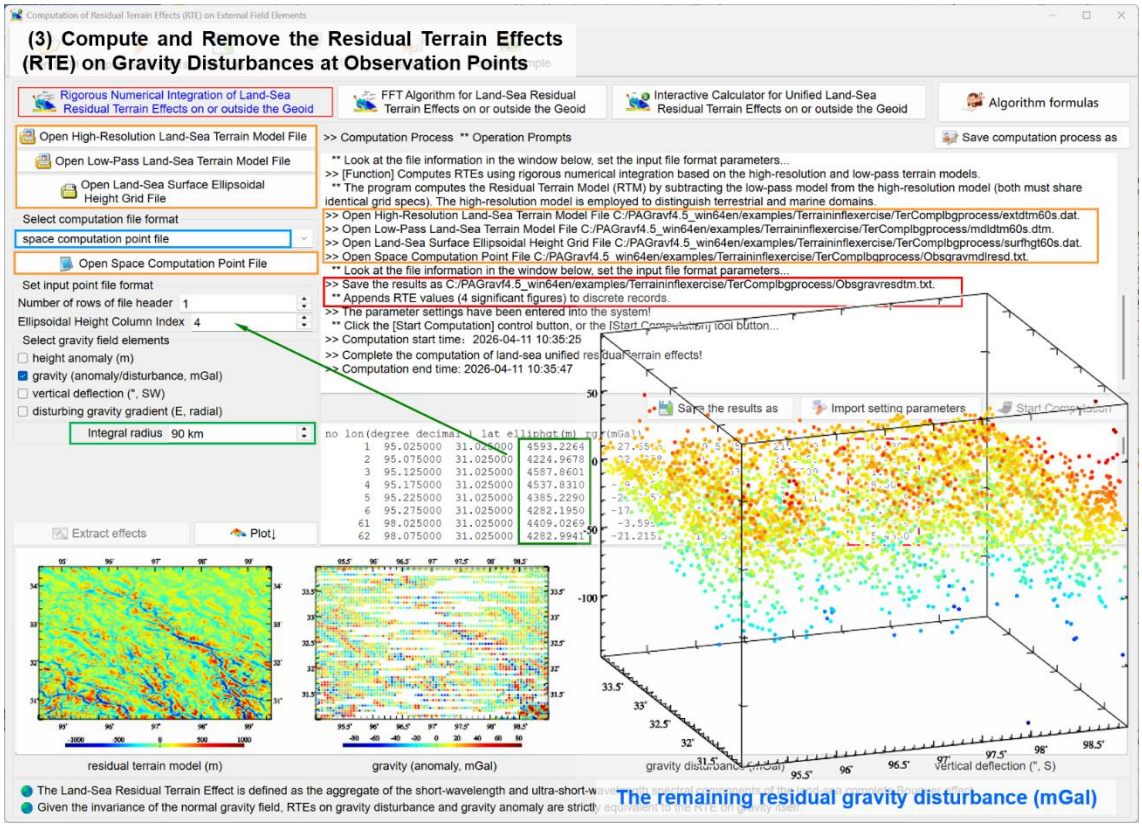

Table 3.10: Statistics for residual gravity disturbances after the residual terrain effects.

Observed points	Mean	STD	Minimum	Maximum
RTE on gravity disturbance (mGal)	4.8843	7.2038	-73.7901	118.6158
Remaining residual gravity disturbance (mGal)	-5.3034	19.7638	-144.5444	92.4782

Note: Tables 3.8 – 3.10 facilitate algorithm optimization based on the terrain effect quantitative criteria. This step is omitted here due to the simulated nature of the data lacking real ultra-short-wavelength content.

Status: Reduction from observation points to the terrain equielevation surface is complete.

(4) Griding on Remaining Residual Gravity Disturbances to 120″×120″ on Terrain Equielevation Surface.

Action: Interpolate heterogeneous residual data onto the target grid.

Function: [Gridding of Heterogeneous Data by Basis Function Weighted Interpolation].

Strategy: Equal weights (or weights estimated via RTE reference attributes).

Input: Column 9 of Obsgravresidual.txt.

Output: 120″×120″ final residual grid distgravresidual.dat.

Specification: Matches the target computation domain and resolution.

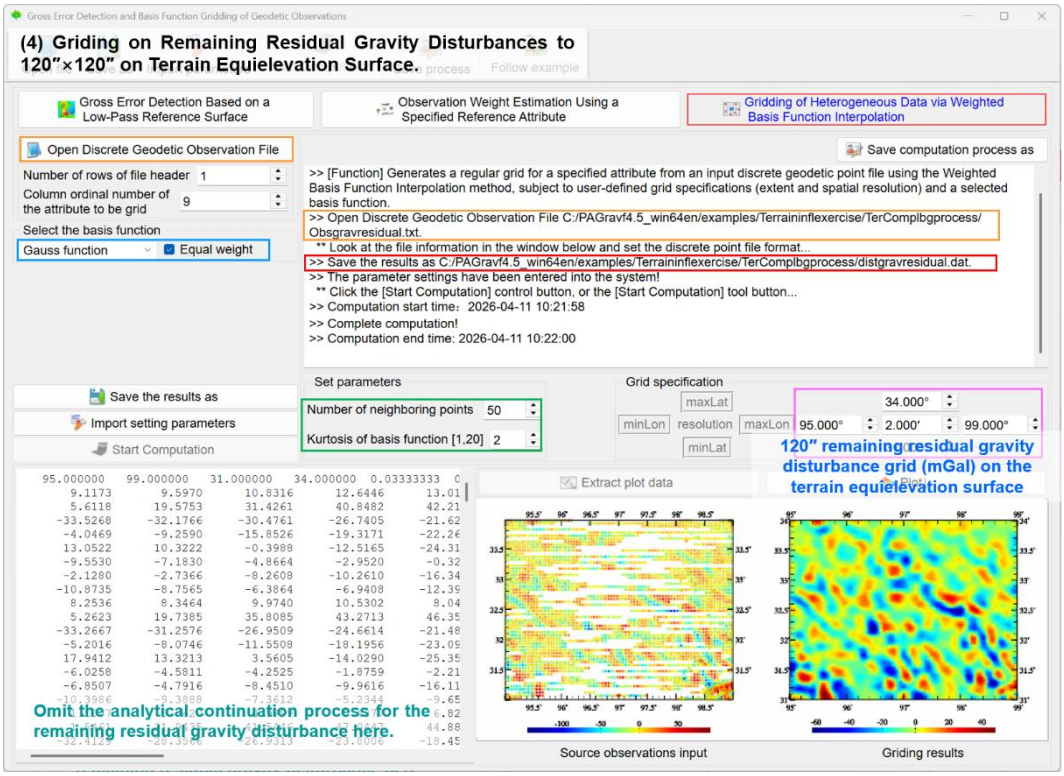

(5) Compute the Ultrahigh-degree Model Gravity Disturbances on Terrain Equielevation Surface

Function Call: [Computation of Gravity Field Elements from a Global Geopotential Model].

Parameters:

- Degree Range: Minimum = 1, Maximum = 720.
- Output Type: Gravity Disturbance.

Inputs:

- Geopotential Model: EGM2008.gfc.
- Computation Surface Grid: equihgt120s1.dat (The terrain equielevation surface, derived from equihgt120s.dat with edge trimming).

Output File: 120″×120″ grid of model gravity disturbances: distgravmdl.rga.

Consistency Constraint: The geopotential model and degree range must strictly match those used in Step (2) to ensure spectral consistency of the reference field model component.

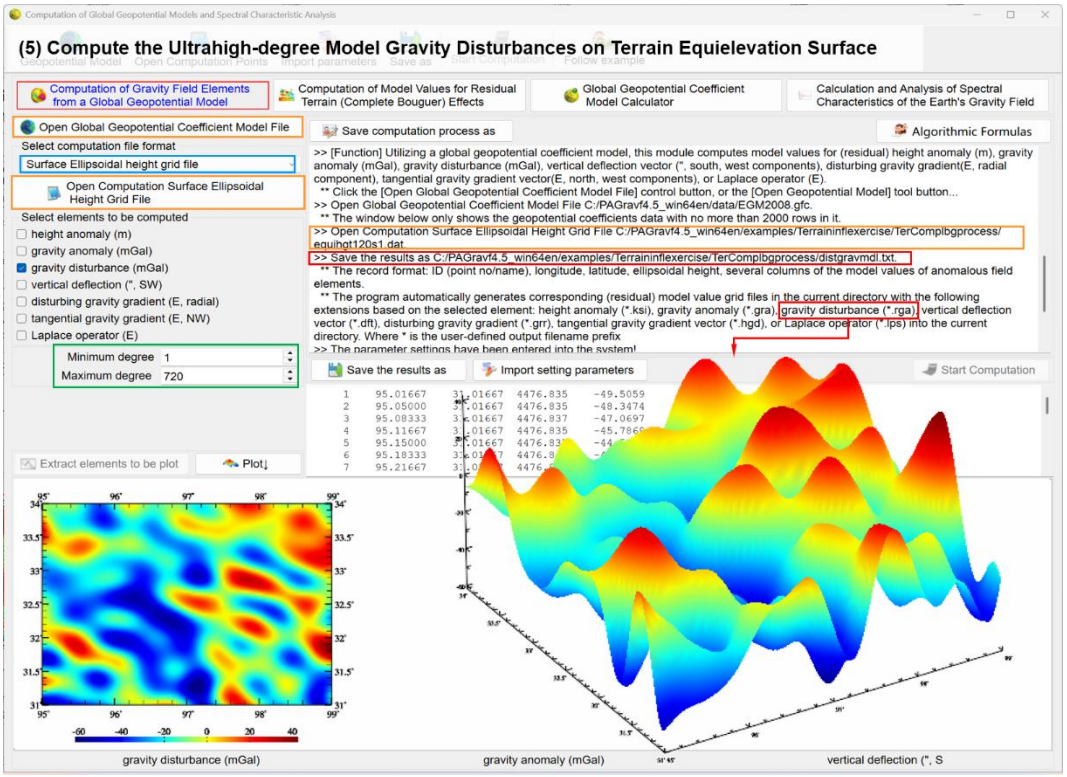

(6) Compute and Restore Model Complete Bouguer Effects on Terrain Equielevation Surface

Objective: Compute the grid of model complete Bouguer effects on gravity disturbances for the terrain equielevation surface (120″×120″).

Function Call: [Computation of Model Values for Complete Bouguer or Residual Terrain Effects].

Parameters:

- Degree Range: Minimum = 1, Maximum = 900.
- Output Type: Gravity Disturbance (effect component).

Inputs:

- Terrain Mass Model: ETOPOcs1800.dat.

○ Surface Elevation Grid: surfhgt120s1.dat (120″×120″ ground ellipsoidal height grid corresponding to the terrain equielevation surface).

Output File: 120″×120″ grid of model complete Bouguer effects: distgravmdlcmpbg.gra.

Consistency Constraint: The terrain mass model and maximum degree must strictly match those used in Step (1) to ensure consistency of the topographic spectrum.

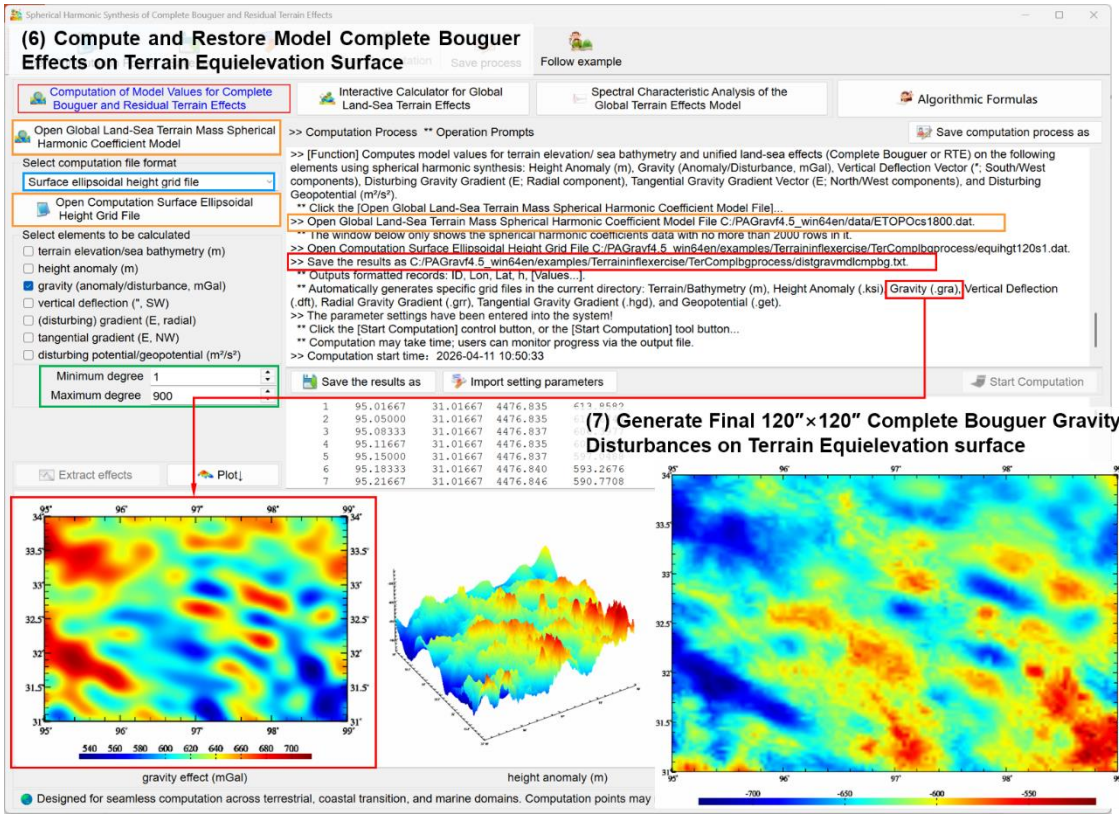

(7) Generate Final 120″×120″ Complete Bouguer Gravity Disturbances on Terrain Equielevation surface

Objective: Assemble the final product by superimposing all processed components.

Operation: Perform an algebraic summation of the following four (120″×120″) gravity disturbance grids:

● Final Residual Grid: distgravresidual.dat (The residual field after remove processing).

● Ultra-High-Degree Model Grid: distgravmdl.rga [The long-wavelength background field restored from Step (5)].

● Restored Residual Terrain Effect (RTE) Grid: distgravresidtm.dat [The short-wavelength terrain signals removed in Step (3), now restored].

● Model Complete Bouguer Effect Grid: distgravmdlcmpbg.gra [The model complete Bouguer effects computed in Step (6)].

Output File: 120″×120″ Complete Bouguer Gravity Disturbance Grid: distgravcmpbg.dat.

Mathematical Formulation: δg^{mcB} (Complete Bouguer gravity disturbance) = δg_{m} (Model gravity disturbance) + δg_{res} (residual gravity disturbance) + RTE (Restored) + g^{cB} (Model complete Bouguer effects).

3.8.2 Demonstration of Land-Sea Bouguer and Isostatic Anomalies/Disturbaces Derived from a Geopotential Model

[Overview] This module demonstrates a rapid workflow for computing classical Bouguer gravity anomalies (or disturbances) and isostatic gravity anomalies (or disturbances) for any global region. Utilizing an Earth geopotential coefficient model and a land-sea terrain mass spherical harmonic coefficient model, the process executes four key steps to synchronously generate unified land-sea anomaly models.

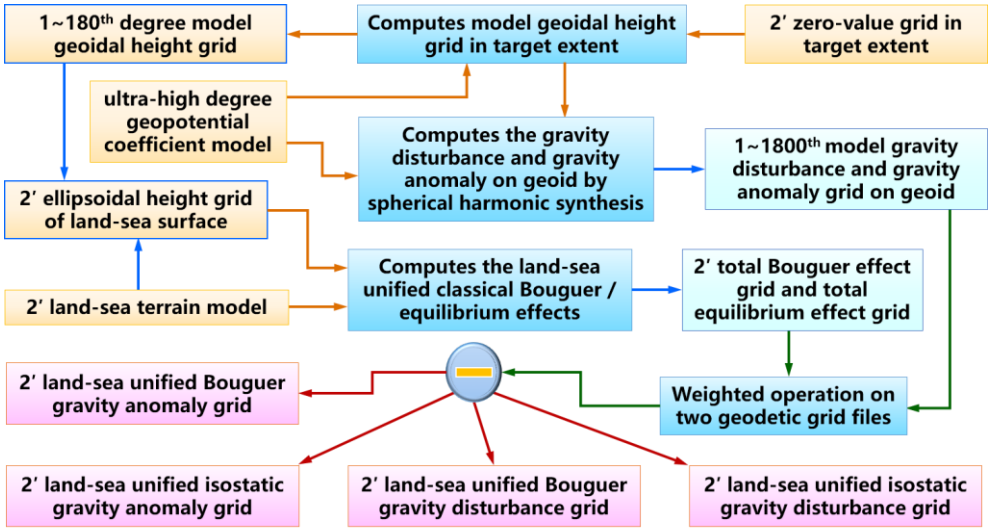

Computation Process of Land-Sea Bouguer and Isostatic Gravity Anomalies/Disturbances Derived from a Geopotential Model

(1) Construction of the Model Geoidal Height Grid (Degrees 1 – 180) as the Reduction Surface

Function Call: [Computation of Gravity Field Elements from a Global Geopotential Model].

Parameters:

- Degree Range: Min = 1, Max = 180.
- Output Type: Height Anomaly (approximating geoidal height in this context).

Inputs:

- Geopotential Model: EGM2008.gfc.
- Target Latitude and Longitude Extent Definition: Zero-value grid file zero2m.dat.

Output File: 2′×2′ Model Geoidal Height Grid: GMgeoidh2m_180.ksi.

Physical Role: This grid serves as the gravity reduction surface and the reference surface for subsequent classical Bouguer and isostatic anomaly computations.

(2) Computation of Gravity Anomaly and Disturbance on the Geoid from a a Global Geopotential Model

Function Call: [Computation of Gravity Field Elements from a Global Geopotential Model].

Parameter Settings:

- Degree Range: Min = 1, Max = 1800.
- Output Elements: Select both Gravity Anomaly and Gravity Disturbance.

Input Files:

○ Geopotential Model: EGM2008.gfc.

○ Computation Surface: The model geoidal height grid GMgeoidh2m_180.ksi generated in Step (1).

Output Files:

● 2′×2′ Gravity Anomaly Grid: EGM2008_2m_1800.gra.

● 2′×2′ Gravity Disturbance Grid: EGM2008_2m_1800.rga.

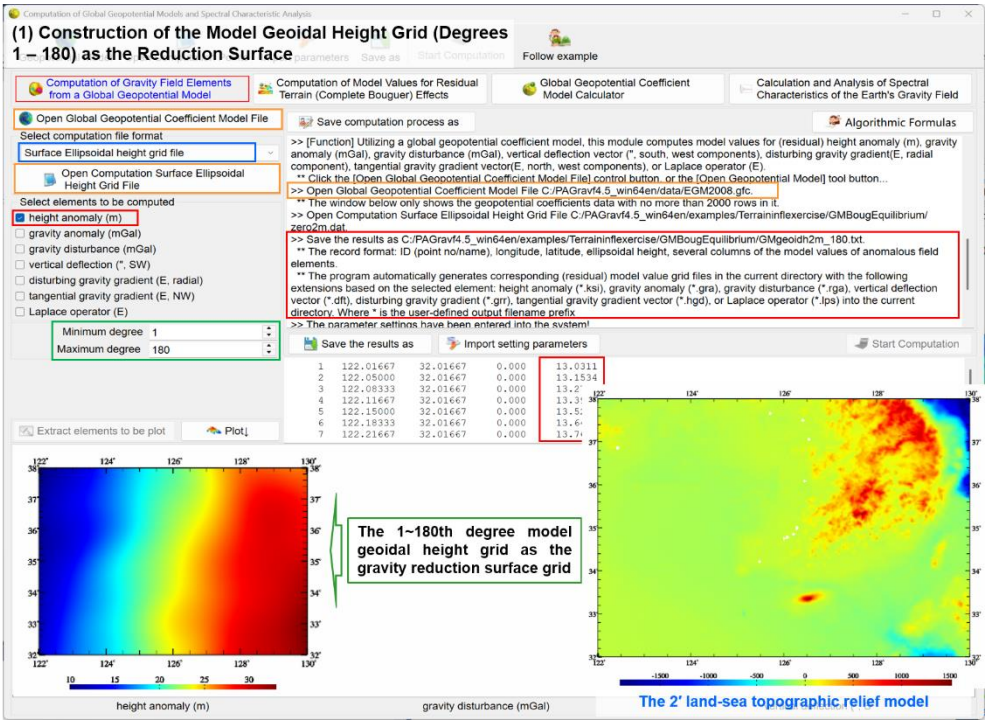

(3) Computation of Total Bouguer and Total Isostatic Effects on Gravity

Function Call: [Integration of Land-Sea Unified Classical Gravity Bouguer / Equilibrium Effect].

Input Files:

● Land-Sea Terrain Model: extlandseadtm2m.dat.

● Land-Sea Surface Ellipsoidal Height Grid: extlandseahgt2m.dat.

Parameter Settings:

● Land Integration Radius: 90 km.

● Sea Integration Radius: 200 km.

● Isostatic Compensation Depth: 30 km.

Output Files:

● 2′×2′ Total Bouguer Effect Grid: BougEquinfl2m.bgr.

● 2′×2′ Total Isostatic Effect Grid: BougEquinfl2m.ist.

Theoretical Note: Given the invariance of the normal gravity field with respect to the chosen reference surface, the computed Bouguer/Isostatic effects are numerically identical for both gravity anomalies and gravity disturbances. Consequently, there is no need to

distinguish between these two quantities in the reduction process.

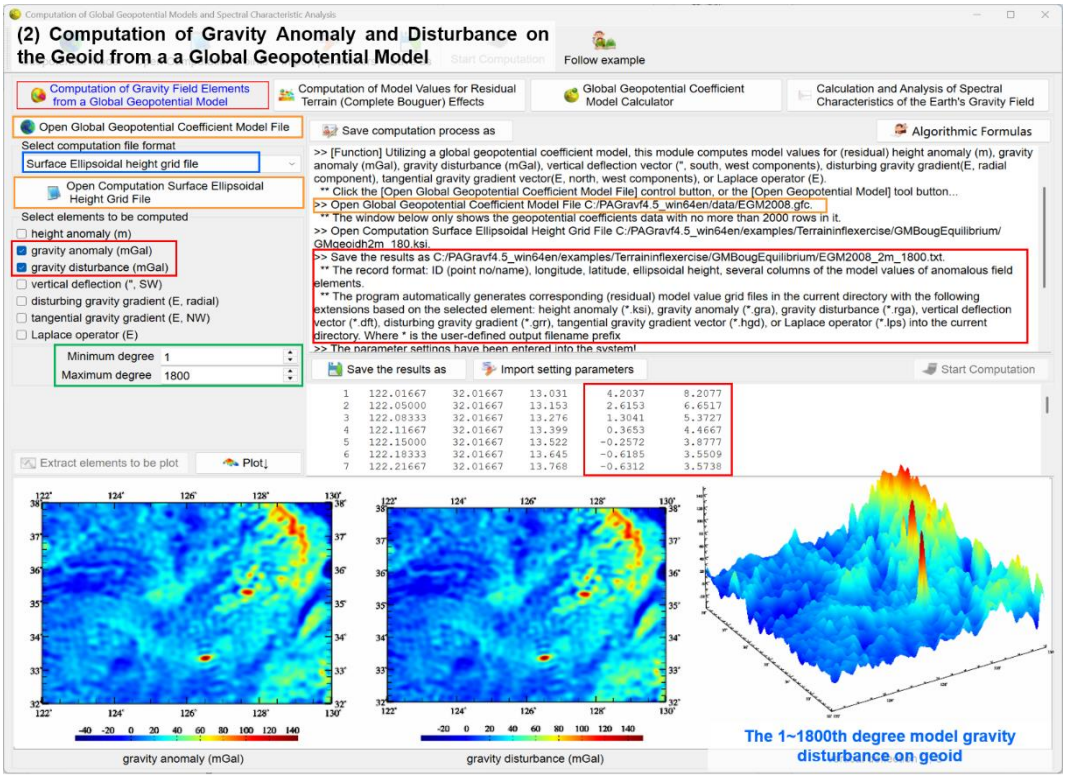

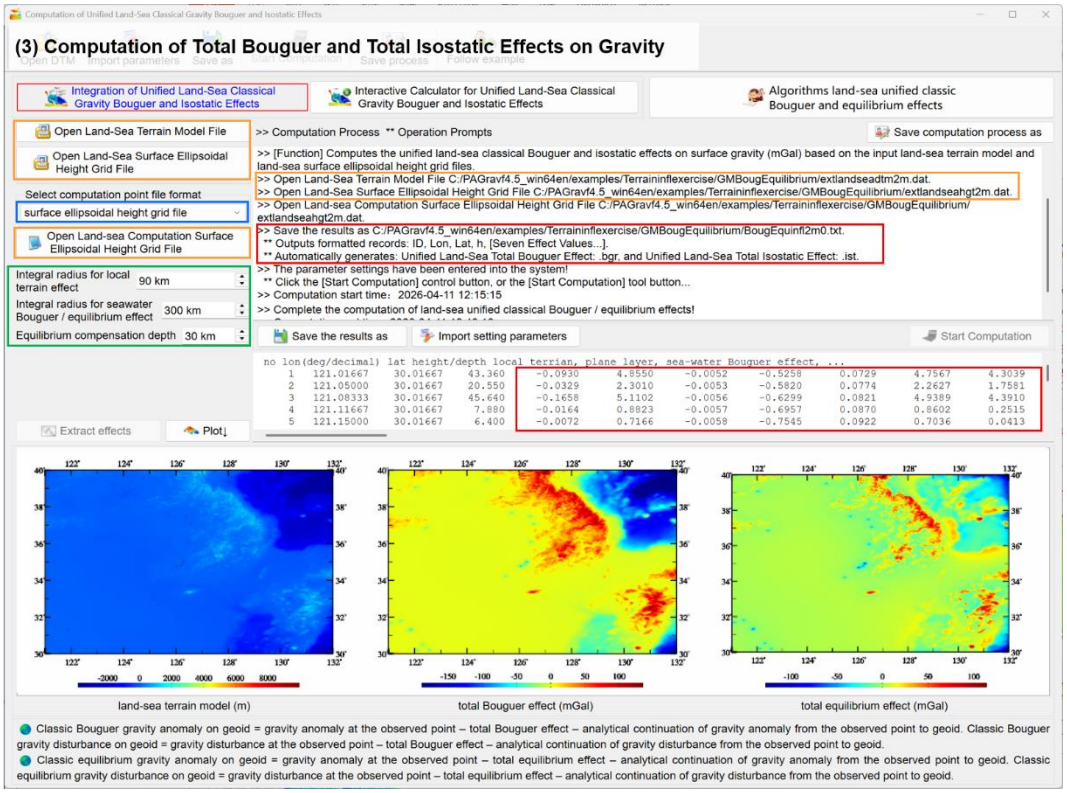

(4) Generation of Land-Sea Unified Classical Bouguer and Isostatic Gravity Anomaly/

Disturbance Grids

Classical Bouguer Anomalies:

● Operation: Subtract the edge-truncated total Bouguer effect grid (BougEquinfl2m0.bgr) from the geoid-based gravity anomaly (EGM2008_2m_1800.gra) and gravity disturbance (EGM2008_2m_1800.rga) grids, respectively.

● Output Models:

○ Classical Bouguer Gravity Anomaly Model: Clsbggravanom2m.dat.

○ Classical Bouguer Gravity Disturbance Model: Clsbgdistgrav2m.dat.

Classical Isostatic Anomalies:

● Operation: Subtract the edge-truncated total isostatic effect grid (BougEquinfl2m0.ist) from the geoid-based gravity anomaly (EGM2008_2m_1800.gra) and gravity disturbance (EGM2008_2m_1800.rga) grids, respectively.

● Output Models:

○ Classical Isostatic Gravity Anomaly Model: Istbggravanom2m.dat.

○ Classical Isostatic Gravity Disturbance Model: Istbgdistgrav2m.dat.

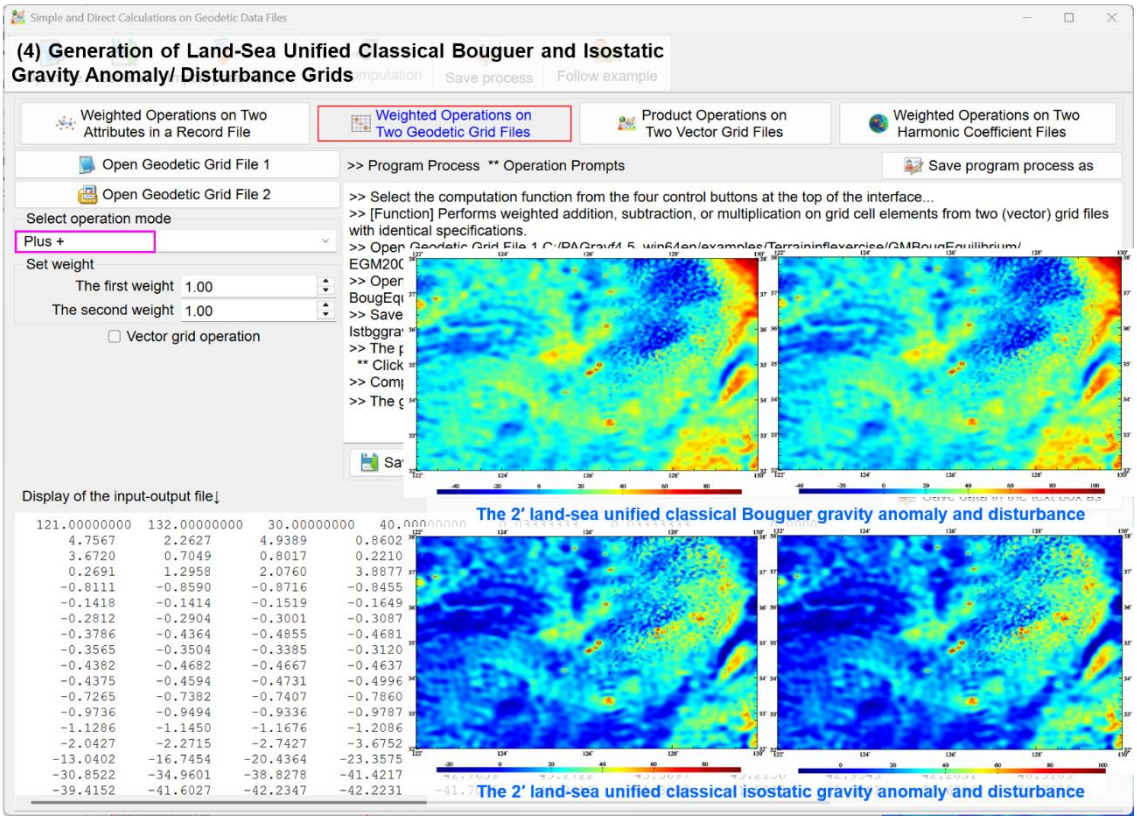

4. High-Precision Gravity Field Approximation and Full-element Modeling

PAGravf4.5 establishes a rigorous gravity field approximation framework. It integrates spatial-domain numerical integration algorithms, based on Boundary Value Theory, with spectral-domain Spherical Radial Basis Function (SRBF) approximation techniques.

Core Objective: To achieve analytical full-element modeling of the gravity field on or outside the geoid. This subsystem seamlessly processes multi-source, heterogeneous data of varying altitudes, cross-distributions, and multiple types, encompassing terrestrial, maritime, aerial, and space-based observations.

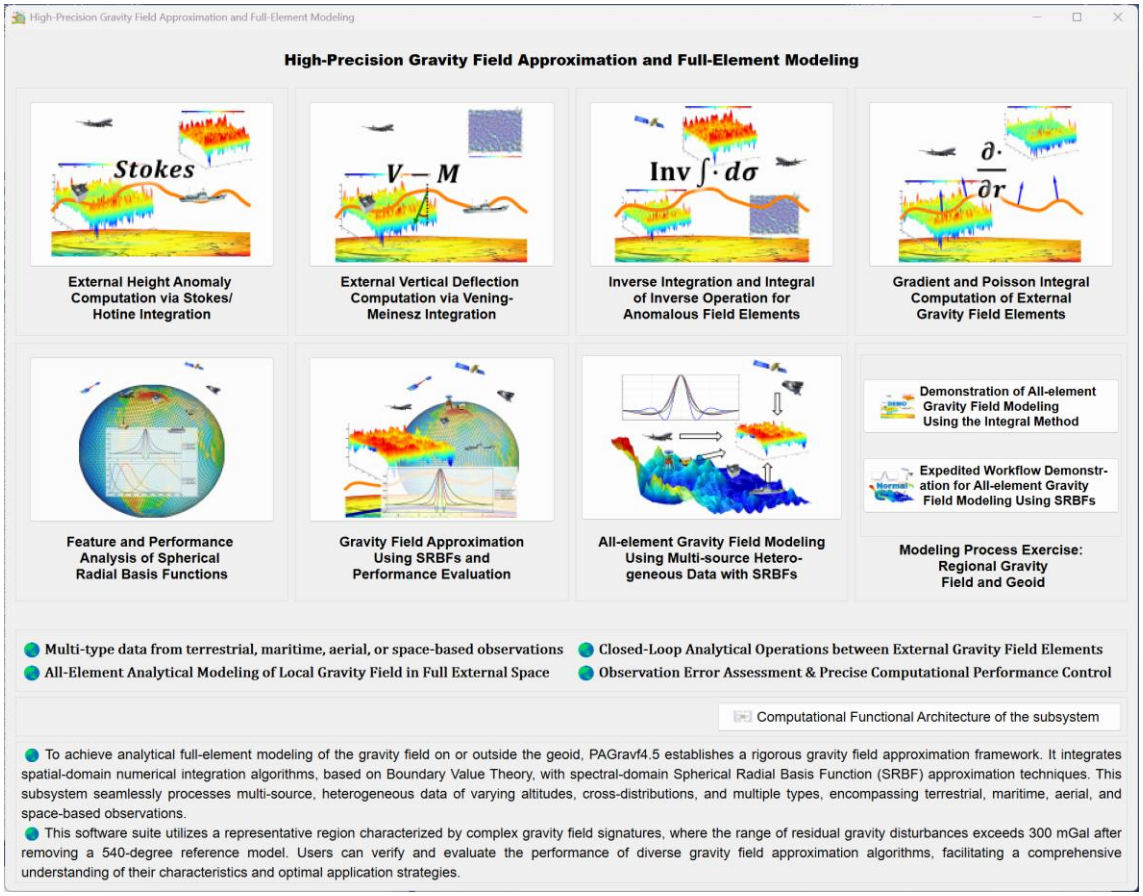

[Demonstration Area & Capabilities]

This software suite utilizes a representative region characterized by complex gravity field signatures, where the range of residual gravity disturbances exceeds 300 mGal after removing a 540-degree reference model. Users can verify and evaluate the performance of diverse gravity field approximation algorithms, facilitating a comprehensive understanding of their characteristics and optimal application strategies.

4.1 External Height Anomaly Computation via Stokes/Hotine Integration

[Purpose] To compute height anomalies (m) on or outside the geoid using generalized rigorous numerical integration or Fast Fourier Transform (FFT) algorithms based on Stokes or Hotine theory. Inputs include an ellipsoidal height grid defining an equipotential boundary

surface and the corresponding gravity anomaly or gravity disturbance grid (mGal) on that surface.

Note: On the geoid, the height anomaly is equivalent to the geoid undulation (geoidal/ellipsoidal height).

[Computational Strategy: Remove-Restore Scheme] To perform integration over a finite radius in local regions, a Remove-Restore scheme based on a reference global geopotential model is employed:

Remove: Subtract the model gravity anomaly/disturbance from the boundary surface data.

Integrate: Perform integration on the residuals to derive the residual height anomaly at the computation point.

Restore: Add the model height anomaly back at the computation point.

[Theoretical Constraints]

Boundary Condition: Stokes Boundary Value Theory mandates that the boundary surface be an equipotential boundary surface; thus, input gravity anomalies/disturbances must reside on such a surface.

Equipotential Surface Construction: Typically constructed from a global geopotential model (degree $\leqslant$ 360). For equipotential surfaces within an altitude of 10 km, a normal (or orthometric) equiheight surface may serve as a valid approximation.

4.1.1 External Height Anomaly Computation via Generalized Stokes Integration

[Function] Computes the external residual height anomaly (m) via Stokes integration, utilizing an ellipsoidal height grid of an equipotential boundary surface and the corresponding residual gravity anomaly grid (mGal) on that surface.

[Input Files]

(1) Equipotential Surface Ellipsoidal Height Grid File: Provides the geodetic coordinates of Equipotential Surface, for deriving integration distances.

(2) Residual Gravity Anomaly Grid File: Must share identical specifications (extent, resolution) with the ellipsoidal height grid.

(3) Computation Point file: a Space Computation Point File or a Computation Surface Ellipsoidal Height grid File.

● Discrete Point record Format: ID (Point No./Name), Longitude (deg), Latitude (deg), Ellipsoidal Height (m), ...

[Parameter Settings]

Define input file parsing rules.

Specify the Integration Radius.

Select the computational algorithm (Numerical Integration or FFT).

[Output Files]

Residual Height Anomaly Results:

● Discrete Input: Appends a column of computed residual height anomalies to the source file, retaining 4 significant figures.

● Grid Input: Generates a residual height anomaly grid file matching the input grid specifications.

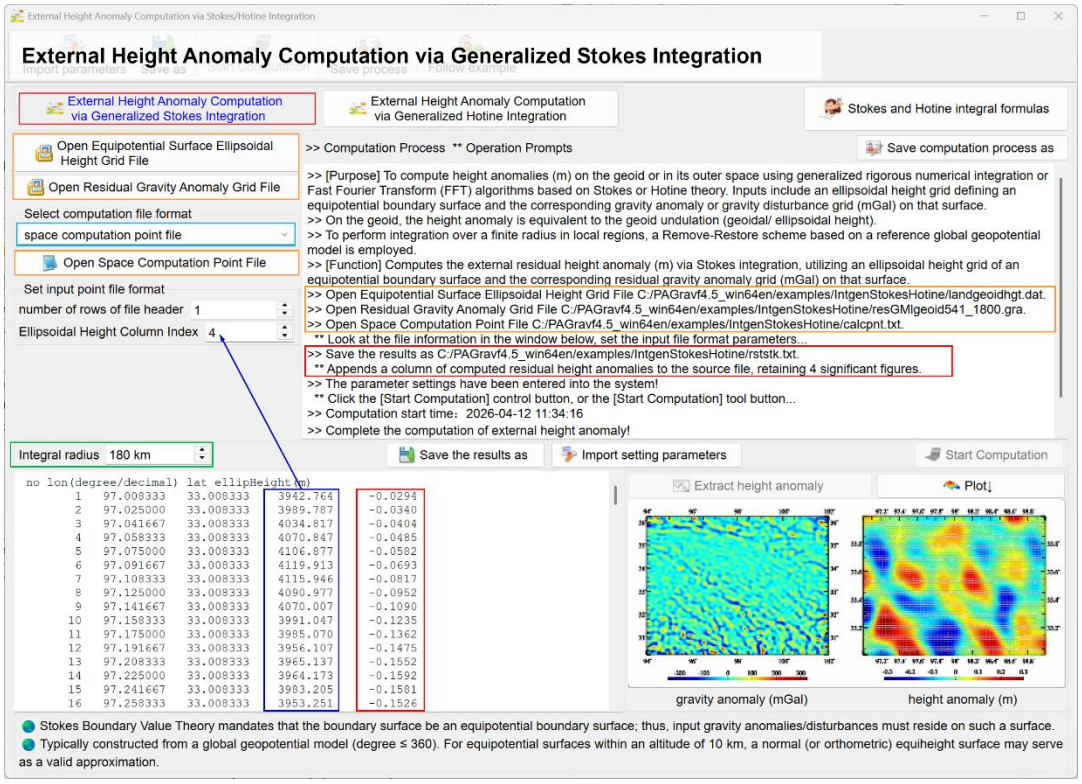

no	lon(degree/decimal)	lat	ellipHeight(m)	
1	97.008333	33.008333	3942.764	-0.0294
2	97.025000	33.008333	3989.787	-0.0340
3	97.041667	33.008333	4034.817	-0.0404
4	97.058333	33.008333	4070.847	-0.0485
5	97.075000	33.008333	4106.877	-0.0582
6	97.091667	33.008333	4119.913	-0.0693
7	97.108333	33.008333	4115.946	-0.0817
8	97.125000	33.008333	4090.977	-0.0952
9	97.141667	33.008333	4070.007	-0.1090
10	97.158333	33.008333	3991.047	-0.1235
11	97.175000	33.008333	3985.070	-0.1362
12	97.191667	33.008333	3956.107	-0.1475
13	97.208333	33.008333	3965.137	-0.1552
14	97.225000	33.008333	3964.173	-0.1592
15	97.241667	33.008333	3983.205	-0.1581
16	97.258333	33.008333	3953.251	-0.1526

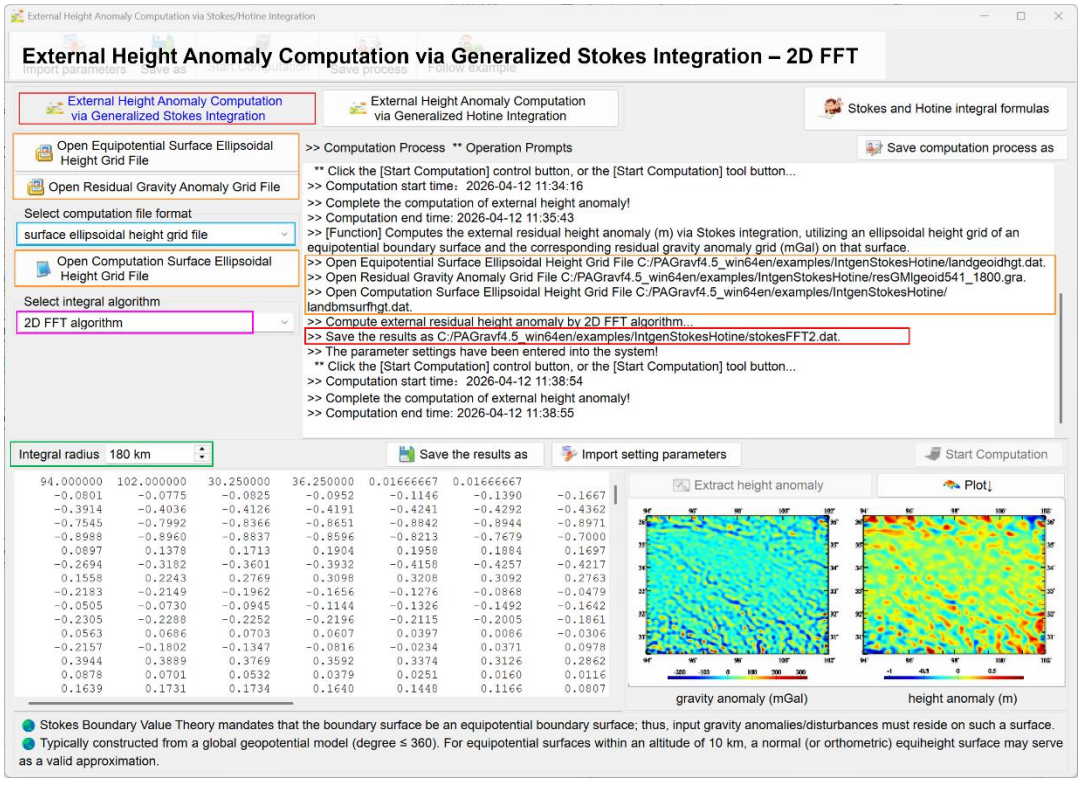

94.000000	102.000000	30.250000	36.250000	0.01666667	0.01666667	
-0.0801	-0.0775	-0.0825	-0.0952	-0.1146	-0.1390	-0.1667
-0.3914	-0.4036	-0.4126	-0.4191	-0.4241	-0.4292	-0.4362
-0.7545	-0.7992	-0.8366	-0.8651	-0.8842	-0.8944	-0.8971
-0.8988	-0.8960	-0.8837	-0.8596	-0.8213	-0.7679	-0.7000
0.0897	0.1378	0.1713	0.1904	0.1958	0.1884	0.1697
-0.2694	-0.3182	-0.3601	-0.3932	-0.4158	-0.4257	-0.4217
0.1558	0.2243	0.2769	0.3098	0.3208	0.3092	0.2763
-0.2183	-0.2149	-0.1962	-0.1656	-0.1276	-0.0868	-0.0479
-0.0505	-0.0730	-0.0945	-0.1144	-0.1326	-0.1492	-0.1642
-0.2305	-0.2288	-0.2252	-0.2196	-0.2115	-0.2005	-0.1861
0.0563	0.0686	0.0703	0.0607	0.0397	0.0086	-0.0306
-0.2157	-0.1802	-0.1347	-0.0816	-0.0234	0.0371	0.0978
0.3944	0.3889	0.3769	0.3592	0.3374	0.3126	0.2862
0.0878	0.0701	0.0532	0.0379	0.0251	0.0160	0.0116
0.1639	0.1731	0.1734	0.1640	0.1448	0.1166	0.0807

[Case Study & Accuracy Assessment]

In this example, residual ground height anomalies are computed via Stokes integration (Radius = 180 km) using residual gravity anomalies (derived from the EGM2008 model, degrees 541 – 1800) on the geoid.

To mitigate integration edge effects, a 2° marginal buffer zone along the grid margins is excluded from statistical analysis. The evaluation compares:

- Reference Truth: Model residual height anomalies (degrees 541 – 1800 EGM2008).
- Algorithm Errors: Differences between computed results (Stokes/FFT) and the reference truth.

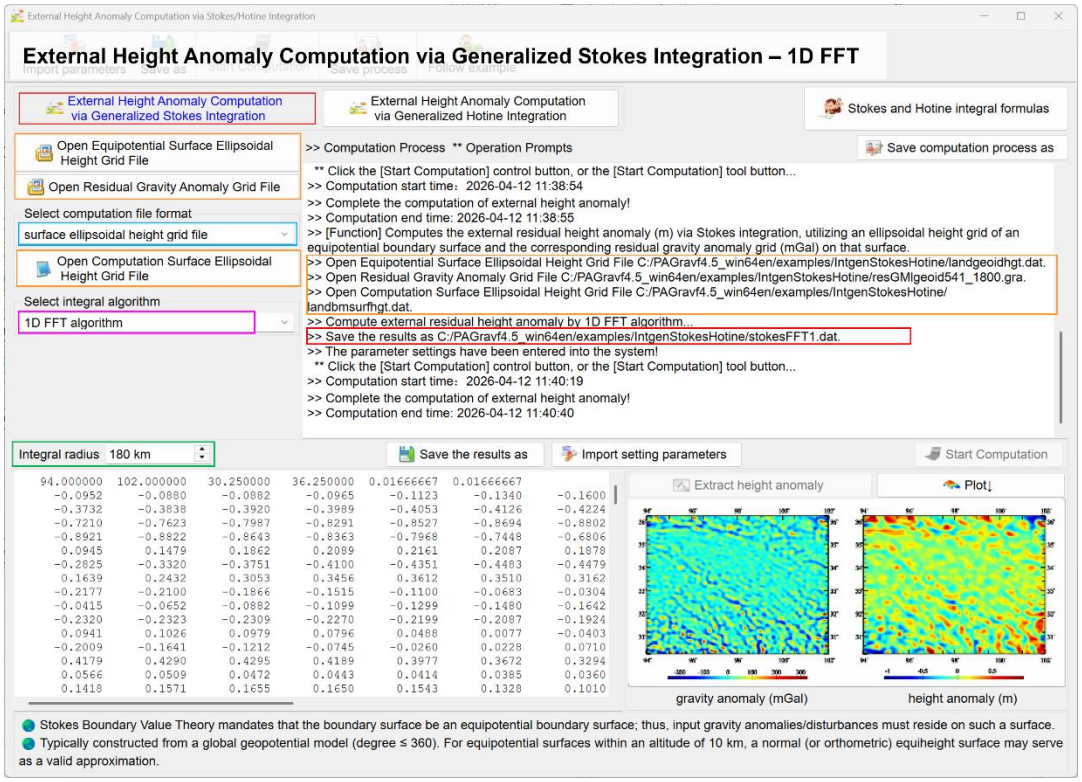

Table 4.1: Statistics of Model Reference Truth (Unit: m)

Item	Mean	Std. Dev.	Minimum	Maximum
Ground Height Anomalies (Deg 541 – 1800)	0.0010	0.1182	-0.6745	0.4760

Table 4.2: Differences between Stokes Computed Results and Reference Truth (Unit: m)

Algorithm	Mean	Std. Dev.	Minimum	Maximum
Numerical Integration	-0.0002	0.0324	-0.1159	0.1211
FFT2	0.0018	0.0326	-0.1150	0.1280
FFT1	0.0018	0.0327	-0.1178	0.1251

Algorithm Performance: The ratio of the standard deviation of Differences in Table 4.2

to the standard deviation of Reference Truths in Table 4.1 reflects the approximation capability of the corresponding algorithm.

Furthermore, inter-algorithm consistency is evaluated by comparing results from Stokes Numerical Integration and FFT methods:

Table 4.3: Inter-Algorithm Differences (Unit: m)

Comparison	Mean	Std. Dev.	Minimum	Maximum
FFT1- numerical integral	0.0021	0.0059	-0.0150	0.0683
FFT2- FFT1	0.0021	0.0059	-0.0150	0.0683

4.1.2 External Height Anomaly Computation via Generalized Hotine Integration

[Function] Computes the external residual height anomaly (m) via Hotine integration, utilizing an ellipsoidal height grid of an equipotential boundary surface and the corresponding residual gravity disturbance grid (mGal) on that surface.

[Input Files]

(1) Equipotential Surface Ellipsoidal Height Grid File: Provides the geodetic coordinates of Equipotential Boundary Surface, for deriving integration distances.

(2) Residual Gravity Disturbance Grid File: Must share identical specifications (extent, resolution) with the ellipsoidal height grid.

(3) Computation Point file: a Space Computation Point File or a Computation Surface Ellipsoidal Height grid File.

[Parameter Settings]

Define input file parsing rules.

Specify the Integration Radius.

Select the computational algorithm (Rigorous Numerical Integration or FFT-based acceleration).

[Output Files]

Residual Height Anomaly Results:

● Discrete Input: Appends a column of computed residual height anomalies to the source file, retaining 4 significant figures.

● Grid Input: Generates a residual height anomaly grid file matching the input grid specifications.

[Case Study & Accuracy Assessment]

Following the methodology established for the Stokes integration analysis, this section evaluates the performance of the Hotine integration by statistically analyzing the differences between the computed results and the model reference truth (degrees 541 – 1800 EGM2008).

Table 4.4: Differences between Hotine Computed Results and Reference Truth (Unit: m)

Algorithm	Mean	Std. Dev.	Minimum	Maximum
Numerical Integration	-0.0001	0.0256	-0.0915	0.0957
FFT2	0.0019	0.0259	-0.0911	0.1065

FFT1	0.0018	0.0261	-0.0934	0.1036

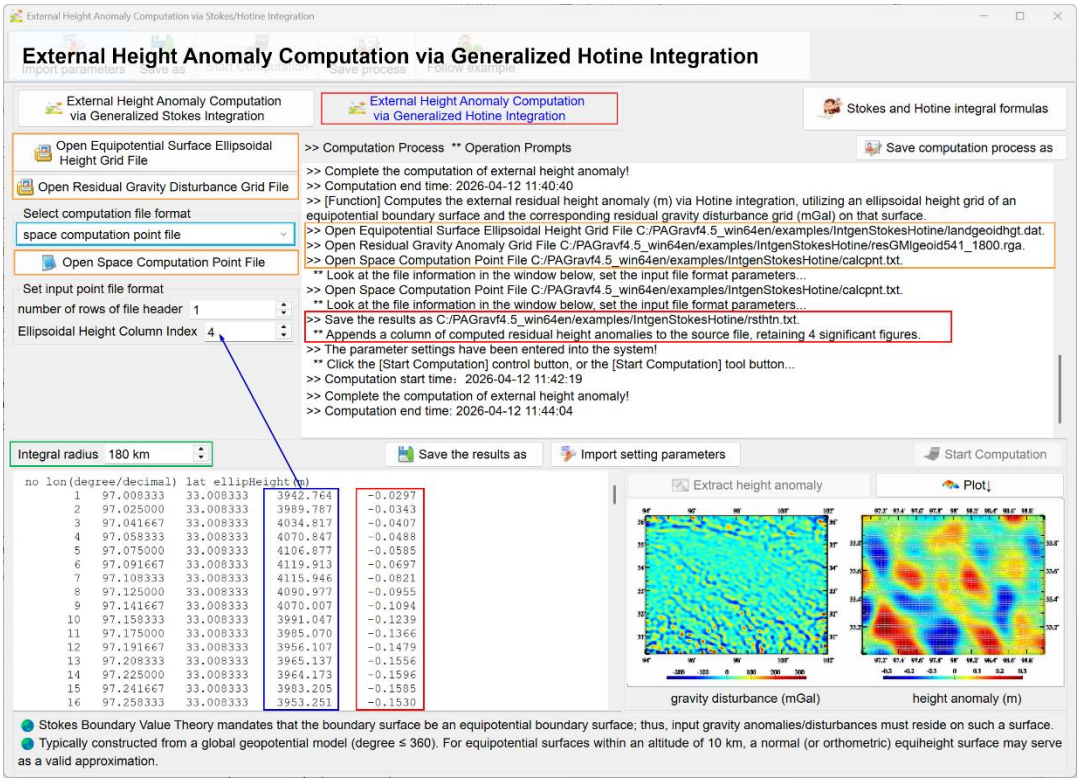

Analysis & Conclusions:

● Algorithm Performance: The ratio of the standard deviation of Differences in Table 4.4 to the standard deviation of Reference Truths in Table 4.1 reflects the approximation ability of the corresponding algorithm.

● By comparing Table 4.2, it can be seen that the performance of the Hotine integration algorithm is slightly better than that of the Stokes integration algorithm.

Furthermore, inter-method consistency is evaluated by comparing the results derived from Stokes and Hotine integrations.

Table 4.5: Differences between Stokes and Hotine Integration Results (Unit: m)

Algorithm	Mean	Std. Dev.	Minimum	Maximum
Numerical Integration	0.0020	0.0090	-0.0264	0.0658
FFT2	-0.0000	0.0067	-0.0239	0.0258
FFT1	-0.0000	0.0068	-0.0245	0.0250

● Analysis: The negligible mean differences (approaching zero) and low standard deviations (~6 – 7 mm) observed in the FFT implementations confirm that, for high-resolution applications, the solutions based on gravity anomalies (Stokes) and gravity disturbances (Hotine) converge to consistent results.

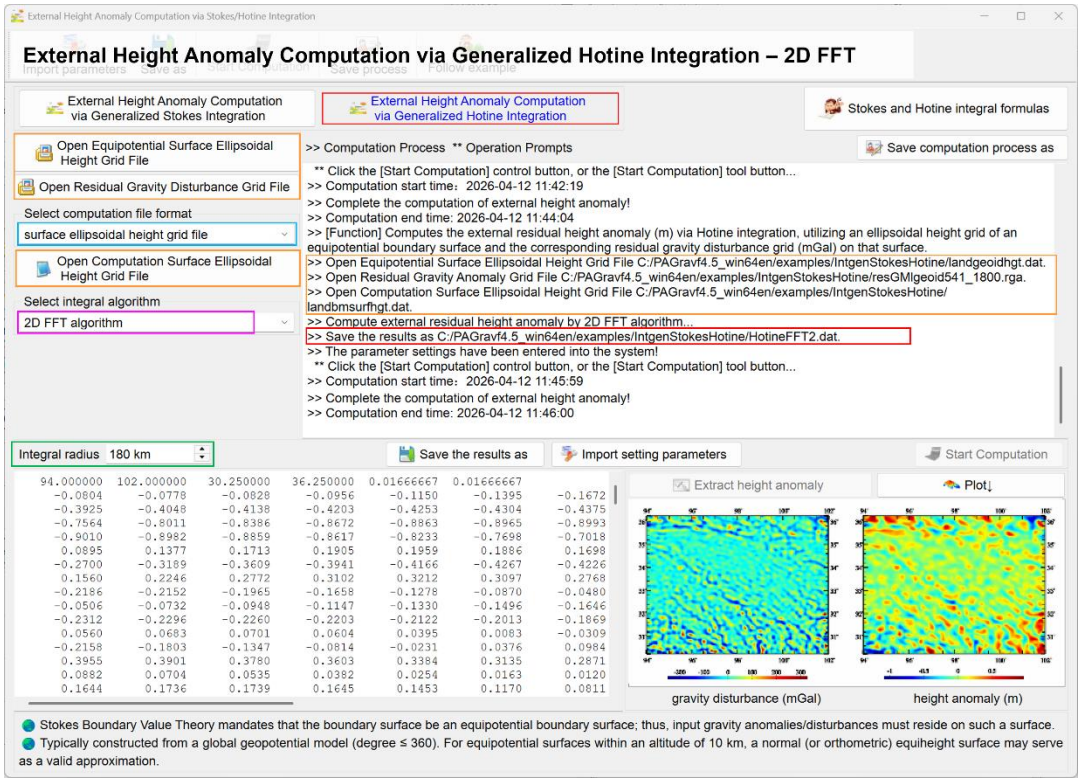

4.2 External Vertical Deflection Computation via Vening-Meinesz Integration

[Purpose] To compute the vertical deflection (″; southward ξ and westward η) on or outside the geoid. This is achieved using generalized rigorous numerical integration or Fast Fourier Transform (FFT) algorithms based on the Vening-Meinesz theory. Inputs include an ellipsoidal height grid defining an equipotential boundary surface and the corresponding gravity anomaly or gravity disturbance grid (mGal) on that surface.

Theoretical Basis: The generalized Vening-Meinesz formula, derived from the generalized Stokes/Hotine formulas, provides a solution to the Stokes Boundary Value Problem. It strictly requires the integrand (i.e., gravity anomaly or disturbance) to be defined on an equipotential boundary surface.

4.2.1 Computation of External Vertical Deflection from Gravity Anomaly

[Function] Computes the external residual vertical deflection (″, south and west components) via the generalized Vening-Meinesz integration, utilizing an ellipsoidal height grid of an equipotential boundary surface and the corresponding residual gravity anomaly grid (mGal).

[Input Files]

(1) Equipotential Surface Ellipsoidal Height Grid: Provides the geodetic coordinates of equipotential boundary surface, for deriving integration distances.

(2) Residual Gravity Anomaly Grid: Must share identical specifications (extent, resolution) with the ellipsoidal height grid.

(3) Computation Point file: a Space Computation Point File or a Computation Surface

Ellipsoidal Height grid File.

● Discrete Point record Format: ID (Point No./Name), Longitude (deg), Latitude (deg), Ellipsoidal Height (m), ...

[Parameter Settings]

Define input file parsing rules.

Specify the Integration Radius.

Select the computational algorithm (Numerical Integration or FFT).

[Output Files]

Residual Vertical Deflection Results:

● Discrete Input: Appends two columns (southward and westward components) of computed residual vertical deflections to the source file, retaining 4 significant figures.

● Grid Input: Generates a residual vertical deflection vector grid file matching the input grid specifications.

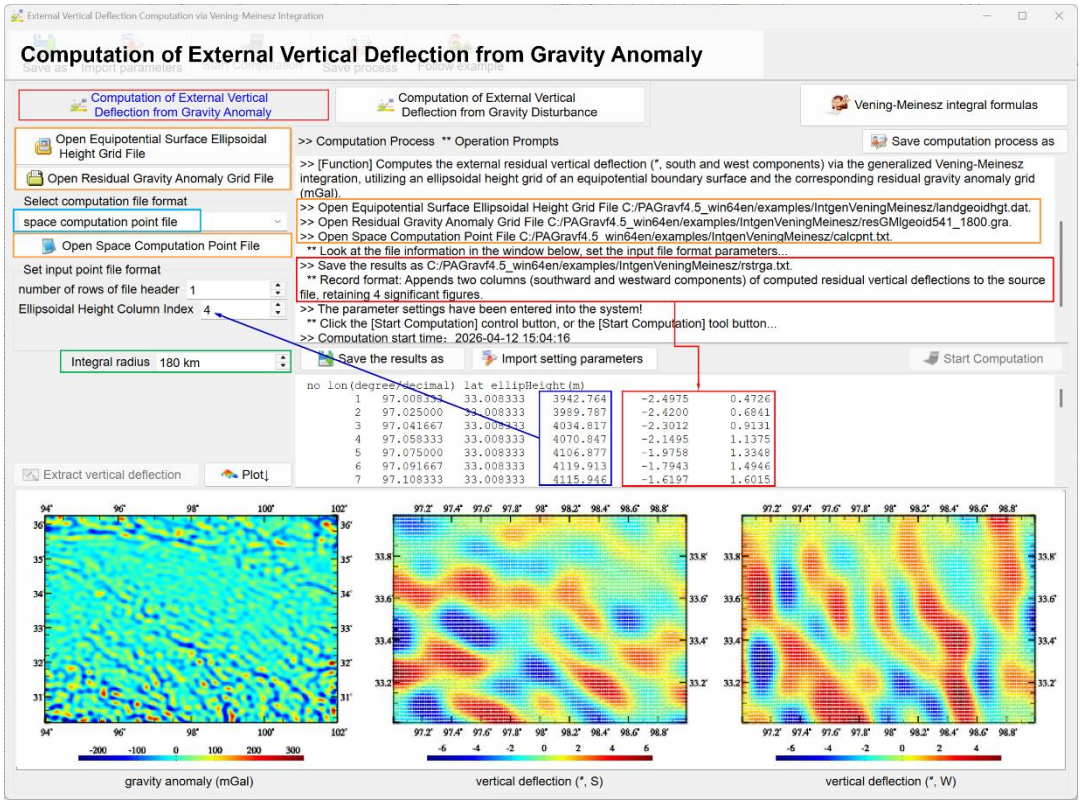

[Case Study & Accuracy Assessment]

In this example, residual ground vertical deflections are computed via generalized Vening-Meinesz integration (Radius = 180 km) using residual gravity anomalies (derived from the EGM2008 model, degrees 541 – 1800) on the geoid.

Excluding a 2° marginal buffer zone to mitigate integration edge effects, statistical analysis compares:

● Reference Truth: Model residual vertical deflections (degrees 541 – 1800 EGM2008).

● Algorithm Errors: Differences between computed results and the reference truth.

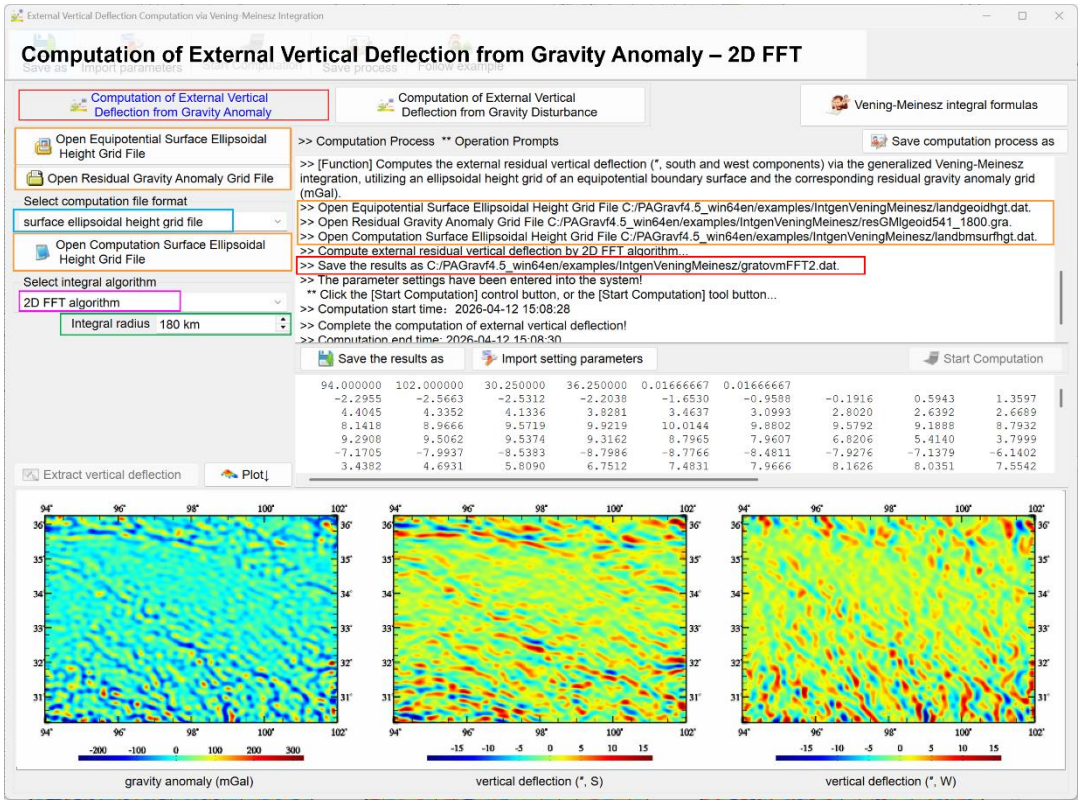

Table 4.6: Statistics of Model Reference Truth (Unit: ″)

Component	Mean	Std. Dev.	Min	Max
Ground Vertical Deflection (South, ξ)	0.0014	2.4951	-12.7789	14.2346
Ground Vertical Deflection (West, η)	0.0097	2.1772	-9.1577	10.4499

Table 4.7: Differences between Computed Results (Anomaly-based) and Reference Truth (Unit: ″)

Algorithm	Component	Mean	Std. Dev.	Min	Max
Numerical integral	South (ξ)	0.0003	0.0380	-0.1061	0.1387
	West (η)	0.0011	0.0289	-0.0830	0.1091
FFT2	South (ξ)	0.0002	0.1107	-0.8974	0.7395
	West (η)	0.0011	0.1003	-0.6887	1.0743
FFT1	South (ξ)	0.0007	0.1090	-0.8189	0.6581
	West (η)	0.0011	0.0984	-0.6078	1.0866

Algorithm Performance: The ratio of the standard deviation of Differences in Table 4.7 to the standard deviation of Reference Truths in Table 4.6 reflects the approximation ability of the corresponding algorithm.

4.2.2 Computation of External Vertical Deflection from Gravity Disturbance

[Function] Computes the external residual vertical deflection (″, south and west components) via the generalized Vening-Meinesz integration, utilizing an ellipsoidal height grid of an equipotential boundary surface and the corresponding residual gravity disturbance grid (mGal).

[Input Files & Parameters]

Identical to Section 4.2.1, except the input gravity field element is residual gravity disturbance.

[Output Files]

Identical to Section 4.2.1, producing southward and westward components.

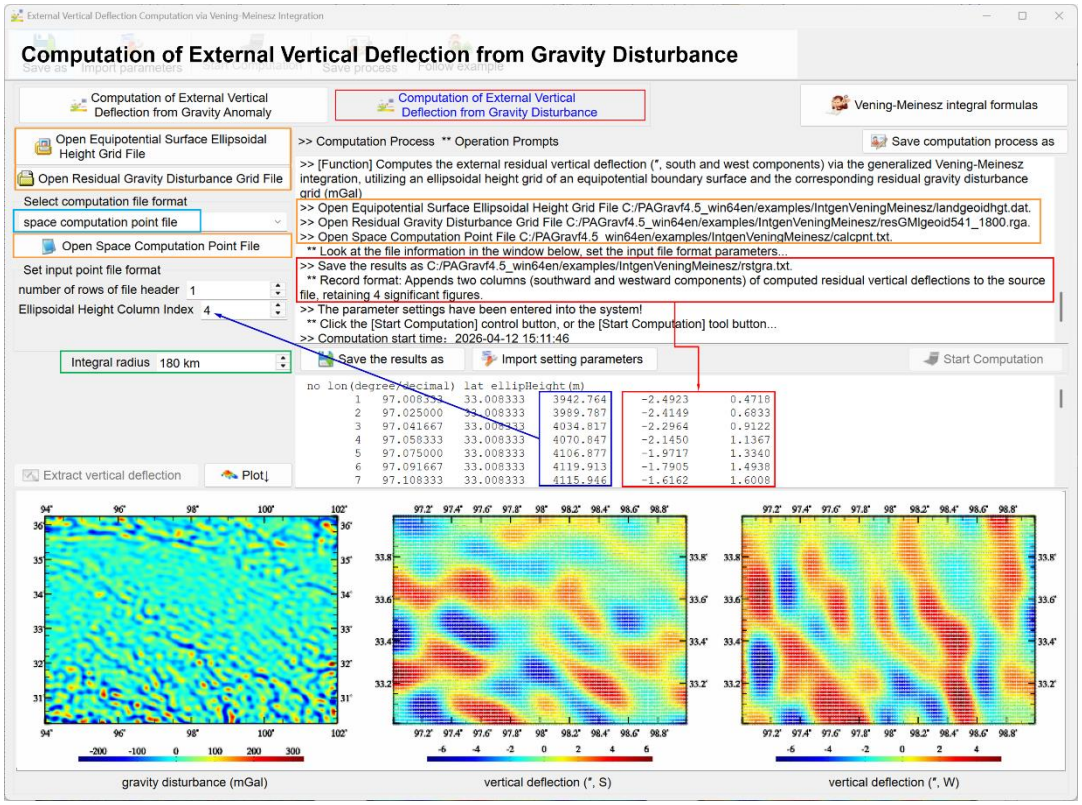

[Case Study & Accuracy Assessment]

Statistical analysis evaluates the differences between the disturbance-based integration results and the model reference truth.

Table 4.8: Differences between Computed Results (Disturbance-based) and Reference Truth (Unit: ″)

Algorithm	Component	Mean	Std. Dev.	Min	Max
Numerical integral	South (ξ)	-0.0003	0.0274	-0.0872	0.0994
	West (η)	0.0005	0.0200	-0.0646	0.0836
FFT2	South (ξ)	0.0002	0.1072	-0.8692	0.7094
	West (η)	0.0010	0.0959	-0.6204	1.0981

FFT1	South (ξ)	0.0007	0.1058	-0.7910	0.6481
	West (η)	0.0010	0.0959	-0.6204	1.0981

Analysis & Conclusions:

● The ratio of the standard deviation of Differences in Table 4.8 to the standard deviation of Reference Truths in Table 4.6 reflects the approximation ability of the corresponding algorithm.

● By comparing Table 4.7, it can be seen that the performance of the integration using gravity disturbance is slightly better than that using gravity anomaly.

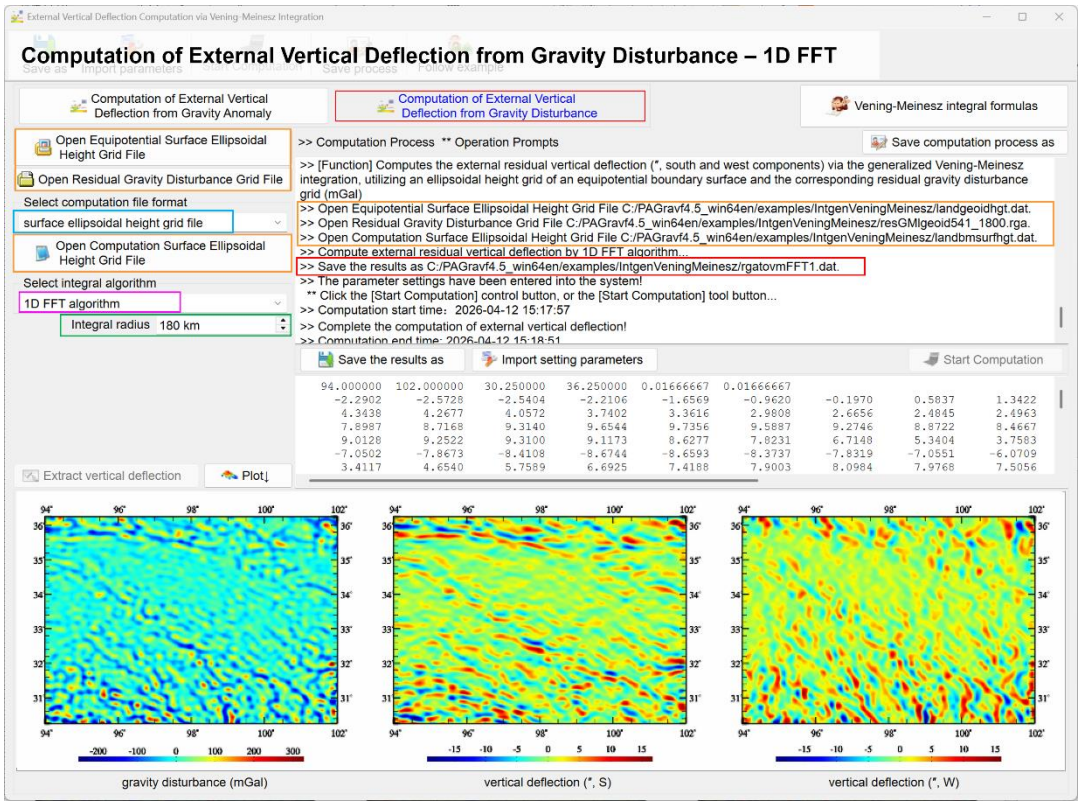

Furthermore, inter-input consistency is evaluated by comparing results derived from gravity anomalies versus gravity disturbances.

Table 4.9: Differences between Anomaly-based and Disturbance-based Results (Unit: ″)

Algorithm	Component	Mean	Std. Dev.	Min	Max
Numerical integral	South (ξ)	-0.0000	0.0062	-0.0286	0.0329
	West (η)	0.0003	0.0059	-0.0206	0.0261
FFT2	South (ξ)	-0.0000	0.0062	-0.0286	0.0329
	West (η)	0.0001	0.0050	-0.0189	0.0244
FFT1	South (ξ)	-0.0000	0.0062	-0.0284	0.0325
	West (η)	0.0001	0.0050	-0.0189	0.0241

● Analysis: The negligible differences (mean ≈ 0, std. dev. ≈ 5 – 6 mas) confirm that, under high-resolution gridding, the Vening-Meinesz solutions driven by gravity anomalies and gravity disturbances are theoretically consistent and numerically equivalent.

4.3 Inverse Integration and Integral of Inverse Operation for Anomalous Field Elements

[Purpose] To compute anomalous gravity field elements (e.g., gravity anomalies or disturbances) from an ellipsoidal height grid defining an equipotential boundary surface and the corresponding height anomaly (m) or vertical deflection vector (″) grid on that surface. This is achieved using either the Inverse Integration method or the Integral of Inverse Operation method.

Integral of Inverse Operation: A rigorous solution to the Stokes-type Boundary Value Problem. It strictly requires the integrand (height anomaly or vertical deflection) to reside on an equipotential boundary surface.

Inverse Integration: Employs a hybrid algorithm combining Poisson integration with the differentiation of anomalous field elements. This approach is more flexible and does not mandate the boundary surface to be an equipotential boundary surface.

[Computational Strategy: Remove-Restore Scheme] To perform integration over a finite radius in local regions, a Remove-Restore scheme based on a reference global geopotential model is employed:

Remove: Subtract the model values of the source field element (e.g., height anomaly) from the boundary surface data.

Invert: Compute the residual values of the target field element (e.g., gravity anomaly) at the computation point via inverse integration or integral of inverse operation.

Restore: Add the model values of the target field element back at the computation point.

4.3.1 Computation of Gravity Anomaly via Inverse Stokes Integration

[Function] Computes the residual gravity anomaly (mGal) on an equipotential boundary surface via Inverse Stokes Integration, utilizing the surface's ellipsoidal height grid and the corresponding residual height anomaly (m) grid.

[Input Files]

(1) Equipotential Surface Ellipsoidal Height Grid: Provides the geodetic coordinates of equipotential boundary surface, for deriving integration distances.

(2) Height Anomaly Grid: Must share identical specifications (extent, resolution) with the ellipsoidal height grid.

(3) Discrete Computation Point File: Discrete points located on the equipotential surface.

● File record Format: ID (Point No./Name), Longitude (deg), Latitude (deg), ...

[Parameter Settings]

Define input file parsing rules.

Specify the Integration Radius.

Select the computational algorithm (Numerical Integration or FFT).

Computation Surface: If no separate computation grid is provided, the program defaults to using the input equipotential surface ellipsoidal height grid as the computation surface.

[Output Files]

Residual Gravity Anomaly Results:

● Discrete Input: Appends two columns to the source file: Interpolated Ellipsoidal Height of the computation point, and Computed Residual Gravity Anomaly value.

● Grid Input: Generates a residual gravity anomaly grid file matching the input grid specifications.

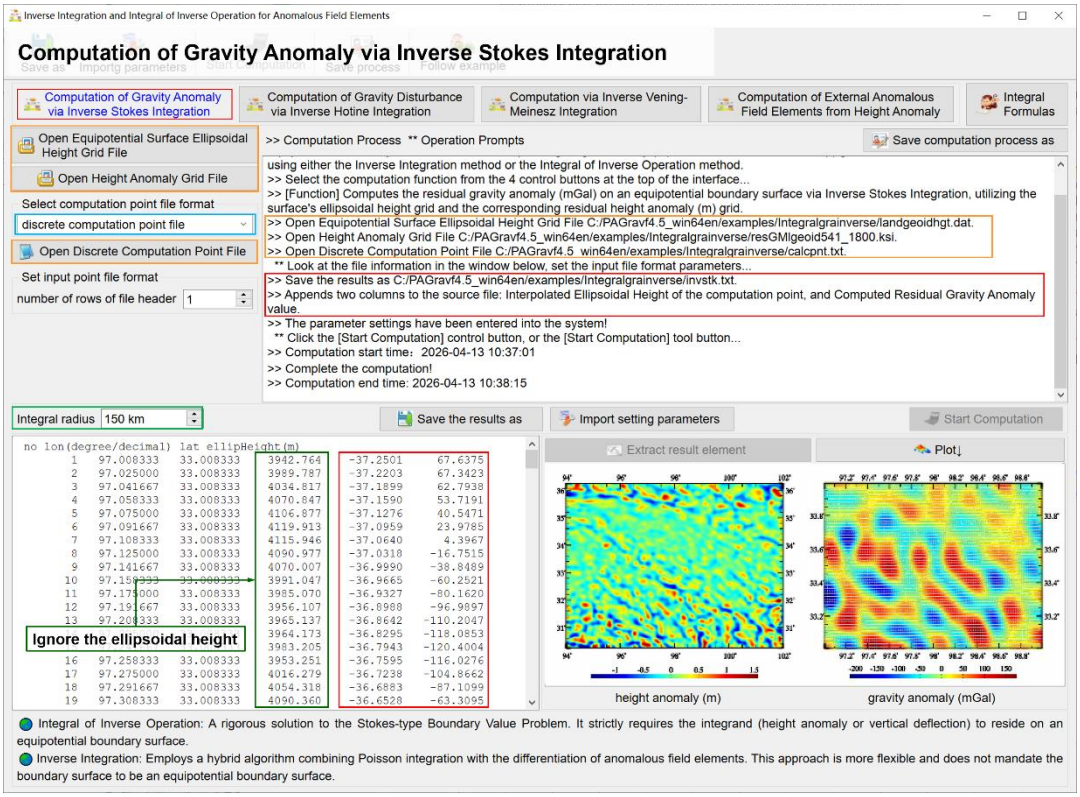

[Case Study & Accuracy Assessment]

In this example, residual gravity anomalies on the geoid are computed via Inverse Stokes Integration (Radius = 150 km) using residual height anomalies (derived from the EGM2008 model, degrees 541 – 1800) on the geoid.

Excluding a 2° marginal buffer zone to mitigate integration edge effects, statistical analysis compares:

Reference Truth: Model residual gravity anomalies (degrees 541 – 1800 EGM2008).

Algorithm Errors: Differences between computed results and the reference truth.

Table 4.10: Statistics of Model Reference Truth (Unit: mGal)

Item	Mean	Std. Dev.	Min	Max
Residual Gravity Anomalies (Deg 541 – 1800)	0.4334	34.0852	-170.9556	177.8780

Table 4.11: Differences between Inverse Operation Integration Results and Reference Truth (Unit: mGal)

Algorithm	mean	standard deviation	minimum	maximum
Numerical Integral	-0.0415	2.9285	-15.2734	14.6970
FFT2	-0.0433	2.8208	-11.9201	13.3607
FFT1	-0.0444	3.0509	-15.7950	15.5242

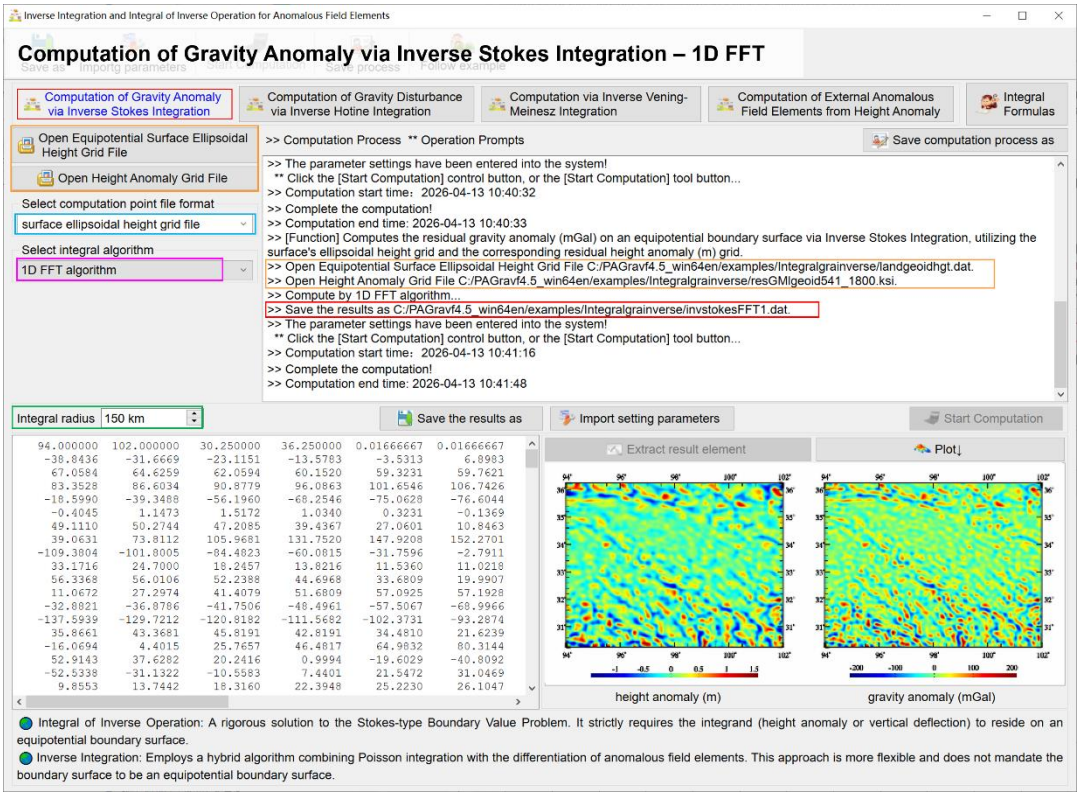

Algorithm Performance: The ratio of the standard deviation of Differences in Table 4.11 to the standard deviation of Reference Truths in Table 4.10 reflects the approximation ability of the corresponding algorithm. Both numerical and FFT algorithms achieve a standard deviation of approximately 3 mGal.

4.3.2 Computation of Gravity Disturbance via Inverse Hotine Integration

[Function] Computes the residual gravity disturbance (mGal) on the surface via the Integral of Inverse Hotine Operation, utilizing the ellipsoidal height grid of the equipotential boundary surface and the corresponding residual height anomaly (m) grid.

[Input Files & Parameters]

Identical to Section 4.3.1, with the target output being gravity disturbance.

[Output Files]

Residual Gravity Disturbance Results:

- Discrete Input: Appends columns for interpolated Ellipsoidal Height and computed

Residual Gravity Disturbance.

● Grid Input: Generates a residual gravity disturbance grid file matching the input specifications.

[Case Study & Accuracy Assessment]

In this example, residual gravity disturbances on the geoid are computed via the Inverse Hotine Operation (Radius = 150 km) using residual height anomalies derived from the EGM2008 model, degrees 541 – 1800.

Statistical analysis evaluates the differences between the computed results and the model reference truth (degrees 541 – 1800 EGM2008).

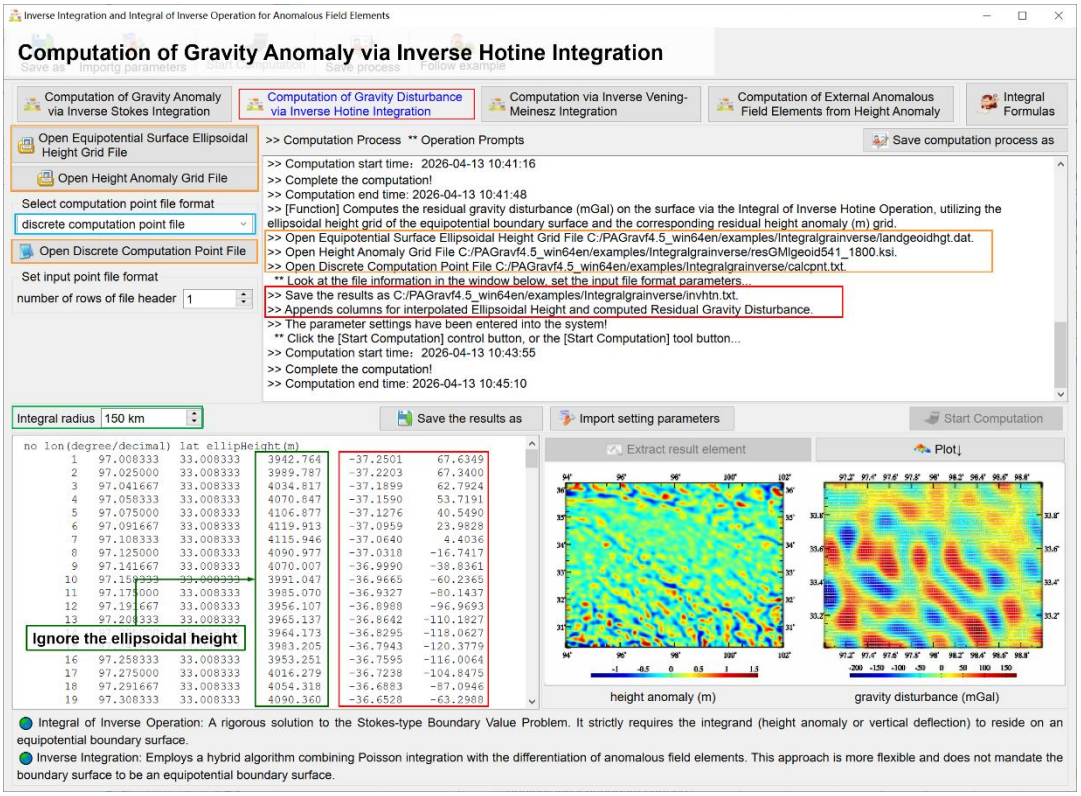

Table 4.12: Statistics of Model Reference Truth (Unit: mGal)

Item	Mean	Std. Dev.	Min	Max
Residual Gravity Disturbances (Deg 541 – 1800)	0.4334	34.0852	-170.9556	177.8780

Table 4.13: Differences between Inverse Operation Integration Results and Reference Truth (Unit: mGal)

Algorithm	Mean	Std. Dev.	Min	Max
Numerical Integral	-0.0415	2.9285	-15.2734	14.6970
FFT2	-0.0433	2.8208	-11.9201	13.3607
FFT1	-0.0444	3.0509	-15.7950	15.5242

Analysis & Conclusions:

● Algorithm Performance: The ratio of the standard deviation of Differences in Table 4.13 to the standard deviation of Reference Truths in Table 4.12 reflects the approximation ability of the corresponding algorithm.

● The Inverse Hotine numerical integration yields a standard deviation of ~2.93 mGal, comparable to the Inverse Stokes method but with a slightly reduced maximum error range (±9.7 mGal vs. ±15.3 mGal). This suggests marginally better numerical stability when solving for gravity disturbances directly.

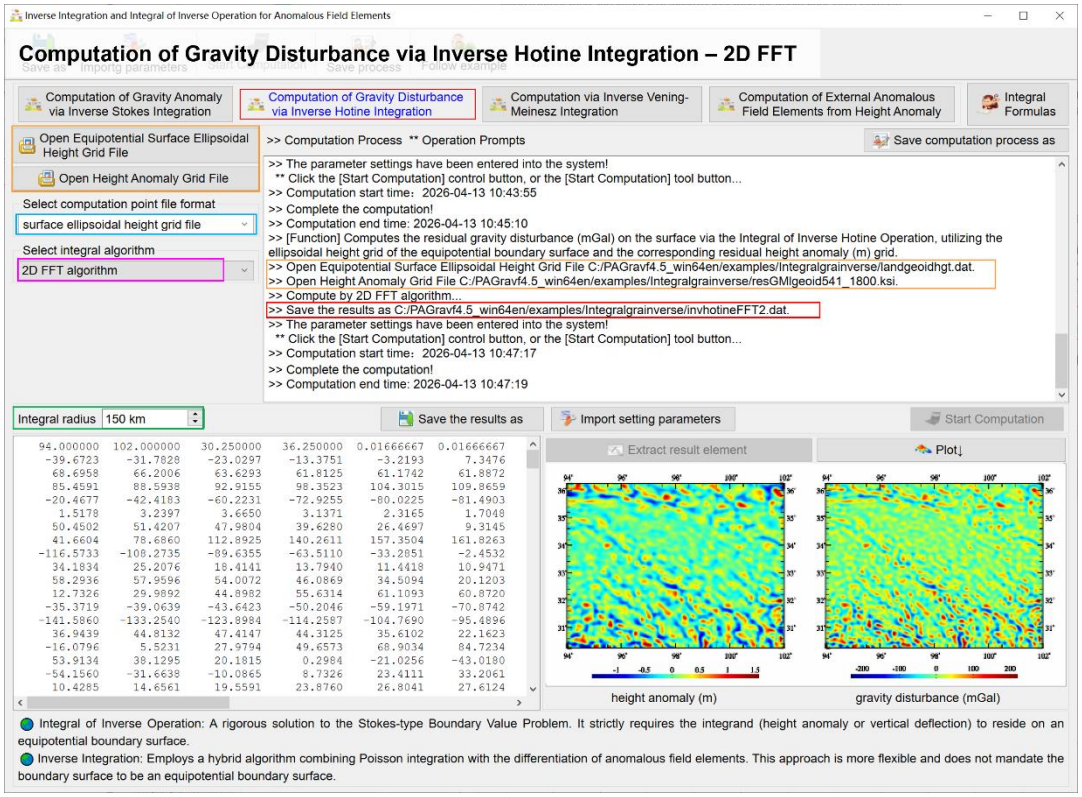

4.3.3 Computation via Inverse Vening-Meinesz Integration

[Function] Computes the residual height anomaly (m), gravity anomaly (mGal), and gravity disturbance (mGal) on an equipotential boundary surface. This is achieved via Inverse Vening-Meinesz Integration, utilizing the surface's ellipsoidal height grid and the corresponding residual vertical deflection vector grid (″, south and west components).

[Input Files]

(1) Equipotential Surface Ellipsoidal Height Grid: Provides the geodetic coordinates of equipotential boundary surface, for deriving integration distances.

(2) Vertical Deflection Vector Grid: Must share identical specifications (extent, resolution) with the ellipsoidal height grid.

(3) Discrete Computation Point File: Discrete points located on the equipotential surface.

● File record Format: ID (Point No./Name), Longitude (deg), Latitude (deg), ...

[Parameter Settings]

Define input file parsing rules.

Specify the Integration Radius.

Select the computational algorithm (Numerical Integration or FFT).

Computation Surface: If no separate computation grid is provided, the program defaults to using the input equipotential surface ellipsoidal height grid.

[Output Files]

● Discrete Input: Appends four columns to the source file: Interpolated Ellipsoidal Height, Residual Height Anomaly, Gravity Anomaly, and Gravity Disturbance.

● Grid Input: Generates a comprehensive result file containing: Point ID, Longitude, Latitude, Ellipsoidal Height, Residual Height Anomaly, Gravity Anomaly, Gravity Disturbance.

○ Additional Grid Files: The program automatically generates three separate grid files in the current directory, prefixed by the user-defined output name (*): Residual Height Anomaly grid (*.ksi), Residual Gravity Disturbance grid (*.rga), and Residual Gravity Anomaly grid (*.gra).

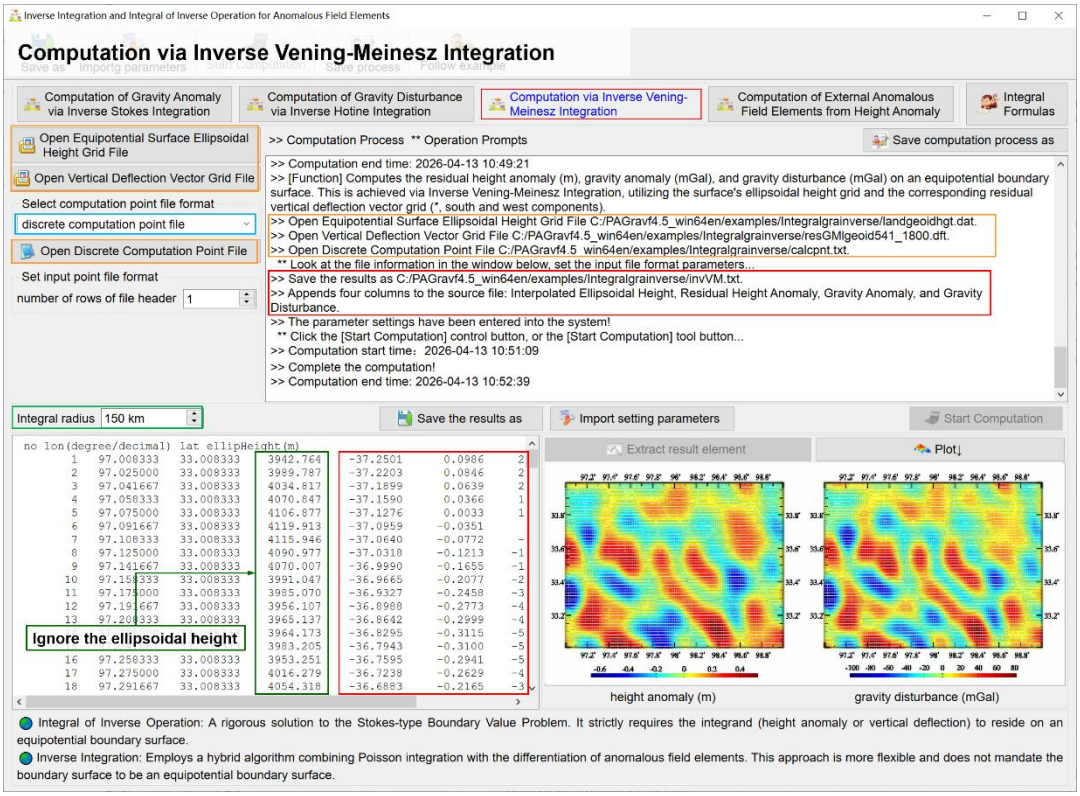

[Case Study & Accuracy Assessment]

In this example, residual geoidal heights (height anomalies), gravity anomalies, and gravity disturbances on the geoid are computed via Inverse Vening-Meinesz Integration (Radius = 150 km) using residual vertical deflection vectors derived from the EGM2008 model, degrees 541 – 1800.

Excluding a 2° marginal buffer zone to mitigate integration edge effects, statistical analysis compares the computed results against the model reference truth (degrees 541 – 1800 EGM2008) for all three field elements.

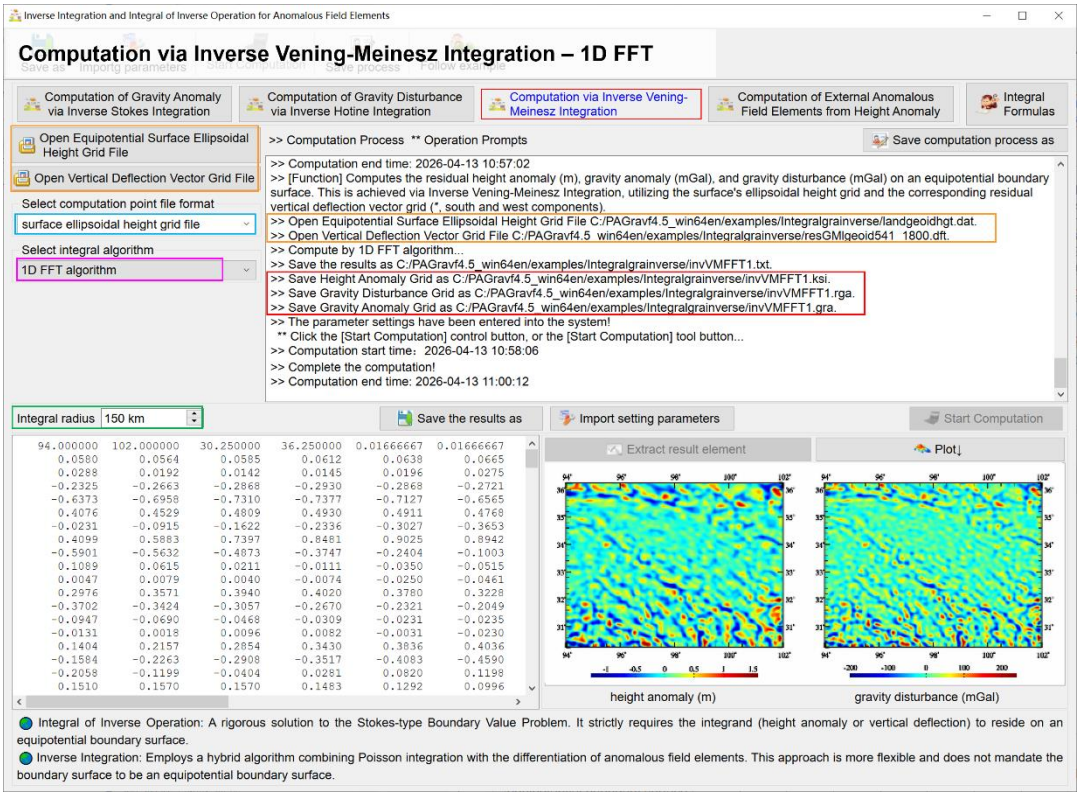

Table 4.14: Statistics of Model Reference Truths

Field Element	Unit	Mean	Std. Dev.	Min	Max
Residual Geoidal Heights	m	0.0045	0.2172	-1.1490	0.9110
Residual Gravity Disturbances	mGal	0.4348	34.1479	-171.3088	178.1561
Residual Gravity Anomalies	mGal	0.4334	34.0852	-170.9556	177.8780

Table 4.15: Differences between Inverse Operation Integration Results and Reference Truth

Algorithm	Field Element	Unit	Mean	Std. Dev.	Min	Max
Numerical integral	Residual Geoidal Heights	m	-0.0002	0.0331	-0.1066	0.1266
	Residual Gravity Disturbances	mGal	-0.0281	3.5304	-19.8306	15.5799
	Residual Gravity Anomalies	mGal	-0.0280	3.5293	-19.8233	15.5701
FFT2	Residual Geoidal Heights	m	0.0001	0.0337	-0.1057	0.1271
	Residual Gravity Disturbances	mGal	-0.0131	2.4732	-12.3026	9.8919
	Residual Gravity Anomalies	mGal	-0.0131	2.4729	-12.2973	9.8831

FFT1	Residual Geoidal Heights	m	-0.0001	0.0332	-0.1068	0.1263
	Residual Gravity Disturbances	mGal	-0.0283	3.5527	-19.9907	15.7164
	Residual Gravity Anomalies	mGal	-0.0283	3.5516	-19.9830	15.7072

Analysis & Conclusions:

● Algorithm Performance: The ratio of the standard deviation of Differences in Table 4.15 to the standard deviation of Reference Truths in Table 4.14 reflects the approximation ability of the corresponding algorithm.

● Geoidal Height Recovery: All three algorithms demonstrate comparable performance in recovering geoidal heights, with standard deviations around 3.3 cm and maximum errors within ±13 cm. This confirms the high stability of the Inverse Vening-Meinesz formula.

● Internal Consistency: The nearly identical error statistics for gravity anomalies and gravity disturbances validate the internal logical consistency of the algorithm implementation.

4.3.4 Computation of External Anomalous Gravity Field Elements from Height Anomaly

[Function] Computes the residual gravity anomaly (mGal), residual gravity disturbance (mGal), and residual vertical deflection vector (″, south and west components) on or outside the geoid. Inputs include an ellipsoidal height grid of a boundary surface and the corresponding residual height anomaly (m) grid.

Algorithmic Basis: The inverse operation for height anomalies employs a hybrid algorithm combining Poisson integration with differentiation. This approach does not require the boundary surface to be an equipotential boundary surface.

[Input Files]

(1) Boundary Surface Ellipsoidal Height Grid File: Provides the geodetic coordinates of Boundary Surface, for deriving integration distances.

(2) Height Anomaly Grid File: Must share identical specifications (extent, resolution) with the ellipsoidal height grid.

(3) Computation Point file: a Space Computation Point File or a Computation Surface Ellipsoidal Height grid File.

● Discrete Point record Format: ID (Point No./Name), Longitude (deg), Latitude (deg), Ellipsoidal Height (m), ...

[Parameter Settings]

Define input file parsing rules.

Specify the Integration Radius.

Select the computational algorithm.

[Output Files]

External Anomalous Field Elements Result File:

● Discrete Input: Appends four attribute columns to the source file: Residual Gravity

Anomaly, Residual Gravity Disturbance, Residual Vertical Deflection (Southward), and Residual Vertical Deflection (Westward).

● Grid Input: Generates a comprehensive result file containing: Point ID, Longitude, Latitude, Ellipsoidal Height, Residual Gravity Anomaly, Residual Gravity Disturbance, Residual Vertical Deflection (S), Residual Vertical Deflection (W).

○ Additional Grid Files: The program automatically generates three separate grid files in the current directory, prefixed by the user-defined output name (*): Residual Gravity Anomaly grid (*.gra), Residual Gravity Disturbance grid (*.rga), and Residual Vertical Deflection Vector grid (*.dft).

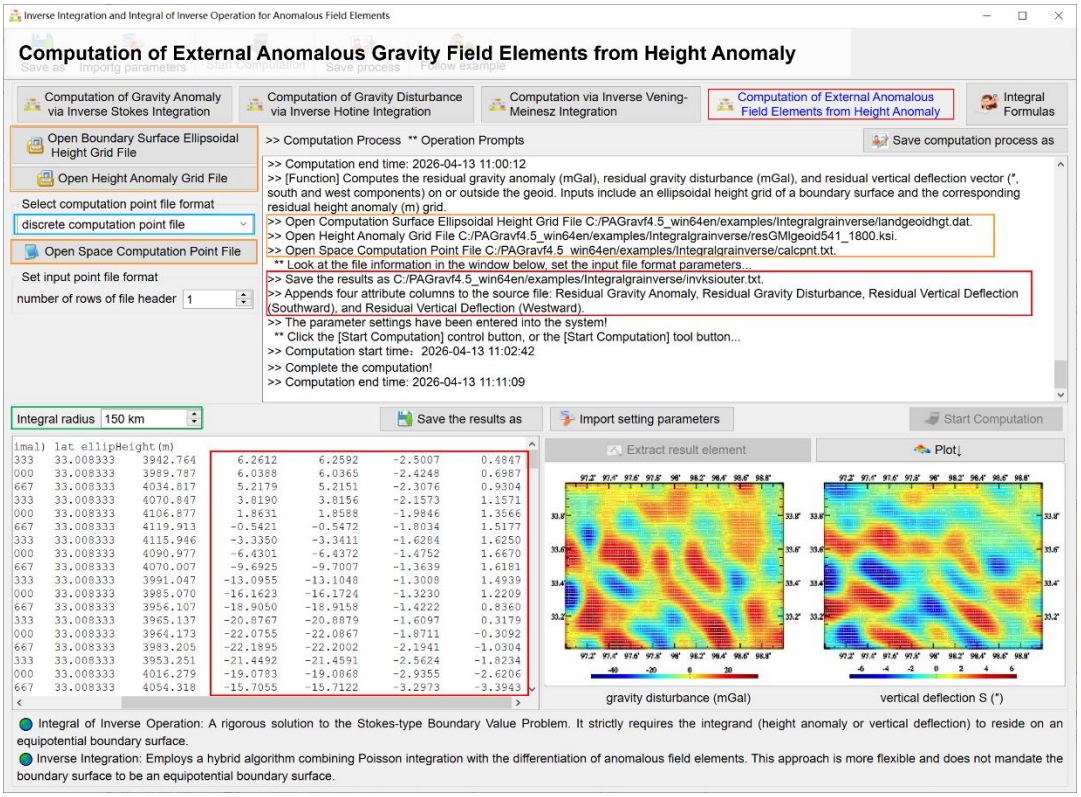

[Case Study & Accuracy Assessment]

In this example, ground residual gravity anomalies, gravity disturbances, and vertical deflections are computed from residual geoidal heights (Radius = 150 km) derived from the EGM2008 model, degrees 541 – 1800.

Excluding a 2° marginal buffer zone to mitigate integration edge effects, statistical analysis compares the computed results against the model reference truth (degrees 541 – 1800 EGM2008) for ground-based field elements.

Table 4.16: Statistics of Model Reference Truths

Field Element	Unit	Mean	Std. Dev.	Min	Max
Ground Residual Gravity anomalies	mGal	-0.0349	15.7184	-93.7784	66.5507
Ground Residual Gravity	mGal	-0.0346	15.7527	-93.9854	66.6638

disturbances					
Ground Residual Vertical Deflection (S)	″	0.0014	2.4951	-12.7789	14.2346
Ground Residual Vertical Veflection (W)	″	0.0097	2.1772	-9.1577	10.4499

Table 4.17: Differences between Computed Results and Reference Truth

Field Element	Unit	Mean	Std. Dev.	Min	Max
Ground Residual Gravity anomalies	mGal	-0.0104	2.0577	-8.2097	10.7064
Ground Residual Gravity disturbances	mGal	-0.0100	2.0929	-8.3217	10.8982
Ground Residual Vertical Deflection (S)	″	0.0004	0.0075	-0.0357	0.0388
Ground Residual Vertical Veflection (W)	″	0.0003	0.0076	-0.0362	0.0358

Analysis & Conclusions:

● Algorithm Performance: The ratio of the standard deviation of Differences in Table 4.17 to the standard deviation of Reference Truths in Table 4.16 reflects the approximation ability of the corresponding algorithm.

● Exceptional Inversion Accuracy: The inversion from height anomalies to ground gravity field elements demonstrates exceptional precision. The standard deviations for gravity anomalies and disturbances are merely ~2.06 – 2.09 mGal, representing a significant signal-to-noise improvement over the original field variability (~15.7 mGal).

● High-Precision Vertical Deflection Recovery: The recovery of vertical deflections is remarkably accurate, with standard deviations of only 0.0075″ (7.5 mas) and maximum errors confined within ±0.04″. This underscores the superior numerical stability and high-frequency preservation capabilities of the combined Poisson integration and differentiation algorithm when transforming geoidal heights to vertical deflections.

● Algorithm Robustness: Given that this method does not require an equipotential boundary, these results further validate the algorithm's robustness and reliability for practical applications involving quasi-geoids or non-strict reference surfaces.

4.4 Gradient and Poisson Integral Computation of External Gravity Field Elements

[Purpose] To perform radial gradient integration, integral inverse operations, inverse operation integrations, and Poisson integrations on anomalous gravity field elements using rigorous numerical integration methods.

● Radial Gradient Integration: Derived from the solution to the Stokes Boundary Value Problem, this algorithm requires the integrand field elements to reside on an equipotential boundary surface.

● Poisson Integration: Constitutes the mathematical solution to the First Boundary Value

Problem. Unlike the Stokes-type problem, it does not require the boundary surface to be an equipotential surface, allowing for application on general reference surfaces (e.g., topographic surfaces).

4.4.1 Radial Gradient Integration of Anomalous Gravity Field Elements

[Function] Computes the radial gradient (/km) of a specific field element on a surface via numerical integration, utilizing the ellipsoidal height grid of the equipotential boundary surface and the corresponding anomalous gravity field element grid.

[Input Files]

(1) Equipotential Surface Ellipsoidal Height Grid: Provides the geodetic coordinates of equipotential boundary surface, for deriving integration distances.

(2) Anomalous Field Element Grid: Must share identical specifications with the height grid.

(3) Discrete Computation Point File: Discrete points located on the equipotential surface.

- File Record Format: ID (Point No./Name), Longitude (deg), Latitude (deg), ...

[Parameter Settings]

Define input file parsing rules.

Specify the Integration Radius.

Computation Surface: Defaults to the input equipotential surface ellipsoidal height grid if no separate computation grid is provided.

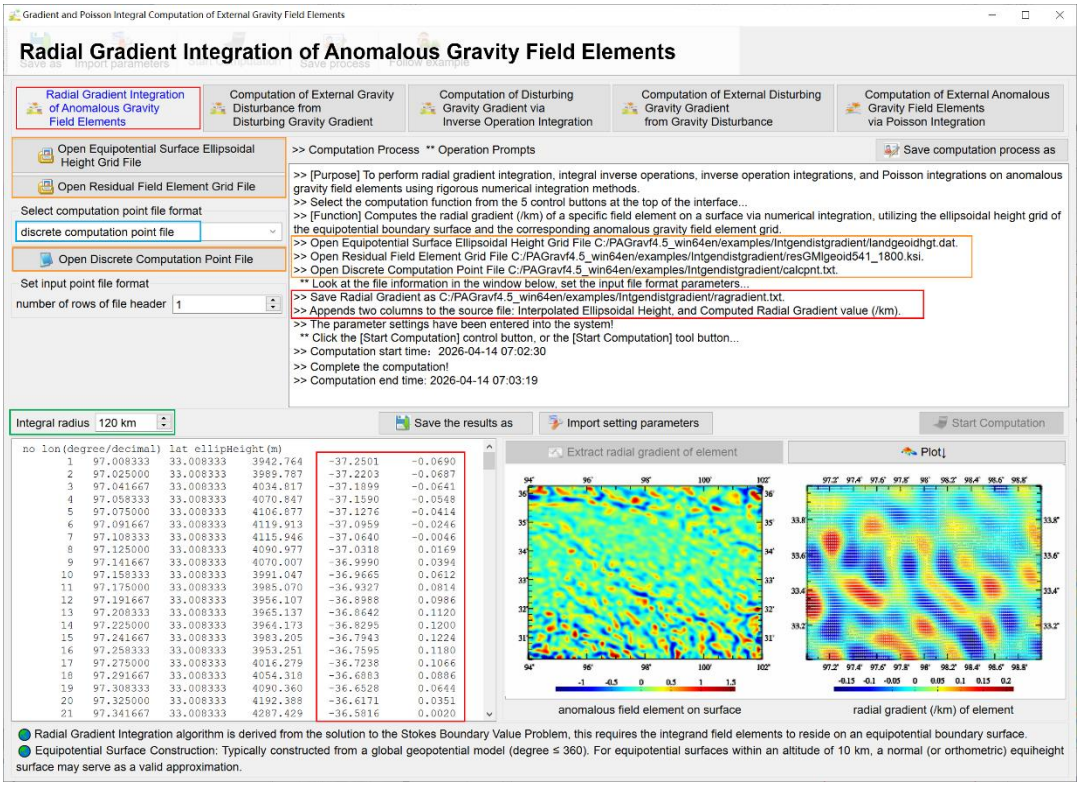

no	lon(degree/decimal)	lat	ellipHeight(m)		
1	97.008333	33.008333	3942.764	-37.2501	-0.0690
2	97.025000	33.008333	3989.787	-37.2203	-0.0687
3	97.041667	33.008333	4034.817	-37.1899	-0.0641
4	97.058333	33.008333	4070.847	-37.1590	-0.0548
5	97.075000	33.008333	4106.677	-37.1276	-0.0414
6	97.091667	33.008333	4119.913	-37.0959	-0.0246
7	97.108333	33.008333	4115.946	-37.0640	-0.0046
8	97.125000	33.008333	4090.977	-37.0318	0.0169
9	97.141667	33.008333	4070.007	-36.9990	0.0394
10	97.158333	33.008333	3991.047	-36.9665	0.0612
11	97.175000	33.008333	3985.070	-36.9327	0.0814
12	97.191667	33.008333	3956.107	-36.8988	0.0986
13	97.208333	33.008333	3965.137	-36.8642	0.1120
14	97.225000	33.008333	3964.173	-36.8295	0.1200
15	97.241667	33.008333	3983.205	-36.7943	0.1224
16	97.258333	33.008333	3953.251	-36.7595	0.1180
17	97.275000	33.008333	4016.279	-36.7238	0.1066
18	97.291667	33.008333	4054.318	-36.6883	0.0886
19	97.308333	33.008333	4090.360	-36.6528	0.0644
20	97.325000	33.008333	4192.388	-36.6171	0.0351
21	97.341667	33.008333	4287.429	-36.5816	0.0020

[Output Files]

Radial Gradient Result File:

- Discrete Input: Appends two columns to the source file: Interpolated Ellipsoidal Height,

and Computed Radial Gradient value (/km).

● Grid Input: Generates a radial gradient grid file (/km) matching the input grid specifications.

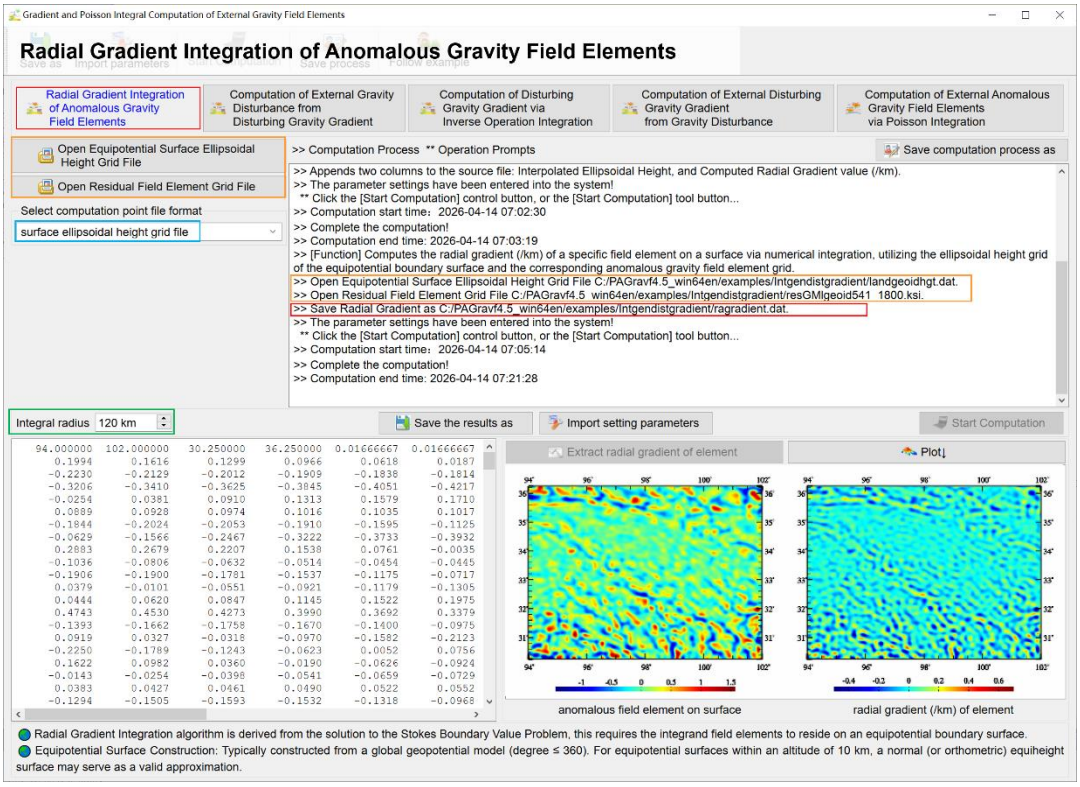

4.4.2 Computation of External Gravity Disturbance from Disturbing Gravity Gradient

[Function] Computes the residual gravity disturbance (mGal) on or outside the geoid via numerical integration, utilizing the ellipsoidal height grid of the equipotential boundary surface and the corresponding residual disturbing gravity gradient grid (E, radial component).

Note: This function performs the inversion (downward/upward continuation) from gravity gradients to gravity disturbances.

[Input Files]

(1) Equipotential Surface Ellipsoidal Height Grid.

(2) Residual Disturbing Gravity Gradient Grid: Must share identical specifications with the height grid.

(3) Computation Point file: a Space Computation Point File or a Computation Surface Ellipsoidal Height grid File.

● Discrete Point record Format: ID (Point No./Name), Longitude (deg), Latitude (deg), Ellipsoidal Height (m), ...

[Parameter Settings]

Define input file parsing rules.

Specify the Integration Radius.

[Output Files]

External Residual Gravity Disturbance Result File:

● Discrete Input: Appends one column containing the residual gravity disturbance value (formatted to four significant digits).

● Grid Input: Generates a residual gravity disturbance grid file matching the input grid specifications.

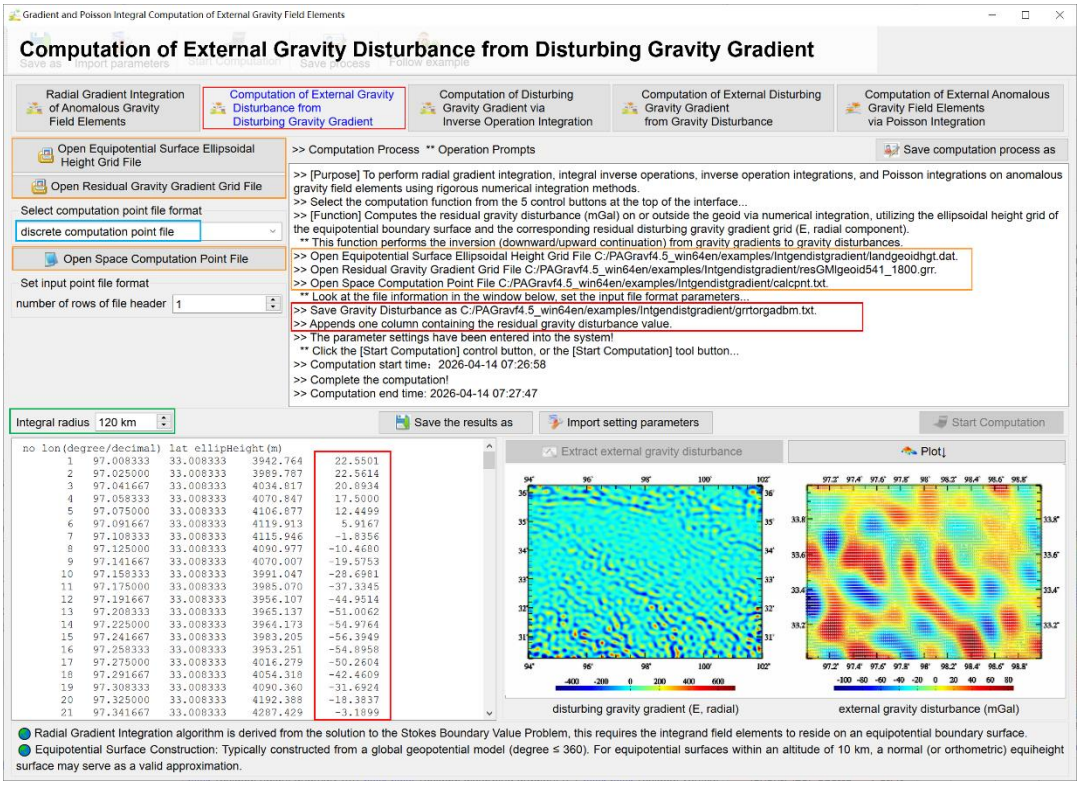

[Case Study & Accuracy Assessment]

In this example, ground residual gravity disturbances are computed from residual disturbing gravity gradients (derived from the EGM2008 model, degrees 541 – 1800) on the geoid via numerical integration (Radius = 120 km).

Excluding a 2° marginal buffer zone to mitigate integration edge effects, statistical analysis compares the results against the model reference truth (degrees 541 – 1800).

Table 4.18: Statistics of Model Reference Truth

Field Element	Unit	Mean	Std. Dev.	Min	Max
Ground Residual Gravity Disturbances	mGal	-0.0346	15.7527	-93.9854	66.6638

Table 4.19: Differences between Computed Results and Reference Truth

Field Element	Unit	Mean	Std. Dev.	Min	Max
Ground Residual Gravity Disturbances	mGal	0.0071	4.2456	-18.5325	16.5266

Analysis & Conclusions:

● Algorithm Performance: The ratio of the standard deviation of Differences in Table 4.19 to the standard deviation of Reference Truths in Table 4.18 reflects the approximation ability of the corresponding algorithm.

● Robustness: The inversion from gravity gradients to disturbances yields a standard deviation of approximately 4.25 mGal. Given the ill-posed nature of differentiation and the high-frequency content of gradient data, this accuracy demonstrates the algorithm's effectiveness in suppressing noise amplification while successfully recovering medium-to-long wavelength gravity signals.

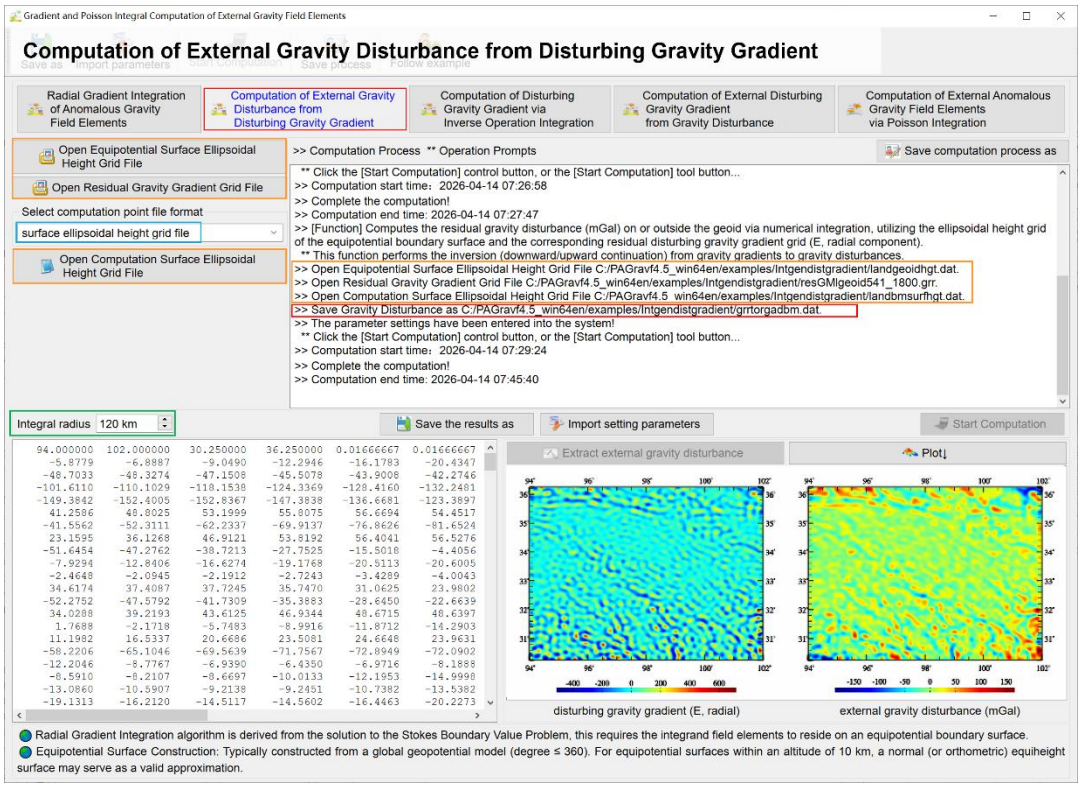

4.4.3 Computation of Disturbing Gravity Gradient via Inverse Operation Integration

[Function] Computes the residual disturbing gravity gradient (E, radial component) on a surface via inverse operation integration, utilizing the ellipsoidal height grid of the equipotential boundary surface and the corresponding residual gravity disturbance grid (mGal).

Note: This function effectively implements the differentiation of gravity field elements through an integral formulation.

[Input Files]

(1) Equipotential Surface Ellipsoidal Height Grid.

(2) Residual Gravity Disturbance Grid: Must share identical specifications with the height grid.

(3) Discrete Computation Point File: Discrete points located on the equipotential boundary surface.

● File Record Format: ID (Point No./Name), Longitude (deg), Latitude (deg), ...

[Parameter Settings]

Define input file parsing rules.

Specify the Integration Radius.

Computation Surface: Defaults to the input equipotential surface ellipsoidal height grid.

[Output Files]

Residual Disturbing Gravity Gradient Result File:

● Discrete Input: Appends two columns to the source file: Interpolated Ellipsoidal Height, and Computed residual disturbing gravity gradient value.

● Grid Input: Generates a residual disturbing gravity gradient grid file matching the input grid specifications.

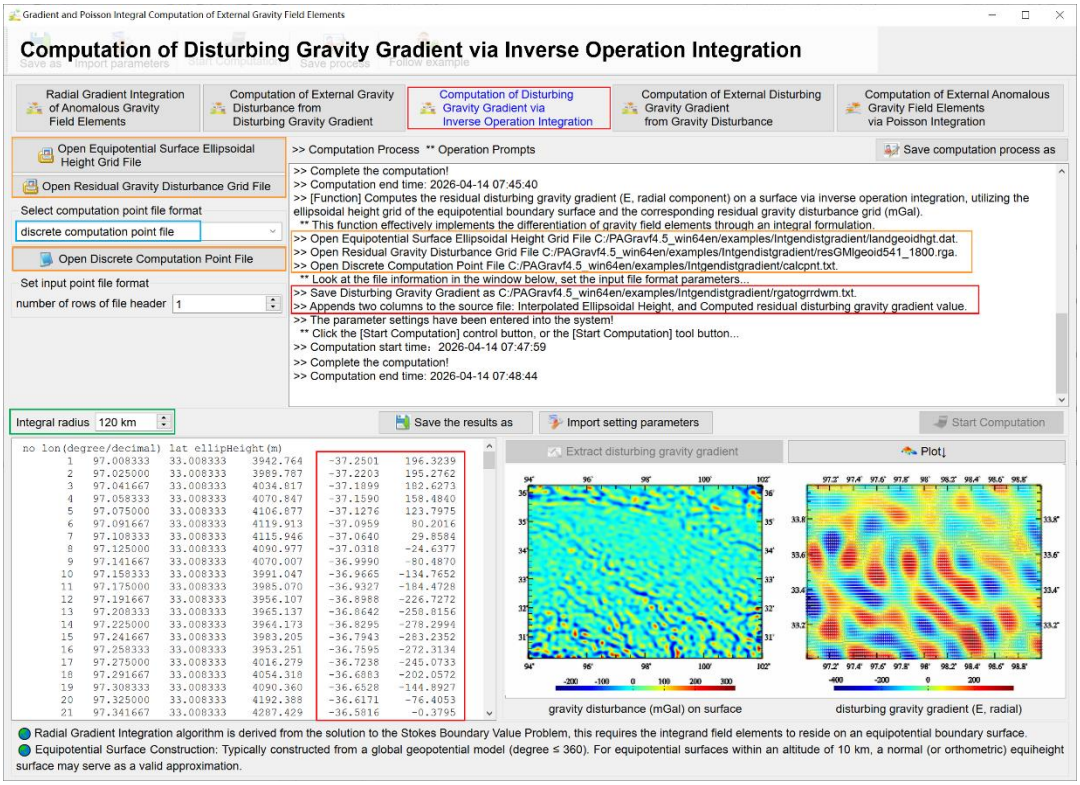

[Case Study & Accuracy Assessment]

In this example, residual disturbing gravity gradients on the geoid are computed from residual gravity disturbances derived from the EGM2008 model, degrees 541 – 1800 via inverse operation integration (Radius = 120 km).

Excluding a 2° marginal buffer zone to mitigate integration edge effects, statistical analysis evaluates the differences between the computed results and the model reference truth (degrees 541 – 1800).

Table 4.20: Statistics of Model Reference Truth

Field Element	Unit	Mean	Std. Dev.	Min	Max
Residual Disturbing Gravity	E	0.4763	68.2499	-288.1750	387.7286

Gradients (Radial) on Geoid					

Table 4.21: Differences between Computed Results and Reference Truth

Field Element	Unit	Mean	Std. Dev.	Min	Max
Residual Disturbing Gravity Gradients (Radial) on Geoid	E	-0.0562	6.6405	-37.1465	28.3557

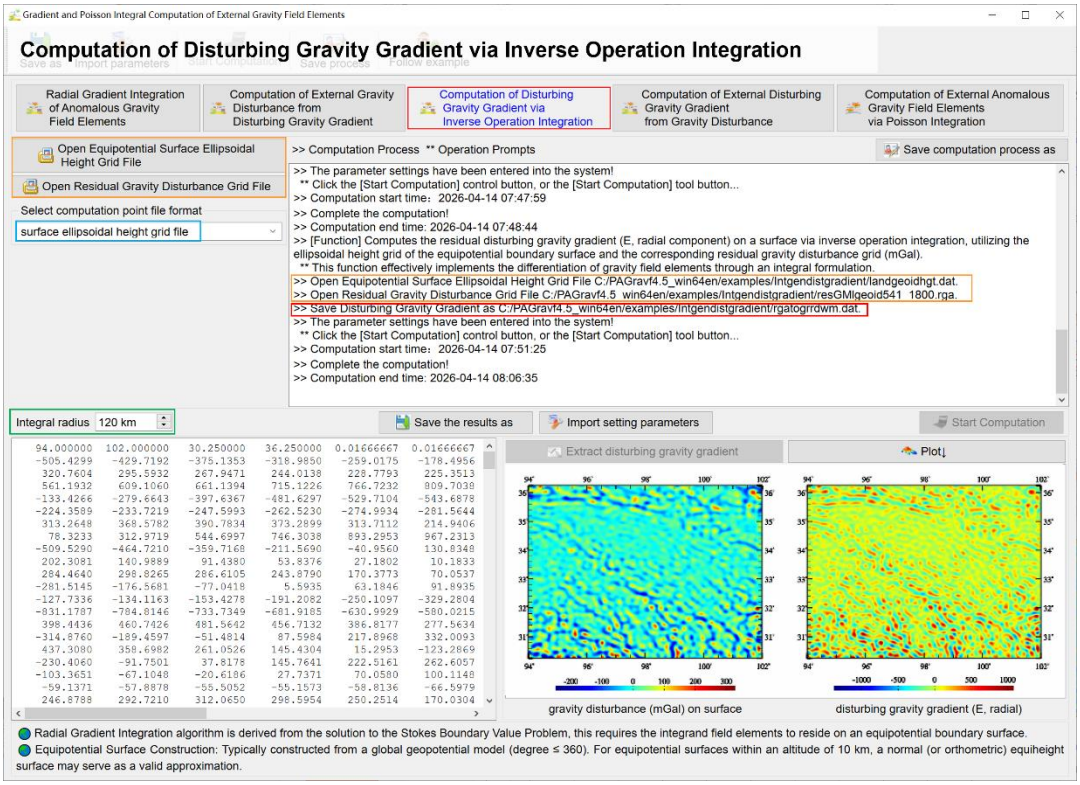

Analysis & Conclusions:

● Algorithm Performance: The ratio of the standard deviation of Differences in Table 4.21 to the standard deviation of Reference Truths in Table 4.20 reflects the approximation ability of the corresponding algorithm.

● Stability of Differentiation: Computing gradients from gravity disturbances is a differentiation process, typically sensitive to high-frequency noise. In this case, while the true signal exhibits a large variability (Std. Dev. = 68.25 E), the error standard deviation is well-controlled at ~6.64 E (approximately 10% of the signal strength).

● Conclusion: These results indicate that the inverse operation integration algorithm offers superior numerical stability for differentiation tasks. It effectively preserves high-frequency signal characteristics while avoiding the severe oscillations often associated with traditional finite difference methods, making it suitable for high-precision gravity gradient field modeling.

4.4.4 Computation of External Disturbing Gravity Gradient from Gravity Disturbance

[Function] Computes the residual disturbing gravity gradient (E, radial component) on or

outside the geoid. Inputs include an ellipsoidal height grid of a boundary surface and the corresponding residual gravity disturbance grid (mGal).

Algorithmic Basis: The inverse integration of gravity disturbances employs a hybrid algorithm combining Poisson integration with differentiation. This approach does not require the boundary surface to be an equipotential surface.

[Input Files]

(1) Boundary Surface Ellipsoidal Height Grid: Provides the geodetic coordinates of Boundary Surface, for deriving integration distances.

(2) Residual Gravity Disturbance Grid: Must share identical specifications with the height grid.

(3) Computation Point file: a Space Computation Point File or a Computation Surface Ellipsoidal Height grid File.

● Discrete Point record Format: ID (Point No./Name), Longitude (deg), Latitude (deg), Ellipsoidal Height (m), ...

[Parameter Settings]

Define input file parsing rules.

Specify the Integration Radius.

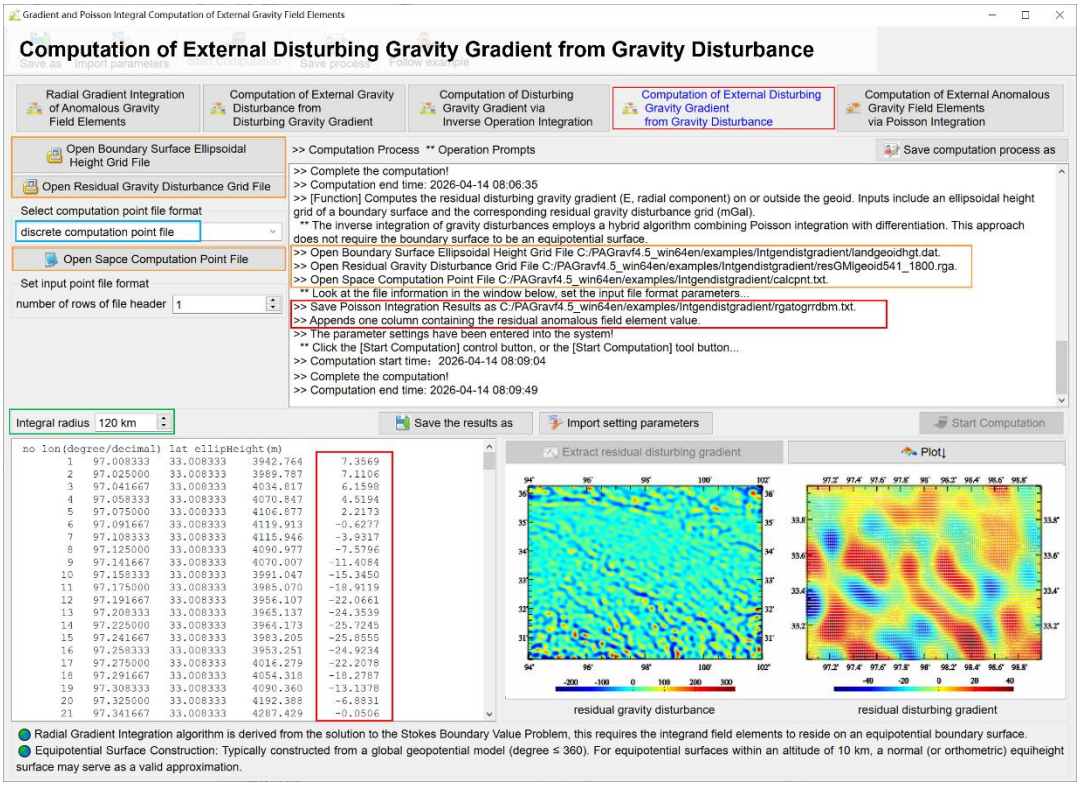

[Output Files]

External Residual Disturbing Gravity Gradient Result File:

● Discrete Input: Appends one column containing the residual disturbing gravity gradient value (formatted to four significant digits).

● Grid Input: Generates a residual disturbing gravity gradient grid file matching the input

grid specifications.

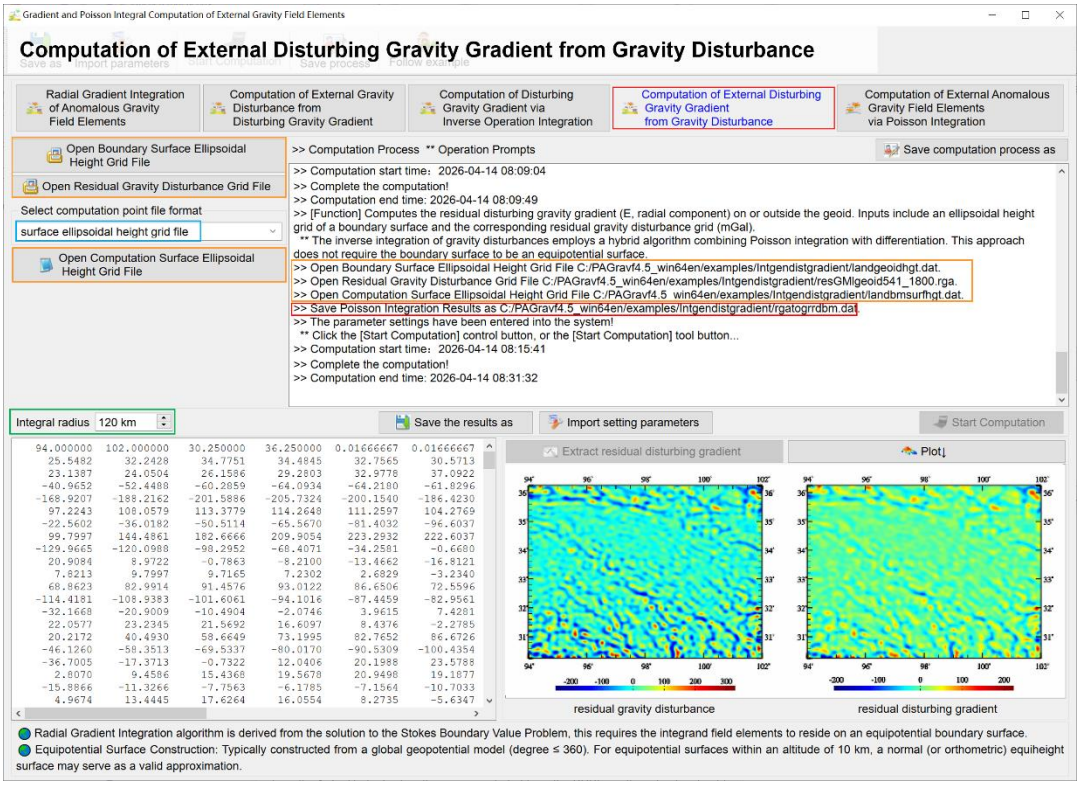

[Case Study & Accuracy Assessment]

In this example, ground residual disturbing gravity gradients are computed from residual gravity disturbances (derived from the EGM2008 model, degrees 541 – 1800) on the geoid via numerical integration (Radius = 120 km).

Excluding a 2° marginal buffer zone to mitigate integration edge effects, statistical analysis compares the results against the model reference truth (degrees 541 – 1800).

Table 4.22: Statistics of Model Reference Truth

Field Element	Unit	Mean	Std. Dev.	Min	Max
Ground Residual Disturbing Gravity Gradients (Radial)	E	-0.2872	26.9448	-148.0282	136.7864

Table 4.23: Differences between Computed Results and Reference Truth

Field Element	Unit	Mean	Std. Dev.	Min	Max
Ground Residual Disturbing Gravity Gradients (Radial)	E	-0.0361	2.7361	-14.2089	13.6802

Analysis & Conclusions:

● Algorithm Performance: The ratio of the standard deviation of Differences in Table 4.23 to the standard deviation of Reference Truths in Table 4.22 reflects the approximation ability of the corresponding algorithm.

● Comparative Analysis: When compared with the inverse operation integration method

described in Section 4.4.3, the inverse integration of gravity disturbance demonstrates comparable performance and accuracy. Both approaches effectively achieve high-precision differential inversion from gravity disturbances to gradients, with error standard deviations controlled to approximately 10% of the signal strength, validating the consistency of the algorithms across different mathematical formulations.

4.4.5 Computation of External Anomalous Gravity Field Elements via Poisson Integration

[Function] Computes residual anomalous gravity field elements on or outside the geoid via Poisson integration. Inputs include an ellipsoidal height grid of a boundary surface and the corresponding residual anomalous field element grid on that surface.

Algorithmic Basis: The Poisson integral constitutes the rigorous mathematical solution to the First Boundary Value Problem (Dirichlet Problem). It does not require the boundary surface to be an equipotential surface, making it ideal for analytical continuation (both upward and downward) across arbitrary geometric boundaries.

[Input Files]

(1) Boundary Surface Ellipsoidal Height Grid File: Provides the geodetic coordinates of Boundary Surface, for deriving integration distances.

(2) Residual Anomalous Field Element Grid File: Must share identical specifications with the height grid.

(3) Computation Point file: a Space Computation Point File or a Computation Surface Ellipsoidal Height grid File.

● Discrete Point record Format: ID (Point No./Name), Longitude (deg), Latitude (deg), Ellipsoidal Height (m), ...

[Parameter Settings]

Define input file parsing rules.

Specify the Integration Radius.

Select the computational algorithm.

[Output Files]

External Residual Anomalous Field Element Result File:

● Discrete Input: Appends one column containing the residual anomalous field element value (formatted to four significant digits).

● Grid Input: Generates a residual anomalous field element grid file matching the input grid specifications.

[Case Study & Accuracy Assessment]

In this example, ground residual height anomalies and ground residual gravity disturbances are computed from residual geoidal heights and residual gravity disturbances (derived from the EGM2008 model, degrees 541 – 1800) on the geoid, respectively, via Poisson integration (Radius = 120 km).

Excluding a 2° marginal buffer zone to mitigate integration edge effects, statistical analysis evaluates the differences between the computed results and the model reference truth (degrees 541 – 1800).

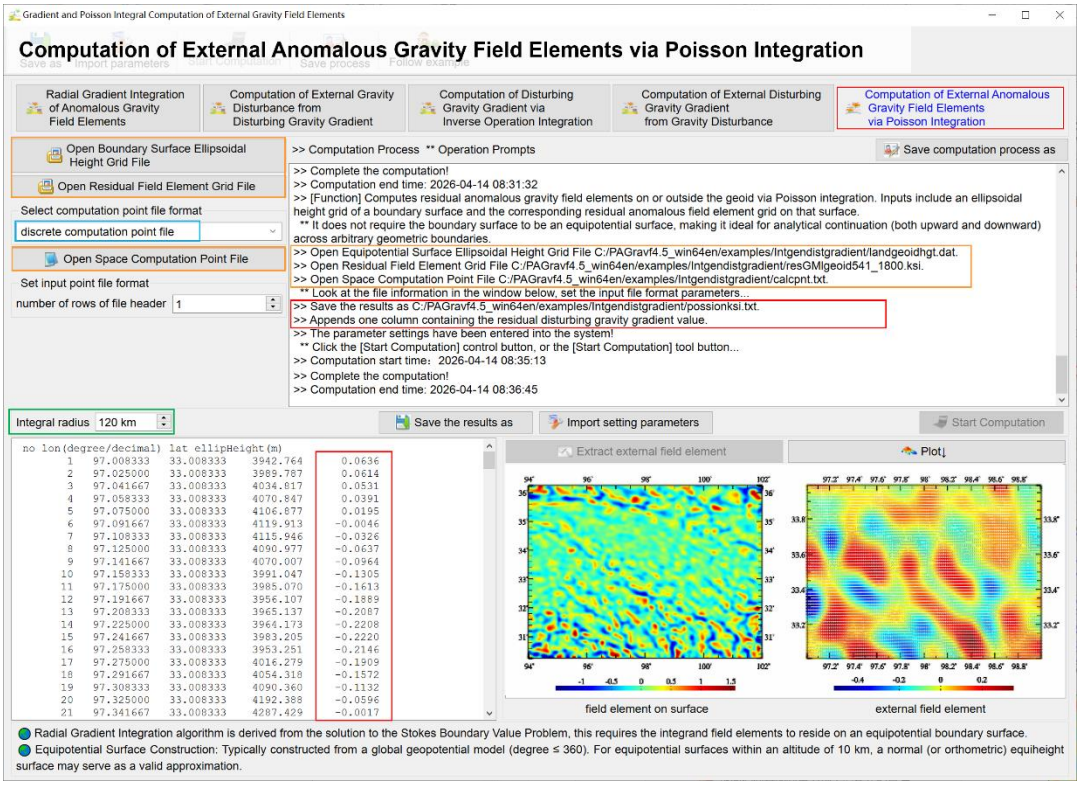

Table 4.24: Statistics of Model Reference Truths

Field Element	Unit	Mean	Std. Dev.	Min	Max
Ground Residual Height Anomalies	m	0.0010	0.1182	-0.6745	0.4760
Ground Residual Gravity Disturbances	mGal	-0.0346	15.7527	-93.9854	66.6638

Table 4.25: Differences between Computed Results and Reference Truth

Field Element	Unit	Mean	Std. Dev.	Min	Max
Ground Residual Height Anomalies	m	0.0004	0.0074	-0.0326	0.0334
Ground Residual Gravity Disturbances	mGal	0.0476	1.1919	-5.0173	6.5138

Analysis & Conclusions:

● Algorithm Performance: The ratio of the standard deviation of Differences in Table 4.19 to the standard deviation of Reference Truths in Table 4.18 reflects the approximation ability of the corresponding algorithm.

● Superior Short-Wavelength Preservation: The algorithm effectively suppresses the attenuation of short-wavelength signals, demonstrating high fidelity for both upward and downward analytical continuation. Notably, the error standard deviation for gravity disturbances is merely 1.19 mGal (~7.5% of the signal), and for height anomalies, it is only

7.4 mm.

● Iterative Strategy: This function supports iterative execution to perform multi-step Poisson integrations. In general, a single iteration suffices to meet accuracy requirements for most applications. In scenarios involving extreme topography or large vertical separations, at most three iterations are typically required to achieve convergence.

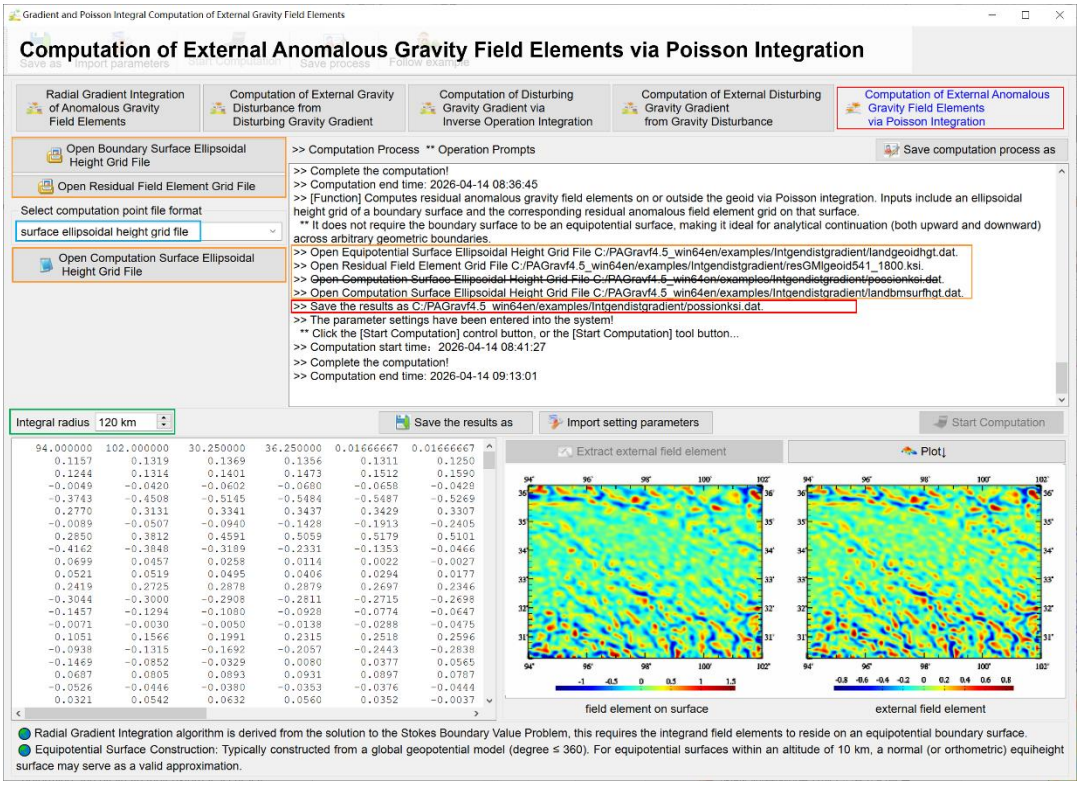

4.5 Feature and Performance Analysis of Spherical Radial Basis Functions

[Purpose] To compute the spatial-domain and spectral-domain response curves for four types of Spherical Radial Basis Functions (SRBFs) for anomalous gravity field elements. Subsequently, the module constructs an equal-area spherical grid based on a specified latitude/longitude extent to facilitate the design of SRBF networks and corresponding gravity field approximation algorithms.

Note: This is a standalone analysis tool; no input files are required.

4.5.1 Spatial and Spectral Performance Analysis of Spherical Radial Basis Functions

[Function] Given the influence radius and sampling interval, this function calculates and visualizes the spatial and spectral curves of SRBFs for gravity disturbance, height anomaly (disturbing potential), total vertical deflection, or disturbing gravity gradient.

By adjusting key parameters – specifically the minimum and maximum degrees of the SRBF Legendre expansion, the burial depth of the reference surface (Bjerhammar sphere), and the order (m) of multipolar SRBFs – users can analyze and characterize the spatial localization and spectral behavior of SRBFs for diverse gravity field elements.

[Parameter Settings]

Field Element Selection: Choose the target anomalous gravity field element.

SRBF Core Parameters:

● Legendre Expansion Degrees: Enter $n_{\min}$ and $n_{\max}$ to control the spectral bandwidth of the SRBF.

● Bjerhammar Sphere Burial Depth: Defines the depth of the Bjerhammar sphere relative to the mean observation surface. Combined with the expansion degrees, this parameter tunes the spectral center and bandwidth.

○ Effect: Greater burial depth yields a smoother SRBF with lower kurtosis, corresponding to a wider spectral bandwidth.

● Multipole/Wavelet Order (m): Set the order m for the radial multipole kernel or Poisson wavelet kernel.

○ Effect: A larger m increases the kurtosis of the SRBF, resulting in a more localized spatial response.

● Action distance of SBRF center: Specified as a spherical angular distance (influence radius), equivalent to the integration radius in regional gravity field modeling.

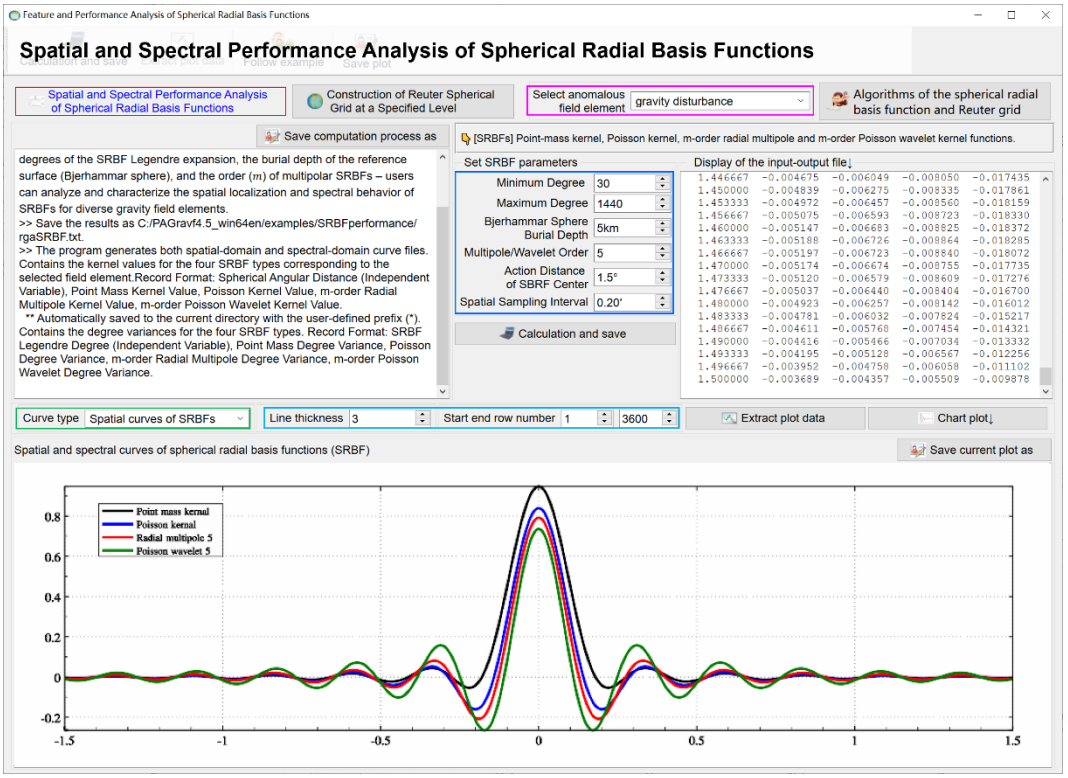

Spatial Sampling Interval: Defines the step size for discretizing the spatial curve.

Plotting Parameters: Configure visualization settings.

[Output Files] The program generates both spatial-domain and spectral-domain curve files.

(1) Spatial Curve File:

Contains the kernel values for the four SRBF types corresponding to the selected field element.

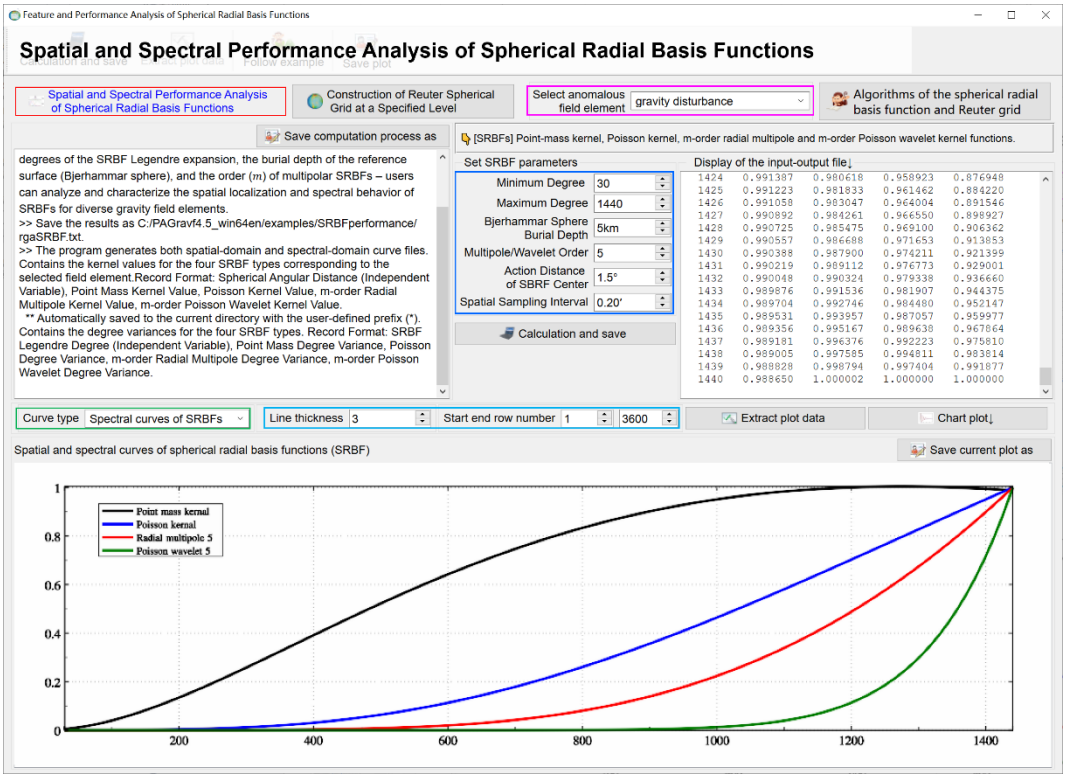

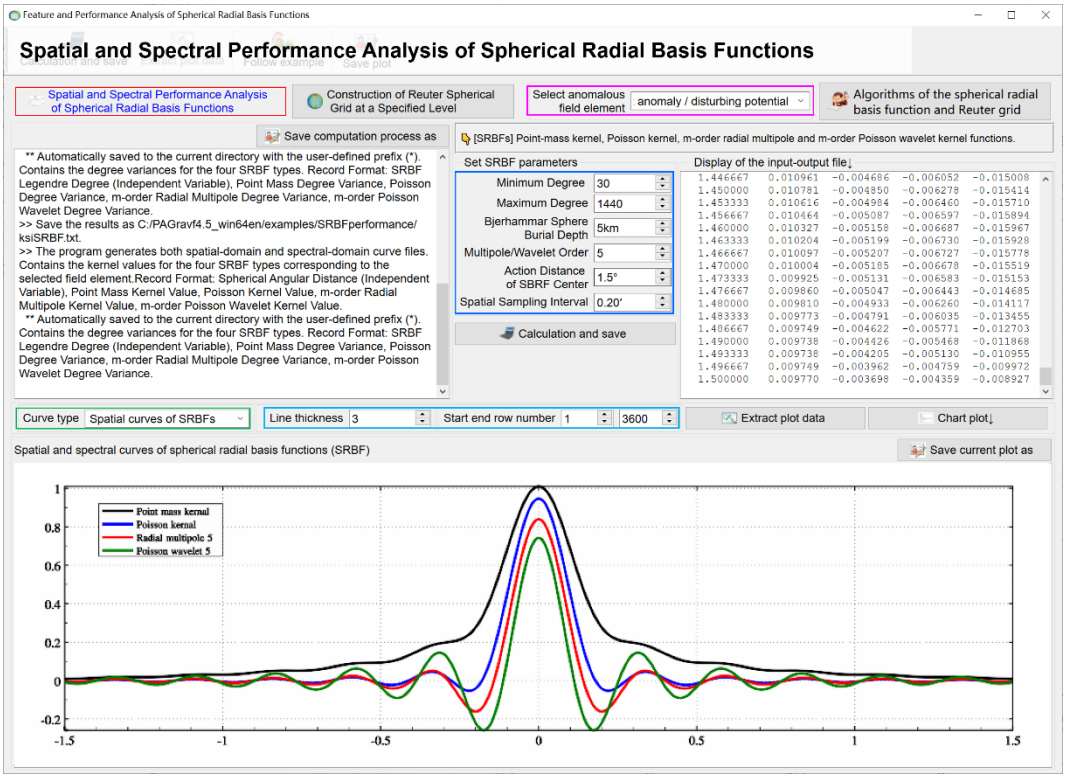

Record Format: Spherical Angular Distance (Independent Variable), Point Mass Kernel Value, Poisson Kernel Value, m-order Radial Multipole Kernel Value, m-order Poisson Wavelet Kernel Value.

(2) Spectral Curve File (*.dgr):

Automatically saved to the current directory with the user-defined prefix (*). Contains the degree variances for the four SRBF types.

Record Format: SRBF Legendre Degree (Independent Variable), Point Mass Degree Variance, Poisson Degree Variance, m-order Radial Multipole Degree Variance, m-order Poisson Wavelet Degree Variance.

4.5.2 Construction of Reuter Spherical Grid at a Specified Level

[Function] Constructs a global or regional Reuter spherical coordinate grid given the Reuter grid level (Q) and a specific latitude/longitude extent.

Spatial Resolution: Approximately π/Q on the unit sphere.

Cell Area Characteristics: Equatorial cell area: $A = \pi^2/Q^2$.

Polar cell area: $\pi A/4$.

Definition of Level Q: The spherical surface is partitioned into Q prime vertical circles with a latitude interval of π/Q. Higher Q values yield finer spatial resolution.

- Examples: Q = 360 corresponds to a resolution of 30 arcminutes; Q = 1800 corresponds to 6 arcminutes.

[Parameter Settings]

Specify the Latitude and Longitude Extent.

Enter the Reuter Grid Level (Q).

Configure Plotting Parameters.

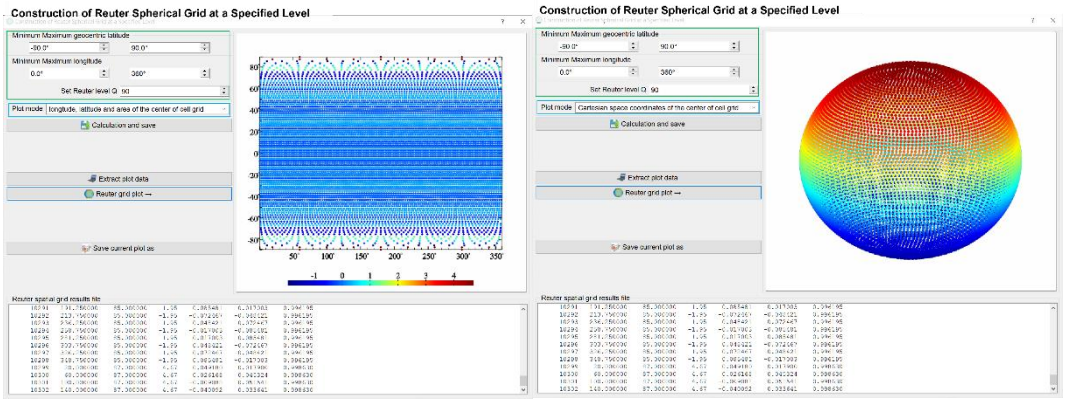

[Output Files]

(1) Reuter Unit Sphere Coordinate Grid File:

Record Format: Cell ID, Central Longitude, Geocentric Latitude, Area Deviation (%), Rectangular Coordinates (X, Y, Z).

Area Deviation Calculation: (Cell Area − Equatorial Cell Area A) / Equatorial Cell Area A × 100

Note: The global Reuter grid excludes singular polar cells.

(2) Reuter Grid Parameter File (*.par): Automatically saved to the current directory with the user-defined prefix (*).

Header Format: Latitude/Longitude Extent, Reuter Grid Level, Total Number of Points.

Record Format: Point ID, Central Latitude of Prime Vertical Circle (°), Prime Vertical Circle Index, Longitude Interval (arcminutes), Cell Area Deviation (%).

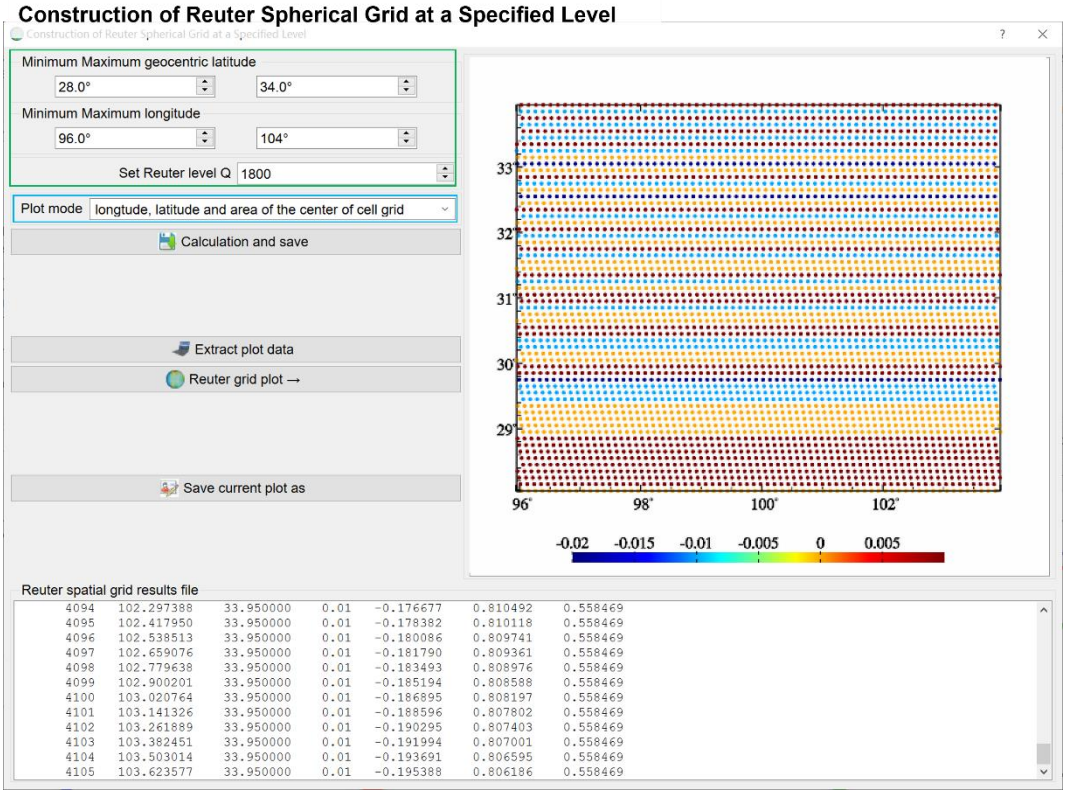

4.6 Gravity Field Approximation Using SRBFs and Performance Evaluation

[Purpose] To evaluate the spatial, spectral, and analytical performance of the Spherical Radial Basis Function (SRBF) approximation algorithm by selecting specific residual observations and SRBF kernel types. This is achieved by estimating specific residual gravity field elements – such as gravity disturbances, height anomalies, gravity anomalies, disturbing potential gradients, or vertical deflections – on or outside the geoid.

Input Strategy: Select a single type of discrete residual observation from the following: gravity disturbance (mGal), height anomaly (m), gravity anomaly (mGal), disturbing gravity gradient (radial, E), or vertical deflection (south/west components, ″).

Kernel Selection: Employ a single type of Spherical Radial Basis Functions (SRBFs) for approximation, chosen from: Point Mass, Poisson, m-order Radial Multipole, or Poisson Wavelet kernel functions.

Comprehensive Testing: By varying input observation types, SRBF configurations, parameters, and target field elements, this module facilitates a rigorous analysis of the spatial, spectral, and analytical properties of SRBFs and their associated approximation algorithms.

Accuracy Assessment & Gross Error Detection:

- Cross-Validation: Set the weight of the target field element's observations to zero to exclude them from coefficient estimation. The program then computes estimates at

these points using the remaining data, enabling effective gross error detection and determination of external accuracy indices.

○ Synchronous Evaluation: Alternatively, use the observation points of the target field element directly as computation points for synchronous evaluation.

Versatile Applications: Supports gridding, analytical continuation, type conversion, external accuracy determination, all-element gravity field modeling, and geoidal model computation based on any single type of observed disturbance field element.

Unified Multi-Platform Processing: PAGravf4.5 adopts a completely unified processing framework for airborne, terrestrial, and marine gravity data. Gravity disturbances from all three platforms are treated as an observation type, requiring no distinction.

[Input Files]

(1) Single-Type Residual Observation File.

(2) Computation Surface Ellipsoidal Height Grid: Provides the geodetic coordinates of Computation Surface for the target field elements.

(3) Synchronous Computation Mode: If selected, requires a Space Computation Point File.

● File Format Convention: Header occupies 1 row. Record format: Point Number, Longitude (decimal degrees), Latitude, Ellipsoidal height (m), ...

● By setting computation points identical to the observation points of the target field element, the program generates SRBF-based estimates using the input observation data. The residuals between the observed and estimated values are then employed for gross error detection and the assessment of external accuracy indices.

[Parameter Settings]

Warning: Inappropriate parameters may lead to an unstable solution. Adjust parameters iteratively until stability criteria are met (refer to "Quantitative Validity Criteria for Single SRBF Approximation").

(1) Weight Attribute Column Index:

● Specify the column index for weights in the observation file record.

● If the index < 1, exceeds the column count, or weights are negative, the program defaults to equal weighting.

● If a weight equals 0, the corresponding observation is excluded for SRBF coefficient estimation, allowing the program can be employed to compute its external accuracy index.

(2) Observation Field Element Type: Select the type and define observation file format parameters.

(3) SRBF Form: Choose between Radial Multipole Kernel or Poisson Wavelet Kernel.

Note: Order 0 Radial Multipole Kernel = Point Mass Kernel; Order 0 Poisson Wavelet Kernel = Poisson Kernel.

(4) Bjerhammar Sphere Burial Depth (km): Depth relative to the mean observation surface.

(5) SRBF Center Action Distance:

● Also known as the influence radius, calculated as spherical angular distance ×

Bjerhammar sphere radius. Equivalent to the integration radius in local gravity field integration algorithm.

● A fixed action distance ensures spectral-spatial consistency in the regional gravity field structure.

● The action distance significantly influences the statistical mean of observation residuals after SRBF approxiation.

(6) Reuter Grid Level (Q):

● Divides the sphere into Q parallel circles with a latitude interval of $180^{\circ}/Q$. Higher Q yields higher resolution.

● Guideline: Set $180^{\circ}/Q$ comparable to the average inter-point distance of observations.

● Adaptive Node Distribution: PAGravf4.5 employs a Reuter grid fitting algorithm to determine the effective number of observations (J) within each basis function's cell. Centers with $J < 1$ are eliminated. This ensures the spatial distribution of SRBF centers mirrors that of the observation points (uniform inputs yield uniform SRBF centers; irregular inputs yield irregular SRBF centers).

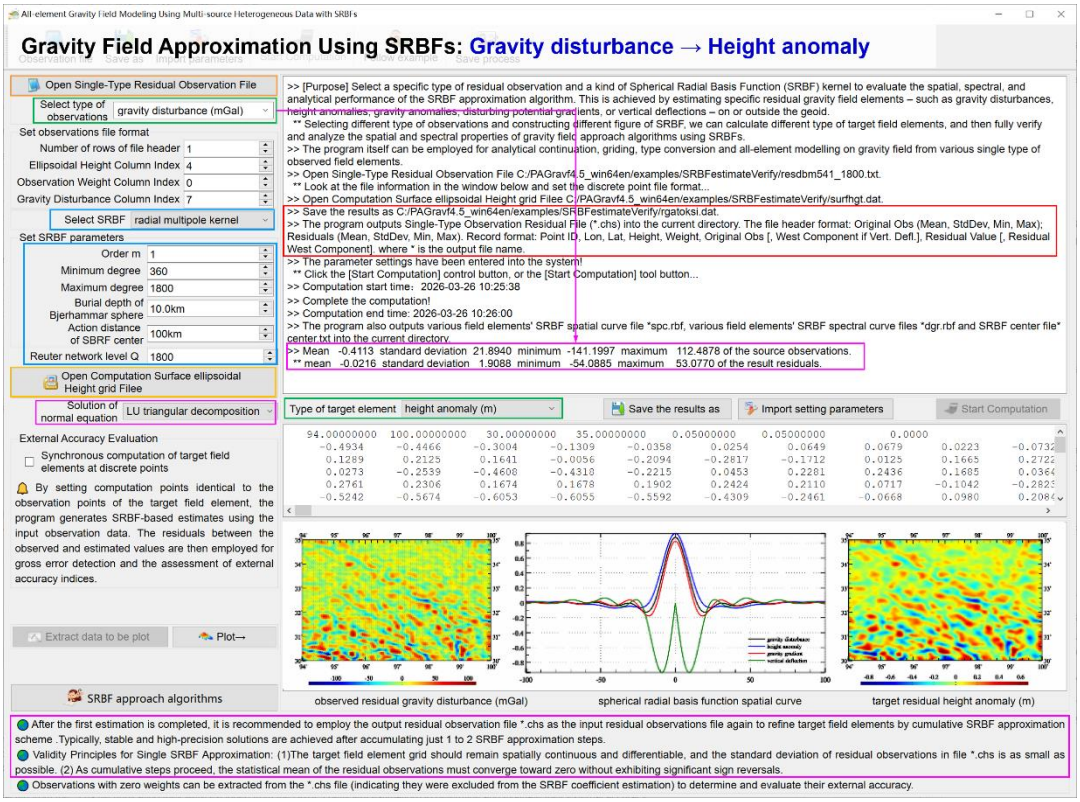

(7) Legendre Expansion Degree Range:

● Minimum Degree: Primarily affects the statistical mean of observation residuals after SRBF approxiation.

● Maximum Degree & Grid Level Q: Significantly affect the statistical standard deviation of observation residuals after SRBF approxiation.

(8) Normal Equation Solver: Select from LU Decomposition, Cholesky Decomposition, or

Minimum Norm Solution.

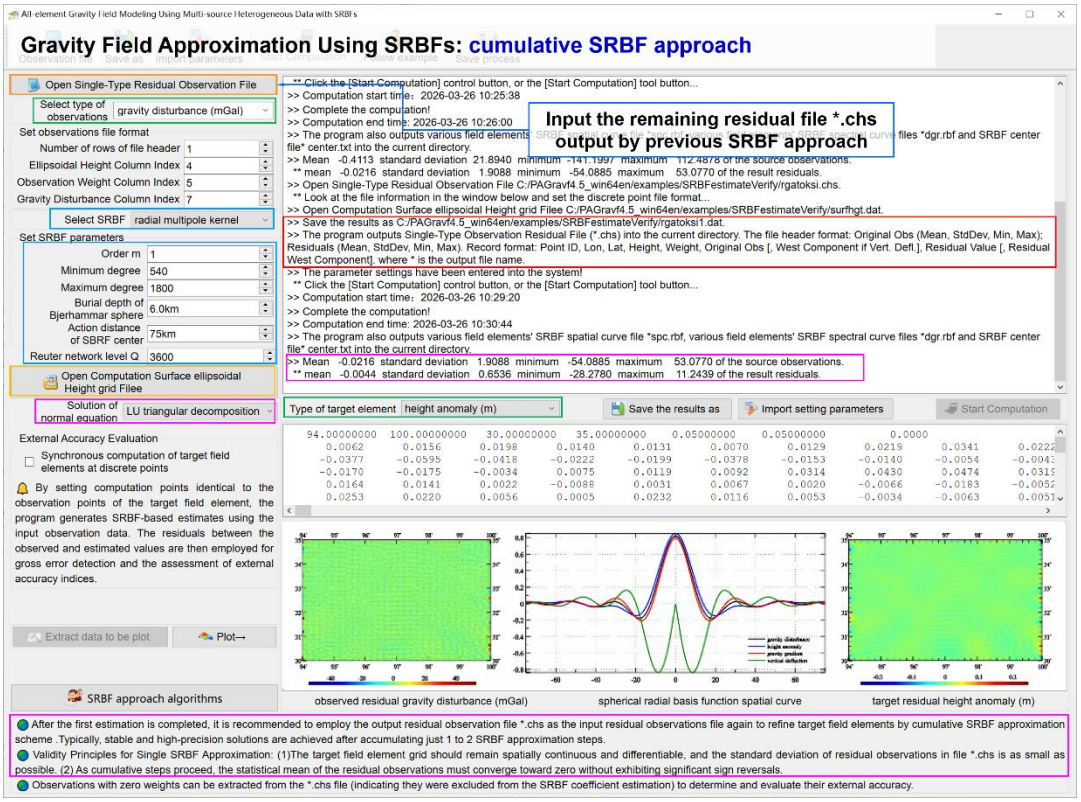

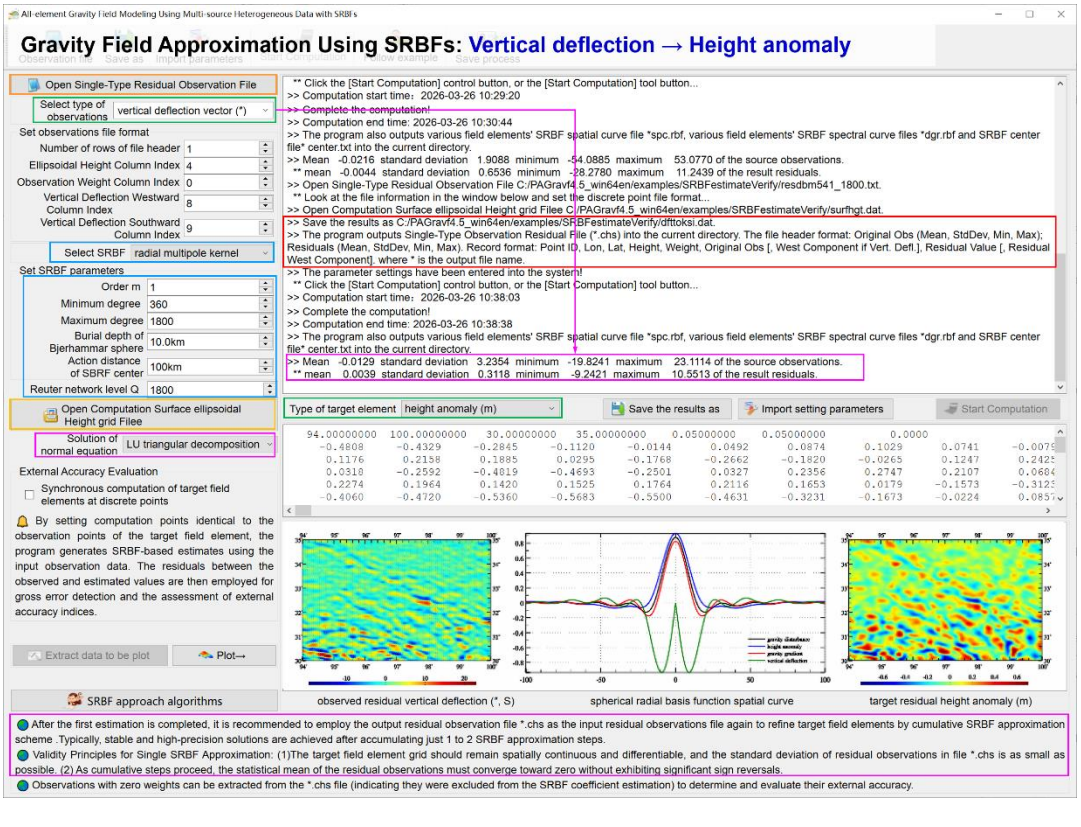

(9) Target Residual Field Element Type: Select the desired output field element.

[Output Files]

(1) Target Residual Field Element Grid File: Matches the specifications of the input ellipsoidal height grid.

(2) Space Point Estimation File (&.tgt): Generated when "Synchronous Computation" is selected (& = input filename).

● Record Format: Appends 1 or 2 columns of computed values (4 significant digits) to the input record.

Appends 2 columns (South & West components) only if the target is Vertical Deflection; otherwise, 1 column.

(3) Single-Type Observation Residual File (*.chs): Essential for gross error detection and accuracy assessment, and can also be employed as next Observations File for next Cumulative SRBF Approximation.

● Header: Original Obs (Mean, StdDev, Min, Max); Residuals (Mean, StdDev, Min, Max).

● Record Format: Point ID, Lon, Lat, Height, Weight, Original Obs [, West Component if Vert. Defl.], Residual Value [, Residual West Component].

● Observations with zero weights can be extracted from the *.chs file (indicating they were excluded for the SRBF coefficient estimation) to determine and evaluate their external accuracy.

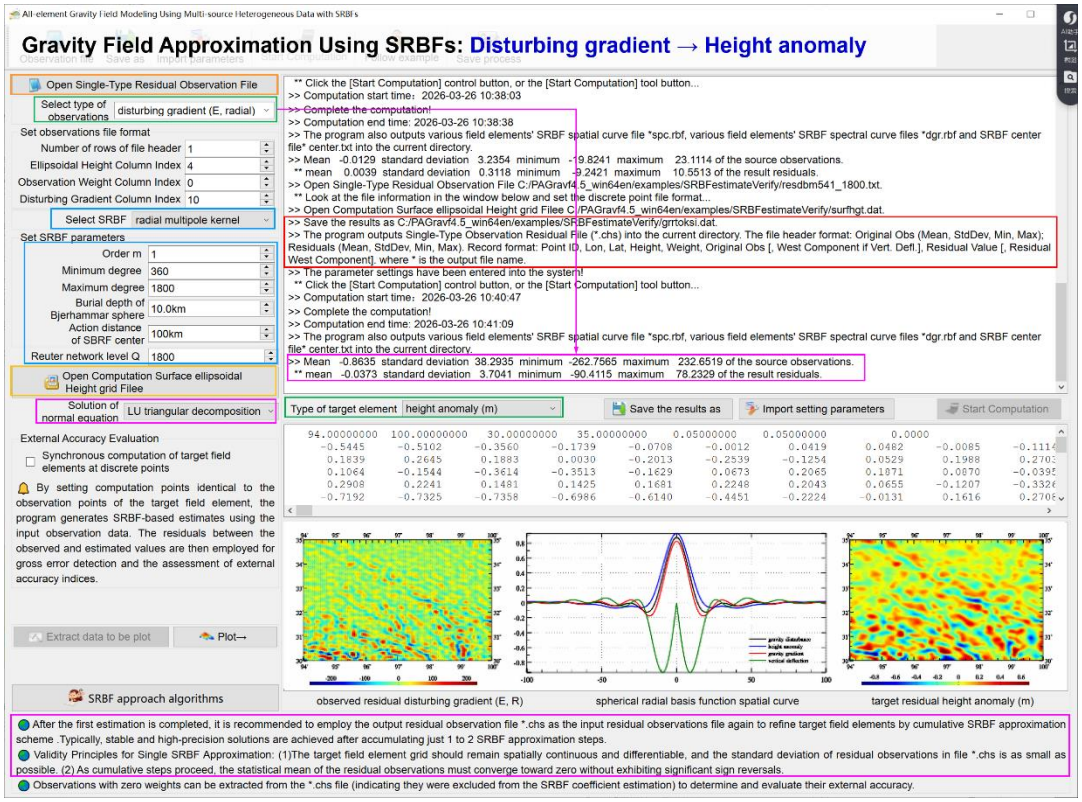

(4) Auxiliary Analysis Files:

● Multi-Element SRBF Spatial Curve (*spc.rbf).

● Multi-Element SRBF Spectral Curve (*dgr.rbf).

● SRBF Center File (*center.txt).

Headers (*spc.rbf, *dgr.rbf): SRBF Type (0-Multipole, 1-Wavelet), Order, Min Degree, Max Degree, Compensation Depth (km).

*spc.rbf Records: Spherical Distance (km), Normalized SRBF Values (Gravity Disturbance, Height Anomaly, Gravity Gradient, Total Vert. Defl.).

*dgr.rbf Records: Degree, Normalized SRBF Values (Gravity Disturbance, Height Anomaly, Gravity Gradient, Total Vert. Defl.).

PAGravf4.5: Edge Effect Suppression and Cumulative SRBF Approximation Algorithm

(a) Edge Effect Suppression Mechanism

PAGravf4.5 introduces a novel algorithm to enhance parameter estimation performance by actively suppressing edge effects. When an SRBF center is located at the margin of the computation area, the program imposes a constraint setting its coefficient to zero.

● Enhanced Stability: This approach significantly improves the stability and reliability of the SRBF coefficient estimation.

● Regularization-Free: With edge effect suppression integrated, the normal equations no longer require explicit regularization. This prevents the analytical structure of the derived gravity field from being distorted by regularization biases or observation errors, preserving the physical integrity of the solution.

(b) Limitations of Single SRBF and Spectral Leakage

The target field element is mathematically defined as the convolution of the observation field element and a filtering SRBF. When the target and observation elements are of different types, a single SRBF often fails to simultaneously match the spectral centers and bandwidths of both fields. This mismatch leads to spectral leakage in the reconstructed target field.

Furthermore, factors such as SRBF type, Legendre expansion degrees (n_{min}, n_{max}), and center distribution critically influence approximation performance. Consequently, optimizing SRBF coefficients using burial depth as the sole parameter is insufficient to guarantee optimal gravity field recovery.

(c) Cumulative SRBF Approximation Strategy

To address this challenge, leveraging the linear superposition principle of the gravity field, PAGravf4.5 proposes a Cumulative SRBF Approximation method. This approach replaces the conventional iterative optimization of burial depth (or width parameters) with a multi-component synthesis strategy.

● Non-Iterative Efficiency: The method eliminates the need for iterative searches for an optimal burial depth.

● Comprehensive Spectral Coverage: Each approximation step employs an SRBF with distinct spectral characteristics. By combining the spectral centers and bandwidths of multiple SRBFs, the method fully resolves the spectral signals of the target field, effectively eliminating spectral leakage and achieving an optimal analytical reconstruction in the spatial domain.

(d) Validity Principles for Single SRBF Approximation

The validity of each iteration within the cumulative scheme is governed by two simple

and intuitive criteria in PAGravf4.5:

● Spatial Regularity & Minimization: The target field element grid should remain spatially continuous and differentiable, and the standard deviation of residual observations in file *.chs is as small as possible.

● Convergence Behavior: As cumulative steps proceed, the statistical mean of the residual observations must converge toward zero without exhibiting significant sign reversals (indicative of over-correction or instability).

(e) Technical Characteristics: Remove-Compute-Restore

The core technical feature of the cumulative SRBF approximation is its implementation of the Remove-Compute-Restore principle. Each residual approximation step utilizes the result of the previous step as the reference gravity field, progressively refining the residual target field element.

● Rapid Convergence: Typically, stable and high-precision solutions are achieved after accumulating just 1 to 2 SRBF approximation steps.

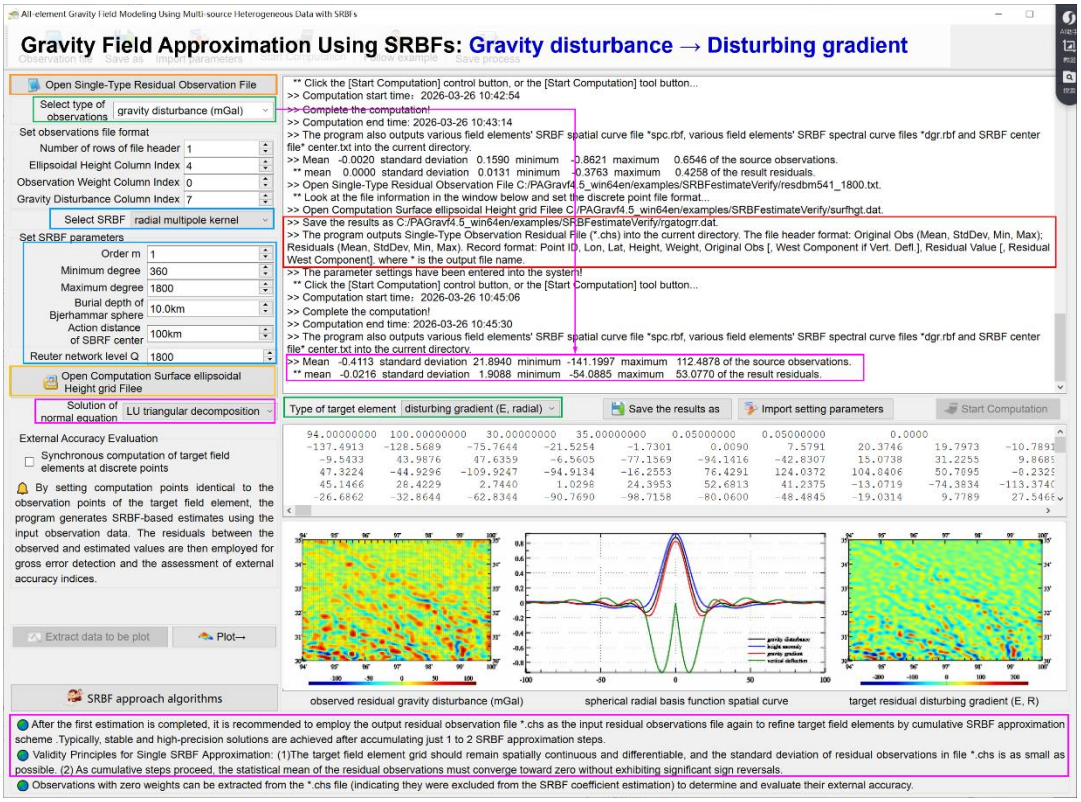

Case Study and Accuracy Assessment

In this case study, with an SRBF center action distance of 120 – 150 km, ground disturbance field elements on a 3′×3′ grid were computed using a single type of observation data (residual height anomalies, gravity anomalies, gravity disturbances, or vertical deflections derived from the EGM2008 model, degrees 541 – 1800). Excluding a 1° peripheral buffer zone to mitigate edge effects, statistical analysis compared:

Reference Truth: Model-derived ground residual disturbance field elements (degrees

541 – 1800).

Approximation Errors: Differences between SRBF approximated values and the reference truth.

Table 4.26: Statistics of Model Reference Truths

Field Element	Unit	Mean	Std. Dev.	Min	Max
Residual Geoidal Heights	m	-0.0020	0.1590	-0.8621	0.6546
Residual Gravity Disturbances	mGal	-0.4113	21.8940	-141.1997	112.4878

Table 4.27: Differences between SRBF Approximation and Reference Model

Observation Residuals	Target Residual Element	1st SRBF Approx.		2nd SRBF Approx.	
		Mean	Std. Dev.	Mean	Std. Dev.
Gravity Disturbance	Ground Height Anomaly (m)	0.0201	0.0185	0.0189	0.0162
Vertical Deflection		0.0058	0.0147	0.0058	0.0072
Disturbing Gradient		-0.0055	0.0202	-0.0056	0.0185
Height Anomaly	Ground Gravity Disturbance (mGal)	0.1731	1.4421	0.2075	1.4382
Vertical Deflection		0.3550	1.6905	0.3566	1.6845
Disturbing Gradient		0.0840	1.5780	0.0906	1.5298

Algorithm Performance: The approximation capability of the algorithm is quantified by the ratio of the standard deviation of the approximation errors (Table 4.27) to the standard deviation of the reference truth (Table 4.26).

Comparative Analysis: Comparative analysis against traditional gravity field integration algorithms reveals that even a single-step SRBF approximation surpasses standard integration methods in accuracy. Furthermore, the cumulative SRBF approximation strategy (specifically the second iteration) yields additional improvements. This is particularly evident in the recovery of ultra-short-wavelength gravity field signals, as demonstrated by the consistent reduction in standard deviations across all test scenarios.

Capabilities in Gross Error Detection and External Accuracy

The program incorporates robust functionalities for the direct detection of gross errors in discrete gravity field observations and the rigorous determination of their external accuracy indices.

- Cross-Type Detection: It enables the detection of gross errors in any specific type of gravity field observation within a region, utilizing any single type of input observational data as the reference basis.
- Unrestricted Applicability: The methodology imposes no stringent constraints on the spatial distribution or density of the observation points, ensuring flexibility across diverse survey configurations.
- Integrated Assessment: Concurrently with gross error detection, the program directly computes reliable external accuracy metrics for the evaluated observations, providing a comprehensive quality control solution in a single processing step.

4.7 All-element Gravity Field Modeling Using Multi-source Heterogeneous Data with SRBFs

[Purpose] Integrating multiple types of discrete residual anomalous field element observations such as gravity disturbances, height anomalies, gravity anomalies, disturbing gravity gradients, or vertical deflection vectors, the program estimates all residual gravity field element grid models on a specified computation surface using the Spherical Radial Basis Function (SRBF) approximation method, thereby achieving unified modeling of the regional gravity field and geoid.

Versatility: An exceptionally robust, all-purpose tool for comprehensive gravity field modeling and quality assessment.

Preprocessing-Free: Observations require no reduction, analytical continuation, or gridding prior to processing.

Multi-Source Fusion: Directly integrates multi-source, heterogeneous, varying-altitude, cross-distributed, and multi-type data encompassing terrestrial, maritime, aerial, or space-based observations.

All-element High-Precision Modeling: Enables high-precision, all-element modeling of the regional gravity field throughout the entire spatial domain.

Complex Scenario Handling: Effectively addresses critical challenges in complex scenarios, including gross error detection for diverse observation types, external accuracy determination, and computational performance control.

[Input Files]

(1) Multi-source Heterogeneous Residual Observations File.

● Record format: Point ID/Station Name, Longitude (deg), Latitude (deg), Ellipsoidal height (m), Residual Observation Value, ..., Field Element Type Code (0 – 5), Observation Weight, System Weight, ...

Note: The position and order of the first five attributes (ID through Residual Value) are fixed.

● Field Element Type Codes & Units:

0: Residual Gravity Disturbance (mGal)

1: Residual Height Anomaly (or Residual Geoidal Height, m)

2: Residual Gravity Anomaly (mGal)

3: Residual Disturbing Gravity Gradient (E, radial)

4: Residual Vertical Deflection, South Component (″)

5: Residual Vertical Deflection, West Component (″)

● Weight Definitions:

○ Observation Weight: Differentiates Observation errors within a single system group; independent of other groups (or systems).

○ System Weight: Differentiates performance and quality disparities between different observation system groups (facilitating variance component estimation).

○ Automatic Grouping Mechanism: The program automatically identifies observation system groups (limit: < 20 groups).

• Observations of different types belong to distinct system groups.

• Observations of the same type but with different system weights are also assigned to separate groups.

• Example: Gravity disturbances and height anomalies form two distinct groups. If gravity disturbances possess two distinct system weights, they are partitioned into two separate groups.

(2) Computation Surface ellipsoidal Height grid File.

Computation Surface Ellipsoidal Height Grid: Provides the geodetic coordinates of Computation Surface for the target field elements. The spatial resolution of the output grid is unrestricted and can be tailored to specific requirements.

[Parameter Settings]

Recommendation: Initially invoke the "[Gravity Field Approximation Using SRBFs and Performance Evaluation]" program. Conduct comprehensive tests on the spectral centers and bandwidths of observation/target elements and SRBFs under various parameter combinations. Optimize parameters based on the principle of fully resolving the spectral structure of the target field elements.

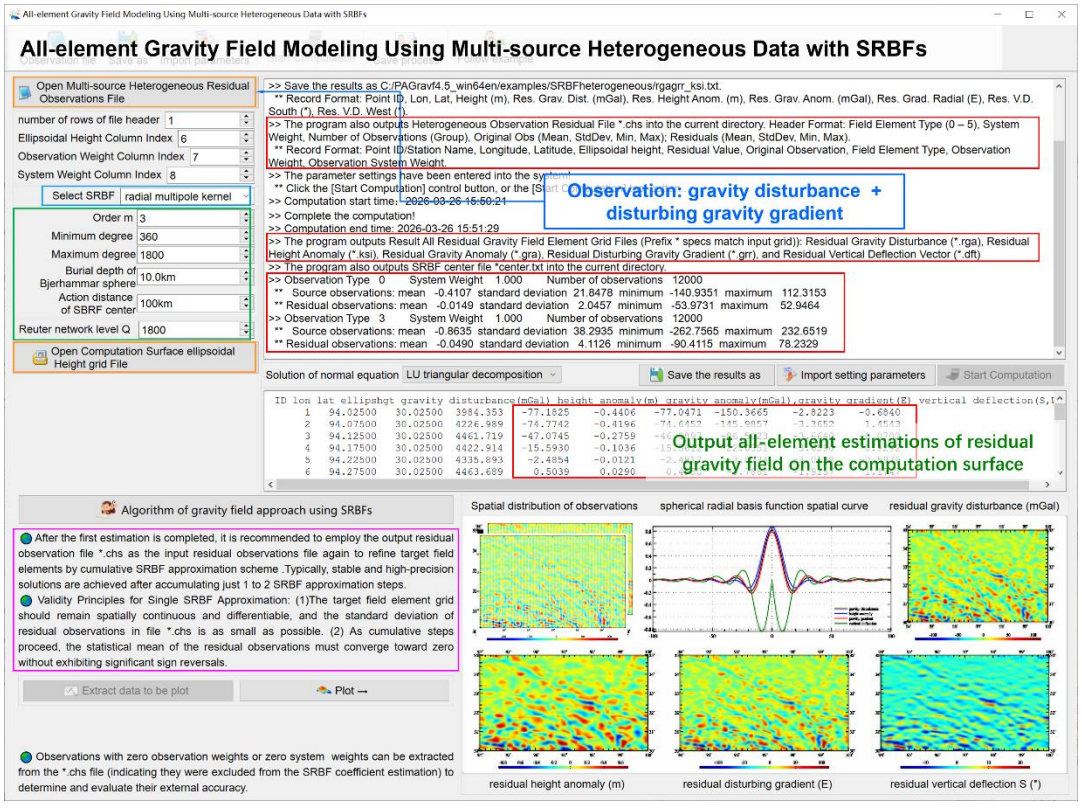

(1) Attribute Column Indices:

● Specify column indices for Ellipsoidal Height, Observation and Observation Weight, and System Weight.

● If the Observation Weight index is invalid (<1 or out of bounds) or values are negative, the program defaults to equal weighting.

● If an Observation Weight equals 0, the corresponding observation is excluded for SRBFcoefficient estimation, can be employed to determination of its external accuracy index.

(2) SRBF Type: Select Radial Multipole Kernel or Poisson Wavelet Kernel.

Note: Order 0 Radial Multipole Kernel = Point Mass Kernel; Order 0 Poisson Wavelet Kernel = Poisson Kernel.

(3) Bjerhammar Sphere Burial Depth (km): Depth relative to the mean observation surface.

(4) SRBF Center Action Distance:

● Also known as influence radius (angular distance × Bjerhammar radius). Equivalent to the integration radius in local modeling.

● A fixed action distance ensures spectral-spatial consistency in the regional gravity field structure.

(5) Reuter Grid Level (Q):

● Partitions the sphere into Q parallel circles (interval 180°/Q). Higher Q yields higher resolution.

● Guideline: Set 180°/Q comparable to the average inter-point distance.

● Adaptive Node Distribution: PAGravf4.5 employs a Reuter grid fitting algorithm to determine the effective number of observations (J) within each basis function's cell.

○ Centers where J is less than the minimum required observations per cell are eliminated. This ensures the spatial distribution of RBF centers strictly mirrors that of the observation points (uniform inputs → uniform centers; irregular inputs → irregular centers).

(6) Legendre Expansion Degree Range:

● Minimum Degree: Significantly influences the statistical mean of residuals.

● Maximum Degree & Grid Level Q: Primarily influence the statistical standard deviation.

● Burial Depth (D): Exhibits no obvious regularity and has low sensitivity.

(7) Normal Equation Solver: Select from LU Decomposition, Cholesky Decomposition, or Minimum Norm Solution.

[Output Files]

(1) Result Residual Gravity Field Element File:

Record Format: Point ID, Lon, Lat, Height (m), Res. Grav. Dist. (mGal), Res. Height Anom. (m), Res. Grav. Anom. (mGal), Res. Grad. Radial (E), Res. V.D. South (″), Res. V.D. West (″).

(2) All Residual Gravity Field Element Grid Files (Saved to current directory; prefix *; specs match input grid): Residual Gravity Disturbance (*.rga), Residual Height Anomaly (*.ksi), Residual Gravity Anomaly (*.gra), Residual Disturbing Gravity Gradient (*.grr), and Residual Vertical Deflection Vector (*.dft).

(3) Remaining Residual Observation File (*.chs): The program generates an observation residual file in the current directory. This file is Essential for gross error detection and accuracy assessment, and can also be employed as next Observations File for next Cumulative SRBF Approximation.

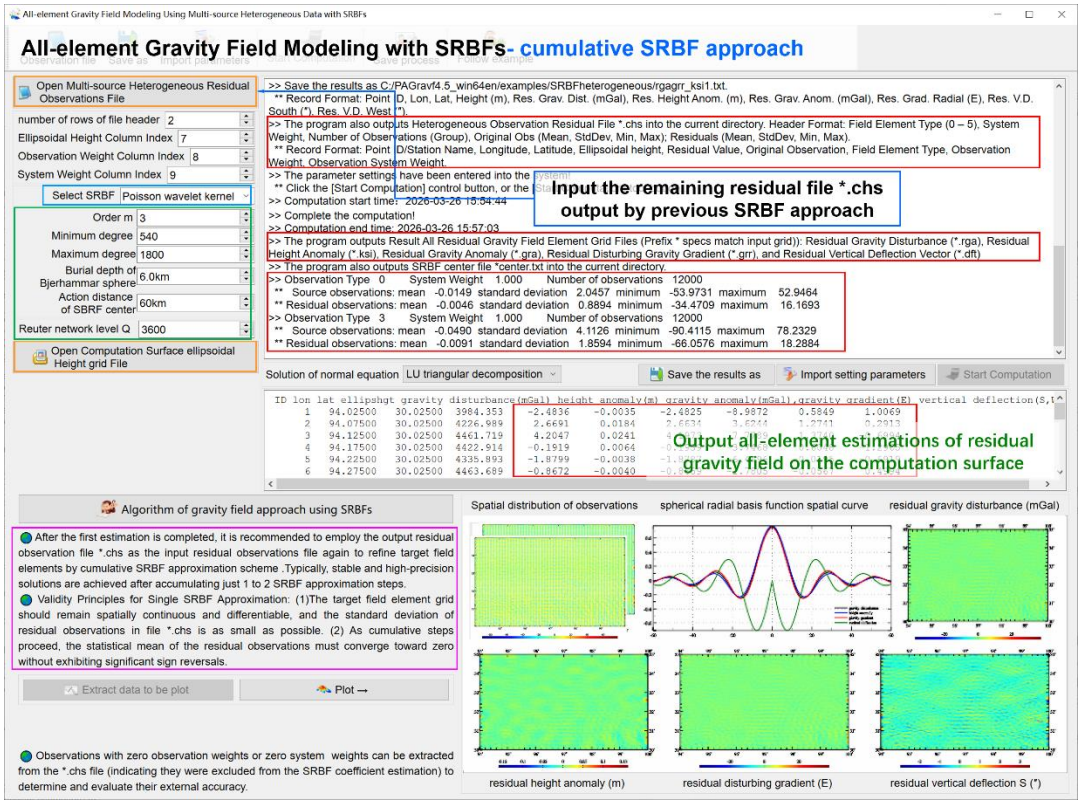

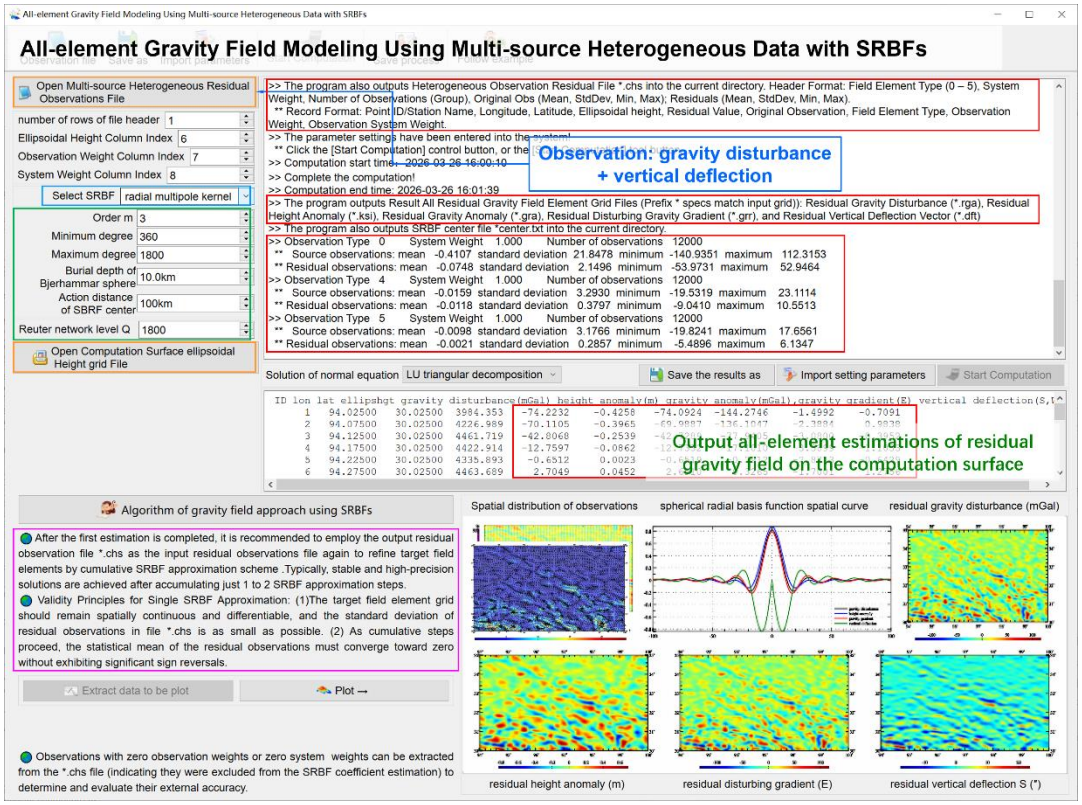

Header Format: Statistical results for each observation type occupy a dedicated row:

Field Element Type (0 – 5), System Weight, Number of Observations (Group), Original Obs (Mean, StdDev, Min, Max); Residuals (Mean, StdDev, Min, Max).

Record Format: Point ID/Station Name, Longitude, Latitude, Ellipsoidal height, Residual Value, Original Observation, Field Element Type, Observation Weight, Observation System Weight.

(4) SRBF Center File (*center.txt): The program outputs the Spherical Radial Basis Function center file to the current directory.

Header Format: Reuter Grid Level, Total RBF Centers, Meridian Cell Count, Max Parallel Circle Cell Count, Latitude Interval (arcminutes).

Record Format: Point ID, Longitude (deg), Geocentric Latitude, Cell Area Deviation (%), Parallel Circle Longitude Interval (arcminutes).

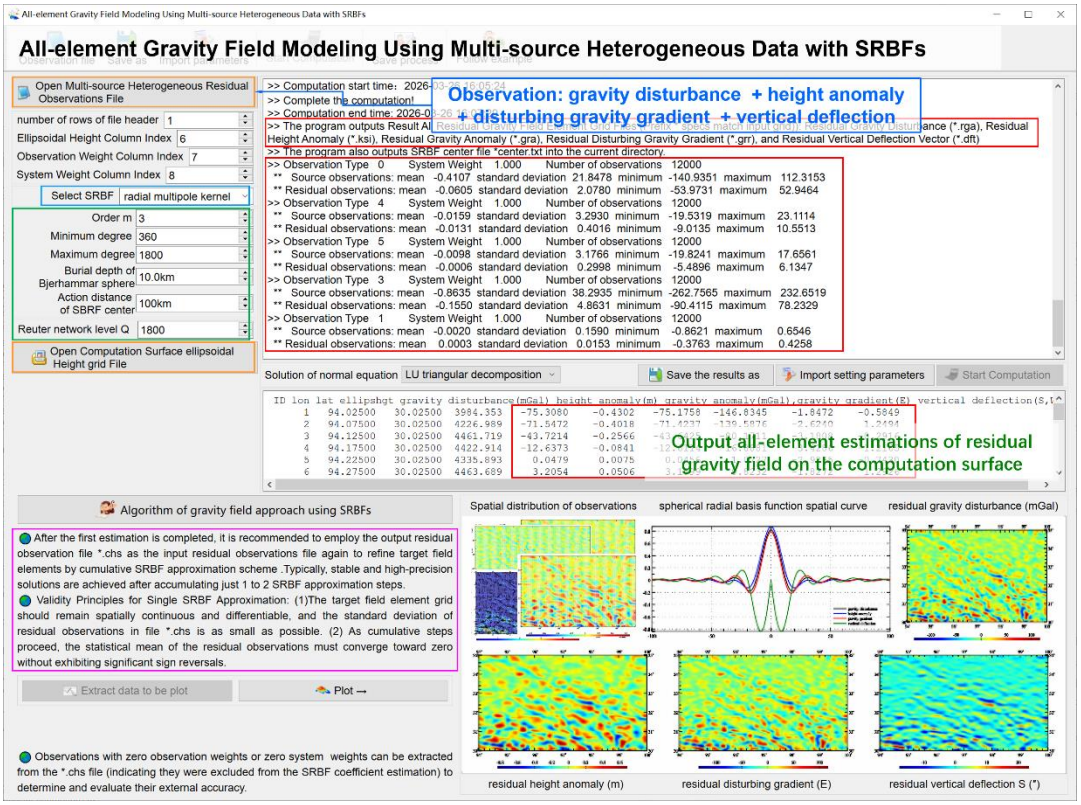

Robust Deep Integration of Multi-source Heterogeneous Systems

PAGravf4.5 implements a robust methodology for the deep integration of multi-source heterogeneous observation systems.

Core Mechanism: By normalizing the normal equations derived from distinct groups, the algorithm effectively controls the fusion of diverse observation types within the covariance structure. This enables precise gravity field approximation through the synthesis of heterogeneous field elements.

Decoupling Model and Quality: This approach completely decouples the influence of the observation system model (sensitivity matrix structure) from the influence of observation quality (errors or gross errors).

Immunity: the fusion process exhibits immunity to observation errors (including gross errors), discrepancies in observation types, and variations in the spatial distribution of observation points.

Strategic Advantages:

● Facilitates the seamless fusion of observation types with extreme spatial distribution disparities (e.g., sparse astronomical vertical deflections or GNSS-leveling data).

● Significantly enhances the precision of gross error detection.

Quantitative Validity Criteria for Single SRBF Approximation

Continuity and Differentiability: Ensure the spatial distribution of residual target field elements is continuous and differentiable, minimizing the residual standard deviation.

Mean Convergence: As cumulative approximations increase, the statistical mean of residuals must converge toward zero without significant sign reversals.

○ Convergence Behavior: Typically, stable solutions are achieved after 1 – 2 iterative approximation steps. The optimally approximated target residual field element grid is obtained by summing the residual grids generated from these iterations.

Case Study: Accuracy Assessment of Multi-source Data Fusion

In this case study, with an SRBF center action distance of 150 km, ground disturbance field elements on a 3′×3′ grid were computed by fusing multiple observation types: residual height anomalies, gravity anomalies, gravity disturbances, and vertical deflections derived from the EGM2008 model, degrees 541 – 1800. Excluding a 1° peripheral buffer zone to mitigate edge effects, statistical analysis compared:

● Reference Truth: EGM2008 Model-derived ground residual disturbance field elements (degrees 541 – 1800).

● Approximation Errors: Differences between SRBF approximated values and the reference truth.

Table 4.28: Statistics of Model Reference Truths

Field Element	Unit	Mean	Std. Dev.	Min	Max
Residual Geoidal Heights	m	-0.0020	0.1590	-0.8621	0.6546
Residual Gravity Disturbances	mGal	-0.4113	21.8940	-141.1997	112.4878
Residual Disturbing Gradients	E	-0.8635	38.2935	-262.7565	232.6519

Table 4.29: Differences between SRBF Approximation and Reference Model

Residual Observations	Target Residual Element	1st SRBF Approx.		2nd SRBF Approx.	
		Mean	Std. Dev.	Mean	Std. Dev.
Gravity Disturbances	Ground Height Anomaly (m)	0.0023	0.0095	0.0005	0.0093
Geoidal Heights					
Gravity Disturbances	Ground Height Anomaly (m)	0.0036	0.0190	0.0031	0.0158
Disturbing Gradients					

Algorithm Performance: The approximation capability of the algorithm is quantified by

the ratio of the standard deviation of the approximation errors (Table 4.29) to the standard deviation of the reference truth (Table 4.28).

Results demonstrate that multi-source fusion combined with a second approximation iteration further reduces standard deviations, enhancing overall accuracy.

Advanced Testing, Verification, and Analytical Capabilities

The program offers powerful capabilities for testing and validating complex geodetic scenarios:

(1) Fusion of Sparse High-Precision Data:

Strategy: Set Observation System Weight > 1.

Application: Test and validate the analytical fusion of sparse but high-precision data (e.g., astronomical vertical deflections or GNSS-leveling sites) to strengthen local constraints.

(2) Gross Error Detection in Mixed Data:

Strategy: Set corresponding Observation System Weight = 0.

Application: Perform gross error detection and external accuracy assessment on multi-source, multi-generation aliased data by treating them as independent check sets.

(3) Sea Surface Topography (SST) Separation:

Strategy: Set Satellite Altimetry System Weight < 1.

Application: Detect coastal boundary currents and effectively separate Sea Surface Topography from shallow-water satellite altimetry data.

(4) Performance Evaluation under Extreme Conditions:

Application: Evaluate the performance characteristics and technical robustness of gravity field approximation when faced with significant disparities in spatial distribution, quality, and accuracy across multiple data sources.

Workflow for Local Accuracy Assessment of New observations

For new airborne gravity observation lines or localized gravity observation point data:

- Method A: Set the Observation Weight (p) for these specific points to zero.
- Method B: Treat these data as an independent observation system group and set its System Weight to zero.
- Outcome: the program directly detects gross errors in the new gravity data and determines their external accuracy indices.

4.8 Modeling Process Exercise: Regional Gravity Field and Geoid

4.8.1 Demonstration of All-element Gravity Field Modeling Using the Integral Method

[Purpose] Using a ground Digital Elevation Model (DEM) and observed gravity disturbances simulated from the EGM2008 geopotential model, this program computes the height anomaly, gravity disturbance, vertical deflection vector and disturbing gravity gradient grid models on the Ground (terrain surace) and on the Geoid.

The computation employs a Remove-Integral-Restore scheme with Residual Terrain Effects (RTE) and the reference field of the EGM2008 model. This demonstration illustrates the critical issues and computational workflow involved in all-element regional gravity field modeling via the spatial-domain integral method.

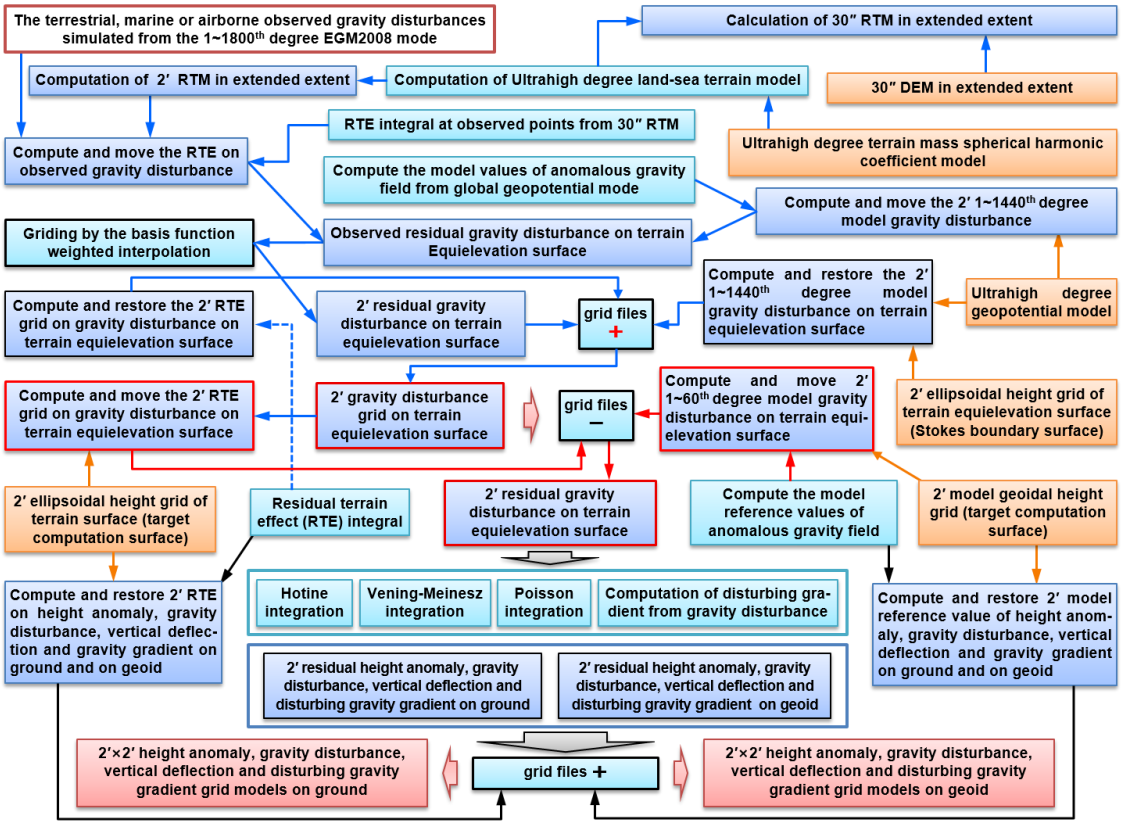

Computation Process of All-element Gravity Field Modeling Using the Integral Method

Input/Output Data and Related Terrain Models

To mitigate edge effects in integration, data extents are defined with the following nested containment: Terrain Data latitude and longitude extent (Extended Extent: E104.0° – 111.0°, N24.0° – 29.0°) ⊃ Computation Extent (Observation Distribution/ Boundary Surface: E104.5° – 110.5°, N24.5° – 28.5°) ⊃ Results Extent (Model Output: E105.0° – 110.0°, N25.0° – 28.0°).

(1) Observed Gravity Disturbance File (Obsgrav.txt)

- Source: Gravity disturbances simulated from EGM2008 (degrees 1 – 1800).
- Unified Processing: PAGravf4.5 applies identical algorithms to terrestrial, marine, and airborne data; no distinction is made based on observation altitude or environment.
- Record Format: ID, Longitude (°), Latitude (°), Ellipsoidal Height (m), Gravity Disturbance (mGal).

(2) Spherical Harmonic Coefficient Models

- Files: ETOPOcs3600.dat (3600-degree global land-sea terrain mass model) and EGM2008.gfc (2190-degree geopotential model).
- Location: C:\PAGravf4.5_win64en\data.

Note: ETOPOcs3600.dat is generated via the [Ultrahigh-Degree Spherical Harmonic Analysis of Global Land-Sea Terrain Model] function using the global 2′×2′ ETOPO2v2g grid model.

(3) Ground Digital Elevation Models (DEM)

Two resolutions are required:

● High-Resolution (30″×30″): Used for observation reduction (computing/removing RTEs on observation field elements). File: extdtm30s.dat.

● Target Resolution (2′×2′): Used for restoring RTEs on target field elements. File: extdtm2m.dat.

(4) Terrain Equielevation Surface Ellipsoidal Height Grid (equihgt30s.dat / equihgt2m.dat)

● Definition: Ellipsoidal Height = EGM2008 Height Anomaly (deg 1 – 360) + Mean Orthometric Height of the terrain surface.

● Dual Role:

○ Reduction Surface: For downward/upward continuing ground observations.

○ Boundary Equipotenial Surface: For solving the Stokes Boundary Value Problem.

● Special Case: If orthometric heights are zero, this equielevation surface coincides with the traditional geoid.

● Advantage: Using the terrain equielevation surface minimizes the vertical distance between observation points and the boundary surface, effectively suppressing the attenuation of ultra-short-wavelength gravity signals.

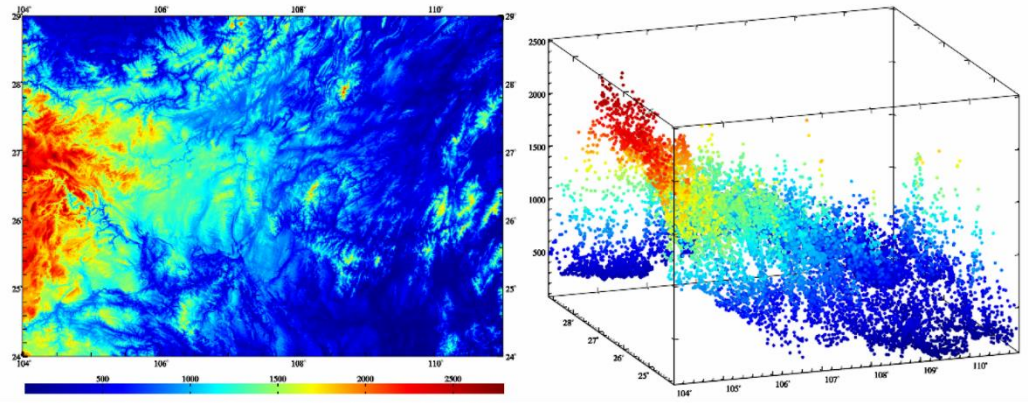

Digital elevation model (m) and gravity observation point distribution (BLH)

(5) Reference Grids

● Geoidal Height Grid (geoidhgt2m.dat): Derived from EGM2008 (deg 1 – 360); and Provides geodetic coordinates of the geoid.

● Ground Ellipsoidal Height Grid (surfhgt2m.dat): Sum of EGM2008 height anomaly (deg 1 – 360) and DEM; provides the geodetic coordinates of ground surface,

(6) Output Products

● Geoid-Level Grids (2′×2′): Geoidal height, gravity disturbance, vertical deflection vector, disturbing gravity gradient.

● Ground-Level Grids (2′×2′): Height anomaly, gravity disturbance, vertical deflection vector, disturbing gravity gradient, plus Ground DEM or Ellipsoidal Height grid.

Workflow: Function Calls and Data Flow

(1) Construct Residual Terrain Models (RTM)

Function: [Computation of Model Values for Complete Bouguer and Residual Terrain Effects].

Settings: Degrees 1 – 1800.

Type: 'Terrain elevation / Bathymetry'.

Input: ETOPOcs3600.dat.

Process: Generate model terrain elevations (mdldtm30s.dat, mdldtm2m.dat) from the respective DEMs. Subtract these from the original DEMs to obtain RTMs (resdtm30s.dat, resdtm2m.dat).

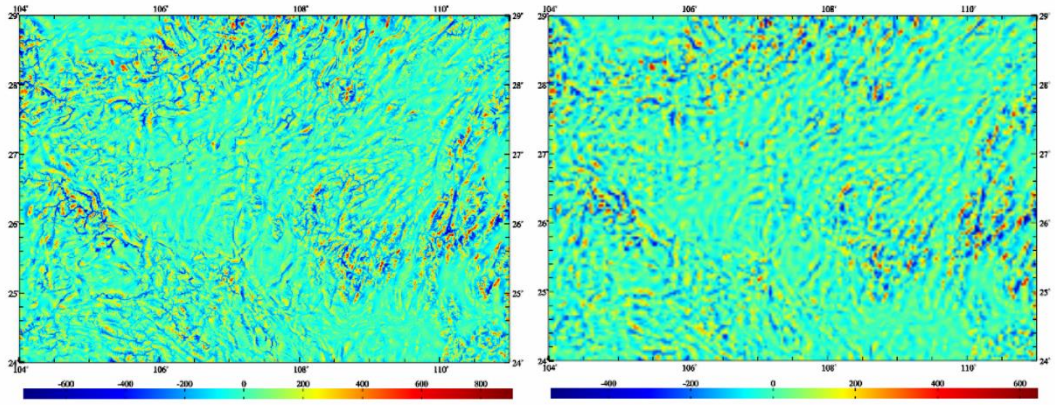

30″×30″ and 2′×2′ residual terrain model (RTM, m)

Table 4.30: Statistics of 30″×30″ and 2′×2′ RTMs (Unit: m)

Model	Mean	Std. Dev.	Min	Max
30″×30″ RTM	-0.4626	137.2485	-746.0400	908.8900
2′×2′ RTM	-0.8250	97.5569	-541.2900	645.0400

(2) Remove Ultra-High-Degree Model Gravity Disturbances

Function: [Computation of Gravity Field Elements from a Global Geopotential Model].

Settings: Degrees 1 – 1440.

Input: EGM2008.gfc, Obsgrav.txt.

Type: 'Gravity Disturbance'.

Process: Compute model values (Obsgravmdl.txt, col 6). Subtract from observations (col 5) to generate model residuals (Obsgravmdlresd.txt, col 7).

Table 4.31: Statistics of Gravity Disturbances at Observation Points Before and After Removal of the 1440-degree Geopotential Model (Unit: mGal)

Statistic	Mean	Std. Dev.	Min	Max
Observed	-27.7853	28.7143	-147.4878	74.7074
Model residuals	-0.3743	6.4755	-35.8263	27.4789

(3) Remove Residual Terrain Effects (RTE) on Observations

Function: [Rigorous Numerical Integration of Land-Sea Residual Terrain Effects].

Inputs: Obsgravmdlresd.txt, extdtm30s.dat, mdldtm30s.dat, surfhgt30s.dat.

Settings: Integration radius = 60 km.

Process: Compute RTE (col 8 in Obsgravresdtm.txt). Subtract RTE from model residuals (col 7) to obtain final residual gravity disturbances (Obsgravresidual.txt, col 9).

Table 4.32: Statistic of Residual Gravity Disturbances at Observation Points Following the Removal of RTEs (Unit: mGal)

Statistic	Mean	Std. Dev.	Min	Max
Final Residuals	6.4474	9.7051	-28.6215	79.6853

Note: Analytical continuation via residual radial gradient is omitted here due to negligible its impact within 1000 m height differences. Thus, residuals at observation points are treated as equivalent to those on the equipotential boundary surface. The reduction to the Terrain Equielevation Surface is now complete.

Optimization Note: Tables 4.28 – 4.29 statistics are typically used to refine RTE algorithms based on the terrain effect quantitative criteria. This step is skipped here as simulated data lacks sufficient real-world ultra-short-wavelength content.

(4) Grid Residual Gravity Disturbances

Function: [Gridding of Heterogeneous Data via Weighted Basis Function Interpolation].

Settings: Select 'Equal Weights' (weights can be pre-estimated using RTE as a reference attribute).

Process: Grid the final residuals (col 9 of Obsgravresidual.txt) onto a 2′×2′ grid on the terrain equielevation surface, generating distgravresidual.dat.

(5) Compute 1440-degree EGM2008 Model Gravity Disturbance Grid on the Terrain Equielevation Surface

Function: [Computation of Gravity Field Elements from a Global Geopotential Model].

Parameters: Min degree = 1, Max degree = 1440.

Inputs: EGM2008.gfc and the ellipsoidal height grid of the terrain equielevation surface (equihgt2m01.dat).

Operation: Select 'Gravity Disturbance' to generate the 2′×2′ model grid distgravmdl.dat.

Consistency Check: The geopotential model and degree range must match those used in Step (2).

Theoretical Basis: Step (2) removed model values at observation points, while Step (5) restores them on the reduction surface. This Remove-Restore mechanism facilitates analytical continuation leveraging the ultra-high-degree geopotential model.

(6) Compute Residual Terrain Effect (RTE) Grid for Gravity Disturbances

Function: [Rigorous Numerical Integration of Land-Sea Residual Terrain Effects].

Inputs:

- ○ High-res DTM: extdtm2m.dat.
- ○ Low-pass DTM: 2′×2′ model terrain mdldtm2m.dat.
- ○ Position Grid: 2′×2′ ground ellipsoidal height surfhgt2m.dat (defines residual mass location).
- ○ Target Surface: Terrain equielevation surface ellipsoidal height equihgt2m01.dat.

Parameters: Element type = ‘Gravity Disturbance’; Integration radius = 60 km (must match Step (3)).

Output: 2′×2′ RTE grid distgravresidtm.dat.

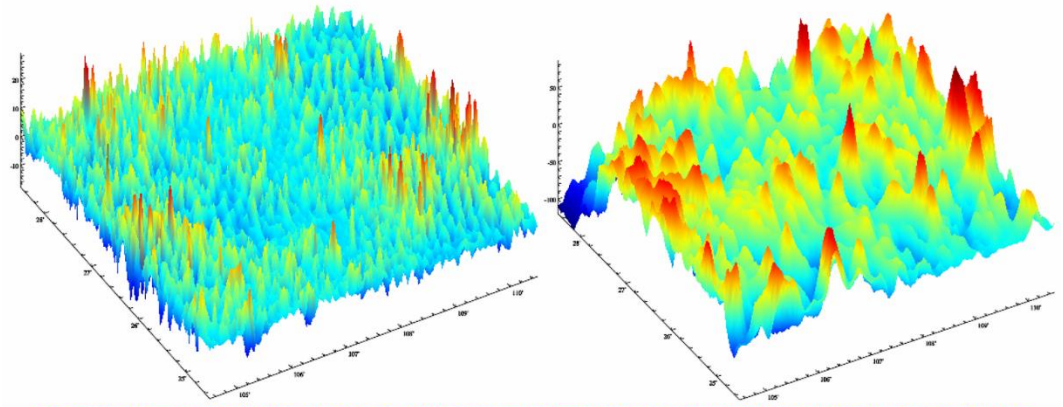

2′×2′ residual gravity disturbance (mGal) and 1440-degree model gravity disturbance (mGal) on terrain equielevation surface

(7) Synthesize Final Gravity Disturbance Grid on the Terrain Equielevation Surface

Synthesis: Sum the following three grids:

- Residual grid: distgravresidual.dat
- Ultra-high-degree model grid: distgravmdl.dat
- RTE grid: distgravresidtm.dat

Result: The 2′×2′ gravity disturbance grid on the terrain equielevation surface.

Workflow Phase: Steps (1) – (7) complete the data reduction and preprocessing phase. Subsequent steps focus on gravity field approximation and modeling based on geodetic boundary value theory.

(8) Reconstruct RTM and RTE for Gravity Field Approximation

Bandwidth Selection: Select the spectral bandwidth for the Residual Terrain Model (RTM) (here, max degree = 1440).

Recomputation: Generate the 2′×2′ RTM file resdtm2m1.dat.

Function: [Rigorous Numerical Integration of Land-Sea Residual Terrain Effects].

Parameters: Integration radius = 60 km.

Output: RTE grid on gravity disturbances equdisgravrtm.dat.

Technical Note: Optimization criteria for gravity field approximation differ from those for gridding. This example directly adopts a max degree of 1440 due to the limited ultra-short-wavelength content in simulated data.

(9) Compute 1st – 720th Degree GM Reference Values

Function: [Computation of Gravity Field Elements from a Global Geopotential Model].

Parameters: Min degree = 1, Max degree = 720.

Inputs: EGM2008.gfc and equihgt2m01.dat.

Output: 2′×2′ model reference grid equdisgravmdl.dat.

Role Differentiation:

- 1440-degree model [Steps (2) & (5)]: Used for analytical continuation (preserving high-frequency signals).

○ 1 – 720-degree model [Step (9)]: Serves as the reference gravity field for local gravity field integrations.

(10) Generate Final Residual Gravity Disturbance Grid

Computation: Subtract the RTE grid (equdisgravrtm.dat) and the 720-degree model reference grid (equdisgravmdl.dat) from the total gravity disturbance grid (equdistgrav.dat).

Output: Final residual grid equgravresidual.dat.

Table 4.33: Statistics of Gravity Field Elements on the Terrain Equielevation Surface (Unit: mGal)

Element	Mean	Std. Dev.	Min	Max
Total Gravity Disturbance	-17.7675	23.3340	-119.4421	86.6984
Residual Terrain Effects	-1.6478	4.5234	-31.5185	22.3032
720-degree Model Values	-23.5523	19.5560	-112.3400	31.4088
Final Residuals	7.4326	13.1966	-56.9378	71.9857

Optimization Objective: The primary goal of these statistics is to refine the RTE algorithm and parameters based on the gravity field approximation optimization criterion.

Note: Detailed optimization analysis is omitted here as the simulated data lacks sufficient real-world ultra-short-wavelength information.

(11) Compute Residual Anomalous Gravity Field Elements via Integration

Utilize the gravity field integration module to compute residual anomalous field elements on both the terrain surface (ground) and the geoid.

Input Configuration:

○ Ground computations: Load the ground ellipsoidal height grid surfhgt2m2.dat.

○ Geoid computations: Load the model geoidal height grid geoidhgt2m2.dat (derived from EGM2008 up to degree 360).

Integration Radius: Set the integration radius to 90 km.

Execution Steps:

○ Height Anomaly: Invoke [External Height Anomaly Computation via Generalized Hotine Integration] to generate surfksiresidual.dat (ground) and geoidhgtresidual.dat (geoid).

○ Vertical Deflection: Invoke [Computation of External Vertical Deflection from Gravity Disturbance] to generate surfdftresidual.dat (ground) and geoiddftresidual.dat (geoid).

○ Gravity Disturbance: Invoke [Computation of External Anomalous Gravity Field Elements via Poisson Integration] to generate surfrgaresidual.dat (ground) and geoidrgaresidual.dat (geoid).

○ Disturbing Gravity Gradient: Invoke [Computation of External Disturbing Gravity Gradient from Gravity Disturbance] to generate surfgrresidual.dat (ground) and geoidgrresidual.dat (geoid).

(12) Compute and Restore Residual Terrain Effects (RTE)

Compute the RTEs on various anomalous field elements on the ground and geoid to facilitate the restoration step.

Function: [Rigorous Numerical Integration of Land-Sea Residual Terrain Effects].

Settings: Select all four element types (Height Anomaly, Gravity Disturbance, Vertical Deflection, Disturbing Gravity Gradient).

○ Ground: Input surfhgt2m.dat.

○ Geoid: Input geoidhgt2m.dat.

Consistency: The integration radius and RTM file (resdtm2m.dat) must match those defined in Step (8).

Output Files (RTE Grids):

○ Ground: surfhgt2mrtm.ksi (Height Anomaly), surfhgt2mrtm.rga (Gravity Disturbance), surfhgt2mrtm.dft (Vertical Deflection), surfhgt2mrtm.grr (Disturbing Gravity Gradient).

○ Geoid: geoidhgtrtm.ksi (Geoidal Height), geoidhgtrtm.rga (Gravity Disturbance), geoidhgtrtm.dft (Vertical Deflection), geoidhgtrtm.grr (Disturbing Gravity Gradient).

(13) Compute and Restore GM Reference Values (GMR)

Compute the 1st – 720th degree GM reference values for various anomalous field elements on the ground and geoid.

Function: [Computation of Gravity Field Elements from a Global Geopotential Model].

Settings: Select all four element types; Min degree = 1, Max degree = 720 [consistent with Step (9)].

○ Ground: Input surfhgt2m.dat.

○ Geoid: Input geoidhgt2m.dat.

Output Files (MRV Grids):

○ Ground: surfhgt2mgm720.ksi, surfhgt2mgm720.rga, surfhgt2mgm720.dft, surfhgt2mgm720.grr.

○ Geoid: geoidh2mgm720.ksi, geoidh2mgm720.rga, geoidh2mgm720.dft, geoidh2mgm720.grr.

(14) Synthesize Final Target Grids for Ground Anomalous Field Elements

Generate the final target grids by summing the residual field, the RTE, and the GMR on the ground for each element type. Generated Products (2′×2′):

- Ground Height Anomaly: surfhgtksi2m.dat
- Ground Gravity Disturbance: surfhgtrga2m.dat
- Ground Vertical Deflection Vector: surfhgtdft2m.dat
- Ground Disturbing Gravity Gradient: surfhgtgrr2m.dat

(Plus the ground ellipsoidal height grid defining ground surface.)

Table 4.34: Statistics of Synthesized Ground Anomalous Gravity Field Elements

Element type	Component	Mean	Std. Dev.	Min	Max
Ground Height Anomaly (m)	Model Ref. Value (MRV)	-27.4261	3.2927	-36.0901	-20.1879
	Residual Terrain Eff. (RTE)	-0.0008	0.0314	-0.1219	0.1363
	Residual Field	0.6136	0.1608	0.2218	1.2427
	Total Synthesized	-26.8133	3.3149	-35.4331	-19.1927

Ground Gravity Disturbance (mGal)	Model Ref. Value (MRV)	-22.4136	15.7881	-76.2475	18.5218
	Residual Terrain Eff. (RTE)	-0.7256	0.6856	-7.8832	1.8187
	Residual Field	6.8912	11.4588	-35.1321	65.7856
	Total Synthesized	-16.2480	18.7702	-81.8505	77.2212
Ground Vert. Deflection (″, S)	Model Ref. Value (MRV)	1.5543	3.0688	-5.7396	14.0662
	Residual Terrain Eff. (RTE)	0.1340	0.7770	-3.5615	3.6938
	Residual Field	-0.0232	1.4285	-7.3171	6.1334
	Total Synthesized	1.6649	3.2346	-9.5143	16.4299
Ground Vert. Deflection (″, W)	Model Ref. Value (MRV)	-4.3753	2.7632	-12.4916	5.1844
	Residual Terrain Eff. (RTE)	-0.0525	0.9824	-4.3215	5.2168
	Residual Field	0.0222	1.6118	-7.6123	6.2307
	Total Synthesized	-4.4050	3.2895	-18.4035	6.0986
Ground Disturbing Gradient (E)	Model Ref. Value (MRV)	-0.2116	9.6634	-34.2497	32.342
	Residual Terrain Eff. (RTE)	-0.0986	49.3177	-269.71	232.31
	Residual Field	-0.0622	15.1553	-62.71	112.45
	Total Synthesized	-0.3736	52.1555	-262.54	253.71

(15) Synthesize Final Target Grids for Geoidal Anomalous Field Elements

Generate the final target grids by summing the residual field, the RTE, and the MRV on the geoid for each element type. Generated Products (2′×2′):

- Geoidal Height: geoidhksi2m.dat
- Geoidal Gravity Disturbance: geoidhrga2m.dat
- Geoidal Vertical Deflection Vector: geoidhdft2m.dat
- Geoidal Disturbing Gravity Gradient: geoidhgrr2m.dat

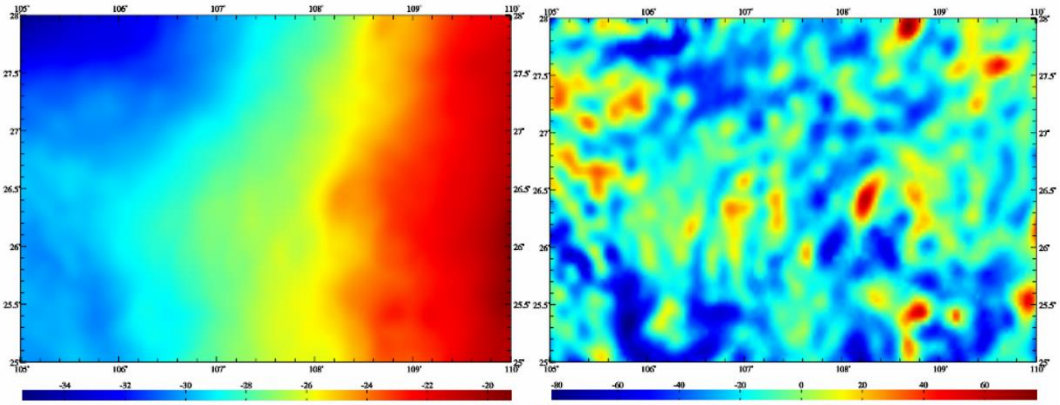

2′×2′ ground height anomaly (m) and ground gravity disturbance (mGal)

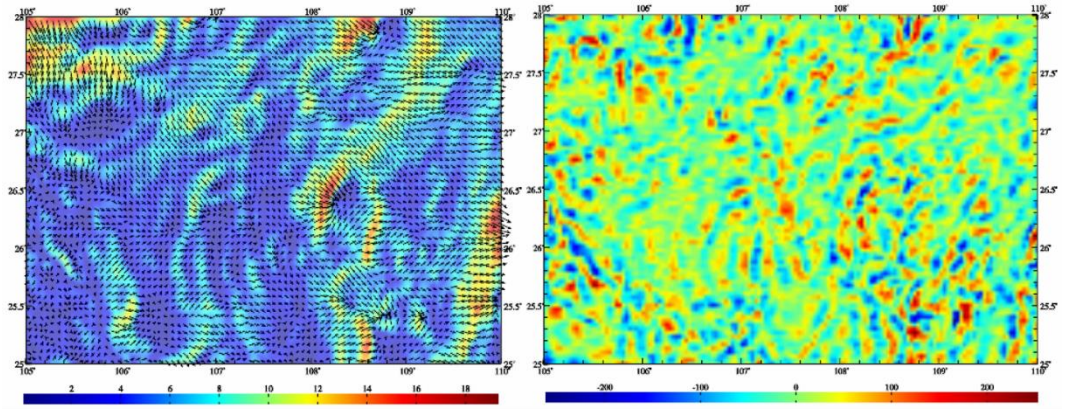

2′×2′ ground vertical deflection (″) and ground disturbing gravity gradient (E)

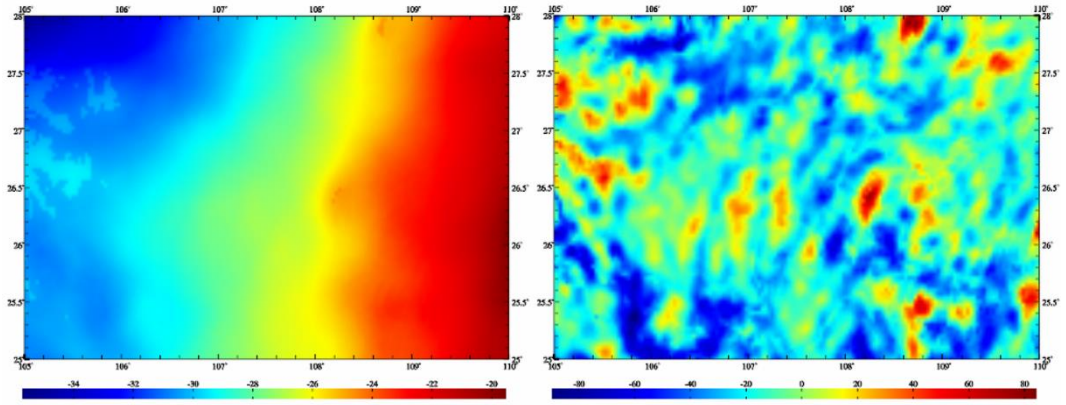

2′×2′ geoidal height (m) and gravity disturbance (mGal)

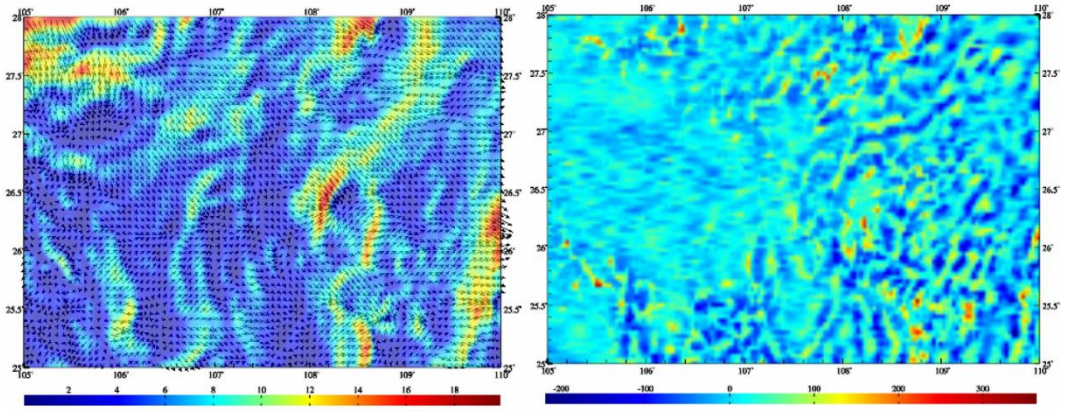

2′×2′ vertical deflection (″) and disturbing gravity gradient (E) on the geoid

4.8.2 Expedited Workflow Demonstration for All-element Gravity Field Modeling Using SRBFs

[Purpose] This example demonstrates a streamlined, six-step workflow for all-element gravity field modeling based on the Spherical Radial Basis Function (SRBF) approximation method on both the ground and the geoid. The approach directly utilizes observed gravity disturbances (terrestrial, marine, and airborne) and GNSS-leveling height anomalies (or

geoidal heights) without employing complex schemes of terrain effects and traditional pre-processing. This workflow aims to facilitate a rapid understanding of key aspects in spectral-domain local SRBF modeling, including observation data analysis, computational quality control, and gravity field reconstruction techniques.

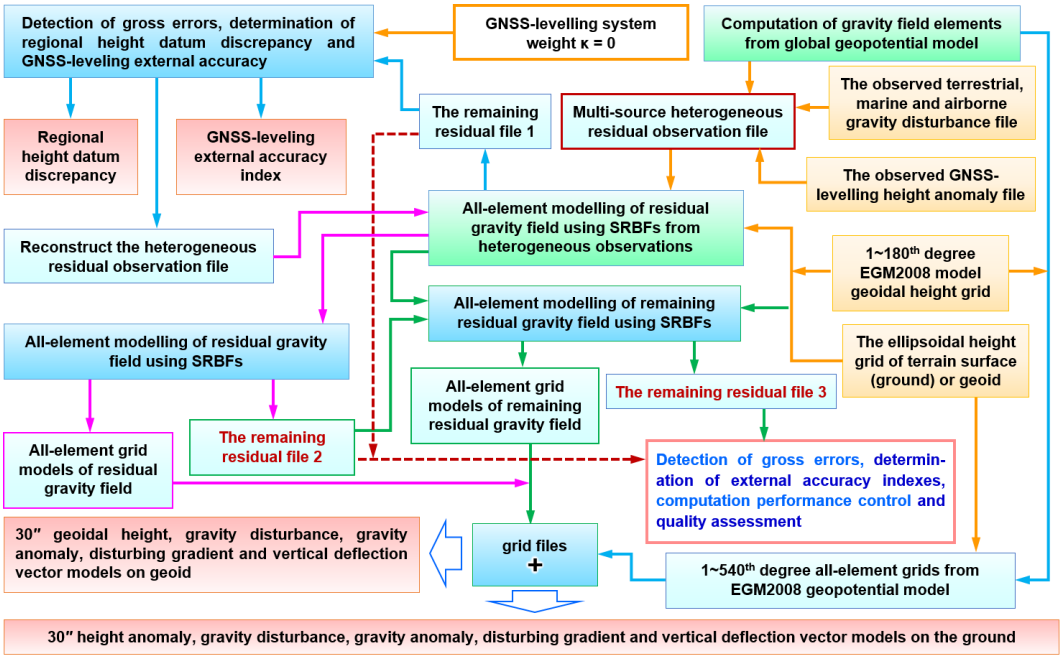

Expedited Workflow for All-element Gravity Field Modeling Using SRBFs

Primary Data Sources

(1) Observed Gravity Disturbances (obsdistgrav.txt)

Format: Point ID/Station Name, Longitude (decimal degrees), Latitude (decimal degrees), Ellipsoidal Height (m), Observation Gravity Disturbance (mGal).

(2) GNSS-Leveling Observation Height Anomalies (obsGNSSlksi.txt)

Format: Point ID/Station Name, Longitude (decimal degrees), Latitude (decimal degrees), Ellipsoidal Height (m), Observation Height Anomaly or Geoidal Height (m).

Normal Height System: The "Ellipsoidal Height" attribute corresponds to the GNSS-derived ellipsoidal height at the GNSS-leveling site.

Orthometric Height System: The observation geoidal height represents the ellipsoidal height of the geoid. In the file record, this value populates the "Ellipsoidal Height" field.

Note: The SRBF-based all-element modeling workflow is identical for both height systems; only the appropriate ellipsoidal heights for the GNSS-leveling sites are required. This example employs observation height anomalies under the Normal Height System. Both datasets are simulated by adding noise to EGM2008 model values (degrees 1 – 1800).

(3) Computation Surface Ellipsoidal Height Grids

For Geoidal Modeling: The computation surface is defined by the model geoidal height grid. In this example: mdlgeoidh30s.dat.

For Ground Modeling: The computation surface is defined by the ground ellipsoidal height grid. In this example: surfhgt30s.dat (= Land-Sea DEM DEM30s.dat + Model Geoidal

Height mdlgeoidh30s.dat).

Model Derivation: Model geoidal heights and ground height anomalies are derived from a 180-degree gravity field model (steps omitted).

Requirement: The extent of the computation surface grid must exceed the target extent to mitigate edge effects.

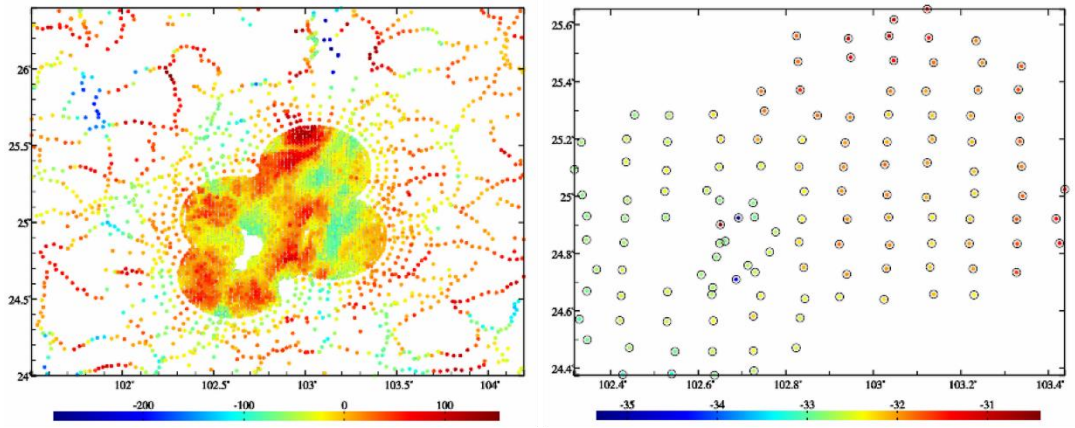

The observed gravity disturbances (mGal) and observed GNSS-levelling height anomalies (m)

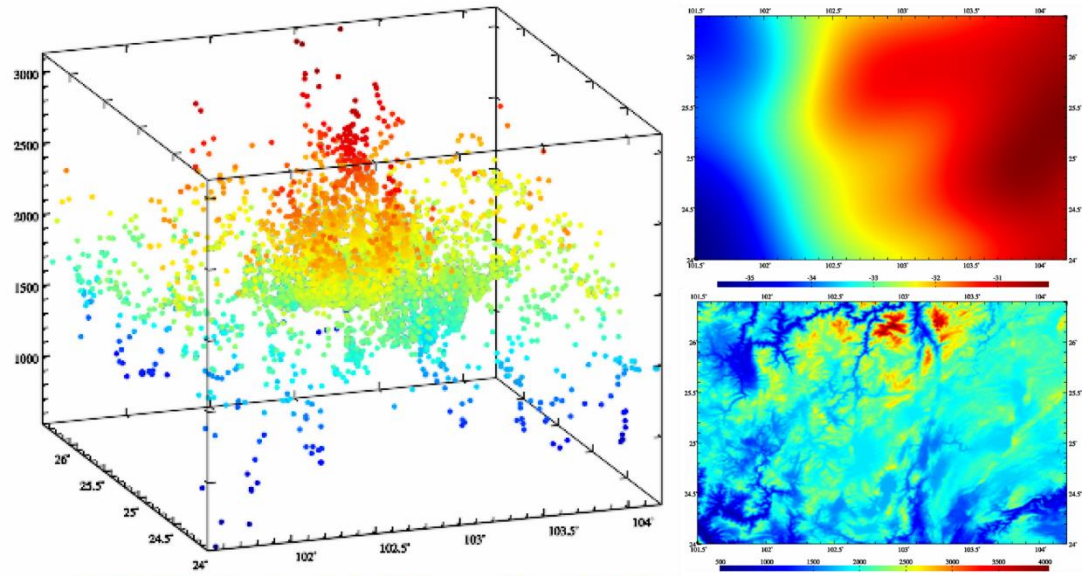

The distribution of gravity points, 1~180th degree model geoidal height and ellipsoidal height of the terrain surface

Step 1: Remove Reference Model Values and Construct Multi-source Heterogeneous Residual Observations

Function: [Computation of Gravity Field Elements from a Global Geopotential Model].

Settings: Maximum degree = 540.

Procedure:

- Compute and remove reference gravity field values from obsdistgrav.txt and obsGNSSlksi.txt.
- Merge results into a Multi-source heterogeneous discrete residual observation file: obsresiduals0.txt.

File Convention (obsresiduals0.txt):

○ Columns: ID, Lon, Lat, Ellipsoidal Height (m), Residual Value, Element Type (0 – 5), Obs Weight, Sys Weight, ...

○ Fixed Attributes: The first five columns are fixed in position and order.

○ Element Types: 0 = Residual Gravity Disturbance (mGal); 1 = Residual Height Anomaly (m).

Critical Action: Set the System Weights for all GNSS-leveling sites in obsresiduals0.txt to zero.

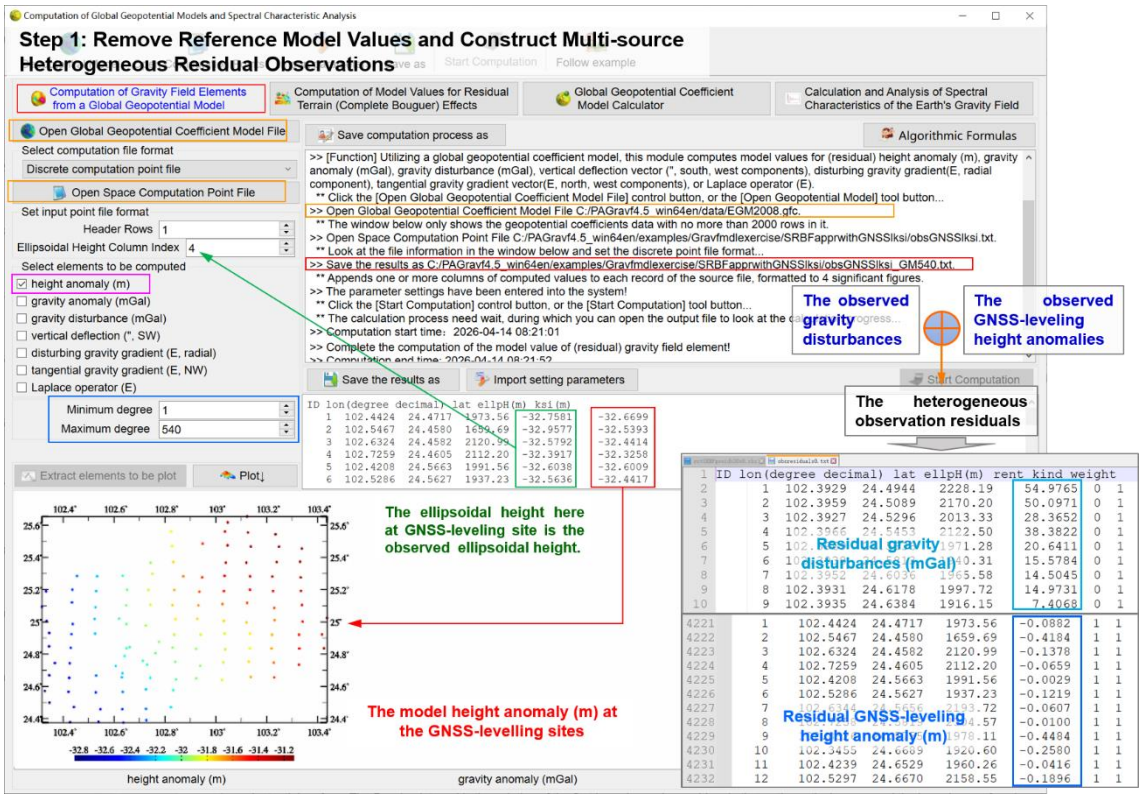

Step 2: Gross Error Detection via SRBF and Data Reconstruction

Function: [All-element Gravity Field Modeling Using Multi-source Heterogeneous Data with SRBFs].

Inputs: obsresiduals0.txt and surfhgt30s.dat.

Outputs:

○ Residual ground all-element grids: SRBFsurfhgt30s0.xxx (.ksi, .rga, .gra, .grr, .dft).

○ Remaining residual observation file: SRBFsurfhgt30s0.chs.

Gross Error Detection Protocol:

○ Extract remaining residual gravity disturbances (rntobsdistgrav0.txt) and GNSS-leveling height anomalies (rntobsGNSSlksi0.txt) from SRBFsurfhgt30s0.chs.

○ Use the remaining residual value (Column 5) as the statistical metric for outlier detection:

• Gravity disturbances: Reject observations exceeding 5σ (5 times the standard

deviation).

• GNSS-Leveling sites: Reject observations exceeding 3σ.

Regenerate the cleaned heterogeneous residual observation file: obsresiduals01.txt.

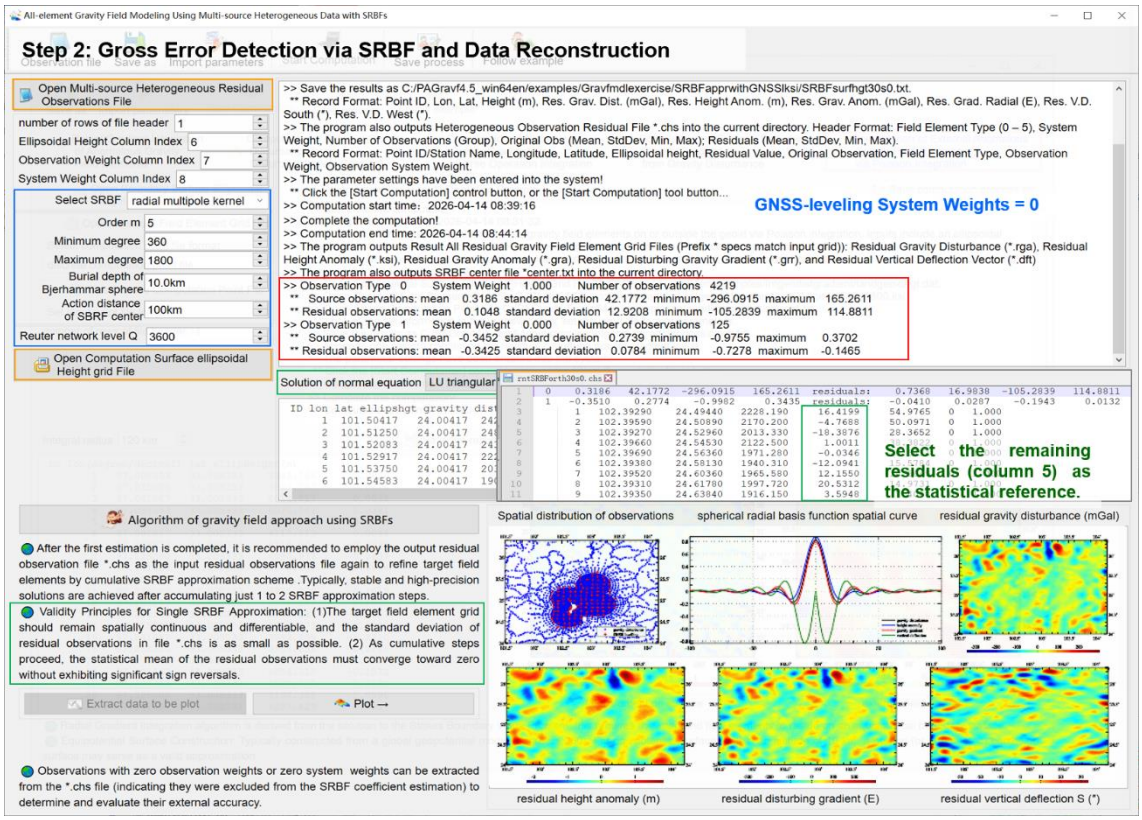

Step 3: Determination of Height Datum Discrepancy and GNSS-Leveling External Accuracy

Input: Cleaned file obsresiduals01.txt.

Procedure: Repeat Step 2 to re-estimate residual grids (rntSRBFdatum30s.xxx) and output the remaining residual observation file rntSRBFdatum30s.chs.

Methodological Note: Since GNSS-leveling sites' system weights were previously set to zero, this step effectively uses only the discrete residual gravity disturbances to evaluate the external accuracy of the GNSS-leveling height anomalies.

Table 4.35: Statistics of Residual Observations before and after Gross Error Detection/Elimination (SRBF Approximation)

Data Type	Stage	Count	Mean	Std. Dev.	Min	Max
Gravity Disturbance (mGal)	Original Residuals	4219	0.3186	42.1772	-296.0915	165.2611
	Post-Rejection Residuals	4215	0.2695	42.0737	-296.0915	165.2611
	Remaining Residuals	4215	-0.5677	13.8957	-80.4161	64.8276

GNSS-Leveling Height Anomaly (m)	Original residuals	125	-0.3452	0.2739	-0.9755	0.3702
	Residuals without error	123	-0.3404(1)	0.2735	-0.9755	0.3702
	Remaining residuals	123	-0.0069(2)	0.0233(3)	-0.1295	0.0528

Regional Height Datum Discrepancy: The statistical mean of the GNSS-leveling residual height anomalies (-0.3404 m marked as (1)) represents the determined discrepancy between the regional height datum and the global height datum (gravimetric geoid). This illustrates the SRBF method for datum unification.

GNSS-Leveling External Accuracy Index: The standard deviation of the remaining residuals (e.g., 0.0233 m marked as (3), corresponding to 2.33 cm) serves as the external accuracy index. This indicates that the external accuracy of the GNSS-leveling data is no worse than this standard deviation value.

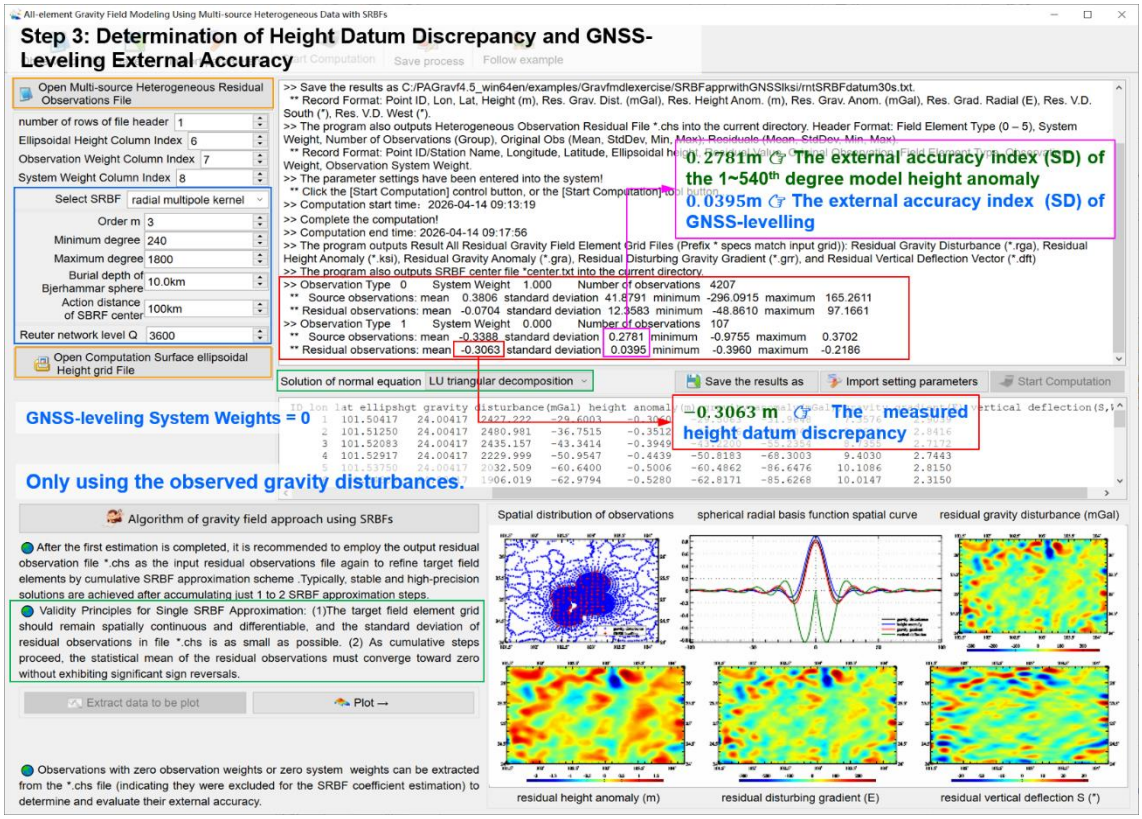

Standard Practice: Typically, one iterates the SRBF approximation 1 – 2 more times using the *.chs file to minimize the standard deviation of remaining residuals, establishing the final accuracy index.

Critical Action:

- Remove the determined regional height datum discrepancy (e.g., -0.3404 m) from the observation GNSS-leveling residual height anomalies.

○ Restore the System Weights for GNSS-leveling sites.

○ Regenerate the final heterogeneous residual observation file: obsresiduals1.txt.

Step 4: Computation of Residual Ground All-Element Gravity Field Models via SRBF Approximation

Function: [All-element Gravity Field Modeling Using Multi-source Heterogeneous Data with SRBFs].

Inputs:

○ Multi-source heterogeneous residual observation file: obsresiduals1.txt.

○ Ground ellipsoidal height grid: surfhgt30s.dat.

Procedure:

○ Estimate the residual ground all-element gravity field grids: SRBFsurfhgt30s1.xxx.

○ Output the remaining residual observation file: SRBFsurfhgt30s1.chs.

Quality Control (QC):

○ The .chs file can be utilized for further gross error detection using the 5σ criterion for gravity disturbances and the 3σ criterion for GNSS-leveling sites.

○ Upon outlier rejection, the workflow should restart from Step 3. This iterative refinement is omitted in the current example.

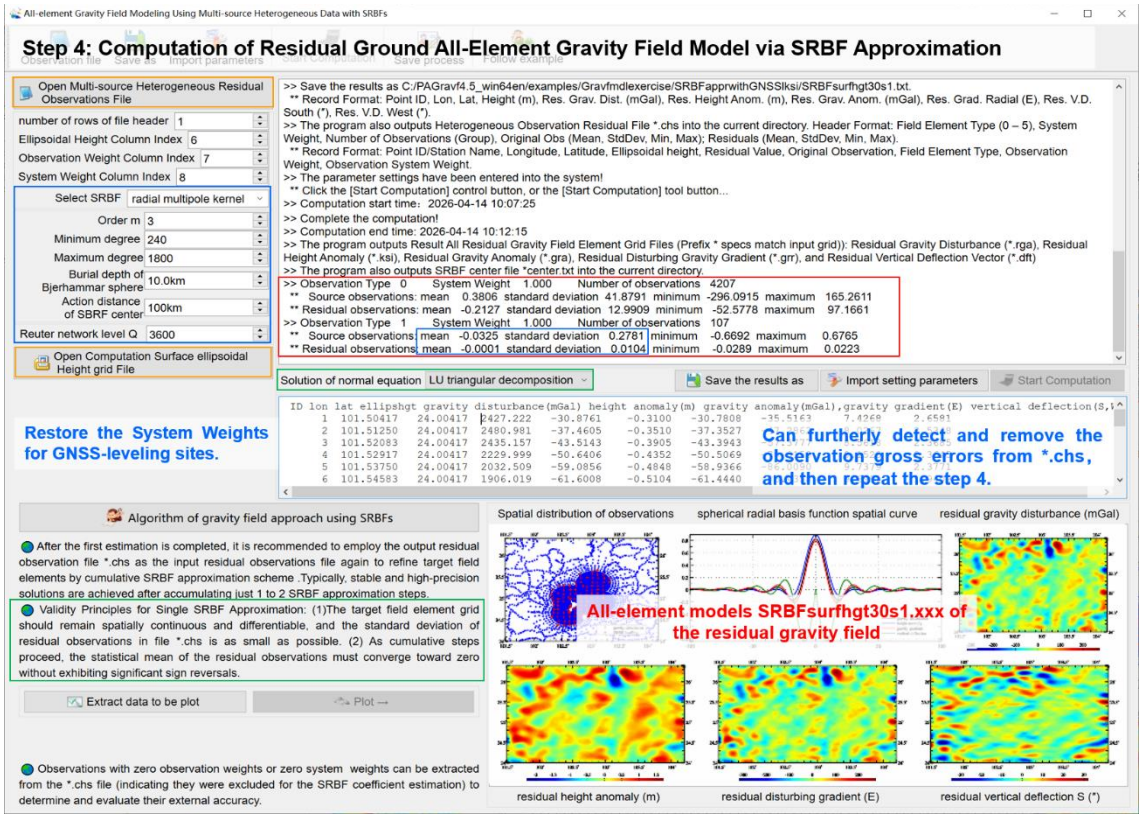

Step 5: Cumulative SRBF Approximation using Remaining Residuals

Function: [All-element Gravity Field Modeling Using Multi-source Heterogeneous Data with SRBFs].

Inputs:

- ○ Remaining residual observation file: SRBFsurfhgt30s1.chs.
- ○ Ground ellipsoidal height grid: surfhgt30s.dat.

Procedure:

- ○ Estimate the higher-order remaining residual ground all-element gravity field grids: SRBFsurfhgt30s2.xxx.
- ○ Output the updated remaining residual observation file: SRBFsurfhgt30s2.chs.

Table 4.36: Statistical Comparison of Residuals Before and after Cumulative SRBF Approximations

Data Type	Stage	Mean	Std. Dev.	Min	Max
Residual gravity disturbance (mGal)	Initial Residuals	0.2695	42.0737	-296.0915	165.2611
	After 1st SRBF	0.0620	12.9866	-80.4161	64.8276
	After 2nd SRBF	0.1309	8.5135	-50.6030	57.3920
Residual GNSS-levelling height anomaly (m)	Initial Residuals	-0.0071	0.2768	-0.6571	0.6846
	After 1st SRBF	-0.0014	0.0291	-0.1886	0.0595
	After 2nd SRBF	-0.0013	0.0154[4]	-0.0708	0.0315

Accuracy Metric: The value 0.0154 m [4] = 1.54 cm cited in the analysis serves as the accuracy index for gravity disturbance-derived ground height anomaly modeling.

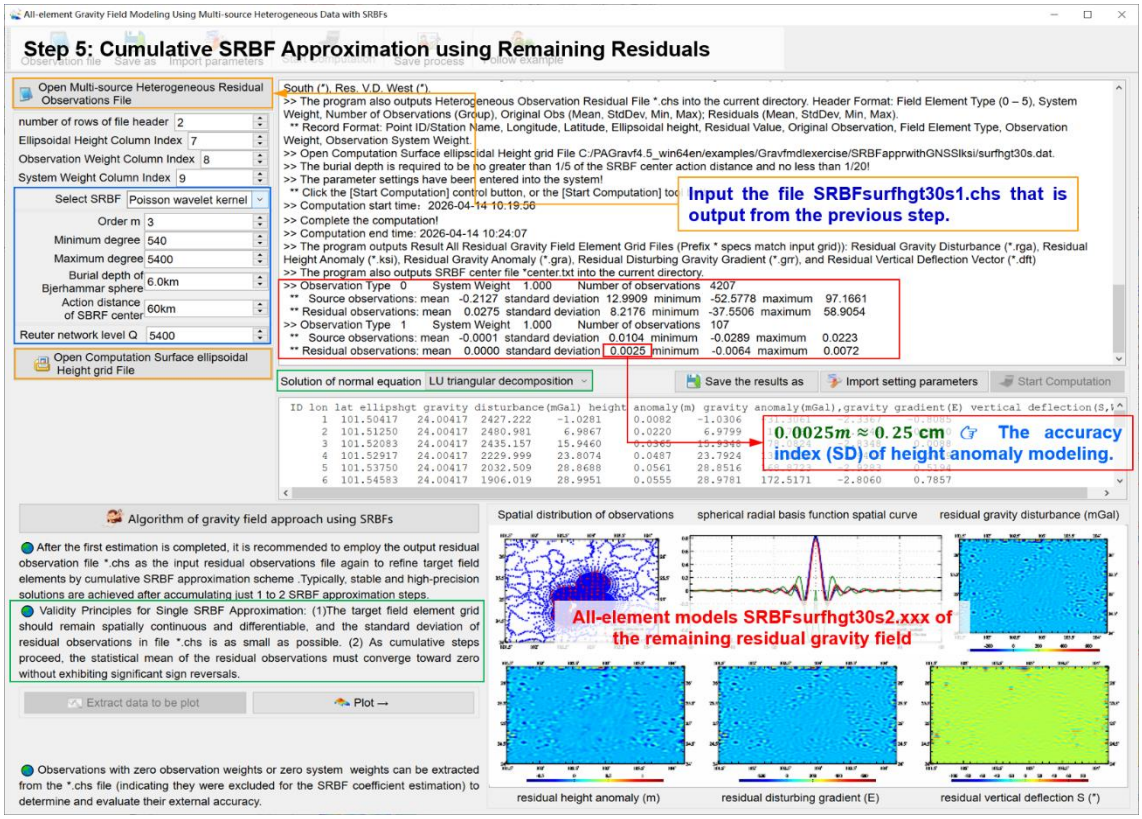

Quality Control (QC) Measures:

- ○ Gross error detection (5σ for gravity disturbances, 3σ for GNSS-leveling sites) can

be repeated using SRBFsurfhgt30s2.chs, necessitating a restart from Step 3 if outliers are found (omitted here).

○ If result quality is insufficient, further cumulative approximations may be performed. This is also omitted for brevity.

Step 6: Restoration of Reference Field Values to Generate Final Ground All-Element Models

Function: [Computation of Gravity Field Elements from a Global Geopotential Model].

Settings: Maximum degree = 540.

Input: Ground ellipsoidal height grid (edge-effect corrected): surfhgt30srst.dat.

Procedure: Compute the 540-degree reference gravity field element grids: GMsurfhgt30s540.ksi (Height Anomaly), GMsurfhgt30s540.rga (Gravity Disturbance), GMsurfhgt30s540.gra (Gravity Anomaly), GMsurfhgts540.grr (Disturbing Gravity Gradient), and GMsurfhgt30s540.dft (Vertical Deflection).

Final Model Synthesis: Sum the following three components (after trimming edges from SRBF grids):

○ 1st SRBF Residuals: surfhgt30s1.xxx (derived from SRBFsurfhgt30s0.xxx).

○ 2nd SRBF Remaining Residuals: surfhgt30s2.xxx (derived from SRBFsurfhgt30s1.xxx).

○ 540-degree Reference Field: GMsurfhgt30s540.xxx.

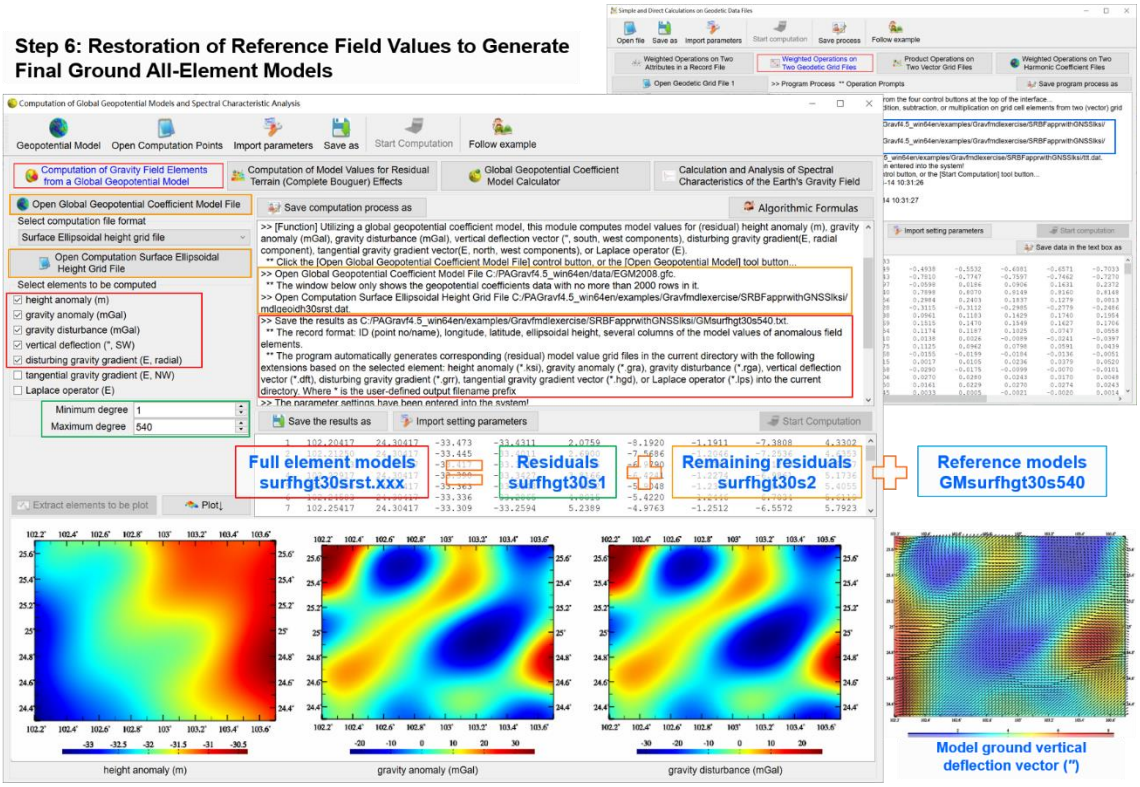

Output Products: The final ground all-element gravity field model grids (30″×30″ resolution) are generated, comprising:

○ Ground Height Anomaly: surfhgt30srst.ksi

○ Ground Gravity Disturbance: surfhgt30srst.rga

○ Ground Gravity Anomaly: surfhgt30srst.gra

○ Ground Disturbing Gravity Gradient: surfhgt30srst.grr

○ Ground Vertical Deflection Vector: surfhgt30srst.dft

○ Regional Datum Application: Add the determined regional height datum discrepancy (-0.3063 m) to surfhgt30srst.ksi to obtain the ground height anomaly grid referenced to the regional height datum: surfhgt30srgn.ksi.

Completion: The ground all-element gravity field modeling is now complete, yielding ground 30″×30″ all-element grid models.

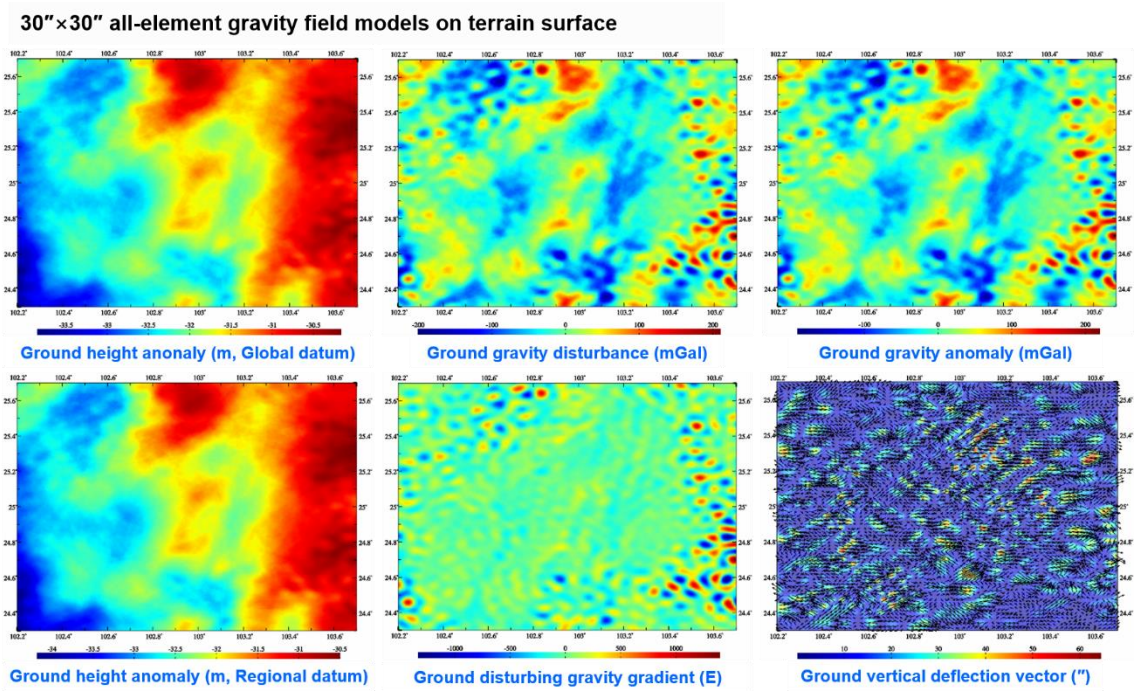

Generation of the Geoidal Model

By switching the computation surface to the geoid, the 30″×30″ all-element gravity field model on the geoid can be directly generated.

Workflow: In Steps 3 through 6, maintain all input data files and parameter settings unchanged. Only replace the computation surface with the model geoidal height grid (e.g., mdlgeoidh30s.dat).

Synchronous Outputs: Following the identical workflow above yields the geoidal all-element model geoidh30srst.xxx, including:

○ Geoidal Height: geoidh30srst.ksi

○ Gravity Disturbance: geoidh30srst.rga

○ Gravity Anomaly: geoidh30srst.gra

○ Disturbing Gravity Gradient: geoidh30srst.grr

○ Vertical Deflection Vector: geoidh30srst.dft

○ Gravimetric Geoid (Regional Datum): geoidh30srgn.ksi

In Steps 3 through 6, maintain all input data files and parameter settings unchanged. Switching computation surface to geoid, 30″×30″ all-element gravity field models on the geoid can be directly generated.

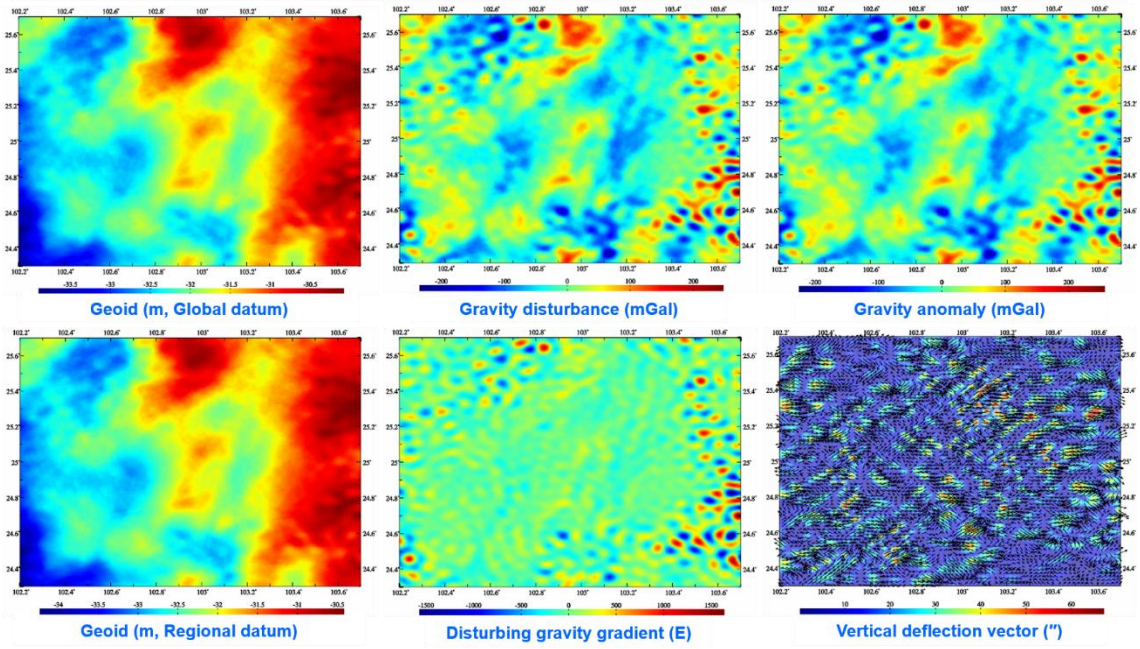

Technical Features of the SRBF Gravity Field Approximation Program

● Rigorous Analytical Relationships: Strict analytical mathematical relationships exist between observation elements, target elements, and among the elements themselves. The algorithm's performance remains robust regardless of the error distribution characteristics within the observation data.

● One-Step Analytical Fusion of Heterogeneous Data: Capable of fusing multiple types of heterogeneous gravity observations (varying heights, cross-distributed, land-sea coexistence) in a single analytical step. No preprocessing such as reduction, continuation, or gridding is required.

● Unified Modeling Framework: Enables synchronous analytical modeling of the geoid and all external gravity field elements. Effectively integrates sparse data sources, such as astronomical vertical deflections and GNSS-leveling observations.

● Robust Quality Control: Possesses advanced capabilities for gross error detection in gravity observations, precise determination of external accuracy indices and height datum discrepancies, and rigorous control over computational performance.

5. Optimization, Unification, and Application of regional height datums

This subsystem implements a suite of ingenious physical geodetic algorithms based on Earth's gravity field theory and observational data. Its primary objective is the optimization and unification of regional height datums, thereby enhancing the precision and applicability of gravity field models and vertical datum products.

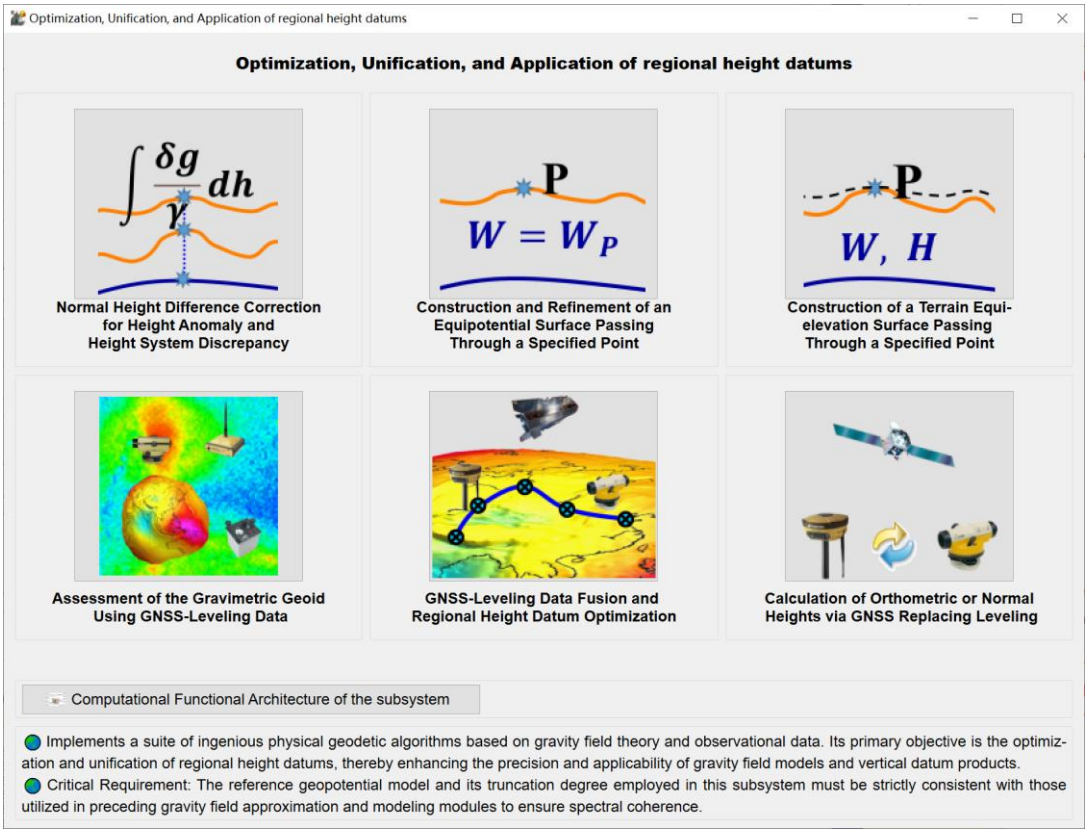

Critical Requirement: The reference geopotential model and its truncation degree employed in this subsystem must be strictly consistent with those utilized in preceding gravity field approximation and modeling modules to ensure spectral coherence.

5.1 Normal Height Difference Correction for Height Anomaly and Height System Discrepancy

[Computation Scheme] This module provides a three-tiered correction strategy for the normal height difference. Users may select one of the following configurations based on accuracy requirements:

- (a) Model Component: Compute the normal height difference correction solely from the reference geopotential model.
- (a)+(b) Model + Residual Component: Refine the correction by adding the residual term derived from regional gravity field data using the remove-restore scheme.
- (a)+(b)+(c) Full Solution: Further refine the result by incorporating a measured adjustment term utilizing in-situ gravity observations at the computation point.

5.1.1 Model-Based Computation of Normal Height Difference Correction

[Function] Computes the model radial gradient (cm/km) of height anomaly and model normal height difference correction (m) using the ellipsoidal heights of the current point and target point in near-Earth space. The computations are based on a reference global geopotential model.

Note: When the current point is on the topographic surface and the target point is on the geoid, the output represents the difference between Normal Height and Orthometric Height. This is numerically equivalent to the difference between Geoidal (Ellipsoidal) Height and Height Anomaly.

[Input Files]

(1) Space Computation Point File: Record Format: ID, Longitude (deg), Latitude (deg), ...

(2) Global Geopotential Coefficient File:

● Header Convention: The first line contains scale parameters: Geocentric Gravitational Constant GM (10^{14} m^3/s^2) and the Earth's semi-major axis a (m).

[Parameter Settings]

Number of header lines in the point file.

Column indices for the ellipsoidal heights of the current and target points.

Maximum computation degree for the geopotential model. The program automatically adopts the smaller of the model's maximum degree and the user-input maximum degree as the actual computation limit.

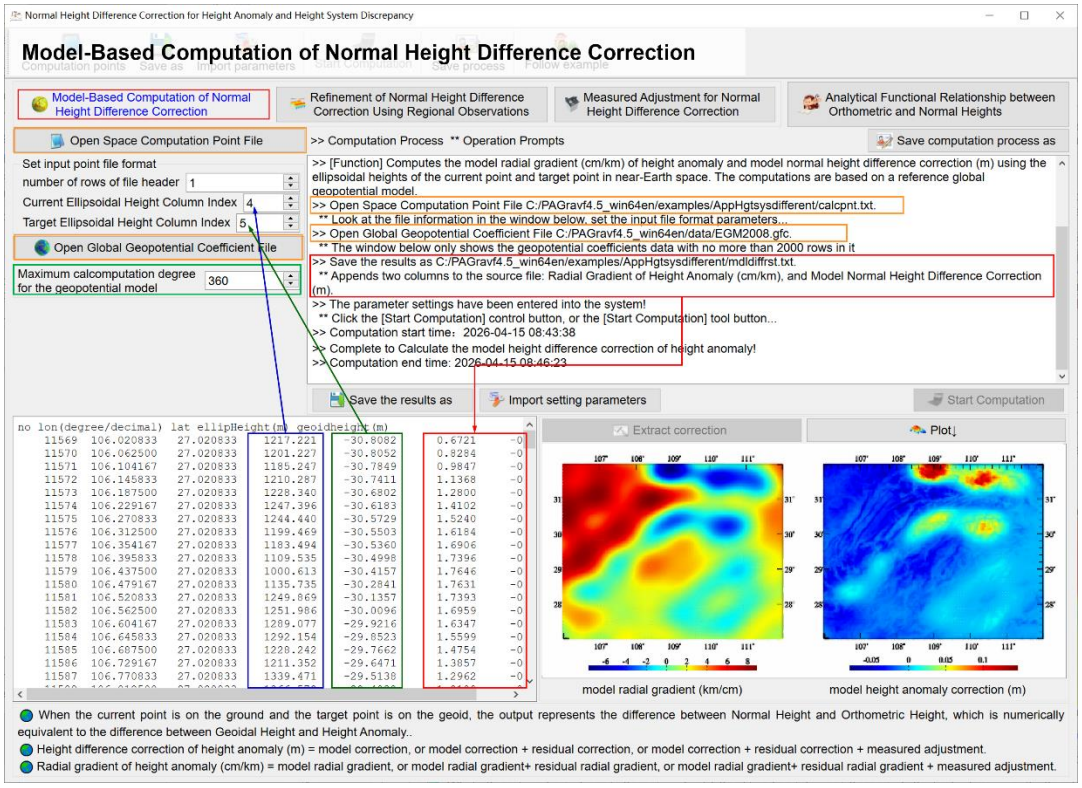

[Output File] Model Height Difference Correction File.

Appends two columns to the source file: Radial Gradient of Height Anomaly (cm/km),

and Model Normal Height Difference Correction (m).

5.1.2 Refinement of Normal Height Difference Correction Using Regional Observations

[Function] Computes the residual radial gradient (cm/km) of height anomaly at the computation point and the residual normal height difference correction (m) for the target point relative to the current point. This utilizes the ellipsoidal height grid of an equipotential surface and the corresponding residual gravity disturbance grid.

[Input Files]

(1) Space Computation Point File.

(2) Equipotential Surface Ellipsoidal Height Grid File.

(3) Residual Gravity Disturbance Grid File (must match the equipotential surface ellipsoidal height grid specifications).

Prerequisite: Residual gravity disturbances should locate on the equipotential boundary surface and be pre-computed via removeing model gravity disturbances.

[Parameter Settings]

Header line count.

Column indices for current and target ellipsoidal heights.

Residual Integration Radius.

[Output File] Residual Normal Height Difference Correction File.

Appends two columns (formatted to 4 significant figures): Residual Radial Gradient, and Residual Normal Height Difference Correction.

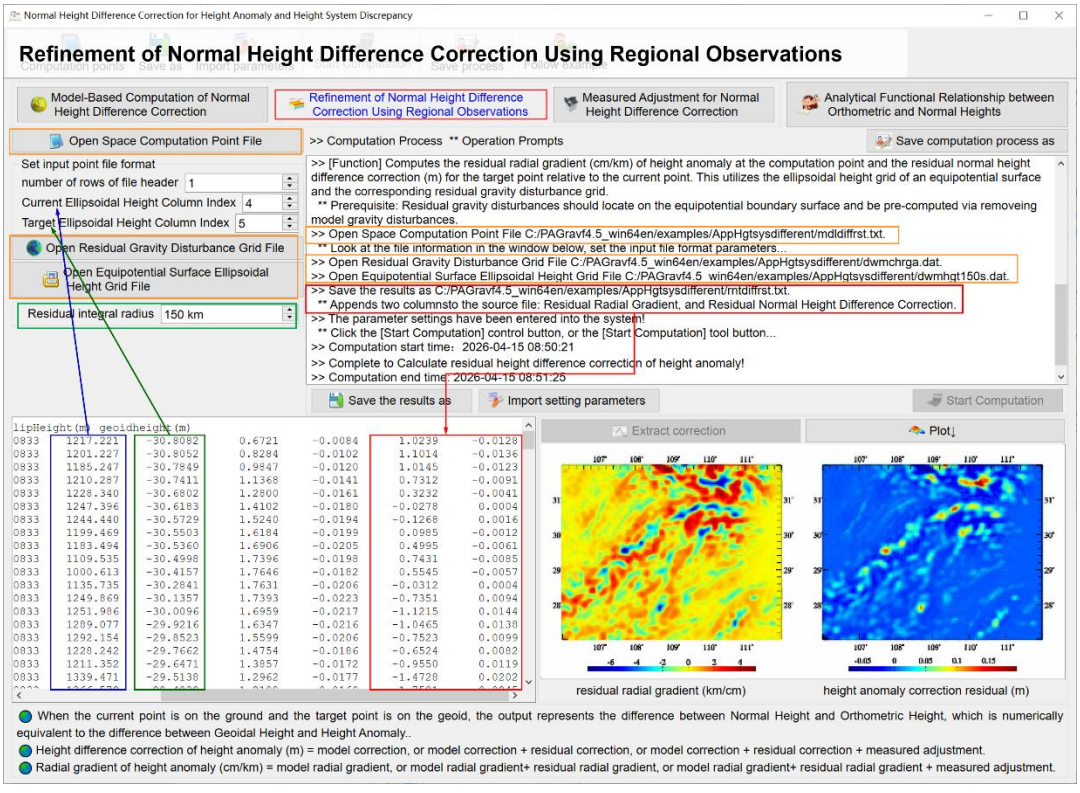

5.1.3 Measured Adjustment for Normal Height Difference Correction

[Function] Sequentially invokes the previous two functions to derive the measured remaining residual measured gravity disturbance: $\delta g_{rem}=\delta g_{obs}-\delta g_{model}-\delta g_{residual}$. Then calculates the “measured adjustment” for the radial gradient (cm/km) of height anomaly and the normal height difference correction (m). This step further refines the solution when in-situ gravity obsvation δg_{obs} is available.

[Input File] Space Computation Point File containing the Measured Remaining Residual Gravity Disturbance attribute.

[Parameter Settings]

Header line count.

Column indices for current/target ellipsoidal heights and the measured remaining residual gravity disturbance.

[Output File] Measured Adjustment File.

Appends two columns (formatted to 4 significant figures): Adjustment to Radial Gradient (cm/km), and Adjustment to Normal Height Difference Correction (m).

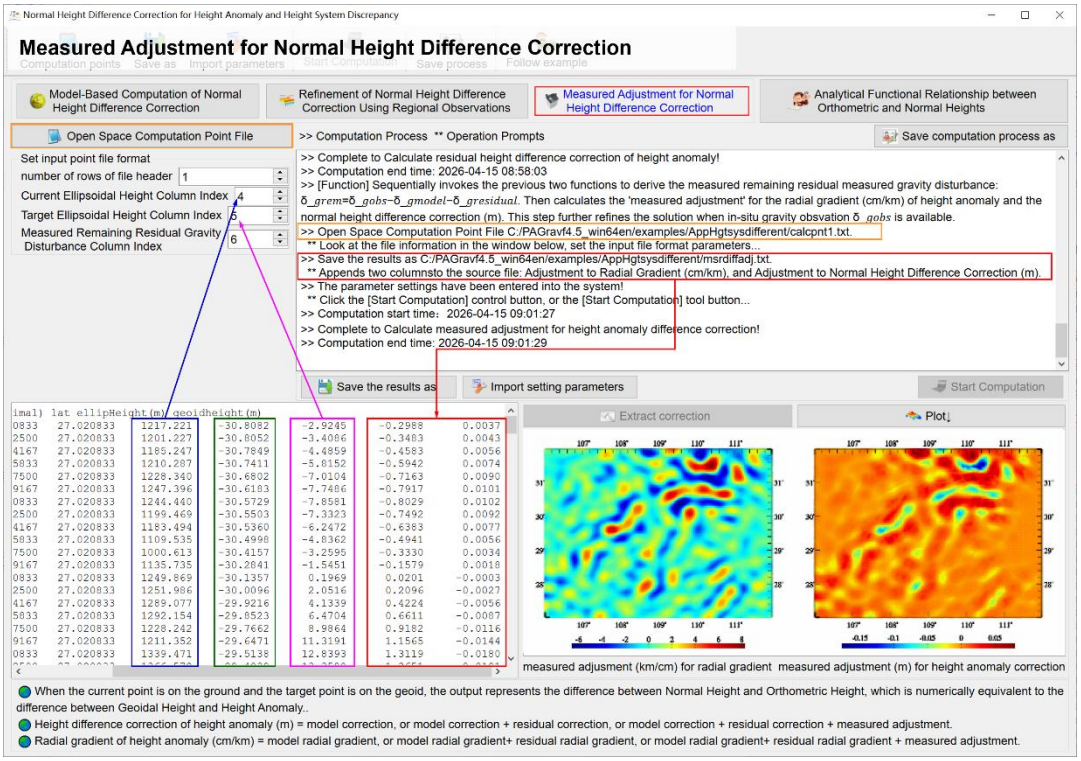

[Final Result Synthesis Formulas]

● Height difference correction of height anomaly (m) = model correction, or model correction + residual correction, or model correction + residual correction + measured adjustment.

● Radial gradient of height anomaly (cm/km) = model radial gradient, or model radial gradient+ residual radial gradient, or model radial gradient+ residual radial gradient + measured adjustment.

5.2 Construction and Refinement of an Equipotential Surface Passing Through a Specified Point

[Purpose] To first compute the model ellipsoidal height of a gravity equipotential surface from a reference global geopotential model, and subsequently refine this surface's ellipsoidal height grid using anomalous field elements via the remove-restore scheme.

5.2.1 Construction of Equipotential Surface from a Global Geopotential Model

[Function] Computes the model gravity (mGal) and model ellipsoidal height (m) grids for the equipotential surface passing through a specified point (B, L, H), based on a global geopotential coefficient model.

[Input Files]

(1) Equipotential Surface Grid Extent: Defines the latitude-longitude extent and resolution.

(2) Global Geopotential Coefficient Model File (Header convention as in 5.1.1).

[Parameter Settings]

Geodetic coordinates (B, L, H) of the specified point (must lie within the grid extent).

Maximum computation degree.

Note: The program uses an iterative approximation method; excessively high degrees will significantly increase computation time.

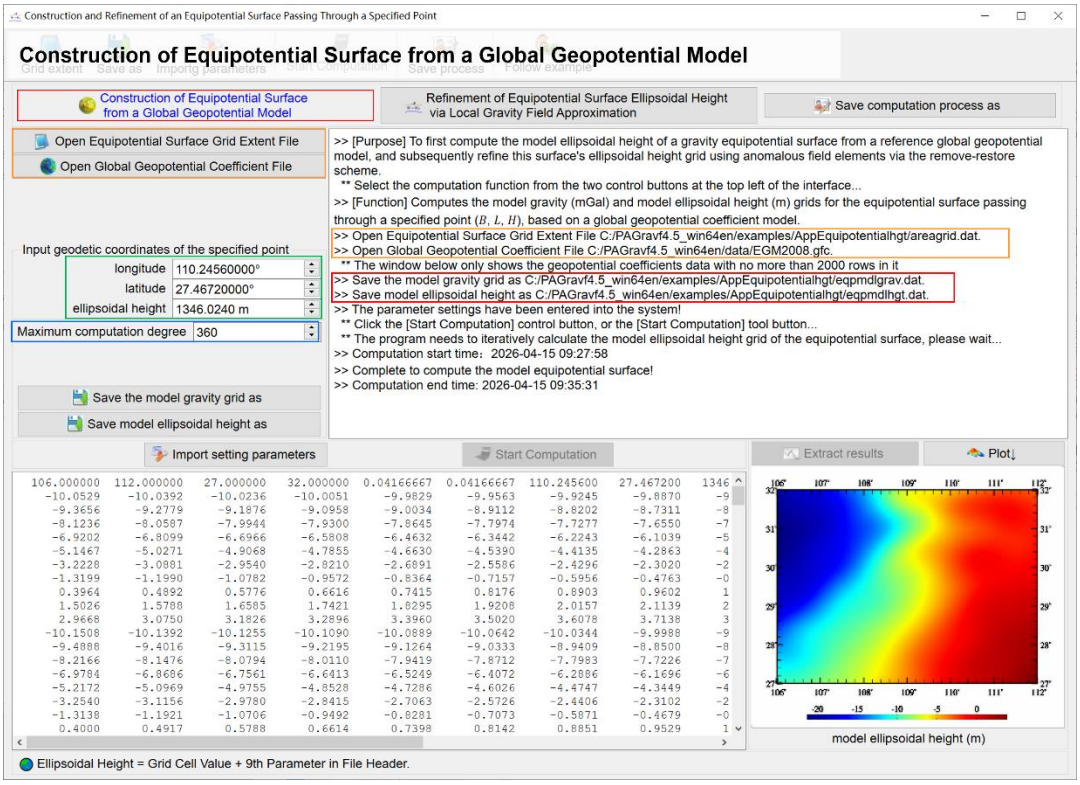

[Output Files]

(1) Model Ellipsoidal Height Grid on Model Equipotential Surface.

● Value Retrieval: Model Ellipsoidal Height = Grid Cell Value + 9th Parameter in File Header.

(2) Model Gravity Grid on Model Equipotential Surface.

- Value Retrieval: Model Gravity = Grid Cell Value + 10th Parameter in File Header.

5.2.2 Refinement of Equipotential Surface Ellipsoidal Height via Local Gravity Field Approximation

[Function] Refines the ellipsoidal height grid of the equipotential surface passing through (B, L, H) using the Hotine Integration. Inputs include the ellipsoidal height of a chosen equipotential boundary surface, the residual gravity disturbance on that surface, and the pre-computed model grids.

Definition: The "equipotential boundary surface" refers specifically to the Stokes boundary surface where residual gravity disturbances are defined, distinct from the target equipotential surface being determined.

[Input Files]

(1) Ellipsoidal Height Grid & Residual Gravity Disturbance Grid of the equipotential boundary surface.

Prerequisite: Residual gravity disturbances should locate on the equipotential boundary surface and be pre-computed via removeing model gravity disturbances.

(2) Model Ellipsoidal Height Grid & Model Gravity Grid of the model equipotential surface.

[Parameter Settings]

Geodetic coordinates of the specified point.

Residual Integration Radius.

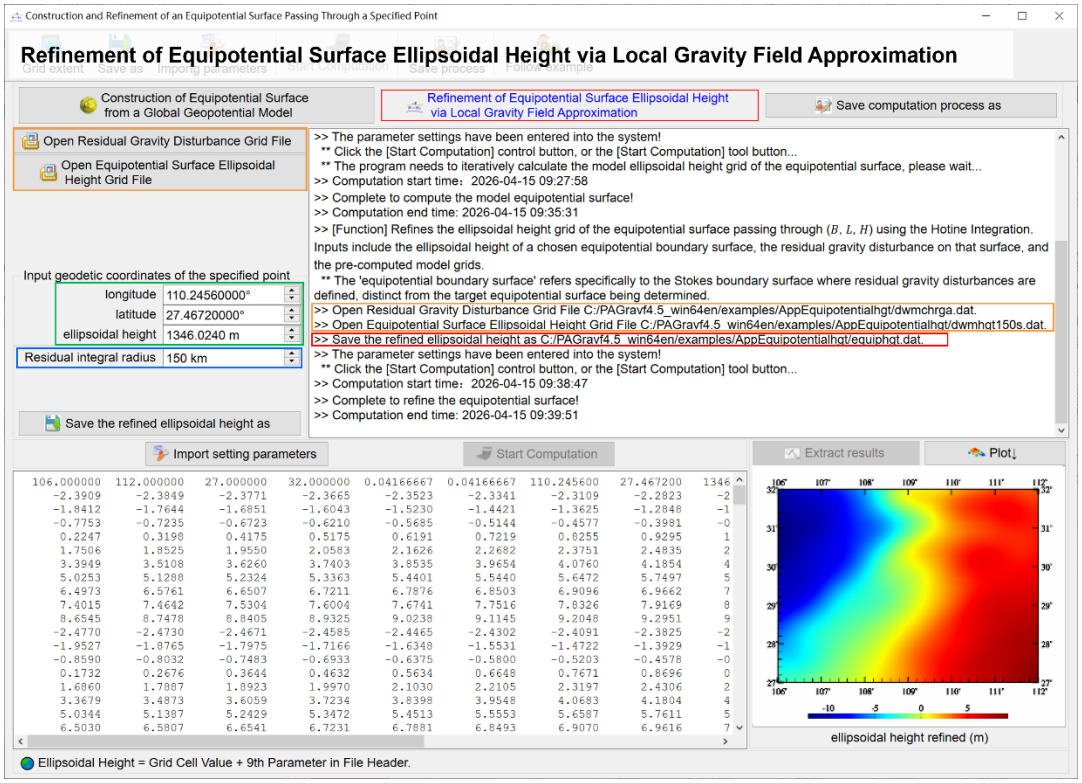

[Output File] Refined Equipotential Surface Ellipsoidal Height Grid.

Value Retrieval: Ellipsoidal Height = Grid Cell Value + 9th Parameter in File Header.

5.3 Construction of a Terrain Equielevation Surface Passing Through a Specified Point

[Purpose] To first compute the model geopotential of an equielevation (normal or orthometric equiheight) surface from a reference global geopotential model, and subsequently refine this terrain equielevation surface using anomalous field elements via the remove-restore scheme.

5.3.1 Computation of Model Geopotential for a Normal or Orthometric Equiheight Surface

[Function] Computes the model geopotential, model ellipsoidal height (m), and model gravity (mGal) grids for the equielevation (normal or orthometric equiheight) surface passing through a specified point (B , L), based on a global geopotential coefficient model.

[Input Files]

(1) Equielevation Surface Grid Extent: Defines the latitude-longitude extent and resolution.

(2) Global Geopotential Coefficient File: Header convention as in 5.1.1.

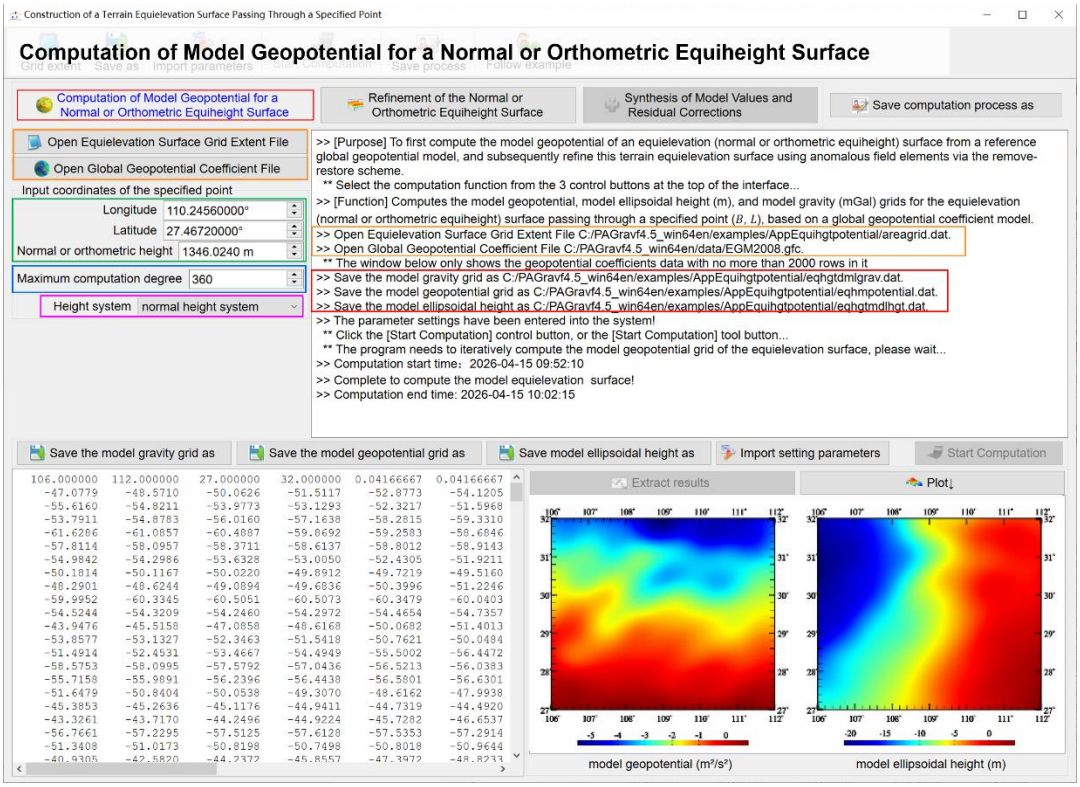

[Parameter Settings]

Geodetic coordinates (B , L) of the specified point (must lie within the grid extent).

Maximum calculation degree for the global geopotential model.

Height System Type: Select either Normal Height or Orthometric Height.

Logic: Due to the use of an iterative approximation method, excessively high degrees are discouraged to avoid excessive computation time.

[Output Files]

(1) Equielevation Surface Model Geopotential Grid

(2) Equielevation Surface Model Ellipsoidal Height Grid

- Value Retrieval: Model Ellipsoidal Height = Grid Cell Value + 9th Parameter in Header.

(3) Equielevation Surface Model Gravity Grid

- Value Retrieval: Model Gravity = Grid Cell Value + 10th Parameter in Header.

5.3.2 Refinement of the Normal or Orthometric Equiheight Surface

[Function] Refines the ellipsoidal height grid of the equielevation (normal or orthometric equiheight) surface passing through (B, L) using the Hotine Integral. Inputs include the ellipsoidal height of a chosen equipotential boundary surface, the residual gravity disturbance on that surface, and pre-calculated model grids.

Methodology: Computes the residual geopotential correction and residual ellipsoidal height correction derived from residual gravity disturbances after removing reference model gravity disturbances.

[Input Files]

(1) Equipotential Boundary Surface: Ellipsoidal Height Grid & Residual Gravity Disturbance Grid.

(2) Model Ellipsoidal Height Grid & Model Gravity Grid on Equielevation Surface.

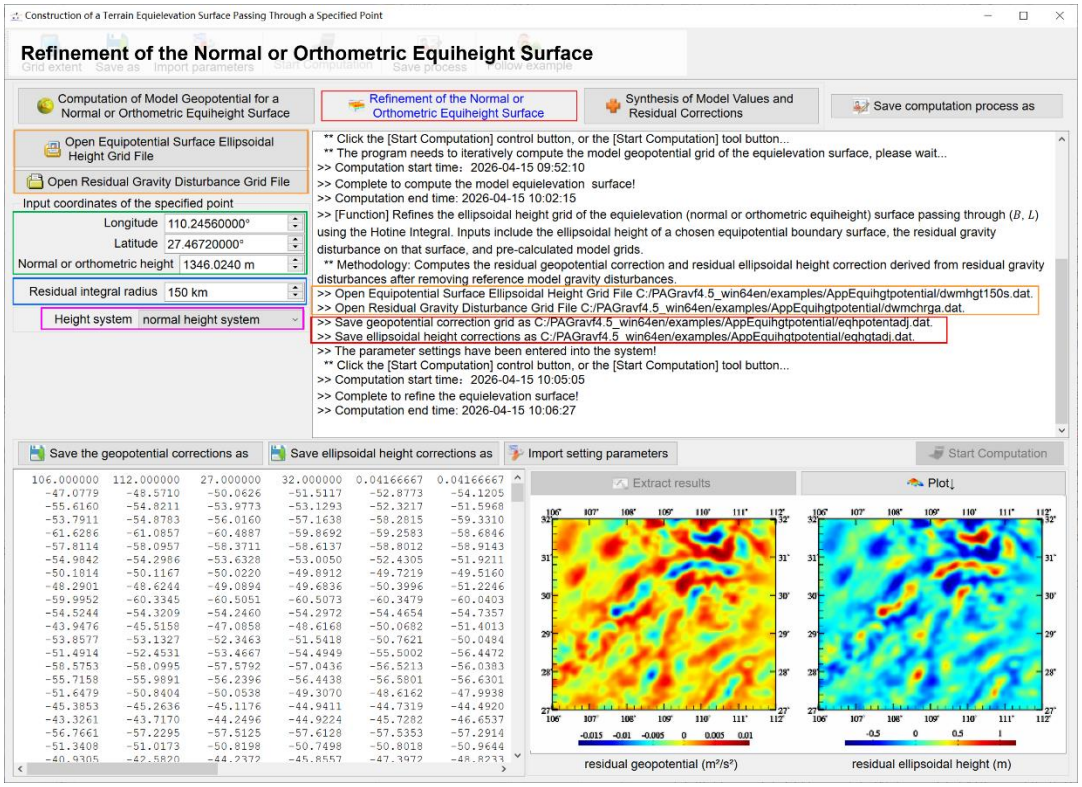

[Parameter Settings]

Geodetic coordinates of the specified point.

Residual Integration Radius.

Height System Type: Normal or Orthometric.

[Output Files]

(1) Equielevation Surface Geopotential Correction Grid

(2) Equielevation Surface Ellipsoidal Height Correction Grid

5.3.3 Synthesis of Model Values and Residual Corrections

[Function] Generates the final refined values for the equielevation (normal or orthometric equiheight) surface by summing the model components and their respective corrections.

[Output Files]

(1) Final Equielevation Surface Geopotential Grid

● Synthesis Formulas: Final Geopotential = Model Geopotential + Geopotential Correction

(2) Final Equielevation Surface Ellipsoidal Height Grid

● Synthesis Formulas: Final Ellipsoidal Height = Model Ellipsoidal Height + Height Correction

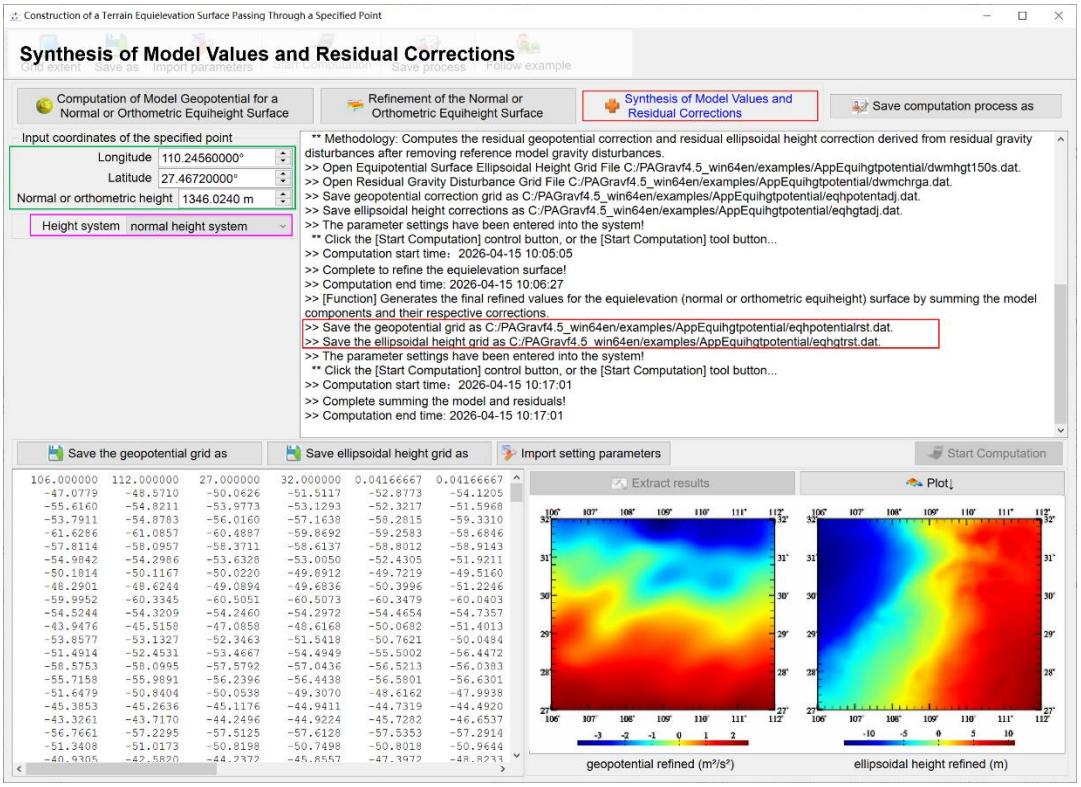

5.4 Assessment of the Gravimetric Geoid Using GNSS-Leveling Data

[Function] Performs a statistical analysis of GNSS-leveling residual height anomalies (m) based on the spectral-domain error characteristics of both GNSS-leveling data and local gravity field. The module estimates: (a) Error of gravimetric height anomalies (cm). (b)

Internal coincidence error of hybrid height anomalies (cm). (c) Error of hybrid height anomaly differences. (d) Error of GNSS-leveling height anomaly differences.

Note: By substituting ground height anomalies with geoidal heights, this program evaluates the gravimetric geoid within the orthometric height system.

Theoretical Basis: The assessment relies on the principle that the error in GNSS-leveling height anomaly differences increases with distance, whereas the error in gravimetric height anomaly differences remains relatively constant regardless of distance.

[Input File] GNSS-Leveling Residual Height Anomaly File.

Normal Height System: GNSS-Leveling Residual = Measured Height Anomaly - Gravimetric Height Anomaly.

Orthometric Height System: GNSS-Leveling Residual = Measured Geoidal Height - Gravimetric Geoidal Height.

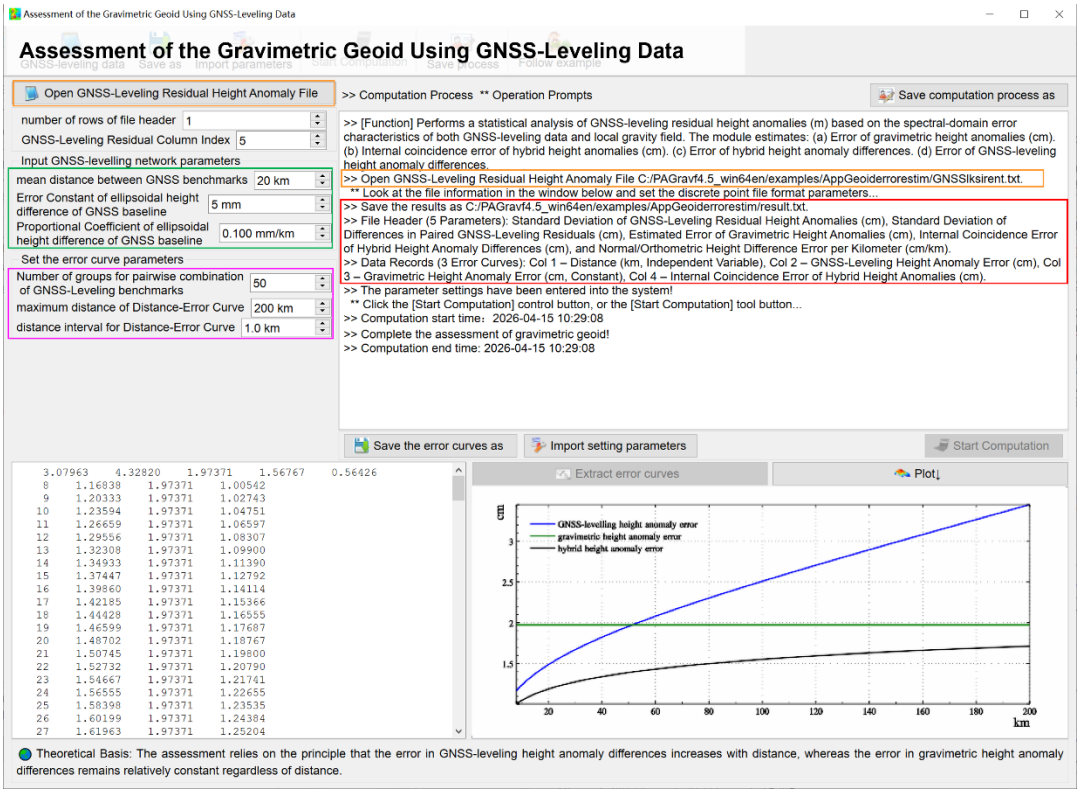

[Parameter Settings]

Input file format configuration.

GNSS Network Parameters: Mean distance between benchmarks; Error Constant (a) and Error Proportional Coefficient (b) for GNSS baseline ellipsoidal height differences.

Grouping Strategy: Number of groups for pairwise combination of GNSS-Leveling benchmarks.

Distance-Error Curve: Maximum distance and distance interval.

Algorithm: The program forms $n(n-1)/2$ baselines from n benchmarks, sorts them by length, groups them, and statistically analyzes the differences in residual height anomalies

for each group.

[Output File] Gravimetric Geoid Error Curve File.

File Header (5 Parameters): Standard Deviation of GNSS-Leveling Residual Height Anomalies (cm), Standard Deviation of Differences in Paired GNSS-Leveling Residuals (cm), Estimated Error of Gravimetric Height Anomalies (cm), Internal Coincidence Error of Hybrid Height Anomaly Differences (cm), and Normal/Orthometric Height Difference Error per Kilometer (cm/km).

Data Records (3 Error Curves): Col 1 – Distance (km, Independent Variable), Col 2 – GNSS-Leveling Height Anomaly Error (cm), Col 3 – Gravimetric Height Anomaly Error (cm, Constant), Col 4 – Internal Coincidence Error of Hybrid Height Anomalies (cm).

5.5 GNSS-Leveling Data Fusion and Regional Height Datum Optimization

[Purpose] To estimate the geopotential difference of the regional height datum and its zero-point parameters using GNSS-leveling residual geoidal heights (or height anomalies). The module calculates corrections for the hybrid geoid, thereby optimizing and unifying the regional height datum (GNSS-leveling network).

5.5.1 Computation of Geopotential for the Zero-Elevation Surface of a Regional Datum

[Function] Estimates the zero-elevation surface geopotential (W_r) of the regional height datum from GNSS-leveling measured geoidal heights (or height anomalies) and their residuals. Given the global geopotential (W_0), it computes the geopotential difference W_r - W_0 representing the discrepancy between the regional and global datums (or geoids).

[Input File] GNSS-Leveling Residual File.

Residual Definition:

- ○ Normal Height System: Measured Height Anomaly minus Gravimetric Height Anomaly.
- ○ Orthometric System: Measured Geoidal Height minus Gravimetric Geoidal Height.

[Parameter Settings]

Configure input file format.

Input the global (zero-elevation surface) geopotential W_0.

[Output File] Remaining GNSS-Leveling Residual File.

File Header (6 Attributes):

- ○ W_r: Regional zero-elevation surface geopotential.
- ○ U_0: Normal potential of the normal ellipsoid, numerically equal to the geoid geopotential / global geopotential W_0.
- ○ W_0: Global geopotential (reference geopotential of global orthometric and normal zero-height surface).
- ○ W_r-U_0: Geopotential difference relative to the normal ellipsoid.
- ○ W_r-W_0: Geopotential difference relative to the global geoid.
- ○ U_0-W_0: Geopotential difference between the normal ellipsoid and the global geoid.

Data Records: Appends a column for the "Correction to Gravimetric Geoid".

Theoretical Note: The normal and orthometric zero-height surfaces are theoretically coincident everywhere; no distinction is required.

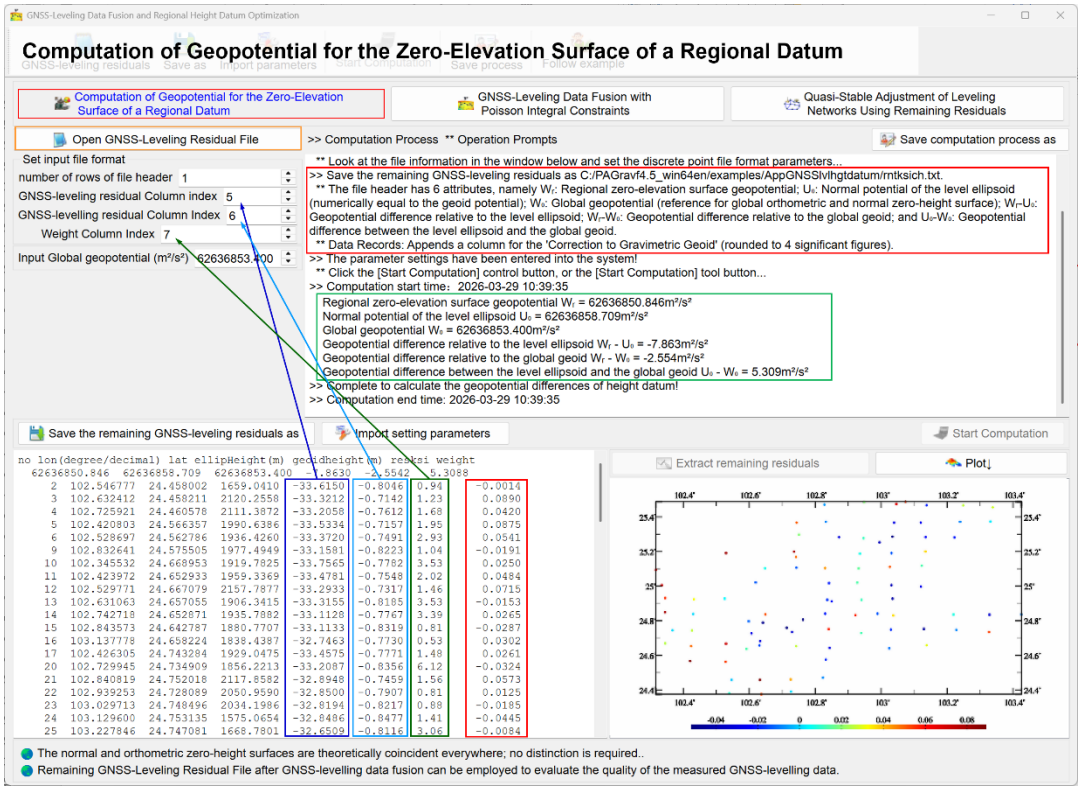

5.5.2 GNSS-Leveling Data Fusion with Poisson Integral Constraints

[Function] Estimates corrections for gravimetric geoidal heights or ground height anomalies by applying Poisson Integral constraints to GNSS-leveling residuals and the ellipsoidal height grid of the fusion surface. This achieves analytical fusion of GNSS-leveling with gravimetric models.

[Input Files]

Remaining GNSS-Leveling Residual File.

Data Fusion Surface Ellipsoidal Height Grid File.

- Normal Height System: Fusion surface is the Ground; input the Ground Ellipsoidal Height Grid.
- Orthometric System: Fusion surface is the Geoid; input the Model Geoidal Height Grid.

[Parameter Settings]

(1) Header line count for the GNSS-Leveling file.

(2) Column indices for Ellipsoidal Height, GNSS Residual, and Weight.

- **Constraint:** The ellipsoidal height column must match the fusion surface definition (Model Geoidal Height for Orthometric; Ellipsoidal Height at benchmarks for Normal).

(3) Iterative Count, Residual Integration Radius, Laplace Operator Parameter, and Edge Effect Suppression Parameter (n).

○ Integration Radius: Smaller radii yield faster computation.

○ Laplace Parameter: Larger values induce stronger smoothing/filtering.

○ Edge Effect Suppression (n): Suppresses edge and far-zone effects by constraining residuals at grid margins to zero via the observation equation.

(4) Systematic Bias Handling: Since local gravity field approximation cannot inherently resolve systematic biases, the program automatically removes the statistical mean of the GNSS-leveling residuals prior to fusion.

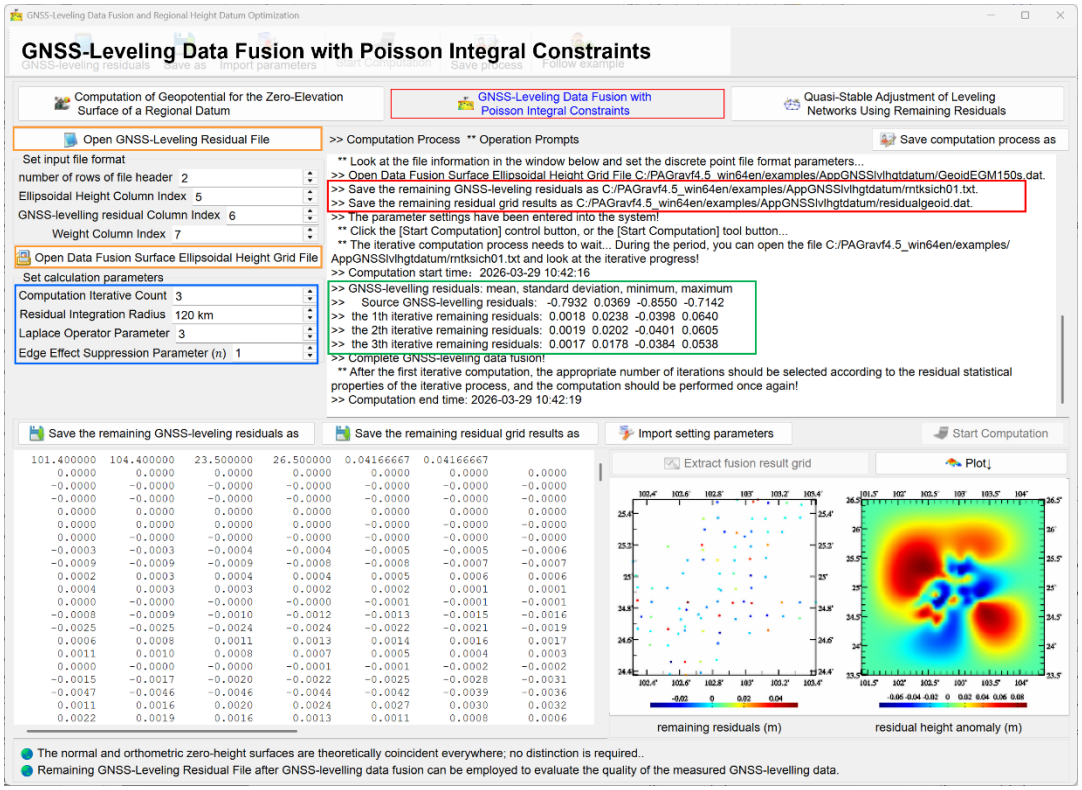

[Output File] Remaining Residual Geoidal Height / Height Anomaly Grid File.

Interface Display: Real-time statistics of remaining residuals during iteration.

Workflow Recommendation: After an initial run, select an optimal number of iterations based on residual statistics and re-run the calculation.

Application: The post-fusion residual file serves as a quality assessment metric for the measured GNSS-leveling data.

5.5.3 Quasi-Stable Adjustment of Leveling Networks Using Remaining Residuals

[Function] Treats all GNSS-leveling sites as quasi-stable benchmarks. Using the method of Indirect Least Squares Adjustment with Quasi-Stable Constraints, it estimates: (a) Normal/Orthometric Height Corrections for leveling benchmarks. (b) Height Anomaly Corrections for GNSS-leveling benchmarks.

[Input Files]

(1) Remaining GNSS-Leveling Residual File.

(2) Leveling Network Route File.

● Leveling Route File (format compliant with [Geodetic Data File Format Convention]).

[Parameter Settings]

GNSS-Leveling Residual File Header line count.

Column indices for Ellipsoidal Height, GNSS Residual, and Weight.

[Output Files]

(1) Leveling Benchmark Height Correction File.

(2) GNSS-Leveling Benchmark Height Anomaly Correction File.

5.6 Calculation of Orthometric or Normal Heights via GNSS Replacing Leveling

[Function] Computes Orthometric or Normal Heights for GNSS positioning points based on regional gravity field and geoid modeling results.

Operational Workflow:

(1) Select Height System:

● Normal Height System: Requires Ground Height Anomaly Grid, Ground Ellipsoidal Height Grid, and Ground Gravity Disturbance Grid.

○ Usage: The ground ellipsoidal height grid is employed to stand for the location of the ground height anomaly; the gravity disturbance grid is employed to calculate the height anomaly correction due to height differences.

● Orthometric Height System: Requires Geoidal Height Grid.

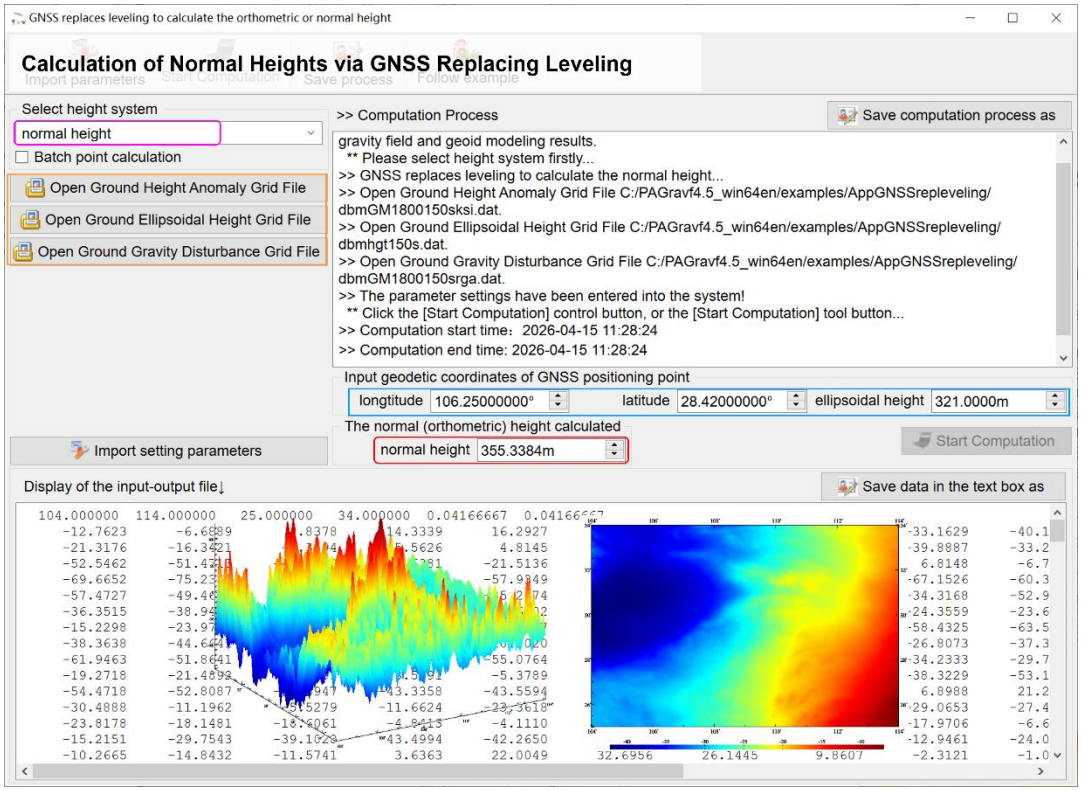

(2) Real-Time Calculation: Users can repeatedly input geodetic coordinates to instantly compute and display the normal or orthometric height for specific GNSS points.

● Constraint: Points must lie within the latitude-longitude extent of the geoid model.

(3) Synchronous Computation: Ground gravity disturbances can be calculated simultaneously during the modelling of ground gravimetric height anomalies.

(4) Batch Processing: By inputting a Space GNSS Position Point File, the program supports batch calculation of the normal or orthometric heights for multiple points.

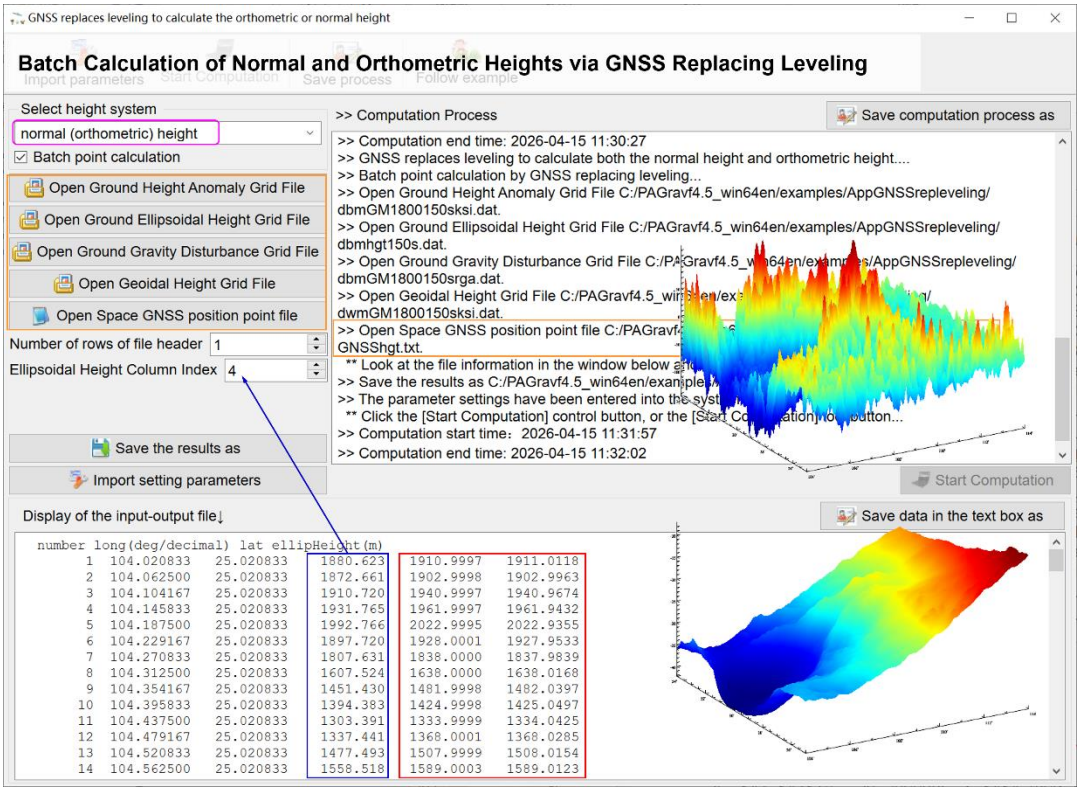

6. Toolkit for Geodetic Data File Editing, Calculation, and Visualization

This subsystem is dedicated to preprocessing and auxiliary computational tasks in physical geodesy. Core functionalities encompass format conversion, interpolation and gridding, data extraction, separation and merging, processing of vector and numerical grid data, weighted arithmetic operations on multiple datasets, and visualization utilities.

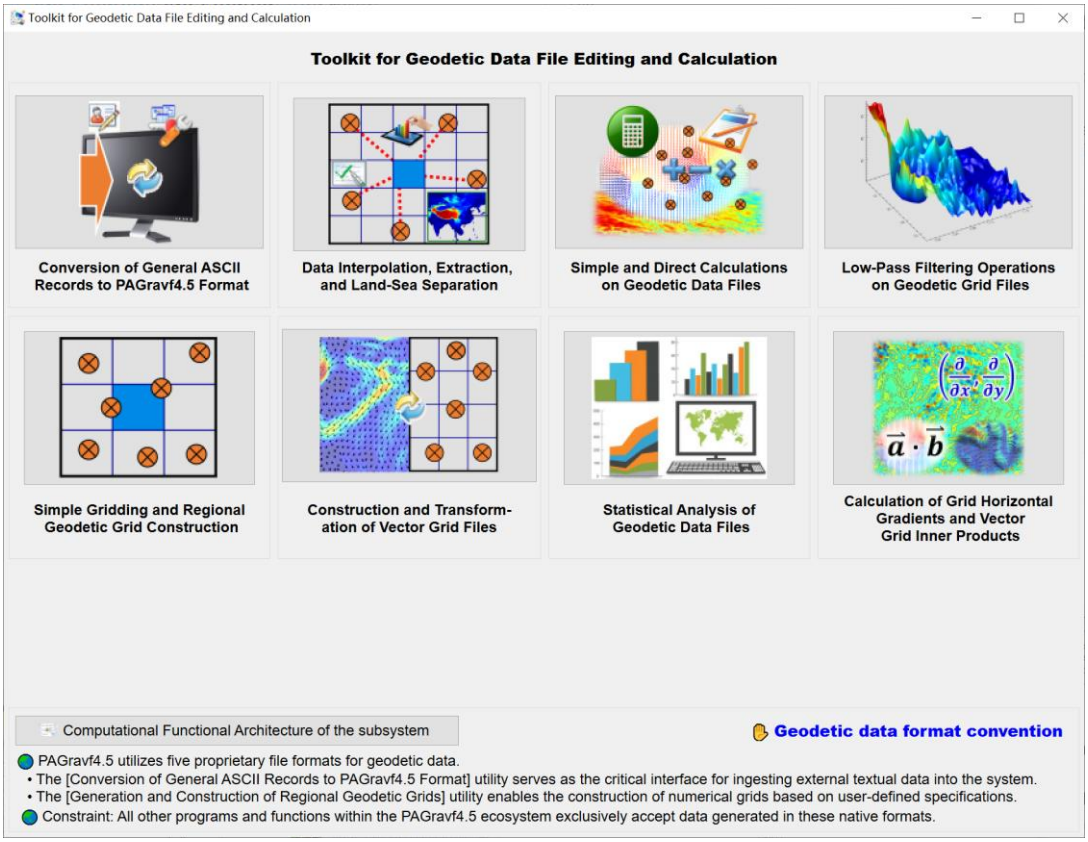

The PAGravf4.5 system employs five proprietary binary formats for geodetic data management.

● The [Conversion of General ASCII Records to PAGravf4.5 Format] utility serves as the primary interface for ingesting external textual data into the system.

● The [Generation and Construction of Regional Geodetic Grids] utility facilitates the construction of numerical grids based on user-defined specifications.

Constraint: All other modules within the PAGravf4.5 ecosystem exclusively process data in these native binary formats.

6.1 Conversion of General ASCII Records to PAGravf4.5 Format

[Function] Converts standard ASCII data records from heterogeneous external sources or non-standard formats into discrete geodetic record files compliant with PAGravf4.5 specifications.

[Procedure]

(1) Load Source: Click the [Open Source ASCII Record File] button to load the raw text

file.

(2) Enter the number of header lines in the input file.

(3) Click [Extract and Edit Data] to open the configuration dialog.

(4) Configuration:

- Define the target file header and record table header.
- Select the target record attributes (columns).
- Note: Clear the header text box if no record table header is required.

(5) Confirm: Click [OK] to close the dialog.

(6) Process: Click [Organize and Display Result File] to initiate processing.

- The program calculates the maximum character width for each target column.
- The upper editable text box displays the formatted target file header, table header, and all records.
- Organizing target record attributes... Please wait.

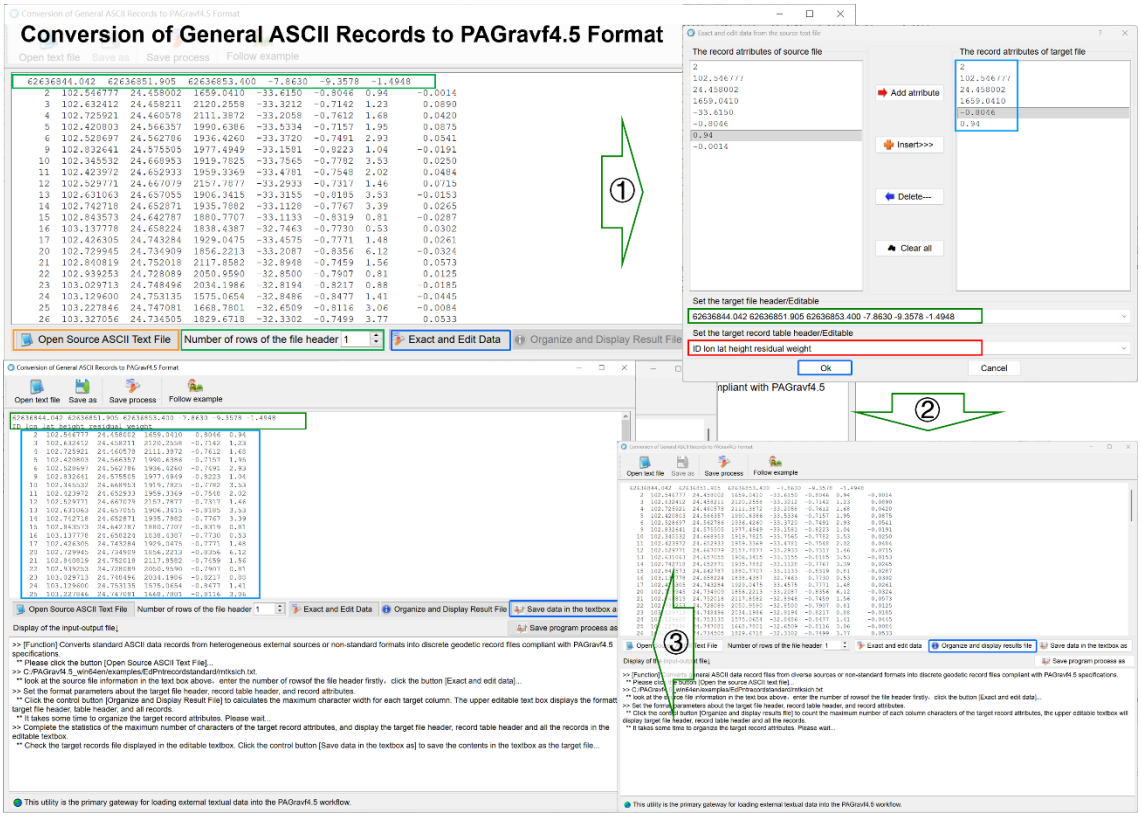

[Output File] Discrete Geodetic Record File (PAGravf4.5 Format).

Review: Inspect the formatted data in the text box.

Export: Click [Save data in the textbox as] to export the final file.

Significance: This utility is the primary gateway for loading external textual data into the PAGravf4.5 workflow.

6.2 Data Interpolation, Extraction, and Land-Sea Separation

6.2.1 Grid Resolution Modification via Interpolation

[Function] Modifies the spatial resolution of a geodetic grid based on a target resolution and a selected interpolation algorithm (Upsampling or Downsampling).

[Input File] Geodetic Grid File.

[Parameter Settings]

Target Spatial Resolution.

Interpolation Mode.

[Output File] Target Geodetic Numerical Grid File.

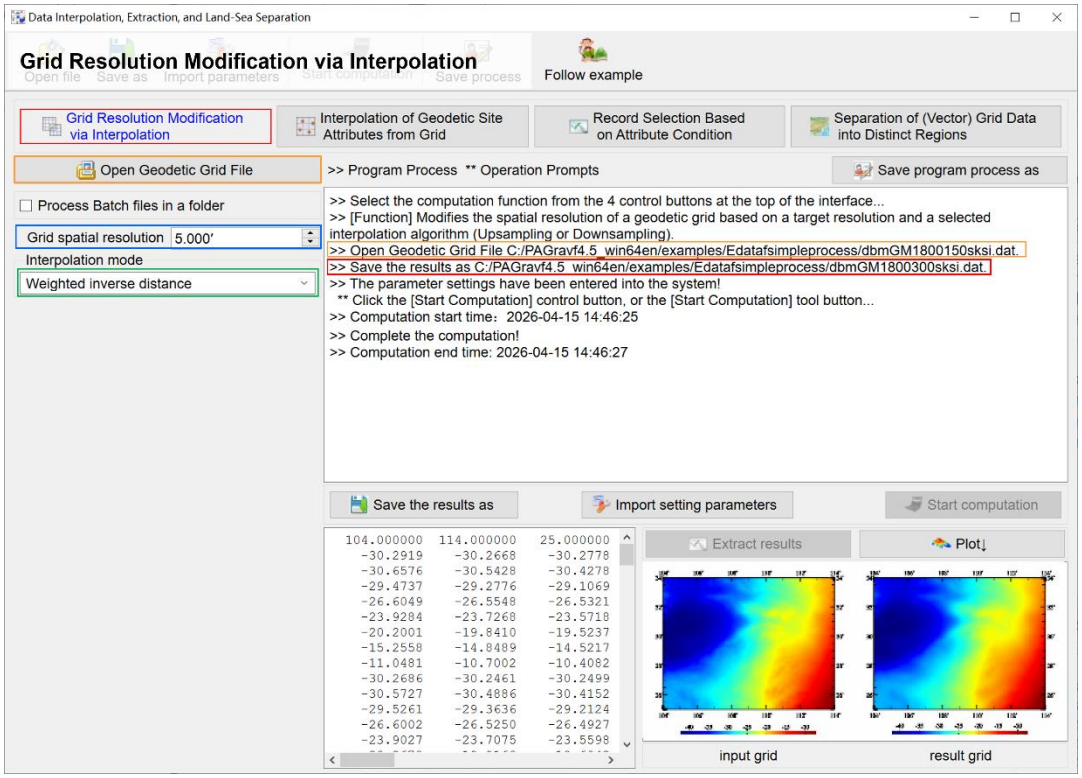

Algorithm Definitions:

● Grid Direct Averaging: Sums all valid source cell values within a target cell and divides by the count of valid source cells.

● Grid Equal-Area Averaging: Sums all valid source cell values within a target cell and divides by the total number of source cells (including invalid/null placeholders).

● Downsampling: Both averaging methods are applicable for reducing resolution.

● Upsampling: When the target resolution is higher than the source resolution, the program automatically employs the Inverse Distance Weighted (IDW) interpolation method.

6.2.2 Interpolation of Geodetic Site Attributes from Grid

[Function] Interpolates attribute values for specific geodetic sites from a numerical grid using a selected spatial interpolation method.

[Input Files]

(1) Discrete Geodetic Point File: Target sites.

(2) Geodetic Grid File: source data.

[Parameter Settings]

Number of header lines in the point file.

Interpolation Mode.

[Output File] Interpolated Discrete Geodetic Point File.

Format matches the input point file.

A new column containing the interpolated values is appended to the records.

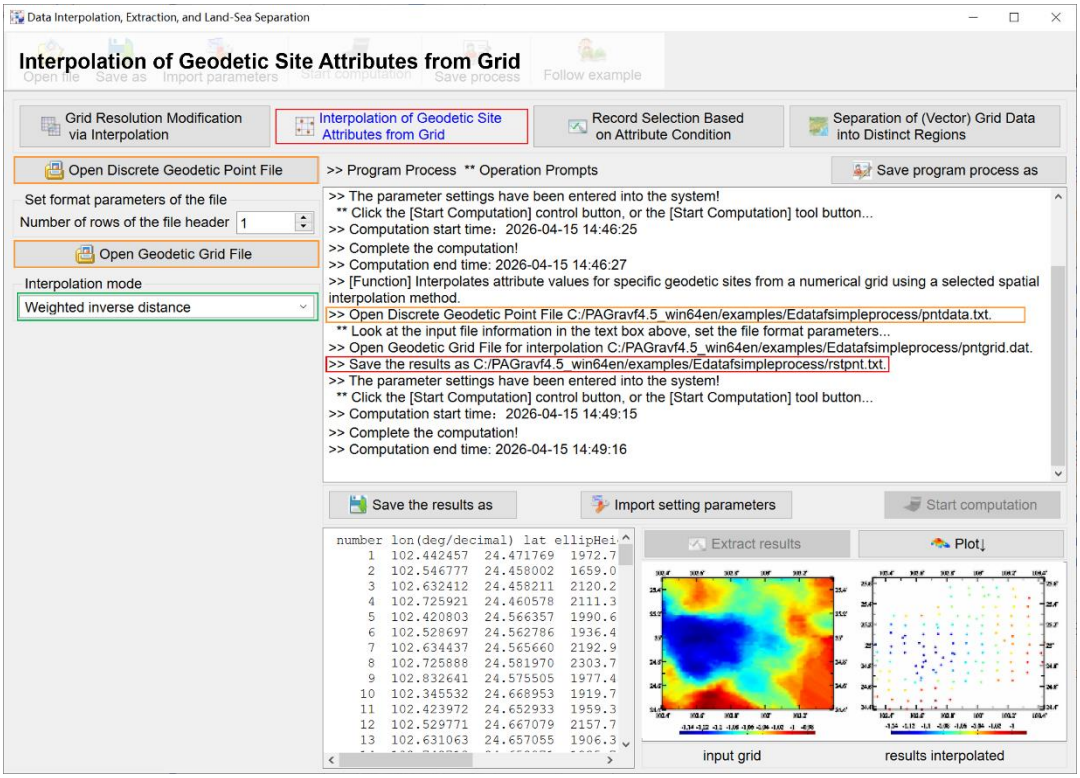

6.2.3 Record Selection Based on Attribute Condition

[Function] Filters geodetic records from a file based on a specified minimum and maximum range for a selected attribute.

[Parameter Settings]

Number of header lines.

Column index of the conditional attribute.

Minimum and Maximum threshold values.

6.2.4 Separation of (Vector) Grid Data into Distinct Regions

[Function] Utilizes a reference grid to delineate distinct regions. Separates the target region (vector) grid data by replacing grid values that do not meet the reference conditions with constant placeholders.

Requirement: The reference grid must effectively delineate the target area via its cell value range.

[Input Files]

(1) Source Geodetic (Vector) Grid File.

(2) Reference Grid File (Spatial extent must be ≥ those of the source grid).

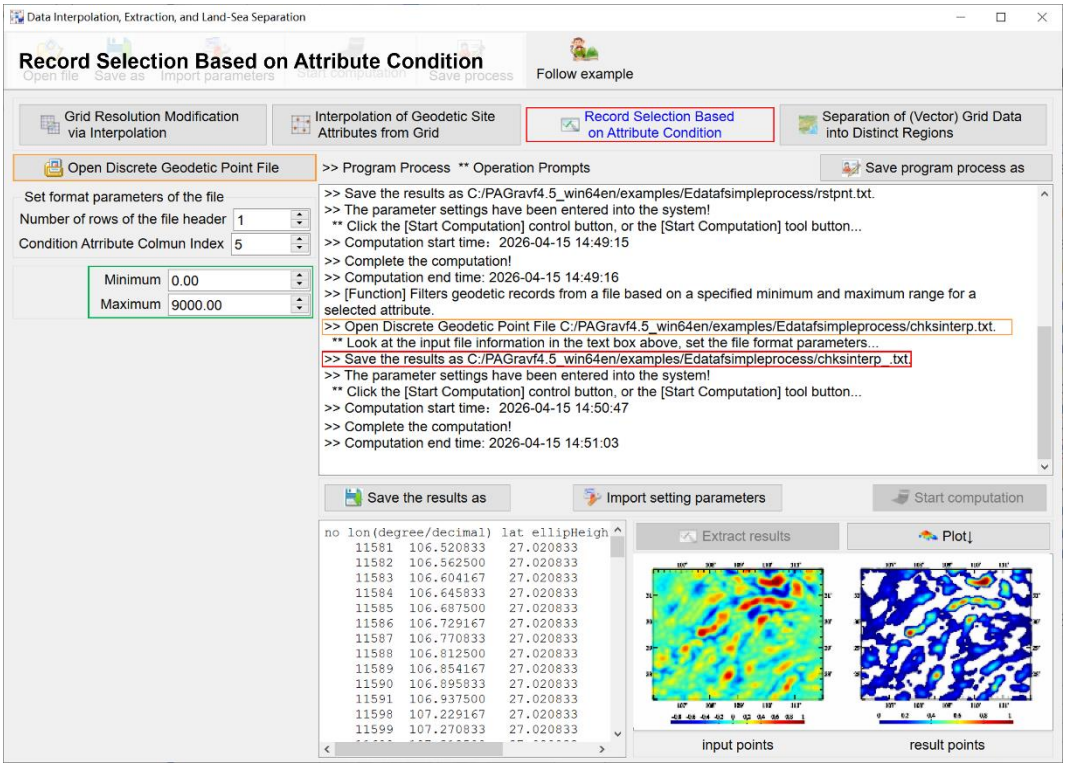

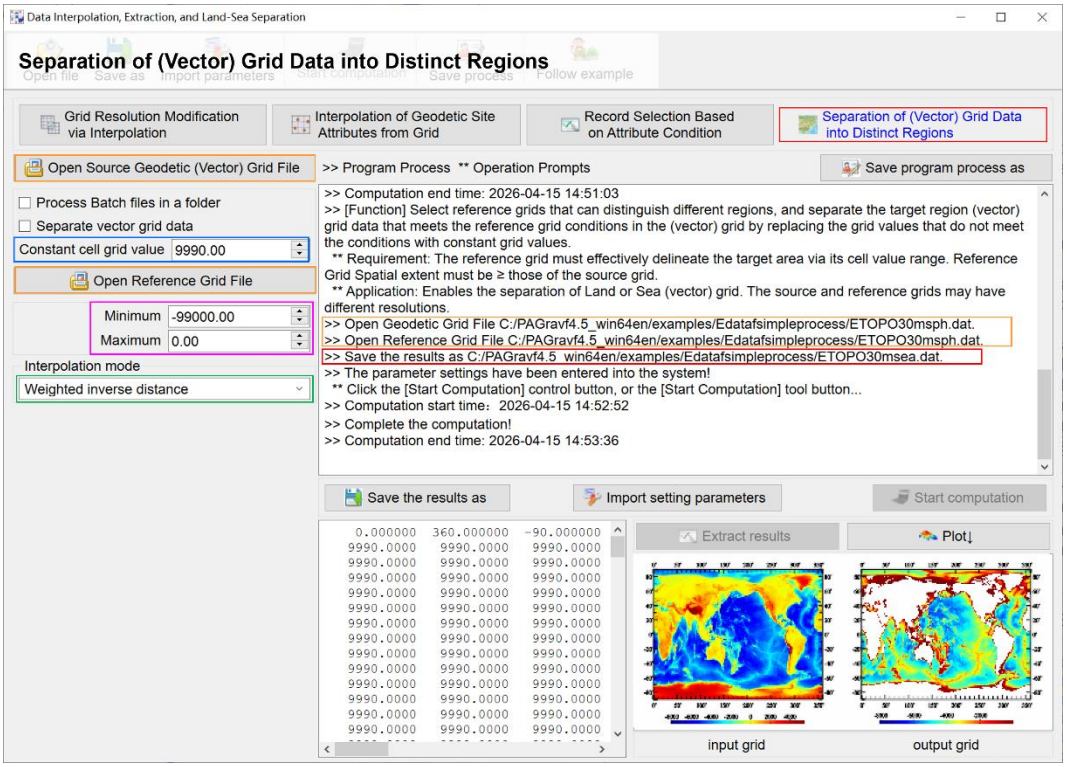

Application: Enables the separation of Land or Sea (vector) grid. The source and reference grids may have different resolutions.

6.3 Simple and Direct Calculations on Geodetic Data Files

6.3.1 Weighted Operations on Two Attributes in a Record File

[Function] Performs weighted addition, subtraction, or multiplication on two specified attributes within a discrete point file.

[Input File] Discrete Geodetic Point File.

[Parameter Settings]

Number of header lines.

Column indices and respective weights for Attribute 1 and Attribute 2.

Operation Mode (Add/Sub/Multiply).

[Output File] Processed Discrete Geodetic Point File.

Format matches the input file; a column with the calculation result is appended.

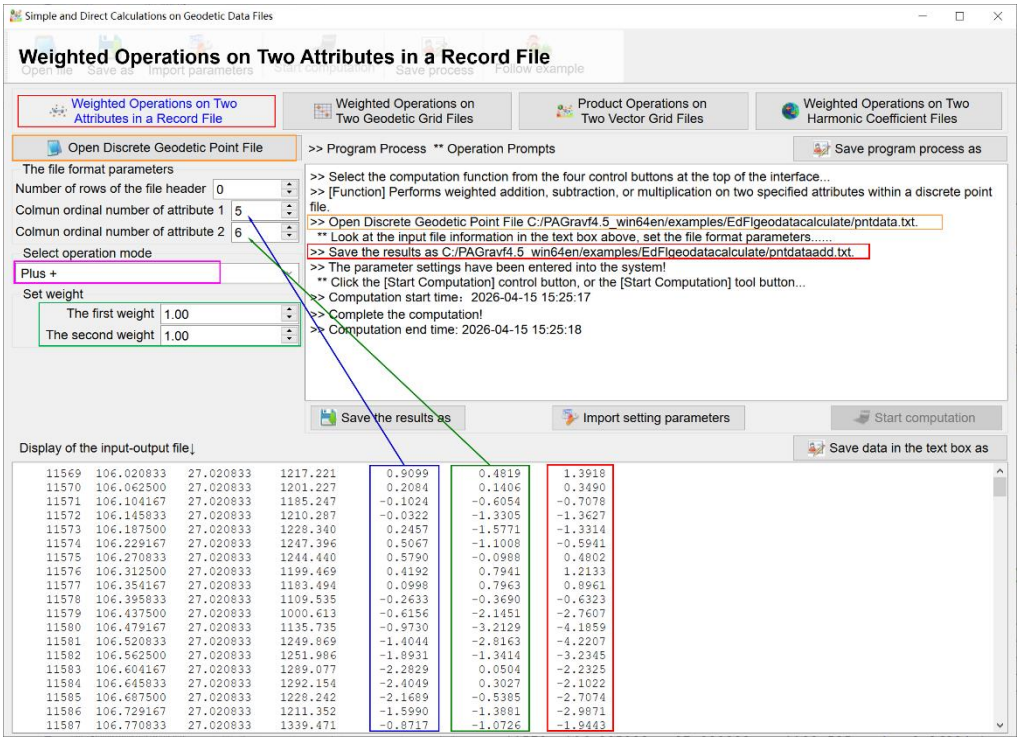

6.3.2 Weighted Operations on Two Geodetic Grid Files

[Function] Performs weighted addition, subtraction, or multiplication on corresponding grid cell elements from two (vector) grid files with identical specifications (extent and resolution).

6.3.3 Product Operations on Two Vector Grid Files

[Function] Computes the outer product or inner product of corresponding cell vector elements from two vector grid files with identical specifications.

6.3.4 Weighted Operations on Two Harmonic Coefficient Files

[Function] Performs weighted operations on two normalized spherical harmonic coefficient

model files.

File Format Specification: File Header: Single row containing the scale parameters: the geocentric gravitational constant GM (10^{14} m³/s²) and the Earth's semi-major axis a (m).

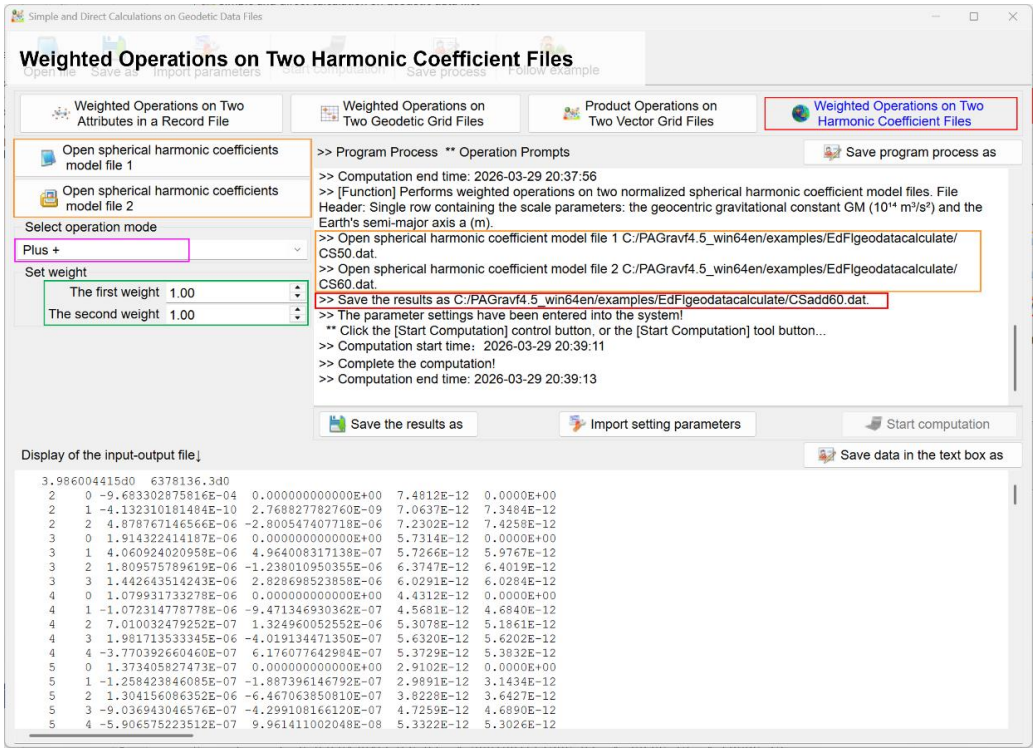

6.4 Low-Pass Filtering Operations on Geodetic Grid File

[Function] Performs low-pass filtering to a geodetic numerical grid file using algorithms such as Moving Average, Gaussian, Exponential, or Butterworth. The grid specification (latitude-longitude extent and spatial resolution) remains invariant before and after filtering.

[Input File] Geodetic Numerical Grid File.

[Parameter Settings]

Select Filter Type.

● Moving Average, Gaussian, Exponential or Butterworth filter.

Set Filter Parameter (n).

● Moving Average: Larger n values yield stronger smoothing (wider kernel).

● Exponential / Butterworth: Smaller n values yield stronger smoothing (lower cutoff frequency).

● Gaussian: Ignores the filtering parameter n.

[Output File] Filtered Geodetic Numerical Grid File.

6.5 Simple Gridding and Regional Geodetic Grid Construction

6.5.1 Gridding of Discrete Geodetic Data via Simple Interpolation

[Function] Generates a grid file for a specified attribute from a discrete geodetic point file based on a selected interpolation method and target grid specification. Supports batch

processing of multiple input files.

[Input Files]

(1) Discrete Geodetic Point File: source data.

(2) Geodetic Numerical Grid File: defines target grid specification (extent and resolution).

[Parameter Settings]

Number of header lines in the point file.

Column index of the target attribute.

Interpolation Search Radius (defined as a multiple of the grid cell size).

Grid specification parameters (target extent and resolution).

Interpolation Mode.

[Output File] Interpolated Geodetic Grid File.

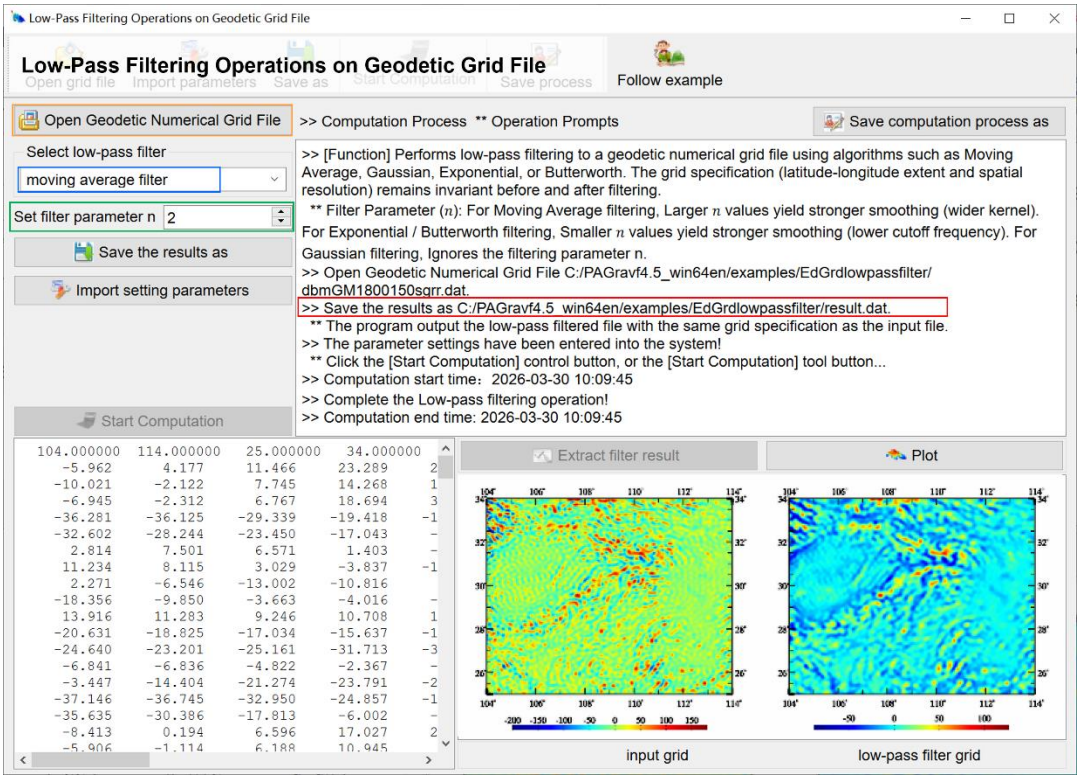

6.5.2 Vector Grid Interpolation from Dual Attribute Records

[Function] Constructs a vector grid file from a discrete geodetic point file by interpolating two specified component attributes (e.g., East/North components) onto a defined grid using a selected interpolation method.

6.5.3 High-Resolution Gridding via Direct Averaging

[Function] Aggregates high-resolution discrete observations into a grid using the Direct Averaging Method (arithmetic mean of valid observations within each cell).

6.5.4 Construction of General Geodetic Grid File

[Function] Generates synthetic grid files based on user-defined extent and resolution. Supported content types include: Constant Values, Random Numbers (stochastic noise), 2D

Array Indices, or Gaussian Surfaces.

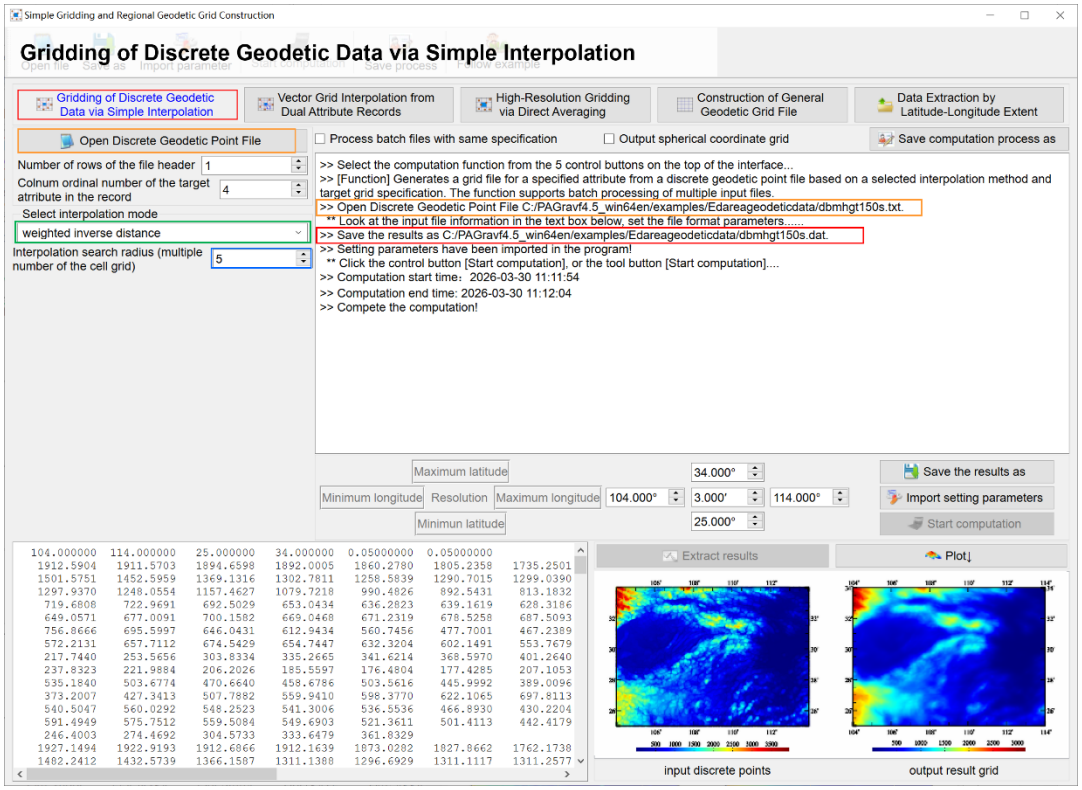

6.5.5 Data Extraction by Latitude-Longitude Extent

[Function] Extracts subsets of data from discrete point file, grid file, or vector grid file based on a specified geographic bounding box (latitude-longitude extent). The function supports batch extraction.

6.6 Construction and Transformation of Vector Grid Files

6.6.1 Synthesis of Vector Grid File from Two Scalar Grids

[Function] Combines two scalar grid files with identical specifications into a single vector grid file, treating them as orthogonal components (e.g., U and V).

6.6.2 Decomposition of Vector Grid File into Scalar Components

[Function] Decomposes a vector grid file into its two constituent scalar grid files.

6.6.3 Vector Grid Representation Transformation

[Function] Transforms vector grid representations within a vector grid file between:

Cartesian Form: In-phase / Quadrature amplitudes (or East-North components).

Polar Form: Amplitude (Magnitude) / Phase (Direction/Azimuth).

6.6.4 Conversion of Vector Grid File to Discrete Point File

[Function] Raster-to-Vector conversion: transforms a (vector) grid file into a discrete point file. The latitude and longitude of each output point correspond to the centric coordinates of the respective grid cell.

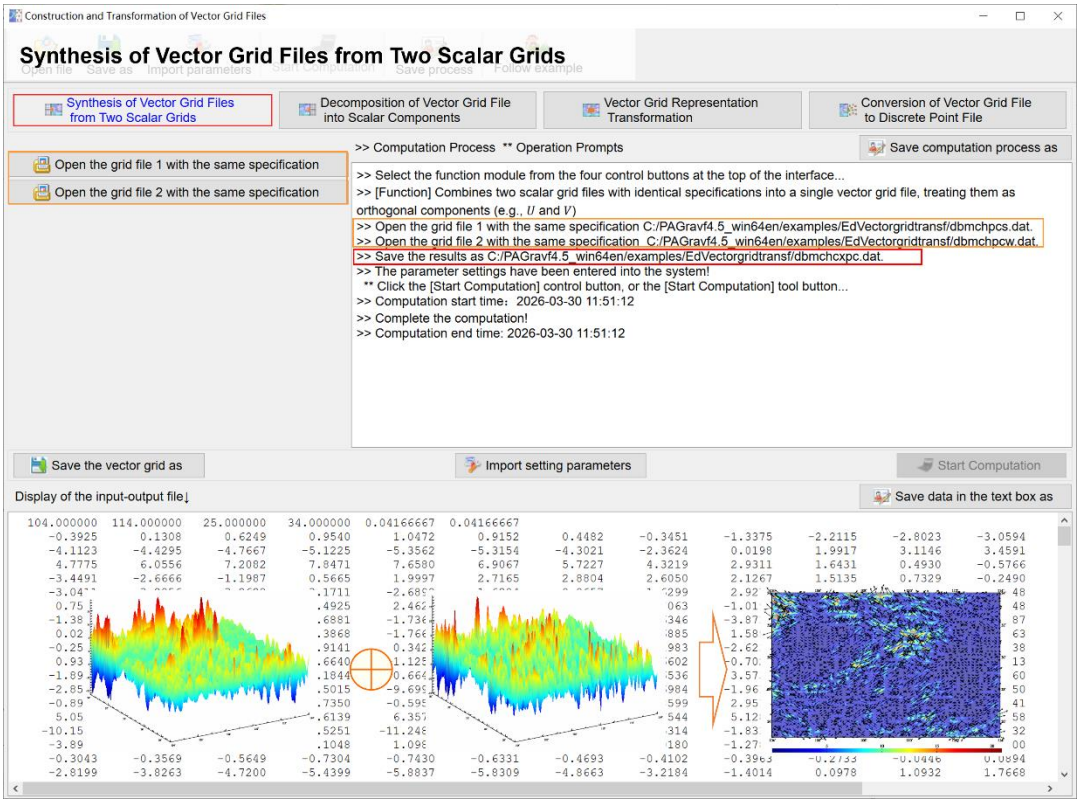
Construction and Transformation of Vector Grid Files
Synthesis of Vector Grid Files from Two Scalar Grids
Synthesis of Vector Grid Files from Two Scalar Grids
Decomposition of Vector Grid File into Scalar Components
Vector Grid Representation Transformation
Conversion of Vector Grid File to Discrete Point File
Open the grid file 1 with the same specification
Open the grid file 2 with the same specification
>> Computation Process ** Operation Prompts
Save computation process as
>> Select the function module from the four control buttons at the top of the interface...
>> [Function] Combines two scalar grid files with identical specifications into a single vector grid file, treating them as orthogonal components (e.g., U and V)
>> Open the grid file 1 with the same specification C:/PAGravf4.5_win64en/examples/EdVectorgridtransf/dbmchpcs.dat.
>> Open the grid file 2 with the same specification C:/PAGravf4.5_win64en/examples/EdVectorgridtransf/dbmchpcw.dat.
>> Save the results as C:/PAGravf4.5_win64en/examples/EdVectorgridtransf/dbmchcxpc.dat.
>> The parameter settings have been entered into the system!
** Click the [Start Computation] control button, or the [Start Computation] tool button...
>> Computation start time: 2026-03-30 11:51:12
>> Complete the computation!
>> Computation end time: 2026-03-30 11:51:12
Save the vector grid as
Import setting parameters
Start Computation
Display of the input-output file↓
Save data in the text box as

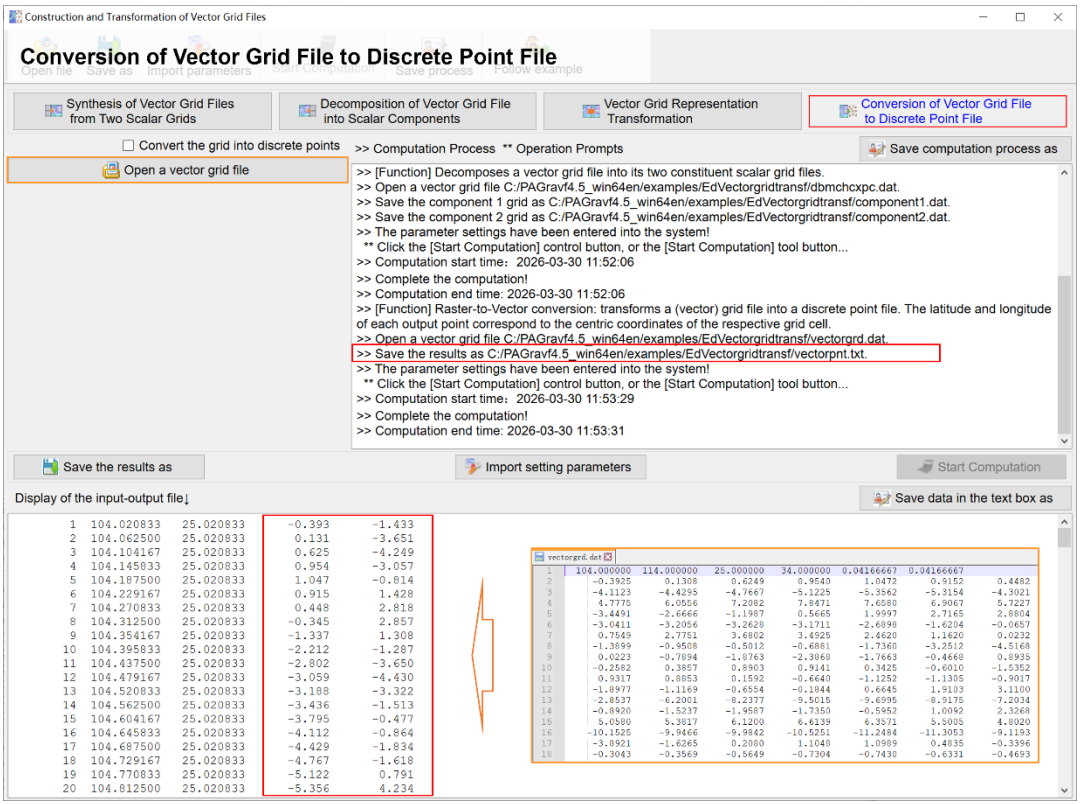
Construction and Transformation of Vector Grid Files
Conversion of Vector Grid File to Discrete Point File
Synthesis of Vector Grid Files from Two Scalar Grids
Decomposition of Vector Grid File into Scalar Components
Vector Grid Representation Transformation
Conversion of Vector Grid File to Discrete Point File
Convert the grid into discrete points
Open a vector grid file
>> Computation Process ** Operation Prompts
Save computation process as
>> [Function] Decomposes a vector grid file into its two constituent scalar grid files.
>> Open a vector grid file C:/PAGravf4.5_win64en/examples/EdVectorgridtransf/dbmchcxpc.dat.
>> Save the component 1 grid as C:/PAGravf4.5_win64en/examples/EdVectorgridtransf/component1.dat.
>> Save the component 2 grid as C:/PAGravf4.5_win64en/examples/EdVectorgridtransf/component2.dat.
>> The parameter settings have been entered into the system!
** Click the [Start Computation] control button, or the [Start Computation] tool button...
>> Computation start time: 2026-03-30 11:52:06
>> Complete the computation!
>> Computation end time: 2026-03-30 11:52:06
>> [Function] Raster-to-Vector conversion: transforms a (vector) grid file into a discrete point file. The latitude and longitude of each output point correspond to the centric coordinates of the respective grid cell.
>> Open a vector grid file C:/PAGravf4.5_win64en/examples/EdVectorgridtransf/vectorgrd.dat.
>> Save the results as C:/PAGravf4.5_win64en/examples/EdVectorgridtransf/vectorpnt.txt.
>> The parameter settings have been entered into the system!
** Click the [Start Computation] control button, or the [Start Computation] tool button...
>> Computation start time: 2026-03-30 11:53:29
>> Complete the computation!
>> Computation end time: 2026-03-30 11:53:31
Save the results as
Import setting parameters
Start Computation
Display of the input-output file↓
Save data in the text box as
vectorgrd.dat

6.7 Statistical Analysis of Geodetic Data File

[Purpose] Performs statistical calculations on the specified record attribute of a discrete point file, the cell values of a geodetic grid file, or the cell values of a vector grid file. Output metrics include: Geographic Extent (Lat/Lon bounds), Mean, Standard Deviation, Minimum, and Maximum values.

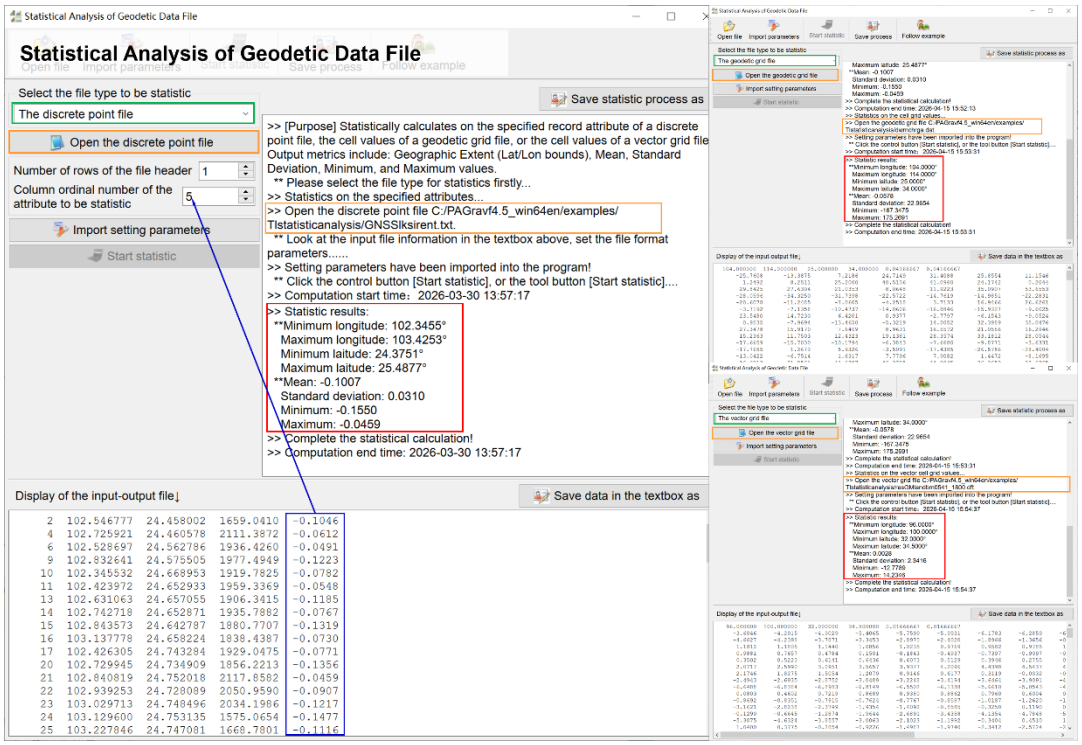

6.8 Calculation of Grid Horizontal Gradients and Vector Grid Inner Products

[Purpose] Estimates first- and second-order horizontal gradients of geodetic grid, or computes the inner product of two vector grids.

6.8.1 Horizontal Gradient Estimation of Geodetic Grid

[Function] Estimates the first-order horizontal gradient vector (units: $/km$) or second-order horizontal gradient vector (units: $/km^2$) grid from a geodetic parameter grid using the Least Squares Method.

[Input Files]

(1) Geodetic Grid File.

(2) Surface Ellipsoidal Height Grid File: Provices the geodetic coordinates of Geodetic Grid, essential for deriving horizontal distances

Output Formats: Results can be exported in Polar Coordinates (Magnitude/Direction) or East-North (EN) Cartesian Coordinates.

6.8.2 Inner Product Operation on Geodetic Vector Grids

[Function] Calculates the inner product (dot product) of two geodetic vector grids with identical specifications.

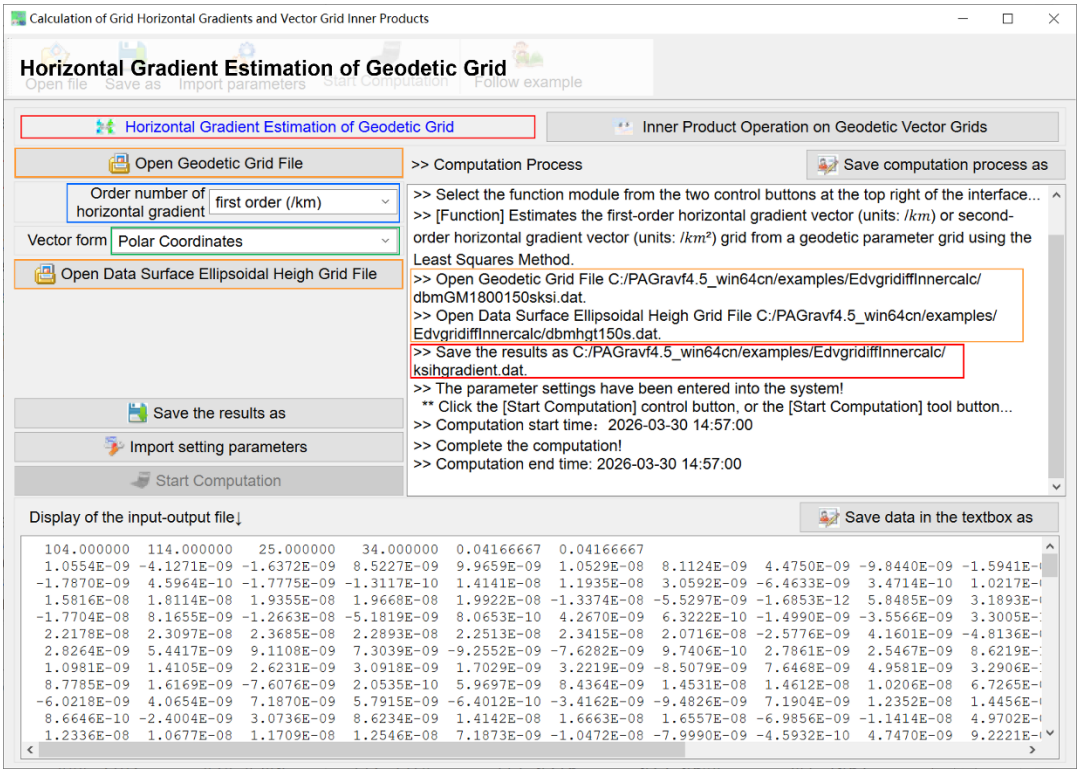

6.9 Visualization and Plotting Tools for Geodetic Data Files

6.9.1 Visualization of Multi-attribute Curves from 2D Geodetic Data

[Function] Renders and plots multiple attribute curves stored within a discrete geodetic point file.

Input File:

- 2D multi-attribute record file

Data Requirements:

- The file header must occupy exactly one row.
- Values in the column designated as the X-axis must be strictly sorted in ascending order.
- Maximum capacity: 15 curves per operation.

Interactive Controls:

- Rotate: Hold and drag the Left Mouse Button.
- Zoom: Hold and drag the Right Mouse Button, or scroll the Middle Mouse Wheel.
- Pan: Hold and drag the Middle Mouse Button.

Optimization Tip: For high-resolution plot, maximize the graphics window below the interface prior to clicking the [Chart Plot] button.

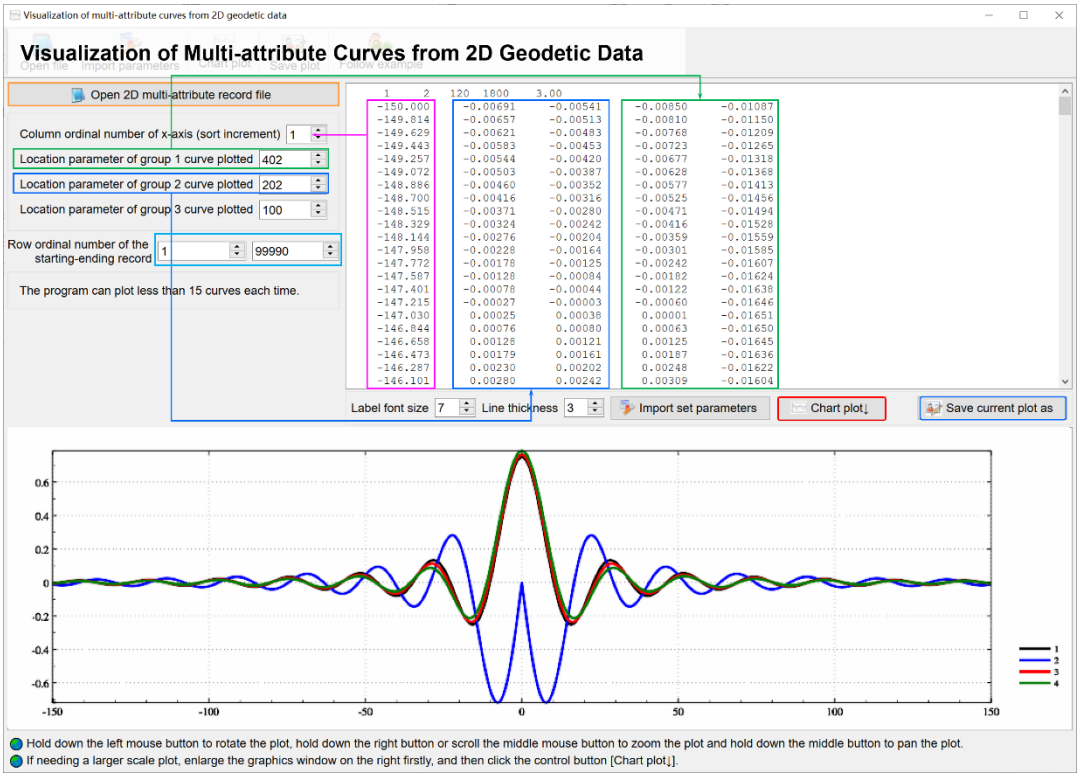

6.9.2 Visualization of Specified Attributes in Discrete Point File

[Function] Displays the geographic distribution and corresponding attribute values (Z-values) from a discrete geodetic point file as a scatter plot.

Interactive Controls:

- Rotate: Hold and drag the Left Mouse Button.
- Zoom: Hold and drag the Right Mouse Button, or scroll the Middle Mouse Wheel.
- Pan: Hold and drag the Middle Mouse Button.

Operational Workflow:

- To generate a high-resolution plot, maximize the graphics window and click [Scatter Plot].
- Refresh Mechanism: Upon changing the input file, Z-attribute, or other parameters, the user should re-click [Import Setting Parameters] to update the visualization.
- Scale Unification: Batch plots can maintain a unified scale range by fixing the Minimum and Maximum threshold values.

Batch Plotting Protocol:

- Preparation: Adjust the graphics window size and plot parameters to the desired state before initiating batch processing.
- Constraint: During batch execution, parameters and window dimensions are locked. Do not perform any mouse interactions on the plot area, as this may interrupt the process or cause rendering errors.

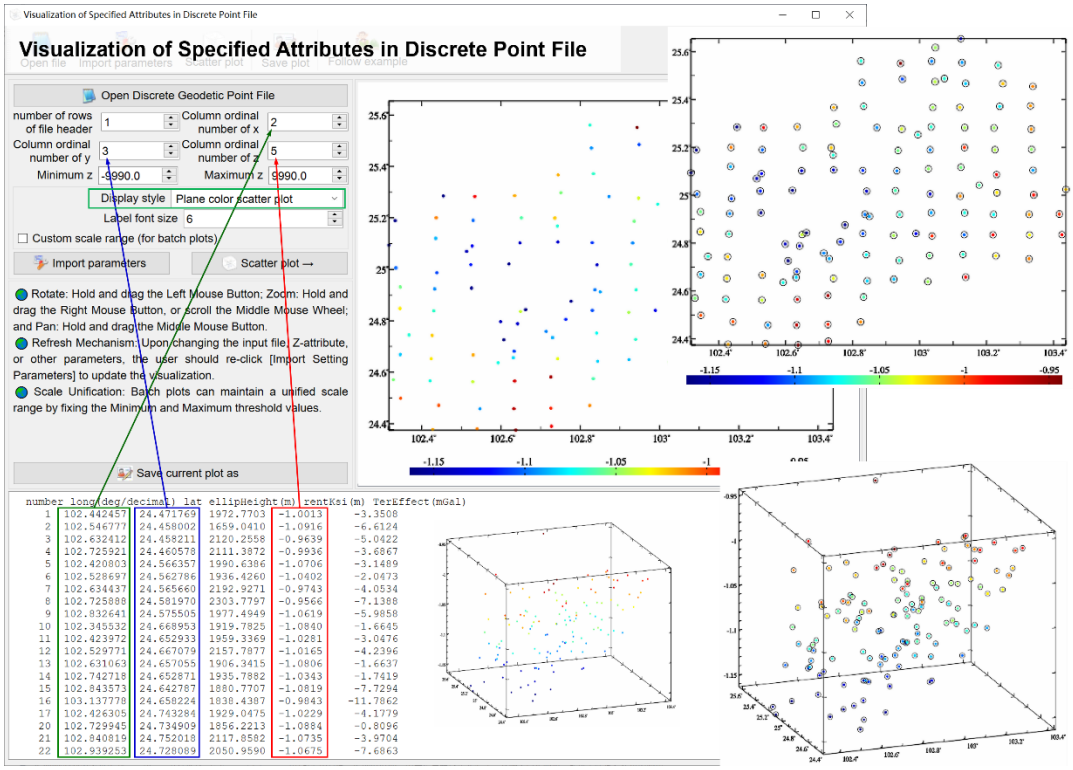

6.9.3 Visualization of Geodetic Grid File

[Function] Renders and plots data from geodetic numerical grid files (e.g., contour maps or color-coded raster images).

[Parameter Settings]

- Select Display Style.
- Enable/Disable [Custom Scale Range].

Vector Grid Support: Capable of displaying the first component of a vector grid as a standard scalar grid.

Batch Plotting Protocol: Same constraints as Section 6.9.2 apply. Ensure window size and scale limits are preset; avoid mouse interaction during batch processing to ensure consistency and stability.

6.9.4 Visualization of Geodetic Vector Grid File

[Function] Renders and plots data from geodetic vector grid file.

Coordinate System Convention:

- X-Axis: Points East.
- Y-Axis: Points North.
- This ENU (East-North-Up) planar convention aligns with the standard definition for horizontal displacement vectors.

Vector Component Definitions:

- East-North (EN): Standard format for Horizontal Displacement Vectors.
- South-West (SW): Traditional format for Vertical Deflection Vectors (ξ , η), where

components are often defined positive towards South and West.

- North-West (NW): Specialized format for Tangential Gravity Gradient Vectors.

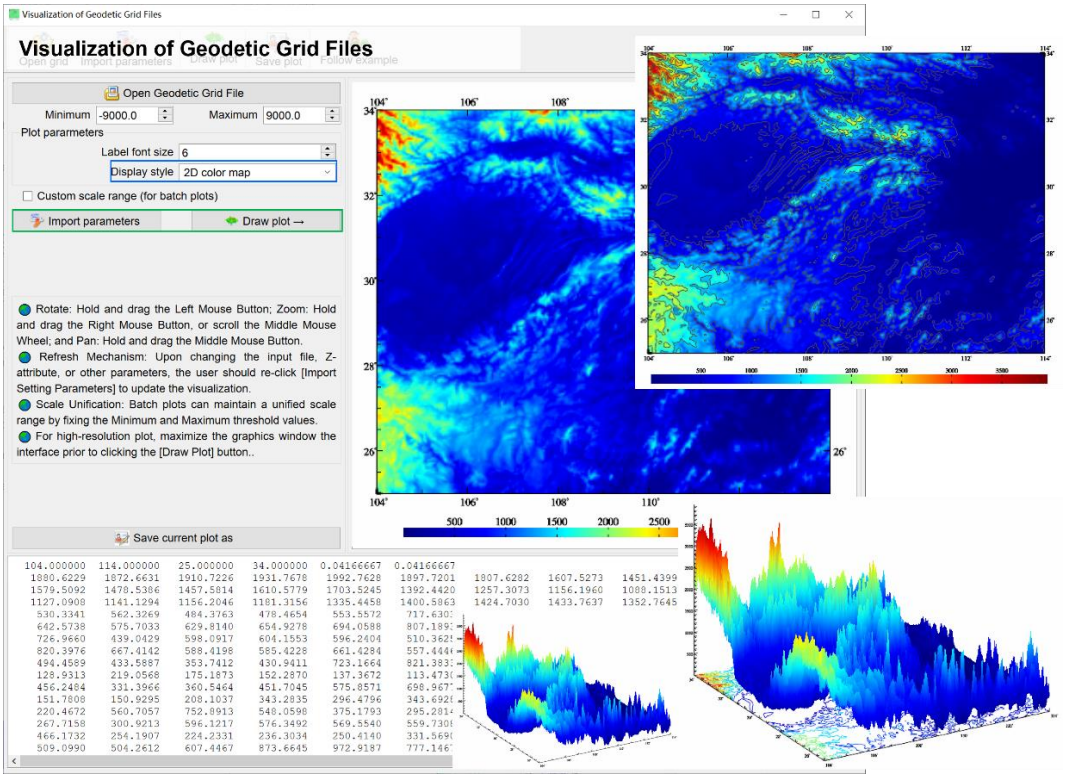

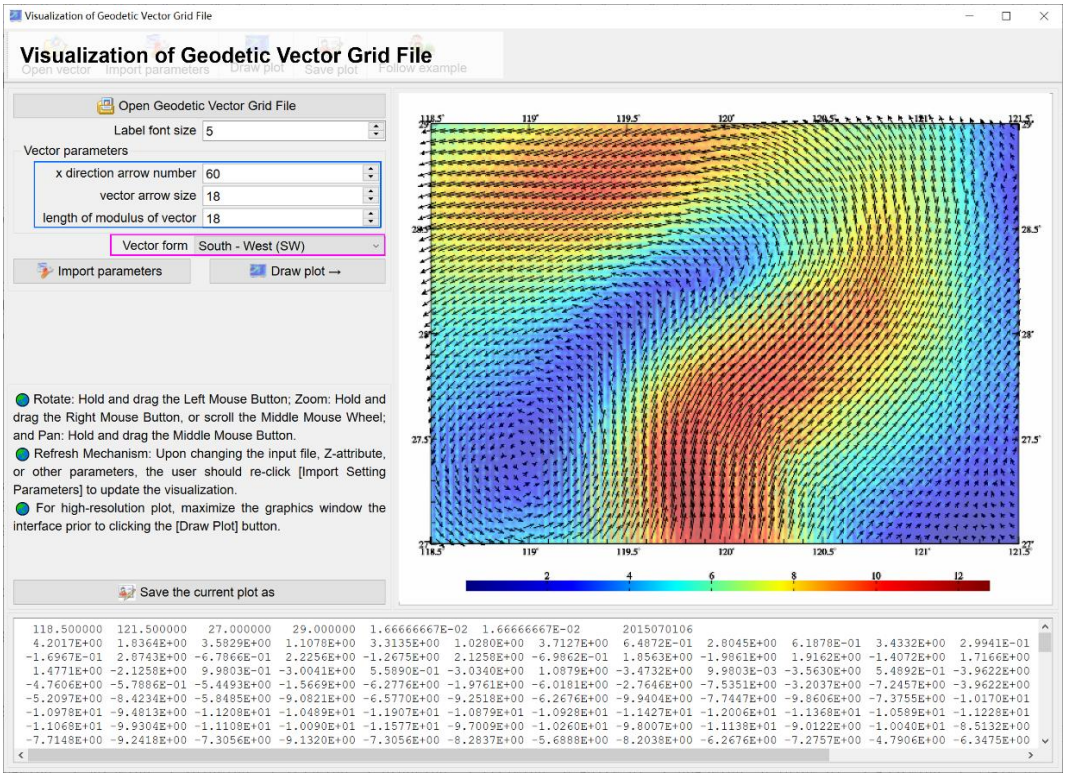

7. Key Formulas and Algorithms of PAGravf4.5

This section details the rigorous mathematical derivations and algorithmic implementations for the core computational modules within the PAGravf4.5 software. Approximately 300 algorithmic formulas are presented, each subjected to strict theoretical verification and cross-validation. The distinctive algorithms proposed herein are specifically designed to address complex computational challenges in physical geodesy based on first principles. The performance and numerical stability of these algorithms can be independently verified through the corresponding module invocation interfaces provided in the software.

7.1 Computation Formulas of Normal Gravity Field

This subsection outlines the algorithms for computing normal gravity quantities and their gradients at arbitrary spatial points.

7.1.1 Formulations for Normal Gravity at Arbitrary Points

The normal geopotential U outside the reference ellipsoid (including its surface) is expressed as a spherical harmonic series:

$$U(\theta,r)=\frac{GM}{r}\left[1-\sum_{n=1}^{\infty}\left(\frac{a}{r}\right)^{2n}J_{2n}P_{2n}(cos\theta)\right]+\frac{1}{2}\omega^2r^2sin^2\theta \tag{1.1}$$

$$J_{2n}=(-1)^{n+1}\frac{3e^{2n}}{(2n+1)(2n+3)}\left(1-n+\frac{5nJ_2}{e^2}\right) \tag{1.2}$$

Notation:

r: Geocentric distance to the computation point.

λ: Longitude.

$\theta=\pi/2-\varphi$: Geocentric co-latitude (φ is geocentric latitude).

a: Semi-major axis of the ellipsoid.

J_2: Dynamical form factor of the Earth.

GM: Geocentric gravitational constant.

ω: Mean angular velocity of Earth's rotation.

e: First eccentricity of the normal ellipsoid.

$P_{2n}(cos\theta)$: Legendre function of degree $2n$.

As illustrated in Figure 7.1, the unit vectors $\boldsymbol{e}_\theta$, $\boldsymbol{e}_\lambda$, and $\boldsymbol{e}_r$ define the local spherical coordinate system at point P. These vectors are mutually orthogonal, corresponding to the directions of co-latitude, longitude, and geocentric radius, respectively. The line elements along these axes are $rd\theta$, $rsin\theta d\lambda$, and dr, respectively. In geodesy, the radial direction $\boldsymbol{e}_r$ is fundamental for defining derivatives.

The normal gravity vector $\boldsymbol{\gamma}$ at point P is derived by taking the total differential of U in this local spherical coordinate system:

$$\boldsymbol{\gamma}=\frac{1}{r}\frac{\partial U}{\partial\theta}\boldsymbol{e}_\theta+\frac{1}{rsin\theta}\frac{\partial U}{\partial\lambda}\boldsymbol{e}_\lambda+\frac{\partial U}{\partial r}\boldsymbol{e}_r \tag{1.3}$$

Substituting Eq. (1.1) into Eq. (1.3) and noting that $\partial U/\partial\lambda=0$ due to rotational symmetry, the normal gravity vector becomes:

$$\boldsymbol{\gamma}(\theta,r)=-\left\{\frac{GM}{r^2}\sum_{n=1}^{\infty}\left(\frac{a}{r}\right)^{2n}J_{2n}\frac{\partial}{\partial\theta}[P_{2n}(cos\theta)]-\omega^2r^2sin\theta cos\theta\right\}\boldsymbol{e}_\theta$$

$$+\left\{\frac{GM}{r^2}\left[1-\sum_{n=1}^{\infty}(2n+1)\left(\frac{a}{r}\right)^{2n}J_{2n}P_{2n}(cos\theta)\right]+\omega^2 rsin^2\theta\right\}\boldsymbol{e}_r \tag{1.4}$$

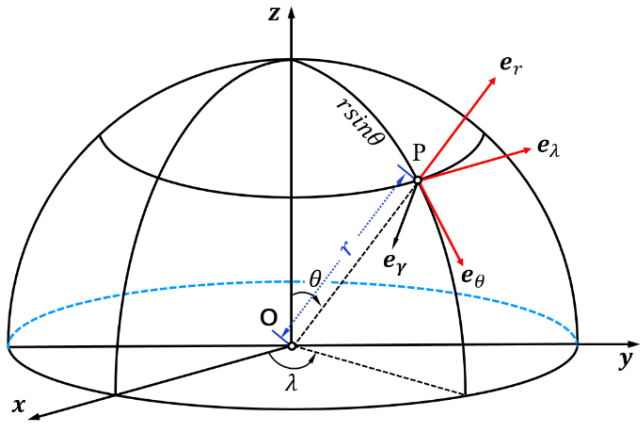

Figure 7.1: Unit vectors in the local spherical coordinate system at computation point P.

In the local spherical coordinate system at point P, by taking partial derivatives of the normal geopotential $U(\theta,r)$ formula (1.1) along the directions of the local coordinate axes, the normal gravity vector at P can be expressed as:

$$\boldsymbol{\gamma}(\theta,r)=\gamma_\theta\boldsymbol{e}_\theta+\gamma_r\boldsymbol{e}_r \tag{1.5}$$

$$\gamma_\theta=\frac{\partial U}{r\partial\theta}=-\frac{GM}{r^2}\sum_{n=1}^{\infty}\left(\frac{a}{r}\right)^{2n}J_{2n}\frac{\partial}{\partial\theta}[P_{2n}(cos\theta)]+\omega^2r^2sin\theta cos\theta \tag{1.6}$$

$$\gamma_r=\frac{GM}{r^2}\left[1-\sum_{n=1}^{\infty}(2n+1)\left(\frac{a}{r}\right)^{2n}J_{2n}P_{2n}(cos\theta)\right]+\omega^2rsin^2\theta \tag{1.7}$$

Since $\boldsymbol{e}_\theta\perp\boldsymbol{e}_r$, the scalar magnitude of normal gravity is:

$$\gamma=\sqrt{\gamma_\theta^2+\gamma_r^2} \tag{1.8}$$

Further, by computing the partial derivatives of the normal gravity vector, the diagonal elements of the normal gravity gradient tensor in this local system are obtained:

$$U_{\theta\theta}=\frac{\partial^2U}{r^2\partial\theta^2}=\frac{\partial\gamma_\theta}{r\partial\theta}=-\frac{GM}{r^3}\left[\sum_{n=1}^{\infty}\left(\frac{a}{r}\right)^{2n}J_{2n}\frac{\partial^2}{\partial\theta^2}P_{2n}(cos\,\theta)\right]+\omega^2cos2\theta \tag{1.9}$$

$$U_{rr}=-2\frac{GM}{r^3}\left[1-\sum_{n=1}^{\infty}(n+1)(2n+1)\left(\frac{a}{r}\right)^{2n}J_{2n}P_{2n}(cos\theta)\right]+\omega^2sin^2\theta \tag{1.10}$$

The scalar magnitude of the normal gravity gradient, derived from the orthogonal components, is given by:

$$U_{EE}=\sqrt{U_{\theta\theta}^2+U_{rr}^2} \tag{1.11}$$

7.1.2 Calculation of the Normal Gravity Line and Normal Gravity Gradient Line

In physical geodesy conventions, the normal gravity line is directed towards the Earth's interior (downward), whereas the normal gravity gradient is directed outward. Consequently, the unit vector $\boldsymbol{e}_r$ of the normal gravity line at P (pointing inward) in the local basis $(\boldsymbol{e}_\theta,\boldsymbol{e}_\lambda,\boldsymbol{e}_r)$ is defined as:

$$\boldsymbol{e}_r=\frac{1}{\gamma}(\gamma_\theta,0,-\gamma_r) \tag{1.12}$$

Let the geocentric direction (inward) be defined as $-\boldsymbol{e}_r=(0,0,-1)$, the deflection angle

ϵ_γ between the normal gravity line and the geocentric direction is computed as:

$$cos\epsilon_\gamma = -\boldsymbol{e}_r \cdot \boldsymbol{e}_{\boldsymbol{\gamma}} = \frac{\gamma_r}{\gamma} \quad \Longrightarrow \quad \epsilon_\gamma = tan^{-1}\frac{\gamma_\theta}{\gamma_r} \tag{1.13}$$

Geometric Analysis: Due to the decrease of ellipsoidal flattening with altitude, normal gravity lines are generally curved outside the reference ellipsoid. Although the normal gravity direction coincides with the surface normal on the ellipsoid itself, in space it aligns with the normal of the level ellipsoid at that specific height. This results in a divergence from the normal of the reference ellipsoid (semi-major axis a), yielding a non-zero deflection angle.

Similarly, the angle ϵ_E between the normal gravity gradient direction $\boldsymbol{e}_{nd}$ and the geocentric radial direction $\boldsymbol{e}_r$ is:

$$cos\epsilon_E = \boldsymbol{e}_r \cdot \boldsymbol{e}_{nd} = \frac{U_{rr}}{U_{EE}} \quad \Longrightarrow \quad \epsilon_E = tan^{-1}\frac{U_{\theta\theta}}{U_{rr}} \tag{1.14}$$

Using the IERS Conventions (2010) constants, the northward deflection angles ϵ_γ and ϵ_E (in arcminutes) were calculated for ellipsoidal heights of 0 km and 900 km, The geocentric co-latitude θ was varied from 0° to 180°. The results are visualized in Figure 7.2.

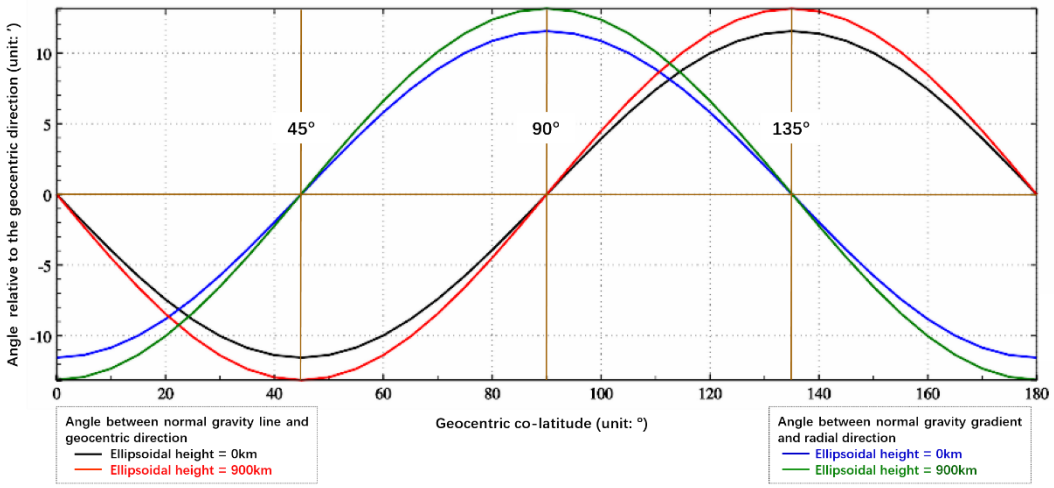

Figure 7.2: Variation of northward deflection angles of the normal gravity line and gradient direction relative to the geocentric direction, versus co-latitude.

Analysis of Figure 7.2:

● The deflection angles for the gravity line and gradient line exhibit distinct variations at different altitudes.

● Both lines are generally curved, except at specific geometric points.

● At the equator and poles (θ = 0°, 180°), the normal gravity lines are straight and intersect the geocenter.

● At co-latitudes of 45° and 135°, the normal gravity gradient lines are straight and parallel to the geocentric radius.

● Crucially, the reference ellipsoid normal, the normal gravity line, and the normal gravity gradient line possess distinct geometric properties and are generally not parallel.

Since the scalar gravity γ is maximized along the gravity line, and the gradient U_{EE} is maximized along the gradient line, their analytical relations to the radial components are:

$$\gamma = \gamma_r cos^{-1}\epsilon_\gamma \quad U_{EE} = U_{rr} cos^{-1}\epsilon_E \tag{1.15}$$

where $cos^{-1}\epsilon_\gamma$ and $cos^{-1}\epsilon_E$ are derived analytically from Eqs. (1.13) and (1.14).

7.1.3 Algorithms for Legendre Functions and Their Derivatives

Let $x = cos\,\theta, \quad \tau = sin\,\theta$. The Legendre function (polynomial) with x as the independent variable is defined as:

$$P_n(x) = \frac{1}{2^n n!}\frac{d^n}{dx^n}(x^2-1)^n = -\frac{(-1)^n}{2^n n!}\frac{d^n}{dx^n}\tau^{2n} \tag{1.16}$$

For efficient numerical computation of $P_n(x)$ and its derivatives with respect to θ, the following recurrence relations are implemented:

$$P_n(x) = \frac{2n-1}{n}xP_{n-1}(x) - \frac{n-1}{n}P_{n-2}(x) \tag{1.17}$$

with initial values $$P_0(x) = 1, \quad P_1(x) = x, \quad P_2(x) = \frac{1}{2}(3x^2-1) \tag{1.18}$$

First-order derivatives:

$$\frac{\partial}{\partial\theta}P_n(x) = \frac{2n-1}{n}x\frac{\partial}{\partial\theta}P_{n-1}(x) - \frac{2n-1}{n}\tau P_{n-1}(x) - \frac{n-1}{n}\frac{\partial}{\partial\theta}P_{n-2}(x) \tag{1.19}$$

with $$\frac{\partial}{\partial\theta}P_1(x) = -\tau, \quad \frac{\partial}{\partial\theta}P_2(x) = -3\tau x \tag{1.20}$$

Second-order derivatives:

$$\frac{\partial^2}{\partial\theta^2}P_n(x) = \frac{2n-1}{n}\left(x\frac{\partial^2}{\partial\theta^2}P_{n-1} - 2\tau\frac{\partial}{\partial\theta}P_{n-1} - xP_{n-1}\right) - \frac{n-1}{n}\frac{\partial^2}{\partial\theta^2}P_{n-2} \tag{1.21}$$

with $$\frac{\partial^2}{\partial\theta^2}P_1(x) = -x, \quad \frac{\partial^2}{\partial\theta^2}P_2(x) = 3(1-2x^2) \tag{1.22}$$

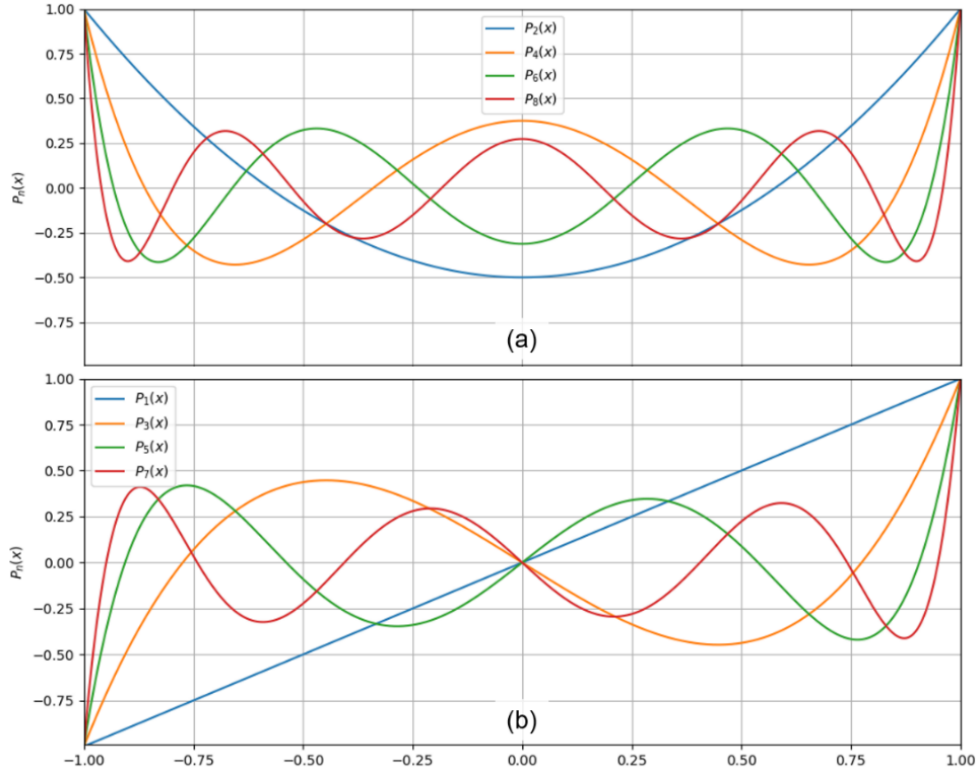

Figure 7.3: Curves of even-order (a) and odd-order (b) Legendre functions

Figure 7.3 illustrates the characteristic curves of even-order and odd-order Legendre

functions.

7.2 Computation Formulas for Earth's Geopotential Coefficient Models

This section details the spherical harmonic synthesis algorithms for computing various gravity field functionals (disturbing potential, gravity anomalies, vertical deflections, and gradients) based on fully normalized geopotential coefficient models.

7.2.1 Spherical Harmonic Synthesis of Gravity Field elements

The disturbing potential T or the height anomaly ζ at an external point (θ, λ, r) is expressed via spherical harmonic expansion as:

$$T(\theta,\lambda,r) = \zeta\gamma = \frac{GM}{r}\sum_{n=1}^{\infty}\left(\frac{a}{r}\right)^n \sum_{m=0}^{n}(\delta\bar{C}_{nm}cosm\lambda + \bar{S}_{nm}sinm\lambda)\bar{P}_{nm}(cos\theta) \tag{2.1}$$

Notation:

$\bar{C}_{nm}, \bar{S}_{nm}$: Fully normalized Stokes coefficients (geopotential coefficients).

$\bar{P}_{nm}(cos\theta)$: Fully normalized associated Legendre functions.

n, m : Degree and order of the expansion, respectively.

Correction terms for zonal coefficients:

$$\delta\bar{C}_{2n,0} = \bar{C}_{2n,0} + \frac{J_{2n}}{\sqrt{4n+1}} \tag{2.2}$$

$$\delta\bar{C}_{2n,m} = \bar{C}_{2n,m}(m>0) \quad \delta\bar{C}_{2n+1,m} = \bar{C}_{2n+1,m} \tag{2.3}$$

In the local spherical coordinate system at point P(θ, λ, r), the spherical harmonic expansions for the gravity disturbance δg, vertical deflections (ξ ,η) , and gravity anomaly Δg implemented as follows:

$$\delta g = \frac{\partial}{\partial r}T =$$
$$\frac{GM}{r^2}\sum_{n=1}^{\infty}(n+1)\left(\frac{a}{r}\right)^n \sum_{m=0}^{n}(\delta\bar{C}_{nm}cosm\lambda + \bar{S}_{nm}sinm\lambda)\bar{P}_{nm}(cos\theta) \tag{2.4}$$

$$\xi = \frac{1}{r\gamma}\frac{\partial}{\partial\theta}T =$$
$$\frac{GM}{\gamma r^2}\sum_{n=1}^{\infty}\left(\frac{a}{r}\right)^n \sum_{m=0}^{n}(\delta\bar{C}_{nm}cosm\lambda + \bar{S}_{nm}sinm\lambda)\frac{\partial}{\partial\theta}[\bar{P}_{nm}(cos\theta)] \tag{2.5}$$

$$\eta = -\frac{1}{r\gamma sin\theta}\frac{\partial}{\partial\lambda}T =$$
$$\frac{GM}{\gamma r^2 sin\theta}\sum_{n=1}^{\infty}\left(\frac{a}{r}\right)^n \sum_{m=1}^{n} m(\delta\bar{C}_{nm}sinm\lambda - \bar{S}_{nm}cosm\lambda)\bar{P}_{nm}(cos\theta) \tag{2.6}$$

$$\Delta g = \frac{GM}{r^2}\sum_{n=2}^{\infty}(n-1)\left(\frac{a}{r}\right)^n \sum_{m=0}^{n}(\delta\bar{C}_{nm}cosm\lambda + \bar{S}_{nm}sinm\lambda)\bar{P}_{nm}(cos\theta) \tag{2.7}$$

where γ is the normal gravity at P. The vector components $(\xi, \eta, \delta g)$ form a right-handed Cartesian local coordinate system.

Similarly, the radial gravity gradient T_{rr} and tangential gravity gradients (T_{nn}, T_{ww}) are computed by:

$$T_{rr} = \frac{\partial^2}{\partial r^2}T =$$
$$\frac{GM}{r^3}\sum_{n=1}^{\infty}(n+1)(n+2)\left(\frac{a}{r}\right)^n \sum_{m=0}^{n}(\delta\bar{C}_{nm}cosm\lambda + \bar{S}_{nm}sinm\lambda)\bar{P}_{nm} \tag{2.8}$$

$$T_{nn} = \frac{1}{r^2}\frac{\partial^2}{\partial\theta^2}T =$$

$$\frac{GM}{r^3}\sum_{n=1}^{\infty}\left(\frac{a}{r}\right)^n\sum_{m=0}^{n}(\delta\bar{C}_{nm}cosm\lambda+\bar{S}_{nm}sinm\lambda)\frac{\partial^2}{\partial\theta^2}\bar{P}_{nm} \tag{2.9}$$

$$T_{ww}=\frac{1}{r^2sin^2\theta}\frac{\partial^2}{\partial\lambda^2}T=$$

$$-\frac{GM}{r^3sin^2\theta}\sum_{n=1}^{\infty}\left(\frac{a}{r}\right)^n\sum_{m=0}^{n}m^2(\delta\bar{C}_{nm}cosm\lambda+\bar{S}_{nm}sinm\lambda)\bar{P}_{nm} \tag{2.10}$$

These components satisfy the Laplace equation:

$$T_{rr}+T_{nn}+T_{ww}\equiv 0,\quad \text{where } T_*=\sum_{n=1}^{\infty}T_*^n \tag{2.11}$$

Eq. (2.11) serves as a rigorous check for the spatial and spectral consistency of the gravity field model. The components (T_{nn},T_{ww},T_{rr}) also form a right-handed system.

7.2.2 Algorithms for Associated Legendre Functions and Their Derivatives

The computation of gravity field functionals necessitates the efficient evaluation of fully normalized Associated Legendre Functions (ALFs) $\bar{P}_{nm}(cos\theta)$ and their derivatives. Define $t=cos\theta,\tau=sin\theta$. The following robust recurrence algorithms are implemented to ensure numerical stability across various degree ranges (Yu Jinhai, Zeng Yanyan et al., 2015).

(1) Standard Forward Column-wise Recurrence for $\bar{P}_{nm}(t)$ (n<1900)

Initial values:
$$\bar{P}_{00}(t)=1,\quad \bar{P}_{10}(t)=\sqrt{3}t,\quad \bar{P}_{11}(t)=\sqrt{3}\tau \tag{2.12}$$

For >1 :
$$\begin{cases}\bar{P}_{nm}(t)=a_{nm}t\bar{P}_{n-1,m}(t)-b_{nm}\bar{P}_{n-2,m}(t) & (m<n)\\ \bar{P}_{nn}(t)=\tau\sqrt{\frac{2n+1}{2n}}\bar{P}_{n-1,n-1}\end{cases} \tag{2.13}$$

where,

$$a_{nm}=\sqrt{\frac{(2n-1)(2n+1)}{(n+m)(n-m)}},\quad b_{nm}=\sqrt{\frac{(2n+1)(n+m-1)(n-m-1)}{(2n-3)(n+m)(n-m)}}.$$

(2) Modified Belikov Recurrence for $\bar{P}_{nm}(t)$ (n<64800)

Optimized for ultra-high degrees. For $n\geq 2$:

$$\bar{P}_{n0}(t)=a_nt\bar{P}_{n-1,0}(t)-b_n\frac{\tau}{2}\bar{P}_{n-1,1}(t),\ m=0 \tag{2.14}$$

$$\bar{P}_{nm}(t)=c_{nm}t\bar{P}_{n-1,m}-d_{nm}\tau\bar{P}_{n-1,m+1}+e_{nm}\tau\bar{P}_{n-1,m-1}(t),m>0 \tag{2.15}$$

where,

$$a_n=\sqrt{\frac{2n+1}{2n-1}},\quad b_n=\sqrt{\frac{2(n-1)(2n+1)}{n(2n-1)}}$$

$$c_{nm}=\frac{1}{n}\sqrt{\frac{(n+m)(n-m)(2n+1)}{2n-1}},\quad d_{nm}=\frac{1}{2n}\sqrt{\frac{(n-m)(n-m-1)(2n+1)}{2n-1}}$$

For $m>0$,

$$e_{nm}=\frac{1}{2n}\sqrt{\frac{2}{2-\delta_0^{m-1}}}\sqrt{\frac{(n+m)(n+m-1)(2n+1)}{2n-1}}$$

(3) Cross-Degree-Order Recurrence for $\bar{P}_{nm}(t)$ (n<20000)

An alternative stable scheme relating degrees n and $n-2$:

$$\bar{P}_{nm}(t)=\alpha_{nm}\bar{P}_{n-2,m}(t)+\beta_{nm}\bar{P}_{n-2,m-2}(t)-\gamma_{nm}\bar{P}_{n,m-2}(t) \tag{2.16}$$

where,

$$\alpha_{nm}=\sqrt{\frac{(2n+1)(n-m)(n-m-1)}{(2n-3)(n+m)(n+m-1)}},\quad \beta_{nm}=\sqrt{1+\delta_0^{m-2}}\sqrt{\frac{(2n+1)(n+m-2)(n+m-3)}{(2n-3)(n+m)(n+m-1)}}$$

$$\gamma_{nm} = \sqrt{1+\delta_0^{m-2}}\sqrt{\frac{(n-m+1)(n+m-3)}{(n+m)(n+m-1)}}$$

(4) Non-Singular Recurrence for First Derivatives $\frac{\partial}{\partial\theta}\bar{P}_{nm}(cos\,\theta)$

To avoid singularities at the polar regions ($\theta\to 0,\pi$), the first derivatives are expressed as linear combinations of adjacent orders:

$$\frac{\partial}{\partial\theta}\bar{P}_{nm}(cos\,\theta) = -sin\,\theta\,\frac{\partial}{\partial t}\bar{P}_{nm}(t) \tag{2.17}$$

$$\begin{cases} \frac{\partial}{\partial\theta}\bar{P}_{n0}(t) = -\sqrt{\frac{n(n+1)}{2}}\bar{P}_{n1}, \quad \frac{\partial}{\partial\theta}\bar{P}_{n1} = \sqrt{\frac{n(n+1)}{2}}\bar{P}_{n0} - \frac{\sqrt{(n-1)(n+2)}}{2}\bar{P}_{n2}(t) \\ \frac{\partial}{\partial\theta}\bar{P}_{nm}(t) = \frac{\sqrt{(n+m)(n-m+1)}}{2}\bar{P}_{n,m-1} - \frac{\sqrt{(n-m)(n+m+1)}}{2}\bar{P}_{n,m+1}(t), \quad m>2 \end{cases} \tag{2.18}$$

Initial values: $\frac{\partial}{\partial\theta}\bar{P}_{00}(t) = 0, \quad \frac{\partial}{\partial\theta}\bar{P}_{10}(t) = -\sqrt{3}\tau, \quad \frac{\partial}{\partial\theta}\bar{P}_{11}(t) = \sqrt{3}t$ (2.19)

Specific forms for $m = 0,1$ and $m > 2$ are provided in Eq. (2.18).

(5) Non-Singular Recurrence for Second Derivatives $\frac{\partial^2}{\partial\theta^2}\bar{P}_{nm}$

Expresses second derivatives using orders $m, m-2, m+2$:

$$\begin{cases} \frac{\partial^2}{\partial\theta^2}\bar{P}_{n0}(t) = -\frac{n(n+1)}{2}\bar{P}_{n0}(t) + \sqrt{\frac{n(n-1)(n+1)(n+2)}{8}}\bar{P}_{n2}(t) \\ \frac{\partial^2}{\partial\theta^2}\bar{P}_{n1}(t) = -\frac{2n(n+1)+(n-1)(n+2)}{4}\bar{P}_{n1}(t) + \frac{\sqrt{(n-2)(n-1)(n+2)(n+3)}}{4}\bar{P}_{n3}(t) \end{cases} \tag{2.20}$$

$$\frac{\partial^2}{\partial\theta^2}\bar{P}_{nm}(t) = \frac{\sqrt{(n-m+1)(n-m+2)(n+m-1)(n+m)}}{4}\bar{P}_{n,m-2}(t) - \frac{(n+m)(n-m+1)+(n-m)(n+m+1)}{4}$$

$$\bar{P}_{nm}(t) + \frac{\sqrt{(n-m-1)(n-m)(n+m+1)(n+m+2)}}{4}\bar{P}_{n,m+2}(t), \quad m>2 \tag{2.21}$$

Initial values: $\frac{\partial^2}{\partial\theta^2}\bar{P}_{00}(t) = 0, \quad \frac{\partial^2}{\partial\theta^2}\bar{P}_{10}(t) = -\sqrt{3}t, \quad \frac{\partial^2}{\partial\theta^2}\bar{P}_{11}(t) = -\sqrt{3}\tau$ (2.22)

These formulations ensure numerical stability across all latitudes, including the geographic poles.

7.3 Boundary Value Corrections for Ellipsoidal and Spherical Surfaces

To transform the Molodensky boundary value problem (defined on a non-equipotential surface) into the classical Stokes problem (defined on an equipotential surface), specific boundary value corrections are required. These corrections depend on the geometric relationship between the boundary surface (ellipsoid or sphere).

(1) Ellipsoidal Correction for Gravity: The correction applied to the gravity value g on a specific ellipsoidal surface of the Earth, from the direction of the vertical to the direction of normal gravity, also known as the vertical deflection correction for gravity:

$$\varepsilon_p = \gamma sin\theta cos\theta\left[3J_2\left(\frac{a}{r}\right)^2 + \frac{\omega^3 r^3}{GM}\right]\xi \tag{3.1}$$

(2) Correction for the gravity value g from the direction of normal gravity to the geocentric direction:

$$\varepsilon_h = \gamma e^2 sin\theta cos\theta\xi \tag{3.2}$$

(3) Correction for the normal gravity value γ from the direction of normal gravity to the geocentric direction:

$$\varepsilon_\gamma = 3\gamma\left[J_2\frac{a^2}{r^3}(3cos^2\theta - 1) - \frac{\omega^3 r^3}{GM}sin^2\theta\right]T \tag{3.3}$$

Implementation Guidelines:

● Ellipsoidal Boundary: Apply only the ellipsoidal correction term (3.1).

● Spherical Boundary: Apply all three corrections (3.1) through (3.3) simultaneously to account for both the ellipsoidal nature of the field and the geometric deviation of the sphere from the equipotential surface.

7.4 Classical Terrestrial Gravity Reduction Schemes and Their Limitations

The classical Stokes boundary value problem defines the geoid as the boundary surface, with both the Bouguer gravity anomaly and isostatic gravity anomaly are strictly defined on this equipotential surface. Traditional gravity reduction essentially involves the analytic downward continuation of gravity observables from the Earth's surface (or near-Earth space) to the geoid, incorporating corrections for topographic mass effects.

7.4.1 Free-Air Correction and Gravity Anomaly

The gravity g on the geoid can be expressed in terms of terrestrial gravity g_s via a Taylor series expansion:

$$g = g_s - \left(\frac{\partial g}{\partial h}\right)_N h - \frac{1}{2}\left(\frac{\partial^2 g}{\partial h^2}\right)_N h^2 - \cdots = g_s + \Delta_1 g \tag{4.1}$$

where $\Delta_1 g$ denotes the Free-Air Correction. This term represents the increment required to analytically continue g_s downward to the geoid when neglecting the topographic masses between the surface and the geoid.

Since the actual vertical gravity gradient on the geoid is unknown, it is conventionally approximated by the normal gravity gradient, truncating higher-order terms (typically retaining up to the second order):

$$\Delta_1 g = -\left(\frac{\partial \gamma}{\partial h}\right)_N h - \frac{1}{2}\left(\frac{\partial^2 \gamma}{\partial h^2}\right)_N h^2 \tag{4.2}$$

Using approximations for the normal gradient, $\Delta_1 g = 0.3086h - 1.5 \times 10^{-7}h^2 \approx 0.3086h$ mGal, where h is the orthometric (or normal) height in meters.

Consequently, the gravity anomaly on the geoid is formulated as:

$$\Delta g = g - \gamma_0 = g_s - \gamma_0 + \Delta_1 g \tag{4.3}$$

where g is the gravity on the geoid, and γ_0 is the normal gravity on the normal ellipsoid.

Comparing the terrestrial gravity anomaly $(\Delta g_s = g_s - \gamma_\zeta)$ with the geoid-defined gravity anomaly $(\Delta g = g - \gamma_0)$, a more rigorous approach than the simplified free-air correction mentioned above is to directly perform analytic continuation on the gravity anomaly field itself, utilizing the functional relationship between Δg_s and Δg.

7.4.2 Bouguer Plate Correction and Local Terrain Correction

Assuming planar geometry for both the Earth's surface (terrain surface) and the geoid, the gravitational attraction of the topographic mass (modeled as an infinite planar slab of thickness h at point P) is $2\pi G\rho h$. Removing this mass yields the Bouguer Plate Correction (or Simple Bouguer Correction):

$$\Delta_2 g = -2\pi G\rho h \tag{4.4}$$

where G is the gravitational constant. With a standard topographic density $\rho = 2.67 \times 10^3$kg/m^3, this simplifies to $\Delta_2 g = -0.1118h$ mGal.

Also known as the Planar Layer Correction, this induces a geopotential change $\Delta_2 V = 2\pi G\rho h S/R$, where S is the base area of the planar layer, and R is the average radius of the Earth. Since $\lim_{s\to\infty} \Delta(\Delta_2 V) \neq 0$, the resulting geopotential is non-harmonic. Thus, the planar Bouguer correction fundamentally violates the harmonic property of the Earth's external gravitational field.

The planar assumption implies a flat surrounding terrain. To account for real topographic relief, one must subsequently remove masses above the computation point and fill voids below it in the vicinity.

This residual term is the Local Terrain Correction ($\Delta_3 g$). Unlike the Bouguer plate correction, both the Free-Air correction ($\Delta_1 g$) and Local Terrain correction ($\Delta_3 g$) are analytic operations that preserve the harmonic nature of the field.

7.4.3 Bouguer Anomaly and Gridding Computation

The Bouguer Gravity Anomaly (or simply Bouguer Anomaly) defined on the geoid, is given by:

$$\Delta g_b = \Delta g + \Delta_2 g + \Delta_3 g = g_s - \gamma_0 + \Delta_1 g + \Delta_2 g + \Delta_3 g \tag{4.5}$$

The sum $\Delta_b g = \Delta_2 g + \Delta_3 g$ constitutes the Bouguer Correction. Due to the planar slab assumption, these are often termed "Simple" or "Planar" anomalies/corrections. Critically, the Bouguer correction alters the Earth's total mass distribution, thereby making the geoid and the external gravity field change.

The Bouguer gravity anomalies, defined on an equipotential surface with topographic masses effects removed, are generally believed to be smoother than the free-air gravity anomalies on the geoid. Consequently, gridding or prediction based on Bouguer gravity anomalies typically yields lower interpolation errors.

Grid averaging usually employs algorithms with translational invariance (isotropy). The mean Bouguer anomaly for a grid cell centered at (λ, φ) is expressed as:

$$\overline{\Delta g_b}(\lambda, \varphi) = \left[\sum_k f(\lambda_k - \lambda, \varphi_k - \varphi)\Delta g_b(\lambda_k, \varphi_k)\right] \tag{4.6}$$

where f is the two-dimensional kernel function. Common kernels include Inverse Distance Weighting, Shepard's Method, Multi-Quadric Interpolation, Kriging, and Radial Basis Functions.

Technical Note: If a gridding algorithm does not inherently satisfy the analytic functional relationships of the gravity field, operations should be performed on a gravity equipotential surface (e.g., the geoid) to minimize signal distortion. Direct gridding of terrestrial gravity anomalies on the non-equipotential terrain surface is theoretically inadvisable without prior rigorous harmonic reduction.

7.4.4 Limitations of Classical Gravity Reduction

Classical reduction schemes rely on the approximation $\Delta_1 g = -0.3086h + O(h^2)$ mGal, which accounts solely for the normal gravity gradient. However, in regions with moderate

relief (hundreds of meters), the contribution of the disturbing gravity gradient can reach or exceed the mGal level. A rigorous workflow should first compute normal gravity and gravity anomalies at observation points using exact formulas, followed by strict analytic continuation of the anomaly field to the geoid.

Furthermore, the classical concept of terrain correction is restricted to terrestrial gravity observations. The classical direct topographic effect specifically refers to the influence of topography on gravity (disturbance/anomaly), while the indirect topographic effect specifically refers to the influence of topography on the geopotential (disturbing potential/height anomaly/geoid undulation). Modern gravimetry encompasses diverse data types from space, airborne, marine, and terrestrial platforms, requiring a unified treatment of topographic effects on all gravity field elements (both on and outside the geoid).

Contemporary physical geodesy demands a comprehensive handling of these topographic effects across all gravity field elements. Traditional concepts like "Free-Air Correction", simple "Terrain Correction", and “Direct/Indirect Topographic Effect” are insufficient for high-precision applications.

PAGravf4.5 addresses these limitations by implementing a comprehensive algorithm framework capable of rigorous analytic treatment to diverse terrain effects on all gravity field elements on and outside the geoid.

7.5 Algorithms for Land-Sea Complete Bouguer Effects and Residual Terrain Effects

In physical geodesy, the treatment of topographic mass effects on various gravity field elements serves two fundamental objectives:

(a) Spectral Separation: To isolate ultra-short-wavelength components from discrete anomalous gravity field elements, thereby enhancing the performance of prediction, gridding, and numerical modeling.

(b) Approximation Enhancement: To improve the approximation of the ultra-short-wavelength gravity field by explicitly modeling the topographic mass contribution during gravity field recovery.

Crucially, for the second objective, maintaining the analytic functional relationships among topographic effects on various gravity field elements across different locations is a mandatory requirement of gravity field approximation theory.

Any anomalous gravity field element at an external point can be expressed as a linear combination of the disturbing potential (T), the gravity disturbance (δg), or their partial derivatives in the local coordinate system defined on the equipotential surface passing through the point. For instance, vertical deflections correspond to horizontal derivatives of T, while disturbing gravity gradients relate to vertical derivatives of δg. Consequently, solving the topographic mass effect problem for T and δg inherently provides the solution for all other gravity field elements.

7.5.1 Spherical Approximation Algorithm for Land Complete Bouguer Effects

The gravitational field generated by land topographic masses is termed the Land

Complete Bouguer Effect. It represents the total effect of masses located between the terrain surface and the geoid on external gravity field elements.

The Unified Land-Sea Complete Bouguer Effect at any external point (See Figure 7.4 for the fundamental principle) is defined as the sum of:

- The effect of land topographic masses (between the surface and the geoid).
- The effect of seawater compensation masses (density change from ρ_w to ρ).

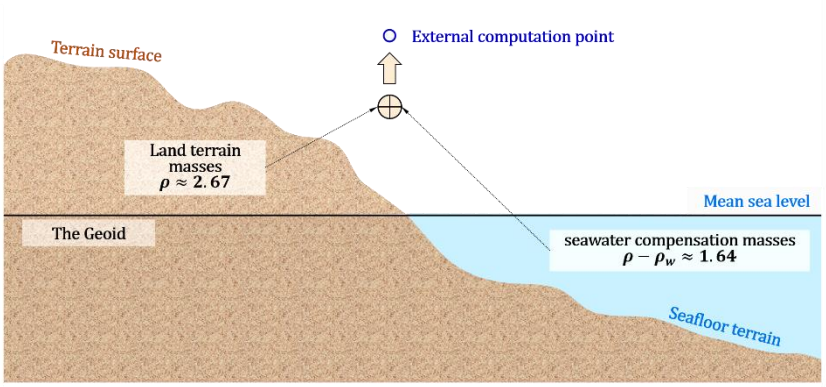

Figure 7.4: Fundamental Principle of Unified Land-Sea Complete Bouguer Effect

Neglecting atmospheric mass, the disturbing potential T at an external point is decomposed as:

$$T = T^{NT} + T^t = T^{NT} + T^B + T^R \tag{5.1}$$

where:

T^t: Gravitational potential of all topographic masses (Complete Bouguer Effect).

T^B: Potential of the spherical shell masses with thickness equal to the topographic elevation (Spherical Shell Bouguer Effect).

T^R : Potential of local topographic masses (Local Terrain Effect).

T^{NT} : Disturbing potential after removing topographic masses (Land Complete Bouguer Disturbing Potential).

Given that T is harmonic in external space, T^B, T^R, and T^t are likewise harmonic. Under the spherical approximation, the complete Bouguer effect on the disturbing potential in near-Earth space ($r \geq R + h$) can be expanded by h/R as:

$$T^t = T^B + T^R = 4\pi G\rho_0 \frac{R^2 h}{r}\left(1 + \frac{h}{R} + \frac{h^2}{3R^2}\right) + T^R \tag{5.2}$$

where: h is the terrain elevation directly beneath the external computation point, r is the geocentric distance of the computation point, and $\rho_0 = 2.67\times10^3 \mathrm{kg/m^3}$ is the mean topography density from the ground to the geoid.

Similarly, the gravity disturbance δg decomposes as:

$$\delta g = -\frac{\partial T^{NT}}{\partial r} - \frac{\partial T^t}{\partial r} = \delta g^{NT} + \delta g^t = \delta g^{NT} + \delta g^B + \delta g^R \tag{5.3}$$

where:

δg^t: Gravity (disturbance) of all topographic masses (Complete Bouguer Effect).

δg^B: Gravity (disturbance) of the spherical shell masses with thickness equal to the terrain elevation (Spherical Shell Bouguer Effect).

δg^R Gravity (disturbance) of local topographic masses (Local Terrain Effect).

δg^{NT}: Gravity disturbance removing topographic masses (Land Complete Bouguer gravity disturbance).

Under spherical approximation, the complete Bouguer effect on gravity disturbance is:

$$\delta g^t = \delta g^B + \delta g^R = 4\pi G\rho_0 \frac{R^2 h}{r^2}\left(1 + \frac{h}{R} + \frac{h^2}{3R^2}\right) + \delta g^R \tag{5.4}$$

Note: Eqs. (5.2) and (5.4) are truncated at the second order of h/R, making them suitable for terrestrial and airborne applications but insufficient for satellite altitudes.

7.5.2 Integral Algorithms for Local Terrain Effects in External Space

(1) Rigorous Integral Formulation

Assuming a constant terrain density $= \rho_0$, the rigorous integral expression for the local terrain effect on the disturbing potential is:

$$T^R = \gamma\zeta^R = G\rho \iint_s \int_{R+h}^{R+h'} L^{-1}(r, \psi, r')\, dr'\, ds \tag{5.5}$$

where $ds = r'^2 cos\varphi' d\varphi' d\lambda'$ is the integration area element, r' is the geocentric distance of the integration area element (the moving point), and $L = \sqrt{r^2 + r'^2 - 2rr' cos\psi}$ is the Euclidean distance between the computation point and the volume element $dV = dr'ds$. The inner integral yields:

$$\int L^{-1}(r, \psi, r')\, dr' = ln(r' - rt + L) + C \tag{5.6}$$

where $t = cos\psi$ and C is the integration constant.

Singularity Handling: When the computation point coincides with the integration moving point, the integral becomes singular. The singular value is:

$$T^R|_0 = \frac{1}{6} G\rho A_0 \sqrt{A_0/\pi}\left(h_{xx} + h_{yy}\right) \tag{5.7}$$

where A_0 is the area of the integration area element at the computation point; h_{xx}, h_{yy} are the second-order horizontal partial derivatives of the terrain elevation at the computation point in the north (x) and east (y) directions, respectively.

The rigorous integral for the local terrain effect on gravity disturbance is:

$$\delta g^R = -T_r^R = -\frac{\partial T^R}{\partial r} = -G\rho \iint_s \int_{R+h}^{R+h'} \frac{\partial L^{-1}(r,\psi,r')}{\partial r} dr' ds \tag{5.8}$$

with the inner integral:

$$\int \frac{\partial L^{-1}(r,\psi,r')}{\partial r} dr' = -\int \frac{r - r't}{L^3} dr' = -\frac{r'}{rL} + C \tag{5.9}$$

The singular value for the effect on gravity disturbance is:

$$\delta g^R|_0 = \frac{1}{2} G\rho \sqrt{\pi A_0}\left(h_x^2 + h_y^2\right) \tag{5.10}$$

where $\left(h_x, h_y\right)$ is the terrain slope vector at the computation point.

Vertical Deflections: Using spherical trigonometry relations for $\partial\psi/\partial\varphi = -cos\alpha$ and $\partial\psi/\partial\lambda = -cos\varphi sin\alpha$, the local terrain effect on vertical deflection vector (ξ^R, η^R) are:

$$\begin{aligned} \xi^R &= -\frac{\partial T^R}{\gamma r \partial\varphi} = -\frac{\partial T^R}{\gamma r \partial\psi}\frac{\partial\psi}{\partial\varphi} = \frac{\partial T^R}{\gamma r \partial\psi} cos\alpha \\ &= \frac{G\rho}{\gamma r} \iint_s \int_{R+h}^{R+h'} \frac{\partial L^{-1}(r,\psi,r')}{\partial\psi} dr' cos\alpha ds \\ \eta^R &= -\frac{\partial T^R}{\gamma r cos\varphi \partial\lambda} = -\frac{\partial T^R}{\gamma r cos\varphi \partial\psi}\frac{\partial\psi}{\partial\lambda} = \frac{\partial T^R}{\gamma r cos\varphi \partial\psi} cos\varphi sin\alpha \end{aligned} \tag{5.11}$$

$$= \frac{G\rho}{\gamma r} \iint_S \int_{R+h}^{R+h'} \frac{\partial L^{-1}(r,\psi,r')}{\partial \psi} dr' sin\alpha ds \tag{5.12}$$

where α is the geodetic azimuth of ψ, and

$$\int \frac{\partial L^{-1}(r,\psi,r')}{\partial \psi} dr' = \frac{r - r't}{L sin\psi} + C \tag{5.13}$$

From spherical trigonometry formulas:

$$sin\psi cos\alpha = cos\varphi sin\varphi' - sin\varphi cos\varphi' cos(\lambda' - \lambda) \tag{5.14}$$

$$sin\psi sin\alpha = cos\varphi' sin(\lambda' - \lambda) \tag{5.15}$$

Gravity Gradients: The radial component T_{rr}^R is given by:

$$T_{rr}^R = \frac{\partial^2}{\partial r^2} T^R = G\rho \iint_S \int_{R+h}^{R+h'} \frac{\partial^2 L^{-1}(r,\psi,r')}{\partial r^2} dr'\, ds \tag{5.16}$$

with the inner integral:

$$\int \frac{\partial^2 L^{-1}(r,\psi,r')}{\partial r^2} dr' = \int \left[-\frac{1}{L^3} + \frac{3(r - r't)^2}{L^5} \right] dr' = \frac{r'}{r^2 L} + \frac{r'(r - r't)}{r L^3} + C \tag{5.17}$$

Similarly, The tangential components (T_{nn}^R, T_{ww}^R) are derived via chain rules involving second derivatives with respect to ψ.

$$T_{nn}^R = \frac{1}{r^2} T_{\varphi\varphi}^R \tag{5.18}$$

$$T_{ww}^R = -\frac{1}{r^2 cos^2\varphi} T_{\lambda\lambda}^R \tag{5.19}$$

where,

$$T_{\varphi\varphi}^R = \frac{\partial^2 T^R}{\partial \psi^2} \frac{\partial^2 \psi}{\partial \varphi^2}, \quad T_{\lambda\lambda}^R = \frac{\partial^2 T^R}{\partial \psi^2} \frac{\partial^2 \psi}{\partial \lambda^2} \tag{5.20}$$

Taking the partial derivative of both sides of Eq. 5.14 with respect to φ:

$$-cos\psi cos^2\alpha + sin\psi \frac{\partial^2 \psi}{\partial \varphi^2} = -\sin\varphi sin\varphi' - cos\varphi cos\varphi' cos(\lambda' - \lambda) \tag{5.21}$$

Thus,

$$sin\psi \frac{\partial^2 \psi}{\partial \varphi^2} = -\sin\varphi sin\varphi' - cos\varphi cos\varphi' cos(\lambda' - \lambda) + cos\psi cos^2\alpha \tag{5.22}$$

Taking the partial derivative of both sides of Eq. 5.15 with respect to λ:

$$-cos\psi cos\varphi sin^2\alpha + sin\psi \frac{\partial^2 \psi}{\partial \lambda^2} = -cos\varphi' sin(\lambda' - \lambda) \tag{5.23}$$

Thus,

$$sin\psi \frac{\partial^2 \psi}{\partial \lambda^2} = -cos\varphi' sin(\lambda' - \lambda) + cos\psi cos\varphi sin^2\alpha \tag{5.24}$$

Taking the second partial derivative of both sides of the integral expression for the local terrain effect on the disturbing potential Eq. 5.5 with respect to the spherical angle distance ψ:

$$\frac{\partial^2 T^R}{\partial \psi^2} = G\rho \iint_S \int_{R+h}^{R+h'} \frac{\partial^2}{\partial \psi^2} \frac{1}{L} dr' ds =$$

$$G\rho \iint_S \int_{R+h}^{R+h'} \frac{\partial^2}{\partial \psi^2} \frac{1}{\sqrt{r^2 + r'^2 - 2rr' cos\psi}} dr' ds \tag{5.25}$$

where:

$$\int \frac{\partial^2}{\partial \psi^2} \frac{1}{L} dr' = \frac{r'(6r^2 + 4r'^2 + 6r^2 cos2\psi - rr' cos3\psi) - rt(4r^2 + 11r'^2)}{4L^3 sin^2\psi} \tag{5.26}$$

Physical Remarks:

- The topographic mass effect on gravity disturbance equals the effect on gravity itself.

● In high-altitude regions, local terrain effects on gravity can be positive or negative.

● These effects are non-zero in coastal zones but vanish in the deep ocean.

(2) Fast Algorithm for Local Terrain Effect Integrals

A Local Horizontal Polar Coordinate System is established with the z-axis directed toward the zenith and the origin O located on the terrain surface directly beneath the computation point. At the origin, $z = 0$. Let $\tilde{h}$ denote the elevation of the computation point relative to the underlying terrain surface O. In this local coordinate system, $dz = dr'$ and $d\tilde{h} = dr$, as illustrated in Figure 7.5. The rigorous integral for the local terrain effect on the disturbing potential Eq. (5.5) transforms into:

$$T^R = G\rho \iint_s \int_0^{\Delta h} \frac{dz}{L} ds = G\rho \iint_s \int_0^{\Delta h} \frac{dz}{\sqrt{(\tilde{h}-z)^2+l^2}} ds$$

$$= G\rho \iint_s \left[ln \frac{\sqrt{(\tilde{h}-\Delta h)^2+l^2}-\tilde{h}+\Delta h}{\sqrt{(\tilde{h}-\Delta h)^2+l^2}+\tilde{h}-\Delta h} - ln \frac{\sqrt{\tilde{h}^2+l^2}-H}{\sqrt{\tilde{h}^2+l^2}+H} \right] ds \quad (5.27)$$

where:

Δh: Height difference of the integration area element ds relative to the terrain surface O directly beneath the computation point.

l: Planar distance from the area element ds to point O on the equielevation surface passing through O.

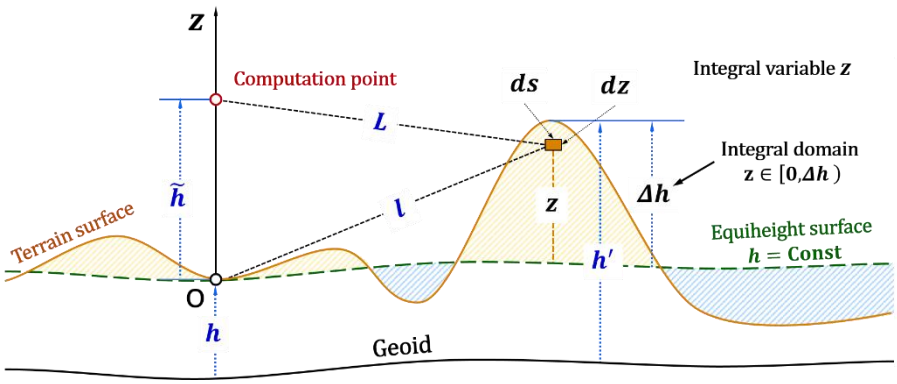

Figure 7.5: Geometric relationships of elements in the rigorous integral for local terrain effects within the local polar coordinate system.

Since the rigor of gravity field integrals depends solely on the accurate calculation of the area element and its spatial distance to the computation point, Eq. (5.27) is mathematically equivalent to Eq. (5.5) and constitutes a rigorous formulation. Expanding the integrand of Eq. (5.27) in a Taylor series around $z = 0$ up to the third order yields:

$$T^R = G\rho \iint_s \left[\frac{1}{\mathcal{L}} \Delta h + \frac{\tilde{h}}{2\mathcal{L}^3} \Delta h^2 + \frac{2\tilde{h}^2-l^2}{6\mathcal{L}^5} \Delta h^3 \right] ds \quad (5.28)$$

Here, $\mathcal{L} = \sqrt{\tilde{h}^2 + l^2}$ represents the spatial distance from the surface element ds (at $z = 0$) to the external computation point. Note that this $\mathcal{L}$ differs from the distance involving the volume element $dzds$.

By substituting the binomial expansions $\Delta h^k = (h' - h)^k$ (where h' is the terrain elevation at ds and h is the elevation at O), each term inside the integral assumes a

convolution form dependent only on the integration variable l (embedded in $\mathcal{L}$) and the terrain elevations. Consequently, the Fast Fourier Transform (FFT) algorithm can be applied term-by-term for rapid computation.

Similarly, the rigorous integral for the local terrain effect on the gravity disturbance (Eq. 5.8) becomes:

$$\delta g^R = \frac{G\rho}{r}\iint_S \left[\frac{(r_0+z)}{\sqrt{(\tilde{h}-z)^2+l^2}}\right]_0^{\Delta h} ds = \frac{G\rho}{r}\iint_S \left[\frac{r_0+\Delta h}{\sqrt{(\tilde{h}-\Delta h)^2+l^2}} - \frac{r_0}{\mathcal{L}}\right] ds \tag{5.29}$$

Expanding the integrand around $z = 0$ up to the fourth order:

$$\delta g^R = \frac{G\rho}{r}\iint_S \left[\begin{array}{c} \frac{r\tilde{h}+\mathcal{L}^2}{\mathcal{L}^3}\Delta h + \frac{2\tilde{h}\mathcal{L}^2+r_0(2\tilde{h}^2-l^2)}{2\mathcal{L}^5}\Delta h^2 + \frac{2\tilde{h}^3 r+\tilde{h}^2 l^2-3r_0\tilde{h}l^2-l^4}{2\mathcal{L}^7} \\ \Delta h^3 + \frac{8r\tilde{h}^4-4\tilde{h}^3 l^2-12\tilde{h}l^4-24r_0\tilde{h}^2 l^2+3l^4 r_0}{8\mathcal{L}^9}\Delta h^4 \end{array}\right] ds \tag{5.30}$$

Equation (5.30) is also amenable to FFT acceleration after expansion.

For the vertical deflection, expanding the integrand up to the third order yields the kernel:

$$-\frac{r^2 sin\psi}{\mathcal{L}^3}\Delta h - \frac{3\tilde{h}r^2 sin\psi}{2\mathcal{L}^5}\Delta h^2 - \left[\frac{r^2 sin\psi}{3\mathcal{L}^5} + \frac{5r^2 sin\psi(2\tilde{h}^2-l^2)}{6\mathcal{L}^7}\right]\Delta h^3 \tag{5.31}$$

Substituting Eq. (5.31) into Eqs. (5.11) and (5.12) enables fast FFT-based computation of the local terrain effect on vertical deflections.

For the disturbing gravity gradient (T_{rr}^R), the equivalent rigorous integral is:

$$T_{rr}^R = G\rho\iint_S \left[\frac{\tilde{h}-\Delta h}{((\tilde{h}-\Delta h)^2+l^2)^{3/2}} - \frac{\tilde{h}}{\mathcal{L}^3}\right] ds \tag{5.32}$$

Expanding up to the third order:

$$T_{rr}^R = G\rho\iint_S \left[\begin{array}{c} \frac{2\tilde{h}^2-l^2}{\mathcal{L}^5}\Delta h - \frac{3\tilde{h}(2\tilde{h}^2-3l^2)}{2\mathcal{L}^7}\Delta h^2 + \\ \frac{4\tilde{h}^4+6r^4-12\tilde{h}^2 l^2-(6r^4+3r^2 l^2)cos\psi}{\mathcal{L}^9}\Delta h^3 \end{array}\right] ds \tag{5.33}$$

The integrand in the rigorous integral expression for the local terrain effect on the tangential gravity gradient (Equation 5.25) is equivalent to:

$$\begin{aligned} \int_{R+h}^{R+h'} \frac{\partial^2}{\partial\psi^2}\frac{1}{L}dr' &= \int_0^{\Delta h} \frac{\partial^2}{\partial\psi^2}\frac{1}{\sqrt{(\tilde{h}-z)^2+4r_0^2 sin^2(\psi/2)}}dz \\ &= \frac{1}{8sin^2\frac{\psi}{2}}\left[\frac{\tilde{h}(2\mathcal{L}^2+r_0^2 sin^2\psi)}{\mathcal{L}^3} - \frac{(\tilde{h}-\Delta h)(2\mathcal{L}^2+r_0^2 sin^2\psi-4\tilde{h}\Delta h+2\Delta h^2)}{(\mathcal{L}^2-2\tilde{h}\Delta h+\Delta h^2)^{3/2}}\right] \end{aligned} \tag{5.34}$$

Expanding around $z = 0$ up to the third order yields:

$$\begin{aligned} \int_{R+h}^{R+h'} \frac{\partial^2}{\partial\psi^2}\frac{1}{L}dr' &= -\frac{2(\tilde{h}^2+2r_0^2)cos\psi+r_0^2(-5+cos2\psi)}{2L^5}r_0^2\Delta h \\ &+ \frac{6(\tilde{h}^2+2r_0^2)cos\psi+3r_0^2(-7+3cos2\psi)}{4\mathcal{L}^7}\tilde{h}r_0^2\Delta h^2 \\ &+ \frac{(8\tilde{h}^4+12\tilde{h}^2 r_0^2-19r_0^4)cos\psi-r_0^2(36\tilde{h}^2-18r_0^2-(24\tilde{h}^2-2r_0^2)cos2\psi+3r_0^2 cos3\psi)}{4\mathcal{L}^9}r_0^2\Delta h^3 \end{aligned} \tag{5.35}$$

If the computation point lies on the terrain surface ($\tilde{h} = 0$, $\mathcal{L} = l$), Eqs. (5.27) – (5.35) simplify significantly.

7.5.3 Integral Algorithm for Land-Sea Complete Bouguer Effects outside the Geoid

In oceanic regions, the topographic gravitational field is modeled as the Seawater Complete Bouguer Effect, defined as the effect resulting from compensating the seawater

density (ρ_w) to the land topographic density (ρ).

The rigorous integral for the Seawater Complete Bouguer Effect on the disturbing potential is:

$$T^o = G\beta \iint_s \int_{R+d}^{R} L^{-1}(r,\psi,r')\, dr'\, ds \tag{5.36}$$

where:

$d < 0$: Bathymetry (sea depth) relative to mean sea level.

$\beta = \rho - \rho_w$ =1.64×10³kg/m³: Seawater compensation density.

L : Spatial distance from the seawater volume element to the computation point.

Using the local horizontal polar coordinate system (z -axis points toward the zenith, $z = 0$ at sea surface), Eq. (5.36) becomes:

$$T^o = G\beta \iint_s \int_d^0 \frac{dz}{L} ds = G\beta \iint_s \int_d^0 \frac{dz}{\sqrt{(\tilde{h}-z)^2+l^2}} ds$$

$$= G\beta \iint_s \left[ln \frac{\sqrt{\tilde{h}^2+l^2}-\tilde{h}}{\sqrt{\tilde{h}^2+l^2}+\tilde{h}} - ln \frac{\sqrt{(\tilde{h}-d)^2+l^2}-\tilde{h}+d}{\sqrt{(\tilde{h}-d)^2+l^2}+\tilde{h}-d} \right] ds \tag{5.37}$$

where $l = 2r_0 \sin(\psi/2)$ is the planar distance on the sea surface, $\tilde{h}$ is the computation point's altitude, and r_0 is the mean geocentric distance of the sea surface.

Similarly, the rigorous integral expression for the seawater complete Bouguer effect on on the gravity disturbance is:

$$\delta g^o = -\frac{\partial T^o}{\partial r} = -G\beta \iint_s \int_{R+d}^{R} \frac{\partial L^{-1}(r,\psi,r')}{\partial r} dr'\, ds \tag{5.38}$$

which is equivalent to:

$$\delta g^o = \frac{G}{r} \iint_s \beta \int_d^0 \frac{(r_0+z)dz}{\sqrt{(\tilde{h}-z)^2+l^2}} ds = \frac{G\beta}{r} \iint_s \left[\frac{r_0}{\mathcal{L}} - \frac{r_0+d}{\sqrt{(\tilde{h}-d)^2+l^2}} \right] ds \tag{5.39}$$

The rigorous integral expressions for the seawater complete Bouguer effect on the vertical deflection are:

$$\xi^o = \frac{T_\theta^o}{\gamma r} = \frac{G\beta}{\gamma r} \iint_s \int_{R+d}^{R} \frac{\partial L^{-1}(r,\psi,r')}{\partial \psi} dr' cos\alpha ds \tag{5.40}$$

$$\eta^o = -\frac{T_\lambda^o}{\gamma r sin\theta} = \frac{G\beta}{\gamma r} \iint_s \int_{R+d}^{R} \frac{\partial L^{-1}(r,\psi,r')}{\partial \psi} dr' sin\alpha ds \tag{5.41}$$

The rigorous integral expression for the complete Bouguer effect of seawater on the disturbing gravity gradient is:

$$T_{rr}^o = \frac{\partial^2}{\partial r^2} T^o = G\beta \iint_s \int_{R+d}^{R} \frac{\partial^2 L^{-1}(r,\psi,r')}{\partial r^2} dr'\, ds \tag{5.42}$$

which is equivalent to:

$$T_{rr}^o = G\beta \iint_s \left[\frac{\tilde{h}-d}{((\tilde{h}-d)^2+l^2)^{3/2}} - \frac{h}{\mathcal{L}^3} \right] ds \tag{5.43}$$

FFT Acceleration:

By expanding the integrands of Eqs. (5.37), (5.39), (5.40 – 41), and (5.43) in Taylor series around the sea surface ($z = 0$), we obtain convolution forms suitable for FFT. For example, the expansion for T^o up to the third order is:

$$T^o = G\beta \int_d^0 \frac{1}{L} dz ds = G\beta \iint_s \left(\frac{1}{\mathcal{L}} d + \frac{\tilde{h}}{2\mathcal{L}^3} d^2 + \frac{2\tilde{h}^2-l^2}{6\mathcal{L}^5} d^3 \right) ds \tag{5.44}$$

Similar expansions for δg^0 (4th order), vertical deflections (3rd order), and T_{rr}^o (3rd order) are provided in Eqs. (5.45) – (5.47). All expanded terms can be computed efficiently using the FFT algorithm.

$$\delta g^0 = \frac{G}{r}\iint_S \beta \left[\begin{matrix} \frac{r\tilde{h}+\mathcal{L}^2}{\mathcal{L}^3}d + \frac{2\tilde{h}\mathcal{L}^2+r_0(\tilde{h}^2+\mathcal{L}^2)}{2\mathcal{L}^5}d^2 + \frac{2\tilde{h}^3 r+\tilde{h}^2 l^2-3r_0\tilde{h}l^2-l^4}{2\mathcal{L}^7} \\ d^3 + \frac{8r\tilde{h}^4-4\tilde{h}^3 l^2-12\tilde{h}l^4-24r_0\tilde{h}^2 l^2+3l^4 r_0}{8\mathcal{L}^9}d^4 \end{matrix}\right] ds \tag{5.45}$$

$$\int_{R+d}^{R} \frac{\partial L^{-1}(r,\psi,r')}{\partial \psi}dr' = -\frac{r^2 sin\psi}{\mathcal{L}^3}d - \frac{3\tilde{h}r^2 sin\psi}{2\mathcal{L}^5}d^2 - \left[\frac{r^2 sin\psi}{3\mathcal{L}^5} + \frac{5r^2 sin\psi(2\tilde{h}^2-l^2)}{6\mathcal{L}^7}\right]d^3 \tag{5.46}$$

$$T_{rr}^o = -\frac{\partial \delta g^o}{\partial r} = G\beta\iint_S \left[\begin{matrix} \frac{2\tilde{h}^2-l^2}{\mathcal{L}^5}d + \frac{3\tilde{h}(2\tilde{h}^2-3l^2)}{2\mathcal{L}^7}d^2 + \\ \frac{4\tilde{h}^4+6r^4-12\tilde{h}^2 l^2-(6r^4+3r^2 l^2)cos\psi}{\mathcal{L}^9}d^3 \end{matrix}\right] ds \tag{5.47}$$

Simplification: If the computation point is on the sea surface ($h = 0$, $\mathcal{L} = l$), all equations simplify considerably.

Magnitude and Computational Strategy for Seawater Complete Bouguer Effects

The magnitude of the Seawater Complete Bouguer Effect on various external gravity field elements is substantial. In practical computations, a sufficiently large integration radius (e.g., ≥250 km) is required to capture these effects accurately. Coastal land areas are influenced by the seawater Bouguer effect, while nearshore waters are affected by the local terrain effect of adjacent land masses. Consequently, the coastal transition zone is subject to both effects simultaneously.

Given the significant magnitude of Spherical Shell Bouguer Effects, approximating topographic reliefs solely via third-order Taylor expansions can introduce errors exceeding the gravity disturbance signal itself in certain regions. Therefore, it is strongly recommended that:

- The Complete Bouguer effect only on gravity may be computed using direct integral methods.
- The Complete Bouguer effects on all other gravity field elements (including gravity, if highest precision is required) should be computed using the Remove-Restore technique. This involves computing the Residual Terrain Effect (RTE) via rigorous integrals, using a global land-sea topographic mass model represented by spherical harmonic coefficients as the reference field.

7.5.4 Integral Algorithms for Residual Terrain Effects (RTE) outside the Geoid

The Land-Sea Residual Terrain Effect is defined as the short- and ultra-short-wavelength components of the Land-Sea Complete Bouguer Effect. The computational workflow involves:

- Constructing a Residual Terrain Model (RTM) by subtracting a low-pass filtered terrain grid from a high-resolution terrain grid (both with identical specifications).
- Computing the effects of this RTM on various field elements using rigorous integral formulas.

The integral formulations for RTE are formally identical to those for local terrain and seawater Bouguer effects, differing only in the density parameter (β') and the radial

integration limits defined by the residual elevation/ bathymetry (δ').

The RTE on the disturbing potential in external space is:

$$T^{\mathrm{rtm}} = G \iint_s \int_R^{R+\delta'} \beta' L^{-1}(r,\psi,r')\, dr'\, ds \tag{5.48}$$

where:

δ': Residual terrain elevation (land) or residual bathymetry (ocean). Note that δ' can be positive or negative.

β': Density parameter. That is topographic density ρ (land) or seawater compensation density $\beta' = \rho - \rho_w$ (ocean).

Similarly, the RTE on other field elements are:

● Gravity Disturbance:

$$\delta g^{\mathrm{rtm}} = -\frac{\partial T^{\mathrm{rtm}}}{\partial r} = -G \iint_s \beta' \int_R^{R+\delta'} \frac{\partial L^{-1}(r,\psi,r')}{\partial r} dr'\, ds \tag{5.49}$$

● Vertical Deflections:

$$\xi^{\mathrm{rtm}} = \frac{G}{\gamma r} \iint_s \beta' \int_R^{R+\delta'} \frac{\partial L^{-1}(r,\psi,r')}{\partial \psi} dr' cos\alpha ds \tag{5.50}$$

$$\eta^{\mathrm{rtm}} = \frac{G}{\gamma r} \iint_s \beta' \int_R^{R+\delta'} \frac{\partial L^{-1}(r,\psi,r')}{\partial \psi} dr' sin\alpha ds \tag{5.51}$$

● Radial Gravity Gradient:

$$T_{rr}^{\mathrm{rtm}} = \frac{\partial^2}{\partial r^2} T^{\mathrm{rtm}} = G \iint_s \beta' \int_R^{R+\delta'} \frac{\partial^2 L^{-1}(r,\psi,r')}{\partial r^2} dr'\, ds \tag{5.52}$$

Rigorous Integral Formulations within a Local Coordinate System:

Adopting a Local Horizontal Polar Coordinate System ($z = 0$ at the surface, z-axis to zenith), let $\mathcal{L} = \sqrt{\tilde{h}^2 + l^2}$ be the distance from the surface element to the computation point. The rigorous integrals can be rewritten in closed form:

● RTE on disturbing Potential:

$$T^{\mathrm{rtm}} = G \iint_s \beta' \int_0^{\delta'} \frac{dz}{\sqrt{(\tilde{h}-z)^2 + l^2}} ds$$

$$= G \iint_s \beta' \left[ln \frac{\sqrt{(\tilde{h}-\delta')^2 + l^2} - \tilde{h} + \delta'}{\mathcal{L} + \tilde{h} - \delta'} - ln \frac{\mathcal{L} - \tilde{h}}{\mathcal{L} + \tilde{h}} \right] ds \tag{5.53}$$

● RTE on Gravity Disturbance:

$$\delta g^{\mathrm{rtm}} = \frac{G}{r} \iint_s \beta' \iint_0^{\Delta h} \frac{\partial}{\partial \tilde{h}} \frac{dz}{\sqrt{(\tilde{h}-z)^2 + l^2}} ds = \frac{G}{r} \iint_s \beta' \left[\frac{1}{\sqrt{(\tilde{h}-\Delta h)^2 + l^2}} - \frac{1}{\mathcal{L}} \right] ds \tag{5.54}$$

● RTE on vertical deflection (Kernel expansion):

$$\int_R^{R+\delta'} \frac{\partial L^{-1}(r,\psi,r')}{\partial \psi} dr' = \frac{1}{2} ctg \frac{\psi}{2} \left[\frac{\tilde{h} - \delta'}{\sqrt{(\tilde{h}-\delta')^2 + l^2}} - \frac{\tilde{h}}{\mathcal{L}} \right] \tag{5.55}$$

● RTE on Radial Gravity Gradient:

$$T_{rr}^{\mathrm{rtm}} = G \iint_s \beta' \left[\frac{\tilde{h} - \delta'}{((\tilde{h}-\delta')^2 + l^2)^{3/2}} - \frac{\tilde{h}}{\mathcal{L}^3} \right] ds \tag{5.56}$$

Fast Computation via Taylor Expansion:

Expanded in a Taylor series around $z = 0$ to derive convolution forms suitable for FFT

acceleration:

To enable fast computation, the integrands in the above rigorous integral expressions are expanded around $z = 0$, which here represents the land terrain / sea surface. Expanding the integrand in Equation (5.53) around $z = 0$ yields:

● Disturbing Potential (3rd order):

$$T^{\mathrm{rtm}} = -G \iint_s \beta' \left(\frac{1}{\mathcal{L}}\delta' + \frac{\tilde{h}}{2\mathcal{L}^3}\delta'^2 + \frac{2\tilde{h}^2 - l^2}{6\mathcal{L}^5}\delta'^3\right) ds \tag{5.57}$$

● Gravity Disturbance (4th order):

$$\delta g^{\mathrm{rtm}} = \frac{G}{r} \iint_s \beta' \left[\frac{\tilde{h}}{\mathcal{L}^3}\delta' + \frac{2\tilde{h}^2 - l^2}{2\mathcal{L}^5}\delta'^2 + \frac{\tilde{h}(2\tilde{h}^2 - 3l^2)}{2\mathcal{L}^7}\delta'^3 + \frac{8\tilde{h}^4 - 24\tilde{h}^2 l^2 + 3l^4}{8\mathcal{L}^9}\delta'^4\right] ds \tag{5.58}$$

● Vertical Deflections (Kernel expansion, 3rd order):

$$\int_R^{R+\delta'} \frac{\partial L^{-1}(r,\psi,r')}{\partial \psi} dr' = -\frac{r^2 sin\psi}{\mathcal{L}^3}\delta' - \frac{3\tilde{h}r^2 sin\psi}{2\mathcal{L}^5}\delta'^2 - \left[\frac{r^2 sin\psi}{3\mathcal{L}^5} + \frac{5r^2 sin\psi(2\tilde{h}^2 - l^2)}{6\mathcal{L}^7}\right]\delta'^3 \tag{5.59}$$

● Radial Gravity Gradient (4th order):

$$T_{rr}^{\mathrm{rtm}} = G \iint_s \beta' \left[\frac{2\tilde{h}^2 - l^2}{\mathcal{L}^5}\delta' + \frac{3\tilde{h}(2\tilde{h}^2 - 3l^2)}{2\mathcal{L}^7}\delta'^2 + \frac{8\tilde{h}^4 - 24\tilde{h}^2 l^2 + 3l^4}{2\mathcal{L}^9}\delta'^3\right] ds \tag{5.60}$$

These expanded terms depend only on the residual elevation powers (δ'^k) and the geometric kernel ($\mathcal{L}$, l , $\tilde{h}$), allowing for efficient evaluation using the Fast Fourier Transform (FFT) algorithm.

7.6 Local Terrain Compensation and Terrain Helmert Condensation

7.6.1 Effects of Terrain Helmert Condensation on Gravity Field elements

The Helmert condensation of topographic masses is based on the concept of topographic mass compensation (referred to henceforth as terrain compensation). For any gravity field element defined on or outside the geoid, terrain compensation is defined as the mass adjustment applied to counteract the gravitational field changes induced by the removal of topographic masses.

The process of Terrain Helmert Condensation comprises two distinct steps:

● Removal: Subtract the gravitational field generated by the actual topographic masses (i.e., subtract the Land Complete Bouguer Effect).

● Compensation: Add the gravitational field generated by the condensed mass layer to compensate for the removal (i.e., add the Terrain Compensation).

The net change in any external gravity field element α due to this process is termed the Terrain Helmert Condensation Effect, expressed uniformly as:

$$\alpha^h = \alpha^t - \alpha^c \tag{6.1}$$

where:

α^h: Terrain Helmert condensation effect on α.

α^t: Land Complete Bouguer effect on α.

α^c: Terrain compensation effect on α.

Unlike local terrain or complete Bouguer effects, Helmert condensation preserves the

total topographic masses. Consequently, the vertical component of the Helmert condensation effect is generally significantly smaller than both the complete Bouguer effect and the local terrain effect.

The space external to the geoid after this transformation is referred to as Helmert Space, and the resulting field is the Helmert Gravity Field. This field differs from the actual Earth's gravity field solely by the harmonic field change induced by the condensation. Notably, the terrain Helmert condensation effect retains the harmonic property in external space.

7.6.2 Algorithms for Terrain Compensation and Helmert Condensation Effects

This section introduces the algorithms for computing terrain compensation on various gravity field elements at arbitrary altitudes within the near-Earth harmonic space.

● Disturbing Potential:

The terrain compensation effect on the external disturbing potential is defined as:

$$T^c = T^B + T^{cR} = T^B + G\iint_S \frac{\mu' - \mu}{L} ds \tag{6.2}$$

where:

T^{cR}: Local Terrain Compensation on the disturbing potential.

ds: Moving area element on the terrain surface.

μ: Topographic mass compensation density. Under spherical approximation:

$$\mu = \rho h\left(1 + \frac{h}{R} + \frac{h^2}{3R^2}\right) \tag{6.3}$$

where h is the ground elevation directly beneath the computation point, and ρ is the topographic density.

By approximating the geocentric distances with mean values for the computaion surface and terrain surfaces, the integral term in Eq. (6.2) can be computed efficiently using the Fast Fourier Transform (FFT) algorithm.

Singularity Handling: When the computation point coincides with the integration moving point, T^{cR} becomes singular. The analytical value of this singular integral is:

$$T^{cR}|_0 = \frac{R^2}{6\bar{r}^2} G A_0 \sqrt{A_0/\pi}\left(\mu_{xx} + \mu_{yy}\right) \tag{6.4}$$

where μ_{xx}, μ_{yy} are the second-order partial derivatives of the topographic mass compensation density at the computation point in the north (x) and east (y) directions, respectively.

● Gravity Disturbance:

Substituting Eq. (6.2) into the definition of gravity disturbance yields:

$$\delta g^c = \delta g^B + \delta g^{cR} = \delta g^B + G\iint_S (\mu' - \mu)\frac{r - r't}{L^3} ds \tag{6.5}$$

where δg^{cR} is the local terrain compensation effect on the gravity disturbance. Its singular value is:

$$\delta g^{cR}|_0 = \frac{R^2}{12\bar{r}^3} G A_0 \sqrt{A_0/\pi}\left(\mu_{xx} + \mu_{yy}\right) \tag{6.6}$$

● General Formulation:

Combining Eqs. (6.2) and (6.5), the Terrain Helmert Condensation effect for any field element α simplifies to:

$$\alpha^h = \alpha^t - \alpha^c = (\alpha^B + \alpha^R) - (\alpha^B + \alpha^{cR}) = \alpha^R - \alpha^{cR} \tag{6.7}$$

Under spherical approximation, the Spherical Shell Bouguer effect (α^B) cancels out. Thus, the Helmert condensation effect is simply the difference between the Local Terrain Effect (α^R) and the Local Terrain Compensation (α^{cR}).

● FFT Implementation Details:

Adopting a Local Horizontal Polar Coordinate System (z-axis to zenith, $dr = d\tilde{h}$), the local terrain compensation on gravity disturbance can be expanded into convolution terms suitable for FFT:

$$\begin{aligned}\delta g^{cR} = -G\iint_s (\mu' - \mu)\frac{\partial}{\partial \tilde{h}}\frac{1}{L}ds &= G\iint_s (\mu' - \mu)\frac{\tilde{h}}{L^3} - \frac{\mu' - \mu}{L^3}(h' - h)ds \\ &= G\iint_s (\mu' - \mu)\frac{\tilde{h}}{L^3}ds - G\iint_s \frac{\mu' h'}{L^3}\frac{t}{L}ds \\ &+ G\iint_s \frac{\mu' h}{L^3}ds + G\iint_s \frac{\mu h'}{L^3}ds - G\iint_s \frac{\mu h}{L^3}ds\end{aligned} \tag{6.8}$$

Note: Eq. 6.8 decomposes the integrand into separate convolutions of compensation densities and geometric kernels, all computable via FFT.

Similarly, using the relation:

$$\frac{\partial L^{-1}(r,\psi,r')}{\partial \psi} = \frac{rr' sin\psi}{L^3},\quad \frac{\partial \psi}{\partial \varphi} = -cos\alpha,\quad \frac{\partial \psi}{\partial \lambda} = -cos\varphi sin\alpha \tag{6.9}$$

the FFT formulas for Vertical Deflections are:

$$\begin{aligned}\xi^{cR} = -\frac{\partial T^{cR}}{\gamma r \partial \varphi} = -\frac{\partial T^{cR}}{\gamma r \partial \psi}\frac{\partial \psi}{\partial \varphi} = \frac{\partial T^{cR}}{\gamma r \partial \psi}cos\alpha &= \frac{G}{\gamma r}\iint_s (\mu' - \mu)\frac{\partial L^{-1}(r,\psi,r')}{\partial \psi}cos\alpha ds \\ &= \frac{G}{\gamma}\int_s (\mu' - \mu)\frac{r' sin\psi}{L^3}cos\alpha ds\end{aligned} \tag{6.10}$$

$$\begin{aligned}\eta^{cR} = -\frac{\partial T^{cR}}{\gamma r cos\varphi \partial \psi}\frac{\partial \psi}{\partial \lambda} = \frac{\partial T^{cR}}{\gamma r \partial \psi}sin\alpha &= \frac{G}{\gamma r}\iint_s \frac{\partial L^{-1}(r,\psi,r')}{\partial \psi}(\mu' - \mu)sin\alpha ds \\ &= \frac{G}{\gamma}\iint_s (\mu' - \mu)\frac{r' sin\psi}{L^3}sin\alpha ds\end{aligned} \tag{6.11}$$

And for the Radial Gravity Gradient:

$$\begin{aligned}T_{rr}^{cR} = \frac{\partial^2}{\partial r^2}T^{cR} = G\iint_s (\mu' - \mu)\frac{\partial^2}{\partial r^2}\left(\frac{1}{L}\right)ds \\ = G\iint_s (\mu' - \mu)\left(3\frac{r - r' cos\psi}{L^5} - \frac{1}{L^3}\right)ds\end{aligned} \tag{6.12}$$

Equations (6.10) through (6.12) provide the rigorous kernel functions required for FFT-based computation of local terrain compensation effects on vertical deflections and gravity gradients.

7.7 Spherical Harmonic Analysis and Synthesis of Land-Sea Terrain Masses

The terrain surface density $q(\theta, \lambda)$ at any point P(θ, λ, R) on the land or sea surface can be expanded in terms of normalized spherical harmonic coefficients as:

$$q(\theta, \lambda) = \beta h = a\sum_{n=1}^{\infty}\sum_{m=0}^{n}[A_{nm}cosm\lambda + B_{nm}sinm\lambda]\,\bar{P}_{nm}(cos\theta) \tag{7.1}$$

where:

a: Semi-major axis of the Earth's ellipsoid (used for consistency with global geopotential model).

A_{nm}, B_{nm}: Normalized spherical harmonic coefficients of the topographic mass of degree n and order m.

$\bar{P}_{nm}$: Fully normalized associated Legendre functions.

Parameters:

○ On land: $h > 0$ is the terrain elevation, and $\beta = \rho = 2.67\times10^3$kg/m^3 is the topographic density.

○ On sea: $h <$ is the bathymetry, and $\beta = \rho - \rho_w = 1.64\times10^3$kg/m^3 is the seawater compensation density.

The Land-Sea Complete Bouguer Effect on the geopotential at an external point (θ, λ, r) is expressed via the global terrain mass spherical harmonic series:

$$V^{\mathrm{tbg}}(\theta,\lambda,r) = \frac{3GM}{r\rho_e}\sum_{n=1}^{\infty}\left(\frac{a}{r}\right)^n \sum_{m=0}^{n}(A_{nm}cosm\lambda + B_{nm}sinm\lambda)\bar{P}_{nm}(cos\theta) \tag{7.2}$$

where $\rho_e = 5.517\times10^3$kg/m^3 is the Earth's mean density.

The Residual Terrain Effect (RTE) on the geopotential is obtained by truncating the series at a minimum degree n_1:

$$V^{\mathrm{rtm}}(\theta,\lambda,r) = \frac{3GM}{r\rho_e}\sum_{n=n_1}^{\infty}\left(\frac{a}{r}\right)^n \sum_{m=0}^{n}(A_{nm}cosm\lambda + B_{nm}sinm\lambda)\bar{P}_{nm}(cos\theta) \tag{7.3}$$

The relationship between the normalized terrain mass coefficients (A_{nm}, B_{nm}) and the normalized terrain gravitational potential coefficients $(\bar{C}^{\mathrm{ter}}_{nm}, \bar{S}^{\mathrm{ter}}_{nm})$ is:

$$\bar{C}^{\mathrm{ter}}_{nm} = \frac{3}{\rho_e}\frac{1}{2n+1}A_{nm}, \quad \bar{S}^{\mathrm{ter}}_{nm} = \frac{3}{\rho_e}\frac{1}{2n+1}B_{nm} \tag{7.4}$$

These coefficients $\bar{C}^{\mathrm{ter}}_{nm}, \bar{S}^{\mathrm{ter}}_{nm}$ represent the Stokes coefficients of the geopotentials generated by the combined land topography and seawater compensation masses. They define the Land-Sea Complete Bouguer Field in the spectral domain.

By substituting Eq. (7.4) into the standard spherical harmonic expansions for anomalous gravity field elements, we derive the synthesis formulas for the Residual Terrain Effects on various gravity field elements in external space:

- Height Anomaly (ζ^{rtm}):

$$\zeta^{\mathrm{rtm}}(\theta,\lambda,r) = \frac{GM}{r\gamma}\frac{3}{\rho_e} \sum_{n=n_1}^{\infty}\left(\frac{a}{r}\right)^n \frac{1}{2n+1}\sum_{m=0}^{n}(A_{nm}cosm\lambda + B_{nm}sinm\lambda)\bar{P}_{nm}(cos\theta) \tag{7.5}$$

- Gravity (Anomaly/Disturbance) (g^{rtm}):

$$g^{\mathrm{rtm}}(\theta,\lambda,r) = \frac{GM}{r^2}\frac{3}{\rho_e}\sum_{n=n_1}^{\infty}\frac{n+1}{2n+1}\left(\frac{a}{r}\right)^n \sum_{m=0}^{n}(A_{nm}cosm\lambda + B_{nm}sinm\lambda)\bar{P}_{nm}(cos\theta) \tag{7.6}$$

- Vertical Deflections ($\xi^{\mathrm{rtm}}, \eta^{\mathrm{rtm}}$):

$$\xi^{\mathrm{rtm}}(\theta,\lambda,r) = \frac{GM}{r^2}\frac{3}{\gamma\rho_e}sin\,\theta\sum_{n=n_1}^{\infty}\frac{1}{2n+1}\left(\frac{a}{r}\right)^n \sum_{m=0}^{n}(A_{nm}cosm\lambda + B_{nm}sinm\lambda)\frac{\partial}{\partial\theta}\bar{P}_{nm}(cos\theta) \tag{7.7}$$

$$\eta^{\mathrm{rtm}}(\theta,\lambda,r) = \frac{GM}{r^2\,sin\,\theta}\frac{3}{\gamma\rho_e}\sum_{n=n_1}^{\infty}\frac{1}{2n+1}\left(\frac{a}{r}\right)^n \sum_{m=1}^{n}m(A_{nm}sinm\lambda - B_{nm}cosm\lambda)\bar{P}_{nm}(cos\theta) \tag{7.8}$$

- Radial Gravity Gradient (V^{rtm}_{rr}):

$$V^{\mathrm{rtm}}_{rr}(\theta,\lambda,r) = \frac{GM}{r^3}\frac{3}{\rho_e}\sum_{n=n_1}^{\infty}\frac{(n+1)(n+2)}{2n+1}\left(\frac{a}{r}\right)^n$$

$$\sum_{m=0}^{n}(A_{nm}cosm\lambda + B_{nm}sinm\lambda)\bar{P}_{nm}(cos\theta) \tag{7.9}$$

● Tangential Gravity Gradients ($V_{nn}^{\mathrm{rtm}}, V_{ww}^{\mathrm{rtm}}$):

$$V_{nn}^{\mathrm{rtm}}(\theta,\lambda,r) = -\frac{GM}{r^3}\frac{3}{\rho_e}\sum_{n=n_1}^{\infty}\frac{1}{2n+1}\left(\frac{a}{r}\right)^n \sum_{m=0}^{n}(A_{nm}cosm\lambda + B_{nm}sinm\lambda)\frac{\partial^2}{\partial\theta^2}\bar{P}_{nm}(cos\theta) \tag{7.10}$$

$$V_{ww}^{\mathrm{rtm}}(\theta,\lambda,r) = -\frac{GM}{r^3 sin^2\theta}\frac{3}{\rho_e}\sum_{n=n_1}^{\infty}\frac{1}{2n+1}\left(\frac{a}{r}\right)^n \sum_{m=1}^{n} m^2(A_{nm}sinm\lambda + B_{nm}cosm\lambda)\bar{P}_{nm}(cos\theta) \tag{7.11}$$

Implementation Notes:

● Setting $n_1 = 1$ yields the formulas for the full Land-Sea Complete Bouguer Effect. The degree-1 term is significant and must be retained.

● For high-precision applications involving short wavelengths, the Remove-Restore technique is recommended: use the spherical harmonic model (Eqs. 7.5 – 7.11) for the long-to-medium wavelengths ($n < n_1$) and rigorous spatial integration (Section 7.5.4) for the residual short wavelengths ($n \geq n_1$).

7.8 Unified Algorithms for Land-Sea Classical Bouguer and Isostatic Effects

7.8.1 Classical Reduction Method for Land Bouguer Gravity Anomalies

The Classical Planar Bouguer Gravity Anomaly is strictly defined on the geoid. It is computed as the gravity anomaly on the geoid minus the gravitational attraction exerted by all topographic masses external to the geoid on the surface gravity. The classical algorithm is expressed as:

$$\Delta g_B = \Delta g - g^R - 2\pi G\rho h \tag{8.1}$$

where:

Δg: Free-air gravity anomaly on the geoid.

$-g^R$: Classical Planar Terrain Correction (g^R represents the planar approximation of the local terrain effect on surface gravity).

$-2\pi G\rho h$: Bouguer Plate Correction ($2\pi G\rho h$ represents the planar approximation of the spherical shell Bouguer effect on surface gravity).

In mountainous regions, the plate correction term is significantly negative, typically resulting in negative Bouguer anomalies. Since observation points are rarely located on the geoid, measured gravity must be analytically continued from the observation attitude down to the geoid to obtain Δg. Only then can Eq. (8.1) be applied.

Thus, the general formula for computing the Planar Bouguer Gravity Anomaly (referenced to the geoid) from ground or airborne observations is:

$$\Delta g_B = \Delta g^s - g^R - 2\pi G\rho h - \Delta g^c \tag{8.2}$$

where Δg^s is the gravity anomaly at the observation point; Δg^c is the analytical continuation term for the gravity anomaly.

Similarly, for the Bouguer Gravity Disturbance:

$$\delta g_B = \delta g^s - g^R - 2\pi G\rho h - \delta g^c \tag{8.3}$$

where: δg^s is the gravity disturbance at the observation point, and $\delta g^c \approx \Delta g^c$.

Critical Implementation Note:

Regardless of whether data are acquired on the ground or from an aircraft, the Bouguer Gravity Anomaly/Disturbance are defined exclusively on the geoid. Furthermore, the topographic correction terms (g^R and the plate correction) specifically represent the effect of topography masses on surface gravity (gravity on the terrain surface), not on gravity at the airborne altitude or on the geoid. Even when processing airborne data, g^R in Eqs. (8.2) and (8.3) must be calculated as the local terrain effect on surface gravity.

7.8.2 Computation of Seawater and Unified Land-Sea Bouguer Anomalies

Over continents, topographic masses external to the geoid are removed (Land Bouguer Effect). Over oceans, the density deficit of seawater relative to crustal rock is compensated (Seawater Bouguer Effect).

The rigorous integral for the Seawater Complete Bouguer Effect on gravity anomaly/disturbance is:

$$g_b^w = \frac{G\beta}{r}\iint_S \left[\frac{r_0}{\mathcal{L}} - \frac{r_0+d}{\sqrt{(\tilde{h}-d)^2+l^2}}\right] ds \tag{8.4}$$

where $d < 0$ is the bathymetry; $\beta = \rho - \rho_w$ is the seawater compensation density; $\tilde{h}$ is the computation point elevation relative to the sea surface; r_0 is the geocentric distance of the sea surface, ds is the area element on the sea surface; $\mathcal{L}$ is the spatial distance from ds to the computation point; and l is the straight-line distance between ds and the projection point of the computation point onto the sea surface.

Since both g^R (Eq. 8.1) and g_b^w (Eq. 8.4) are regional integrals:

- In nearshore waters, $g^R \neq 0$ due to the influence of adjacent land topography..
- In coastal lands, $g_b^w \neq 0$ due to the influence of adjacent ocean basins.

This necessitates a Land-Sea Unified Bouguer effect Algorithm. Noting that terrain elevation $h = 0$ over the ocean and bathymetry $d = 0$ over land, the integration domains for g^R and g_b^w are disjoint yet seamlessly contiguous. Summing these integrals yields the unified formulas for the Bouguer gravity anomaly and disturbance:

$$\Delta g_B = \Delta g^s - g^R - 2\pi G\rho h - g_b^w - \Delta g^c \tag{8.5}$$

$$\delta g_B = \delta g^s - g^R - 2\pi G\rho h - g_b^w - \delta g^c \tag{8.6}$$

Defining the total Classical Bouguer Effect on Gravity as:

$$g^B = g_b + g_b^w = g^R + 2\pi G\rho h + g_b^w \tag{8.7}$$

it follows that the classical Bouguer correction is unified for both gravity anomalies and gravity disturbances across land and sea.

7.8.3 Land Airy-Heiskanen Crustal Isostatic Effect

Large negative Bouguer anomalies in mountainous regions suggest compensation by mass deficits (roots) in the underlying mantle (magma layer). The Airy-Heiskanen Isostatic Model assumes:

- Floating Crust: Mountains (density $\rho = 2.67\times10^3$kg/m^3) float on the denser mantle (mantle density $\rho_1 = 3.27\times10^3$kg/m^3).

● Root Formation: Topographic elevations h are compensated by mountain roots of depth b extending into the mantle.

● Hydrostatic equilibrium: The mass of the root compensates the topographic load:

$$b\Delta\rho_1 = \rho_0 h \quad \Longrightarrow \quad b = \frac{\rho_0}{\Delta\rho_1} h = 4.45h \tag{8.8}$$

where $\Delta\rho_1 = \rho_1 - \rho = 0.6\times10^3$kg/m^3.

The Crustal Isostatic Effect (g_I) is the gravitational attraction of this compensating root mass (which fills the density deficit). It generally opposes the sign of the Bouguer effect. With the z-axis vertical and origin O at sea level the effect is expressed as:

$$g_I = -G\Delta\rho_1 \iint_\sigma \int_D^{D+b} \frac{z-z'}{L^3} dz\, d\sigma \tag{8.9}$$

Note: The negative sign indicates the direction relative to the removal logic; physically, the root adds mass, increasing gravity compared to the Bouguer-reduced field.

7.8.4 Calculation of Marine and Unified Land-Sea Isostatic Gravity Anomalies

The oceanic column consists of a low-density seawater layer (ρ_w =1.03×10^{3}kg/m^3) and an oceanic crust layer with density ρ. The combined weight of these layers is insufficient to balance the buoyancy force from the underlying mantle (magma), necessitating an upward displacement of mantle material into the oceanic region, forming an anti-root.

Compensation for the seawater density deficit ($\beta = \rho - \rho_w$ =1.64×10^{3}kg/m^3) generates the Seawater Bouguer Effect, as defined in Eq. (8.4). Let d denote the bathymetry (depth). After accounting for seawater compensation, the hydrostatic equilibrium condition for the oceanic anti-root depth b' is:

$$b'\Delta\rho_1 = \beta d \quad \Longrightarrow \quad b' = \frac{\beta}{\Delta\rho_1} d = 2.73d \tag{8.10}$$

Just as the land mountain root requires mass compensation, the oceanic anti-root represents a mass excess that must be removed to achieve isostatic equilibrium. Consequently, the Oceanic Crustal Isostatic Effect (g_I^o) generally opposes the sign of the Seawater Bouguer Effect. It is expressed as:

$$g_I^o = -G\Delta\rho_1 \iint_\sigma \int_{D-b'}^{D} \frac{z-z'}{L^3} dz\, d\sigma \tag{8.11}$$

Note: The integration limits reflect the anti-root extending upwards from the compensation depth D towards the seabed.

Since both the Land Isostatic Effect (Eq. 8.9) and the Oceanic Isostatic Effect (Eq. 8.11) are regional integrals:

● In nearshore waters, the land isostatic effect is non-zero (influence of distant land roots).

● In coastal land areas, the oceanic isostatic effect is non-zero (influence of distant oceanic anti-roots).

This necessitates a Unified Land-Sea Crustal Isostatic Algorithm. Following the same logic as the unified Bouguer algorithm:

● Over the ocean ($h = 0$), there is no land root; thus, the land isostatic integral contributes zero over oceanic cells.

● Over land ($d = 0$), there is no oceanic anti-root; thus, the oceanic isostatic integral

contributes zero over land cells.

The integration domains are disjoint yet seamlessly contiguous. Summing the two integrals yields the unified formulas for the Isostatic Gravity Anomaly (Δg_I) and Isostatic Gravity Disturbance (δg_I):

$$\Delta g_I = \Delta g^s - g^B - g_I - g_I^o - \Delta g^c \tag{8.12}$$

$$\delta g_I = \delta g^s - g^B - g_I - g_I^o - \delta g^c \tag{8.13}$$

Defining the total Classical Unified Land-Sea Isostatic Effect as:

$$g^I = g_I + g_I^o \tag{8.14}$$

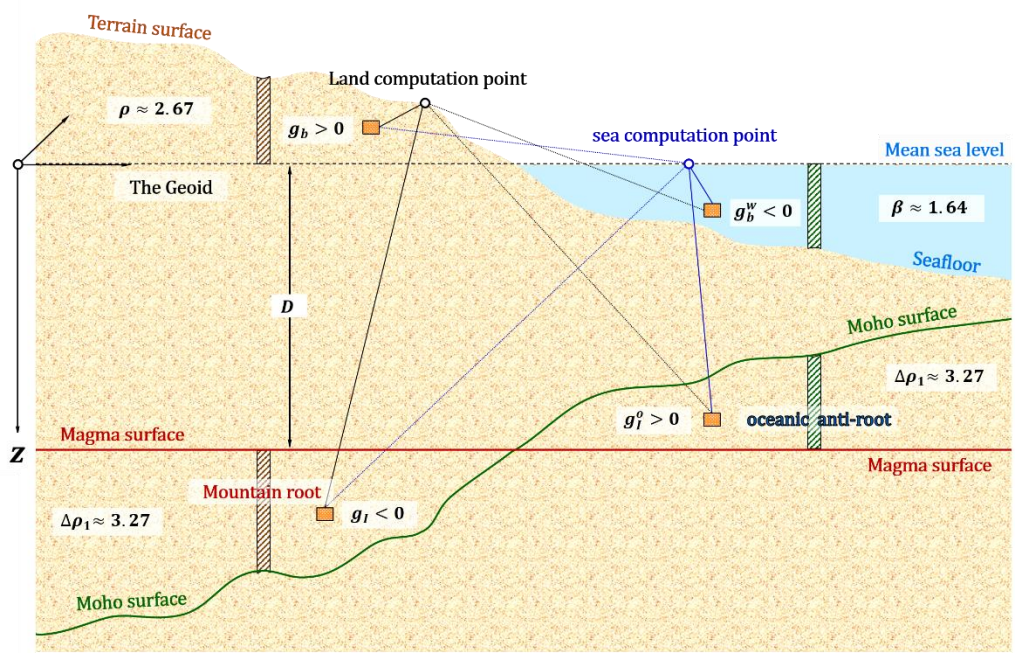

Figure 7.6: Calculation Principle for Unified Land-Sea Bouguer and Isostatic Effects on Surface Gravity

7.8.5 Physical Interpretation of Sign Conventions for Bouguer and Isostatic Effects

The sign conventions for these effects are derived from their physical mechanisms:

(a) Land Bouguer Effect ($g_b > 0$): Involves removing the excess topographic mass external to the geoid. Since topography attracts gravity positively, removing it requires a negative correction to the observed gravity. Conversely, the "effect" value g_b (the magnitude of the terrain attraction) is positive. In the reduction formula $\Delta g_B = \Delta g - g^B$, a positive g^B reduces the anomaly.

(b) Seawater Bouguer Effect ($g_b^w < 0$): Involves compensating the seawater density deficit (replacing water with rock). This adds mass, increasing gravity. However, relative to the land convention, or considering the deficit nature, the effect is defined with an opposite sign in the unified framework.

(c) Land Isostatic Effect ($g_I < 0$): Involves filling the root deficit with compensating mass. This adds mass (increasing gravity), opposing the removal logic of the Bouguer effect. Thus, its sign is opposite to that of the Bouguer effect.

(d) Oceanic Isostatic Effect ($g_I^o > 0$): Involves removing the excess mass of the anti-root. This reduces mass (decreasing gravity), opposing the addition logic of the seawater Bouguer effect g_b^w.

● **Summary of Signs (as illustrated in Figure 7.6):**

Land Bouguer Effect: Positive (+); Seawater Bouguer Effect: Negative (−); Land Isostatic Effect: Negative (−); and Oceanic Isostatic Effect: Positive (+).

● **Magnitude Relationships:**

Principles of isostasy dictate that the compensation is partial or local.

○ On land: $|g_b| > |g_I|$. The effects partially cancel, making the Isostatic Anomaly smaller than the Bouguer Anomaly.

○ At sea: $|g_b^w| > |g_I^o|$. Similarly, the effects partially cancel.

Consequently, Isostatic Anomalies are generally smoother and smaller in magnitude than Bouguer Anomalies in most regions.

Equivalence of Topographic Effects on Gravity Field elements

● Invariance Principle: Given the invariance of the normal gravity field, various terrain effects on gravity disturbance and on gravity anomaly are strictly equal to the effects on gravity itself.

● Implementation Note: Software modules computing Local Terrain Effects, Helmert Condensation, Unified Bouguer Effects, Unified Isostatic Effects, or Residual Terrain Effects need not distinguish between anomalies and disturbances; the computed topographic correction value is the same for both.

Critical Mathematical Distinction:

While various terrain effects on δg and Δg are equal, their relationship does not satisfy the fundamental equation of physical geodesy (which relates vertical derivatives). The relationship between the terrain effects on gravity anomalies and those on height anomalies are governed by the Hotine Formula, not the Stokes Formula.

7.9 Integral Algorithm Formulas for the Anomalous Earth Gravity Field

While the global gravity field is typically modeled in the spectral domain, spatial integral algorithms are essential for local gravity field approximation. To perform integration over a finite radius in local regions, the Remove-Restore Method, based on a reference global geopotential model, is standard practice:

(1) Remove: Compute and subtract the model values of the anomalous field elements on the boundary surface to obtain residual field elements.

(2) Integrate: Apply a spatial integral algorithm with a finite radius to these residuals to derive the target residual field element at the computation point.

(3) Restore: Add the model value of the target element at the computation point to obtain the final local approximation.

7.9.1 Generalized Stokes and Hotine Integral Formulas

Given the gravity anomaly Δg on the geoid or an external equipotential surface S the

disturbing potential T or height anomaly ζ at an external point $T(\theta,\lambda,r)$ is computed via the Generalized Stokes Integral:

$$T(\theta,\lambda,r)=\gamma\zeta(\theta,\lambda,r)=\frac{1}{4\pi}\iint_S \Delta g' S(r,\psi,r')ds \tag{9.1}$$

where r' is the geocentric distance of the moving element ds, and $S(r,\psi,r')$ is the Generalized Stokes Kernel:

$$S(r,\psi,r')=\frac{2}{L}+\frac{1}{r}-\frac{3L}{r^2}-\frac{5r'cos\psi}{r^2}-\frac{3r'}{r^2}cos\psi ln\frac{r-r'cos\psi+L}{2r} \tag{9.2}$$

where L being the Euclidean distance between the computation and moving points.

Singularity Handling: When the computation point coincides with the moving point, the integral becomes singular. The analytical value for this singular term is:

$$\zeta|_0=\frac{A_0}{\gamma}\Delta g_0 \tag{9.3}$$

where A_0, Δg_0, and γ are the area, gravity anomaly, and normal gravity at the computation point, respectively.

Similarly, given the gravity disturbance δg on S, the Generalized Hotine Integral is used:

$$T(\theta,\lambda,r)=\gamma\zeta(\theta,\lambda,r)=\frac{1}{4\pi}\iint_S \delta g' H(r,\psi,r')ds \tag{9.4}$$

where the Generalized Hotine Kernel $H(r,\psi,r')$ is:

$$H(r,\psi,r')=\frac{2}{L}-\frac{1}{r'}ln\frac{r-r'cos\psi+L}{r(1-cos\psi)} \tag{9.5}$$

The corresponding singular value is:

$$\zeta|_0=\frac{A_0}{\gamma}\delta g_0 \tag{9.6}$$

FFT Implementation: By approximating the geocentric distances r and r' as constant mean values, these integrals transform into convolution forms, enabling rapid computation via the Fast Fourier Transform (FFT) algorithm.

Note: The Stokes boundary value problem strictly requires the boundary surface S to be an equipotential surface (e.g., the geoid which can be constructed from a global geopotential model up to degree ~360). For equipotential surfaces within an altitude of 10 km, a normal (or orthometric) equiheight surface may serve as a valid approximation.

7.9.2 Generalized Vening-Meinesz Integral Formulas

Taking horizontal derivatives of the generalized Stokes formula (9.1) in a local horizontal coordinate system yields the Generalized Vening-Meinesz Formulas for vertical deflections (ξ,η):

$$\xi=-\frac{1}{4\pi r\gamma}\iint_S \Delta g'\frac{\partial S(r,\psi,r')}{\partial\psi}\frac{\partial\psi}{\partial\varphi}ds,\quad \eta=-\frac{1}{4\pi r cos\varphi\gamma}\iint_S \Delta g'\frac{\partial S(r,\psi,r')}{\partial\psi}\frac{\partial\psi}{\partial\lambda}ds \tag{9.7}$$

From the relation:

$$cos\psi=sin\varphi sin\varphi'+cos\varphi cos\varphi' cos(\lambda'-\lambda) \tag{9.8}$$

taking horizontal derivatives on both sides gives:

$$-sin\psi\frac{\partial\psi}{\partial\varphi}=cos\varphi sin\varphi'-sin\varphi cos\varphi' cos(\lambda'-\lambda) \tag{9.9}$$

$$-sin\psi\frac{\partial\psi}{\partial\lambda}=cos\varphi cos\varphi' sin(\lambda'-\lambda) \tag{9.10}$$

Using spherical trigonometric formulas:

$$sin\psi cos\alpha = cos\varphi sin\varphi' - sin\varphi cos\varphi' cos(\lambda' - \lambda) \tag{9.11}$$

$$sin\psi sin\alpha = cos\varphi' sin(\lambda' - \lambda) \tag{9.12}$$

Combining Equations (9.9) through (9.12), we have:

$$\frac{\partial\psi}{\partial\varphi} = -cos\alpha, \quad \frac{\partial\psi}{\partial\lambda} = -cos\varphi sin\alpha \tag{9.13}$$

Substituting into Equation (9.7) yields:

$$\xi = \frac{1}{4\pi r\gamma}\iint_S \Delta g' \frac{\partial S(r,\psi,r')}{\partial\psi} cos\alpha ds, \quad \eta = \frac{1}{4\pi r\gamma}\iint_S \Delta g' \frac{\partial S(r,\psi,r')}{\partial\psi} sin\alpha ds \tag{9.14}$$

Considering $= \sqrt{r^2 + r'^2 - 2rr'cos\psi}$, we have:

$$\frac{\partial}{\partial\psi}L = \frac{rr'}{L} sin\psi, \quad \frac{\partial}{\partial\psi}\left(\frac{1}{L}\right) = -\frac{1}{L^2}\frac{\partial}{\partial\psi}L = -\frac{rr'}{L^3} sin\psi \tag{9.15}$$

$$\frac{\partial}{\partial\psi} ln\frac{r - r'cos\psi + L}{2r} = \frac{1}{r - r'cos\psi + L}\left(\frac{rr'}{L} sin\psi + r' sin\psi\right) = \frac{r' sin\psi}{r + L - r'cos\psi}\frac{L + r}{L} \tag{9.16}$$

$$\begin{aligned}
\frac{\partial}{\partial\psi}S(r,\psi,r') &= \frac{\partial}{\partial\psi}\left(\frac{2}{L} + \frac{1}{r} - \frac{3L}{r^2} - \frac{5r'cos\psi}{r^2} - \frac{3r'cos\psi}{r^2} ln\frac{r - r'cos\psi + L}{2r}\right) \\
&= \frac{\partial}{\partial\psi}\frac{2}{L} - \frac{3}{r^2}\frac{\partial}{\partial\psi}L + \frac{5r' sin\psi}{r^2} + \frac{3r' sin\psi}{r^2} ln\frac{r + L - r'cos\psi}{2r} - \frac{3r'cos\psi}{r^2}\frac{\partial}{\partial\psi} ln\frac{r + L - r'cos\psi}{2r} \\
&= \left(-\frac{2rr'}{L^3} - \frac{3r'}{rL} + \frac{5r'}{r^2} + \frac{3r'}{r^2} ln\frac{r - r'cos\psi + L}{2r} - \frac{3r'cos\psi}{r^2}\frac{r'}{r - r'cos\psi + L}\frac{L + r}{L}\right) sin\psi \\
&= \left[-\frac{2r}{L^3} - \frac{3}{rL} + \frac{5}{r^2} + \frac{3}{r^2} ln\frac{r - r'cos\psi + L}{2r} - \frac{3r'(L + r)cos\psi}{r^2 L(r - r'cos\psi + L)}\right] r' sin\psi
\end{aligned} \tag{9.17}$$

Similarly, deriving from the Hotine formula (9.4) using gravity disturbances δg:

$$\xi = \frac{1}{4\pi r\gamma}\iint_S \delta g' \frac{\partial H(r,\psi,r')}{\partial\psi} cos\alpha ds, \quad \eta = \frac{1}{4\pi r\gamma}\iint_S \delta g' \frac{\partial H(r,\psi,r')}{\partial\psi} sin\alpha ds \tag{9.18}$$

Since: $\frac{\partial}{\partial\psi} ln\frac{r - r'cos\psi + L}{r(1 - cos\psi)} = \frac{r(1 - cos\psi)}{r - r'cos\psi + L}\frac{\left(\frac{rr'}{L} sin\psi + r' sin\psi\right) r(1 - cos\psi) + (r - r'cos\psi + L) r sin\psi}{r^2(1 - cos\psi)^2}$

$$= \frac{sin\psi}{r - r'cos\psi + L}\frac{\frac{L + r}{L} r'(1 - cos\psi) + (r - r'cos\psi + L)}{1 - cos\psi} = \left[\frac{r'(L + r)}{(r - r'cos\psi + L)L} + \frac{1}{1 - cos\psi}\right] sin\psi \tag{9.19}$$

Therefore: $\frac{\partial}{\partial\psi}H(r,\psi,r') = \frac{\partial}{\partial\psi}\left(\frac{2}{L} - \frac{1}{r'} ln\frac{r - r'cos\psi + L}{r(1 - cos\psi)}\right) = \frac{\partial}{\partial\psi}\frac{2}{L} - \frac{1}{r'}\frac{\partial}{\partial\psi} ln\frac{r - r'cos\psi + L}{r(1 - cos\psi)}$

$$= \left[-\frac{2rr'}{L^3} - \frac{L - r}{(r - r'cos\psi + L)L} + \frac{1}{r'(1 - cos\psi)}\right] sin\psi \tag{9.20}$$

These formulas allow the computation of vertical deflections at any point on the Earth's surface or in external space from gravity anomalies or disturbances defined on an equi-potential surface. Like the Stokes/Hotine integrals, they can be accelerated using FFT under the constant-radius approximation.

7.9.3 Poisson Integral Algorithm and Applications

The Poisson Integral solves the First Boundary Value Problem (Dirichlet Problem), performing analytical continuation of an anomalous field element μ (e.g., δg or ζ) from a source surface S to a target surface D at a different attitude:

$$\mu(\theta,\lambda,r) = \frac{1}{4\pi r}\int_S (\theta',\lambda',r')\frac{r^2 - r'^2}{L^3} ds \tag{9.21}$$

Singularity neutralization:

When $r \to r'$ (computation point on the source surface), the kernel becomes undefined (0/0) and singular ($L \to 0$). To resolve this, we apply an identity transformation (Hofmann, 2006) to obtain the Modified Poisson Integral:

$$\mu(\theta,\lambda,r)=\frac{r'^2}{r^2}\mu(\theta,\lambda,r')+\frac{1}{4\pi r}\int_s\ [\mu(\theta',\lambda',r')-\mu(\theta',\lambda',r)]\frac{r^2-r'^2}{L^3}ds \tag{9.22}$$

Here, the difference term $[\mu-\mu']\to 0$ as $L\to 0$, effectively neutralizing the singularity of the kernel and ensuring numerical stability.

Application to Gravity Gradients:

The radial disturbing gravity gradient T_{rr} can be derived by taking the radial derivative of the Poisson integral for gravity disturbance δg.

Applying the Poisson integral to the gravity disturbance δg yields:

$$\delta g(\theta,\lambda,r)=\frac{1}{4\pi r}\iint_s\ \delta g'\frac{r^2-r'^2}{L^3}ds \tag{9.23}$$

Considering $T_{rr}=\frac{\partial}{\partial r}\left(\frac{\partial}{\partial r}T\right)=-\frac{\partial}{\partial r}(\delta g)$, taking the radial partial derivative of both sides of Equation (9.23) gives:

$$\begin{aligned}T_{rr}&=-\frac{1}{4\pi r}\iint_s\ \delta g'\frac{\partial}{\partial r}\frac{r^2-r'^2}{L^3}ds\\&=\frac{1}{4\pi r}\iint_s\ \delta g'\frac{r^3-5rr'^2+(r^2+3r'^2)r'^2cos\psi}{L^5}ds\end{aligned} \tag{9.24}$$

Similar modification techniques (subtracting the computation point value inside the integral) should be applied to Eq. (9.24) to suppress singularities when computing gradients on or near the source surface.

7.9.4 Forward and Inverse Integral Operations for the Anomalous Gravity Field

(1) Computing Gravity Disturbance from Height Anomaly

Differentiating the Poisson integral for the disturbing potential T along the vertical direction yields the gravity disturbance $\delta\ g$:

$$\delta g=\frac{\partial T}{\partial n}\approx-\frac{\gamma\partial\zeta}{\partial r}=-\frac{\gamma}{2\pi}\iint_s\ \frac{\zeta-\zeta_p}{l^3}ds \tag{9.25}$$

where ∂n denotes differentiation along the vertical direction, and l is the straight-line distance between the computation point and the moving element on the equipotential boundary.

Singularity: When the computation point coincides with the moving point, the singular value is:

$$\delta g|_0=\frac{\gamma\sqrt{A_0/\pi}}{4}(\zeta_{xx}+\zeta_{yy}) \tag{9.26}$$

where ζ_{xx}, ζ_{yy} are the second-order horizontal derivatives of the height anomaly.

Eq. (9.25) is known as the Inverse Hotine Integral. It computes gravity disturbance on an equipotential surface from height anomalies defined on the same surface.

Note: The boundary must be an equipotential surface.

(2) Computing Gravity Anomaly from Height Anomaly

Substituting the fundamental equation of physical geodesy into Eq. (9.25) yields the Inverse Stokes Integral:

$$\Delta g=-\frac{\gamma}{2\pi}\iint_s\ \frac{\zeta-\zeta_p}{l^3}ds-\frac{\zeta\gamma}{2r} \tag{9.27}$$

This formula derives gravity anomaly from height anomaly on an equipotential surface.

(3) Computing Height Anomaly from Vertical Deflection

$$\zeta=\frac{r}{4\pi}\iint_\sigma\ ctg\frac{\psi}{2}(\xi cos\alpha+\eta sin\alpha)\,d\sigma \tag{9.28}$$

Singularity:

$$\zeta|_0 = \frac{A_0}{4\pi}(\xi_y + \eta_x) \tag{9.29}$$

where ξ_y, η_x are are the cross-derivatives of the vertical deflection components.

(4) Computing Gravity Anomaly from Vertical Deflection

$$\Delta g = -\frac{\gamma}{4\pi}\iint_\sigma \left(3csc\psi - csc\psi csc\frac{\psi}{2} - tg\frac{\psi}{2}\right)(\xi cos\alpha + \eta sin\alpha)\, d\sigma \tag{9.30}$$

Singularity:

$$\Delta g|_0 = -\frac{\gamma\sqrt{A_0/\pi}}{4}(\xi_y + \eta_x) \tag{9.31}$$

(5) Computing Gravity Disturbance from Vertical deflection Integral

Combining the fundamental differential equation with Eqs. (9.28) and (9.30) yields:

$$\delta g = -\frac{\gamma}{4\pi} \iint_\sigma \left(3csc\psi - csc\psi csc\frac{\psi}{2} - tg\frac{\psi}{2} - 2ctg\frac{\psi}{2}\right)(\xi cos\alpha + \eta sin\alpha)\, d\sigma \tag{9.32}$$

Singularity:

$$\delta g|_0 = -\frac{\gamma}{2\pi}\left(\sqrt{\pi A_0} + \frac{A_0}{r}\right)(\xi_y + \eta_x) \tag{9.33}$$

Eqs. (9.28), (9.30), and (9.32) constitute the Inverse Vening-Meinesz Integrals. Under the constant-radius approximation ($r \approx$const), all inverse formulas (9.25 – 9.32) can be efficiently computed using the FFT algorithm.

(6) Forward and Inverse Computation of Disturbing Gravity Gradients

Forward (Gradient to Disturbance): Compute δg at an external point from T_{rr} on an equipotential surface using the Generalized Hotine Integral:

$$\delta g(\theta, \lambda, r) = \frac{1}{4\pi}\iint_s T_{rr} H(r, \psi, r') ds \tag{9.34}$$

Inverse (Disturbance to Gradient): Compute T_{rr} on the surface from δg via the radial gradient integral:

$$T_{rr} = \frac{1}{2\pi}\iint \frac{\delta g - \delta g'}{l^3} ds \tag{9.35}$$

Optimization Strategy:

Optimal combination of these algorithms with "1-to-2-step residual cumulative approximation" scheme can enhance the accuracy and stability of boundary value problem solutions and short-wavelength field approximations.

7.9.5 Analytical Properties of Gravity Field Integral Kernel Functions

The kernel functions depend on the straight-line distance l, expressible via the spherical angular distance ψ. Two major challenges arise in numerical integration:

- Spectral Leakage: Due to convergence issues in the kernel functions.
- Singularity: When the computation point lies on the boundary surface ($\psi \to 0$), leading to resolution-dependent jumps in numerical results.

(1) Analysis under Spherical Approximation ($r' = r = R$):

Let $l = 2Rsin(\psi/2)$. The kernel functions on the boundary sphere are:

- Stokes Kernel:

$$S(\psi) = R \cdot S(R,\psi,R) = sin^{-1}\frac{\psi}{2} + 1 - 6sin\frac{\psi}{2} - 5cos\psi - 3cos\psi ln\frac{1-cos\psi+2sin(\psi/2)}{2}$$
$$= 1 + sin^{-1}\frac{\psi}{2} - 6sin\frac{\psi}{2} - 5cos\psi - 3cos\psi ln\left(sin\frac{\psi}{2} + sin^2\frac{\psi}{2}\right) \quad (9.36)$$

● Hotine kernel:

$$H(\psi) = R \cdot H(R,\psi,R) = 2 - ln\left(1 + sin^{-1}\frac{\psi}{2}\right) \quad (9.37)$$

● Vening-Meinesz Kernel (Derivative of Hotine):

$$V(\psi) = \frac{\partial}{\partial\psi}H(\psi) = \frac{1}{2}\frac{ctg\frac{\psi}{2}}{1+sin\frac{\psi}{2}} \quad (9.38)$$

As shown in Figure 7.7, all three kernels diverge to infinity as $\psi \to 0$ $(S, H, V \to \infty)$, necessitating singularity handling.

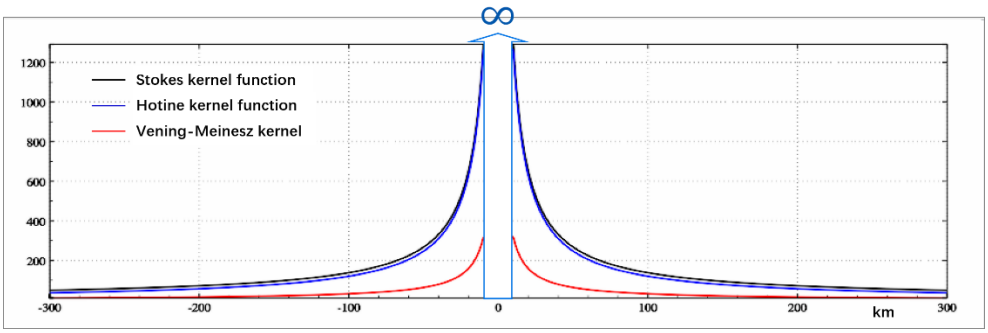

Figure 7.7: Curves of Major Gravity Field Integral Spherical Kernel Functions

(2) The Poisson Kernel Instability:

For the Poisson integral (Eq. 9.21) used for same-type continuation:

● If $r = r'$, the kernel $P(\psi) = (r^2 - r'^2)/L^3$ becomes identically zero/undefined.

● If points coincide $(L \to 0)$, it becomes singular (0/0 form).

Consequently, direct Poisson integration on the same surface is numerically unstable. Effective analytical continuation requires restricting the integration range and employing modified forms (e.g., Eq. 9.22) to neutralize singularities.

(3) Recommendation on Kernel Modification:

While the Poisson integral theoretically underpins Stokes, Hotine, and Vening-Meinesz solutions, its severe high-order oscillations and non-convergence on the boundary introduce uncontrollable uncertainties. Historically, two approaches were used to mitigate this:

● Assuming isotropic random statistical properties for residual fields.

● Kernel Modification: Altering kernel functions based on spectral approximations.

However, these modification techniques rely on assumptions (statistical or data-driven) that lack a rigorous foundation in analytical gravity field theory, compromising their universality. Consequently, PAGravf4.5 does not recommend the use of gravity field integral kernel modification algorithms.

Despite numerical challenges, spatial integral formulas remain indispensable for explicitly expressing the analytical relationships between gravity field elements, serving as the cornerstone of physical geodesy and gravity field approximation theory.

7.10 Spherical Radial Basis Function Algorithms for Gravity Field Approximation

Classical spatial gravity field boundary value theory relies on a single type of observation gravity field element on a single boundary surface. In contrast, spectral domain gravity field approximation theory does not involve boundary surfaces or boundary value conditions. It can directly approximate the all-element gravity field using multi-source heterogeneous observations via the Least Squares Method, making it the mainstream approach in modern physical geodesy. This section introduces the theory and methodology of Spherical Radial Basis Function (SRBF) spectral domain approximation.

7.10.1 Representation of the External Disturbing Potential Using SRBFs

The disturbing potential $T(\boldsymbol{x})$ at an external point $\boldsymbol{x}$ can be expressed as a linear combination of fully normalized surface spherical harmonics:

$$T(\boldsymbol{x}) = \frac{GM}{r}\sum_{n=1}^{N}\left(\frac{a}{r}\right)^n \sum_{m=-n}^{n}\bar{F}_{nm}\bar{Y}_{nm}(\boldsymbol{e}) \tag{10.1}$$

where $\boldsymbol{x} = \boldsymbol{r}\cdot\boldsymbol{e} = r(sin\theta cos\lambda, sin\theta sin\lambda, cos\theta)$ represents geocentric spherical coordinates (θ, λ, r); $\bar{F}_{nm}$ are the fully normalized Stokes coefficients (geopotential coefficients); and a is the Earth's semi-major axis. The the normalized surface spherical harmonic basis functions $\bar{Y}_{nm}(\boldsymbol{e})$ are defined on the sphere of radius a:

$$\begin{aligned} \bar{Y}_{nm}(\boldsymbol{e}) &= \bar{P}_{nm}(cos\theta)cosm\lambda, \quad \bar{F}_{nm} = \delta\bar{C}_{nm}, \quad m \geq 0 \\ \bar{Y}_{nm}(\boldsymbol{e}) &= \bar{P}_{n|m|}(cos\theta)sin|m|\lambda, \quad \bar{F}_{nm} = \bar{S}_{n|m|}, \quad m < 0 \end{aligned} \tag{10.2}$$

where $\bar{P}_{nm}(cos\theta)$ is the fully normalized associated Legendre function; n is the degree and m is the order of the geopotential coefficients.

Equivalently, these basis functions $\bar{Y}_{nm}(\boldsymbol{e})$ can be defined on a Bjerhammar sphere of radius $\mathcal{R}$. Thus, $T(\boldsymbol{x})$ can also be written as:

$$T(\boldsymbol{x}) = \frac{GM}{r}\sum_{n=1}^{N}\left(\frac{\mathcal{R}}{r}\right)^n \sum_{m=-n}^{n}\bar{E}_{nm}\bar{Y}_{nm}(\boldsymbol{e}) \tag{10.3}$$

Here, $\mathcal{R} \in (a-\delta, a+\delta)$ with $\delta \ll a$. The relationship between coefficients is $a^n\bar{F}_{nm} = \mathcal{R}^n\bar{E}_{nm}$, and the surface spherical harmonics basis functions $\{\bar{Y}_{nm}(\boldsymbol{e})\}$ in Equations (10.3) and (10.1) is identical.

Alternatively, $T(\boldsymbol{x})$ can be represented as a linear combination of K Spherical Radial Basis Functions (SRBFs):

$$T(\boldsymbol{x}) = \frac{GM}{r}\sum_{k=1}^{K} d_k\Phi_k(\boldsymbol{x}, \boldsymbol{x}_k) = \frac{GM}{r}\sum_{k=1}^{K} d_k\Phi_k(\boldsymbol{x}, \psi_k) \tag{10.4}$$

where:

$\boldsymbol{x}_k = \mathcal{R}\cdot\boldsymbol{e}_k$: The SRBF node (center) on the Bjerhammar sphere.

ψ_k: The spherical angular distance between $\boldsymbol{x}_k$ and $\boldsymbol{x}$ (the argument of the SRBF).

d_k: The SRBF coefficient.

K: The number of nodes, i.e., the number of SRBF coefficients, determining the spatial resolution.

$\Phi_k(\boldsymbol{x}, \boldsymbol{x}_k) = \Phi_k(\boldsymbol{x}, \psi_k)$: The radial basis function for the disturbing potential, which can be abbreviated as $\Phi_k(\boldsymbol{x}) = \Phi_k(\boldsymbol{x}, \boldsymbol{x}_k)$.

The SRBF can be expanded into a Legendre series:

$$\Phi_k(\boldsymbol{x},\boldsymbol{x}_k)=\Phi_k(\boldsymbol{x},\psi_k)=\sum_{n=1}^{N}\phi_n P_n(\psi_k)=\sum_{n=1}^{N}\frac{2n+1}{4\pi}B_n\left(\frac{\mathcal{R}}{r}\right)^n P_n(\psi_k) \tag{10.5}$$

where ϕ_n is the n-th degree Legendre coefficient (or shape factor), characterizing the spectral properties of the SRBF, and $\mu=\mathcal{R}/r$ is the bandwidth parameter.

Note that N (maximum degree) and K (number of nodes) are independent parameters. The N in Equation (10.5) is the maximum degree of the Legendre functions. Although it is the maximum degree in the surface spherical harmonic expansion of the disturbing potential (Equation 10.3), there is no explicit functional relationship with K, the number of SRBF coefficients representing spatial resolution.

Substituting Eq. (10.5) into (10.4) and applying the Spherical Harmonic Addition Theorem:

$$P_n(\psi_k)=P_n(\boldsymbol{e},\boldsymbol{e}_k)=\frac{4\pi}{2n+1}\sum_{m=-n}^{n}\bar{Y}_{nm}(\boldsymbol{e})\bar{Y}_{nm}(\boldsymbol{e}_k) \tag{10.6}$$

$$\begin{aligned}T(\boldsymbol{x})&=\frac{GM}{4\pi r}\sum_{n=1}^{N}(2n+1)B_n\left(\frac{\mathcal{R}}{r}\right)^n\sum_{k=1}^{K}d_k P_n(\psi_k)\\&=\frac{GM}{4\pi r}\sum_{k=1}^{K}d_k\sum_{n=1}^{N}(2n+1)B_n\left(\frac{\mathcal{R}}{r}\right)^n P_n(\psi_k)\end{aligned} \tag{10.7}$$

$$T(\boldsymbol{x})=\frac{GM}{r}\sum_{n=1}^{N}B_n\left(\frac{\mathcal{R}}{r}\right)^n\sum_{m=-n}^{n}\sum_{k=1}^{K}d_k\bar{Y}_{nm}(\boldsymbol{e})\bar{Y}_{nm}(\boldsymbol{e}_k) \tag{10.8}$$

yields the relationship between geopotential coefficients and SRBF coefficients:

$$\bar{F}_{nm}=\left(\frac{\mathcal{R}}{a}\right)^n\bar{E}_{nm}=B_n\left(\frac{\mathcal{R}}{a}\right)^n\sum_{k=1}^{K}d_k\bar{Y}_{nm}(\boldsymbol{e}_k) \tag{10.9}$$

This relation holds for global domain ($\psi_k\in[0,\pi)$). For local gravity field approximation, ψ_k acts analogously to the integration radius in spatial methods. The distribution and number K of SRBF centers determine the spatial degrees of freedom.

7.10.2 Suitable Spherical Radial Basis Functions for Gravity Field Approximation

SRBFs must satisfy Laplace's equation ($\Delta\Phi=0$). Common harmonic kernels include the Point-Mass kernel, Poisson kernel, Radial Multipole kernel, and Poisson Wavelet kernel.

(1) Analytical Forms and Normalized Representation

Let $\boldsymbol{x}$ be the computation point and $\boldsymbol{x}_k$ the SRBF node on the Bjerhammar sphere $\Omega_{\mathcal{R}}$.

● Point-Mass Kernel: An inverse multiquadric (Newtonian) kernel.

$$\Phi_{IMQ}(\boldsymbol{x},\boldsymbol{x}_k)=\frac{1}{L}=\frac{1}{|\boldsymbol{x}-\boldsymbol{x}_k|} \tag{10.10}$$

where: L is the spatial distance from $\boldsymbol{x}_k$ to $\boldsymbol{x}$. The point-mass function is also known as the Newtonian kernel function. Since $\Delta(1/L)=0$, the point-mass kernel function $\Phi_{IMQ}(\boldsymbol{x},\boldsymbol{x}_{\mathrm{k}})$ satisfies Laplace's equation.

● Poisson Kernel: Derived from the Poisson integral.

$$\Phi_P(\boldsymbol{x},\boldsymbol{x}_k)=-2r\frac{\partial}{\partial r}\left(\frac{1}{L}\right)-\frac{1}{L}=\frac{r^2-r_k^2}{L^3} \tag{10.11}$$

● Radial Multipole Kernel (Order m):

$$\Phi_{RM}^{m}(\boldsymbol{x},\boldsymbol{x}_k)=\frac{1}{m!}\left(\frac{\partial}{\partial r_k}\right)^m\frac{1}{L} \tag{10.12}$$

Note: $m=0$ yields the point-mass kernel: $\Phi_{IMQ}(\boldsymbol{x},\boldsymbol{x}_k)=\Phi_{RM}^{0}(\boldsymbol{x},\boldsymbol{x}_k)$.

● Poisson Wavelet Kernel (Order m):

$$\Phi_{PW}^{m}(\boldsymbol{x},\boldsymbol{x}_k) = 2(\chi_{m+1} - \chi_m), \quad \chi_m = \left(r_k \frac{\partial}{\partial r_k}\right)^m \frac{1}{L} \tag{10.13}$$

Note: $m = 0$ yields the Poisson kernel: $\Phi_P(\boldsymbol{x},\boldsymbol{x}_k) = \Phi_{PW}^{0}(\boldsymbol{x},\boldsymbol{x}_k)$.

(2) Computation of Spherical Radial Basis Functions

To highlight spectral properties and simplify multi-type data processing, SRBFs can be computed via their normalized Legendre series. A normalization coefficient Φ^0 is defined by evaluating the series at $\psi_k = 0$ ($P_n(1) = 1$):

$$\Phi^0 = \sum_{n=1}^{N} \frac{2n+1}{4\pi} B_n \mu^n \tag{10.14}$$

The Normalized SRBF is then:

$$\Phi_k(\boldsymbol{x},\boldsymbol{x}_k) = \frac{1}{\Phi^0}\sum_{n=1}^{N} \phi_n P_n(\psi_k) = \frac{1}{\Phi^0}\sum_{n=1}^{N} \frac{2n+1}{4\pi} B_n \mu^n P_n(\psi_k) \tag{10.15}$$

This normalization preserves the linear functional relationships between different gravity field elements (e.g., potential, anomaly, and disturbance).

Table 7.2: Disturbing Potential Spherical Radial Basis Functions and Their Legendre Coefficients

SRBF Type	Analytical Form Φ_k	Legendre Coeff. ϕ_n	Parameter B_n
Point mass kernel	$\frac{1}{L} = \frac{1}{\lvert x - x_k \rvert}$	μ^n	$\frac{1}{2n+1}$
Poisson kernel	$\frac{r^2 - r_k^2}{L^3}$	$(2n+1)\mu^n$	1
Radial multipole kernel (m)	$\frac{1}{m!}\left(\frac{\partial}{\partial r_k}\right)^m \frac{1}{L}$	$C_n^m \mu^{n-m}$ $(n \geq m)$	$\frac{C_n^m}{2n+1}\mu^{-m}$
Poisson wavelet kernel (m)	$2(\chi_{m+1} - \chi_m)$ $\chi_m = \left(r_k \frac{\partial}{\partial r_k}\right)^m \frac{1}{L}$	$(-nln\mu)^m (2n+1)\mu^n$	$(-nln\mu)^m$

(3) Series Representation of Various Anomalous Field elements Using SRBFs

Based on the definitions of anomalous field elements, the parameterized forms of SRBFs for other field types can be derived from the SRBF expansion of the disturbing potential (Eq. 10.6). By applying appropriate differential operators, we obtain:

- Disturbing Potential (Height Anomaly):

$$T(\boldsymbol{x}) = \gamma\zeta(\boldsymbol{x}) = \frac{GM}{4\pi r}\sum_{k=1}^{K} d_k \sum_n (2n+1) B_n \left(\frac{\mathcal{R}}{r}\right)^n P_n(\psi_k) \tag{10.16}$$

- Gravity Disturbance:

$$\delta g(\boldsymbol{x}) = -\frac{\partial T}{\partial r} = \frac{GM}{4\pi r^2}\sum_{k=1}^{K} d_k \sum_n (2n+1)(n+1) B_n \left(\frac{\mathcal{R}}{r}\right)^{n-1} P_n(\psi_k) \tag{10.17}$$

- Gravity Anomaly:

$$\Delta g(\boldsymbol{x}) = \frac{GM}{4\pi r^2}\sum_{k=1}^{K} d_k \sum_n (2n+1)(n-1) B_n \left(\frac{\mathcal{R}}{r}\right)^{n-1} P_n(\psi_k) \tag{10.18}$$

- Vertical Deflection Components (ξ: North-South, η: East-West):

$$\xi(\boldsymbol{x}) = \frac{GM}{4\pi r^2 \gamma}\sum_{k=1}^{K} d_k \cos\alpha_k \sum_n (2n+1) B_n \left(\frac{\mathcal{R}}{r}\right)^n \frac{\partial P_n(\psi_k)}{\partial \psi_k} \tag{10.19}$$

$$\eta(\boldsymbol{x}) = \frac{GM}{4\pi r^2 \gamma}\sum_{k=1}^{K} d_k \sin\alpha_k \sum_n (2n+1) B_n \left(\frac{\mathcal{R}}{r}\right)^n \frac{\partial P_n(\psi_k)}{\partial \psi_k} \tag{10.20}$$

- Radial Disturbing Gravity Gradient:

$$T_{rr}(\boldsymbol{x}) = \frac{GM}{4\pi r^3}\sum_{k=1}^{K} d_k \sum_n (2n+1)(n+1)(n+2)B_n \left(\frac{\mathcal{R}}{r}\right)^{n-1} P_n(\psi_k) \tag{10.21}$$

where $\mu = \mathcal{R}/r$ is the bandwidth parameter, and α_k is the geodetic azimuth of ψ_k.

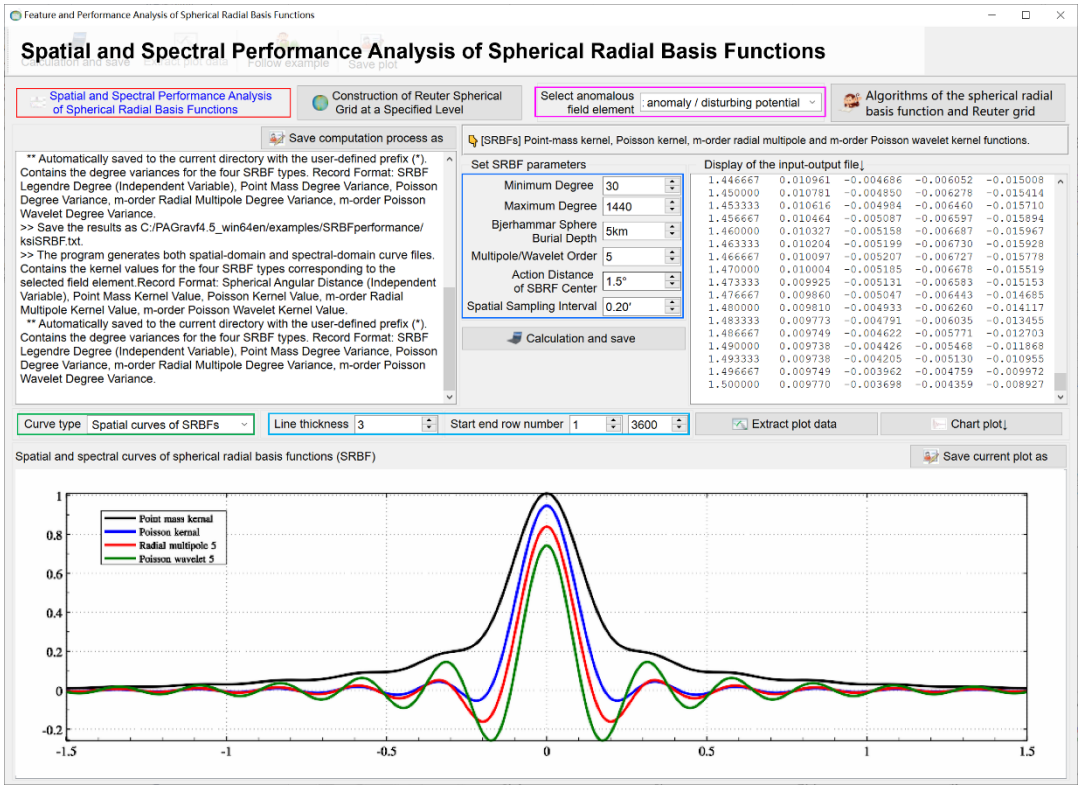

Figure 7.8: Calculation of curves of the four normalized SRBF types

Parameter Selection for Local Approximation:

In local gravity field modeling, a Remove-Restore technique is typically employed: medium-to-low frequency signals are removed using a reference global geopotential model, and residuals are approximated regionally. Consequently, the spectral bandwidth (range of degree n) and the domain of the argument ψ_k in Eqs. (10.16) – (10.21) depend critically on:

- The chosen reference global geopotential model.
- The target regional gravity field structure.
- The desired spatial resolution (controlled by the number of SRBF nodes K or the Reuter grid level Q).

These parameters should be optimized through empirical testing with actual gravity field observation data in target region.

(4) Reuter Grid Construction and Adaptive SRBF Node Design

A Spherical Equal-Area Reuter Grid provides a globally and regionally consistent framework for node distribution. Given a grid level Q, SRBF nodes (centers) are constructed such that their spatial density adapts to the distribution of observations. The level Q acts as the spatial resolution indicator, analogous to the maximum degree N_{max} of a global geopotential model.

● Unit Sphere Reuter Grid Algorithms

For an even integer level Q, the geocentric latitude interval $d\varphi$ and the latitude φ_i of the i-th row center are:

$$d\varphi = \frac{\pi}{Q}, \quad \varphi_i = -\frac{\pi}{2} + \left(i - \frac{1}{2}\right) d\varphi, \quad 1 \le i < Q \tag{10.22}$$

The number of cells J_i along the parallel at φ_i, the longitude interval $d\lambda_i$, and the approximate side length dl_i are:

$$J_i = \left[\!\left[\frac{2\pi cos\varphi_i}{d\varphi}\right]\!\right] = [\![2Qcos\varphi_i]\!], \quad d\lambda_i = \frac{2\pi}{J_i}, \quad dl_i = d\lambda_i cos\varphi_i \tag{10.23}$$

where $[\![\cdot]\!]$ denotes the floor function. Note that $dl_i \approx d\varphi$.

The relative area deviation ε_i from the equatorial cell area ds is:

$$\varepsilon_i = \frac{ds_i - ds}{ds} = \frac{dl_i - d\varphi}{d\varphi} = \frac{d\lambda_i}{d\varphi} cos\varphi_i - 1 \tag{10.24}$$

Typically, ε_i is negligible (order of 10^{-4}), ensuring near-perfect equal-area properties. For regional applications, indices i and J_i are restricted to the target latitude/longitude bounds, avoiding global grid computation.

● Adaptive SRBF Center Design

PAGravf4.5 implements an adaptive algorithm to align SRBF nodes with observation distribution density:

○ Construct a regional Reuter grid at level Q.

○ Count the number of effective observations j within each grid cell containing a potential SRBF node.

○ Pruning Rule: If j is below a user-defined minimum threshold, the corresponding SRBF node is discarded.

○ The remaining nodes form an adaptive SRBF network.

This ensures that SRBF node distribution mirrors observation distribution: regular grids yield regular nodes; irregular or clumped observations yield irregular nodes.

Global Node Count Estimate:

Setting $Q = N_{max}$, the total number of SRBF nodes K for a global grid satisfies:

$$K = \sum_{i=1}^{Q} J_i = \sum_{i=1}^{Q} [\![2Qcos\varphi_i]\!] > N_{maxn}(N_{maxn} + 2) \tag{10.25}$$

Thus, the number of SRBF coefficients slightly exceeds the number of spherical harmonic coefficients for equivalent resolution.

7.10.3 Local Gravity Field Approximation Using the Spectral Domain SRBF Method

Gravity field approximation is essentially a linear spatial transformation. Removing constant factors $(GM/(4\pi))$ and common radial terms $(1/r)$ simplifies the observation equations without altering analytical relationships. Eqs. (10.16) – (10.21) simplify to:

$$\zeta(\boldsymbol{x}) = \frac{1}{\gamma}\sum_{k=1}^{K} d_k \sum_n (2n+1) B_n \mu^n P_n(\psi_k) \tag{10.26}$$

$$\delta g(\boldsymbol{x}) = \frac{1}{r}\sum_{k=1}^{K} d_k \sum_n (2n+1)(n+1) B_n \mu^{n-1} P_n(\psi_k) \tag{10.27}$$

$$\Delta g(\boldsymbol{x}) = \frac{1}{r}\sum_{k=1}^{K} d_k \sum_n (2n+1)(n-1) B_n \mu^{n-1} P_n(\psi_k) \tag{10.28}$$

$$\xi(\boldsymbol{x}) = \frac{1}{r\gamma}\sum_{k=1}^{K} d_k \, cos\alpha_k \sum_n (2n+1) B_n \mu^n \frac{\partial P_n(\psi_k)}{\partial \psi_k} \tag{10.29}$$

$$\eta(\boldsymbol{x}) = \frac{1}{r\gamma}\sum_{k=1}^{K} d_k \, sin\alpha_k \sum_n (2n+1) B_n \mu^n \frac{\partial P_n(\psi_k)}{\partial \psi_k} \tag{10.30}$$

$$T_{rr}(\boldsymbol{x}) = \frac{1}{r^2}\sum_{k=1}^{K} d_k \sum_n (2n+1)(n+1)(n+2) B_n \mu^{n-1} P_n(\psi_k) \tag{10.31}$$

Substituting the specific B_n from Table 7.2 yields the fundamental observation equations:

$$\boldsymbol{L} = \{F(\boldsymbol{x}_i)\}^T = \boldsymbol{A}\{d_k\}^T + \boldsymbol{\varepsilon} \quad (i = 1, \cdots, M; k = 1, \cdots, K) \tag{10.32}$$

where M is the number of observations, K is the number of SRBF centers, and:

$\boldsymbol{L} = \{F(\boldsymbol{x}_1), \cdots, F(\boldsymbol{x}_M)\}^T$: Vector of observed (residual) field elements.

$\boldsymbol{d} = \{d_1, \cdots, d_K\}^T$: Vector of unknown SRBF coefficients.

$\boldsymbol{A}$: The $M \times K$ design matrix, containing the SRBF functions.

$\boldsymbol{\varepsilon}$: The $M \times 1$ observation error vector

● Technical Constraint: Uniform Action Distance

To ensure spatial consistency in the approximation quality, a critical requirement in constructing Eq. (10.32) is that all SRBF centers share an identical Action Distance (or Influence Radius) $d\,r$.

○ Definition: An observation at $\boldsymbol{x}_i$ is influenced only by SRBF nodes k satisfying $\psi_{i,k} \leq dr/\mathcal{R}$.

○ Implication: The support domain of SRBFs is truncated uniformly. This parameter $d\,r$ is conceptually equivalent to the integration radius in spatial local gravity field methods.

7.10.4 Parameter Estimation via Grouped Synergistic Adjustment of Multi-Source Heterogeneous Observations

Observations of gravity field elements exhibit distinct spatial distributions and sensitivity characteristics relative to Spherical Radial Basis Function (SRBF) coefficients. Consequently, the design matrices (sensitivity matrices) within their respective observation equations often possess disparate structural features. Formulating separate normal equations for each observation type and combining them through standard Variance Component Estimation (VCE) frequently results in unstable solutions for the SRBF coefficients due to ill-conditioning.

To address this numerical instability, a Grouped Synergistic Adjustment strategy is employed:

(a) System Grouping: Observation equations are partitioned into distinct groups based on their sensitivity patterns (design matrix $\boldsymbol{A}$) to SRBF coefficients. Observations across different groups are statistically independent, while the design matrices within a single group exhibit homogeneity. Each partition constitutes a distinct Observation System.

(b) Normalization: Normal equations for each system are formed via the Least Squares Principle and subsequently normalized to eliminate magnitude discrepancies arising from differing physical units or sensitivities.

(c) Weighted Combination: System weights are assigned based on observational quality. The normalized normal equations are weighted and summed to form a Combined Normal Equation:

$$\sum_k \left(\frac{w_k}{Q_k}\boldsymbol{A}_k^{\mathrm{T}}\boldsymbol{P}_k\boldsymbol{A}_k\right)\{d_k\}^{\mathrm{T}} = \sum_k \left(\frac{w_k}{Q_k}\boldsymbol{A}_k^{\mathrm{T}}\boldsymbol{P}_k\boldsymbol{L}_k\right) \tag{10.34}$$

where:

k =1,⋯,K : Index of the observation system; K denotes the total number of system groups..

$\boldsymbol{d} = \{d_k\}^{\mathrm{T}}$: Vector of unknown SRBF coefficients.

$\boldsymbol{A}_k, \boldsymbol{P}_k, \boldsymbol{L}_k$: Design matrix, weight matrix, and observation vector for system k, respectively.

Q_k: Normalization parameter, defined as the Root Mean Square (RMS) of the diagonal elements of $\boldsymbol{A}_k^{\mathrm{T}}\boldsymbol{P}_k\boldsymbol{A}_k$. This factor mitigates scale differences in sensitivity between disparate observation systems.

w_k: System weight, reflecting the relative quality of system k compared to others.

Key Properties:

● Independence: The internal weights P_{ki} affect only system k. Normalization via Q_k ensures that systems with sparse observations do not lose sensitivity when combined with dense systems.

● System Weight Determination: The weights w_k are estimated via a simplified Iterative VCE process:

○ Initialization: Set $w_k = 1$ and solve for preliminary SRBF coefficient vector $\boldsymbol{d}$.

○ Variance Estimation: Compute the posteriori variance σ_k^2 for each system using observation residuals.

○ Influence Propagation: Estimate the influence of σ_k^2 on the unknowns (approximated via error propagation):

$$\tilde{\sigma}_{k,s}^2 = \frac{1}{(\boldsymbol{A}_k^T\boldsymbol{A}_k)_s}\sigma_k^2, \quad w_k = \left(\sum_s \tilde{\sigma}_{k,s}^2\right)^{-1} \tag{10.35}$$

where s indexes the SRBF coefficients.

○ Iteration: Update w_k and resolve. This process typically converges within one iteration.

Note: One may analyze the variance function curves $\tilde{\sigma}_{k,s}^2$ with s as the independent variable across different systems to optimize system weights based on specific sensitivity requirements.

7.10.5 Zero-Constraint Method for SRBF Coefficients at Distant Outer Boundaries

In local gravity field approximation, Outer Boundary Constraints are necessary to suppress edge effects and stabilize the solution in regions with sparse data.

Methodology:

$$[\boldsymbol{A}^T\boldsymbol{P}\boldsymbol{A} + \epsilon\boldsymbol{\Xi}]\{d_k\}^T = \boldsymbol{A}^T\boldsymbol{P}\boldsymbol{L} \tag{10.33}$$

where:

$\boldsymbol{\Xi}$: A diagonal constraint matrix. $\Xi_{vv} = 1$ if node v is at or outside the boundary of target region; otherwise 0.

ϵ: A scaling factor, defined as the reciprocal of the RMS of the diagonal elements of $\boldsymbol{A}^T\boldsymbol{P}\boldsymbol{A}$, ensuring numerical balance between data and constraints.

Advantages: The addition of boundary conditions can weaken the need for Tikhonov-type regularization, which might otherwise distort the analytical relationships between field elements. Thus, the intrinsic functional relationships derived from potential theory are

preserved.

7.10.6 Cumulative SRBF Approximation Scheme for Residual Gravity Field elements

From a signal processing perspective, the target field element is effectively the convolution of the observed field element and the SRBF filter kernel. When the target and observed elements differ in type (e.g., approximating gravity anomalies from gravity gradients), a single SRBF function often fails to simultaneously match the spectral center and bandwidth of both elements. This mismatch can lead to spectral leakage, degrading the fidelity of the target field reconstruction. Furthermore, SRBF approximation performance depends on multiple factors beyond the Bjerhammar sphere burial depth $\mathcal{R}$ (or bandwidth parameter $\mu = \mathcal{R}/r$), including:

- The specific SRBF kernel type (Poisson, Radial multipole kernel, etc.).
- The spectral truncation limits (n_{min}, n_{max}).
- The Reuter grid level (Q) and node distribution.
- The effective action distance.

Consequently, optimizing SRBF coefficients solely by tuning the bandwidth parameter μ is insufficient to guarantee an optimal solution.

(1) Proposed Solution: Cumulative SRBF Approximation

To address this limitation, we propose a Cumulative SRBF Approximation Scheme based on the linear additivity of gravity field functionals. Unlike traditional methods that seek a single optimal μ , this scheme employs a multi-step iterative strategy:

- Multi-Spectral Fusion: Each approximation step utilizes SRBFs with distinct spectral characteristics (different centers and bandwidths).
- Parameter Flexibility: Individual steps do not require a fixed, globally optimal Bjerhammar radius $\mathcal{R}$ or μ .
- Signal Resolution: By accumulating contributions from multiple spectral bands, the method can fully resolve the target field's signal content, mitigate spectral leakage, and achieve superior approximation accuracy.

(2) Algorithmic Interpretation

Each step in the Cumulative SRBF method functions equivalently as a Remove-Restore process:

- Remove: The residual field from the previous step serves as the input.
- Restore: The current SRBF approximation models a specific spectral band of the residuals.
- Update: The new approximation is added to the cumulative model, updating the reference field for the next iteration.

This approach ensures that complex gravity field signals, which cannot be captured by a single scale parameter, are reconstructed progressively and robustly.

(3) Quantitative Criteria for Single-Step Effectiveness

The validity of each iteration within the cumulative scheme is governed by two simple and intuitive criteria:

● Spatial Regularity & Minimization: The target field element grid should remain spatially continuous and differentiable, and the standard deviation of residual observations is as small as possible.

● Convergence Behavior: As cumulative steps proceed, the statistical mean of the residual observations must converge toward zero without exhibiting significant sign reversals (indicative of over-correction or instability).

(4) Distinctive Technical Features of the PAGravf4.5 SRBF Module

(a) Strict Analytical Consistency and Error Immunity:

The approximation scheme strictly adheres to the intrinsic analytical functional relationships between gravity field elements. The approximation performance is mathematically decoupled from random observational errors, guaranteeing the internal consistency of the physical-mathematical model.

(b) Full-Space, All-Element Modeling Without Traditional Pre-processing:

Capable of directly utilizing multi-source heterogeneous observations to construct all-element gravity field models on or outside the geoid. No traditional gravity reduction, upward/downward continuation, or gridding interpolation is required, thereby eliminating signal attenuation and non-analytical distortions at the source.

(c) Robust Fusion of Sparse observations:

Exhibits superior capability in leveraging and fusing sparse high-precision observation data (e.g., limited astronomical vertical deflections or GNSS-leveling sites).

(d) Advanced Quality Control and Performance Assessment:

Equipped with high-precision mechanisms for detecting observational gross errors, quantitatively assessing external accuracy metrics, and comprehensively monitoring and optimizing computational performance.

7.11 Height Systems and Height Datum: Theory and Concepts

The fundamental essence of geodetic elevation is the geopotential difference. In geodesy, elevation serves as the geometric approximation of the geopotential number in Earth's gravity field space, defined in an Earth-fixed coordinate reference system. By selecting the geoid potential W_G as the constant reference datum, the geopotential number of a terrain point represents its potential energy relative to the geoid. This constitutes a physically meaningful "physical elevation", an objective quantity inherent to the gravity field. The corresponding height system is termed the Geopotential Number System.

7.11.1 Rigorous Geodetic Definitions of Height Systems

The definition of geometric geodetic elevation must satisfy three fundamental conditions:

● Uniqueness: The elevation of any point must be single-valued.

● Measurability: Reduction corrections should be minimal to avoid significant deviations from observed leveling elevations, in local, low-order levelings.

● Equipotential Consistency: Points on an equipotential surface should possess almost identical elevations.

Geodetic elevation (orthometric or normal height) is the geometric realization of the

geopotential number within the Earth-fixed reference system, adhering to the constraints of uniqueness and measurability. The height difference between two points represents the geometric realization of their geopotential difference. The two primary forms are Orthometric Height and Normal Height, both referred to collectively as "geometric elevations."

Let W_A be the geopotential of terrain point A. Let point Q share the same ellipsoidal coordinates (latitude, longitude) as A, with its normal potential U_Q equal to W_A. By gravity field theory, the segment QA represents the height anomaly ζ_A at point A (see Figure 7.9).

All elements in Figure 7.9 reside within a unified Earth-fixed reference system with a consistent geometric scale. Arrows indicate the direction of measurement. This establishes the Earth-fixed reference system theory as the indispensable foundation for modern height systems.

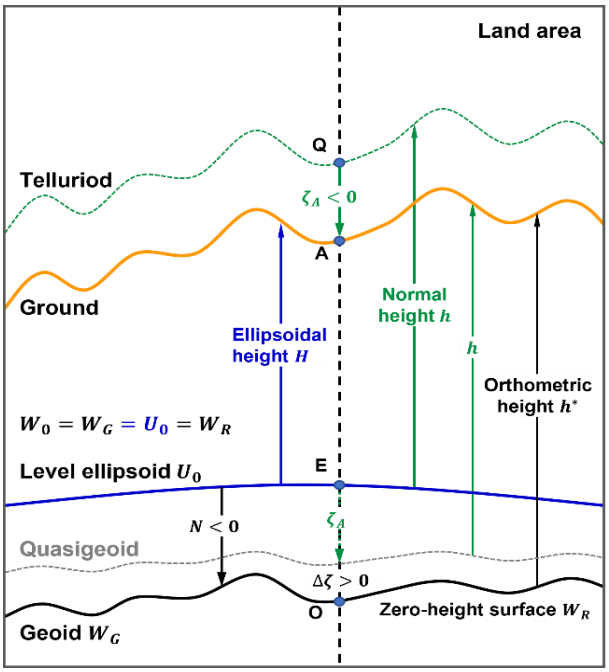

Figure 7.9: Geometric Relationships among Ellipsoidal Height, Orthometric/Normal Height, and Geoidal Height in an Earth-Fixed Reference System

(1) Physical-Geodetic Definition of the Orthometric Height System

Orthometric height h^* is defined as the ratio of the geopotential number c_A of point A to the mean gravity $\bar{g}_A$ between A and the geoid G:

$$h_A^* = \frac{W_G - W_A}{\bar{g}_A} = \frac{c_A}{\bar{g}_A} \tag{11.1}$$

The mean gravity $\bar{g}_A$ is physically defined as:

$$\bar{g}_A = \frac{1}{h_A^*}\int_0^{h^*} g(h)dh \tag{11.2}$$

where dh is the line element between the terrain surface and the geoid. Assuming a constant crustal density ρ, the mean gravity $\bar{g}_A$ can be approximated using the Prey reduction formula:

$$\bar{g}_A = g_A - \left(\frac{1}{2}\frac{\partial\gamma}{\partial h} + 2\pi G\rho\right)h_A^* \tag{11.3}$$

where g_A is the observed gravity at A, G is the gravitational constant, and $\partial\gamma/\partial h$ is the normal

gravity gradient. The resulting elevation is known as the Helmert Orthometric Height.

(2) Physical-Geodetic Definition of the Normal Height System

Normal height h is defined as the ratio of the normal geopotential number of point Q $(U_0 - U_Q)$ to the mean normal gravity $\bar{\gamma}_Q$ between Q and the normal ellipsoid E:

$$h_A = \frac{U_0 - U_Q}{\bar{\gamma}_Q} \tag{11.4}$$

According to the Molodensky condition, the normal geopotential number at Q equals the actual geopotential number at A $(U_0 - U_A = c_A = W_G - W_A)$. Substituting this yields the Molodensky Normal Height:

$$h_A = \frac{U_0 - U_Q}{\bar{\gamma}_Q} = \frac{W_G - W_A}{\bar{\gamma}_Q} = \frac{C_A}{\bar{\gamma}_Q} \tag{11.5}$$

where $\bar{\gamma}_Q$ is the Molodensky mean normal gravity. Given $W_G = U_0$, it follows that

$$U_Q = W_A \tag{11.6}$$

Equation (11.6) confirms that point Q lies on the equipotential surface passing through A (Fig. 7.9). China's national height system is based on this definition.

Note: The Molodensky condition here is distinct from the Molodensky Boundary Value Problem; it is the geometric realization of Bruns' formula at point A.

Since $\bar{\gamma}_Q$ $(\bar{g}_A)$ is constant, normal (orthometric) height is also unique, path-independent, and measurable.

7.11.2 Concept of the Analytical Geoid and Analytical Orthometric Height

The so-called "true" geoid (or terrain-corrected geoid), which attempts to account for the topographic mass effects through reduction, suffers from decimeter-level uncertainties in continental mountainous regions. These uncertainties stem from necessary approximations in terrain density models and assumptions regarding methods of terrain mass reduction (e.g., Helmert condensation or complete Bouguer reduction). At the centimeter-level precision demanded, such a geoid fails to meet the fundamental constraints of uniqueness and precise measurability required for valid geodetic elements. Consequently, the geoidal height derived following such terrain adjustments is metrologically undefined; it is neither uniquely determinable nor does it possess an accepted concept of accuracy.

To resolve this fundamental theoretical and practical impasse, PAGravf4.5 introduces the Analytical Geoid, a well-defined geodetic element achieved via specific, theoretically consistent terrain mass reduction that preserves the potential field's invariance. Crucially, before and after this mass reduction, the geopotential (or the disturbing potential T) remains invariant everywhere across the entire ground surface and throughout the external space (or any closed surface outside the geoid). This geoidal height is defined as the Analytical Geoidal Height, which is mathematically equivalent to the analytical continuation of the height anomaly (ζ) from the ground surface (or exterior) down to the geoid.

In metrological sense, helmert orthometric height fails to qualify as a general geodetic element satisfying the uniqueness and measurability requirement. Furthermore, it does not meet the datum conditions necessary for GNSS Replacing Leveling, since rendering the relationship ($H = h^* + N$) between ellipsoidal height (H), orthometric height (h^*), and geoidal

height (N) ambiguous.

PAGravf4.5 addresses this long-standing deficiency by introducing the Analytical Orthometric Height. In this formulation, the gravity at any point along the theoretical path from the ground to the geoid is not approximated by a constant or a simplified density model. Instead, it is defined as the gravity value obtained via the analytical continuation of the external gravity field to that specific point (i.e., the analytical gravity). The mean gravity along this path is then rigorously defined as the geometric mean of these continuously varying analytical gravity values. The orthometric height derived from this rigorously defined mean gravity constitutes the Analytical Orthometric Height.

Unlike the Helmert orthometric height, both the Analytical Orthometric Height and the Normal Height strictly satisfy the datum conditions for GNSS Replacing Leveling. And the fundamental equation $H = h$ (normal height) + ζ holds with analytical rigor. Furthermore, these two height systems share a rigorous analytical functional relationship within the framework of gravity field theory. This robust and consistent theoretical foundation is not Earth-specific, two height systems can be directly extended and applied to other celestial bodies, such as the Moon and terrestrial planets.

The Analytical Orthometric Height requires no assumptions regarding crustal density. Its mean gravity can be continuously refined and updated using the latest gravity field data and models, making it a dynamic and improvable geodetic element. From the perspective of the uniqueness and measurability of geodetic elements, the Analytical Orthometric Height is more suitable for modern height datum purposes than other types of orthometric heights.

Simple calculations using global geopotential models demonstrate that, numerically, the values of the Analytical Orthometric Height and the Normal Height are globally much closer to each other than either is to the Helmert orthometric height. The discrepancy between the Analytical Orthometric Height and the Helmert orthometric height can reach approximately 60 cm at an elevation of 3,000 meters.

7.11.3 Analytical Functional Relationship between Orthometric and Normal Heights

Geodetic elevation (orthometric or normal height) is the geometric expression of geopotential in the Earth-fixed reference system. Both orthometric and normal heights are objectively unique and precisely measurable.

The ellipsoidal height H relates to orthometric height h^* and geoidal height (geoid undulation) N, as well as normal height h and height anomaly ζ, via:

$$H = h^* + N = h + \zeta \tag{11.7}$$

Equation (11.7) provides the theoretical basis for determining h^* (or h) using GNSS-derived H and a geoid model (N or ζ). The difference between orthometric and normal heights is:

$$h^* - h = \zeta - N = \Delta\zeta \tag{11.8}$$

That is, the discrepancy between the orthometricl height h^* and normal height h equals the difference between the height anomaly ζ and geoidal height N.

The integral solution to the Stokes Boundary Value Problem determines the disturbing potential everywhere outside the geoid, yielding both ζ and N (Generalized Stokes Formula).

Crucially, this solution constrains the analytical relationship between ζ and N (Zhang Chuanyin, 2017):

$$\zeta = N + \Delta\zeta = N + \int_0^{h^*} \frac{\partial \zeta}{\partial h} dh = N - \int_0^{h^*} \frac{\delta g}{\gamma} dh \tag{11.9}$$

where δg is the gravity disturbance and γ are is the normal gravity along the line element dh.

7.11.4 Applicability of the Geoid as the Zero-Elevation Surface

While orthometric and normal heights are unique and measurable geometric quantities, their physical representation (the geopotential number) involves approximations. This is an inherent characteristic of their geodetic definitions.

(1) Geodetic Basis for the Uniqueness of the Height Datum

If the normal height of point A is zero ($h_A = 0$), Substituting equation (11.5), we can obtain:

$$h_A = \frac{U_0 - U_Q}{\bar{\gamma}_Q} = \frac{W_G - W_A}{\bar{\gamma}_Q} = \frac{c_A}{\bar{\gamma}_Q} = 0 \quad \Longrightarrow \quad c_A = 0, \quad W_A = W_G \tag{11.10}$$

This indicates that a point with zero normal height has zero geopotential number, thus the point should lie on the geoid ($W_A = W_G$).

Substituting $c_A = 0$ into the orthometric height definition (11.1) yields:

$$h_A^* = \frac{W_G - W_A}{\bar{g}_A} = \frac{c_A}{\bar{g}_A} = \frac{0}{\bar{g}_A} = 0 \tag{11.11}$$

Equation (11.11) shows that the orthometric height of point A also equals zero, $h_A^* = 0$. Consequently, a point with zero normal height also has zero orthometric height.

Conclusion: The zero-orthometric-height surface, zero-normal-height surface, zero-geopotential-number surface, and the Geoid are coincident. They all share the constant geopotential W_G. Therefore, regardless of the specific height system (Orthometric Height, Normal Height, or Geopotential Number), the geodetic height starting datum surface is only the (global or regional) Geoid.

(2) Analysis of Geoidal Geopotential Properties and Datum Nature

The geodetic definitions of orthometric and normal heights [Eqs. (11.1) and (11.5)] constitute the sole theoretical foundation in geodesy for elucidating the nature of the height starting datum and geodetic elevation. All formulas for leveling elevation difference corrections are derived from these definitions.

The definition of height system can be uniformly expressed as:

$$\mathcal{H} = \frac{W_G - W}{\mathcal{g}} = \frac{c}{\mathcal{g}} \tag{11.12}$$

where:

- ○ If $\mathcal{g}$ represents the mean gravity between the terrain point and the geoid, Eq. (11.12) defines the Orthometric Height System.
- ○ If $\mathcal{g}$ represents the Molodensky mean normal gravity, it defines the Molodensky Normal Height System.
- ○ If $\mathcal{g} = 1$, it defines the Geopotential Number System.

A unique and time-invariant reference datum is a mandatory constraint for the entire geodetic discipline. Examining Eq. (11.12), since $\mathcal{g} \neq 0$, the geopotential W of a terrain point is the sole independent variable determining its orthometric (or normal) height, whereas the

geoidal geopotential W_G is a pre-defined constant. Consequently, Eq. (11.12) dictates that only the constant W_G can serve as the unique, invariant starting datum value for orthometric and normal height systems.

(3) Definition of Geoidal Geometric Deformation

The elevation of any terrain point is an objective quantity uniquely defined by its geopotential number. For a deforming Earth, the geopotential W changes objectively with time due to the redistribution of internal mass, inducing temporal variations in the geopotential number (and thus geometric elevation) at any point. Earth's deformation directly causes discrepancies in the spatial distribution of geopotential between two time epochs. This means that in the Earth-fixed reference system, the geometric positions of the geoid (W_G remains unchanged) at two epochs differ, and this difference represents the geoid's geometric deformation.

7.11.5 Issues with the Quasi-Geoid as a Datum Surface

In traditional physical geodesy, the closed surface where the ellipsoidal height equals the ground height anomaly is termed the quasi-geoid. Historically, this surface was regarded as the datum for normal heights. However, this perception contradicts the rigorous definition of normal height [Eq. (11.5)] for two reasons:

(a) Physical Inconsistency: The geopotential number on the zero-normal-height surface is zero; thus, the zero-normal-height surface is the geoid, not the quasi-geoid.

(b) Violation of Uniqueness: For two points with identical latitude and longitude but different attitudes, their height anomalies (ζ) differ. If normal heights were referenced to the quasi-geoid, there would exist two non-coincident starting points in the vertical direction for the same location, violating the uniqueness requirement of the normal height system.

Actual observation points rarely lie precisely on the specific Digital Elevation Model (DEM) surface employed to construct the ground height anomaly model. For centimeter-level applications, a height-dependent correction $\delta\zeta$, accounting for the height anomaly gradient (or gravity disturbance), should be applied:

$$\zeta = \zeta_0 + \delta\zeta = \zeta_0 + \int_{h_0}^{h} \frac{\partial \zeta}{\partial h} dh = \zeta_0 - \int_{h_0}^{h} \frac{\delta g}{\gamma} dh = \zeta_0 - \left[\frac{\delta g}{\gamma}\right](h - h_0) \tag{11.13}$$

where:

ζ: Height anomaly at the actual observation point (elevation h).

ζ_0: Height anomaly interpolated from the ground height anomaly model to the point's horizontal location.

h_0: Terrain elevation interpolated from the DTM.

$\delta g, \gamma$: Gravity disturbance and normal gravity, respectively, along the vertical segment.

$[\cdot]$: Averaging operator.

Practical Implication: For instance, using a 1′×1′ ground height anomaly model to represent the quasi-geoid can result in correction terms $\delta\zeta$ reaching decimeter-level magnitudes in regions like western China. Thus, while the normal height system is theoretically rigorous, looking the quasi-geoid as its datum surface fails to meet geodetic requirements at decimeter-level accuracy and contradicts Eq. (11.5).

Consequently, PAGravf4.5 comprehensively deemphasizes the concept of the quasi-geoid and related legacy knowledge.

7.11.6 Geometric Properties of Height Systems and Conceptual Updates

Both orthometric and normal height systems are strictly defined within the Earth-fixed reference system based on gravity field theory.

(1) Geometric Parallelism of Orthometric Heights:

Consider two surfaces of constant orthometric height, h_1' and h_2', such that their difference $\Delta h_{12}' = h_2' - h_1' = C \neq 0$ is constant. From Eq. (11.7), the ellipsoidal height difference ΔH_{12} between the two surfaces is:

$$\Delta H_{12} = H_2 - H_1 = (h_2' + N) - (h_1' + N) = h_2' - h_1' = \Delta h_{12}' = C \tag{11.14}$$

Eq. (11.14) demonstrates that the ellipsoidal height difference between two constant orthometric height surfaces equals their orthometric height difference, independent of the geoidal height N. This implies that orthometric equiheight surfaces are parallel within the Earth-fixed reference system.

● **Revised Definition:** Orthometric height is rigorously the distance from a terrain point to the geoid measured along a straight line perpendicular to the geoid. A direct corollary is that the integration path in the mean gravity definition [Eq. (11.2)] should be treated as a straight line.

● **Correction of Misconception:** The conventional view that orthometric height is the irregular curvilinear distance along the plumb line is incorrect. Due to the deflection of the vertical and the curvature of the normal gravity line, the plumb line is an irregular curve whose length exceeds the straight-line distance. This traditional interpretation lacks a rigorous geodetic foundation.

● **Limitation:** Globally parallel closed surfaces do not exist in external Earth space. Parallelism holds only in infinitesimally local spaces; thus, orthometric height possesses typical local properties.

(2) Geometric Behavior of Normal Heights:

Normal height is also unique and measurable. However, since the height anomaly ζ varies with attitude (elevation), normal equiheight surfaces are not strictly parallel in the Earth-fixed reference system. The signal of the height anomaly attenuates with increasing elevation. Consequently, the geometric shape of a normal equiheight surface becomes progressively smoother relative to the geoid as elevation increases.

(3) Conclusion:

● Orthometric Height: Offers intuitive geometric measurement properties due to the parallelism of its equipheight surfaces with the geoid.

● Normal Height: aligns more closely with gravity field properties, as its equipheight surfaces smooth out with elevation increase, reflecting the attenuation of gravitational signals.

● Both height systems possess distinct advantages, limitations, and scientific applicability. Their coexistence is both necessary and scientifically justified.

Index for PAGravf4.5 scientific computation functions

Names table of the sample directories and executable files

No	Program name	Sample directory name / Executable program name
1	PAGravf4.5 system parameter settings	Systemparameterset
2	Computation of Normal Earth Gravity Field and Ellipsoid Constants	PrNormalgravfdcalc
3	Computation of Global Geopotential Models and Spectral Characteristic Analysis	PrModelgravfdcalc
4	Computation of Observed Anomalous Field Elements and Error Analysis of Gravimetric Geoid	ProbsAnomousgrav
5	Correction of Boundary Value Problems for Gravity Field Elements on Non-Equipotential Surfaces	PrBoundaryvalueAdj
6	Analytical Continuation of Anomalous Field Elements Using Multi-Order Radial Gradients	PrGradicontinuation
7	Gross Error Detection and Basis Function Gridding of Geodetic Observations	PrGerrweighgridate
8	Computation of Local Terrain Effects on Field Elements on or outside the Geoid	TerLocalterraininfl
9	Computation of Unified Land, Ocean, and Lake Complete Bouguer Effects on External Gravity	TerCompleteBougure
10	Computation of Terrain Helmert Condensation Effects on External Field Elements	TerHelmertcondensat
11	Computation of Residual Terrain Effects (RTE) on External Field Elements	Renterraineffect

12	Computation of Unified Land-Sea Classical Gravity Bouguer and Isostatic Effects	TerSurfacegravinfl
13	Ultra-High-Degree Spherical Harmonic Analysis and Construction of Land-Sea Terrain Model	TerGloharmanalysis
14	Spherical Harmonic Synthesis of Complete Bouguer or Residual Terrain Effects	TerHarmrntinfluence
15	Demonstration of Terrain Effect Computation Processes on or outside the Geoid	Terraininflexercise
16	External Height Anomaly Computation via Stokes/Hotine Integration	IntgenStokesHotine
17	External Vertical Deflection Computation via Vening-Meinesz Integration	IntgenVeningMeinesz
18	Inverse Integration and Integral of Inverse Operation for Anomalous Field Elements	Integralgrainverse
19	Gradient and Poisson Integral Computation of External Gravity Field Elements	Intgendistgradient
20	Feature and Performance Analysis of Spherical Radial Basis Functions	SRBFperformance
21	Gravity Field Approximation Using SRBFs and Performance Evaluation	SRBFestimateVerify
22	All-element Gravity Field Modeling Using Multi-source Heterogeneous Data with SRBFs	SRBFheterogeneous
23	Modeling Process Exercise: Regional Gravity Field and Geoid	Gravfmdlexercise
24	Normal Height Difference Correction for Height Anomaly and Height System Discrepancy	AppHgtsysdifferent
25	Construction and Refinement of an Equipotential Surface Passing Through a Specified Point	AppEquipotentialhgt
26	Construction of a Terrain Equielevation Surface Passing Through a Specified Point	AppEquihgtpotential
27	Assessment of the Gravimetric Geoid Using GNSS-Leveling Data	AppGeoiderrorestim
28	GNSS-Leveling Data Fusion and Regional Height Datum Optimization	AppGNSSlvlhgtdatum
29	Calculation of Orthometric or Normal Heights via GNSS Replacing Leveling	AppGNSSrepleveling

30	Conversion of General ASCII Records to PAGravf4.5 Format	EdPntrecordstandard
31	Data Interpolation, Extraction, and Land-Sea Separation	Edatafsimpleprocess
32	Simple and Direct Calculations on Geodetic Data Files	EdFlgeodatacalculate
33	Low-Pass Filtering Operations on Geodetic Grid File	EdGrdlowpassfilter
34	Simple Gridding and Regional Geodetic Grid Construction	Edareageodeticdata
35	Construction and Transformation of Vector Grid Files	EdVectorgridtransf
36	Statistical Analysis of Geodetic Data File	Tlstatisticanalysis
37	Calculation of Grid Horizontal Gradients and Vector Grid Inner Products	AppGerrweighgridate
38	Visualization of Multi-attribute Curves from 2D Geodetic Data	multicurvesplot
39	Visualization of Specified Attributes in Discrete Point File	Viewpntdata
40	Visualization of Geodetic Grid File	Viewgridata
41	Visualization of Geodetic Vector Grid File	Viewvectgrd

References

Hofmann-Wellenhof B. and Moritz H. 2006. Physical Geodesy, 2nd edn. New York: Springer Wien.

Ihde J., Sánchez L. 2005. A unified global height reference system as a basis for IGGOS [J]. Journal of Geodynamics. 40: 400-413

Laura Sánchez1, Jonas Agren, et al. 2021, Strategy for the realisation of the International Height Reference System (IHRS), J. Geod., 95: 33

Petit G., Luzum B. 2010. IERS Conventions 2010 [S]. International Earth Rotation and Reference Systems Service. IERS Technical Note No. 36.

Sandwell, David T. 1991, Geophysical Applications of Satellite Altimetry. RvGeo. 05, 29 (S1): 132-137

Seeber G. 2003. Satellite Geodesy [M]. 2nd edition, Water de Gruyter, Berlin New York.

Zhang Chuanyin, Dang Yamin, Jiang Tao, et al. Heterogenous gravity data fusion and gravimetric quasi-geoid computation in the coastal area of China, Marine Geodesy, 2017, 40(2): 142-159

The following in Chinese:

Shen Yunzhong, 2017. Characteristics and improvement ideas of satellite gravity inversion algorithm by dynamic method [J]. Acta Geodaetica et Cartographica Sinica, 46(10): 1038-1315.

Tian Jialei, Li Xinxing, Wu Xiaoping, et al., 2018. Least-squares fast implementation of ultra-high-order gravity field model [J]. Acta Geodaetica et Cartographica Sinica, 47(11): 1437-1445.

Yu Jinhai, Zeng Yanyan, Zhu Yongchao, Meng Xiangchao, 2015. Cross-order recursive algorithm for ultra-high-degree Legendre functions [J]. Chinese Journal of Geophysics, 58(3): 46-53.

Zhang Chuanyin, 2025. Geodesy for a Deforming Earth [M]. Science Press.

Zhang Chuanyin, 2026. Physical Geodesy [M]. Science Press.

Zhang Chuanyin, Chao Dingbo, Ding Jian, et al., 2009. Topographic effects on arbitrary field elements in the space outside the earth under spherical approximation [J]. Acta Geodaetica et Cartographica Sinica, 38(1): 28-34.

Zhang Chuanyin, Guo Chunxi, Chen Junyong, et al., 2009. Analysis on the applicability of EGM2008 gravity field model in mainland China [J]. Acta Geodaetica et Cartographica Sinica, 38(4): 283-289.

Zhang Chuanyin, Jiang Tao, Ke Baogui, 2025a. Theoretical Foundation of Gravity Field and Improvement of Classical Concepts for Geodetic Height Datum unified in the Terrestrial reference System [J]. Acta Geodaetica et Cartographica Sinica, 54(9): 1561-1571.

Zhang Chuanyin, Jiang Tao, Ke Baogui, Wang Wei, 2017. The Analysis of Height System Delinition and the High Precision GNSS Replacing Leveling Method [J]. Acta Geodaetica et Cartographica Sinica, 46(8): 945-951.

Zhang Chuanyin, Ma Xu, Zhang Lei, et al., 2021. Geoid accuracy evaluation method based on GNSS leveling and gravity field error characteristics [J]. Acta Geodaetica et Cartographica Sinica, 50(1): 12-17.

Zhang Chuanyin, Wang Wei, Jiang Tao, 2025b. Monitoring method of Earth's center of mass, figure pole and various rotational dynamics parameters [J]. Acta Geodaetica et Cartographica Sinica, 54(7): 1157-1169.